PART I. RHODIUM-CATALYZED ASYMMETRIC FUNCTIONALIZATION OF ALLYLIC AMINES
PART II. HARNESSING KINETIC DRIVING FORCES IN ALKYNE METATHESIS FOR THE SYNTHESIS OF COMPLEX MOLECULAR ARCHITECTURES

BY

JOSHUA DONN LAFFOON

DISSERTATION

Submitted in partial fulfillment of the requirements
for the degree of Doctor of Philosophy in Chemistry
in the Graduate College of the
University of Illinois at Urbana-Champaign, 2020

Urbana, Illinois

Doctoral Committee:

Professor Jeffrey S. Moore, Chair
Professor Scott E. Denmark
Associate Professor Alison R. Fout
Professor Steven C. Zimmerman

Abstract

Part I of this Dissertation describes the rhodium catalyzed asymmetric functionalization of allylic amines to form chiral products such as β-branched amides and esters, and γ-branched amines. We developed a modular synthetic strategy that enables the diversification of a single allylic amine scaffold into many value-added products. Chiral, β-branched carbonyl compounds are valuable bioactive products as well as useful intermediates in synthetic pathways toward complex chiral products. Inspired by the work of Noyori and Otsuka, we envisioned that the rhodium-catalyzed isomerization of allylic amines to chiral enamines would serve as a powerful platform for the modular functionalization of a general electrophile. Nucleophilic attack onto an enamine in the presence of water leads to the formation of a hemiaminal or hemiacetal depending on the nucleophile. The hydrogen on the methine carbon in the resulting intermediate is hydridic in nature. We hypothesized that the Rh(I) catalyst could perform a dual role in the reaction where after the allylic isomerization, it could then reengage the hemiaminal or hemiacetal intermediate and dehydrogenate leading to an amide or ester respectively. We found that this reaction proceeded with high efficiency in the presence of a suitable hydrogen acceptor and base. The conditions were elaborated with a series of nucleophiles to demonstrate the modularity of this synthetic tool.

Designing a method with modularity in mind, we were motivated to find an allylic amine substrate that could be general with a variety of exogenous amine and alcohol nucleophiles. Noyori established that the steric bulk of the diethyl amine group was necessary for good stereoselectivity in the allylic isomerization of geranyl diethyl amine, but we found that it prevented the rhodium-catalyzed dehydrogenation of the resulting intermediate. When using diethyl allylic amines, the oxidized amide product was not observed; however, saturated aldehyde was observed, indicating

that the isomerization did proceed. We hypothesized that an exogenous, less sterically hindered amine could exchange with the diethyl iminium intermediate to allow the oxidation to the amide to occur. When we added morpholine to the reaction, we observed formation of a single morpholino amide, with no detectable diethyl amide. Diethyl amine is non-competitive even with alcohols or hindered α-branched amines as nucleophiles. This modularity allows rapid diversification of a single prochiral allylic amine into a variety of enantioenriched (90% to 99.9% e.e.) amides and esters via largely commercially available nucleophiles. The reaction generally affords good yields where yield trends correlate with nucleophile strength. Suitable nucleophiles include primary and cyclic secondary amines, anilines, α-branched chiral amines with excellent diastereoselectivity, and alkyl and benzyl alcohols. We also explored reductive conditions. By introducing formic acid as a hydrogen donor, γ-branched, chiral amines formed as the major product. We demonstrated this method for the synthesis of pharmaceuticals such as (*R*)-Tolterodine and Terikalant. The development of this synthetic strategy also contributes to a broader understanding of the tolerance and scope of rhodium hydride transfer methods.

Part II of this Dissertation describes the synthesis of a molecular Möbius strip under alkyne metathesis with kinetic diastereoselectivity. In 1858, mathematicians Möbius and Listing discovered the Möbius strip, a single-sided, unorientable surface. The intriguing Möbius topology would eventually make its way into the consciousness of chemists as a hypothetical molecular topology that had never been observed in nature. The first successful synthesis of a Möbius aromatic hydrocarbon was not achieved until 2003 by Herges and co-workers, paving the way for experimental validation of what was previously only a theoretical understanding of Möbius aromaticity. Over the past 17 years, other macrocycles with Möbius topology have been synthesized while researchers developed new tools for experimentally probing the aromaticity of

these structurally fascinating molecules. Unfortunately, the syntheses of Möbius macrocycles to date have been limited by lengthy routes with low overall yields. We demonstrate that a cyclooligomerization strategy with alkyne metathesis provides high yields of a Möbius macrocycle in up to 84% in a single step. Of two possible diastereomers, only one was observed as a product of the reaction. Intriguingly, the major product was kinetically, rather than thermodynamically, favored, an unexpected result considering that alkyne metathesis is a reversible process. We provide computational justification for the kinetic selectivity which arises from differences in strain energy in the transition state of metallacyclobutadiene formation. Through the aid of calculations such as electron density of delocalized bonds (EDDB) and anisotropic induced current density (ACID), we observed that the Möbius macrocycle does not have global aromaticity but rather localized aromaticity in the helicene subunits. This work will facilitate future syntheses of Möbius macrocycles for structure-aromaticity studies and other applications.

Acknowledgements

I am tremendously grateful to every person who has shepherded me through my education which has ultimately culminated in this body of work. Never once have I accomplished any milestone alone, and I have many people to thank for molding me into the person and scientist I am today.

I am fortunate to have had two scientists whom I deeply admire, Professor Kami L. Hull and Professor Jeffrey S. Moore, as graduate advisors. Kami taught me to think critically and scientifically and to interrogate all sides of a problem. Jeff has set an example of strong and empathetic leadership that I hope to live up to in my own career. As a student in the Moore group, I have always felt empowered to pursue opportunities from internships to teaching appointments to new research projects that have all bolstered my confidence as a scientist and communicator.

My thesis committee has been consistently encouraging and supportive over the years as I have worked through all the stages of this PhD. Thank you to Professor Scott E. Denmark, Professor Alison R. Fout, and Professor Steven C. Zimmerman for always setting the bar high and giving me an education that fills me with pride. More importantly, thank you for your allyship with the students as we have fought to make the department more inclusive.

Most of my training as a chemist has been in the lab under the guiding hands of several incredible mentors. Dr. Zhao Wu taught me nearly everything I know and showed a great deal of patience with me while I was still a novice. Much of the work that is included in this Dissertation would not have been possible without Zhao as a collaborator, and I hope to honor his incredible training throughout my career. I am privileged to have worked alongside Dr. Shashank Shekhar at AbbVie, Inc., an expert chemist who taught me a hypothesis-driven approach to experimental

design. Dr. Christopher C. Pattillo kindly welcomed me into the Moore group and showed me how to build incredible things out of challenging circumstances. I am grateful to Dr. Xing Jiang for enthusiastically taking me on as a collaborator. Xing's imagination brought us the synthesis of the most interesting molecule of my career thus far, a molecular Möbius strip.

I hope someday to be as impactful of an educator as those who I have learned from along the way. First and foremost, Dr. Jose Zavala showed me how to teach from the heart in CHEM 232. As an undergraduate, Professor Charles Mebi, Professor Franklin D. Hardcastle, and Professor Stewart R. Hart all encouraged me to embrace my love of chemistry and pursue this exciting career.

The amazing administrators and support staff in our department have consistently worked to keep us all organized and sane. Without Ashley Trimmell, Kara Metcalf, Lori Johnson, Katriena Knights, Sarah Bransley, Connie Knight, and Patricia Simpson, I would have dropped the ball a long time ago.

Outside of my formal studies, my time in graduate school has taught me the importance of standing up for what I believe in and fighting the good fight. It has been my honor to stand alongside an amazing cohort like Lauren, Jose, Ceci, Abby, Marina, Tabitha, Effie, Thomas, Elizabeth, Edzna, Hailey, Ephraim, Suds, David, and many others. I am a better person because of these people who have all shown me how to do the right thing even when it means putting up a fight.

My amazing friends and coworkers have carried me through every trial and given me wonderful memories to cherish. To Lauren, Raundi, Hannah, Ian, Ceci, Kelly, Neil, Kyle, Andrew, Katie, Morgan, Shuo, and Betty, I love you all and am so thankful to have met you on this journey. I owe a special thanks to everyone who helped build Out in Chem from the ground up including

Hannah, Kris, Ian, Imran, Noah, Annie, Alison, Elise, Lisa, Lloyd, Kyle, and Nick. Thank you for believing and dreaming with me.

Most importantly, I would not be where I am today without the support of my amazing family. To Mom, Autie, and Sim, I feel like I can do anything knowing you will always have my back. Thank you to my wonderful grandparents, Mimi, Papa, MeeMaw, and Khaki for loving and supporting me when I needed you most. Kathryn and Jaime, you are my best friends and my chosen family, and I am unbelievably lucky to have you by my side.

Getting an education has been the adventure of a lifetime. The path to who am I as a scientist as I write this in 2020 has been complex and unpredictable. I am proud of who I am, what I have learned, and what I have to show for it. I am not the same person I was when I first stepped onto the UIUC campus, still closeted at the time, completely out of my depth as a student, and terrified that graduate school might hurt me more than it helped me. But now all the trials that marked the path to a PhD are in my past. I beat the final boss. Thank you to everyone who ushered me along.

With love,

Josh

Dedicated to Autie and Mom

Listen to the MUSTN'TS, child,
Listen to the DON'TS
Listen to the SHOULDN'TS
The IMPOSSIBLES, the WON'TS
Listen to the NEVER HAVES
Then listen close to me—
Anything can happen, child,
ANYTHING can be.

Shel Silverstein

TABLE OF CONTENTS

CHAPTER 1: INTRODUCTION TO PART I

1.1 Importance of Amides and Esters in Biologically Active Compounds and their Syntheses

Amides and esters are potent functionalities in biological settings and are prevalent in pharmaceuticals and agrochemicals (Figure 1.1).[1–3] Of the 100 top grossing pharmaceuticals of 2013, 34 contained either an amide or an ester,[3] and most of those moieties were constructed through acylation with an acyl chloride or some coupling reagent.[4] Figure 1.1 highlights the common feature of β-branching that is found in many biologically active amides and esters. The syntheses of such compounds are further complicated by this added structural component wherein two key steps must be performed independently: setting the stereocenter at the β-position and installing the desired carbonyl functionality. The synthetic overhead required to perform these two steps in separate transformations can be quite significant particularly if several variations of a compound are needed to build a compound library. There has been intense investigation into establishing more efficient routes toward amide and ester incorporation into complex molecular scaffolds.[5,6]

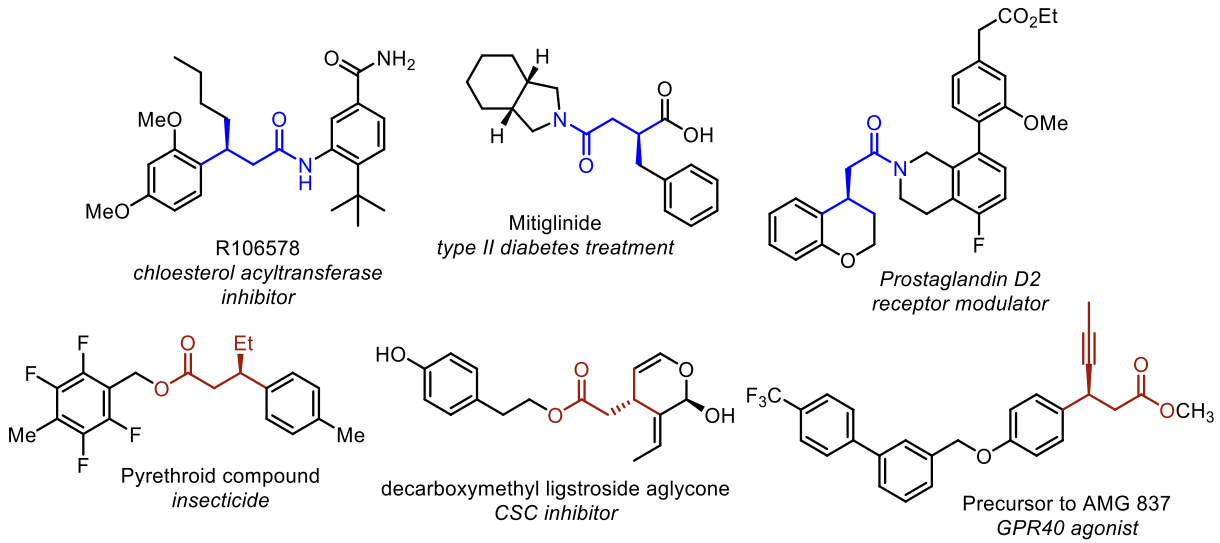

Figure 1.1. Examples of amides and esters in biologically active compounds.

A recent patent demonstrates the synthesis of a library of pyrethroid compounds, useful as household insecticides, through a diastereoselective 1,4-selective Grignard addition followed by a Steglich esterification (Scheme 1.1).[7] This strategy is resource intensive in that it requires stoichiometric chiral auxiliaries and stoichiometric coupling reagents for the conversion of the acid into the ester. Furthermore, the use of Grignard reagents limits the scope of substrates to those devoid of functionality that is sensitive to hard organometallic nucleophiles. The synthesis of the desired β-branched ester requires at least four chemical transformations. This does not include the chemical manipulation that was required to obtain the necessary coupling partners.

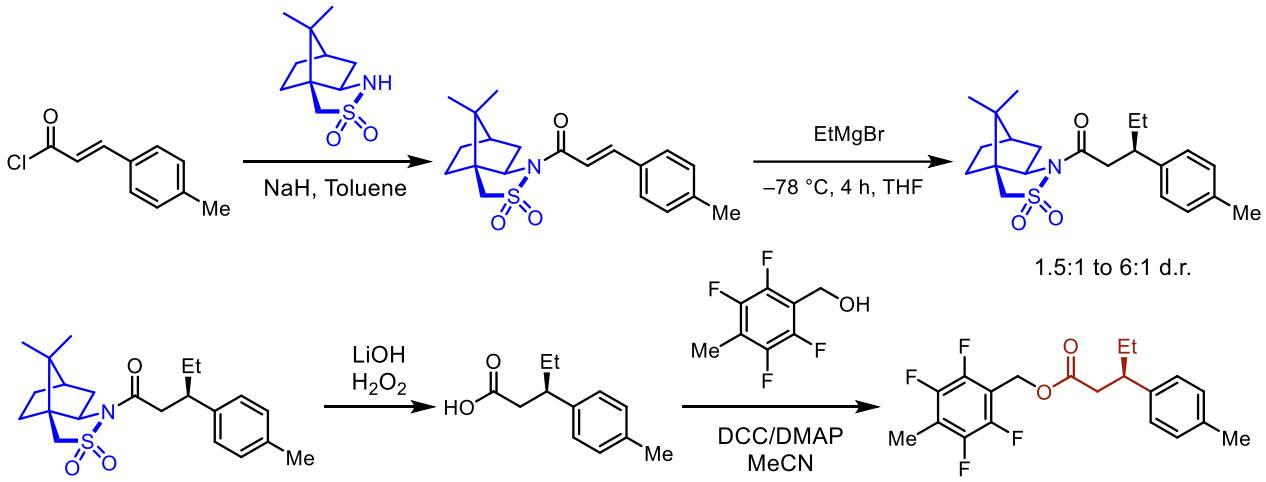

Scheme 1.1. Diastereoselective synthesis of pyrethroid compounds.

Chiral, β-branched esters can also serve as synthetic precursors to pharmaceuticals containing the corresponding carboxylic acid, as is seen in the synthesis of AMG 837 (Scheme 1.2).[8,9] AMG 837 is a GPR40 partial agonist which has shown activity for the treatment of Type II diabetes. The target compound is a β-branched carboxylic acid with an internal alkyne at the β-position. The process scale synthesis published by Amgen is a racemic synthesis involving a chiral resolution.[8] A methodology that directly generates enantioenriched β-branched esters would improve the synthesis by reducing step count and conserving the material that is lost during the chiral separation.

The aforementioned examples demonstrate the common synthetic strategies that have been applied to the synthesis of amide- and ester-containing pharmaceuticals and agrochemicals. Each of these approaches requires several chemical transformations to construct the key β-branched carbonyl compound. Many syntheses are either racemic requiring a chiral resolution or diastereoselective using stoichiometric chiral auxiliaries. To address this synthetic challenge, many researchers have developed catalytic methods for the asymmetric synthesis of chiral, β-branched carbonyl compounds and for the catalytic construction of amide and ester moieties.

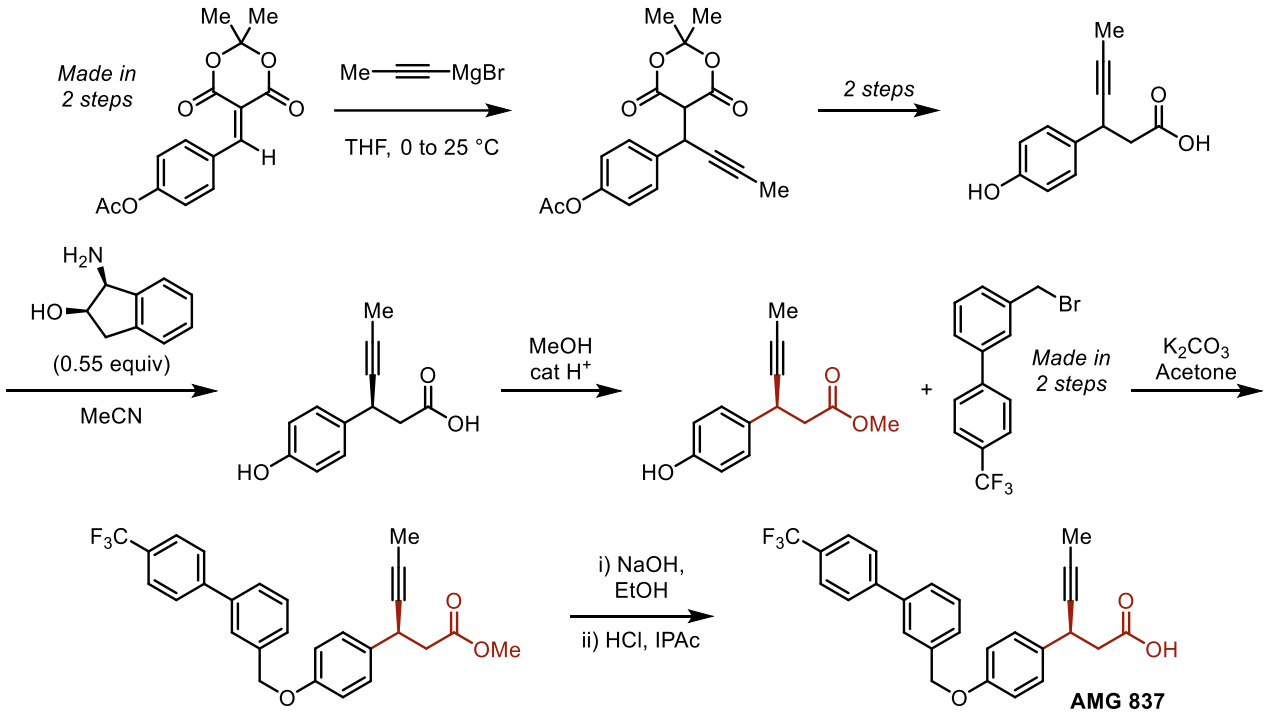

Scheme 1.2. Process route toward AMG 837.

1.1.1 Significant Advances in the Synthesis of Chiral, β-Branched Amides and Esters

Many industrial syntheses of β-branched carbonyl compounds have proceeded through the chiral resolution of a racemic intermediate; however, several methods have sought to establish more general access to this valuable molecular scaffold. In particular, enantioselective functionalization of α,β-unsaturated amides and esters have shown the most promise in achieving

this goal. The most well-established methods are asymmetric conjugate addition (ACA), enantioselective conjugate reduction, and asymmetric hydrogenation.

ACA has been widely developed as a method for constructing both β-branched amides and esters; however, rendering the CA to α,β-unsaturated amides to be asymmetric has presented particularly significant challenges. Amides are the least electrophilic carbonyl compound due to the high degree of resonance delocalization of the lone pair on the Lewis basic nitrogen atom into the carbonyl. This serves to raise the LUMO of the β-position thereby requiring more forcing conditions to effect 1,4-addition of nucleophiles (Scheme 1.3). At the elevated temperatures required for these transformations, the uncatalyzed background reaction becomes competitive with the enantioselective catalytic reaction leading to an erosion of enantioselectivity.[10] In order to circumvent this challenge, two major strategies have been devised: placing electron-withdrawing substituents on the nitrogen atom or appending a chiral auxiliary to the substrate itself.

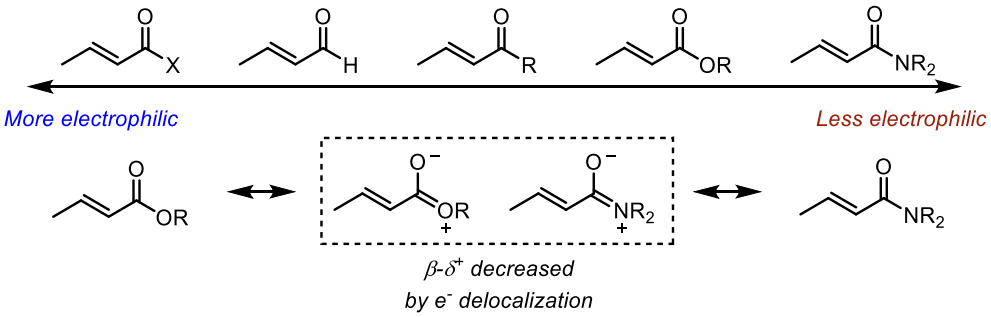

Scheme 1.3. Electrophilicities of various carbonyl compounds.

Electron-deficient enamides, particularly α,β-unsaturated imides, have been widely investigated as surrogate substrates for amides in ACA. Chiral oxazolidinones serve as excellent directing groups for the 1,4-cuprate addition to α,β-unsaturated imides (Scheme 1.4).[11,12] In addition to being electronically activated toward nucleophilic attack, the bidentate coordination of the imide to the Cu species establishes a highly organized transition state where one face of the

olefin is blocked by the substituent on the auxiliary providing access to a single diastereomer after nucleophilic attack. A similar approach has been demonstrated with chiral 1,2-amino alcohol-

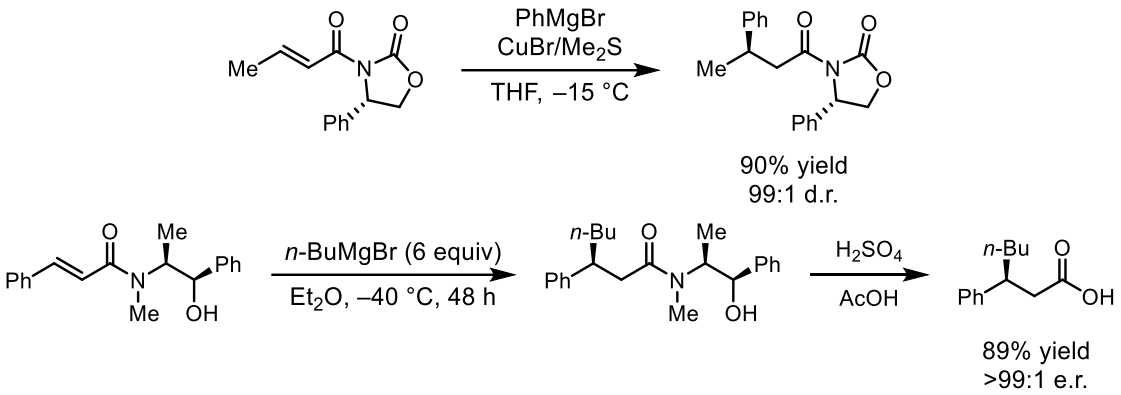

Scheme 1.4. Diastereoselective conjugate additions to α,β-unsaturated imides and amides.

based auxiliaries and Grignard reagents as nucleophiles.[13] It should be noted that auxiliary-based methods require cleavage of the auxiliary followed by subsequent functionalization of the resulting acid to access more general amide or ester products.

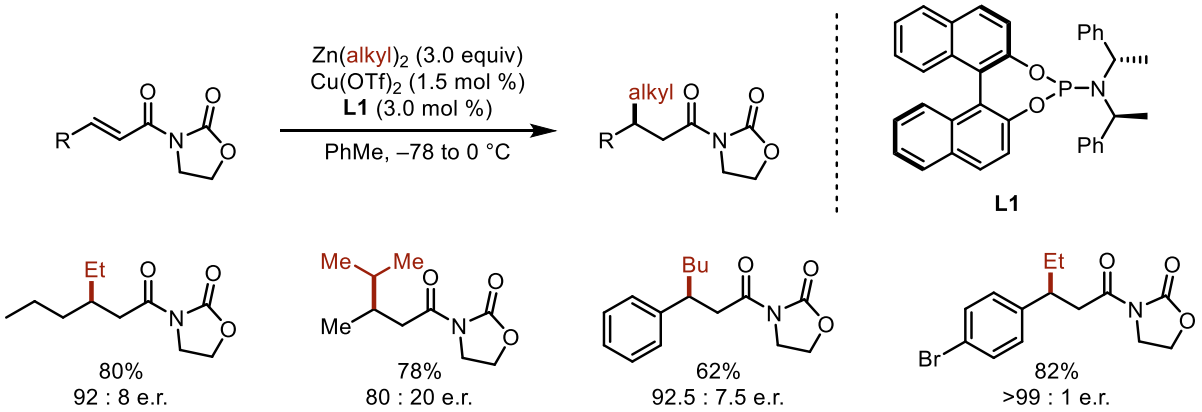

Scheme 1.5. Copper-Catalyzed Enantioselective Conjugate Addition

Catalytic variants of ACA to amides have been enabled by copper and rhodium complexes. Pineschi *et al.* have developed a Cu-phosphoramidite catalyst for the 1,4-addition of dialkyl zinc reagents to α,β-unsaturated imides. The reaction is limited to simple unhindered nucleophiles in order to achieve high selectivities (Scheme 1.5).[14] The first asymmetric rhodium-catalyzed 1,4-addition to amides was published by Miyaura and Sakuma in 2001.[15] In this transformation, a Rh-BINAP complex utilizes aryl boronic acids as nucleophiles for the Michael addition into a variety

of α,β-unsaturated 2° amides. Yields and enantioselectivities are generally high, though the reaction scope is very limited.

Very recently, the conjugate addition of Grignard reagents to acyclic α,β-unsaturated amides facilitated by a chiral copper catalyst and a Lewis acid activator has been reported (Scheme 1.6).[10] In this transformation, either TMSOTf or BF_3•Et_2O serve to activate the substrate toward nucleophilic attack at cryogenic temperatures where the uncatalyzed nucleophilic attack is not kinetically competent. The Lewis acid additive has enabled an unprecedent substrate scope for an asymmetric conjugate addition to a variety of α,β-unsaturated amides, although diaryl-substituted stereocenters are still not accessible.

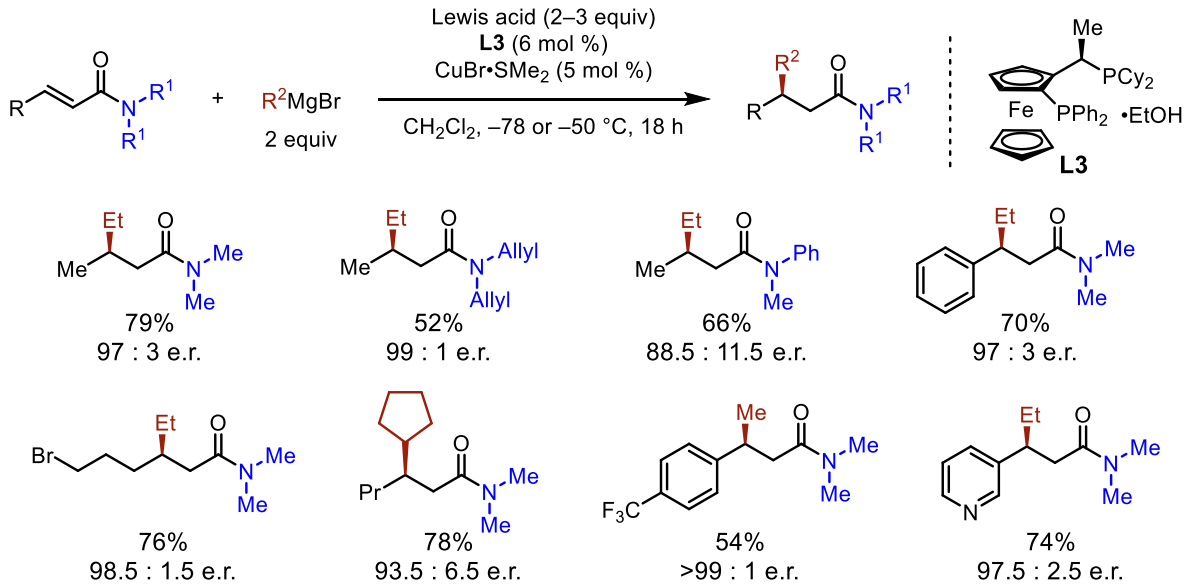

Scheme 1.6. Copper-catalyzed enantioselective conjugate addition to α,β-unsaturated amides.

The enantioselective conjugate addition (ECA) to esters has been more broadly developed than additions to amides, likely due to their increased electrophilicity.[16–20] Feringa *et al.* have shown the use of Cu-phosphine complexes along with Grignard reagents for the synthesis of chiral, β-branched esters (Scheme 1.7).[20] In contrast, Rh-BINAP complexes are known to effect the 1,4-addition of lithium arylborates[17] and aryl boronic acids[19] to α,β-unsaturated esters.

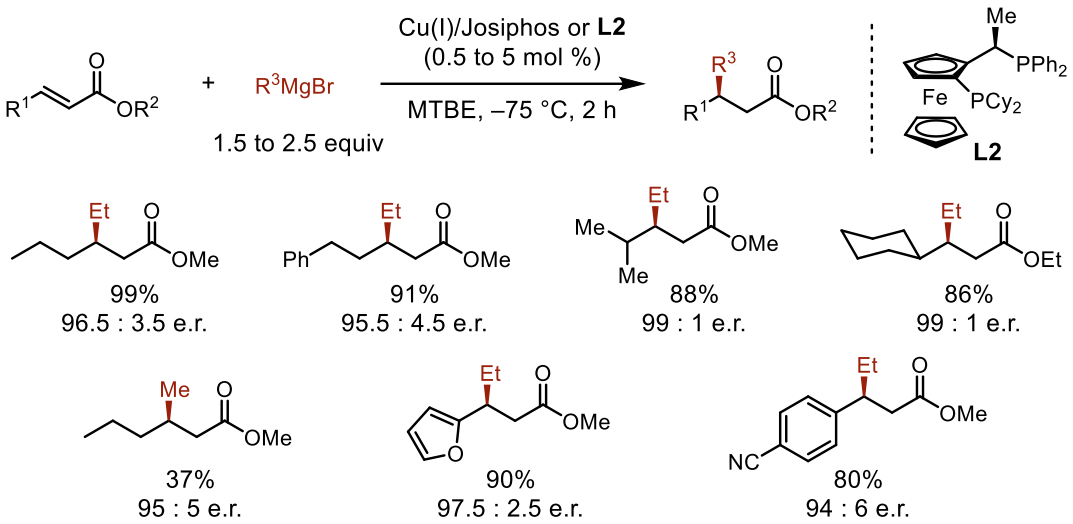

Scheme 1.7. Copper ECA to α,β-unsaturated esters.

In addition to ACA, chiral, β-branched esters can also be accessed from enantioselective conjugate reduction. Conjugate reduction is the 1,4-addition of a hydride into a Michael acceptor. These reactions are typically mediated by a transition metal catalyst in the presence of a hydride source. The most prominent examples of this methodology have been published by Buchwald and coworkers and Lipshutz and coworkers (Scheme 1.8).[21–26] These methods typically employ a Cu-phosphine complex along with polymethylhydrosiloxane (PMHS) for the conjugate reduction of β-disubstituted enoates. In addition to copper-catalysis, a Rh-PheBOX complex has been applied to a similar substrate scope leading to excellent enantioselectivities in most cases.[27] More recently, a Ni-catalyzed transfer hydrogenation approach has been applied toward the synthesis of products containing functional group patterns that are rarely demonstrated within the realm of this chemistry, namely β-cyclic and β-ester substituted carbonyl compounds setting both an α- and a β-stereocenter (Scheme 1.9).

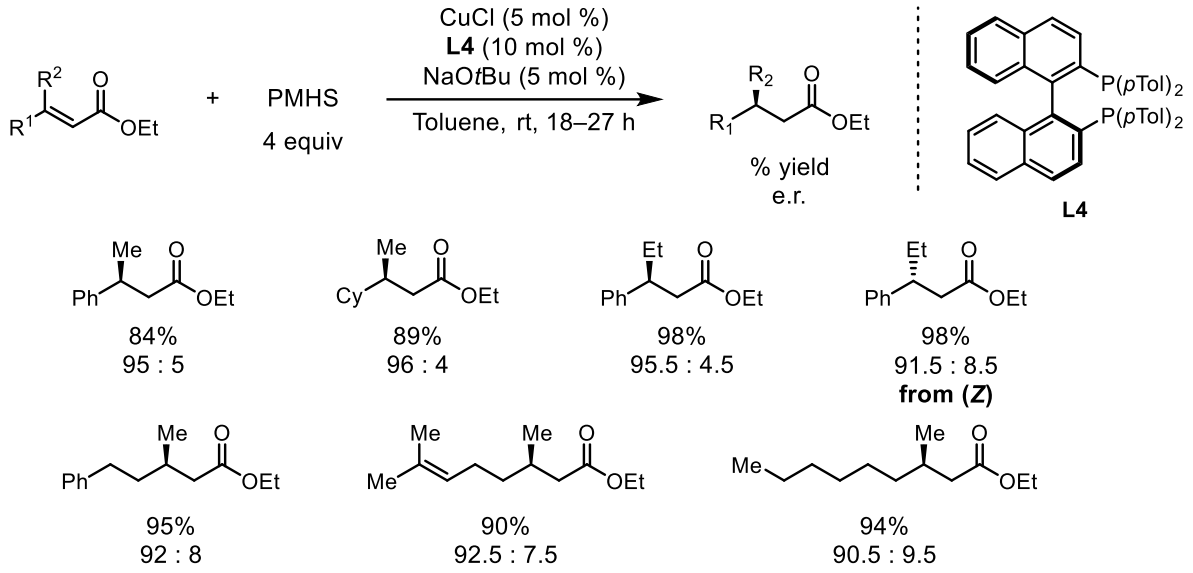

Scheme 1.8. Copper-catalyzed conjugate reduction of enoates.

Generally, for enantioselective conjugate reduction, β-alkyl-β-aryl and β,β-dialkyl substrates are demonstrated where good steric differentiation between the substituents on the olefin is required to obtain high enantioselectivities. This highlights a significant limitation that is general to most methods that form β-branched carbonyl compounds as products. Because the chiral catalyst must distinguish between the substituents at the β-position, one of the substituents is often limited to a small methyl or ethyl group. For this reason, enantioselective routes that might establish a β-diaryl stereocenter are vastly underexplored.

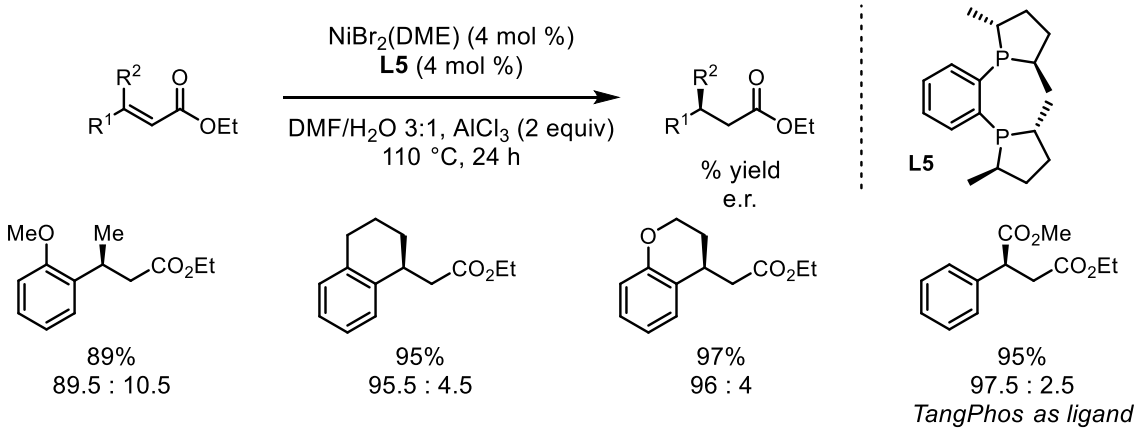

Scheme 1.9. Transfer hydrogenation to enoates.

Asymmetric hydrogenations of α,β-unsaturated esters and carboxylic acids have been extensively studied; however, investigations are typically within the context of catalyst development rather than reaction design.[28] When new catalysts are discovered, they are usually screened with a variety of olefin classes with standard substrates serving as representatives for each class. For this reason, catalysts that are capable of asymmetric hydrogenation of enoates are only demonstrated on a limited number of substrates. There are, of course, rare exceptions to this general trend. In 2012, Andersson *et al*. demonstrated the hydrogenation of α,β-unsaturated esters with a Crabtree-type catalyst yielding complete conversion of starting material and good to excellent enantioselectivities in all cases (Scheme 10).[29]

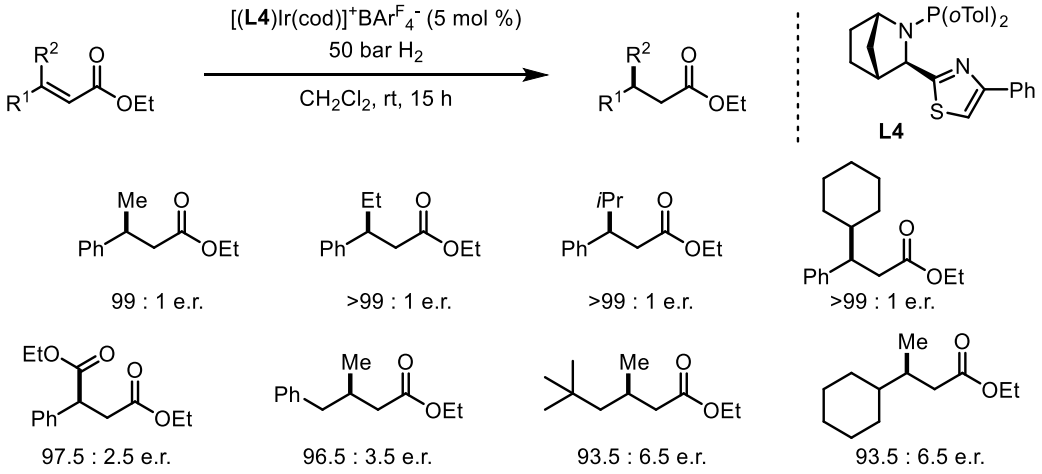

Scheme 1.10. Iridium-catalyzed hydrogenation of α,β-unsaturated esters.

Carboxylic acids are generally superior substrates for asymmetric hydrogenations due to their ability to form tight coordinations to the electrophilic iridium complexes that typically serve as catalysts for the transformations.[28] Currently, the most reliable route to utilizing asymmetric hydrogenation as a synthetic strategy toward chiral, β-branched carbonyl compounds may be through hydrogenation of the α,β-unsaturated carboxylic acid followed by conversion of the acid into the ester or amide derivative. Though this route can provide access to excellent enantioselectivities, it introduces additional synthetic steps into a sequence and is not tolerant of

hydrogenation-sensitive functionalities. Moreover, results with a given catalyst tend to be substrate dependent, and extensive screening may be required to identify an appropriate catalyst for the substrate of interest.

Though previous approaches have made strides in enabling the study and mass production of important biologically active compounds, we recognize the paucity of methods that would allow for a more streamlined synthesis of chiral, β-branched carbonyl compounds. It has been our goal to develop a modular, one-pot protocol for the synthesis of chiral, β-branched amides or esters from easily accessible starting materials.

1.1.2 Dehydrogenative Strategies for Amidation and Esterification

Amide bond formation *via* stoichiometric coupling of carboxylic acids and amines is the most commonly used acylation reaction in the pharmaceutical industry by an astonishing margin.[1] Schneider *et al.* suggest that this favor shown to stoichiometric amide synthesis is due to the operational simplicity of such reactions. However, these strategies often require harsh conditions or generate high molecular weight byproducts that are difficult to separate from the desired compound. Due to the challenges associated with stoichiometric amidation and esterification, catalytic variants have been investigated in recent years.[6,30–32] One such strategy involves the dehydrogenative coupling of alcohols or aldehydes with exogeneous nucleophiles to form the corresponding carbonyl compounds. These reactions can either be acceptorless wherein the only byproduct is H_2 or transfer hydrogenative with a stoichiometric hydride acceptor acting as the terminal oxidant.

Ru-pincer complexes sit at the forefront of dehydrogenative coupling catalysis. Pioneered by Milstein, these complexes facilitate H_2 extrusion from a 1° alcohol to form an amide or ester.[33–

[35] Several analogs of this catalyst have been developed since the seminal report,[36] many of which are capable of both amidation and esterification.

Early esterification reports were limited to the formation of homocoupled (formal Tishchenko) products; however, cross-coupling of 1° alcohols with 2° alcohols have more recently been disclosed.[37] In addition to the cross-coupling of alcohols, transesterification reactions utilizing 2° alcohols as nucleophiles have been achieved with high chemoselectivity.[38] Amidation with both primary[39–43] and secondary[44–48] amines have been optimized where the steric properties of the ligand scaffold play a critical role in achieving high yields (Scheme 1.11). Very recently, pincer complexes derived from base metals such as manganese[48] and iron[47] have been enabled for similar amidation procedures.

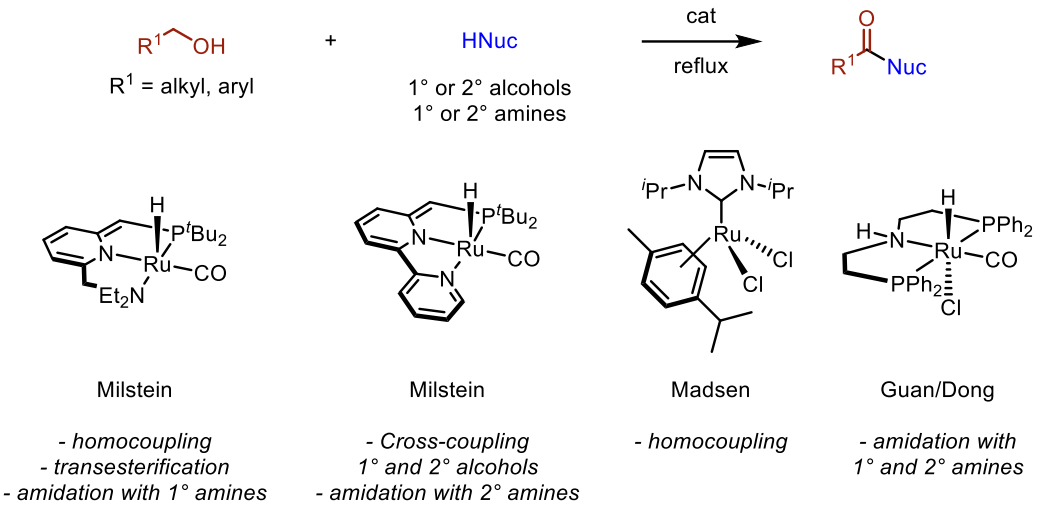

Scheme 1.11. Catalysts for dehydrogenative amidation and esterification.

Transfer hydrogenation has been enabled for the synthesis of both amides and esters under mediation of a variety of metal complexes. Transfer hydrogenation approaches commonly utilize aldehydes as substrates in the presence of stoichiometric hydrogen acceptors. Dong *et al.* have developed a Ni–NHC complex suitable for the coupling of aromatic and aliphatic aldehydes with alcohols, aryl amines, or aliphatic amines with trifluoroacetophenone as a stoichiometric hydrogen acceptor (Scheme 1.12).[49] Molander *et al.* have demonstrated the oxidative esterification of

aliphatic and aromatic aldehydes under palladium catalysis; however, this method requires solvent quantities of alcohol nucleophile.[50]

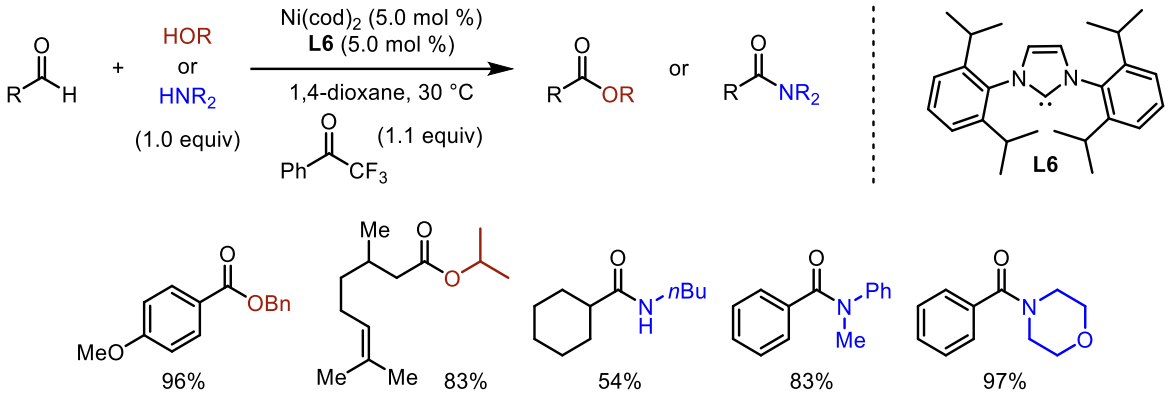

Scheme 1.12. Nickel-catalyzed amidation and esterification of aldehydes.

Considering the valuable complexity of chiral, β-branched carbonyl compounds and the roundabout methods by which they are often synthesized, we have considered the need for more streamlined access to these molecular scaffolds. The state-of-the-art methods in enantioselective β-branched carbonyl synthesis, even after years of extensive development, are still plagued with a fundamental limitation: lack of significant substrate variation. Specifically, current methods only provide access to β-dialkyl or β-alkyl-β-aryl substituted products. Furthermore, one of the β-substituents is almost always a methyl group, and β-diaryl products are virtually never demonstrated outside of the context of hydrogenations of α,β-unsaturated carboxylic acids.[51]

1.2 γ-Branched, Chiral Amines in Biologically Active Compounds

Aliphatic amines with adjacent stereocenters are prevalent in natural products and pharmaceuticals and are often key contributors to their potent biological activity.[52] In particular, enantiopure γ-branched amines represent an important subclass of bioactive amines, including many pharmaceutical agents (Figure 1.2). Despite the generality of this structure, the direct synthesis of chiral, γ-branched amines remains underdeveloped compared to the well-established

methods for constructing α- and β-branched amines,[53–56] as well as distal stereocenters to other function groups such as ketones,[57] aldehydes,[58–61] and amides.[62]

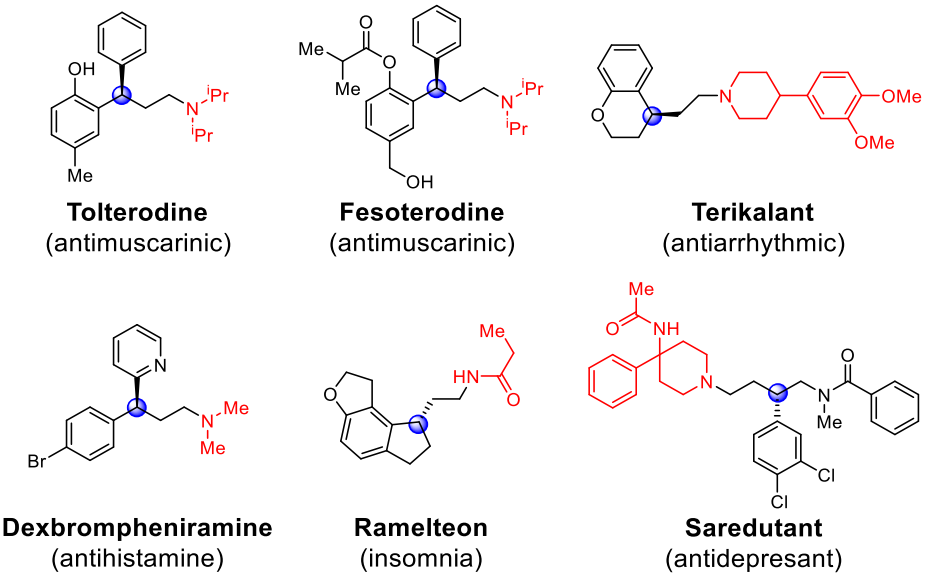

Figure 1.2. Biologically active molecules containing chiral γ-branched amine moiety.

1.2.1 Catalytic Methods for Installing γ-Branched Chiral Amines

Known catalytic approaches to install this subunit often require multistep synthetic sequences via chiral, β-branched carbonyl intermediates, which can hinder the rapid generation of compound libraries for high throughput screening in medicinal chemistry. For example, transition metal-catalyzed asymmetric hydrogenation of α,β-unsaturated acids or esters[63–65] affords the enantiopure β-branched carbonyl intermediates, followed by a reductive amination to install the desired chiral γ-branched amines (Scheme 1.13.1). However, varying substituents at the newly introduced stereocenters, such as aryl vs. alkyl, acyclic vs. cyclic, or carbon atom vs. heteroatom, often requires different metal/ligand scaffolds to achieve high enantioselectivity.[63–65] The redox neutral isomerization of allylic amines[66,67] or alcohols[68–70] provides a solution to this problem; however, current methods suffer from very limited substrate scope.[60–64] To the best of our knowledge, there is only one reported method for the direct synthesis of chiral γ-branched amines

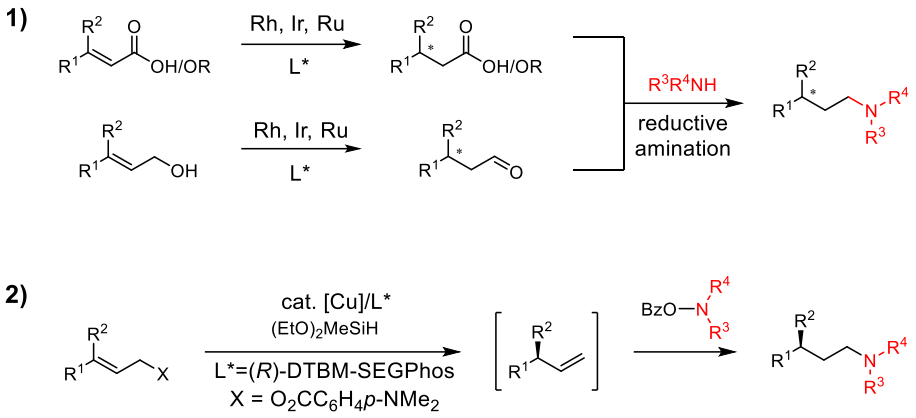

Scheme 1.13. 1) Asymmetric hydrogenation or isomerization followed by reductive amination for the multistep synthesis. 2) Direct synthesis via a Cu—H catalyzed relay hydroamination reaction.

(Scheme 1.13.2). Buchwald et al. have shown that 3,3-disubstituted allylic esters can undergo an enantioselective hydrocupration followed by β-alkoxide elimination and subsequent anti-Markovnikov hydroamination of the intermediate terminal olefin to afford γ-branched amines in one step.[71] Although this method demonstrates high enantioselectivity under a ligand-controlled hydrocupration of allylic esters, the preparation of electrophilic amines requires additional synthetic operations and limits the substrate scope to secondary alkyl amines.[71]

1.3 Research Hypothesis

In each of the examples described above, a chiral catalyst is required to distinguish between the steric environments of the substituents on the olefin to select a face from which to deliver a nucleophile. Enantioselectivity is often improved when one of the substituents is a methyl group because the steric differences between the two β-substituents are more marked. At the outset of our investigation, we believed that an intramolecular hydride transfer from an allylic directing group would allow us to overcome the common limitations of current methods in favor of accessing more nuanced molecular scaffolds (Scheme 1.14).

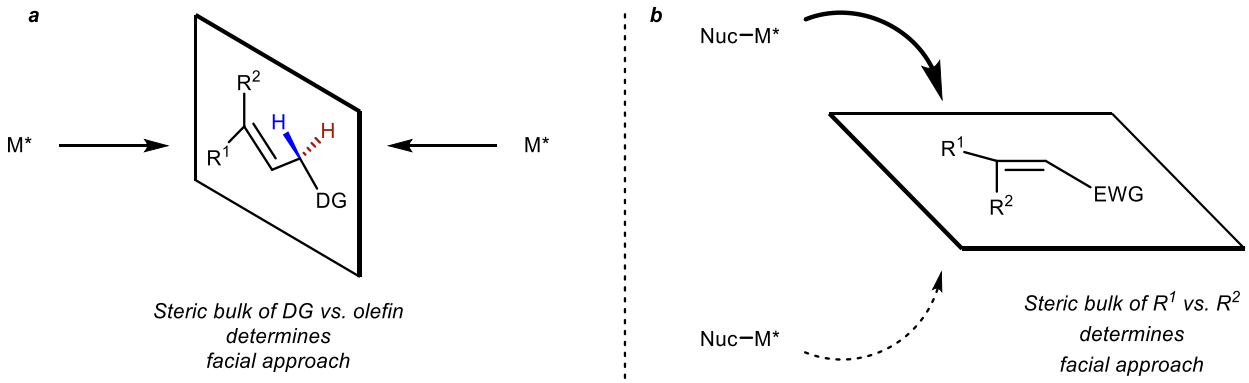

Scheme 1.14. Facial selectivity of olefin functionalizations. a) Stereochemistry of 1,3-hydride shift is determined by directing group and olefin geometry. b) stereochemistry of external nucleophile delivery is determined only by R^1 and R^2.

Allylic Lewis basic groups appealed to us as a substrate class because we envisioned that these would bind the catalyst *via* a two-point binding mode, constraining the conformational freedom of the substrate.[72–76] The facial selectivity of the approach of the substrate to the catalyst would not depend on the substituents on the disubstituted position of the olefin but rather on the combined orientation of the Lewis basic group and olefin. In addition, we have demonstrated that an allylic alcohol may be directly converted to an amide *via* rhodium catalysis[77]The isomerization of an allylic alcohol to form an aldehyde is well-studied,[73–76] and we discovered conditions that would convert the *in situ* formed aldehyde into an amide in the presence of a nucleophile, hydrogen acceptor, and rhodium catalyst. The method we developed provided access to a variety of amides derived from aliphatic or aryl amine nucleophiles; however, when prochiral allylic amines were employed, low enantioselectivities were observed (70:30 e.r.) (Scheme 1.15).

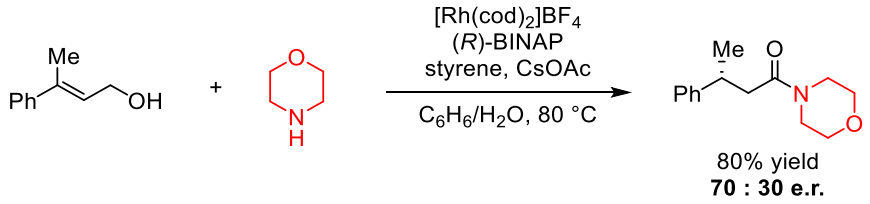

Scheme 1.15. Tandem isomerization/amidation of prochiral allylic alcohols.

The enantioselective isomerization of allylic alcohols is a known challenge in the literature; these methods are often limited in substrate scope.[73–75,78,79] We envisioned that we might render

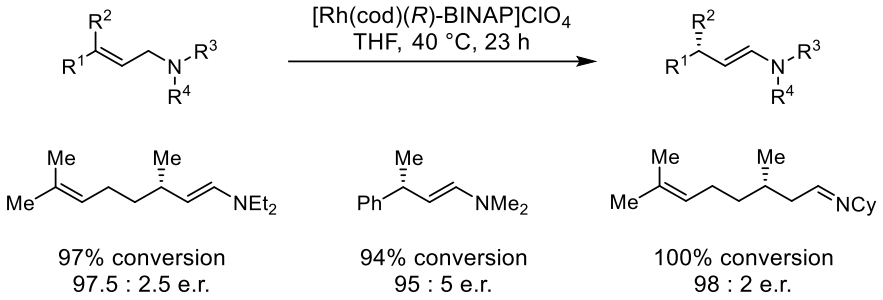

Scheme 1.16. Asymmetric isomerization of allylic amines.

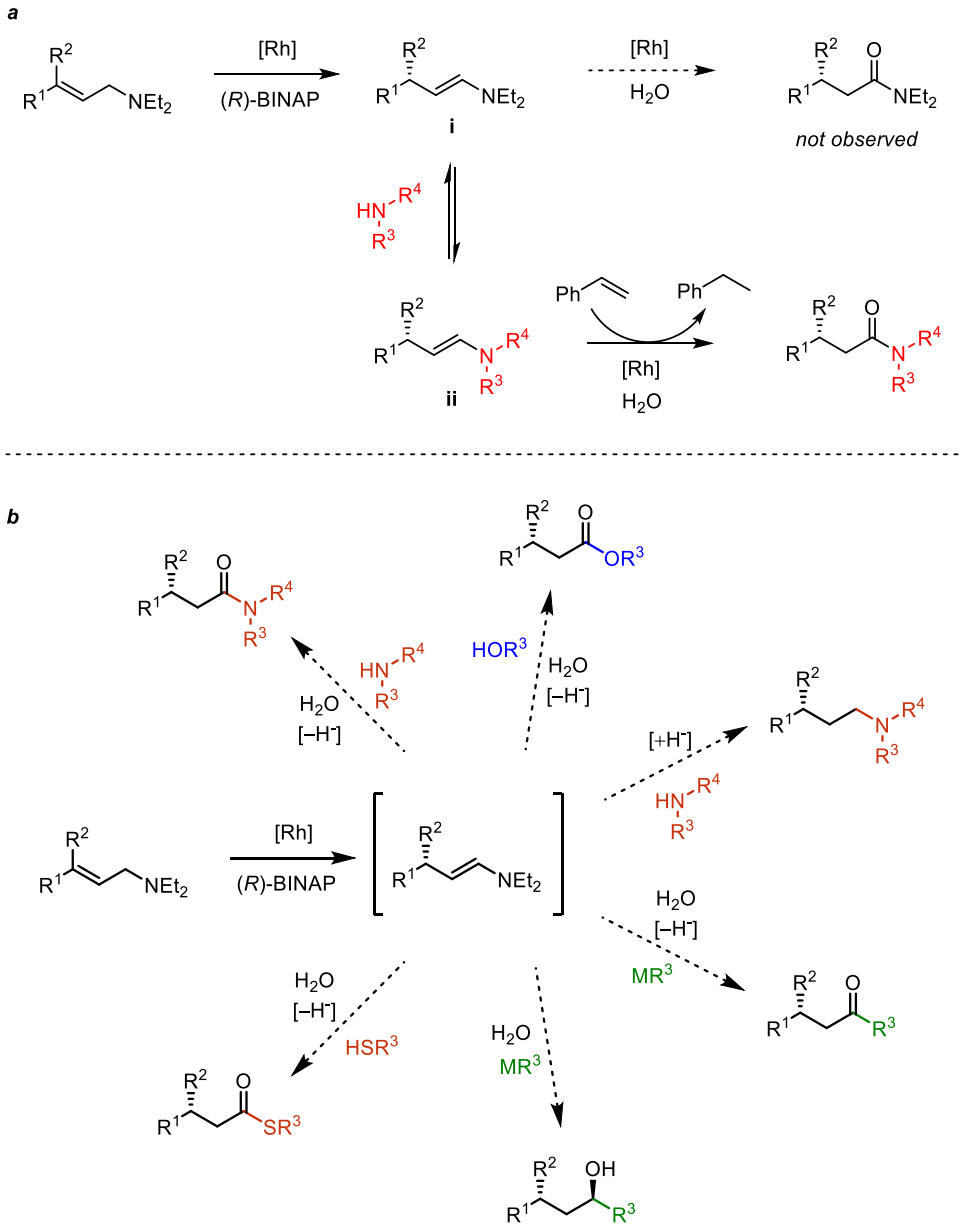

Scheme 1.17. Functionalization of optically pure enamines. a) Proposed enamine exchange of diethyl enamine. b) Proposed functionalizations of diethyl enamine intermediate.

our amidation methodology asymmetric through the allylic isomerization of some functional group that yielded an intermediate that is isoelectronic to an aldehyde, such as an imine. The asymmetric isomerization of allylic amines to generate optically pure enamines proceeds with excellent enantiocontrol under mediation of a Rh-BINAP complex (Scheme 1.16).[72,80–82] Noyori and coworkers have demonstrated that allylic diethyl amines are excellent substrates for the asymmetric isomerization leading to chiral enamines. Our previous results have demonstrated that diethyl amine is not a competent nucleophile for the dehydrogenative amidation of aldehydes, likely due to its steric bulk. Considering this, we propose that the addition of exogeneous amine nucleophiles to diethyl enamine intermediate (**i**) might allow enamine exchange to form (**ii**) followed by oxidation enabling a selective, modular synthesis of chiral, β-branched amides (Scheme 1.17 a). Furthermore, functionalizing the enamine intermediate with a variety of nucleophiles would lead to the formation of several classes of carbonyl compounds from a common starting material (Scheme 1.17 b).

1.4 Literature Cited

(1) Schneider, N.; Lowe, D. M.; Sayle, R. A.; Tarselli, M. A.; Landrum, G. A. Big Data from Pharmaceutical Patents: A Computational Analysis of Medicinal Chemists' Bread and Butter. *J. Med. Chem.* **2016,** *59,* 4385–4402.

(2) Brown, D. G.; Boström, J. Analysis of Past and Present Synthetic Methodologies on Medicinal Chemistry: Where Have All the New Reactions Gone? *J. Med. Chem.* **2016,** *59,* 4443–4458.

(3) Top 100 Drugs by Retail Sales. Poster. http://njardarson.lab.arizona.edu/sites/njardarson.lab.arizona.edu/files/Top%20US%20Pharmaceutical%20Products%20of%202013.pdf [accessed October 10, 2020].

(4) Carey, J. S.; Laffan, D.; Thomson, C.; Williams, M. T. Analysis of the Reactions Used for the Preparation of Drug Candidate Molecules. *Org. Biomol. Chem.* **2006,** *4,* 2337–2347.

(5) Pattabiraman, V. R.; Bode, J. W. Rethinking Amide Bond Synthesis. *Nature* **2011,** *480,* 471–479.

(6) Tsakos, M.; Schaffert, E. S.; Clement, L. L.; Villadsen, N. L.; Poulsen, T. B. Ester Coupling Reactions – An Enduring Challenge in the Chemical Synthesis of Bioactive Natural Products. *Nat. Prod. Rep.* **2015,** *32,* 605–632.

(7) Cao, X.; Li, H.; Han, X.; Wang, M.; Xu, S.; Chen, C. Pyrethroid Compound, and Preparation Method and Applications Thereof. *CN103319343A* **2013.**

(8) Walker, S. D.; Borths, C. J.; DiVirgilio, E.; Huang, L.; Liu, P.; Morrison, H.; Sugi, K.; Tanaka, M.; Woo, J. C. S.; Faul, M. M. Development of a Scalable Synthesis of a GPR40 Receptor Agonist. *Org. Process Res. Dev.* **2011,** *15,* 570–580.

(9) Yazaki, R.; Kumagai, N.; Shibasaki, M. Enantioselective Synthesis of a GPR40 Agonist AMG 837 via Catalytic Asymmetric Conjugate Addition of Terminal Alkyne to α,β-Unsaturated Thioamide. *Org. Lett.* **2011,** *13,* 952–955.

(10) Rodríguez-Fernández, M.; Yan, X.; Collados, J. F.; White, P. B.; Harutyunyan, S. R. Lewis Acid Enabled Copper-Catalyzed Asymmetric Synthesis of Chiral β-Substituted Amides. *J. Am. Chem. Soc.* **2017,** *139,* 14224–14231.

(11) Byrd, K. M. Diastereoselective and Enantioselective Conjugate Addition Reactions Utilizing α,β-Unsaturated Amides and Lactams. *Beilstein J. Org. Chem.* **2015,** *11,* 530–562.

(12) Nicolás, E.; Russell, K. C.; Hrubry, V. J. Asymmetric 1,4-Addition of Organocuprates to Chiral α,β-Unsaturated *N*-Acyl-4-phenyl-2-oxazolidinones: A New Approach to the Synthesis of Chiral β-Branched Carboxylic Acids. *J. Org. Chem.* **1993,** *58,* 766–770.

(13) Mukaiyama, T.; Iwasawa, N. A Facile Asymmetric Synthesis of β-Substituted Alkanoic Acid: The Highly Stereoselective Michael Addition of Grignard Reagents to α,β-Unsaturated Carboxylic Amides Derived from (L)-Ephedrine. *Chem. Lett.* **1981,** *10,* 913–916.

(14) Pineschi, M.; Del Moro, F.; Di Bussolo, V.; Macchia, F. Highly Enantioselective Copper-Phosphoramidite-Catalyzed Conjugate Addition of Dialkylzinc Reagents to Acyclic α,β-Unsaturated Imides. *Adv. Synth. Catal.* **2006,** *348,* 301–304.

(15) Sakuma, S.; Miyaura, N. Rhodium(I)-Catalyzed Asymmetric 1,4-Addition of Arylboronic Acids, to α,β-Unsaturated Amides. *J. Org. Chem.* **2001,** *66,* 8944–8946.

(16) Wang, S.-Y.; Ji, S.-J.; Loh, T.-P. Cu(I) Tol-BINAP-Catalyzed Enantioselective Michael Reactions of Grignard Reagents and Unsaturated Esters. *J. Am. Chem. Soc.* **2007,** *129,* 276–277.

(17) Takaya, Y.; Senda, T.; Kurushima, H.; Ogasawara, M.; Hayashi, T. Rhodium-catalyzed asymmetric 1,4-addition of arylboron reagents to α,β-unsaturated esters. *Tetradhedron: Asymmetry* **1999,** *10,* 4047–4056.

(18) Harutyunyan, S. R.; Hartog, T. d.; Geurts, K.; Minnaard, A. J.; Feringa, B. L. Catalytic Asymmetric Conjugate Addition and Allylic Alkylation with Grignard Reagents. *Chem. Rev.* **2008,** *108,* 2824–2852.

(19) Sakuma, S.; Sakai, M.; Itooka, R.; Miyaura, N. Asymmetric Conjugate 1,4-Addition of Arylboronic Acids to α,β-Unsaturated Esters Catalyzed by Rhodium(I)/(*S*)-binap. *J. Org. Chem.* **2000,** *65,* 5951–5955.

(20) López, F.; Harutyunyan, S. R.; Meetsma, A.; Minnaard, A. J.; Feringa, B. L. Copper-Catalyzed Enantioselective Conjugate Addition of Grignard Reagents to α,β-Unsaturated Esters. *Angew. Chem. Int. Ed.* **2005,** *44*, 2752–2756.

(21) Appella, D. H.; Moritani, Y.; Shintani, R.; Ferreira, E. M.; Buchwald, S. L. Asymmetric Conjugate Reduction of α,β-Unsaturated Esters Using a Chiral Phosphine–Copper Catalyst. *J. Am. Chem. Soc.* **1999,** *121*, 9473–9474.

(22) Hughes, G.; Kimura, M.; Buchwald, S. L. Catalytic Enantioselective Conjugate Reduction of Lactones and Lactams. *J. Am. Chem. Soc.* **2003,** *125*, 11253–11258.

(23) Rainka, M. P.; Aye, Y.; Buchwald, S. L. Copper-Catalyzed Asymmetric Conjugate Reduction as a Route to Novel β-Azaheterocyclic Acid Derivatives. *Proc. Natl. Acad. Sci.* **2004,** *101*, 5821–5823.

(24) Jurkauskas, V.; Sadighi, J. P.; Buchwald, S. L. Conjugate Reduction of α,β-Unsaturated Carbonyl Compounds Catalyzed by a Copper Carbene Complex. *Org. Lett.* **2003,** *5*, 2417–2420.

(25) Lipshutz, B. H.; Keith, J.; Papa, P.; Vivian, R. A Convenient, Efficient Method for Conjugate Reductions Using Catalytic Quantities of Cu(I). *Tetrahedron Lett.* **1998,** *39*, 4627–4630.

(26) Lipshutz, B. H.; Servesko, J. M.; Taft, B. R. Asymmetric 1,4-Hydrosilylations of α,β-Unsaturated Esters. *J. Am. Chem. Soc.* **2004,** *126*, 8352–8353.

(27) Kanazawa, Y.; Tsuchiya, Y.; Kobayashi, K.; Shiomi, T.; Itoh, J.-i.; Kikuchi, M.; Yamamoto, Y.; Nishiyama, H. Asymmetric Conjugate Reduction of α,β-Unsaturated Ketones and Esters with Chiral Rhodium(2,6-bisoxazolinylphenyl) Catalysts. *Chem. Eur. J.* **2005,** *12*, 63–71.

(28) Khumsubdee, S.; Burgess, K. Comparison of Asymmetric Hydrogenations of Unsaturated Carboxylic Acids and Esters. *ACS Catal.* **2013,** *3*, 237–249.

(29) Li, J.-Q.; Quan, X.; Andersson, P. G. Highly Enantioselective Iridium-Catalyzed Hydrogenation of α,β-Unsaturated Esters. *Chem. Eur. J.* **2012,** *18,*10609–10616.

(30) Pattabiraman, V. R.; Bode, J. W. Rethinking Amide Bond Synthesis. *Nature,* **2011,** *480,* 471–479.

(31) Figueiredo, R. M. d.; Suppo, J.-S.; Campagne, J.-M. Nonclassical Routes for Amide Bond Formation. *Chem. Rev.* **2016,** *116,* 12029–12122.

(32) Dunetz, J. R.; Magano, J.; Weisenburger, G. A. Large-Scale Applications of Amide Coupling Reagents for the Synthesis of Pharmaceuticals. *Org. Process Res. Dev.* **2016,** *20,* 140–177.

(33) Gunanathan, C.; Milstein, D. Applications of Acceptorless Dehydrogenation and Related Transformations in Chemical Synthesis. *Science* **2013,** *341,* 1229712.

(34) Gunanathan, C.; Milstein, D. Bond Activation and Catalysis by Ruthenium Pincer Complexes. *Chem. Rev.* **2014,** *114,* 12024–12087.

(35) Werkmeister, S.; Neumann, J.; Junge, K.; Beller, M. Pincer-Type Complexes for Catalytic (De)Hydrogenation and Transfer (De)Hydrogenation Reaction: Recent Progress. *Chem. Eur. J.* **2015,** *21,* 12226–12250.

(36) Zhang, J.; Leitus, G.; Ben-David, Y.; Milstein, D. Facile Conversion of Alcohols into Esters and Dihydrogen Catalyzed by New Ruthenium Complexes. *J. Am. Chem. Soc.* **2005,** *127,* 10840–10841.

(37) Srimani, D.; Balaraman, E.; Gnanaprakasam, B.; Ben-David, Y.; Milstein, D. Ruthenium Pincer-Catalyzed Cross-Dehydrogenative Coupling of Primary Alcohols with Secondary Alcohols under Neutral Conditions. *Adv. Synth. Catal.* **2012,** *354,* 2403–2406.

(38) Gnanaprakasam, B.; Ben-David, Y.; Milstein, D. Ruthenium Pincer-Catalyzed Acylation of Alcohols Using Esters with Liberation of Hydrogen under Neutral Conditions. *Adv. Synth. Catal.* **2010,** *352,* 3169–3173.

(39) Naota, T.; Murahashi, S.-I. Ruthenium-Catalyzed Transformations of Amino Alcohols to Lactams. *Synlett* **1991,** 693–694.

(40) Gunanathan, C.; Ben-David, Y.; Milstein, D. Direct Synthesis of Amides from Alcohols and Amines with Liberation of H_2. *Science* **2007,** *317,* 790–792.

(41) Kim, K.; Kang, B.; Hong, S. H. *N*-Heterocyclic Carbene-Based Well-Defined Ruthenium Hydride Complexes for Direct Amide Synthesis from Alcohols and Amines Under Base-Free Condtions. *Tetrahedron* **2015,** *71,* 4565–4569.

(42) Gusev, D. G. Rethinking the Dehydrogenative Amide Synthesis. *ACS Catal.* **2017,** *7,* 6656–6662.

(43) Makarov, I. S.; Fristrup, P.; Madsen, R. Mechanistic Investigation of the Ruthenium–N-Heterocyclic-Carbene-Catalyzed Amidation of Amines with Alcohols. *Chem. Eur. J.* **2012,** *18,* 15683–15692.

(44) Ortega, N.; Richter, C.; Glorius, F. *N*-Formylation of Amines by Methanol Activation. *Org. Lett.* **2013,** *15,* 1776–1779.

(45) Srimani, D.; Balaraman, E.; Hu, P.; Ben-David, Y.; Milstein, D. Formation of Tertiary Amides and Dihydrogen by Dehydrogenative Coupling of Primary Alcohols with Secondary Amines Catalyzed by Ruthenium Bipyridine-Based Pincer Complexes. *Adv. Synth. Catal.* **2013,** *355,* 2525–2530.

(46) Oldenhius, N. J.; Dong, V. M.; Guan, Z. Catalytic Acceptorless Dehydrogenations: Ru-Macho Catalyzed Construction of Amides and Imines. *Tetrahedron* **2014,** *70,* 4213–4218.

(47) Lane, E. M.; Uttley, K. B.; Hazari, N.; Bernskoetter, W. Iron-Catalyzed Amide Formation from the Dehydrogenative Coupling of Alcohols and Secondary Amines. **2017,** *36,* 2020–2025.

(48) Kumar, A.; Espinosa-Jalapa, N. A.; Leitus, G.; Diskin-Posner, Y.; Avram, L.; Milstein, D. Direct Synthesis of Amides by Dehydrogenative Coupling of Amines with either Alcohols or Esters: Manganese Pincer Complex as Catalyst. *Angew. Chem. Int. Ed.***2017,** *129,* 15188–15192.

(49) Whittaker, A. M.; Dong, V. M. Nickel-Catalyzed Dehydrogenative Cross-Coupling: Direct Transformation of Aldehydes into Esters and Amides. *Angew. Chem. Int. Ed.* **2015,** *54,* 1312–1315.

(50) Tschaen, B. A.; Schmink, J. R.; Molander, G. A. Pd-Catalyzed Aldehyde to Ester Conversion: A Hydrogen Transfer Approach. *Org. Lett.* **2013,** *15,* 500–503.

(51) Yan, Q.; Kong, D.; Zhao, W.; Zi, G.; Hou, D. Enantioselective Hydrogenation of β,β-Disubstituted Unsaturated Carboxylic Acids under Base-Free Conditions. *J. Org. Chem.* **2016,** *81,* 2070–2077.

(52) Nugent, T. C. Chiral Amine Synthesis: Methods, Developments and Applications. Chiral Amine Synthesis: Methods, Developments and Applications. (**2010**). doi:10.1002/9783527629541

(53) Hoffmann, S., Nicoletti, M. & List, B. Catalytic Asymmetric Reductive Amination of Aldehydes via Dynamic Kinetic Resolution. *J. Am. Chem. Soc.* **2006,** *128,* 13074–13075.

(54) Lu, Z., Wilsily, A. & Fu, G. C. Stereoconvergent Amine-Directed Alkyl-Alkyl Suzuki Reactions of Unactivated Secondary Alkyl Chlorides. *J. Am. Chem. Soc.* **2011,** *133,* 8154–8157.

(55) Zhu, S. & Buchwald, S. L. Enantioselective Cu–H-catalyzed Anti-Markovnikov Hydroamination of 1,1-Disubstituted Alkenes. *J. Am. Chem. Soc.* **2014,** *136,* 15913–15916.

(56) Czekelius, C. & Carreira, E. M. Catalytic Enantioselective Conjugate Reduction of β,β-Disubstituted Nitroalkenes. *Angew. Chem. Int. Ed.* **2003,** *42,* 4793–4795.

(57) Werner, E. W., Mei, T. S., Burckle, A. J. & Sigman, M. S. Enantioselective Heck Arylations of Acyclic Alkenyl Alcohols Using a Redox-Relay Strategy. *Science* **2012,** *338,* 1455–1458.

(58) Mei, T. S., Werner, E. W., Burckle, A. J. & Sigman, M. S. Enantioselective Redox-Relay Oxidative Heck Arylations of Acyclic Alkenyl Alcohols Using Boronic Acids. *J. Am. Chem. Soc.* **2013,** *135,* 6830–6833.

(59) Mei, T. S., Patel, H. H. & Sigman, M. S. Enantioselective Construction of Remote Quaternary Stereocenters. *Nature* **2014,** *508,* 340–344.

(60) Patel, H. H. & Sigman, M. S. Palladium-Catalyzed Enantioselective Heck Alkenylation of Acyclic Alkenols Using a Redox-Relay Strategy. *J. Am. Chem. Soc.* **2015,** *137,* 3462–3465.

(61) Zhang, C., Santiago, C. B., Kou, L. & Sigman, M. S. Alkenyl Carbonyl Derivatives in Enantioselective Redox Relay Heck Reactions: Accessing α,β-Unsaturated Systems. *J. Am. Chem. Soc.* **2015,** *137,* 7290–7293.

(62) Wang, Z. X., Bai, X. Y., Yao, H. C. & Li, B. J. Synthesis of Amides with Remote Stereocenters by Catalytic Asymmetric γ-Alkynylation of α,β-Unsaturated Amides. *J. Am. Chem. Soc.* **2016,** *138,* 14872–14875.

(63) Verendel, J. J., Pàmies, O., Diéguez, M. & Andersson, P. G. Asymmetric Hydrogenation of Olefins Using Chiral Crabtree-Type Catalysts: Scope and Limitations. *Chem. Rev.* **2014,** *114,* 2130–2169.

(64) Khumsubdee, S. & Burgess, K. Comparison of Asymmetric Hydrogenations of Unsaturated Carboxylic Acids and Esters. *ACS Catal.* **2013,** *3*, 237–249.

(65) Li, J.-Q.; Liu, J.; Krajangsri, S.; Chumnavej, N.; Singh, T.; Andersson, P. G. Asymmetric Hydrogenation of Allylic Alcohols Using Ir–N,P-Complexes. *ACS Catal.* **2016,** *6*, 8342–8349.

(66) Tani, K.; Yamagata, T.; Akutagawa, S.; Kumobayashi, H.; Taketomi, T.; Takaya, H.; Miyashita, A.; Noyori, R.; Otsuka, S. Highly Enantioselective Isomerization of Prochiral Allylamines Catalyzed by Chiral Diphosphine Rhodium(I) Complexes. Preparation of Optically Active Enamines. *J. Am. Chem. Soc.* **1984,** *106*, 5208–5217.

(67) Inoue, S.; Takaya, H.; Tani, K.; Otsuka, S.; Sato, T.; Noyori, R. Mechanism of the Asymmetric Isomerization of Allylamines to Enamines Catalyzed by 2,2'-Bis(diphenylphosphino)-1,1'-binaphthyl-rhodium Complexes. *J. Am. Chem. Soc.* **1990,** *112*, 4897–4905.

(68) Tanaka, K., Qiao, S., Tobisu, M., Lo, M. M. C. & Fu, G. C. Enantioselective Isomerization of Allylic Alcohols Catalyzed by a Rhodium/Phosphaferrocene Complex. *J. Am. Chem. Soc.* **2000,** *122*, 9870–9871.

(69) Mantilli, L., Gérard, D., Torche, S., Besnard, C. & Mazet, C. Iridium-Catalyzed Asymmetric Isomerization of Primary Allylic Alcohols. *Angew. Chem. Int. Ed.* **2009,** *48*, 5143–5147.

(70) Arai, N., Sato, K., Azuma, K. & Ohkuma, T. Enantioselective Isomerization of Primary Allylic Alcohols into Chiral Aldehydes with the Tol-binap/dbapen/ruthenium(II) Catalyst. *Angew. Chem. Int. Ed.* **2013,** *52*, 7500–7504.

(71) Zhu, S., Niljianskul, N. & Buchwald, S. L. A Direct Approach to Amines with Remote Stereocenters by Enantioselective Cu–H-catalyzed Reductive Relay Hydroamination. *Nat. Chem.* **2016,** *8,* 144–150.

(72) Inoue, S.-i.; Takaya, H.; Tani, K.; Otsuka, S.; Sato, T.; Noyori, R. Mechanism of the Asymmetric Isomerization of Allylamines to Enamines Catalyzed by 2,2'-Bis(diphenylphosphino)-1,1'-binaphthyl-rhodium Complexes. *J. Am. Chem. Soc.* **1990,** *112,* 4897–4905.

(73) Tanaka, K.; Fu, G. C. A Versatile New Catalyst for the Enantioselective Isomerization of Allylic Alcohols to Aldehydes: Scope and Mechanistic Studies. *J. Org. Chem.* **2001,** *66,* 8177–8186.

(74) Cahard, D.; Gaillard, S.; Renaud, J.-L. Asymmetric Isomerization of Allylic Alcohols. *Tetrahedron Lett.* **2015,** *56,* 6159–6169.

(75) Li, H.; Mazet, C. Iridium-Catalyzed Selective Isomerization of Primary Allylic Alcohols. *Acc. Chem. Res.* **2016,** *49,* 1232–1241.

(76) Liu, T.-L.; Ng, T. W.; Zhao, Y. Rhodium-Catalyzed Enantioselective Isomerization of Secondary Allylic Alcohols. *J. Am. Chem. Soc.* **2017,** *139,* 3643–3646.

(77) Wu, Z.; Hull, K. L. Rhodium-Catalyzed Oxidative Amidation of Allylic Alcohols and Aldehydes: Effective Conversion of Amines and Anilines into Amides. *Chem. Sci.* **2016,** *7,* 969–975.

(78) Liu, T.-L.; Ng, T. W.; Zhao, Y. Rhodium-Catalyzed Enantioselective Isomerization of Secondary Allylic Alcohols. *J. Am. Chem. Soc.* **2017,** *139,* 3643–3646.

(79) Li, H.; Mazet, C. Catalyst-Directed Diastereoselective Isomerization of Allylic Alcohols for the Stereoselective Construction of C(20) in Steroid Side Chains: Scope and Topological Diversification. *J. Am. Chem. Soc.* **2015,** *137,* 10720–10727.

(80) Tani, K.; Yamagata, T.; Akutagawa, S.; Kumobayashi, H.; Taketomi, T.; Takaya, H.; Miyashita, A.; Noyori, R.; Otsuka, S. Highly Enantioselective Isomerization of Prochiral Allylamines Catalyzed by Chiral Diphosphine Rhodium(I) Complexes. Preparation of Optically Active Enamines. *J. Am. Chem. Soc.* **1984,** *106,* 5208–5217.

(81) Tani, K.; Yamagata, T.; Otsuka, S.; Akutagawa, S.; Kumobayashi, H.; Taketomi, T.; Takaya, H.; Miyashita, A.; Noyori, R. Cationic Rhodium(I) Complex-catalysed Asymmetric Isomerization of Allylamines to Optically Active Enamines. *J. Chem. Soc., Chem. Commun.* **1982,** 600–601.

(82) Noyori, R.; Takaya, H. BINAP: An Efficient Chiral Element for Asymmetric Catalysis. *Acc. Chem. Res.* **1990,** *23,* 345–350.

(83) Wu, Z.; Laffoon, S. D.; Nguyen, T. T.; McAlpin, J. D.; Hull, K. L. Rhodium-Catalyzed Asymmetric Synthesis of β-Branched Amides. *Angew. Chem. Int. Ed.* **2017,** *56,* 1371–1375.

(84) Aissaoui, H.; Boss, C.; Richard-Bildstein, S.; Siegrist, R. Heterocyclic Derivatives and Their Use as Prostaglandin d2 Receptor Modulators. *WO2013093842A1* **2013.**

(85) Nova, A.; Ujaque, G.; Albéniz, A. C.; Espinet, P. Mechanism of the Rhodium-Catalyzed Asymmetric Isomerization of Allylamines to Enamines. *Chem. Eur. J.* **2008,** *14,* 3323–3329.

CHAPTER 2: RHODIUM CATALYZED ISOMERIZATION AND AMIDATION OF ALLYLIC AMINES WITH AMINE NUCLEOPHILES TO FORM CHIRAL, β-BRANCHED AMIDES

This chapter has been adapted from the following publication:

Wu, Z.; Laffoon, S. D.; Nguyen, T. T.; McAlpin, J. D.; Hull, K. L. Rhodium-Catalyzed Asymmetric Synthesis of β-Branched Amides. *Angew. Chem. Int. Ed.* **2017,** *56,* 1371-1375.

2.1 Abstract

This chapter describes a general asymmetric route for the one-step synthesis of chiral β-branched amides. A cationic Rh(I)-BINAP catalyst facilitates the highly enantioselective isomerization of allylamines and subsequent oxidation following enamine exchange. The enamine exchange allows for a rapid and modular synthesis of various amides, including challenging β-diaryl and β-cyclic from an allylic diethyl amine scaffold. Several combinations of allylic amine substrates and amine nucleophiles were investigated in the transformation totaling 37 examples. Yields ranged from 38% to 82% and e.r. ranging from 94:6 to >99:1.

2.2 Motivation and Background

Enantiopure β-branched amides are common motifs in natural products and biologically active molecules[1] (Figure 2.1) and are useful synthetic intermediates for the construction of γ-branched chiral amines.[2] However, examples of the direct asymmetric synthesis of chiral β-branched amides are rare. Chapter 1 of this Thesis details various catalytic approaches to installing chiral, β-branched amide functionality Although asymmetric hydrogenation or conjugate addition

of α,β-unsaturated carbonyls are common strategies toward β-stereocenters, α,β-unsaturated amides intrinsically display low reactivity.[3] Only a few examples of

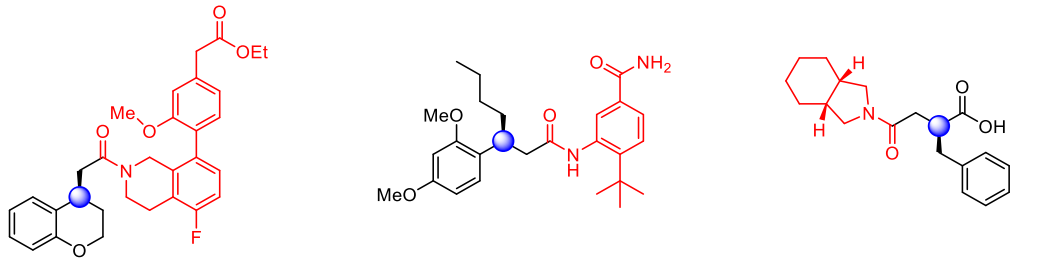

Prostaglandin D2 receptor modulator

R106578
Cholesterol acyltransferase inhibitor

Mitiglinide
Type II diabetes treatment

Figure 2.1. Biologically active compounds containing chiral β-branched amides.

unsaturated acyclic amides have been documented, including Co-catalyzed asymmetric reduction[4] and Rh-catalyzed conjugate addition.[5] For a general and modular synthesis of enantiopure β-branched amides, a multistep sequence is often required via carboxylic acid intermediates (Scheme 2.1).[1c] For example, asymmetric hydrogenation of β,β-disubstituted

a) Asymmetric hydrogenation:

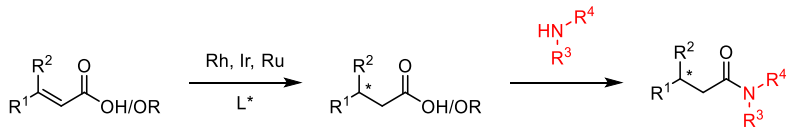

b) Asymmetric conjugate addition:

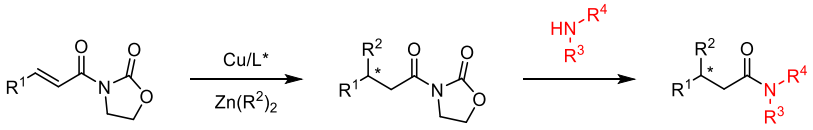

c) Asymmetric isomerization/oxidation:

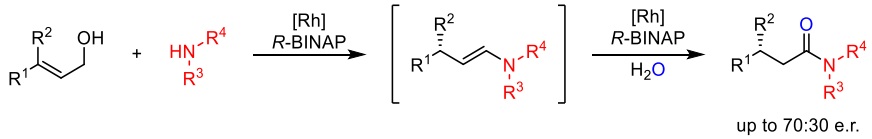

up to 70:30 e.r.

d) This work:

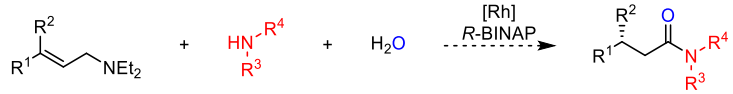

Scheme 2.1. Enantioselective β-branched amide syntheses.

unsaturated acrylic acid or ester has been extensively studied to reach high conversion and excellent enantioselectivity via Rh, Ir, and Ru catalysis (Scheme 2.1a).[6] The same chiral acid intermediate could be prepared through a copper-catalyzed asymmetric 1,4-addition of an alkylzinc to a unsaturated *N*-acyloxazolidione followed by hydrolysis (Scheme 2.1b).[7] For the synthesis of the desired amide products, stoichiometric coupling reagents are often required which leads to poor atom economy.[8]

2.3 Investigating Allylic Amine Substrates

Considering the dearth of approaches for the direct asymmetric synthesis of chiral β-branched amides, we proposed that allylic alcohols could serve as a chiral aldehyde precursor, which upon asymmetric isomerization and subsequent oxidative amidation with an amine, affords the desired product in a single step (Scheme 2.1c). The Hull group reported a cationic Rh/BINAP complex as an effective catalyst for this transformation, converting primary and secondary amines as well as anilines into amides.[9] However, only moderate e.r. was observed when using trisubstituted allylic alcohols as substrates.[10] As an enamine intermediate is formed over the course of the reaction, we hypothesized that utilizing Noyori's asymmetric isomerization of allyl amines, a highly enantioselective process and the key step in the Takasago Process, could allow for the formation of identical intermediates with improved enantioselectivity.[11] To avoid preinstallation of the amine functionality on the substrate, we further proposed a domino process: enantioselective isomerization of an allylic amine, enamine exchange with an external amine nucleophile, and oxidation of enamine to afford enantiopure β-branched amides in a single step (Scheme 2.1d).

The key challenge for this tandem process is identifying an appropriate allyl amine precursor, as it must: isomerize with high enantioselectivity, afford an enamine (**ii**) which is slow

to oxidize and instead undergo enamine exchange with an external amine nucleophile to afford the desired intermediate (**i**) (Scheme 2.2). We hypothesized that acyclic dialkyl amines

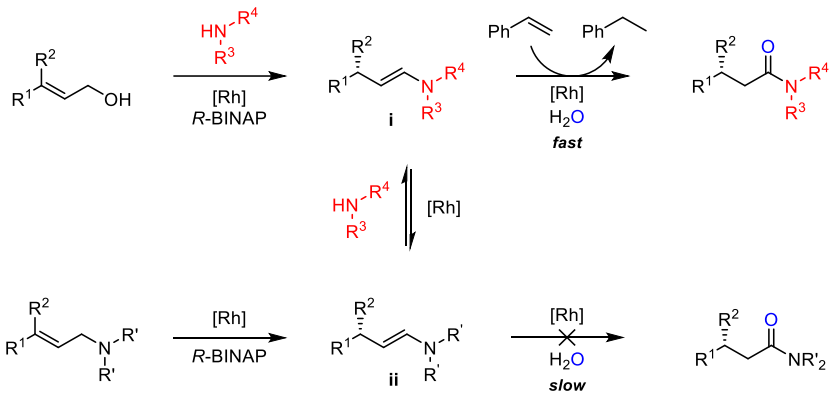

Scheme 2.2. Proposed reaction pathway.

could serve as precursors as they are good substrates in related Rh-catalyzed asymmetric isomerization reactions[11] and are not reactive in the oxidative amidation of allyl alcohols.[9] Several allylic dialkyl amines (**1a–1d**) were screened for this tandem process (Table 2.1). Under slightly modified conditions from the allylic alcohol amidation,[12] the desired morpholine amide (**3a**) was formed in moderate yields from all the allylic amine precursors. Only cinnamyl dimethylamine

Table 2.1. Rhodium-catalyzed allylic dialkylamine amidation.[a]

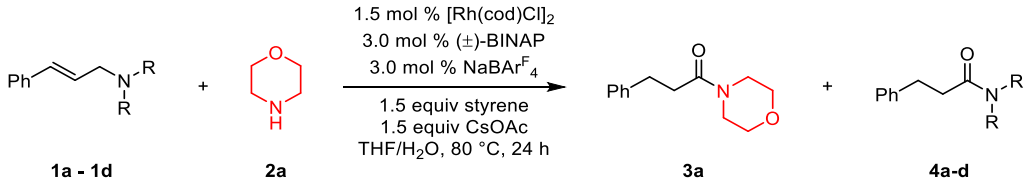

Entry	R	Yield of **3a** (%)[b]	Yield of **4a-d** (%)[c]
1	Me	64	9
2	Et	77	<1%
3	*i*-Pr	71	<1%
4	Bn	74	<1%

a) General reaction conditions: cinnamyl dialkylamine (**1**) (0.12 mmol, 1.0 equiv), morpholine (**2a**) (1.5 equiv), CsOAc (1.5 equiv), styrene (1.5 equiv), THF (1.2 M), DI H_2O. b) *In situ* yield determined by GC analysis. c) *In situ* yield determined by NMR.

(**1a**) provided 9% byproduct **4a**, consistent with dimethyl amine being an effective nucleophile in our allylic alcohol amidation.[9] We chose to further optimize this reaction with cinnamyl diethylamine (**1b**), as it forms a low molecular weight byproduct ($NHEt_2$) which is easily removed.

2.4 Optimized Reaction Conditions

After further optimization of reaction conditions Cs_2CO_3 proved superior to CsOAc for secondary amine nucleophiles and only sub-stoichiometric amount (20 mol%) is required. A variety of hydrogen acceptors were examined showing styrene to be superior, as it was reduced faster than the substrate. Further, decreasing the equivalents of amine nucleophile (1.05 equiv) led to only slightly diminished yields.

2.5 Substrate Scope

Slight modification of the reaction conditions was required for other amine nucleophiles. For less nucleophilic aniline derivatives, excess nucleophile (3.0 equiv) and increased base (0.9 equiv) were required to prevent unproductive reaction pathways. With primary alkyl amine nucleophiles, a stronger base and higher temperature were essential, which presumably aid in the conversion of the less electrophilic imine intermediate to the hemiaminal intermediate. Additionally, acetone proved to be the better hydrogen acceptor, consistent with our allylic alcohol amidation.[9] With the optimized conditions in hand, the amine nucleophile scope was investigated (Table 2.2): cyclic amines such as piperidine (**2b**), indoline (**2e**), and 2-(piperazin-1-yl) pyrimidine (**2f**) and acyclic amines, including dimethyl amine (**2c**) and N-benzyl methyl amine (**2d**) all gave excellent yields of desired products. Moderate yields were obtained with aniline derivatives (**2g–2j**). Electron-deficient (**2i**) and sterically hindered anilines (**2j**) afford slightly diminished yields.

Primary amines are relatively challenging nucleophiles for this reaction and **3k** and **3l** were obtained in 64% and 39%, respectively. Unsurprisingly, diethyl and dibenzyl amines showed no reactivity under optimized conditions, consistent with results in Table 2.1.

Table 2.2. Scope of amine nucleophiles.

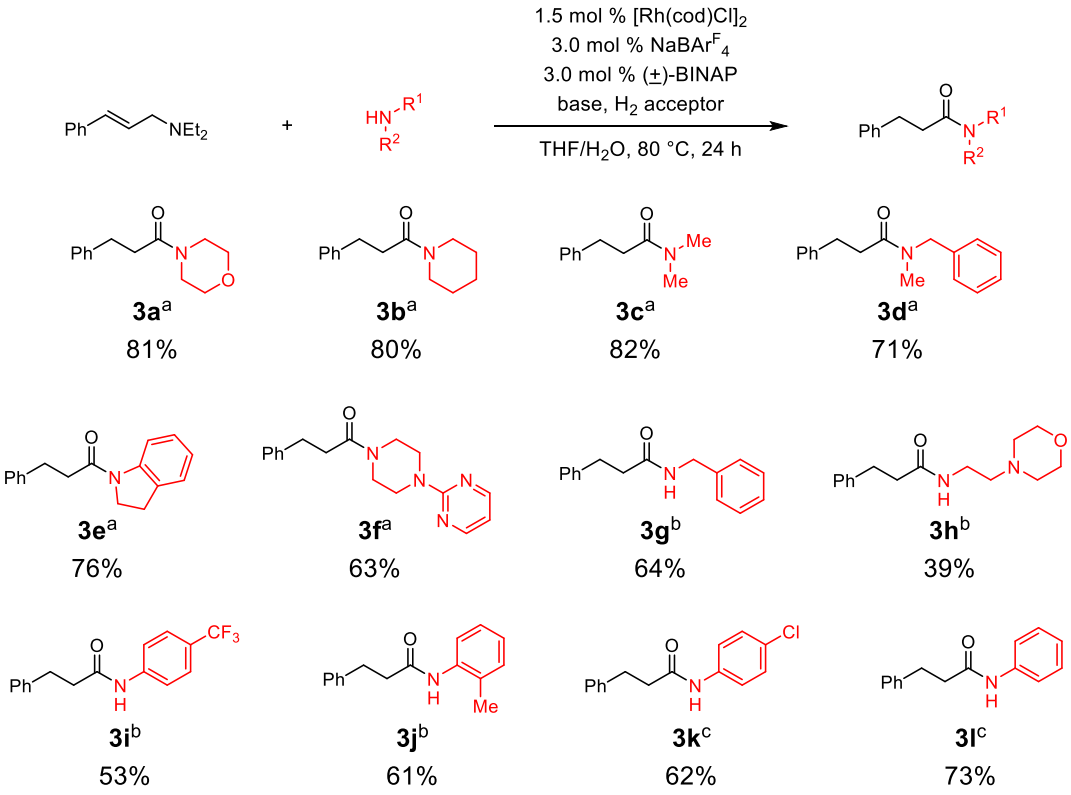

a) **Condition a**: 2° amines (1.05 equiv), Cs_2CO_3 (20 mol %), styrene (1.5 equiv), THF/H_2O (1:0.2). b) **Condition b**: anilines (3.0 equiv), Cs_2CO_3 (90 mol %), styrene (1.5 equiv), THF/H_2O (1:0.3). c) **Condition c**: 1° alkyl amine (1.0 equiv), KOH (2.5 equiv), acetone (1.0 equiv), THF/H_2O (1:1), 100 °C.

The enantioselectivity of this transformation was explored under optimized conditions with different amine nucleophiles (Table 2.3). Excellent enantioselectivities (>96:4 e.r.) were observed in the asymmetric oxidative amidation of (*E*)-geranyl diethyl amine with morpholine, aniline, and benzyl amine, affording **6aa**, **6af**, and **6ak** in fair to excellent yields. Using either (*S*)-BINAP or the (*Z*)-allyl diethylamine affords the opposite enantiomer in identically excellent enantioselectivity.[13]

Focusing our efforts on substrates not previously shown in the Noyori isomerization, the scope of prochiral allylamines was next explored (Table 2.4). A variety of substrates were transformed to the corresponding β-branched amides with high enantioselectivities in moderate to very good yields. Various 3,3-aryl,alkyl allylic diethylamines were investigated (**5b–5h**); stereocenters bearing both small (Me, Et) and large (*i*-Pr) substituents uniformly give excellent enantiomeric ratios (**6ba-6da**).[16] Aryl halides were tolerated under the optimized conditions,

Table 2.3. Enantioselective isomerization/amidation of (*E*)-geranyl diethyl amine.

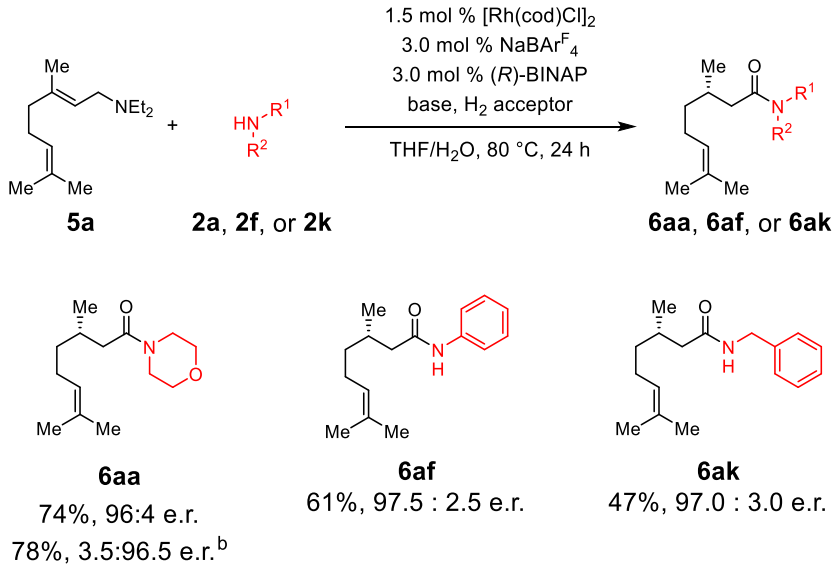

a) For conditions see Table 2.14 Isolated yield, average of two runs. Absolute configuration is assigned by analogy to **6oa** (vide infra). b) With (*S*)-BINAP.

although some protodebromination product was observed from aryl bromides (**6gg**). When bdialkyl allylic diethylamines (**5i–5l**) were exposed to the reaction conditions, chiral amides bearing a dialkyl stereocenter were obtained with excellent enantioselectivity, even with minimally differentiated substituents (**6la**, *n*-Bu vs. *n*-Pent).

Additionally, 3,3-diaryl allylic diethylamines also undergo this asymmetric isomerization/oxidation reaction. Substrates bearing electron-rich (**6ma**) and electron-poor (**6na**) aryl substituents afforded good yields and enantiomeric ratios. Heterocycles such as thiophene were tolerated and compatible with both secondary cyclic (**6oa**) and acyclic (**6od**) amine

nucleophiles. Further, a chroman-derived β-cyclic substrate (**5p**) afforded the chiral amide product with excellent enanotioselectivity, demonstrating an improvement over other approaches, for example, chiral resolution.[16]

The diastereoselectivity of this reaction was investigated with enantiopure amine nucleophiles (Table 2.5). When chiral α-branched amines **2m** and **2n** were used as nucleophiles, **6bm** and **6bn** were formed in high e.r. (>99:1) and d.r. (>96:4). Further, both the enantiomer of ligand, (*R*)- or (*S*)-BINAP, and the enantiomer of amine employed dictate which diastereomer

Table 2.4. Scope of one-step asymmetric isomerization/amidation of allylic amines.

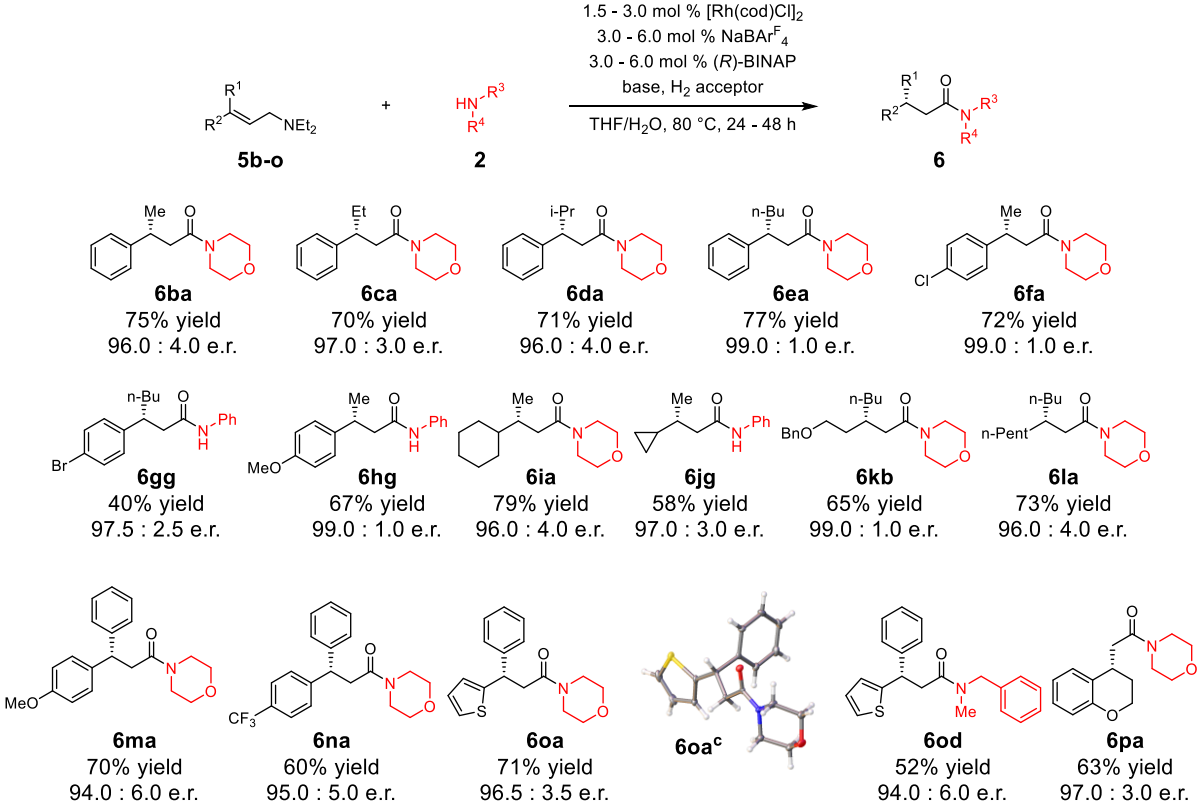

a) For conditions see Table 2.2.[14] Isolated yield, average of two runs. b) Determined from the d.r. of transamidation product from **6la**.[14] c) Absolute configuration of **6oa** was determined by X-ray crystallography. [14]. d) 96:4 *E*/*Z* ratio of starting material.

is formed. This indicates both that the stereocenter α to the amine are unepimerized under the reaction conditions, even with the relatively activated chiral benzylic amine (**2m**), and that it has no effect on the selectivity of the isomerization reaction.

Table 2.5. Diastereoselectivity with enantiopure amine nucleophiles.[14]

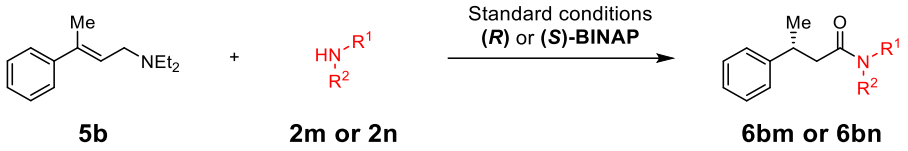

5b **2m or 2n** **6bm or 6bn**

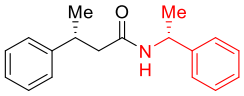

(*R*,*R*)-6bm[a]
44%, 96 : 4 d.r.
99 : 1 e.r.

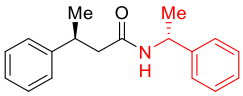

(*S*,*R*)-6bm[b]
46%, 2 : 98 d.r.
>99 : 1 e.r.

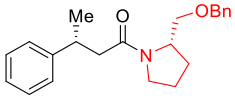

(*R*,*S*)-6bn[a]
38%, 99 : 1 d.r.
>99 : 1 e.r.

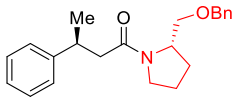

(*S*,*S*)-6bn[b]
42%, 3 : 97 d.r.
>99 : 1 e.r.

a) with (*R*)-BINAP. b) with (*S*)-BINAP.

Next the isomerization of allylic amine with proximal stereocenters was examined (Scheme 2.3). Interestingly, the diastereoselecitivity of the isomerization of **5q** and **5r** with (±)-BINAP favored the formation of (3*S*,5*R*)-**6qa** (56:44 d.r.) and (3*S*,4*S*)-**6ra** (14:85 d.r.), respectively, where the closer stereocenter in **5r** has a greater effect on the diastereoselectivity of the reaction. Excitingly, both **5q** and **5r** undergo the Rh-catalyzed isomerization/oxidation to afford desired products with excellent diastereoselectivities (>97.5:2.5) when enantioenriched ligands are employed. The isomerization reaction proved to be ligand-controlled, as the mismatched combination of (*R*)-BINAP and **5r** decreased the yield of (3*R*,4*S*)-**6ra**, rather than the diastereoselectivity.

As shown in Scheme 2.4, isotope labelling studies were carried out using $H_2{}^{18}O$ and D_2O respectively. The $H_2{}^{18}O$ labelling study (Scheme 2.4a) confirms that the oxygen in the product originates from the water. Similarly, deuterium incorporation at the α-position of the amide was observed (Scheme 2.4b), as it was in the allylic alcohol amidation,[9] supporting the reversible formation of enamine intermediate **i** (Scheme 2.2).

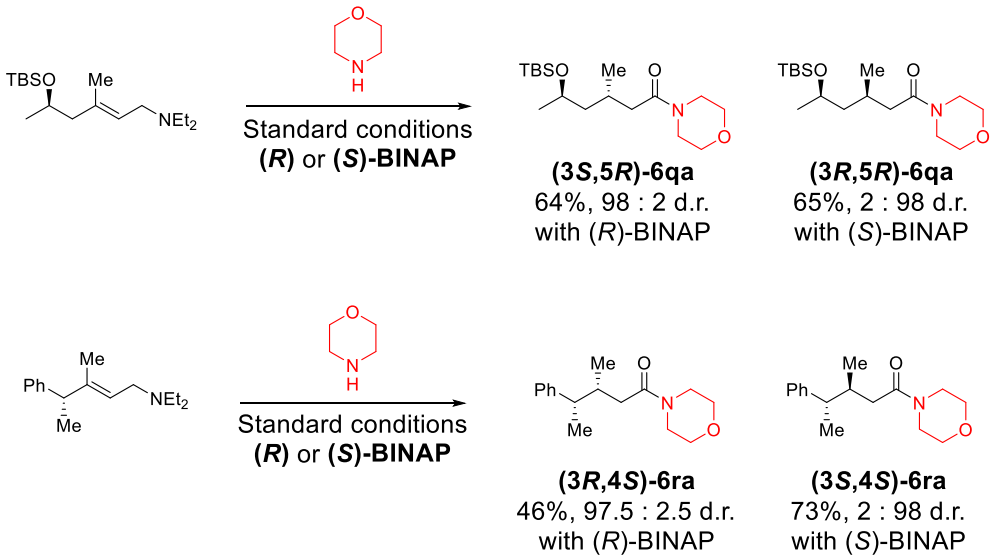

Scheme 2.3. Diastereoselectivity with enantiopure allyl amines. [14]

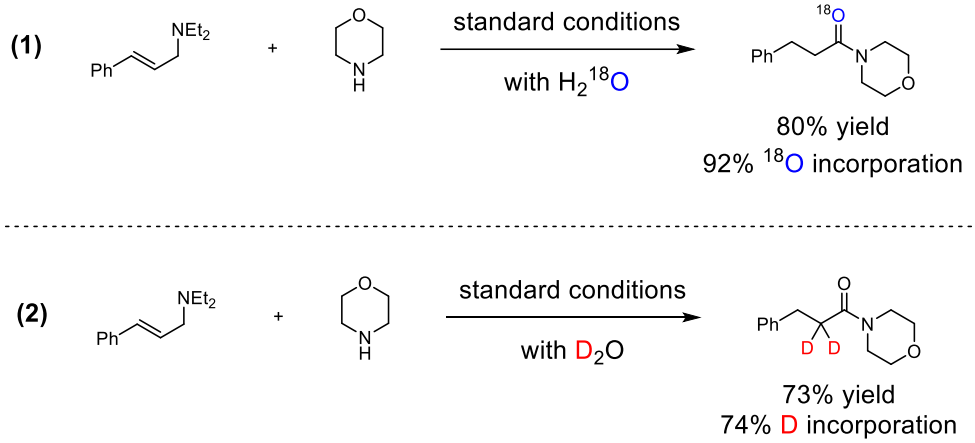

Scheme 2.4. Isotope labelling study.

2.6 Conclusion

We have developed a Rh-catalyzed one-step synthesis of chiral β-branched amides. This method allows for the installation of a stereocenter and amide functionality in a single step under mild conditions. Excellent enantio- and diastereoselectivity was observed for a variety of allylic amine substrates and amine nucleophiles.

2.7 Supporting Information

General Experimental Procedures

All reactions were carried out in flame-dried (or oven-dried at 140 °C for at least 2 h) glassware under an atmosphere of nitrogen unless otherwise indicated. Nitrogen was dried using a drying tube equipped with Drierite™ unless otherwise noted. Air- and moisture-sensitive reagents were handled in a nitrogen-filled glovebox (working oxygen level ~ 0.1 ppm; working water level ~ 0.1 ppm). Column chromatography was performed with silica gel from Grace Davison Discovery Sciences (35-75 μm) with a column mixed as a slurry with the eluent and was packed, rinsed, and run under air pressure. Analytical thin-layer chromatography (TLC) was performed on precoated glass silica gel plates (by EMD Chemicals Inc.) with F-254 indicator. Visualization was either by short wave (254 nm) ultraviolet light, or by staining with potassium permanganate followed by brief heating on a hot plate or by a heat gun. Distillations were performed using a 3 cm shortpath column under reduced pressure or by using a Hickman still at ambient pressure.

Instrumentation

^{1}H NMR and ^{13}C NMR were recorded on a Varian Unity 400/500 MHz (100/125 MHz respectively for 13C) spectrometer, a VXR-500 MHz spectrometer, or a Bruker 500 MHz spectrometer equipped with a CryoProbe. Spectra were referenced using either $CDCl_3$ as solvent (unless otherwise noted) with the residual solvent peak as the internal standard (^{1}H NMR: δ 7.26 ppm, ^{13}C NMR: δ 77.16 ppm for $CDCl_3$). Chemical shifts were reported in parts per million and multiplicities are as indicated: s (singlet,) d (doublet,) t (triplet,) q (quartet,) p (pentet,) m (multiplet,) and br (broad). Coupling constants, *J*, are reported in Hertz and integration is provided, along with assignments, as indicated. Analysis by Gas Chromatography-Mass Spectrometry (GC-

MS) was performed using a Shimadzu GC-2010 Plus Gas chromatograph fitted with a Shimadzu GCMS-QP2010 SE mass spectrometer using electron impact (EI) ionization after analytes traveled through a SHRXI–5MS- 30m x 0.25 mm x 0.25 μm column using a helium carrier gas. Data are reported in the form of m/z (intensity relative to base peak = 100). Gas Chromatography (GC) was performed on a Shimadzu GC-2010 Plus gas chromatograph with SHRXI–MS- 15m x 0.25 mm x 0.25 μm column with nitrogen carrier gas and a flame ionization detector (FID). Enantiomeric ratios were measured *via* High Performance Liquid Chromatography (HPLC) using a Shimadzu Prominence HLPC system with SPD-M20A UV/VIS Photodiode array detector. Low-resolution Mass Spectrometry and High Resolution Mass Spectrometry were performed in the Department of Chemistry at University of Illinois at Urbana-Champaign. The glove box, MBraun LABmaster sp, was maintained under nitrogen atmosphere.

Materials

Solvents used for extraction and column chromatography were reagent grade and used as received. Reaction solvents tetrahydrofuran (Fisher, unstabilized HPLC ACS grade), diethyl ether (Fisher, BHT stabilized ACS grade), methylene chloride (Fisher, unstabilized HPLC grade), dimethoxyethane (Fisher, certified ACS), toluene (Fisher, optima ACS grade), 1,4-dioxane (Fisher, certified ACS), acetonitrile (Fisher, HPLC grade), and hexanes (Fisher, ACS HPLC grade) were dried on a Pure Process Technology Glass Contour Solvent Purification System using activated Stainless Steel columns while following manufacture's recommendations for solvent preparation and dispensation unless otherwise noted. All alcohols were distilled and degassed by the freeze-pump-thaw method, and were stored under an atmosphere of nitrogen in glove box before use. All amines were distilled and degassed by the freeze-pump-thaw method, and were

stored under an atmosphere of nitrogen in glove box before use. All liquid aldehydes were distilled prior to use, and ketones, benzophenone and cyclohexanone, were used as received.

2.7.1 Amidation Experimental Procedure, Isolation, and Characterization

General procedure for Rh-catalyzed isomerization and oxidation of allylic amine with secondary amines (General procedure A)

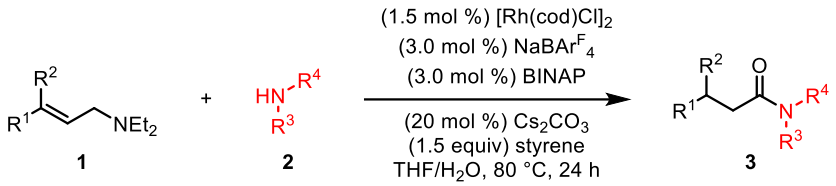

$[Rh(COD)Cl]_2$ (2.0 mg, 0.0036 mmol, 1.5 mol %), (±)-BINAP or (*R*)-BINAP (4.5 mg, 0.0072 mmol, 3.0 mol %), $NaBAr_4^F$ (6.4 mg, 0.0072 mmol, 3.0 mol %), and Cs_2CO_3 (16 mg, 0.048 mmol, 20 mol %) were added to a 4-mL vial equipped with a stir bar under N_2 atmosphere. THF (0.2 mL), cinnamyl diethylamine **1a** (46 mg, 0.24 mmol, 1.0 equiv), styrene (42 µL, 0.36 mmol, 1.5 equiv), secondary amine **2** (0.25 mmol, 1.05 equiv), and DI water (0.04 mL) were added to the vial sequentially. The resulting solution was stirred for 24 h at 80 °C. The reaction vial was cooled to room temperature followed by the addition of diphenylmethane as an internal standard for analysis of the crude reaction mixture. The biphasic solution was diluted with EtOAc, dried over anhydrous $MgSO_4$, concentrated in vacuo and then purified by silica gel chromatography (hexanes/EtOAc) to afford the desired product **3**.

General procedure for Rh-catalyzed isomerization and oxidation of allylic amine with primary anilines (General procedure B)

$[Rh(COD)Cl]_2$ (4.4 mg, 0.009 mmol, 1.5 mol %), (±)-BINAP or (*R*)-BINAP (11.2 mg, 0.018 mmol, 3.0 mol %), $NaBAr^F_4$ (16.0 mg, 0.018 mmol, 3.0 mol %), and Cs_2CO_3 (175.9 mg, 0.54 mmol, 0.9 equiv) were added to a 20-mL vial equipped with a stir bar under N_2 atmosphere. THF (0.5 mL), cinnamyl diethylamine **1a** (113.6 mg, 0.60 mmol, 1.0 equiv), styrene (103 μL, 0.54 mmol, 1.5 equiv), primary aniline **2** (1.8 mmol, 3.0 equiv), and DI water (0.15 mL) were added to the vial sequentially. The resulting solution was stirred for 24 h at 80 °C. The reaction vial was cooled to room temperature followed by the addition of diphenylmethane as an internal standard for analysis of the crude reaction mixture. The biphasic solution was diluted in EtOAc, washed with HCl 1N (2 x 20 mL), dried over anhydrous $MgSO_4$, concentrated *in vacuo* and then purified by silica gel chromatography (hexanes/EtOAc) to afford the desired product **3**.

General procedure for Rh-catalyzed isomerization and oxidation of allylic amine with alkyl primary amines (General procedure C)

$[Rh(COD)Cl]_2$ (2.0 mg, 0.0036 mmol, 1.5 mol %), (±)-BINAP or (*R*)-BINAP (4.5 mg, 0.0072 mmol, 3.0 mol %), and $NaBAr^F_4$ (6.4 mg, 0.0072 mmol, 3.0 mol %) were added to a 4-mL vial equipped with a stir bar under N_2 atmosphere. Cinnamyl diethylamine **1a** (57 mg, 0.36 mmol, 1.25 equiv), primary amine **2** (0.24 mol, 1.0 equiv), acetone (19.4 μL, 0.264 mmol, 1.1 equiv), THF (0.2 mL), and 3 M KOH (0.2 mL, 2.5 equiv KOH) were added sequentially to the vial. The resulting solution was stirred at 80 °C for 24 h. The reaction vial was cooled to room temperature followed by the addition of diphenylmethane as an internal standard for analysis of the crude reaction mixture. The biphasic solution was diluted with EtOAc, dried over anhydrous $MgSO_4$,

concentrated in vacuo, and purified by silica gel chromatography (hexanes/EtOAc) to afford the desired product **3**.

Rh-catalyzed isomerization and oxidation of geranyl diethylamine with benzylamine (General procedure D)

$[Rh(COD)Cl]_2$ (2.0 mg, 0.0036 mmol, 1.5 mol %), (±)-BINAP or (*R*)-BINAP (4.5 mg, 0.0072 mmol, 3.0 mol %), and $NaBAr^F{}_4$ (6.4 mg, 0.0072 mmol, 3.0 mol %), cinnamyl diethylamine **1a** (57 mg, 0.36 mmol, 1.25 equiv), and THF (0.2 mL) were added to a 4-mL vial equipped with a stir bar in a nitrogen filled glovebox. The vial was stirred at 40 °C for 24 hours. The vial was then brought back into the glovebox where KO^{t}Bu (40 mg, 0.36 mmol, 1.5 equiv), benzylamine (39 µL, 0.36 mmol, 1.5 equiv), acetone (53 µL, 0.72 mmol, 3 equiv) were added. The reaction was taken out of the glovebox, DI water (0.2 mL) was added by syringe through a Teflon septum, and the reaction stirred at 80 °C for 24 hours. The reaction vial was cooled to room temperature followed by the addition of diphenylmethane as an internal standard for analysis of the crude reaction mixture. The biphasic solution was diluted with EtOAc, dried over anhydrous $MgSO_4$, concentrated *in vacuo*, and purified by silica gel chromatography (hexanes/EtOAc) to afford the desired product **3**.

Characterization of Final Compounds

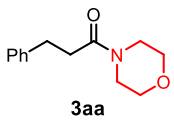

3aa

1-morpholino-3-phenylpropan-1-one $C_{13}H_{17}NO_2$

81 % isolated yield. **R_f** = 0.15 (1:1 hexane/EtOAc)

^{1}H NMR (400 MHz, $CDCl_3$) δ 7.33 – 7.27 (m, 2H), 7.25 – 7.17 (m, 3H), 3.68 – 3.57 (m, 4H), 3.55 – 3.48 (m, 2H), 3.40 – 3.31 (m, 2H), 2.98 (t, *J* = 7.8 Hz, 2H), 2.61 (t, *J* = 7.8 Hz, 2H).

^{13}C NMR (101 MHz, $CDCl_3$) δ 170.97, 141.14, 128.64, 128.56, 126.37, 66.95, 66.56, 46.06, 42.03, 34.92, 31.58.

IR: ν 2927, 2858, 1642, 1432 cm^{-1}.

HRMS (ESI-TOF) m/z: [M+H+] calculated for $C_{13}H_{17}NO_2$, 220.1338; found, 220.1334.

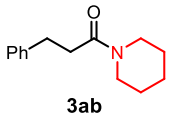

3ab

3-phenyl-1-(piperidin-1-yl)propan-1-one $C_{14}H_{19}NO$

80% isolated yield. **R_f** = 0.05 (5:1 hexane/EtOAc)

^{1}H NMR (500 MHz, $CDCl_3$) δ 7.32 – 7.27 (m, 2H), 7.25 – 7.17 (m, 3H), 3.61 – 3.51 (m, 2H), 3.44 – 3.27 (m, 2H), 2.97 (t, *J* = 8.0 Hz, 2H), 2.62 (t, *J* = 8.0 Hz, 2H), 1.64 – 1.58 (m, 2H), 1.55 – 1.49 (m, 2H), 1.49 – 1.43 (m, 2H).

^{13}C NMR (101 MHz, $CDCl_3$) δ 170.52, 141.57, 128.56, 128.53, 126.18, 46.72, 42.83, 35.31, 31.73, 26.49, 25.65, 24.63.

IR: ν 2937, 2856, 1639, 1437 cm^{-1}.

HRMS (ESI-TOF) m/z: [M+H+] calculated for $C_{14}H_{20}NO$, 218.1545; found, 218.1543.

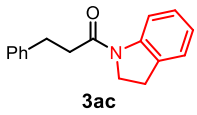

3ac

1-(indolin-1-yl)-3-phenylpropan-1-one $C_{17}H_{17}NO$

76% isolated yield. **R_f** = 0.1 (10:1 hexane/EtOAc). mp =110-112 °C

^{1}H NMR (500 MHz, $CDCl_3$, mixture of amide rotamers) δ 8.26 (d, *J* = 8.1 Hz, 1H), 7.34 – 7.26 (m, 4H), 7.24 – 7.14 (m, 3H, overlapping peaks), 7.01 (t, *J* = 7.3 Hz, 1H), 4.17 (t, *J* = 8.1 Hz, 0.2H, minor rotamer), 3.97 (t, *J* = 8.5 Hz, 2H, ma*J*or rotamer), 3.15 (t, *J* = 8.5 Hz, 2H), 3.12 – 3.05 (m, 2H, ma*J*or rotamer), 2.98 (t, *J* = 8.0 Hz, 0.2H minor rotamer), 2.74 (dd, *J* = 8.7, 7.0 Hz, 2H).

^{13}C NMR (101 MHz, $CDCl_3$) (ma*J*or rotamer) δ 170.48, 143.07, 141.33, 131.16, 128.66, 128.56, 127.64, 126.30, 124.61, 123.68, 117.10, 48.01, 38.02, 30.85, 28.09.

IR: ν 3065, 2929, 1654, 1483 cm^{-1}.

HRMS (ESI-TOF) m/z: [M+H+] calculated for $C_{17}H_{18}NO$, 252.1388; found, 252.1388.

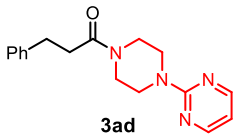

3ad

3-phenyl-1-(4-(pyrimidin-2-yl)piperazin-1-yl)propan-1-one $C_{17}H_{20}N_4O$

63% isolated yield (acid/base workup followed by recrystallization from DCM/pentane). **mp** =74-76 °C

^{1}H NMR (500 MHz, $CDCl_3$) δ 8.31 (d, *J* = 4.7 Hz, 2H), 7.33 – 7.27 (m, 2H), 7.25 – 7.18 (m, 3H), 6.53 (t, *J* = 4.7 Hz, 1H), 3.84 – 3.76 (m, 2H), 3.74 – 3.67 (m, 4H), 3.47 – 3.40 (m, 2H), 3.01 (t, *J* = 7.8Hz, 2H), 2.68 (t, *J* = 7.9 Hz, 2H).

^{13}C NMR (126 MHz, $CDCl_3$) δ 171.00, 161.55, 157.87, 141.25, 128.66, 128.59, 126.37, 110.53, 45.44, 43.69, 43.60, 41.54, 35.27, 31.65.

IR: ν 3030, 2964, 2865, 1632, 1587, 1548, 1496, 1500, 1435, 1355 cm^{-1}.

HRMS (ESI-TOF) m/z: [M+H+] calculated for $C_{17}H_{21}N_4O$, 297.1715; found, 297.1720.

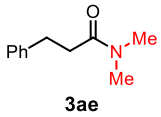

3ae

***N,N*-dimethyl-3-phenylpropanamide** $C_{11}H_{15}NO$

82% isolated yield. **R_f** = 0.25 (1:1 hexane/EtOAc)

^{1}H NMR (500 MHz, $CDCl_3$) δ 7.32 – 7.26 (m, 2H), 7.25 – 7.17 (m, 3H), 2.97 (t, *J* = 7.6 Hz, 2H), 2.95 (s, 3H), 2.93 (s, 3H), 2.61 (t, *J* = 7.9 Hz, 2H).

^{13}C NMR (126 MHz, $CDCl_3$) δ 172.29, 141.62, 128.58, 128.54, 126.20, 37.28, 35.56, 35.45, 31.50.

IR: ν 2933, 2893, 1645, 1496, 1398 cm^{-1}.

HRMS (ESI-TOF) m/z: [M+H+] calculated for $C_{11}H_{26}NO$, 178.1232; found, 178.1235.

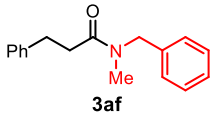

3af

***N*-benzyl-*N*-methyl-3-phenylpropanamide** $C_{17}H_{19}NO$

71% isolated yield. **R_f** = 0.2 (6:1 hexane/EtOAc)

^{1}H NMR (400 MHz, $CDCl_3$, mixture of amide rotamers) δ 7.38 – 7.15 (m, 9H), 7.12 – 7.05 (m, 1H), 4.60 (s, 1.1H), 4.47 (s, 0.8H), 3.09 – 2.97 (m, 2H), 2.96 (s, 1.1H), 2.85 (s, 1.8H), 2.76 – 2.61 (m, 2H).

^{13}C NMR (101 MHz, $CDCl_3$, mixture of amide rotamers) δ 172.72, 172.39, 141.50, 141.41, 137.47, 136.64, 129.03, 128.69, 128.60, 128.58, 128.16, 127.69, 127.43, 126.35, 126.24, 53.37, 50.98, 35.54, 35.11, 34.90, 34.15, 34.11, 31.68, 31.50.

IR: ν 3031, 2933, 1643, 1495, 1453 cm^{-1}.

HRMS (ESI-TOF) m/z: [M+H+] calculated for $C_{17}H_{20}NO$, 254.1545; found, 254.1542.

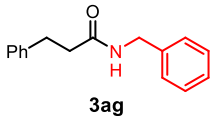

3ag

***N*-benzyl-3-phenylpropanamide** $C_{16}H_{17}NO$

64% isolated yield. **R_f** = 0.3 (1.5:1 hexane/EtOAc) **mp** =77-81 °C

^{1}H NMR (500 MHz, $CDCl_3$) δ 7.32 – 7.15 (m, 10H), 5.81 (s, broad, 1H), 4.39 (d, *J* = 5.7 Hz, 2H), 2.99 (t, *J* = 7.6 Hz, 2H), 2.51 (t, *J* = 7.6 Hz, 2H).

^{13}C NMR (126 MHz, $CDCl_3$) δ 172.01, 140.87, 138.25, 128.73, 128.64, 128.50, 127.81, 127.52, 126.34, 43.64, 38.57, 31.82.

IR: ν 3284, 3028, 1636, 1539, 1218, 693 cm^{-1}.

HRMS (ESI-TOF) m/z: [M+H+] calculated for $C_{16}H_{18}NO$, 240.1388; found, 240.1389.

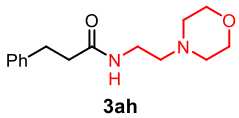

3ah

***N*-(2-morpholinoethyl)-3-phenylpropanamide** $C_{15}H_{22}N_2O_2$

39% isolated yield. **mp** = 94-95 °C

^{1}H NMR (400 MHz, $CDCl_3$) δ 7.29 – 7.17 (m, 5H), 5.89 (s, broad, 1H), 3.65 (t, *J* = 4.7 Hz, 4H), 3.30 (q, *J* = 5.6 Hz, 2H), 2.96 (t, *J* = 7.6 Hz, 2H), 2.49 (t, *J* = 7.6 Hz, 2H), 2.40 – 2.35 (m, 6H).

^{13}C NMR (126 MHz, $CDCl_3$) δ 172.14, 140.98, 128.55, 128.44, 126.27, 66.94, 56.98, 53.30, 38.50, 35.60, 31.84.

IR: ν 3307, 2932, 1637, 1546, 1115, 698 cm^{-1}.

HRMS (ESI-TOF) m/z: [M+H+] calculated for $C_{15}H_{23}N_2O_2$, 263.1760; found, 263.1761.

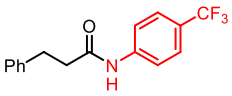

3ai

***N*-(4-(trifluoromethyl)phenyl)-3-phenylpropanamide** $C_{16}H_{14}F_3NO$

53% isolated yield. **R_f** = 0.3 (4:1 hexane/EtOAc). **mp** = 142-145 °C

^{1}H NMR (500 MHz, $CDCl_3$) δ 7.54 (s, 4H), 7.31 (t, *J* = 7.6 Hz, 2H), 7.23 (d, *J* = 7.5 Hz, 3H), 3.06 (t, *J* = 7.7 Hz, 2H), 2.69 (t, *J* = 7.5 Hz, 2H).

^{13}C NMR (126 MHz, $CDCl_3$) δ 170.79, 140.82, 140.42, 128.86, 128.48, 126.68, 126.35 (q, J_{CF} = 3.8 Hz), 126.29 (q, J_{CF} = 32.9 Hz), 124.15 (q, J_{CF} = 272.4 Hz), 125.2, 123.0, 119.4, 39.63, 31.53.

^{19}F NMR (470 MHz, $CDCl_3$) δ -62.20.

IR: ν 3327, 3030, 2926, 1672, 1600, 1524, 1408, 1319, 1164, 1065 cm^{-1}.

HRMS (ESI-TOF) m/z: [M+H+] calculated for $C_{16}H_{14}F_3NO$, 294.1106; found, 294.1106.

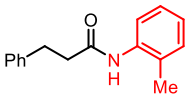

3aj

***N*-(2-methylphenyl)-3-phenylpropanamide** $C_{16}H_{17}NO$

61% isolated yield. **R_f** = 0.4 (2:1 hexane/EtOAc). **mp** = 119-121 °C

^{1}H NMR (500 MHz, $CDCl_3$) δ 7.70 (d, *J* = 8.1 Hz, 1H), 7.30 (d, *J* = 7.5 Hz, 2H), 7.20 (m, 6H, integration gives 1 extra proton due to solvent peak), 7.06 (t, *J* = 7.4 Hz, 1H), 6.97 (s, broad, 1H), 3.06 (t, *J* = 7.6 Hz, 2H), 2.69 (t, *J* = 7.6 Hz, 2H), 2.06 (s, 3H).

^{13}C NMR (126 MHz, $CDCl_3$) δ 170.55, 140.68, 135.59, 130.50, 129.48, 128.75, 128.51, 126.73, 126.50, 125.35, 123.53, 39.26, 31.81, 17.66.

IR: ν 3338, 3289, 3030, 1673, 1601, 1524, 1409, 1320, 1162 cm^{-1}.

HRMS (ESI-TOF) m/z: [M+H+] calculated for $C_{16}H_{17}NO$, 240.1388; found, 240.1387.

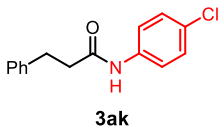

3ak

***N*-(4-chlorophenyl)-3-phenylpropanamide** $C_{15}H_{14}ClNO$

62% isolated yield. **R_f** = 0.3 (3:1 hexane/EtOAc). **mp** = 138-139 °C

^{1}H NMR (500 MHz, $CDCl_3$) δ 7.46 (s, broad, 1H), 7.36 (d, *J* = 8.5 Hz, 2H), 7.29 (t, *J* = 7.4 Hz, 2H), 7.21 (m, 5H), 3.02 (t, *J* = 7.6 Hz, 2H), 2.64 (t, *J* = 7.6 Hz, 2H).

^{13}C NMR (126 MHz, $CDCl_3$) δ 170.76, 140.51, 136.38, 129.38, 129.02, 128.77, 128.43, 126.56, 121.39, 39.39, 31.60.

IR: ν 3299, 3029, 2931, 1658, 1593, 1522, 1491, 1397, 1091 cm^{-1}.

HRMS (ESI-TOF) m/z: [M+H+] calculated for $C_{15}H_{14}ClNO$, 260.0842; found, 260.0838.

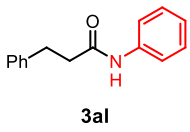

3al

***N*-phenyl-3-phenylpropanamide** $C_{15}H_{15}NO$

73% isolated yield. **R_f** = 0.3 (4:1 hexane/EtOAc). **mp** = 92-93 °C

^{1}H NMR (500 MHz, $CDCl_3$) δ 7.44 (m, 3H), 7.28 (m, 4H), 7.22 (m, *J* = 7.6 Hz, 3H), 7.09 (t, *J* = 7.4 Hz, 1H), 3.04 (t, *J* = 7.7 Hz, 2H), 2.65 (t, *J* = 7.3 Hz, 2H).

^{13}C NMR (126 MHz, $CDCl_3$) δ 170.68, 140.71, 137.86, 129.03, 128.72, 128.47, 126.46, 124.40, 120.13, 39.47, 31.67.

IR: ν 3323, 2924, 2856, 1651, 1599, 1526, 1440 cm^{-1}.

HRMS (ESI-TOF) m/z: [M+H+] calculated for $C_{15}H_{15}NO$, 226.1232; found, 226.1231.

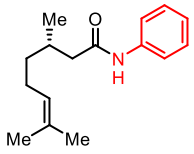

3bl

(*S*)-3,7-dimethyl-*N*-phenyloct-6-enamide $C_{16}H_{23}NO$

61% isolated yield. **R_f** = 0.4 (4:1 hexane/EtOAc). **mp** = 46-48 °C

^{1}H NMR (500 MHz, $CDCl_3$) δ 7.52 (d, *J* = 8.0 Hz, 2H), 7.43 (s, 1H), 7.30 (t, *J* = 7.9 Hz, 2H), 7.09 (t, *J* = 7.4 Hz, 1H), 5.09 (t, *J* = 6.8 Hz, 1H), 2.37 (dd, *J* = 13.2, 5.3 Hz, 1H), 2.07 (m, 4H), 1.68 (s, 3H), 1.60 (s, 3H), 1.42 (ddt, *J* = 12.3, 9.6, 5.9 Hz, 1H), 1.26 (m, 1H), 1.00 (d, *J* = 6.2 Hz, 3H).

^{13}C NMR (101 MHz, $CDCl_3$) δ 171.12, 138.08, 131.72, 129.06, 124.37, 124.29, 120.00, 45.63, 37.00, 30.70, 29.82, 25.84, 25.61, 19.69, 17.80.

IR: ν 3291, 2963, 2915, 2849, 1652, 1599, 1534, 1444, 1374 cm^{-1}.

HRMS (ESI-TOF) m/z: [M+H+] calculated for $C_{16}H_{23}NO$, 246.1858; found, 246.1855.

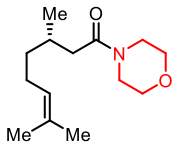

3ba

(*S*)-3,7-dimethyl-1-morpholinooct-6-en-1-one $C_{14}H_{25}NO_2$

74% isolated yield. **R_f** = 0.1 (2:1 hexane/EtOAc)

^{1}H NMR (500 MHz, $CDCl_3$) δ 5.09 (tsept, *J* = 7.1, 1.4 Hz, 1H), 3.71 – 3.57 (m, 6H), 3.50 – 3.43 (m, 2H), 2.31 (dd, *J* = 14.5, 5.8 Hz, 1H), 2.12 (dd, *J* = 14.5, 8.3 Hz, 1H), 2.07 – 1.91 (m, 3H), 1.67 (d, *J* = 1.4 Hz, 3H), 1.60 (s (br), 3H), 1.44 – 1.34 (m, 1H), 1.24 – 1.17 (m, 1H), 0.96 (d, *J* = 6.6 Hz, 3H).

^{13}C NMR (101 MHz, $CDCl_3$) δ 171.40, 131.67, 124.48, 67.16, 66.86, 46.40, 42.02, 40.45, 37.20, 30.17, 25.85, 25.61, 19.92, 17.86.

IR: ν 2966, 2927, 2859, 1644, 1434 cm^{-1}.

HRMS (ESI-TOF) m/z: [M+H+] calculated for $C_{14}H_{26}NO_2$, 240.1964; found, 240.1963.

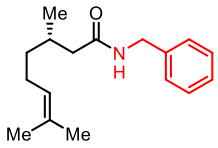

3bg

(*S*)-*N*-benzyl-3,7-dimethyloct-6-enamide $C_{17}H_{25}NO$

47% isolated yield. **R_f** = 0.3 (3:1 hexane/EtOAc) **mp** =54-58 °C

^{1}H NMR (400 MHz, $CDCl_3$) δ 7.37 – 7.25 (m, 5H), 5.72 (s, borad, 1H), 5.08 (tt, *J* = 7.2, 1.5 Hz), 4.45 (dd, *J* = 5.7, 2.9 Hz, 2H), 2.26 – 2.20 (m, 1H), 2.07 – 1.94 (m, 4H), 1.67 (s, 3H), 1.59 (s, 3H), 1.42 – 1.34 (m, 1H), 1.26 – 1.16 (m, 1H), 0.95 (d, *J* = 6.2 Hz, 3H).

^{13}C NMR (126 MHz, $CDCl_3$) δ 172.51, 138.58, 131.58, 128.76, 127.92, 127.54, 124.43, 44.59, 43.65, 37.02, 30.60, 25.81, 25.56, 19.68, 17.76.

IR: ν 3285, 2913, 1631, 1544, 731, 693 cm^{-1}.

HRMS (ESI-TOF) m/z: [M+H+] calculated for $C_{17}H_{26}NO$, 260.2014; found, 260.2013.

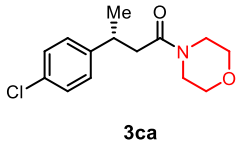

3ca

(*R*)-1-morpholino-3-(4-chlorophenyl)butan-1-one $C_{14}H_{18}ClNO_2$

72% isolated yield. **R_f** = 0.2 (1:2 hexane/EtOAc).

^{1}H NMR (500 MHz, $CDCl_3$) δ 7.26 (d, *J* = 8.1 Hz, 2H), 7.16 (d, *J* = 8.1 Hz, 2H), 3.57 (m, 5H), 3.33 (m, 4H), 2.57 (dd, *J* = 14.9, 7.1 Hz, 1H), 2.50 (dd, *J* = 15.0, 7.2 Hz, 1H), 1.31 (d, *J* = 7.0 Hz, 3H).

^{13}C NMR (126 MHz, $CDCl_3$) δ 170.19, 144.71, 132.14, 128.71, 128.39, 66.97, 66.57, 46.24, 42.04, 41.30, 36.23, 21.86.

IR: ν 2964, 2926, 2857, 1638, 1493, 1434, 1273, 1223, 1113 cm^{-1}.

HRMS (ESI-TOF) m/z: [M+H+] calculated for $C_{14}H_{18}ClNO_2$, 268.1104; found, 268.1101.

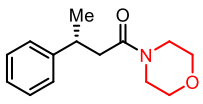

3da

(*R*)-1-morpholino-3-phenylbutan-1-one $C_{14}H_{19}NO_2$

75% isolated yield. **R_f** = 0.1 (2:1 hexane/EtOAc)

^{1}H NMR (400 MHz, $CDCl_3$) δ 7.34 – 7.27 (m, 2H), 7.25 – 7.18 (m, 3H), 3.72 – 3.57 (m, 2H), 3.57 – 3.42 (m, 3H), 3.39 – 3.28 (m, 2H), 3.27 – 3.17 (m, 2H), 2.62 (dd, *J* = 14.5, 7.0 Hz, 1H), 2.50 (dd, *J* = 14.5, 7.4 Hz, 1H), 1.35 (d, *J* = 7.0 Hz, 3H).

^{13}C NMR (126 MHz, $CDCl_3$) δ 170.54, 146.15, 128.67, 127.04, 126.62, 66.96, 66.55, 46.33, 42.02, 41.54, 37.05, 21.76.

IR: ν 2967, 2961, 1640, 1429 cm^{-1}.

HRMS (ESI-TOF) m/z: [M+H+] calculated for $C_{14}H_{20}NO_2$, 234.1494; found, 234.1492.

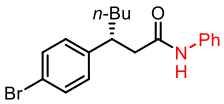

3el

(*R*)-3-(4-bromophenyl)-*N*-phenylheptanamide $C_{19}H_{22}BrNO$

40% isolated yield. **R_f** = 0.2 (8:1 hexane/EtOAc) **mp** = 86-89 °C

^{1}H NMR (500 MHz, $CDCl_3$) δ 7.43 (d, *J* = 8.0 Hz, 2H), 7.33 (d, *J* = 8.0 Hz, 2H), 7.31 – 7.26 (m, 2H), 7.15 – 7.01 (m, 3H), 6.82 (brs, 1H), 3.25 – 3.09 (m, 1H), 2.64 (dd, *J* = 14.3, 6.3 Hz, 1H), 2.50 (dd, *J* = 14.3, 8.4 Hz, 1H), 1.73 (ddt, *J* = 14.5, 10.4, 10.4, 5.3, 1H), 1.61 (dtd, *J* = 14.5, 9.8, 5.0 Hz, 2H), 1.37 – 1.04 (m, 4H), 0.83 (t, *J* = 7.1 Hz, 3H).

^{13}C NMR (126 MHz, $CDCl_3$) δ 169.66, 143.38, 137.63, 131.87, 129.39, 129.09, 124.53, 120.06, 109.90, 45.70, 42.32, 35.78, 29.67, 22.69, 14.09.

IR: ν 3249, 2960, 2929, 2860, 1657, 1597, 1550, 1489, 1445 cm^{-1}.

HRMS (ESI-TOF) m/z: [M+H+] calculated for $C_{19}H_{23}NOBr$, 360.0963; found, 360.0958.

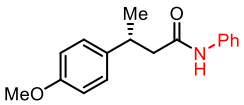

3fl

(*R*)-3-(4-methoxyphenyl)-*N*-phenylbutanamide $C_{17}H_{19}NO_2$

67% isolated yield. **R_f** = 0.5 (2:1 hexane/EtOAc). **mp** = 127-128 °C

^{1}H NMR (500 MHz, $CDCl_3$) δ 7.37 (d, *J* = 8.0 Hz, 2H), 7.26 (t, *J* = 8.4 Hz, 3H, a broad singlet overlapping the triplet, total integration is 3), 7.17 (d, *J* = 8.2 Hz, 2H), 7.07 (t, *J* = 7.4 Hz, 1H),

6.85 (d, *J* = 8.2 Hz, 2H), 3.78 (s, 3H), 3.33 (h, *J* = 7.1 Hz, 1H), 2.57 (h, *J* = 7.2 Hz, 2H), 1.33 (d, *J* = 7.0 Hz, 3H).

^{13}C NMR (126 MHz, $CDCl_3$) δ 170.30, 158.28, 137.85, 137.80, 128.98, 127.84, 124.33, 120.10, 114.17, 55.38, 47.03, 36.34, 22.02.

IR: ν 3299, 3000, 2957, 2837, 1651, 1599, 1512, 1442, 1366, 1306, 1183 cm^{-1}.

HRMS (ESI-TOF) m/z: [M+H+] calculated for $C_{17}H_{19}NO_2$, 270.1494; found, 270.1489.

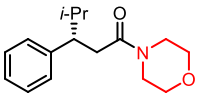

3ga

(*S*)-4-methyl-1-morpholino-3-phenylpentan-1-one $C_{16}H_{23}NO_2$

71% isolated yield. **R_f** = 0.2 (1:1 hexane/EtOAc)

^{1}H NMR (500 MHz, $CDCl_3$) δ: 7.30 – 7.23 (m, 2H), 7.22 – 7.13 (m, 3H), 3.65 – 3.52 (m, 2H), 3.51 – 3.44 (m, 1H), 3.41 – 3.25 (m, 3H), 3.24 – 3.17 (m, 1H), 3.13 – 3.03 (m, 1H), 2.91 (td, *J* = 8.6, 5.6 Hz, 1H), 2.67(dd, *J* = 14.3, 5.5 Hz, 1H), 2.64(dd, *J* = 14.3, 8.9 Hz, 1H), 1.94 (dsep, *J* = 8.4, 6.7 Hz, 1H), 1.01 (d, *J* = 6.6 Hz, 3H), 0.75 (d, *J* = 6.7 Hz, 3H).

^{13}C NMR (126 MHz, $CDCl_3$) δ 171.02, 143.54, 128.45, 128.34, 126.52, 66.93, 66.56, 50.03, 46.42, 42.02, 36.95, 32.82, 21.20, 20.79.

IR: ν 2965, 2930, 2872, 1636, 1453, 1428 cm^{-1}.

HRMS (ESI-TOF) m/z: [M+H+] calculated for $C_{16}H_{24}NO_2$, 262.1807; found, 262.1813.

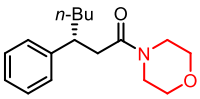

3ha

(*R*)-1-morpholino-3-phenylheptan-1-one $C_{17}H_{25}NO_2$

77% isolated yield. **R_f** = 0.1 (2.5:1 hexane/EtOAc)

^{1}H NMR (500 MHz, $CDCl_3$) δ 7.32 – 7.27 (m, 2H), 7.23 – 7.16 (m, 3H), 3.69 – 3.55 (m, 2H), 3.51 – 3.37 (m, 3H), 3.33 – 3.25 (m, 1H), 3.22 – 3.08 (m, 3H), 2.60 (dd, *J* = 14.4, 7.9 Hz, 1H), 2.52

(dd, *J* = 14.4, 6.5 Hz, 1H), 1.74 (ddt, *J* = 13.0, 10.3, 5.4 Hz, 1H), 1.65 (dtd, *J* = 13.1, 9.8, 5.0 Hz, 1H), 1.36 – 1.04 (m, 4H), 0.82 (t, *J* = 7.2 Hz, 3H).

^{13}C NMR (126 MHz, $CDCl_3$) δ 170.68, 144.61, 128.61, 127.73, 126.61, 66.94, 66.53, 46.38, 42.99, 42.01, 40.44, 35.80, 29.84, 22.76, 14.11.

IR: ν 2936, 2930, 2859, 1640, 1455, 1427 cm^{-1}.

HRMS (ESI-TOF) m/z: [M+H+] calculated for $C_{17}H_{26}NO_2$, 276.1964; found, 276.1962.

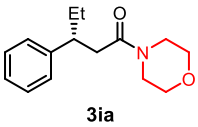

3ia

(*R*)-1-morpholino-3-phenylpentan-1-one $C_{15}H_{21}NO_2$

70% isolated yield. **R_f** = 0.2 (1:1 hexane/EtOAc)

^{1}H NMR (500 MHz, $CDCl_3$) δ 7.33 – 7.27 (m, 2H), 7.23 – 7.16 (m, 3H), 3.70 – 3.56 (m, 2H), 3.53 – 3.37 (m, 3H), 3.35 – 3.26 (m, 1H), 3.24 – 3.10 (m, 2H), 3.08 – 3.02 (m, 1H), 2.60 (dd, *J* = 14.4, 7.8 Hz, 1H), 2.54 (dd, *J* = 14.4, 6.5 Hz, 1H), 1.80 (ddq, *J* = 14.3, 5.1, 7.3 Hz, 1H), 1.66 (ddq, *J* = 14.3, 9.8, 7.3 Hz, 1H), 0.80 (t, *J* = 7.3 Hz, 3H).

^{13}C NMR (126 MHz, $CDCl_3$) δ 170.71, 144.30, 128.61, 127.80, 126.65, 66.95, 66.54, 46.39, 44.75, 42.02, 40.11, 29.00, 12.29.

IR: ν 2964, 2927, 2858, 1638, 1454, 1425 cm^{-1}.

HRMS (ESI-TOF) m/z: [M+H+] calculated for $C_{15}H_{22}NO_2$, 248.1651; found, 248.1616.

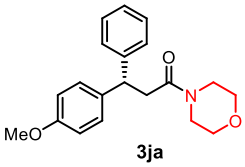

3ja

(*S*)-3-(4-methoxyphenyl)-1-morpholino-3-phenylpropan-1-one

$C_{20}H_{23}NO_3$

70% isolated yield. **R_f** = 0.2 (1:2 hexane/EtOAc)

^{1}H NMR (500 MHz, $CDCl_3$) δ 7.29 – 7.25 (m, 2H), 7.23 – 7.12 (m, 2H), 6.84 – 6.81 (m, 2H), 4.60 (t, *J* = 7.6 Hz, 1H), 3.76 (s, 3H), 3.58 – 3.50 (m, 4H), 3.38 – 3.29 (m, 4H), 3.01 (d, *J* = 7.6 Hz, 2H).

^{13}C NMR (126 MHz, $CDCl_3$) δ 170.14, 158.25, 144.39, 136.14, 128.87, 128.63, 127.86, 126.56, 114.00, 66.90, 66.50, 55.34, 46.76, 46.32, 42.11, 38.84.

IR: ν 2952, 2918, 2851, 1627, 1513, 1242, 1114, 701 cm^{-1}.

HRMS (ESI-TOF) m/z: [M+H+] calculated for C20H24NO3, 326.1756; found, 326.1752.

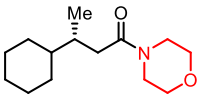

3ka

(*R*)-3-cyclohexyl-1-morpholinobutan-1-one $C_{14}H_{25}NO_2$

79% isolated yield. **R_f** = 0.1 (2:1 hexane/EtOAc)

^{1}H NMR (500 MHz, $CDCl_3$) δ 3.70 – 3.58 (m, 6H), 3.50 – 3.43 (m, 2H), 2.37 (dd, *J* = 14.5, 4.7 Hz, 1H), 2.08 (dd, *J* = 14.5, 9.4 Hz, 1H), 1.88 (dqt, *J* = 9.2, 6.8, 4.6 Hz, 1H), 1.78 – 1.70 (m, 2H), 1.69 – 1.58 (m, 3H), 1.31 – 1.15 (m, 3H), 1.12 (tt, *J* = 12.7, 3.3 Hz, 1H), 1.07 – 0.94 (m, 2H), 0.90 (d, *J* = 6.8 Hz, 3H).

^{13}C NMR (101 MHz, $CDCl_3$) δ 171.93, 67.15, 66.85, 46.41, 42.97, 42.06, 37.55, 35.49, 30.54, 29.07, 26.86, 26.80, 26.75, 16.59.

IR: ν 2923, 2852, 1642, 1426 cm^{-1}.

HRMS (ESI-TOF) m/z: [M+H+] calculated for $C_{14}H_{26}NO_2$, 240.1964; found, 240.1963.

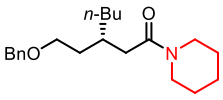

3lb

(*S*)-3-(2-(benzyloxy)ethyl)-1-(piperidin-1-yl)heptan-1-one $C_{21}H_{31}NO_2$

65% isolated yield. **R_f** = 0.2 (3:1 hexane/EtOAc)

^{1}H NMR (500 MHz, $CDCl_3$) δ 7.36 – 7.30 (m, 3H), 7.30 – 7.25 (m, 2H), 4.48 (s, 2H), 3.60 – 3.48 (m, 4H), 3.41 – 3.31 (m, 2H), 2.32 (dd, *J* = 14.7, 6.9 Hz, 1H), 2.25 (dd, *J* = 14.7, 7.0 Hz, 1H), 2.03

(hept, *J* = 6.4 Hz, 1H), 1.69 (tt, *J* = 12.8, 6.4 Hz, 1H), 1.63 – 1.57 (m, 3H), 1.56 – 1.46 (m, 4H), 1.39 – 1.19 (m, 6H), 0.88 (t, *J* = 6.7 Hz, 3H).

^{13}C NMR (126 MHz, $CDCl_3$) δ 170.98, 138.78, 128.45, 127.75, 127.59, 73.02, 68.80, 46.97, 42.79, 38.46, 34.14, 33.94, 32.60, 29.03, 26.73, 25.80, 24.76, 23.12, 14.26.

IR: ν 2933, 2857, 1640, 1436 cm^{-1}.

HRMS (ESI-TOF) m/z: [M+H+] calculated for $C_{21}H_{34}NO_2$, 332.2590; found, 332.2586.

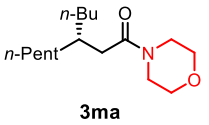

3ma

(*S*)-3-butyl-1-morpholinooctan-1-one $C_{11}H_{20}NO_2$

73% isolated yield. **R_f** = 0.2 (2:1 hexane/EtOAc)

^{1}H NMR (500 MHz, $CDCl_3$) δ 3.68 – 3.64 (m, 4H), 3.64 – 3.60 (m, 2H), 3.47 (t, *J* = 4.8 Hz, 2H), 2.22 (d, *J* = 6.9 Hz, 2H), 1.92 – 1.79 (m, 1H), 1.36 – 1.19 (m, 14H), 0.93 – 0.81 (m, 6H).

^{13}C NMR (126 MHz, $CDCl_3$) δ δ 171.79, 67.17, 66.87, 46.41, 42.07, 37.97, 35.10, 34.02, 33.76, 32.32, 28.99, 26.45, 23.16, 22.81, 14.27, 14.24.

IR: 2958, 2928, 2858, 1647, 1459, 1428 cm^{-1}.

HRMS (ESI-TOF) m/z: [M+H+] calculated for $C_{16}H_{32}NO_2$, 270.2433; found, 270.2433.

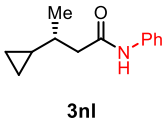

3nl

(*R*)-3-cyclopropyl-N-phenylbutanamide $C_{13}H_{17}NO$

58% isolated yield. **R_f** = 0.4 (3:1 hexane/EtOAc). **mp** = 68-70 °C

^{1}H NMR (500 MHz, $CDCl_3$) δ 7.63 (s, 1H), 7.51 (d, *J* = 8.0 Hz, 2H), 7.28 (t, *J* = 7.8 Hz, 2H), 7.07 (t, *J* = 7.4 Hz, 1H), 2.45 (dd, *J* = 13.8, 6.4 Hz, 1H), 2.26 (dd, *J* = 13.8, 7.8 Hz, 1H), 1.30 (m, 1H), 1.05 (d, *J* = 6.7 Hz, 3H), 0.56 (dp, *J* = 13.4, 4.9, 4.3 Hz, 1H), 0.40 (dd, *J* = 8.1, 4.3 Hz, 2H), 0.17 (dd, *J* = 9.4, 4.7 Hz, 1H), 0.08 (dd, *J* = 9.2, 4.6 Hz, 1H).

^{13}C NMR (126 MHz, $CDCl_3$) δ 171.18, 138.12, 129.02, 124.27, 120.12, 45.77, 36.71, 20.02, 17.91, 4.31, 3.71.

IR: ν 3296, 3076, 2959, 2924, 1655, 1599, 1443, 1164 cm^{-1}.

HRMS (ESI-TOF) m/z: [M+H+] calculated for $C_{13}H_{17}NO$, 204.1388; found, 204.1387.

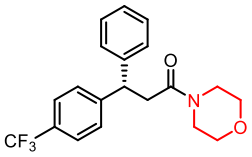

3oa

(*S*)-1-morpholino-3-phenyl-3-(4-(trifluoromethyl)phenyl)propan-1-one

$C_{20}H_{20}F_3NO_2$

60% isolated yield. **R_f** = 0.2 (1:1 hexane/EtOAc)

^{1}H NMR (500 MHz, $CDCl_3$) δ 7.54 (d, *J* = 8.1 Hz, 2H), 7.36 (d, *J* = 8.1 Hz, 2H), 7.33 – 7.28 (m, 2H), 7.24 – 7.18 (m, 3H), 4.74 (t, *J* = 7.4 Hz, 1H), 3.76 – 3.42 (m, 5H), 3.41 – 3.32 (m, 3H), 3.06 (d, *J* = 7.4 Hz, 2H).

^{13}C NMR (126 MHz, $CDCl_3$) δ 169.46, 148.17, 143.27, 128.92, 128.90 (q, J_{CF} = 32.5 Hz) 128.27, 127.95, 127.05, 125.64 (q, J_{CF} = 3.8 Hz), 124.28 (q, J_{CF} = 271.9 Hz), 66.95, 66.54, 47.16, 46.25, 42.22, 38.55.

^{19}F NMR (470 MHz, $CDCl_3$) δ -62.48.

IR: ν 2919, 2855, 1732, 1635, 1324, 1108 cm^{-1}.

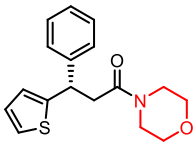

3pa

(*S*)-1-morpholino-3-phenyl-3-(thiophen-2-yl)propan-1-one $C_{17}H_{19}NO_2S$

71% isolated yield. **R_f** = 0.15 (2:1 hexane/EtOAc) **mp** = 102-104 °C

^{1}H NMR (500 MHz, $CDCl_3$) δ 7.35 – 7.29 (m, 4H), 7.25 – 7.20 (m, 1H), 7.15 (dd, *J* = 5.1, 1.2 Hz, 1H), 6.92 (dd, *J* = 5.1, 3.5 Hz, 1H), 6.84 (dt, *J* = 3.5, 1.0 Hz, 1H, allylic coupling with 3° H), 4.90 (t, *J* = 7.4 Hz, 1H), 3.64 – 3.43 (m, 5H), 3.42 – 3.35 (m, 1H), 3.35 – 3.26 (m, 2H), 3.09 (dd, *J* = 14.7, 7.1 Hz, 1H), 3.03 (dd, *J* = 14.7, 7.7 Hz, 1H).

^{13}C NMR (126 MHz, $CDCl_3$) δ 169.43, 148.10, 143.67, 128.78, 127.84, 127.15, 126.82, 124.49, 124.03, 66.93, 66.57, 46.34, 43.36, 42.21, 40.29.

IR: 2921, 2859, 2855, 1630, 1437 cm^{-1}.

HRMS (ESI-TOF) m/z: [M+H+] calculated for $C_{17}H_{20}NO_2S$, 302.1215; found, 302.1218.

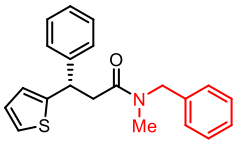

3pf

(*S*)-*N*-benzyl-*N*-methyl-3-phenyl-3-(thiophen-2-yl)propanamide

$C_{21}H_{21}NOS$

52% isolated yield. **R_f** = 0.2 (5:1 hexane/EtOAc)

^{1}H NMR (500 MHz, $CDCl_3$, mixture of amide rotamers) δ 7.38 – 7.19 (m, 8H), 7.16 (dd, *J* = 5.1, 1.2 Hz, 0.6H, ma*J*or rotamer), 7.13 (dd, *J* = 5.1, 1.2 Hz, 0.4H, minor rotamer), 7.04 – 7.00 (m, 1H), 6.99 – 6.96 (m, 1H), 6.92 (dd, *J* = 5.1, 3.5 Hz, 0.6H, ma*J*or rotamer), 6.89 (dd, *J* = 5.1, 3.5 Hz, 0.4H, minor rotamer), 6.85 (dt, *J* = 3.5, 1.0 Hz, 0.6H, ma*J*or rotamer, allyic coupling), 6.78 (dt, *J* = 3.7, 1.0 Hz, 0.4H, minor rotamer, allyic coupling), 4.58 (d, *J* = 14.7 Hz, 0.7H, ma*J*or rotamer), 4.50 (d, *J* = 14.7 Hz, 0.7H, ma*J*or rotamer), 4.47 (d, *J*=17 Hz, 0.4H, minor rotamer), 4.43 (d, *J* = 16.9 Hz, 0.4H, minor rotamer), δ 2.89 (s, 1.2H, minor rotamer), 2.85 (s, 2.0H, ma*J*or rotamer).

^{13}C NMR (126 MHz, $CDCl_3$, mixture of amide rotamers) δ 170.95, 170.79, 148.48, 148.42, 143.91, 143.84, 137.18, 136.54, 129.05, 128.74, 128.70, 128.63, 127.94, 127.92, 127.91, 127.73, 127.32, 126.99, 126.93, 126.78, 126.75, 126.40, 124.49, 124.38, 123.90, 123.87, 53.29, 51.05, 43.24, 42.92, 40.92, 40.81, 35.11, 34.26.

IR: 3063, 3031, 2968, 1641, 1437 cm^{-1}.

HRMS (ESI-TOF) m/z: [M+H+] calculated for $C_{21}H_{22}NOS$, 336.1422; found, 336.1418.

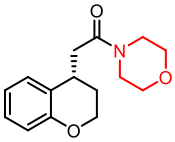

3qa

(*R*)-2-(chroman-4-yl)-1-morpholinoethan-1-one $C_{15}H_{19}NO_3$

63% isolated yield. **R_f** = 0.1 (1:1 hexane/EtOAc)

^{1}H NMR (500 MHz, $CDCl_3$) δ 7.13 – 7.09 (m, 2H), 6.86 (td, *J* = 7.4, 1.2 Hz, 1H), 6.81 (dd, *J* = 8.7, 1.4 Hz, 1H), 4.23 (ddd, *J* = 11.3, 5.4, 3.8 Hz, 1H), 4.16 (ddd, *J* = 11.1, 9.7, 2.8 Hz, 1H), 3.77 – 3.58 (m, 5H), 3.58 – 3.32 (m, 4H), 2.76 (dd, *J* = 15.5, 5.1 Hz, 1H), 2.54 (dd, *J* = 15.5, 9.3 Hz, 1H), 2.23 (dddd, *J* = 13.7, 9.6, 5.7, 3.8 Hz, 1H), 1.85 (dtd, *J* = 14.0, 5.1, 2.8 Hz, 1H).

^{13}C NMR (126 MHz, $CDCl_3$) δ 170.01, 154.74, 129.10, 127.98, 125.13, 120.50, 117.20, 67.01, 66.61, 63.34, 46.18, 42.15, 39.82, 30.44, 27.66.

IR: 2966, 2927 2860, 1638, 1489 cm^{-1}.

HRMS (ESI-TOF) m/z: [M+H+] calculated for $C_{15}H_{20}NO_3$, 262.1443; found, 262.1440.

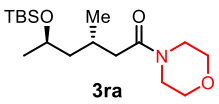

3ra

(3*S*,5*R*)-5-((tert-butyldimethylsilyl)oxy)-3-methyl-1-morpholinohexan-1-one $C_{17}H_{35}NO_3Si$

64% isolated yield. **R_f** = 0.2 (30% EtOAc/Hex).

^{1}H NMR (500 MHz, $CDCl_3$) δ 3.93 – 3.85 (m, 1H), 3.73 – 3.56 (m, 6H), 3.46 (t, *J* = 4.9 Hz, 2H), 2.33 – 2.28 (m, 1H), 2.20 – 2.07 (m, 2H), 1.57 (s, 1H), 1.51 (ddd, *J* = 13.2, 8.9, 4.1 Hz, 1H), 1.29 – 1.17 (m, 2H), 1.13 (dd, *J* = 6.0, 0.8 Hz, 3H), 0.96 (d, *J* = 6.2 Hz, 3H), 0.88 (d, *J* = 0.8 Hz, 9H), 0.06 (s, 3H), 0.05 (s, 3H).

^{13}C NMR (125 MHz, $CDCl_3$) δ 171.02, 67.06, 66.79, 66.24, 47.08, 46.36, 41.88, 41.45, 27.03, 25.89, 24.58, 19.66, 18.06, -4.05, -4.74.

IR: ν 2958, 2928, 2894, 2856, 1645, 1462, 1429, 1252 cm^{-1}.

HRMS (EDI-TOF) m/z: [M+H+] calculated for $C_{17}H_{36}NO_3Si$, 330.2464; found, 330.2460.

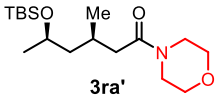

(3R,5R)-5-((tert-butyldimethylsilyl)oxy)-3-methyl-1-morpholinohexan-1-one $C_{17}H_{35}NO_3Si$

65% isolated yield. **R_f** = 0.2 (30% EtOAc/Hex).

^{1}H NMR (500 MHz, $CDCl_3$) δ 3.91 (q, *J* = 6.2 Hz, 1H), 3.72 – 3.58 (m, 6H), 3.51 – 3.43 (m, 2H), 2.44 – 2.30 (m, 1H), 2.20 – 1.99 (m, 2H), 1.40 (hept, *J* = 7.0, 6.6 Hz, 2H), 1.29 – 1.22 (m, 1H), 1.14 (d, *J* = 6.0 Hz, 3H), 0.96 (d, *J* = 6.2 Hz, 3H), 0.88 (s, 9H), 0.05 (s, 6H).

^{13}C NMR (125 MHz, $CDCl_3$) δ 171.16, 67.18, 67.11, 66.86, 47.15, 46.37, 42.04, 40.62, 27.47, 26.06, 23.64, 20.54, 18.27, -4.17, -4.49.

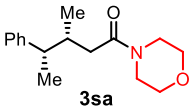

(3*R*,4*S*)-3-methyl-1-morpholino-4-phenylpentan-1-one $C_{16}H_{23}NO_2$

46% isolated yield. **R_f** = 0.1 (3:1 hexane/EtOAc).

^{1}H NMR (500 MHz, $CDCl_3$) δ 7.30 – 7.22 (m, 2H), 7.20 – 7.13 (m, 3H), 3.70 – 3.38 (m, 6H), 3.28 – 3.10 (m, 2H), 2.53 (p, *J* = 7.2 Hz, 1H), 2.20 (dd, *J* = 14.4, 3.5 Hz, 1H), 2.17 – 2.09 (m, 1H), 1.93 (dd, *J* = 14.3, 9.3 Hz, 1H), 1.24 (d, *J* = 7.1 Hz, 3H), 0.99 (d, *J* = 6.5 Hz, 3H).

^{13}C NMR (125 MHz, $CDCl_3$) δ 171.41, 146.37, 128.47, 127.70, 126.30, 67.06, 66.73, 46.12, 45.43, 41.97, 38.50, 36.97, 18.57, 17.53.

IR: ν 2966, 2956, 2863, 1640, 1453, 1429 cm^{-1}.

HRMS (ESI-TOF) m/z: [M+H+] calculated for $C_{16}H_{24}NO_2$, 262.1807; found, 262.1805.

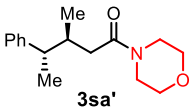

(3*S*,4*S*)-3-methyl-1-morpholino-4-phenylpentan-1-one $C_{16}H_{23}NO_2$

73% isolated yield. **R_f** = 0.1 (3:1 hexane/EtOAc).

^{1}H NMR (500 MHz, $CDCl_3$) δ 7.31 – 7.27 (m, 2H), 7.21 – 7.14 (m, 3H), 3.70 – 3.54 (m, 6H), 3.29 – 3.17 (m, 2H), 2.76 (p, *J* = 6.9 Hz, 1H), 2.35 (dd, *J* = 14.5, 4.5 Hz, 1H), 2.29 – 2.16 (m, 1H), 2.00 (dd, *J* = 14.5, 9.2 Hz, 1H), 1.27 (d, *J* = 7.1 Hz, 3H), 0.89 (d, *J* = 6.8 Hz, 3H).

^{13}C NMR (125 MHz, $CDCl_3$) δ 171.50, 145.18, 128.27, 128.07, 126.27, 67.10, 66.76, 46.16, 44.49, 42.05, 37.06, 36.71, 17.72, 17.50.

IR: ν 2968, 2927, 2862, 1641, 1453, 1429 cm^{-1}.

HRMS (ESI-TOF) m/z: [M+H+] calculated for $C_{16}H_{24}NO_2$, 262.1807; found, 262.1806.

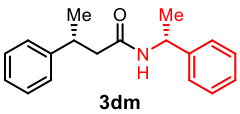

3dm

(*R*)-3-phenyl-*N*-((*R*)-1-phenylethyl)butanamide $C_{18}H_{21}NO$

44% isolated yield (eluent: 3:1 hexane/EtOAc). **R_f** = 0.1 (4:1 hexane/EtOAc)

^{1}H NMR (500 MHz, $CDCl_3$) δ 7.37 – 7.15 (m, 8H), 7.05 – 6.94 (m, 2H), 5.57 – 5.40 (m, 1H), 5.04 (p, *J* = 7.1 Hz, 1H), 3.30 (h, *J* = 7.1 Hz, 1H), 2.55 – 2.33 (m, 2H), 1.39 (d, *J* = 6.9 Hz, 3H), 1.32 (d, *J* = 7.0 Hz, 3H).

^{13}C NMR (126 MHz, $CDCl_3$) δ 170.71, 145.83, 143.00, 128.76, 128.63, 127.23, 126.99, 126.57, 126.12, 48.50, 46.12, 37.25, 21.98, 21.70.

IR: ν 3291, 3067, 3062, 2967, 2929, 2897, 1635, 1547, 1450 cm^{-1}.

HRMS (ESI-TOF) m/z: [M+H+] calculated for $C_{18}H_{22}NO$, 268.1701; found, 268.1697.

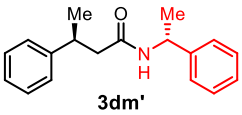

3dm'

(*S*)-3-phenyl-*N*-((*R*)-1-phenylethyl)butanamide $C_{18}H_{21}NO$

46% isolated yield (eluent: 3:1 hexane/EtOAc). **R_f** = 0.1 (4:1 hexane/EtOAc)

^{1}H NMR (500 MHz, $CDCl_3$) δ 7.34 – 7.27 (m, 4H), 7.25 – 7.20 (m, 4H), 7.19 – 7.16 (m, 2H), 5.39 – 5.30 (br, 1H), 5.01 (p, *J* = 7.1 Hz, 1H), 3.29 (h, *J* = 7.2 Hz, 1H), 2.46 – 2.38 (m, 2H), 1.30 (d, *J* = 6.9, Hz, 3H), 1.24 (d, *J* = 6.9 Hz, 3H).

^{13}C NMR (126 MHz, $CDCl_3$) δ 170.73, 145.92, 143.22, 128.79, 128.74, 127.43, 127.02, 126.64, 126.26, 48.63, 46.27, 37.47, 21.98, 21.52.

IR: ν 3277, 3070, 3054, 2964, 2930, 2869, 1633, 1551, 1448 cm^{-1}.

HRMS (ESI-TOF) m/z: [M+H+] calculated for $C_{18}H_{22}NO$, 268.1701; found, 268. 1703.

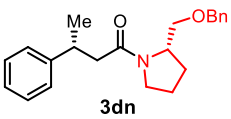

3dn

(*R*)-1-((*S*)-2-((benzyloxy)methyl)pyrrolidin-1-yl)-3-phenylbutan-1-one

$C_{22}H_{27}NO_2$

44% yield. **R_f** = 0.2 (30% EtOAc/Hex).

^{1}H NMR (500 MHz, $CDCl_3$ mixture of rotamers) δ 7.36 – 7.23 (m, 8H), 7.22 – 7.16 (m, 2H), 4.53 (dd, *J* = 12.0, 15.3 Hz, 2H), 4.42 (s, 1H), 4.26 (tt, *J* = 6.6, 2.9 Hz, 1H), 3.64 (dd, *J* = 9.3, 3.3 Hz, 1H), 3.52 (dq, *J* = 8.5, 6.6 Hz, 1H), 3.46 – 3.34 (m, 3H), 3.19 – 3.10 (m, 2H), 2.58 – 2.44 (m, 3H), 2.02 – 1.68 (m, 6H), 1.33 (d, *J* = 6.9 Hz, 3H), 1.29 (d, *J* = 7.0 Hz, 1H), 1.26 (s, 1H).

^{13}C NMR (125 MHz, $CDCl_3$ mixture of rotamers) δ 170.87, 170.75, 146.72, 146.64, 138.75, 137.98, 128.60, 128.53, 128.46, 127.94, 127.67, 127.60, 127.13, 127.04, 126.36, 126.25, 73.33, 73.30, 71.11, 70.32, 57.21, 56.58, 47.61, 45.72, 43.90, 43.10, 36.47, 29.84, 28.94, 27.66, 24.26, 21.93, 21.48, 21.39.

IR: ν 2957, 2918, 2851, 1630, 1560, 1454, 1411, 1376 cm^{-1}.

HRMS (EDI-TOF) m/z: [M+H+] calculated for $C_{22}H_{27}NO_2$, 338.2120; found, 338.2119.

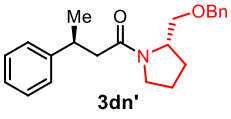

3dn'

(*S*)-1-((*S*)-2-((benzyloxy)methyl)pyrrolidin-1-yl)-3-phenylbutan-1-one

$C_{22}H_{27}NO_2$

42% yield. **R_f** = 0.2 (30% EtOAc/Hex).

^{1}H NMR (500 MHz, $CDCl_3$ mixture of rotamers) δ 7.41 – 7.27 (m, 6H), 7.25 – 7.22 (m, 2H), 7.21 – 7.12 (m, 2H), 4.49 (d, *J* = 13.0 Hz, 1.3H), 4.42 (d, *J* = 12.0 Hz, 0.7H), 4.34 – 4.27 (m, 0.6H), 3.73 – 3.66 (m, 0.4H), 3.59 (dd, *J* = 9.4, 3.3 Hz, 0.6H), 3.45 – 3.29 (m, 3.4H), 3.28 – 3.20 (m, 1.0H), 2.61 – 2.49 (m, 1.4H), 2.46 (dd, *J* = 14.7, 8.0 Hz, 0.6H), 2.03 – 1.68 (m, 4H), 1.34 (d, *J* = 7.0 Hz, 1.8H), 1.28 (d, *J* = 7.0 Hz, 1.2H).

^{13}C NMR (125 MHz, $CDCl_3$, mixture of rotamers) δ 171.21, 170.73, 146.55, 146.28, 138.72, 137.96, 128.62, 128.50, 128.47, 128.43, 127.98, 127.77, 127.62, 127.58, 127.05, 127.02, 126.35, 73.45, 73.25, 71.52, 70.03, 56.99, 56.50, 47.54, 45.48, 43.82, 43.50, 37.09, 36.61, 28.62, 27.58, 24.22, 21.97, 21.70, 21.31.

IR: ν 2957, 2918, 2851, 1630, 1560, 1454, 1411, 1376 cm^{-1}.

2.7.2 HPLC Traces of Isolated Amides

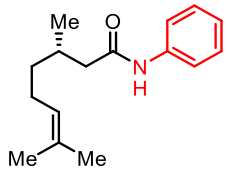

3bl

CHIRALPAK® ID-3, 1.0 mL/min, 30 °C, 99:1 Hexanes: MeOH, er = 97.5:2.5

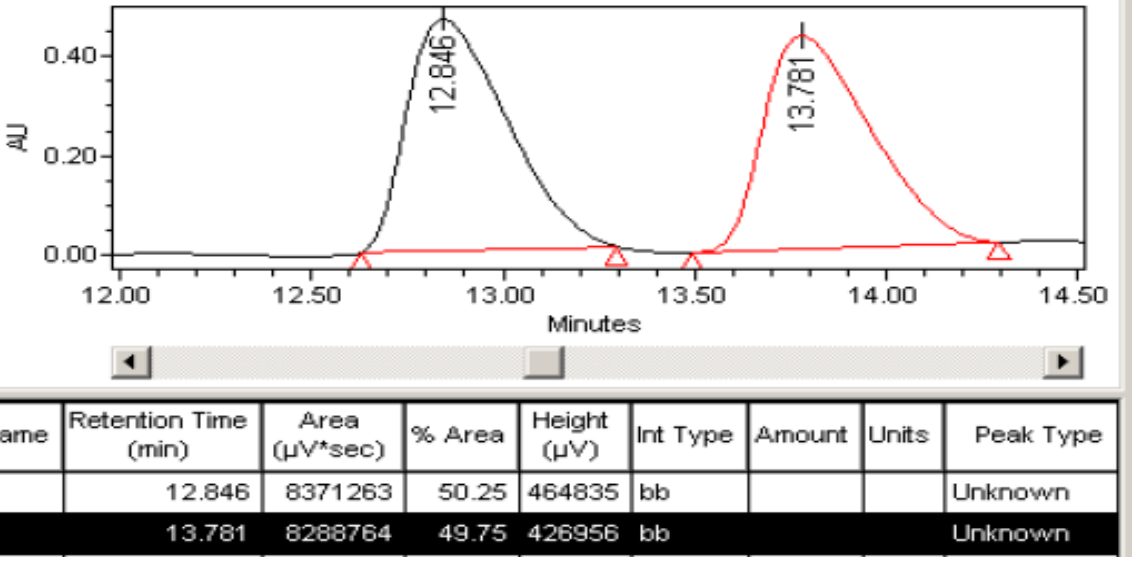

	Name	Retention Time (min)	Area (μV*sec)	% Area	Height (μV)	Int Type	Amount	Units	Peak Type
1		12.846	8371263	50.25	464835	bb			Unknown
2		13.781	8288764	49.75	426956	bb			Unknown

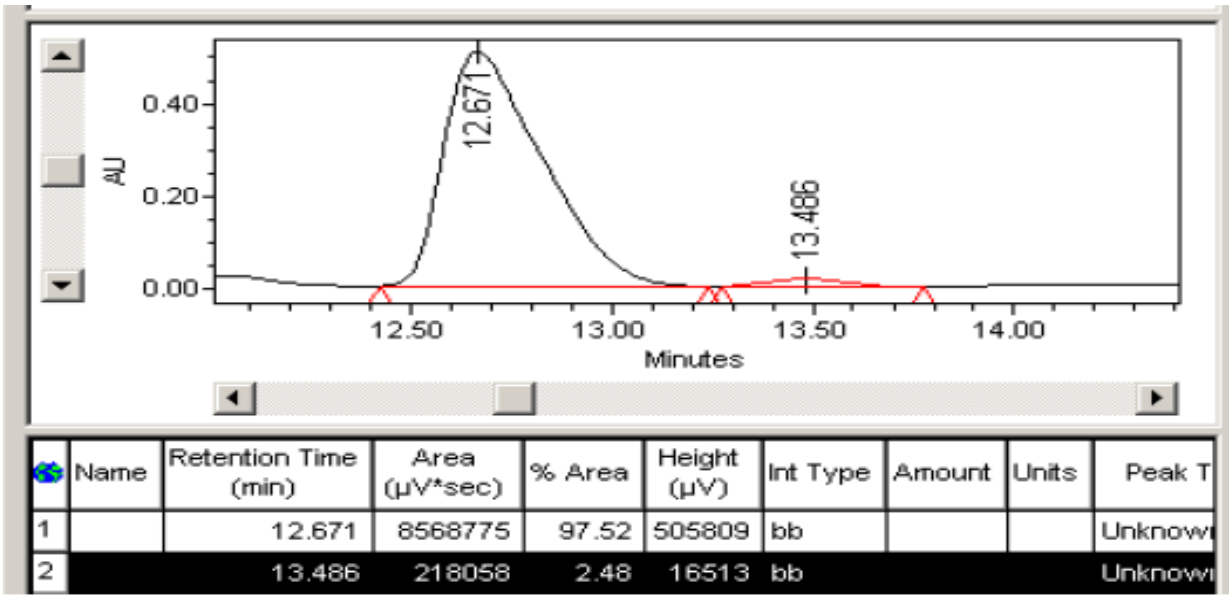

	Name	Retention Time (min)	Area (μV*sec)	% Area	Height (μV)	Int Type	Amount	Units	Peak T
1		12.671	8568775	97.52	505809	bb			Unknown
2		13.486	218058	2.48	16513	bb			Unknown

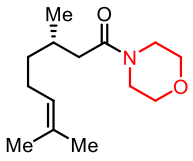

3ba

CHIRALPAK® ID-3, 1.0 mL/min, 30 °C, 97 : 3 Hexanes: *i*-PrOH

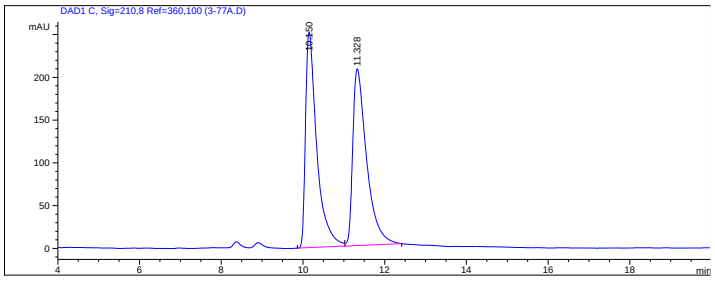


```
================================================================================
                          Area Percent Report
================================================================================

Sorted By             :      Signal
Multiplier            :      1.0000
Dilution              :      1.0000
Use Multiplier & Dilution Factor with ISTDs


Signal 1: DAD1 C, Sig=210,8 Ref=360,100

Peak RetTime Type  Width     Area      Height     Area
  #   [min]        [min]   [mAU*s]     [mAU]       %
----|-------|----|-------|----------|----------|--------|
   1  10.150 BV    0.2835 4827.35059  251.65883  49.8009
   2  11.328 VB    0.3493 4865.95215  206.69400  50.1991

Totals :                  9693.30273  458.35283

 Results obtained with standard integrator!
================================================================================
                          *** End of Report ***
```

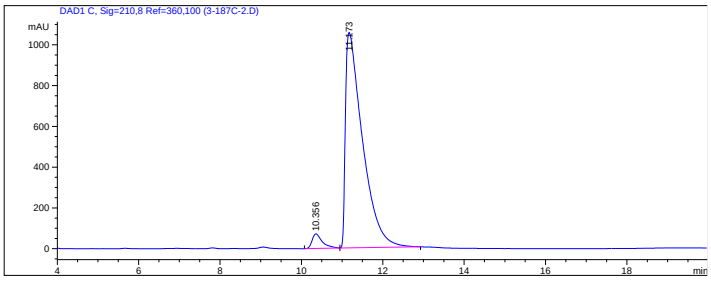


```
================================================================================
                          Area Percent Report
================================================================================

Sorted By             :      Signal
Multiplier            :      1.0000
Dilution              :      1.0000
Use Multiplier & Dilution Factor with ISTDs


Signal 1: DAD1 C, Sig=210,8 Ref=360,100

Peak RetTime Type  Width     Area      Height     Area
  #   [min]        [min]   [mAU*s]     [mAU]       %
----|-------|----|-------|----------|----------|--------|
   1  10.356 BV    0.2604 1252.65405   71.64041   3.9129
   2  11.173 VB    0.4241 3.07608e4  1057.20764  96.0871

Totals :                  3.20135e4  1128.84805

 Results obtained with standard integrator!
================================================================================
                          *** End of Report ***
```

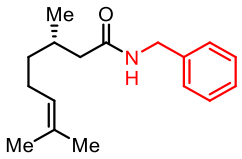

3bg

CHIRALPAK® ID-3, 1.0 mL/min, 30 °C, 90:10 Hexanes: *i*-PrOH, er = 97:3

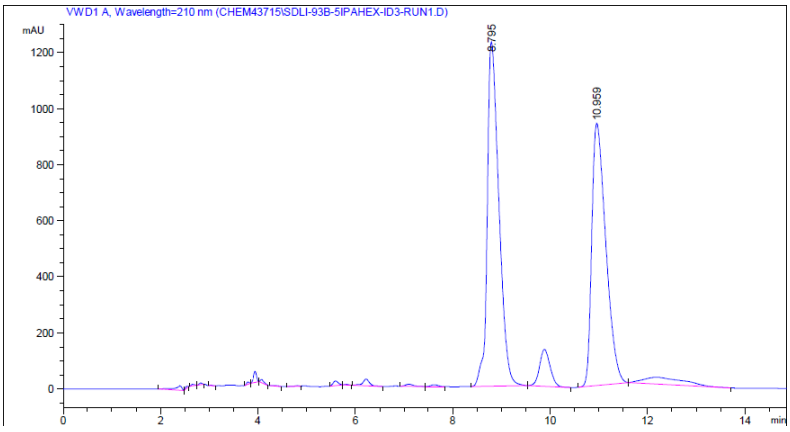

Peak #	RetTime [min]	Type	Width [min]	Area mAU *s	Height [mAU]	Area %
16	8.795	BB	0.2531	2.03647e4	1228.58691	46.8059
18	10.959	BB	0.3079	1.87306e4	935.36475	43.0501

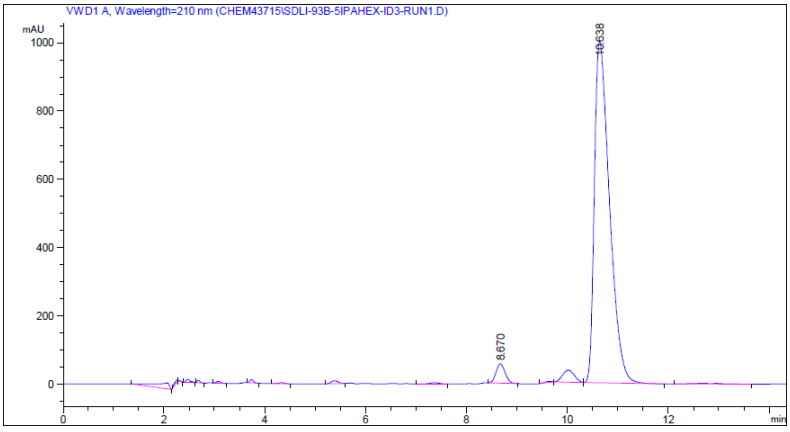

Peak #	RetTime [min]	Type	Width [min]	Area mAU *s	Height [mAU]	Area %
11	8.670	BB	0.1952	706.72205	56.60861	3.0794
14	10.638	BB	0.3164	2.08110e4	1002.51825	90.6783

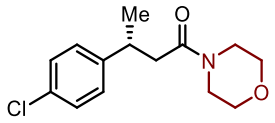

3ca

CHIRALPAK® ID-3, 1.0 mL/min, 30 °C, 95:5 Hexanes: *i*-PrOH, er = 99:1

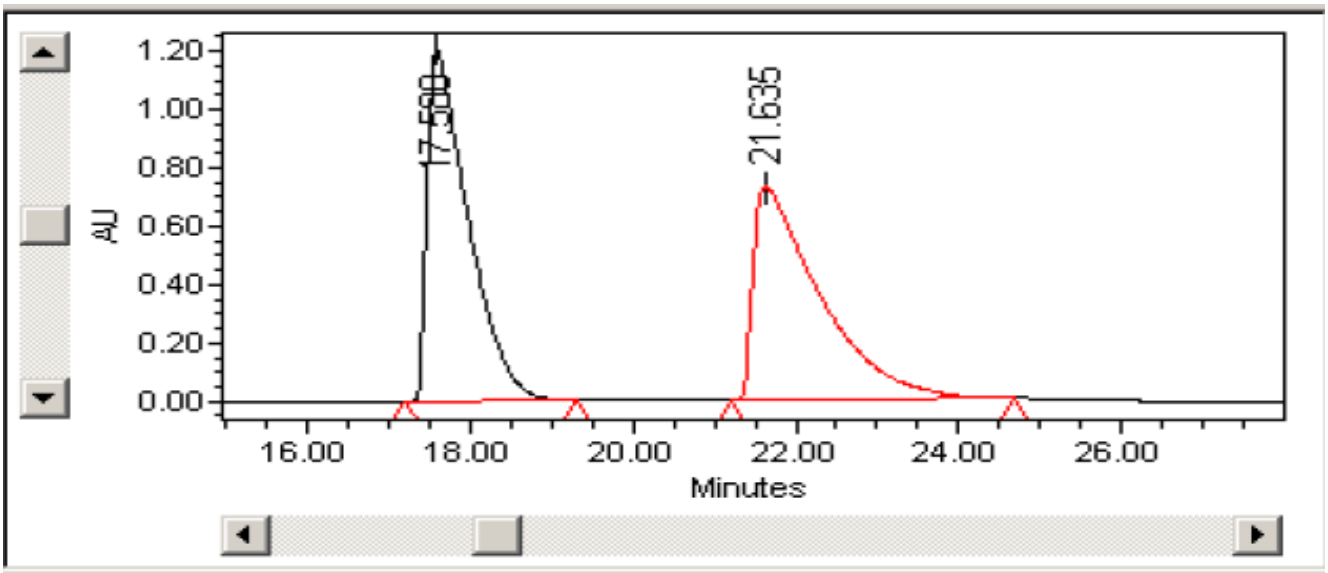

	Name	Retention Time (min)	Area (μV*sec)	% Area	Height (μV)	Int Type	Amount	Units	
1		17.588	42058501	50.43	1202587	bb			Un
2		21.635	41337829	49.57	731545	bb			Un

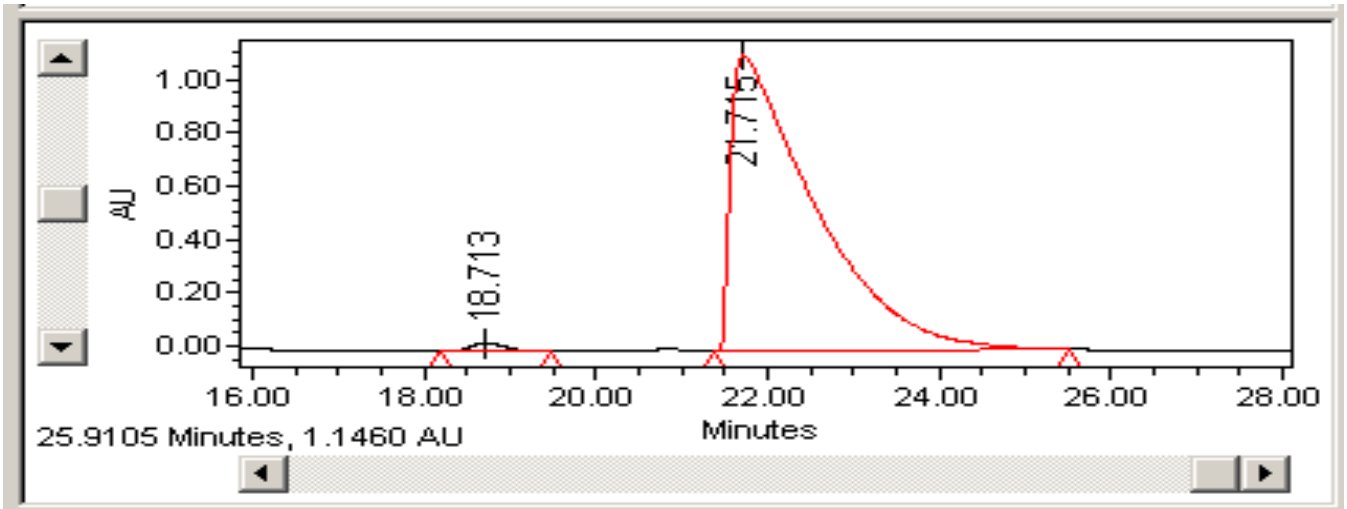

	Name	Retention Time (min)	Area (μV*sec)	% Area	Height (μV)	Int Type	Amount	Units	
1		18.713	778876	1.04	29502	bb			Un
2		21.715	74428060	98.96	1109874	bb			Un

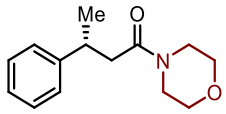

3da

CHIRALPAK® ID-3, 1.0 mL/min, 30 °C, 96:4 Hexanes: *i*-PrOH, er = 96:4

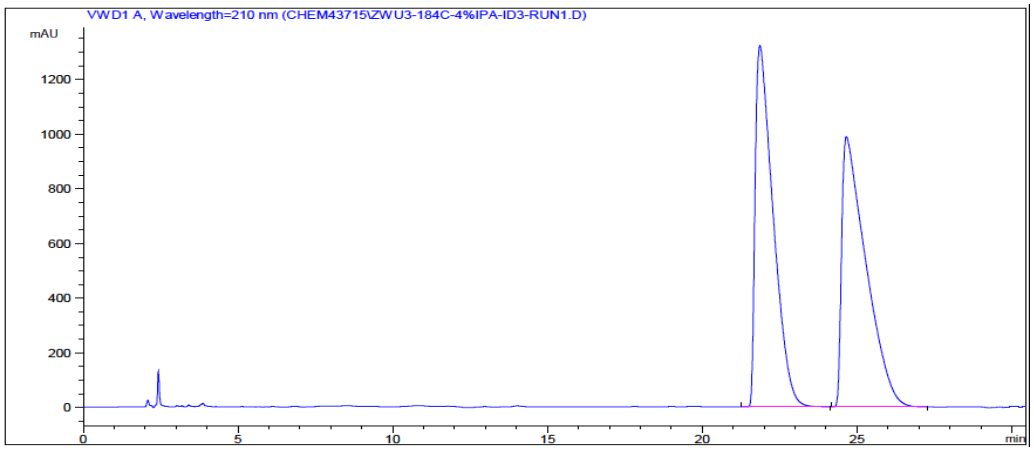

Peak #	RetTime [min]	Sig	Type	Area	Area %	Name
1	21.858	1	VB	5.32616e4	49.7785	?
2	24.653	1	BB	5.37356e4	50.2215	?

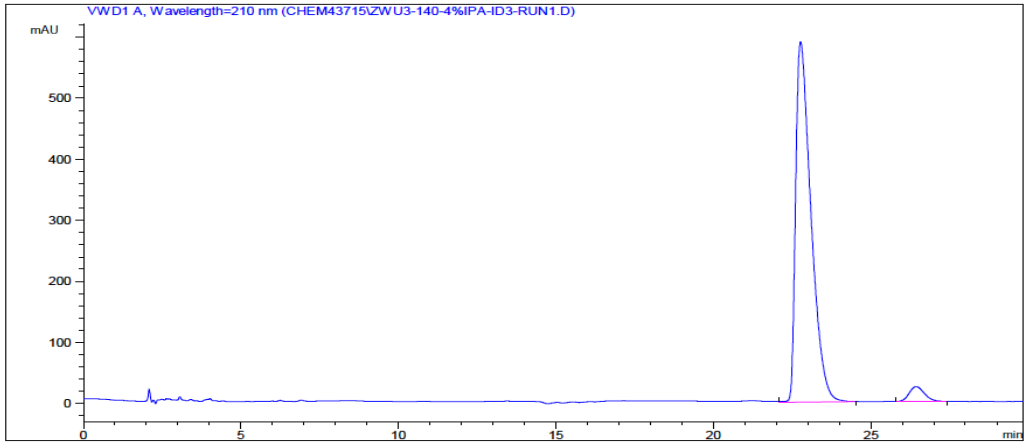

Peak #	RetTime [min]	Sig	Type	Area	Area %	Name
1	22.769	1	VB	1.99553e4	95.9303	?
2	26.437	1	VV	846.56464	4.0697	?

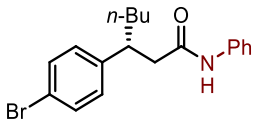

3el

CHIRALPAK® ID-3, 1.0 mL/min, 30 °C, 97:3 Hexanes: *i*-PrOH, er = 97.5:2.5

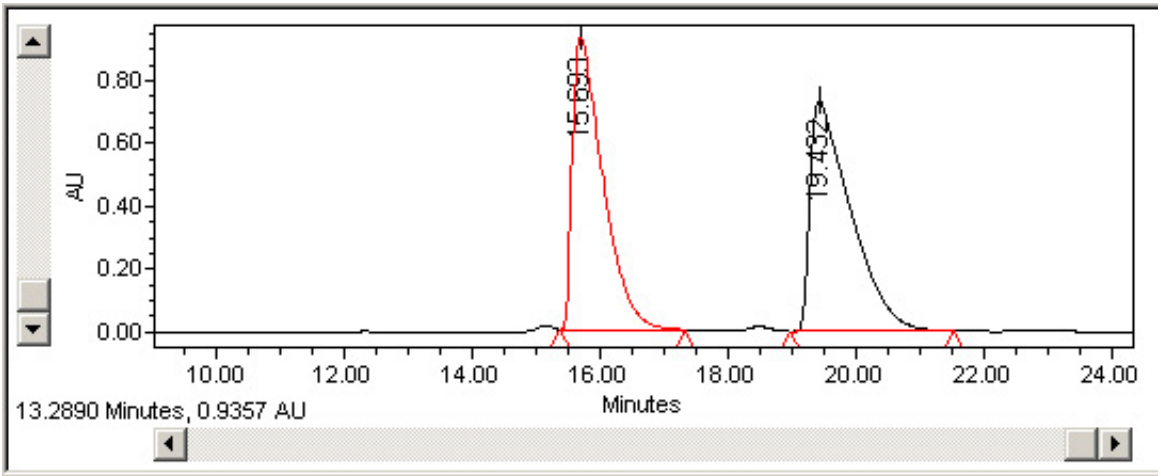

	Name	Retention Time (min)	Area (μV*sec)	% Area	Height (μV)	Int Type	Amount	Units	Peak Type	Peak Codes
1		15.693	31109931	48.91	929179	bb			Unknown	
2		19.432	32502785	51.09	734430	bb			Unknown	

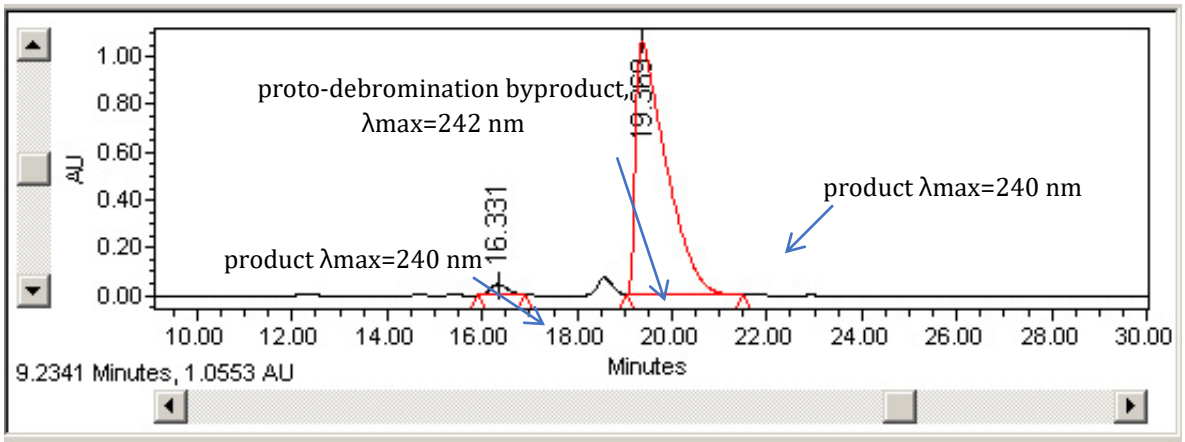

	Name	Retention Time (min)	Area (μV*sec)	% Area	Height (μV)	Int Type	Amount	Units	Peak Type	Peak Codes
1		16.331	1143606	2.36	44432	bb			Unknown	
2		19.369	47285181	97.64	1062476	bb			Unknown	

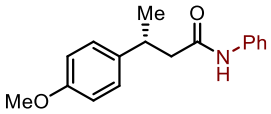

3fl

CHIRALPAK® ID-3, 1.0 mL/min, 30 °C, 95:5 Hexanes: *i*-PrOH, er = 99:1

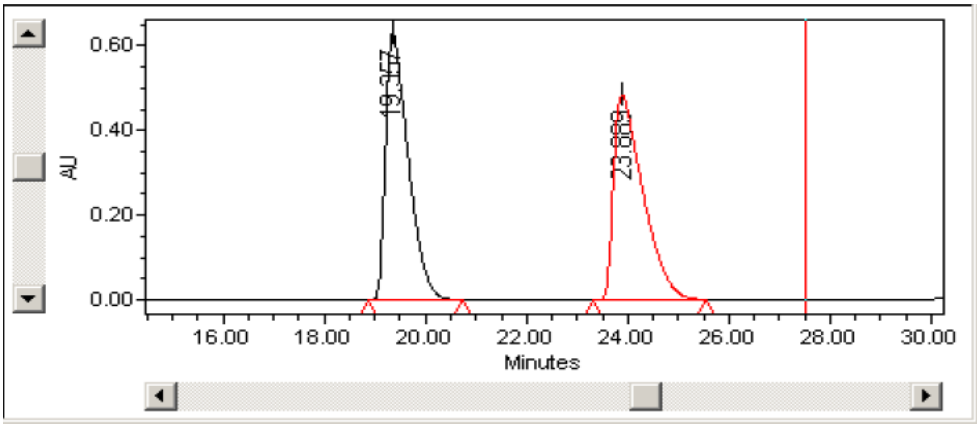

	Name	Retention Time (min)	Area (µV*sec)	% Area	Height (µV)	Int Type	Amount	Units	Peak Type
1		19.357	19611967	50.15	629619	bb			Unknown
2		23.889	19495068	49.85	482976	bb			Unknown

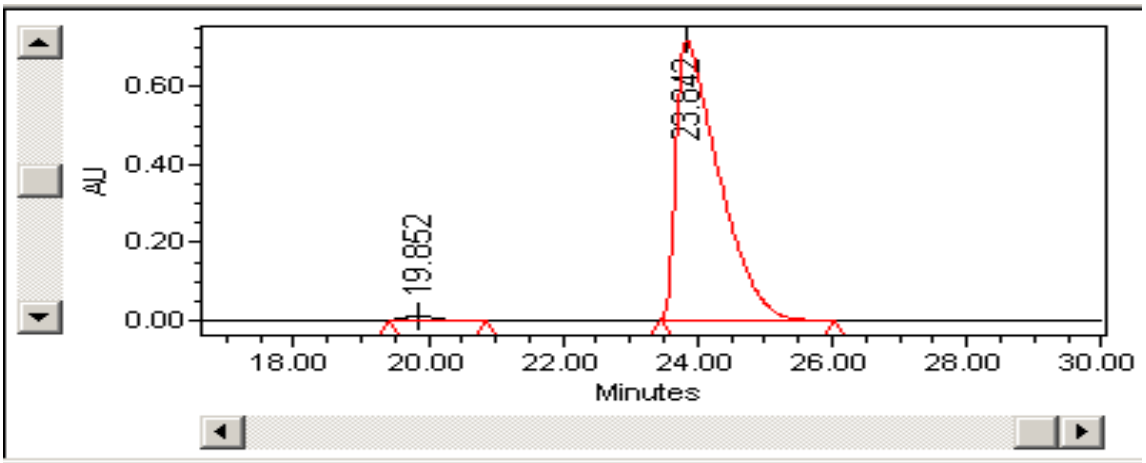

	Name	Retention Time (min)	Area (µV*sec)	% Area	Height (µV)	Int Type	Amount	Units
1		19.852	322075	1.01	11949	bb		
2		23.842	31460285	98.99	715834	bb		

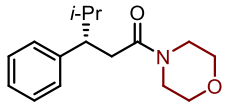

3ga

CHIRALPAK® ID-3, 1.0 mL/min, 30 °C, 97:3 Hexanes: *i*-PrOH, er = 96:4

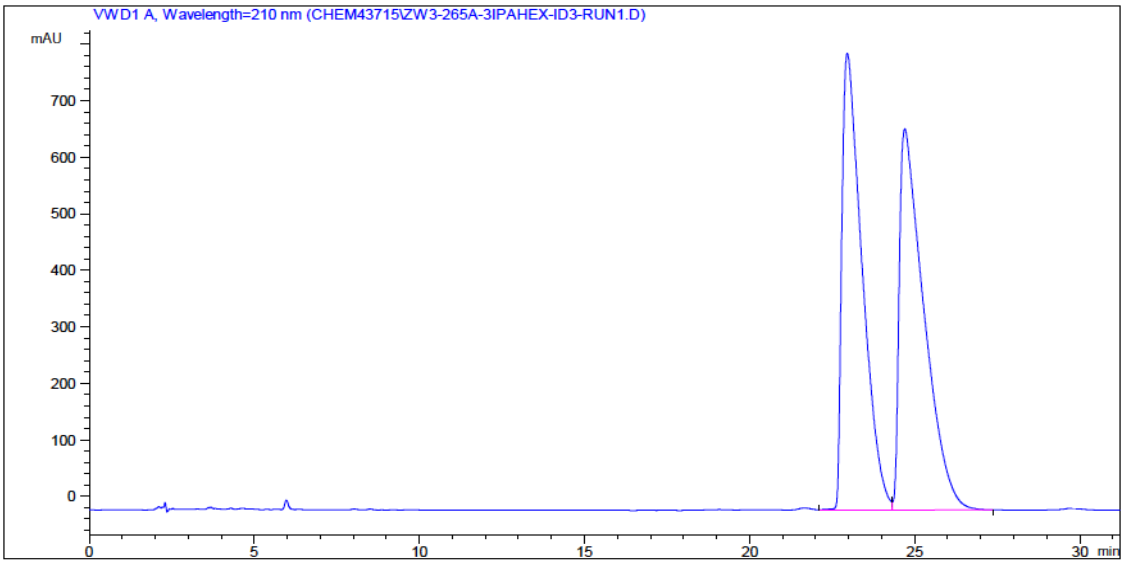

Peak #	RetTime [min]	Sig	Type	Area	Area %	Name
1	22.957	1	VV	3.45078e4	49.6665	?
2	24.698	1	VB	3.49713e4	50.3335	?

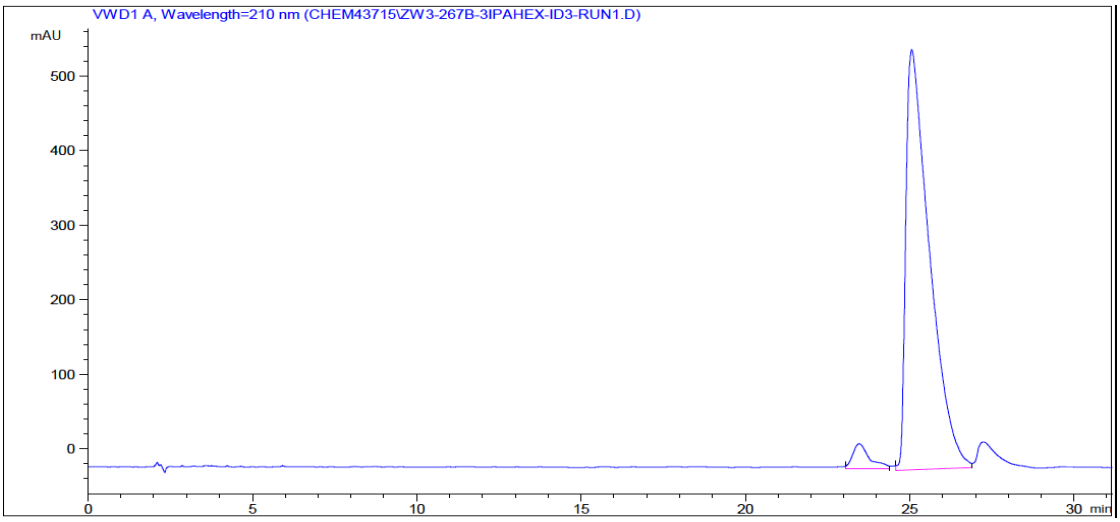

Peak #	RetTime [min]	Sig	Type	Area	Area %	Name
1	23.464	1	MM	1158.81763	3.9530	?
2	25.061	1	MM	2.81560e4	96.0470	?

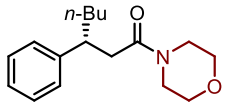

3ha

CHIRALPAK® ID-3, 1.0 mL/min, 30 °C, 96:4 Hexanes: *i*-PrOH, er = 99:1

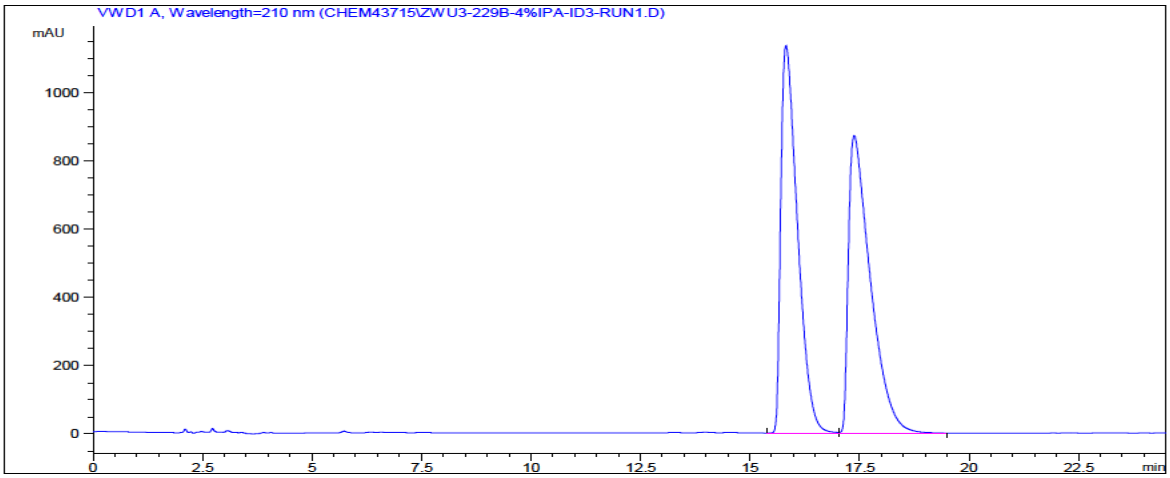

Peak #	RetTime [min]	Sig	Type	Area	Area %	Name
1	15.825	1	VV	3.01186e4	49.7550	?
2	17.382	1	VB	3.04153e4	50.2450	?

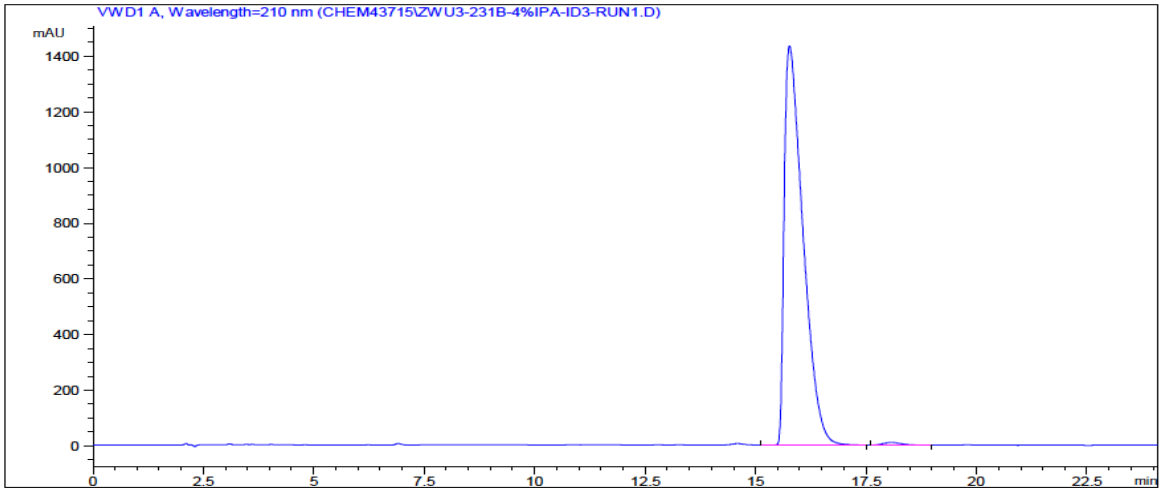

Peak #	RetTime [min]	Sig	Type	Area	Area %	Name
1	15.770	1	VB	4.24359e4	99.2672	?
2	18.075	1	BV	313.28009	0.7328	?

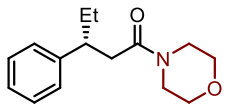

3ia

CHIRALPAK® ID-3, 1.0 mL/min, 30 °C, 97:3 Hexanes: *i*-PrOH, er = 97:3

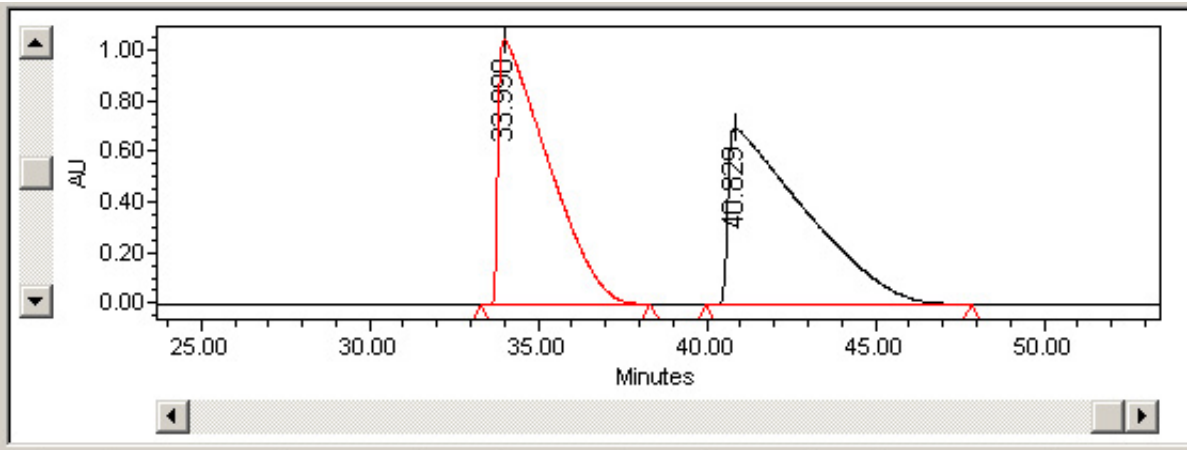

	Name	Retention Time (min)	Area (µV*sec)	% Area	Height (µV)	Int Type	Amount	Units	Peak Type	Peak Codes
1		33.998	106649974	49.22	1049362	bb			Unknown	
2		40.829	110019902	50.78	697362	bb			Unknown	

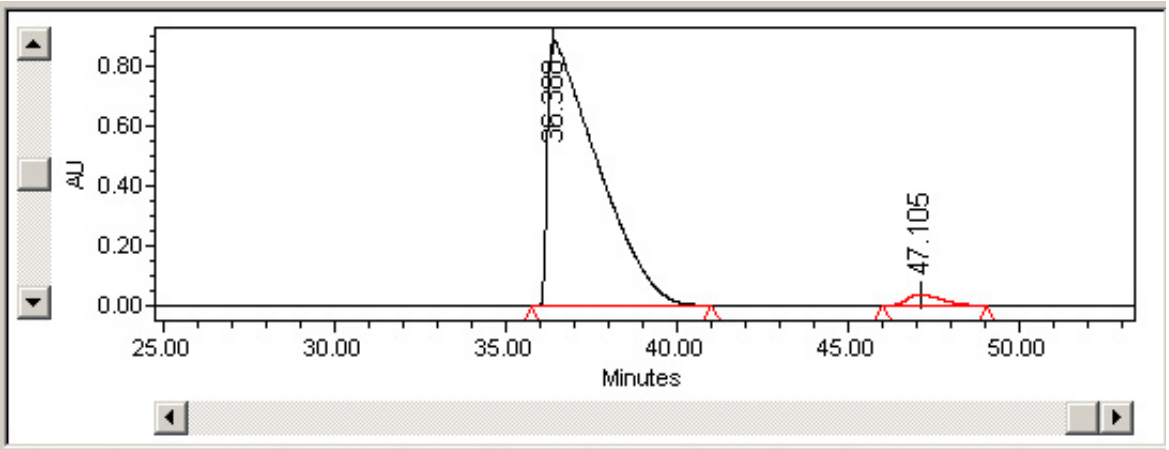

	Name	Retention Time (min)	Area (µV*sec)	% Area	Height (µV)	Int Type	Amount	Units	Peak Type	Peak Codes
1		36.388	90059850	97.16	884461	bb			Unknown	
2		47.105	2634201	2.84	38180	bb			Unknown	

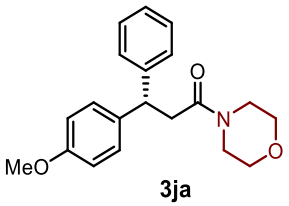

3ja

CHIRALPAK® ID-3, 1.0 mL/min, 30 °C, 80:20 Hexanes: *i*-PrOH, er = 94:6

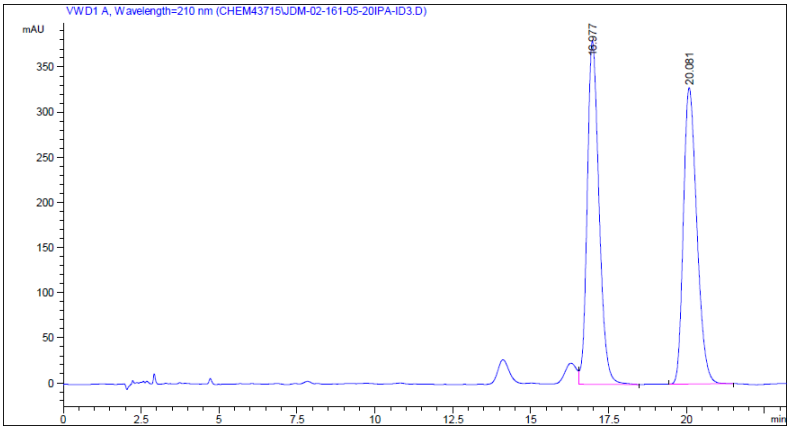

Peak #	RetTime [min]	Type	Width [min]	Area mAU *s	Height [mAU]	Area %
1	16.977	VB	0.4050	1.00284e4	380.51529	50.4556
2	20.081	BB	0.4649	9847.28516	328.36530	49.5444

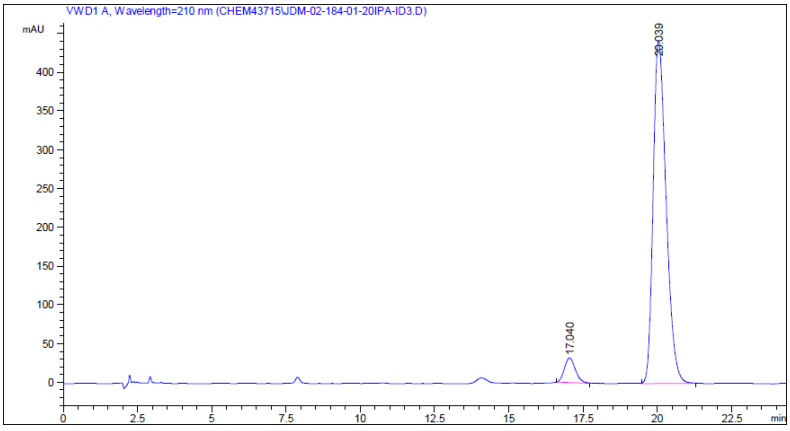

Peak #	RetTime [min]	Type	Width [min]	Area mAU *s	Height [mAU]	Area %
1	17.040	MM	0.4264	809.44543	31.63626	5.6946
2	20.039	MM	0.5054	1.34047e4	442.06891	94.3054

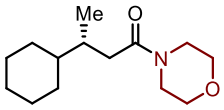

3ka

CHIRALPAK® ID-3, 1.0 mL/min, 30 °C, 96:4 Hexanes: *i*-PrOH, er = 96:4

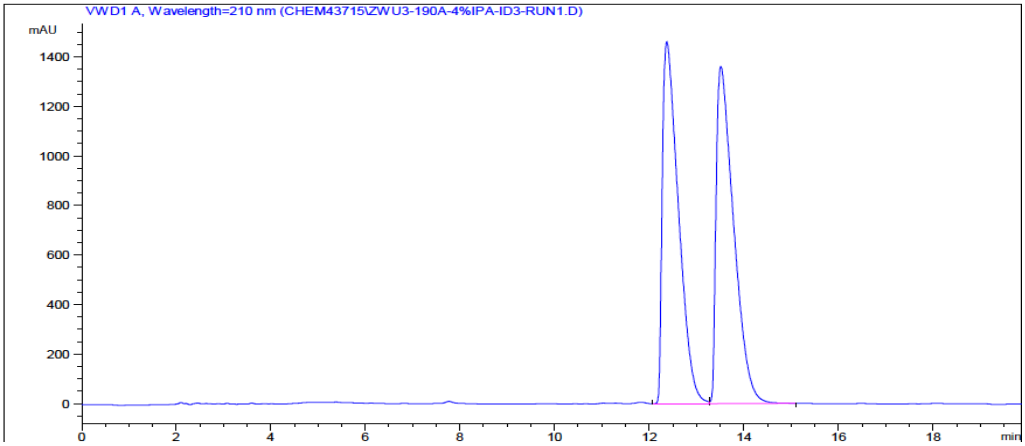

Peak #	RetTime [min]	Sig	Type	Area	Area %	Name
1	12.372	1	VV	3.46205e4	49.7047	?
2	13.515	1	VB	3.50318e4	50.2953	?

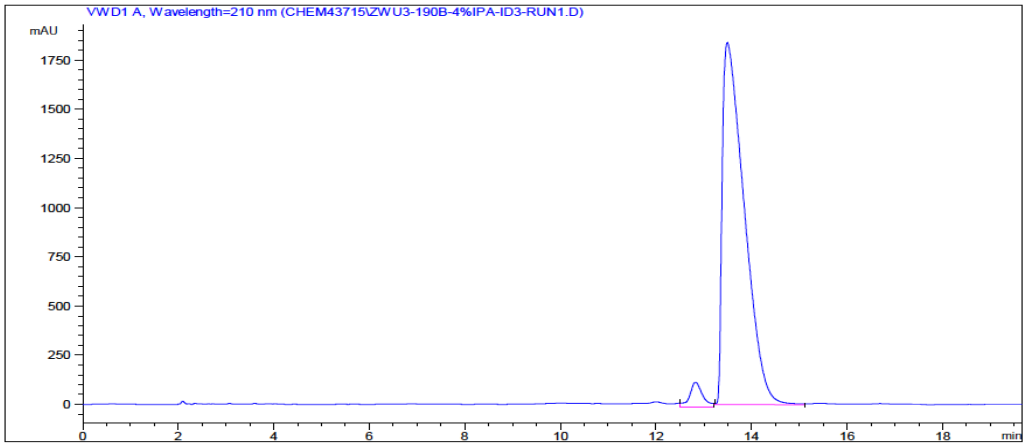

Peak #	RetTime [min]	Sig	Type	Area	Area %	Name
1	12.827	1	MM	2346.90918	3.8451	?
2	13.494	1	VV	5.86902e4	96.1549	?

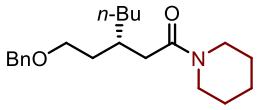

3lb

CHIRALPAK® ID-3, 1.0 mL/min, 30 °C, 97:3 Hexanes: *i*-PrOH, er = 99:1

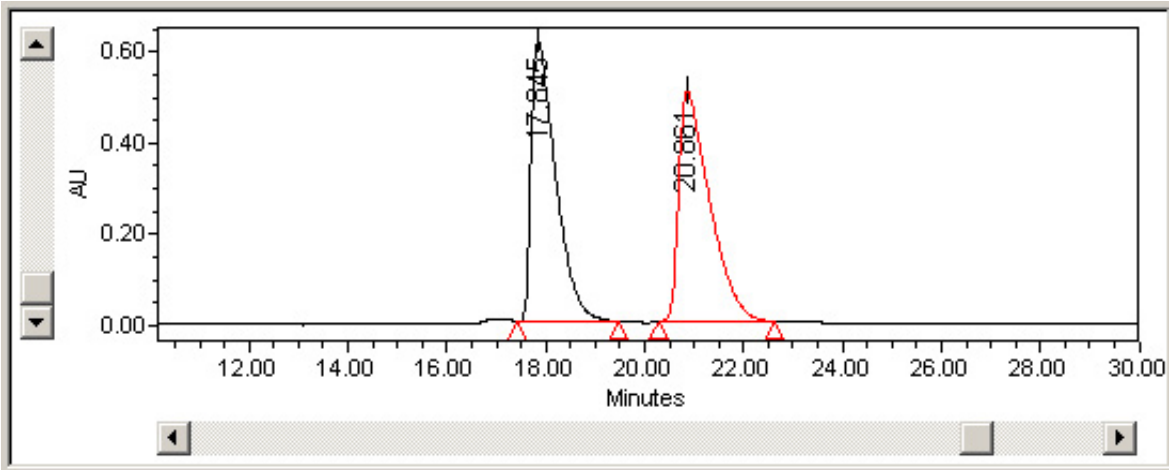

	Name	Retention Time (min)	Area (μV*sec)	% Area	Height (μV)	Int Type	Amount	Units	Peak Type	Peak Codes
1		17.845	21281765	49.14	620215	bb			Unknown	
2		20.861	22024369	50.86	505966	bb			Unknown	

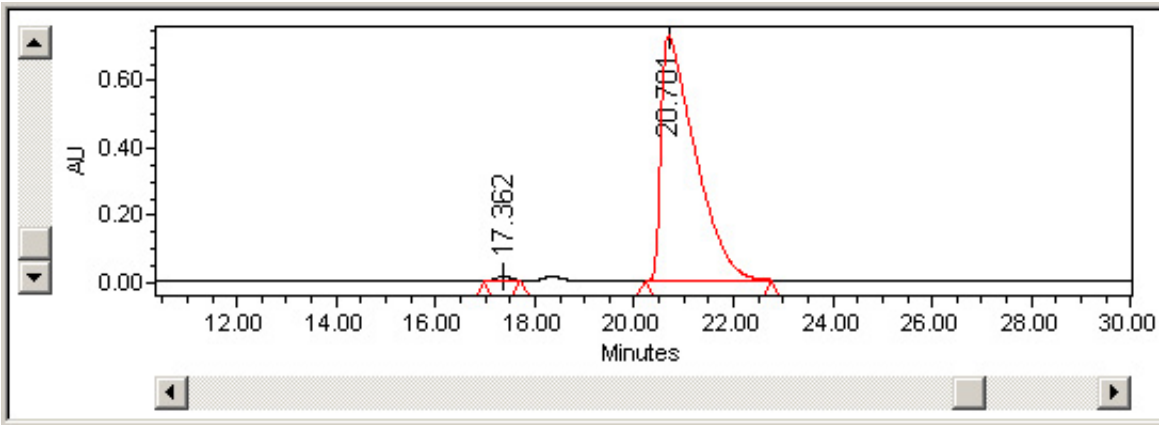

	Name	Retention Time (min)	Area (μV*sec)	% Area	Height (μV)	Int Type	Amount	Units	Peak Type	Peak Codes
1		17.362	298681	0.85	14183	bb			Unknown	
2		20.701	34850855	99.15	728537	bb			Unknown	

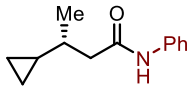

3nl

CHIRALPAK® ID-3, 1.0 mL/min, 30 °C, 99:1 Hexanes: MeOH, er = 97:3

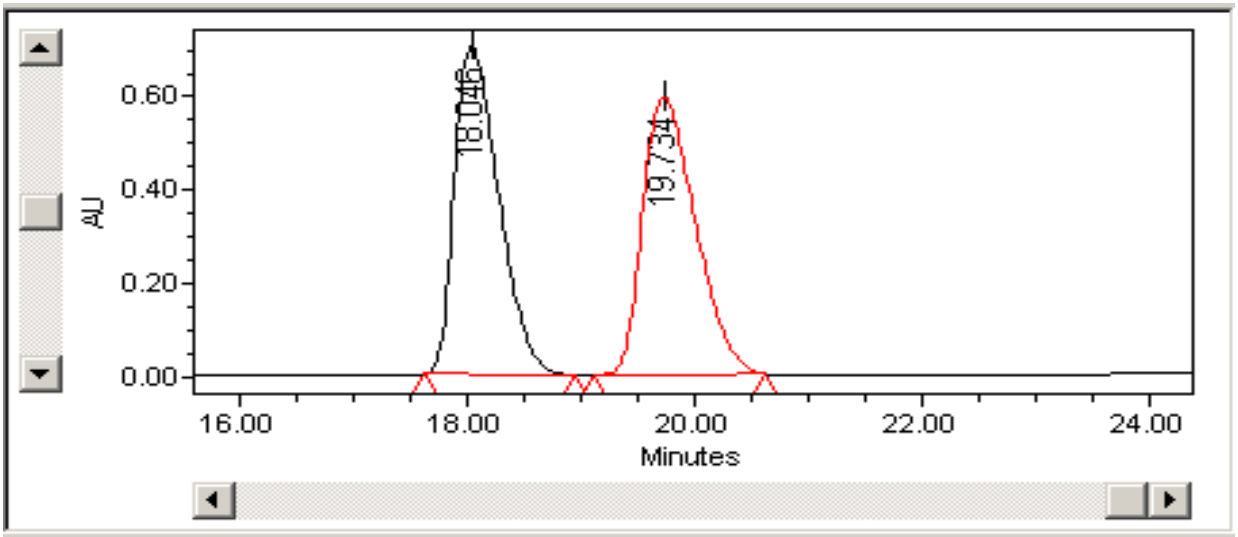

	Name	Retention Time (min)	Area (μV*sec)	% Area	Height (μV)	Int Type	Amount	Units	Peak Typ
1		18.046	19011172	49.84	703162	bb			Unknown
2		19.734	19131979	50.16	594217	bb			Unknown

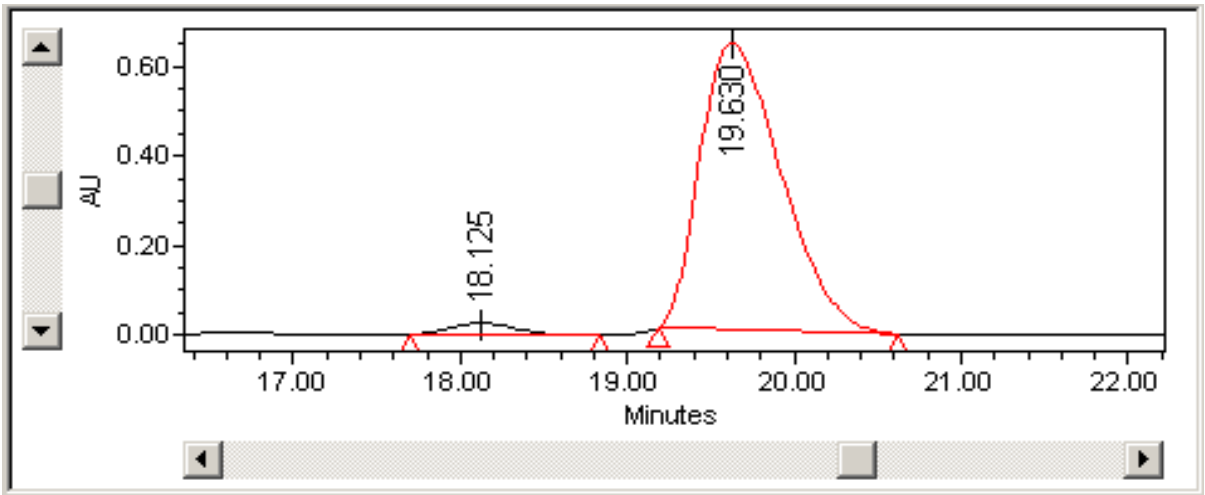

	Name	Retention Time (min)	Area (μV*sec)	% Area	Height (μV)	Int Type	Amount	Units	Peak Type
1		18.125	661692	2.97	25225	bb			Unknown
2		19.630	21590671	97.03	637500	bb			Unknown

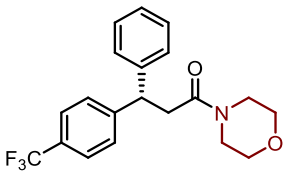

3oa

CHIRALPAK® ID-3, 1.0 mL/min, 30 °C, 95:5 Hexanes: *i*-PrOH, er = 95:5

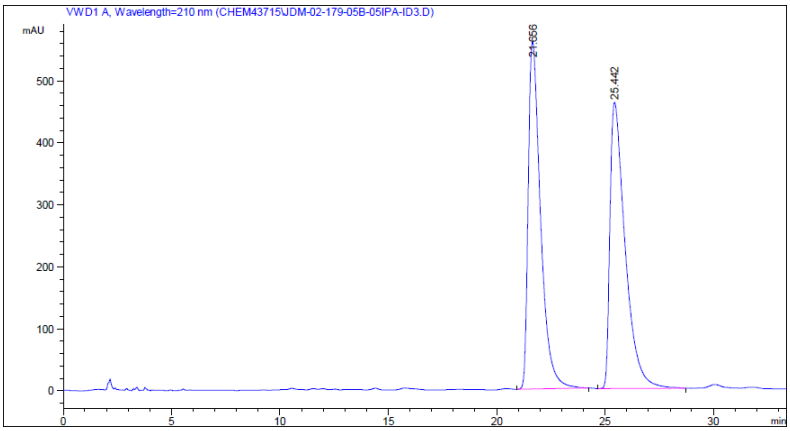

Peak #	RetTime [min]	Type	Width [min]	Area mAU *s	Height [mAU]	Area %
1	21.656	BB	0.5982	2.21596e4	560.43512	49.6326
2	25.442	BB	0.7240	2.24877e4	461.74872	50.3674

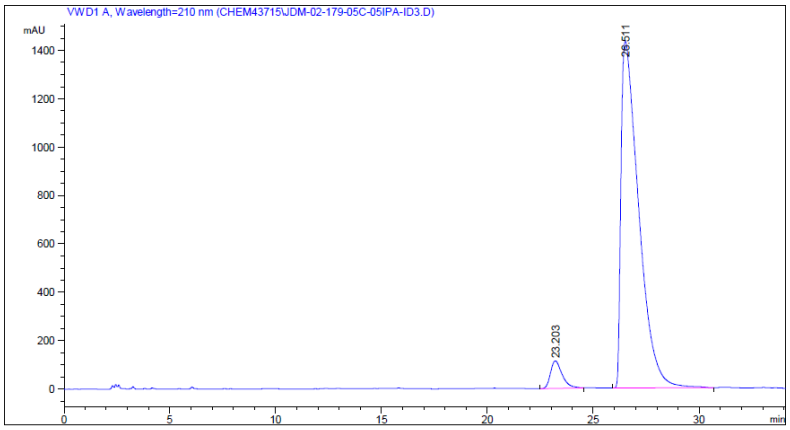

Peak #	RetTime [min]	Type	Width [min]	Area mAU *s	Height [mAU]	Area %
1	23.203	BV	0.5714	4350.99463	113.76025	4.9681
2	26.511	BB	0.8365	8.32280e4	1432.47009	95.0319

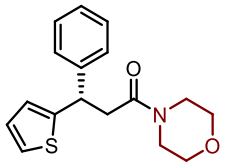

3pa

CHIRALPAK® IC-3, 1.0 mL/min, 30 °C, 90:10 Hexanes: *i*-PrOH, er = 96.5:3.5

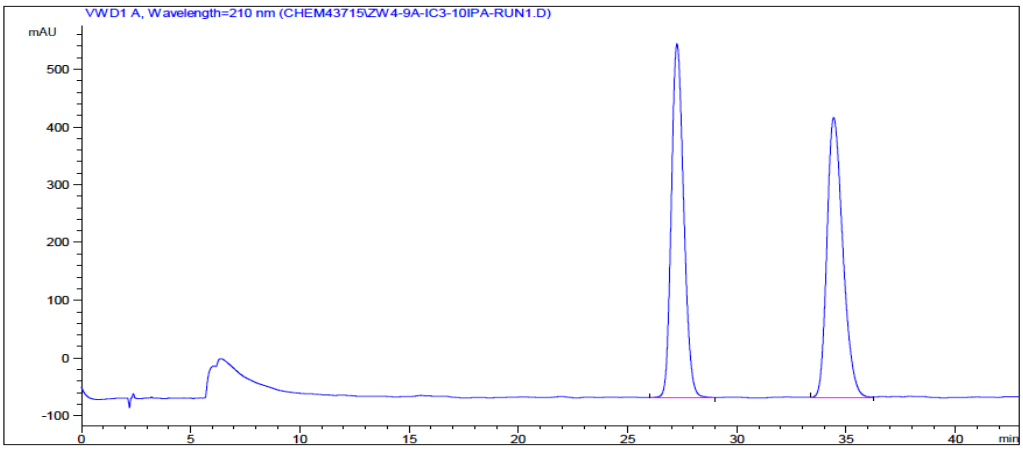

Peak #	RetTime [min]	Sig	Type	Area	Area %	Name
1	27.254	1	VB	2.41505e4	49.4755	?
2	34.424	1	VB	2.46625e4	50.5245	?

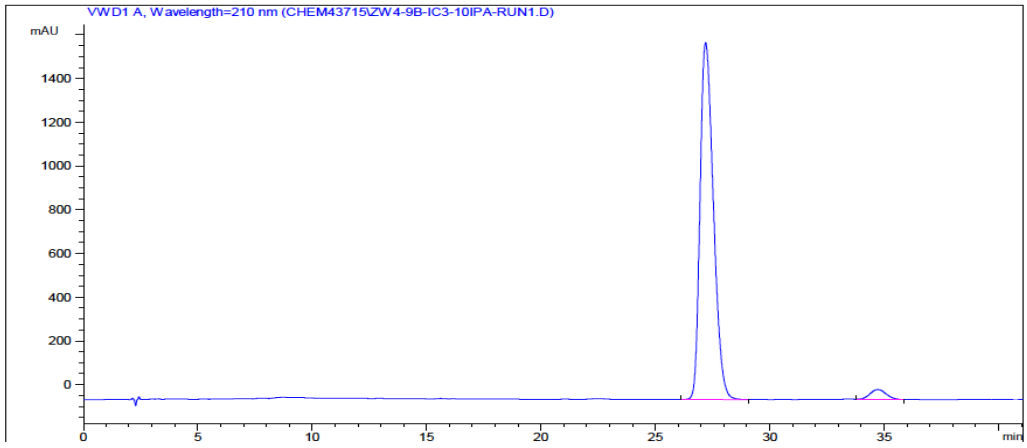

Peak #	RetTime [min]	Sig	Type	Area	Area %	Name
1	27.196	1	VB	6.61592e4	96.6572	?
2	34.723	1	VV	2288.06152	3.3428	?

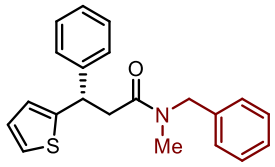

3pf

CHIRALPAK® IC-3, 1.0 mL/min, 30 °C, 90:10 Hexanes: *i*-PrOH, er = 94:6

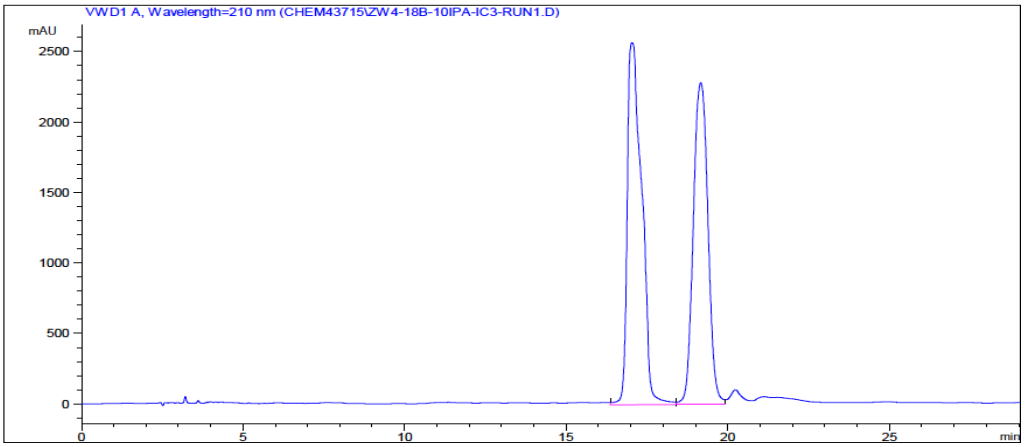

Peak #	RetTime [min]	Sig	Type	Area	Area %	Name
1	17.040	1	VV	7.99294e4	52.5148	?
2	19.163	1	VV	7.22740e4	47.4852	?

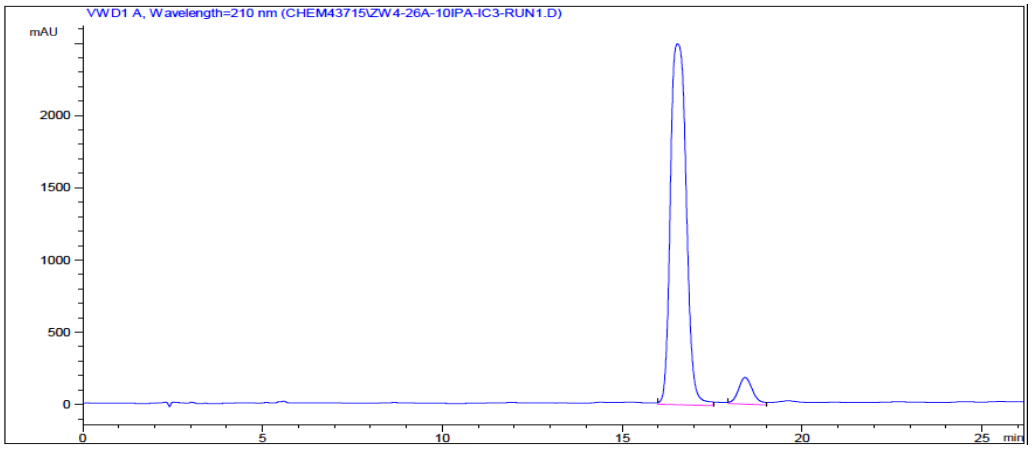

Peak #	RetTime [min]	Sig	Type	Area	Area %	Name
1	16.541	1	MM	7.62152e4	93.7162	?
2	18.418	1	MM	5110.35449	6.2838	?

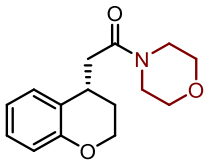

3qa

CHIRALPAK® ID-3, 1.0 mL/min, 30 °C, 90:10 Hexanes: *i*-PrOH, er = 97:3

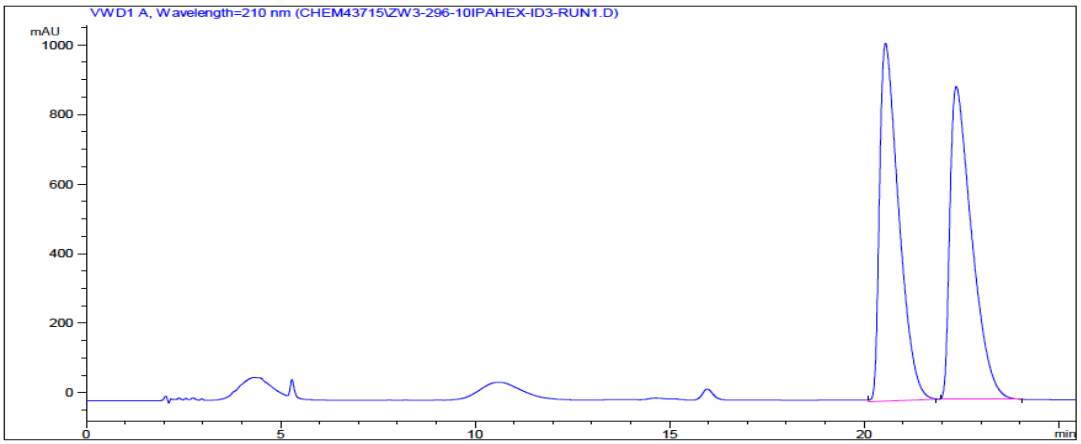

Peak #	RetTime [min]	Sig	Type	Area	Area %	Name
1	20.552	1	MM	3.51960e4	50.2945	?
2	22.372	1	MM	3.47838e4	49.7055	?

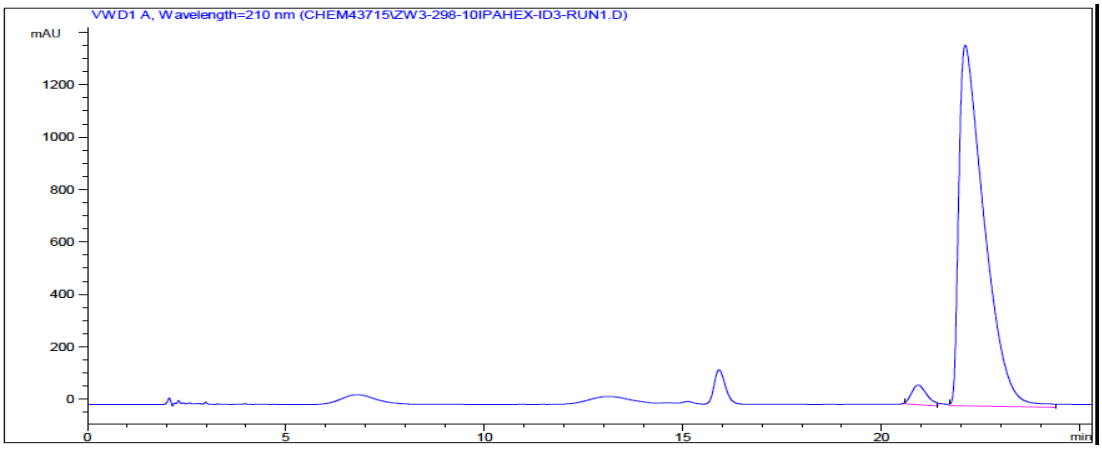

Peak #	RetTime [min]	Sig	Type	Area	Area %	Name
1	20.928	1	MM	1999.15344	3.1793	?
2	22.112	1	MM	6.08813e4	96.8207	?

2.8 Literature Cited

(1) a) McGrath, N. A.; Brichacek, M.; Njardarson, J. T. *J. Chem. Ed.* **2010**, *87*, 1348-1349. b) Aissaoui, H.; Boss, C.; Richard-Bildstein, S.; Siegrist,R. *PTC Int. Appl.* **2013**, WO 2013093842. c) Murakama, M.; Kobayashi, K.; Hirai, K. *Chem. Pharm. Bull*. **2000**, *48*, 1567-1569. d) Yamaguchi, T.; Yanagi, T.; Hokari, H.; Mukaiyama, Y.; Kamijo, T.; Yamamoto, I. *Chem. Pharm. Bull*. **1997**, *45*, 1518-1520.

(2) a) Nugent, T. C. *Chiral Amine Synthesis: Methods, Developments and Applications;* Wiley-VCH, Weinheim, **2010.** b) Shibuya, M.; Taniguchi, T.; Takahashi, M.; Ogasawara, K. *Tetrahedron Lett*. **2002**, *43*, 4145-4147.

(3) For recent reviews, see: a) Khumsubdee, S.; Burgess, K. *ACS Catal*. **2013**, *3*, 237-249. b) Verendel, J. J.; Pamies, O.; Dieguez, M.; Andersson, P. G. *Chem Rev*. **2014**, *114*, 2130-2169. c) Byrd, K. M. *Beilstein J. Org. Chem*. **2015**, *11*, 530-562.

(4) von Matt, P.; Pfaltz, A. *Tetrahedron: Asymmetry* **1991**, *2*, 691-700.

(5) a) Sakuma, S.; Miyaura, N. *J. Org. Chem*. **2001**, *66*, 8944-8946. b) Defieber, C.; Paquin,J.-F.; Serna, S.; Carreira, E. M. *Org. Lett.* **2004**, *6*, 3873-3876.

(6) Ref 3a, 3b and references therein.

(7) Hird, A. W.; Hoveyda, A. H. *Angew. Chem. Int. Ed*. **2003**, *42*, 1276-1279.

(8) a) Coin, I.; Beyermann, M.; Bienert, M. *Nat. Protoc*. **2007**, *2*, 3247-3256. (b) Constable, D. J. C.; Dunn, P. J.; Hayler, J. D.; Humphrey, G. R.; Leazer, Jr. J. L.; Linderman, R. J.; Lorenz, K.; Manley, J.; Pearlman, B. A.; Wells, A.; Zaks, A.; Zhang, T. Y. *Green Chem*. **2007**, *9*, 411-420.

(9) Wu, Z.; Hull, K. L. *Chem. Sci*. **2016**, 7, 969-975.

(10) Rh-catalyzed enantioselective isomerization of allylic alcohols: (a) Tanaka, K.; Fu, G. C. *J. Org. Chem*. **2001**, *66*, 8177-8186. (b) Tanaka, K.; Qiao, S.; Tobisu, M.; Lo, M. M.-C.; Fu, G. C. *J. Am. Chem. Soc*. **2000**, *122*, 9870-9871.

(11) a) Tani, K.; Yamagata, T.; Akutagawa, S.; Kumobayashi, H.; Taketomi, T.; Takaya, H.; Miyashita, A.; Noyori, R.; Otsuka, S. *J. Am. Chem. Soc*. **1984**, *106*, 5208-5217. b) Inoue, S.-I.; Takaya, H.; Tani, K.; Otsuka, S.; Satao, T.; Noyori, R. *J. Am. Chem. Soc*. **1990**, *112*, 4897-4905.

(12) Initial counter ion screens show BAr_4^{F-} gives much higher reactivity for allylic amine isomerization. See Table S1 for details.

(13) (*Z*)-Geranyl diethyl amine combined with (*R*)-BINAP under optimized conditions afforded (*R*)-**6aa** in 78% yield and 3.5:96.5 er.

(14) See Supporting Information for details.

(15) a) Mantilli, L.; Gerard, D.; Torche, S.; Besnard, C.; Mazet, C. *Angew. Chem.* **2009**, *121*, 5245-5249. b) Arai, N.; Sato, K.; Azuma, K.; Ohkuma, T. *Angew. Chem. Int. Ed.* **2013**, *52*, 7500-7504.

(16) Wickens, P.; Cantin, L.-D.; Chuang, C.-Y.; Dai, M.; Hentemann, M. F.; Kumarasinghe, E.; Liang, S. X.; Lowe, D. B.; Shelekhin, T. E.; Wang, Y.; Zhang, C.; Zhang, H.-J.; Zhao, Q. WO2004011446 A1, Feb 5, 2004.

CHAPTER 3: RHODIUM CATALYZED ISOMERIZATION AND ESTERIFICATION OF ALLYLIC AMINES WITH ALCOHOL NUCLEOPHILES TO FORM CHIRAL, β-BRANCHED ESTERS

This chapter has been adapted from the following publication:

Laffoon, S. D.; Wu, Z.; Hull, K. L. Rhodium-Catalyzed Asymmetric Synthesis of β-Branched Esters from Allylic Amines. *Chem. Commun.* **2018**, *54*, 7814–7817.

3.1 Abstract

Allylic amines are converted to chiral, β-branched esters under rhodium catalysis in the presence of alcohol nucleophiles. A cationic Rh(I)/BINAP catalyst facilitates the asymmetric isomerization 3,3'-disubstituted allylic amines. The resulting enamine intermediate is then oxidized in the presence of nucleophilic alcohols, water, and a hydrogen acceptor to form chiral, β-branched esters in a tandem catalytic process. Allylic amines with aliphatic and aromatic vinylic substituents are converted to ester products with excellent enantioselectivities in all cases. Several alcohol nucleophiles have been utilized in the reaction including 1° and 2° derivatives.

3.2 Motivation and Background

The installation of esters into complex molecular scaffolds has been the subject of much investigation in recent years.[1] Chiral, β-branched esters are prevalent moieties in pharmaceuticals, fragrances, materials, and agrochemicals (Figure 3.1), and esters themselves serve as versatile synthetic handles for further functionalization.[2] Inspired by the amidation procedure described in Chapter 2, we set out to develop a method that engages alcohol nucleophiles rather than amines to for the selective synthesis of chiral, β-branched esters in a modular fashion.

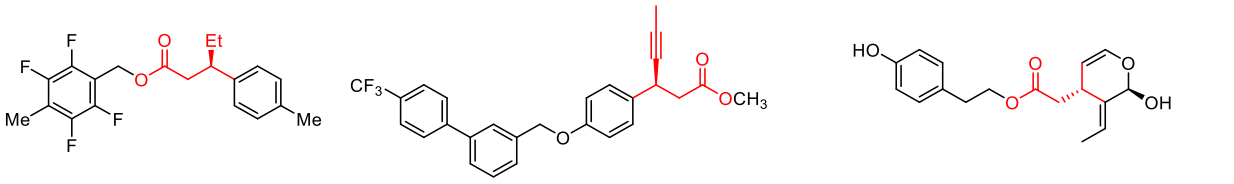

Figure 3.1. Biologically active β-branched esters.

Traditionally, esters are generated through reactive intermediates, such as acyl halides, or carboxylic acids paired with stoichiometric coupling reagents (Steglich esterification) as well as via strong acid catalysis (Fischer esterification). Though these approaches generally proceed with high conversion, the conditions required to generate acyl halides or strongly acidic conditions are not amenable to sensitive functionalities. Stoichiometric coupling reagents generate high molecular weight byproducts that can be challenging to separate from the desired product. Early reports of catalytic esterification, such as the Tishchenko reaction, generate simple homocoupled products (Scheme 3.1a).[3] In recent years, the catalytic esterification of aldehydes via transfer hydrogenation has emerged as a meaningful alternative to stoichiometric coupling reactions; however, many of these reactions require solvent quantities of the alcohol nucleophile and are

a) Oxidative esterification:

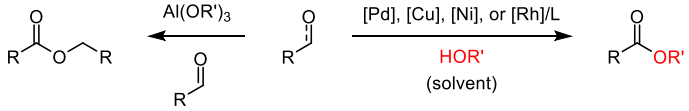

b) Synthesis of chiral, β-branched esters:

Enantioselective conjugate reduction:

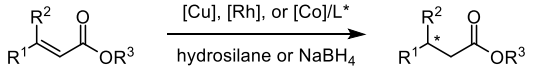

Enantioselective conjugate addition (ECA):

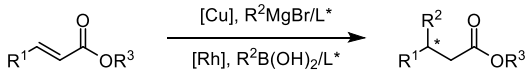

c) Our approach:

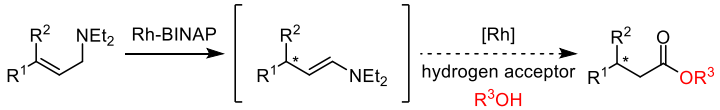

Scheme 3.1. Precedent for the catalytic synthesis of chiral, β-branched esters.

generally sterically limited such that β-branched esters as products are difficult to obtain in synthetically useful yields.[4–6]

Much of the work in generating chiral, β-branched esters has focused on asymmetric conjugate reduction[7] and enantioselective conjugate addition (ECA)[8] to α,β-unsaturated esters (Scheme 3.1b) as described in Chapter 1. The major limitation of such strategies is poor substrate scope for individual catalysts. Changes to the substitution pattern of the substrate can require a different metal/ligand scaffold,[9] and these methods often rely on significant steric differentiation between the substituents at the β-position or are dependent on olefin geometry to achieve high stereoselectivity.[7a,c,e,f]

3.3 Optimization of Reaction Conditions

To overcome the limitations of previous reports, we drew inspiration from the asymmetric isomerization of allylic amines to optically pure enamines, developed by Noyori and Otsuka.[10] Because the enantioselectivity of the isomerization of the allylic amine proceeds via a suprafacial 1,3-hydride shift and the initial binding of the substrate to the catalyst is facially selective,[10e] steric differentiation between the substituents at the prochiral center is not required to achieve enantiopurity. This isomerization approach could pave the way for a critical advance in the asymmetric synthesis of β-branched esters. We envisioned the resulting enantioenriched enamines undergoing a dehydrogenative coupling with alcohol nucleophiles in the presence of water to produce esters (Scheme 3.1c). Furthermore, allylic amines are compelling substrates as they are readily accessed in a diastereomerically pure fashion through a variety of methods (Scheme 3.2).

Experiments described in Chapter 2 reveal that a Rh-BINAP complex with $NaBArF_4$ in ethereal solvents were the ideal conditions for the clean conversion of allylic amines to amides.

One-pot synthesis of allylic amines from alkynes:

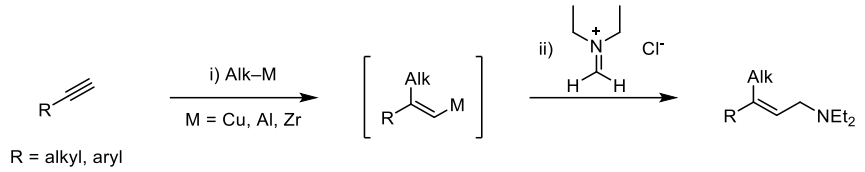

Allylic amines via cross-coupling:

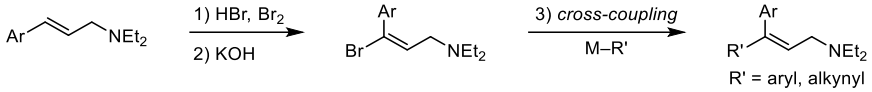

Scheme 3.2. Synthesis of diastereomerically pure allylic amines. See Supporting Information for details of substrate synthesis.

To modify this method for the synthesis of esters, we believed we could replace amine nucleophiles with alcohols; however, there are some inherent challenges with such an approach. Alcohols are less nucleophilic than amines, disfavoring the formation of the hemiacetal intermediate necessary for the final dehydrogenation.[6] For this reason, we were particularly concerned with identifying conditions for the selective synthesis of esters over other byproducts such as alcohol nucleophile homocoupling, aldol condensation, or deleterious reduction pathways in the presence of a Rh–H species.

When our catalytic amidation conditions were employed with 1-hexanol as a nucleophile instead of an amine, a tertiary amine byproduct **4** was observed along with the desired ester product **3a**, consistent with our earlier hypotheses (Table 3.1). We found that the identity of the solvent played a key role in improving the chemoselectivity of the reaction. Changing the solvent from THF to DME limited the formation of **4** to trace quantities. Further modification of the reaction conditions identified Na_3PO_4 as an effective base (Table 3.1, entry 4) with styrene as a sufficient hydrogen acceptor necessary for catalyst turnover (see Supporting Information).

3.4 Evaluating Reaction Scope

After optimizing the reaction conditions, we investigated the nucleophile scope of the reaction (Table 3.2). A variety of 1° alcohol nucleophiles including 1-hexanol (**3a**), ethanol (**3b**), and methanol (**3c**) are well-suited for the reaction providing esters in good yields. Nucleophiles containing heterocycles such as a pendant morpholino group (**3e**) are well-tolerated under the

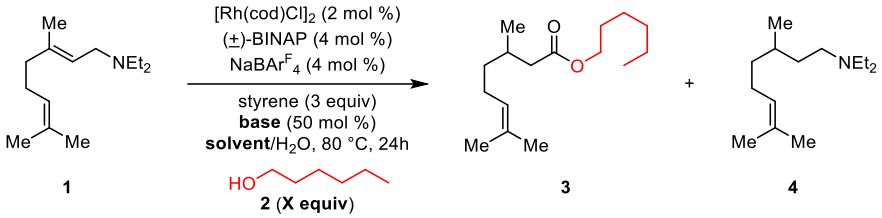

Table 3.1. Optimization of reaction conditions.

Entry	Base	Solvent	X	**3a** yield (%)[b]	**4** yield (%)[b]
1	Cs_2CO_3	THF	3	52	12
2	Cs_2CO_3	DME	3	56	<5
3	Na_3PO_4	THF	3	79	17
4	**Na_3PO_4**	**DME**	**3**	**91**	**<5**
5	Na_3PO_4	DME	2	82	13
6	Na_3PO_4	DME	1.5	71	10.5
7	Na_3PO_4	DME	1	49	17

a) $[Rh(cod)Cl]_2$ (2 mol %), (±)-BINAP (4 mol %), $NaBAr^F_4$ (4 mol %), **1** (0.12 mmol), **2** (1–3 equiv), styrene (3.0 equiv), base (50 mol %), solvent (0.100 mL), H_2O (1.5 equiv), 80 °C, 24 h. b) *In situ* yield determined by gas chromatography with comparison to diphenyl methane (10 μL) as an internal standard.

reaction conditions despite the ability of 3° amines to strongly coordinate to many transition metal catalysts. Benzyl alcohol and its derivatives demonstrate the effect of electronic variation on the yield of the reaction; electron neutral and slightly electron deficient alcohols are most efficient (**3f-3j**). More hindered nucleophiles give slightly diminished yields, demonstrating some sensitivity to steric hinderance (**3k-3m**). Unfortunately, phenols are not competent nucleophiles under the current reaction conditions. This may be attributed to the competitive binding of the phenol to the cationic Rh(I) species.[12]

We were pleased to discover that the reaction is amenable to a broad range of substitution patterns on the allylic amine (Table 3.3). Several β,β-dialkyl esters, such as those containing silyl

Table 3.2. Scope of 1° and 2° alcohols for the esterification of allylic amines.

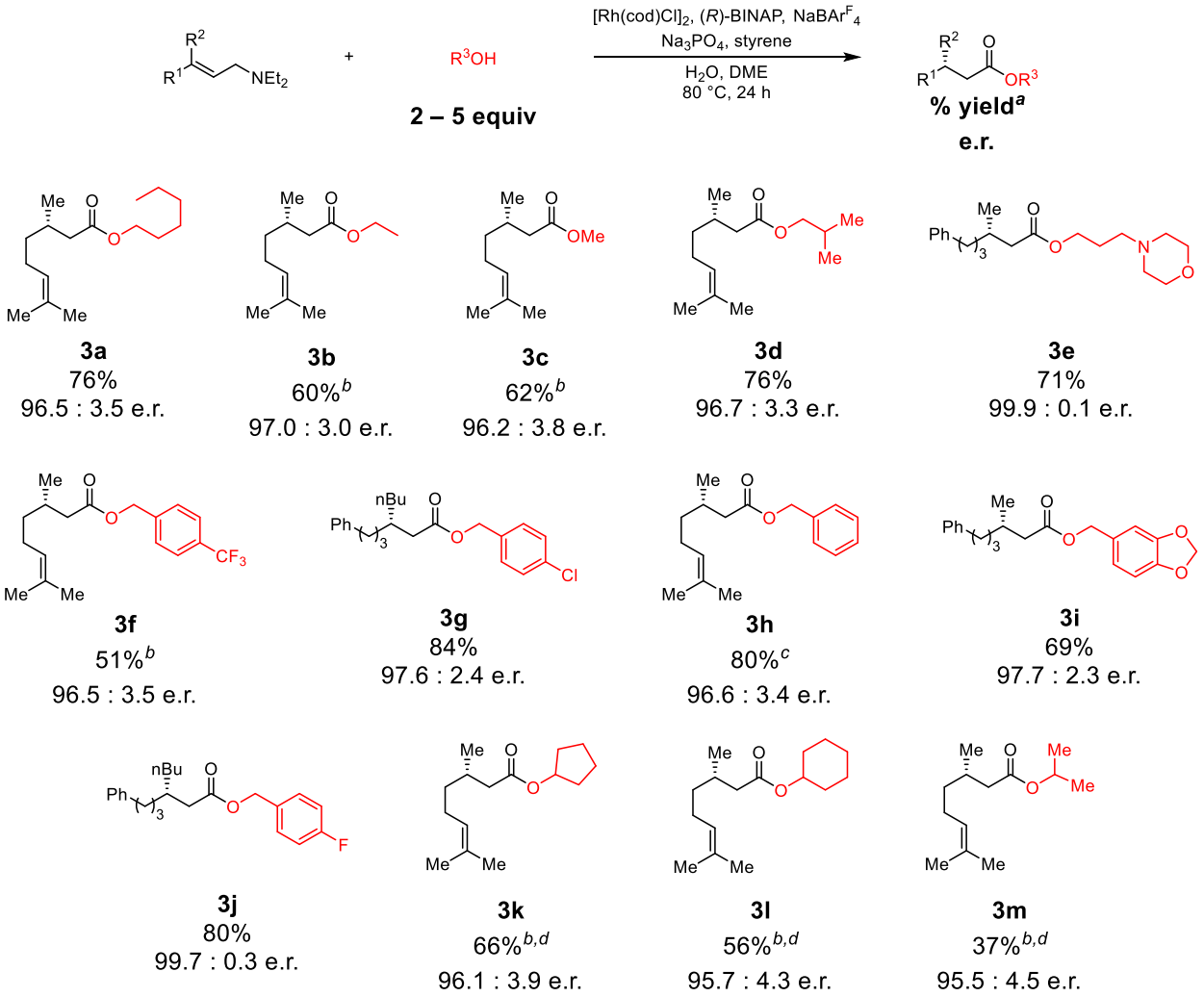

[a] $[Rh(cod)Cl]_2$ (2 mol %), (*R*)-BINAP (4 mol %), $NaBAr^F_4$ (4 mol %), Na_3PO_4 (50 mol %), allylic amine (0.12 mmol), alcohol nucleophile (3.0 equiv), styrene (3.0 equiv), H_2O (1.5 equiv), DME (1.2 M), 80 °C, 24 h. [b] with 5.0 equiv nucleophile. [c] with 2.0 equiv nucleophile. [d] at 100 °C.

ethers (**3n**)‡ or distal arenes (**3o, 3p**), can be accessed from the corresponding allylic amines with excellent enantiomeric excess in all cases. Even when the substituents on the starting alkene are sterically similar, the catalyst maintains high enantiocontrol (**3q**). 3,3-diaryl allylic amines show good reactivity and enantioselectivity; however, increased catalyst loading and temperature are necessary to establish good conversion of starting material to product. Electron-rich furyl rings are well-tolerated under the reaction conditions (**3r**). Excitingly, we have found that substrates containing exocyclic alkenes, a substrate class rarely demonstrated for asymmetric synthesis of β-

Table 3.3. Scope of allylic amines for asymmetric oxidative esterification.

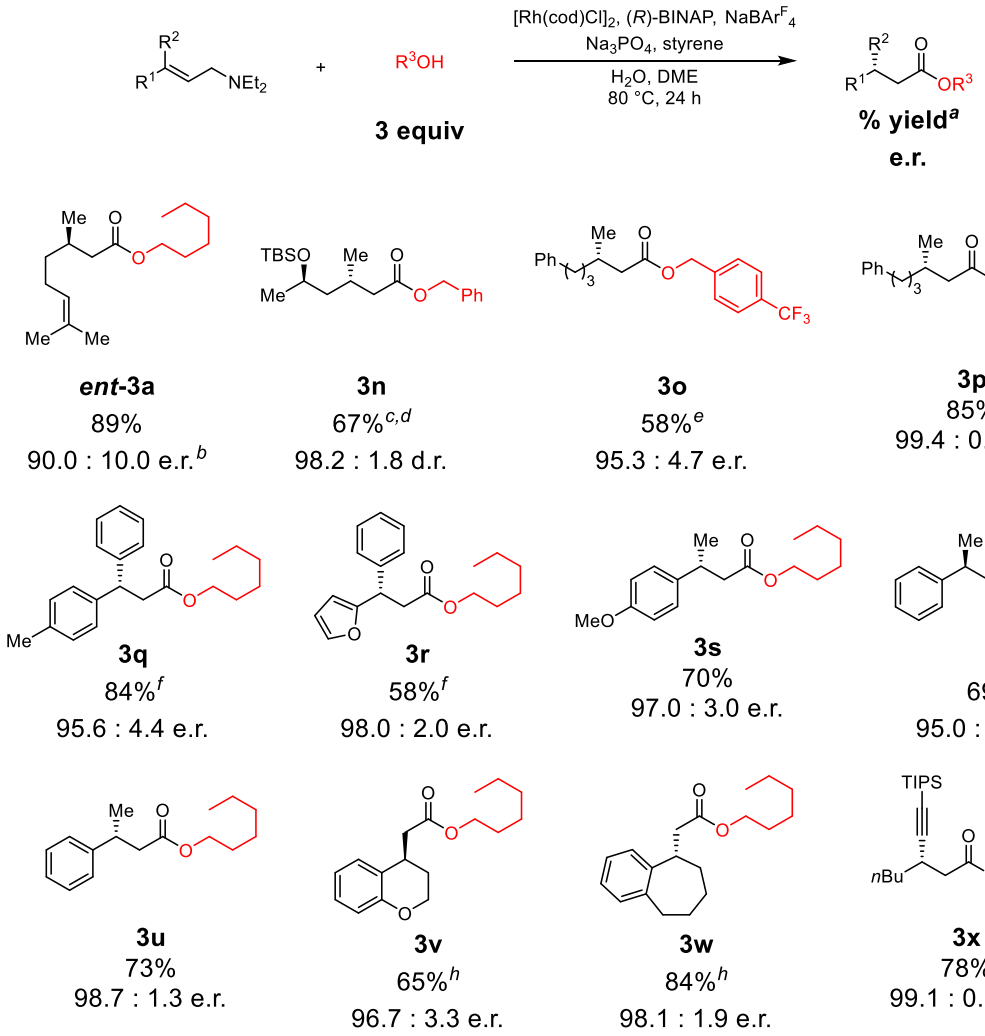

a) $[Rh(cod)Cl]_2$ (2 mol %), (*R*)-BINAP (4 mol %), $NaBAr^F_4$ (4 mol %), Na_3PO_4 (50 mol %), allylic amine (0.12 mmol), alcohol nucleophile (3 equiv), styrene (3.0 equiv), H_2O (1.5 equiv), DME (1.2 M), 80 °C, 24 h. b) from the *Z* isomer of **1** (91.7 : 8.3 *Z*/*E*) c) with 2.0 equiv nucleophile. d) 68% and 5.5 : 94.5 d.r. with *S*-BINAP e) with 5.0 equiv nucleophile. f) at 100 °C. g) with (*S*)-BINAP. h) at 100 °C for 48 h with 8 mol % catalyst.

substituted carbonyl compounds,[7g] are reactive leading to good yields and enantioselectivities (**3v**-**3w**). Allylic amines with π-functionality are not only limited to aryl substituents. When a substrate containing an enyne is subjected to the reaction conditions, no hydrogenation of the alkyne is observed (**3x**). Finally, the absolute stereochemistry has previously been unambiguously determined by X-ray crystallography.[11a]

3.5 Mechanistic Discussion

To probe the chemoselectivity of the transformation, we subjected allylic amine **1a** to the reaction conditions with a 1:1 ratio of 1° alcohol 1-hexanol to a variety of 2° alcohols (Scheme 3.3). Primary alcohols were preferentially incorporated, with selectivities ranging from 5.3:1 for the least sterically hindered cyclopentanol to 16.7:1 for the most sterically hindered α-hydroxyethylbenzene. In an intramolecular competition study between a 1° and 3° alcohol, the 1° alcohol was exclusively incorporated (see Supporting Information).

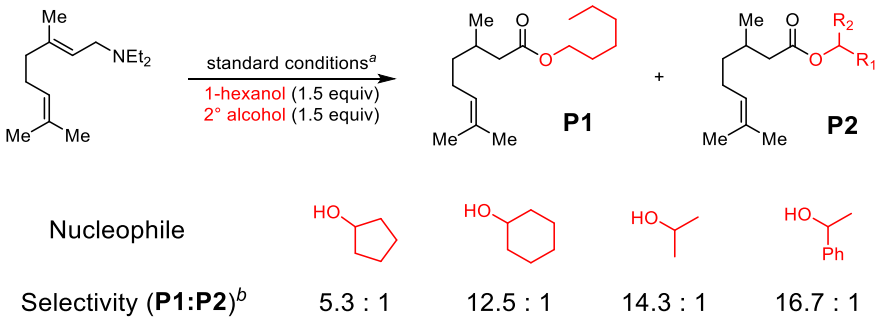

Scheme 3.3. a) General reaction conditions: see Table 3.2. b) Chemoselectivity determined by ^{1}H NMR of the crude reaction mixture.

Our mechanistic hypothesis draws inspiration from the work of Noyori, Otsuka, and Tani (Scheme 3.4a).[10] Cationic Rh(I)-BINAP complexes are known to facilitate an isomerization of allylic amines to form optically pure enamines. The initial β-hydride elimination to form **II** is the enantiodetermining step.[10c,e] Under our reaction conditions, the intermediate enamine **II** can participate in several equilibrium-controlled processes with in situ H_2O and nucleophile to form a Rh-alkoxide species **III**.[13] This intermediate can then undergo a β-hydride elimination to form the final ester product **IV** and a Rh–H species. Styrene acts as a hydrogen acceptor to regenerate the active catalyst. Though we believe this process to be redox neutral, a Rh(I)/(III) cycle for the oxidation of intermediate **III** cannot be ruled out. Furthermore, when citronellal was employed as the substrate under standard reaction conditions, the yield of the reaction diminished (Scheme 3.4b). While no definitive mechanistic conclusion can be drawn by this data alone, it suggests that

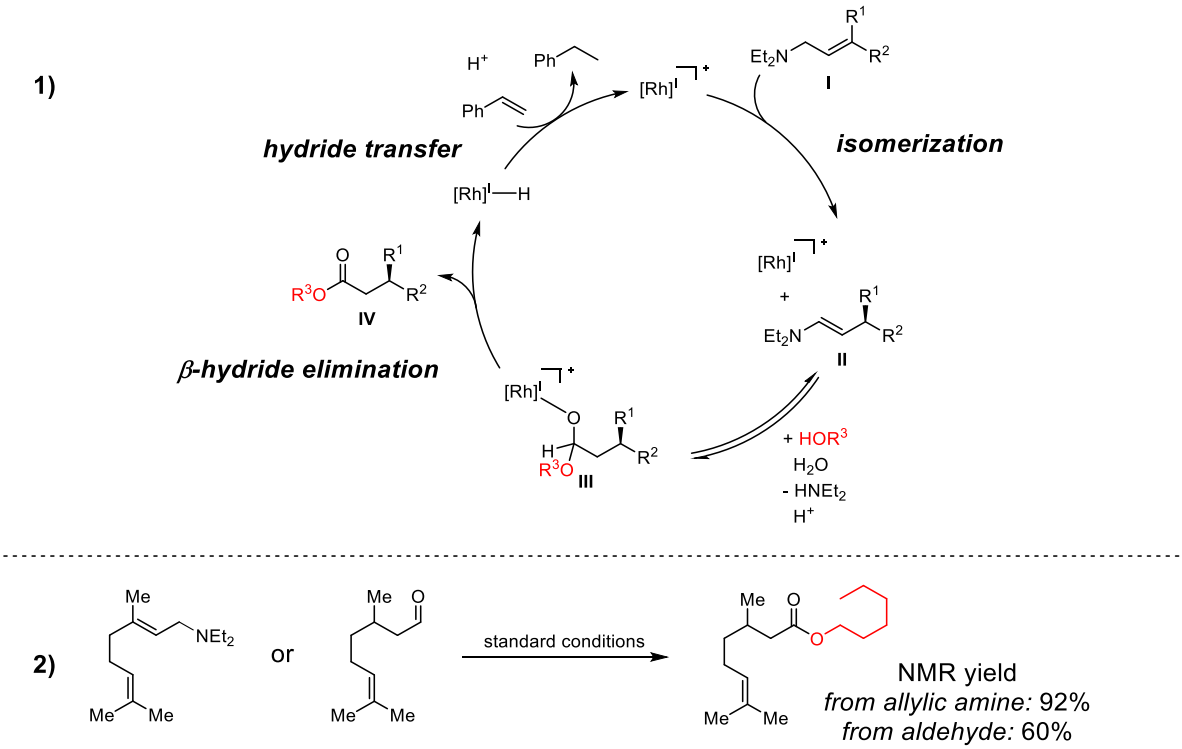

Scheme 3.4. a) Proposed mechanism. b) Comparison of aldehydes and allylic amines as substrates for the reaction.

the reaction does not proceed through build-up of large quantities of a discrete aldehyde intermediate. In fact, crude NMR reveals evidence of aldehyde decomposition under standard conditions (see Supporting Information). Instead, the catalytically formed aldehyde may immediately react with the alcohol to yield the final product, or the alcohol may attack the iminium intermediate directly without proceeding through the aldehyde.

3.6 Conclusion

This Chapter describes a method by which chiral, β-branched esters can be synthesized in one pot with a broad scope of nucleophiles and substrates. Utilizing an isomerization strategy has enabled enantioinduction that is not limited by the steric differentiation of the substituents at the prochiral center. This method has been demonstrated for the asymmetric synthesis of β,β-dialkyl, β,β-diaryl, and β-alkyl-β-aryl-substituted esters, a breadth of substrate scope not commonly

observed in methods for the synthesis of similar compounds. Primary and secondary alcohols are competent reaction partners without need for solvent quantities of nucleophile. This method performs similarly under a variety of steric environments, giving good to excellent yields with excellent enantioselectivities in all cases.

‡ When the desilylated analogue of **6** was subjected to the reaction, only the volatile 4,6-dimethyltetrahydro-2H-pyran-2-one was observed by GC/MS of the crude reaction mixture.

3.7 Supporting Information

Table 3.4. Ethereal Solvents for esterification of allylic amines.

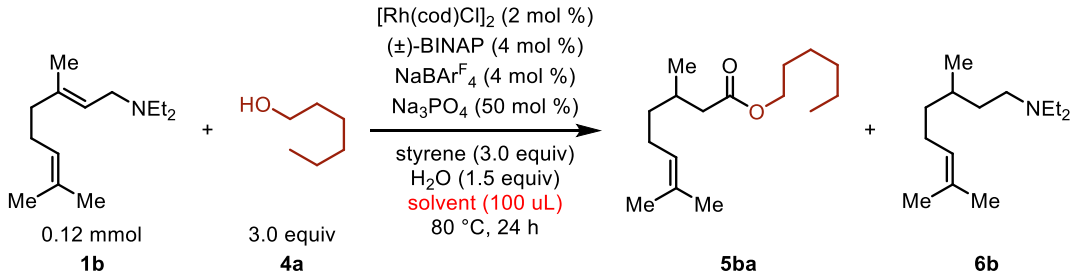

Entry	Solvent	5ba% yield (GC)	6b% yield (GC)
1	DME	96	2
2	Et_2O	85	25
3	THF	83	13
4	1,4-dioxane	75	26

Table 3.5. Base loading screen for esterification of allylic amines.

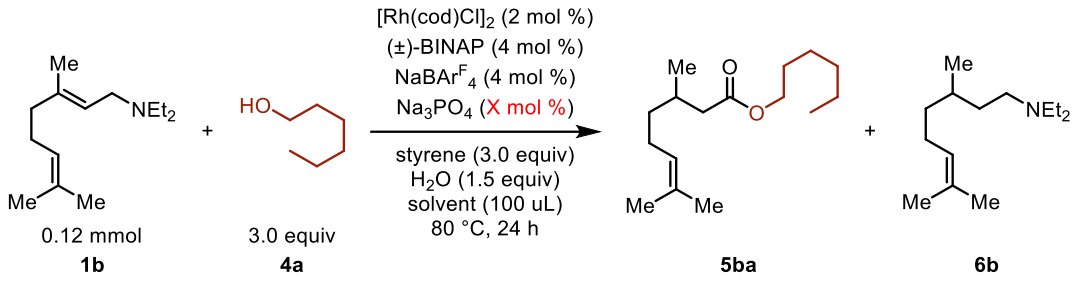

Entry	Base loading (mol %)	5ba% yield (GC)	6b% yield (GC)
1	0	49	28
2	5	63	25
3	15	83	10
4	50	89	8
5	100	90	7

Table 3.6. Nucleophile equivalence screen for esterification of allylic amines.

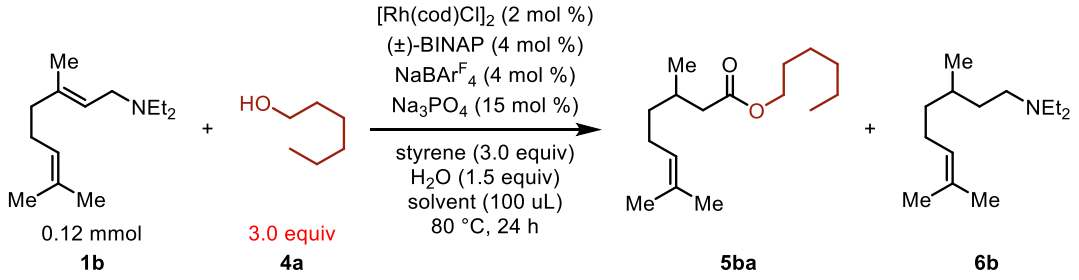

Entry	4a equiv	5ba% yield (GC)	6b% yield (GC)
1	1.0	49	17
2	1.5	71	10
3	2.0	82	13
4	3.0	89	6

Table 3.7. Base screen for esterification of allylic amines.

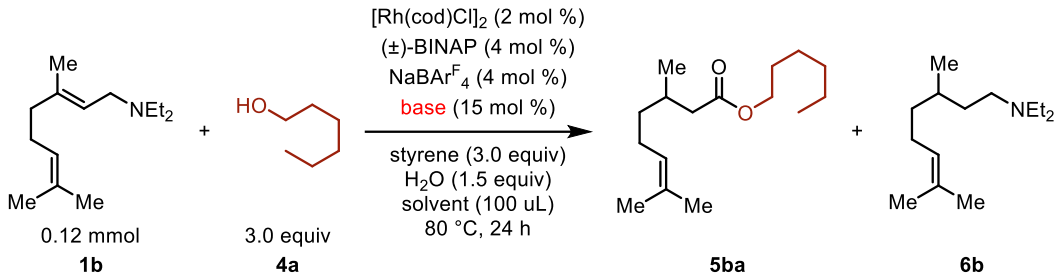

Entry	Base	5ba% yield (GC)	6b% yield (GC)
1	Na_3PO_4	84	8
2	K_3PO_4	26	5
3	K_2CO_3	49	5
4	NaH_2PO_4	20	19
5	Na_2HPO_4	55	29
6	Li_3PO_4	54	30

Table 3.8. Time screen for esterification of allylic amines.

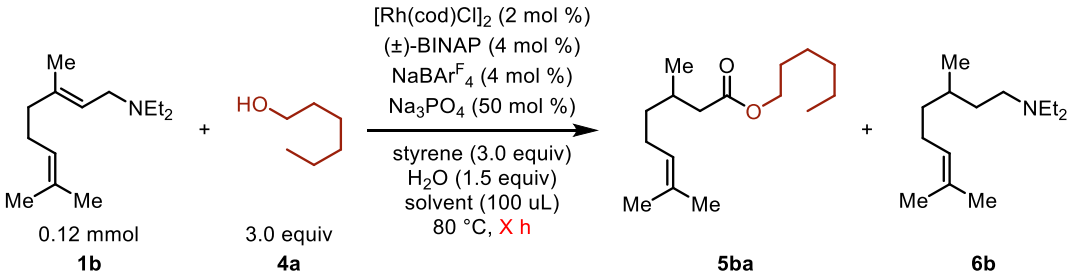

Entry	Time (h)	5ba% yield (GC)
1	0.08	2
2	0.17	3
3	0.33	6
4	0.67	9
5	1	15
6	2	22
7	4	45
8	6	46
9	12	70
10	24	91

3.8 Esterification Experimental Procedure, Isolation, and Characterization

3.8.1 General procedure for Rh-catalyzed isomerization and esterification of allylic amines with alcohols.

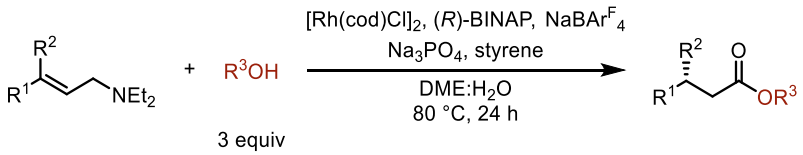

Under atmosphere of nitrogen, $[Rh(cod)Cl]_2$ (1.2 mg, 0.0024 mmol, 2.0 mol %), (*R*)-BINAP (3.0 mg, 0.0048 mmol, 4.0 mol %), $NaBAr^F_4$ (4.3 mg, 0.0048 mg, 4.0 mol %), and Na_3PO_4 (9.8 mg, 0.060 mmol, 50 mol %) were added to a 4-mL vial equipped with a stir bar. Allylic amine **1b** (25.1 mg, 0.12 mmol, 1.0 equiv) was then added to the reaction vial followed by addition of 1-hexanol **4a** (45 µL, 0.36 mmol, 3.0 equiv), styrene (42 µL, 0.36 mmol, 3.0 equiv), and dimethoxyethane (0.100 mL, 0.120 M). The vial was then sealed with a plastic cap fitted with a PTFE-lined septum and removed from the glovebox. H_2O (10.0 µL, 0.18 mmol, 1.5 equiv) was added to the reaction mixed *via* syringe through the septum. The reaction vial was placed on a hot plate with stirring at 80 °C for 24 h. The reaction vial was cooled to room temperature followed by the addition of diphenylmethane (10.0 µL) as an internal standard for analysis of the crude reaction mixture. The crude reaction mixture was diluted with methylene chloride prior to analysis. Celite was added to the reaction mixture which was then concentrated *in vacuo* and purified directly *via* flash column chromatography without further work-up procedures.

3.8.2 Characterization of Final Compounds

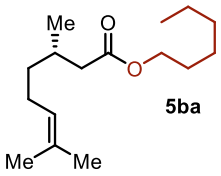

5ba

Hexyl (*S*)-3,7-dimethyloct-6-enoate $C_{16}H_{30}O_2$

Isolation: 60 mL silica gel, dry load on celite. Load column with DCM. Eluent: 10% (5% Et_2O/DCM)/Hex. R_f = 0.07

26.3 mg of inseparable mixture of product (**5ba**) and hydrogenated product (**5ba'**) in a ratio of 8:1. Corrected MW = 254.65 g/mol. **5ba (76%)**; 5ba' (10%).

^{1}H NMR (500 MHz, $CDCl_3$) δ 5.09 (t, *J* = 7.1 Hz, 1H), 4.06 (t, *J* = 6.7 Hz, 2H), 2.30 (dd, *J* = 14.6, 5.9 Hz, 1H), 2.11 (dd, *J* = 14.6, 8.2 Hz, 1H), 2.06 – 1.90 (m, 3H), 1.68 (s, 3H), 1.61 (d, *J* = 7.8 Hz, 4H), 1.40 – 1.13 (m, 9H), 0.94 (d, *J* = 6.6 Hz, 3H), 0.93 – 0.85 (m, 4H).

Note: Integration values are higher than expected due to partial hydrogenation of the final product.

^{13}C NMR (126 MHz, $CDCl_3$) δ 173.54 (**5ba**), 131.65 (**5ba**), 124.45 (**5ba**), 64.49 (**5ba**), 42.16 (**5ba'**), 42.06 (**5ba**), 39.22 (**5ba'**), 37.10 (**5ba'**), 36.94 (**5ba**), 31.59 (**5ba**), 30.58 (**5ba'**), 30.23 (**5ba**), 28.79 (**5ba**), 28.08 (**5ba'**), 25.86 (**5ba**), 25.78 (**5ba**), 25.58 (**5ba**), 24.80 (**5ba'**), 22.81 (**5ba'**), 22.70, 19.90 (**5ba'**), 19.78 (**5ba**), 17.79 (**5ba**), 14.15 (**5ba**).

HRMS: (ESI-TOF) *m/z*: [M+H$^+$] calculated for $C_{16}H_{31}O_2$, 255.2324; found, 255.2327.

IR: ν 2936, 2927, 2858, 1735 cm^{-1}.

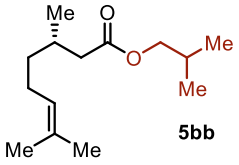

5bb

Isobutyl (*S*)-3,7-dimethyloct-6-enoate $C_{14}H_{26}O_2$

Isolation: 60 mL silica gel, dry load on celite. Load column with DCM. Eluent: 10% (5% Et_2O/DCM)/Hex. R_f = 0.08

22.3 mg of inseparable mixture of product (**5bb**) and hydrogenated product (**5bb'**) in a ratio of 14:1. Corrected MW = 226.50 g/mol. **5bb (76%)**; **5bb'** (6%).

^{1}H NMR (500 MHz, $CDCl_3$) δ 5.09 (tp, *J* = 7.1, 1.4 Hz, 1H), 3.85 (dd, *J* = 6.7, 1.0 Hz, 2H), 2.32 (dd, *J* = 14.6, 6.0 Hz, 1H), 2.12 (dd, *J* = 14.6, 8.2 Hz, 1H), 2.07 – 1.85 (m, 4H), 1.68 (d, *J* = 1.4 Hz, 3H), 1.60 (s, 3H), 1.42 – 1.11 (m, 4H), 0.95 (d, *J* = 6.6 Hz, 3H), 0.93 (d, *J* = 6.7 Hz, 6H), 0.86 (dd, *J* = 6.6, 0.8 Hz, 1H).

Note: Integration values are higher than expected due to partial hydrogenation of the final product.

^{13}C NMR (126 MHz, $CDCl_3$) δ 173.53 (**5bb**), 131.67 (**5bb**), 124.44 (**5bb**), 70.52 (**5bb**), 42.15 (**5bb'**), 42.06 (**5bb**), 39.22 (**5bb'**), 37.12 (**5bb'**), 36.94 (**5bb**), 30.59 (**5bb'**), 30.21 (**5bb**), 28.08 (**5bb'**), 27.88 (**5bb**), 25.86 (**5bb**), 25.58 (**5bb**), 24.80 (**5bb'**), 22.81 (**5bb'**), 22.72 (**5bb'**), 19.92 (**5bb'**), 19.80 (**5bb**), 19.28 (**5bb**), 17.79 (**5bb**).

HRMS (ESI-TOF) *m/z*: [M+H$^+$] calculated for $C_{14}H_{26}O_2$, 249.1831; found, 249.1835.

IR: ν 2961, 2916, 2875, 2850, 1735 cm^{-1}

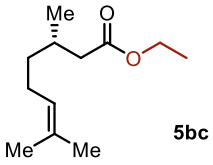

Ethyl (*S*)-3,7-dimethyloct-6-enoate $C_{12}H_{22}O_2$

Isolation: 60 mL silica gel, dry load on celite. Load column with DCM. Eluent: 20% (5% Et_2O/DCM)/Hex. R_f = 0.08

16.2 mg of inseparable mixture of product (**5bc**) and hydrogenated product (**5bc'**) in a ratio of 7:1. Corrected MW = 198.55 g/mol. **5bc (60%)**; 5bc' (8%).

^{1}H NMR (500 MHz, $CDCl_3$) δ 5.09 (tdt, *J* = 7.1, 2.8, 1.4 Hz, 1H), 4.13 (q, *J* = 7.1 Hz, 2H), 2.30 (dd, *J* = 14.6, 6.0 Hz, 1H), 2.10 (dd, *J* = 14.6, 8.2 Hz, 1H), 2.05 – 1.90 (m, 3H), 1.68 (d, *J* = 1.3 Hz, 3H), 1.60 (s, 3H), 1.40 – 1.11 (m, 7H), 0.94 (d, *J* = 6.7 Hz, 3H), 0.86 (dd, *J* = 6.6, 0.9 Hz, 1H) (5bc').

Note: Integration values are higher than expected due to partial hydrogenation of the final product.

^{13}C NMR (126 MHz, $CDCl_3$) δ 173.44 (**5bc**), 131.67 (**5bc**), 124.45 (**5bc**), 60.24 (**5bc**), 42.13 (**5bc'**), 42.02 (**5bc**), 39.21 (**5bc'**), 37.11 (**5bc'**), 36.94 (**5bc**), 30.55 (**5bc'**), 30.20 (**5bc**), 29.86 (**5bc'**), 28.07 (**5bc'**), 25.86 (**5bc**), 25.58 (**5bc**), 24.79 (**5bc'**), 22.81 (**5bc'**), 22.72 (**5bc'**), 19.89 (**5bc'**), 19.76 (**5bc**), 17.79 (**5bc**), 14.44 (**5bc**).

HRMS (ESI-TOF) *m/z*: [M+H$^+$] calculated for $C_{12}H_{22}O_2$, 197.1542; found, 197.1541.

IR: ν 2960, 2861, 2851, 1733 cm^{-1}.

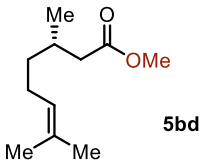

5bd

Methyl (*S*)-3,7-dimethyloct-6-enoate $C_{11}H_{20}O_2$

Isolation: 60 mL silica gel, dry load on celite. Load column with DCM. Eluent: 10% (5% Et_2O/DCM)/Hex. R_f = 0.9

15.9 mg of inseparable mixture of product (**5bd**) and hydrogenated product (**5bd'**) in a ratio of 6:1. Corrected MW = 184.54 g/mol. **5bd (62%)**; 5bd' (9%).

^{1}H NMR (500 MHz, $CDCl_3$) δ 5.09 (ddq, *J* = 8.5, 5.7, 1.4 Hz, 1H), 3.67 (s, 3H), 2.32 (dd, *J* = 14.7, 5.9 Hz, 1H), 2.12 (dd, *J* = 14.7, 8.3 Hz, 1H), 2.06 – 1.91 (m, 3H), 1.68 (d, *J* = 1.4 Hz, 3H), 1.60 (s, 3H), 1.39 – 1.12 (m, 3H), 0.94 (d, *J* = 6.7 Hz, 3H), 0.86 (dd, *J* = 6.6, 1.0 Hz, 1H) (**5bd'**).

Note: Integration values are inflated due to presence of the hydrogenated product.

^{13}C NMR (126 MHz, $CDCl_3$) δ 173.88 (**5bd**), 131.71 (**5bd**), 124.41 (**5bd**), 51.52 (**5bd**), 41.86 (**5bd'**), 41.75 (**5bd**), 39.19 (**5bd'**), 37.11 (**5bd'**), 36.93 (**5bd**), 30.53 (**5bd'**), 30.20 (**5bd**), 28.07 (**5bd'**), 25.86 (**5bd**), 25.58 (**5bd**), 24.80 (**5bd'**), 22.81 (**5bd'**), 22.72 (**5bd'**), 19.91 (**5bd'**), 19.78 (**5bd**), 17.79 (**5bd**).

IR: ν 2956, 2920, 2852, 1739 cm^{-1}.

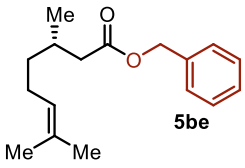

5be

Benzyl (*S*)-3,7-dimethyloct-6-enoate $C_{17}H_{24}O_2$

Isolation: 60 mL silica gel, dry load on celite. Load column with DCM. Eluent: 10% (5% Et_2O/DCM)/Hex. R_f = 0.1

25.0 mg (**5be**); 80% yield

^{1}H NMR (500 MHz, $CDCl_3$) δ 7.41 – 7.29 (m, 5H), 5.12 (s, 2H), 5.07 (tdq, *J* = 7.0, 2.8, 1.3 Hz, 1H), 2.37 (dd, *J* = 14.7, 6.0 Hz, 1H), 2.17 (dd, *J* = 14.8, 8.2 Hz, 1H), 2.05 – 1.90 (m, 3H), 1.67 (d,

J = 1.4 Hz, 3H), 1.59 (s, 3H), 1.35 (dddd, *J* = 13.4, 9.5, 6.5, 5.8 Hz, 1H), 1.22 (dddd, *J* = 13.6, 9.3, 7.9, 6.2 Hz, 1H), 0.94 (d, *J* = 6.6 Hz, 3H).

^{13}C NMR (126 MHz, $CDCl_3$) δ 173.22, 136.29, 131.69, 128.68, 128.34, 128.29, 124.39, 66.18, 41.95, 36.91, 30.22, 25.86, 25.55, 19.77, 17.79.

HRMS (ESI-TOF) *m/z*: [M+H$^+$] calculated for $C_{17}H_{24}O_2$, 283.1674; found, 283.1667.

IR: ν 2957, 2925, 2855, 1730 cm^{-1}.

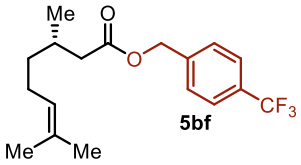

5bf

4-(trifluoromethyl)benzyl (*S*)-3,7-dimethyloct-6-enoate $C_{18}H_{23}F_3O_2$

Isolation: 60 mL silica gel, dry load on celite. Load column with DCM. Eluent: 20% (5% Et_2O/DCM)/Hex. R_f = 0.1

23.2 mg of inseparable mixture of product (**5bf**) and hydrogenated product (**5bf'**) in a ratio of 7:1. Corrected MW = 328.64 g/mol. **Product yield (51%)**; byproduct yield (8%).

^{1}H NMR (500 MHz, $CDCl_3$) δ 7.62 (d, *J* = 8.0 Hz, 2H), 7.46 (d, *J* = 7.9 Hz, 2H), 5.16 (s, 2H), 5.06 (ddt, *J* = 8.5, 5.8, 1.4 Hz, 1H), 2.38 (dd, *J* = 14.8, 5.9 Hz, 1H), 2.19 (dd, *J* = 14.8, 8.1, Hz, 1H), 1.98 (tq, *J* = 14.2, 7.6, 7.0 Hz, 3H), 1.67 (s, 3H), 1.58 (s, 3H), 1.56 – 1.42 (m, 1H), 1.35 (ddt, *J* = 12.5, 9.5, 6.1 Hz, 1H), 1.30 – 1.06 (m, 2H), 0.95 (dd, *J* = 6.7, 0.9 Hz, 3H), 0.85 (dd, *J* = 6.5, 0.8 Hz, 1H) (**5bf'**).

Note: integration values are inflated due to presence of hydrogenated byproduct.

^{13}C NMR (126 MHz, CDCl3) δ 173.01 (**5bf**), 140.28 (**5bf**), 131.79 (**5bf**), 130.47 (q, *J* = 32.6 Hz) (**5bf**), 128.29 (**5bf**), 125.65 (q, *J* = 3.8 Hz) (**5bf**), 124.27 (**5bf**), 124.16 (q, *J* = 272.1 Hz) (**5bf**), 65.20 (**5bf**), 41.92 (**5bf**), 41.82 (**5bf**), 39.17 (**5bf'**), 37.05 (**5bf'**), 36.88 (**5bf**), 30.59 (**5bf'**), 30.22 (**5bf**), 28.05 (**5bf'**), 25.84 (**5bf**), 25.54 (**5bf**), 24.77 (**5bf'**), 22.79 (**5bf'**), 22.70 (**5bf'**), 19.92 (**5bf'**), 19.79 (**5bf**), 17.79 (**5bf**).

^{19}F NMR (471 MHz, $CDCl_3$) δ -62.65.

HRMS (ESI-TOF) *m/z*: [M+H$^+$] calculated for $C_{18}H_{23}F_3O_2$, 351.1548; found, 351.1545.

IR: ν 2959, 2918, 2855, 1738 cm^{-1}.

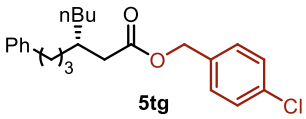

5tg

4-chlorobenzyl (*S*)-3-(3-phenylpropyl)heptanoate $C_{23}H_{29}ClO_2$

Isolation: 60 mL silica gel, dry load on celite. Load column with DCM. Eluent: 20% (5% Et_2O/DCM)/Hex. R_f = 0.11

37.6 mg (**5tg**); 84% yield.

^{1}H NMR (500 MHz, $CDCl_3$) δ 7.34 – 7.24 (m, 6H), 7.20 – 7.13 (m, 3H), 5.05 (s, 2H), 2.56 (t, *J* = 7.8 Hz, 2H), 2.28 (dd, *J* = 6.9, 2.3 Hz, 2H), 1.89 (hept, *J* = 6.2 Hz, 1H), 1.59 (p, *J* = 8.0 Hz, 2H), 1.40 – 1.15 (m, 8H), 0.86 (t, *J* = 6.9 Hz, 3H).

^{13}C NMR (126 MHz, $CDCl_3$) δ 173.36, 142.63, 134.79, 134.22, 129.82, 128.86, 128.49, 128.41, 125.84, 65.33, 39.28, 36.27, 35.16, 33.70, 33.66, 28.86, 28.59, 23.03, 14.19.

HRMS (ESI-TOF) *m/z*: [M+H$^+$] calculated for $C_{23}H_{29}ClO_2$, 395.1754; found, 395.1759.

IR: ν 2945, 2926, 2856, 1733 cm^{-1}.

Specific optical rotation: -1.1200°, C = 0.750g/100mL, 23.2 °C, $CHCl_3$, 589 nm.

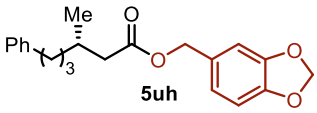

5uh

Benzo[d][1,3]dioxol-5-ylmethyl (*S*)-3-methyl-6-phenylhexanoate $C_{21}H_{24}O_4$

Isolation: 60 mL silica gel, dry load on celite. Load column with DCM. Eluent: 30% (5% Et_2O/DCM)/Hex. R_f = 0.15

24.5 mg (**5uh**); 60% yield.

^{1}H NMR (500 MHz, $CDCl_3$) δ 7.27 (d, *J* = 0.0 Hz, 2H), 7.20 – 7.13 (m, 3H), 6.84 – 6.75 (m, 3H), 5.96 (s, 2H), 5.00 (s, 2H), 2.62 – 2.52 (m, 2H), 2.32 (dd, *J* = 14.8, 6.2 Hz, 1H), 2.15 (dd, *J* = 14.7, 8.0 Hz, 1H), 1.99 (tq, *J* = 13.6, 7.0 Hz, 1H), 1.70 – 1.54 (m, 2H), 1.36 (ddt, *J* = 13.4, 10.9, 5.6 Hz, 1H), 1.28 – 1.19 (m, 1H), 0.93 (d, *J* = 6.6 Hz, 3H).

^{13}C NMR (126 MHz, $CDCl_3$) δ 173.18, 147.92, 147.71, 142.66, 130.03, 128.50, 128.41, 125.82, 122.40, 109.18, 108.37, 101.29, 66.16, 41.97, 36.43, 36.16, 30.48, 28.97, 19.86.

HRMS (ESI-TOF) *m/z*: [M+H$^+$] calculated for $C_{21}H_{24}O_4$, 363.1586; found, 363.1584.

IR: ν 2920, 2852, 1731, 1243, 1039 cm^{-1}.

Specific optical rotation: -3.5958°, C = 1.580g/100mL, 23.2 °C, $CHCl_3$, 589 nm.

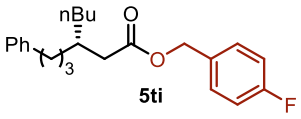

5ti

4-fluorobenzyl (*S*)-3-(3-phenylpropyl)heptanoate $C_{23}H_{29}FO_2$

Isolation: 60 mL silica gel, dry load on celite. Load column with DCM. Eluent: 20% (5% Et_2O/DCM)/Hex. R_f = 0.11

34.2 mg (**5ti**); 80% yield.

^{1}H NMR (500 MHz, $CDCl_3$) δ 7.34 – 7.26 (m, 4H), 7.20 – 7.13 (m, 3H), 7.06 – 7.01 (m, 2H), 5.05 (s, 2H), 2.55 (t, *J* = 7.8 Hz, 2H), 2.27 (dd, *J* = 6.9, 2.1 Hz, 2H), 1.89 (hept, *J* = 6.2 Hz, 1H), 1.59 (p, *J* = 8.0 Hz, 2H), 1.40 – 1.16 (m, 8H), 0.85 (t, *J* = 6.9 Hz, 3H).

^{13}C NMR (126 MHz, $CDCl_3$) δ 173.41, 162.75 (d, *J* = 246.7 Hz), 142.65, 132.14 (d, *J* = 3.3 Hz), 130.42 (d, *J* = 8.35 Hz), 128.45 (d, *J* = 10.0 Hz), 125.83, 115.58 (d, *J* = 21.6 Hz), 65.44, 39.32, 36.27, 35.16, 33.71, 33.66, 28.85, 28.59, 23.03, 14.19.

^{19}F NMR (471 MHz, $CDCl_3$) δ -113.79.

HRMS (ESI-TOF) *m/z*: [M+H$^+$] calculated for $C_{23}H_{29}FO_2$, 379.2049; found, 379.2057.

IR: ν 2945, 2928, 2857, 1734 cm^{-1}.

Specific optical rotation: -1.3800°, C = 1.40g/100mL, 23.2 °C, $CHCl_3$, 589 nm.

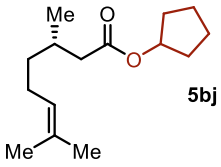

5bj

Cyclopentyl (*S*)-3,7-dimethyloct-6-enoate $C_{15}H_{26}O_2$

Isolation: 60 mL silica gel, dry load on celite. Load column with DCM. Eluent: 20% (5% Et_2O/DCM)/Hex. R_f = 0.1

21.5 mg of inseparable mixture of product (**5b*J***) and hydrogenated product (**5b*J*'**) in a ratio of 8:1. Corrected MW = 238.61 g/mol. **5b*J* (66%)**; 5b*J*' (9%).

^{1}H NMR (500 MHz, $CDCl_3$) δ 5.16 (tt, *J* = 5.7, 2.7 Hz, 1H), 5.09 (dddd, *J* = 7.1, 5.7, 2.9, 1.5 Hz, 1H), 2.26 (dd, *J* = 14.4, 6.1 Hz, 1H), 2.07 (dd, *J* = 14.5, 8.1 Hz, 1H), 2.04 – 1.79 (m, 5H), 1.76 – 1.63 (m, 7H), 1.63 – 1.52 (m, 5H), 1.39 – 1.11 (m, 4H), 0.94 (d, *J* = 6.7 Hz, 3H), 0.86 (d, *J* = 6.6 Hz, 1H) (**5b*J*'**).

Note: Integration values are inflated due to presence of the hydrogenated product.

^{13}C NMR (126 MHz, $CDCl_3$) δ 173.25 (**5b*J***), 131.64 (**5b*J***), 124.48 (**5b*J***), 42.39 (**5b*J*'**), 42.30 (**5b*J***), 39.24 (**5b*J*'**), 37.09 (**5b*J*'**), 36.92 (**5b*J***), 32.85 (**5b*J***), 32.81 (**5b*J***), 30.63 (**5b*J*'**), 30.26 (**5b*J***), 28.08 (**5b*J*'**), 25.86 (**5b*J***), 25.57 (**5b*J***), 24.78 (**5b*J*'**), 23.87 (**5b*J***), 22.81 (**5b*J*'**), 22.73 (**5b*J*'**), 19.87 (**5b*J*'**), 19.74 (**5b*J***), 17.79 (**5b*J***).

HRMS (ESI-TOF) *m/z*: [M+H$^+$] calculated for $C_{15}H_{26}O_2$, 237.1855; found, 237.1846.

IR: ν 2957, 2918, 2856, 2849, 1729 cm^{-1}.

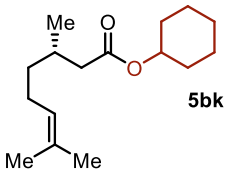

5bk

Cyclohexyl (*S*)-3,7-dimethyloct-6-enoate $C_{16}H_{28}O_2$

Isolation: 60 mL silica gel, dry load on celite. Load column with DCM. Eluent: 20% (5% Et_2O/DCM)/Hex. R_f = 0.1

19.1 mg of inseparable mixture of product (**5bk**) and hydrogenated product (**5bk'**) in a ratio of 8:1.

Corrected MW = 252.62 g/mol. **5bk (56%)**; 5bk' (7%).

^{1}H NMR (500 MHz, $CDCl_3$) δ 5.09 (ddt, *J* = 7.2, 5.7, 1.5 Hz, 1H), 4.77 (tt, *J* = 8.9, 3.8 Hz, 1H), 2.28 (dd, *J* = 14.4, 6.1 Hz, 1H), 2.09 (dd, *J* = 14.4, 8.1 Hz, 1H), 2.05 – 1.91 (m, 3H), 1.88 – 1.78 (m, 2H), 1.77 – 1.69 (m, 2H), 1.68 (s, 3H), 1.60 (s, 3H), 1.58 – 1.50 (m, 2H), 1.46 – 1.11 (m, 9H), 0.94 (d, *J* = 6.6 Hz, 3H), 0.86 (d, *J* = 6.6 Hz, 1H) (**5bk'**).

Note: Integration values are higher than expected due to partial hydrogenation of the final product.

^{13}C NMR (126 MHz, $CDCl_3$) δ 172.86 (**5bk**), 131.59 (**5bk**), 124.47 (**5bk**), 72.38 (**5bk**), 42.46 (**5bk'**), 42.37 (**5bk**), 39.21 (**5bk'**), 37.07 (**5bk'**), 36.90 (**5bk**), 31.84 (**5bk**), 31.80 (**5bk**), 30.64 (**5bk'**), 30.27 (**5bk**), 28.04 (**5bk'**), 25.83 (**5bk**), 25.55 (**5bk**), 24.76 (**5bk'**), 23.90 (**5bk**), 22.78 (**5bk'**), 22.70 (**5bk'**), 19.81 (**5bk'**), 19.69 (**5bk**), 17.77 (**5bk**).

HRMS (ESI-TOF) *m/z*: [M+H$^+$] calculated for $C_{16}H_{28}O_2$, 251.2011; found, 251.2017.

IR: ν 2930, 2859, 1730 cm^{-1}.

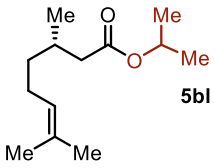

5bl

Isopropyl (*S*)-3,7-dimethyloct-6-enoate $C_{13}H_{24}O_2$

Isolation: 60 mL silica gel, dry load on celite. Load column with DCM. Eluent: 10% (5% Et_2O/DCM)/Hex. R_f = 0.7

11.0 mg of inseparable mixture of product (**5bl**) and hydrogenated product (**5bl'**) in a ratio of 6:1.

Corrected MW = 212.60 g/mol. **5bl (37%)**; 5bl' (6%).

^{1}H NMR (500 MHz, $CDCl_3$) δ 5.09 (tdt, *J* = 7.1, 2.9, 1.4 Hz, 1H), 5.01 (hept, *J* = 6.3 Hz, 1H), 2.27 (dd, *J* = 14.5, 6.0 Hz, 1H), 2.07 (dd, *J* = 14.4, 8.2 Hz, 1H), 2.04 – 1.92 (m, 3H), 1.68 (d, *J* =

1.3 Hz, 3H), 1.60 (s, 3H), 1.39 – 1.27 (m, 3H), 1.23 (d, *J* = 6.3 Hz, 6H), 0.94 (d, *J* = 6.7 Hz, 3H), 0.86 (d, *J* = 6.5 Hz, 1H) (**5bl'**).

Note: Integration values are inflated due to presence of the hydrogenated product.

^{13}C NMR (126 MHz, $CDCl_3$) δ 172.96 (**5bl**), 131.63 (**5bl**), 124.49 (**5bl**), 67.43 (**5bl**), 42.45 (**5bl**), 42.35 (**5bl**), 39.23 (**5bl'**), 37.10 (**5bl'**), 36.94 (**5bl**), 30.61 (**5bl'**), 30.26 (**5bl**), 29.86 (**5bl'**), 28.07 (**5bl'**), 25.86 (**5bl**), 25.57 (**5bl**), 24.78 (**5bl'**), 22.81 (**5bl'**), 22.73 (**5bl'**), 22.05 (**5bl**), 22.02 (**5bl**), 19.83 (**5bl'**), 19.71 (**5bl**), 17.79 (**5bl**).

IR: ν 2962, 2920, 2854, 1731 cm^{-1}.

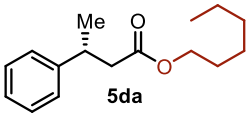

Hexyl (*R*)-3-phenylbutanoate $C_{16}H_{24}O_2$

Isolation: 60 mL silica gel, dry load on celite. Load column with DCM. Eluent: 20% (5% Et_2O/DCM)/Hex. R_f = 0.9

21.8 mg (**5da**); 73% yield.

^{1}H NMR (500 MHz, $CDCl_3$) δ 7.32 – 7.27 (m, 2H), 7.24 – 7.17 (m, 3H), 4.01 (t, *J* = 6.7 Hz, 2H), 3.28 (h, *J* = 7.1 Hz, 1H), 2.62 (dd, *J* = 15.0, 7.0 Hz, 1H), 2.54 (dd, *J* = 15.0, 8.1 Hz, 1H), 1.57 – 1.50 (m, 2H), 1.32 – 1.22 (m, 9H), 0.88 (t, *J* = 6.9 Hz, 3H).

^{13}C NMR (126 MHz, $CDCl_3$) δ 172.64, 145.90, 128.61, 126.89, 126.52, 77.41, 77.16, 76.91, 64.65, 43.16, 36.71, 31.56, 28.71, 25.69, 22.67, 22.04, 14.16.

HRMS (ESI-TOF) *m/z*: [M+H$^+$] calculated for $C_{16}H_{24}O_2$, 271.1674; found, 271.1685.

IR: ν 2956, 2930, 2858, 1733, 1165 cm^{-1}.

Specific optical rotation: -18.1065°, C = 1.340g/100mL, 23.1 °C, $CHCl_3$, 589 nm.

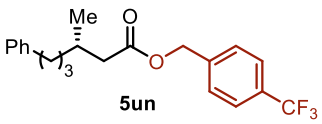

4-(trifluoromethyl)benzyl (*S*)-3-methyl-6-phenylhexanoate

$C_{21}H_{23}F_3O_2$

Isolation: 60 mL silica gel, dry load on celite. Load column with DCM. Eluent: 20% (5% Et_2O/DCM)/Hex. R_f = 0.09

28.0 mg (**5un**); 64% yield.

^{1}H NMR (500 MHz, $CDCl_3$) δ 7.62 (d, *J* = 8.0 Hz, 2H), 7.45 (d, *J* = 8.1 Hz, 2H), 7.31 – 7.26 (m, 2H), 7.20 – 7.13 (m, 3H), 5.15 (s, 2H), 2.64 – 2.52 (m, 2H), 2.37 (dd, *J* = 14.8, 6.1 Hz, 1H), 2.19 (dd, *J* = 14.9, 8.0 Hz, 1H), 2.01 (ddt, *J* = 20.4, 13.7, 6.8 Hz, 1H), 1.72 – 1.54 (m, 2H), 1.37 (ddt, *J* = 13.3, 10.8, 5.6 Hz, 1H), 1.25 (dddd, *J* = 13.3, 10.5, 7.7, 5.4 Hz, 1H), 0.94 (d, *J* = 6.6 Hz, 3H).

^{13}C NMR (126 MHz, $CDCl_3$) δ 172.97, 142.57, 140.25, 130.48 (q, *J* = 32.5 Hz), 128.49, 128.43, 128.42, 128.30, 125.86, 125.66 (q, *J* = 3.82 Hz), 124.16 (q, *J* = 272.18 Hz), 65.21, 41.81, 36.42, 36.14, 30.47, 28.95, 19.87.

^{19}F NMR (471 MHz, $CDCl_3$) δ -62.64.

HRMS (ESI-TOF) *m/z*: [M+H$^+$] calculated for $C_{21}H_{23}F_3O_2$, 387.1548; found, 387.1546.

IR: ν 2927, 2851, 1736, 1323, 1124, 1067 cm^{-1}.

Specific optical rotation: -3.0616°, C = 1.320g/100mL, 23.2 °C, $CHCl_3$, 589 nm.

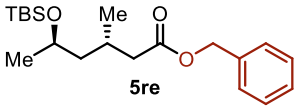

Benzyl (3*S*,5*R*)-5-((tert-butyldimethylsilyl)oxy)-3-methylhexanoate

$C_{20}H_{34}O_3Si$

Isolation: 60 mL silica gel, dry load on celite. Load column with DCM. Eluent: 20% (5% Et_2O/DCM)/Hex. R_f = 0.1

28.2 mg (**5re**); 67% yield.

^{1}H NMR (500 MHz, $CDCl_3$) δ 7.42 – 7.28 (m, 5H), 5.11 (dd, *J* = 22.5, 12.4 Hz, 2H), 3.86 (dddt, *J* = 7.9, 5.9, 4.6, 1.9 Hz, 1H), 2.36 (q, *J* = 9.2 Hz, 1H), 2.22 – 2.11 (m, 1H), 1.48 (ddd, *J* = 13.2, 8.6, 4.4 Hz, 1H), 1.18 (dq, *J* = 13.7, 4.3 Hz, 1H), 1.11 (d, *J* = 6.0 Hz, 3H), 0.93 (d, *J* = 6.2 Hz, 3H), 0.87 (s, 9H), 0.04 (d, *J* = 4.0 Hz, 6H).

^{13}C NMR (126 MHz, $CDCl_3$) δ 172.94, 136.30, 128.66, 128.32, 128.25, 66.39, 66.15, 46.84, 42.65, 27.22, 26.03, 24.57, 19.77, 18.22, -3.95, -4.66.

HRMS (ESI-TOF) *m/z*: [M+H$^+$] calculated for $C_{20}H_{34}O_3Si$, 373.2175; found, 373.2170.

IR: ν 2955, 2929, 2896, 2856, 1736, 1255, 1155, 1065, 835, 774 cm^{-1}.

Specific optical rotation: -12.4766°, C = 1.27g/100mL, 23.1 °C, $CHCl_3$, 589 nm.

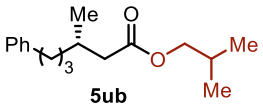

5ub

Isobutyl (*S*)-3-methyl-6-phenylhexanoate $C_{17}H_{26}O_2$

Isolation: 60 mL silica gel, dry load on celite. Load column with DCM. Eluent: 20% (5% Et_2O/DCM)/Hex. R_f = 0.08

26.8 mg (**5ub**); 85% yield.

^{1}H NMR (500 MHz, $CDCl_3$) δ 7.31 – 7.26 (m, 2H), 7.20 – 7.15 (m, 3H), 3.84 (d, *J* = 6.7 Hz, 2H), 2.66 – 2.53 (m, 2H), 2.30 (dd, *J* = 14.6, 6.1 Hz, 1H), 2.12 (dd, *J* = 14.6, 8.0 Hz, 1H), 1.99 (dq, *J* = 14.0, 7.7, 7.2 Hz, 1H), 1.91 (dp, *J* = 13.4, 6.7 Hz, 1H), 1.72 – 1.55 (m, 2H), 1.38 (ddt, *J* = 13.4, 11.0, 5.6 Hz, 1H), 1.25 (dtt, *J* = 10.5, 7.8, 5.4 Hz, 1H), 0.94 (d, *J* = 6.7 Hz, 3H), 0.93 (d, *J* = 6.7 Hz, 6H).

^{13}C NMR (126 MHz, $CDCl_3$) δ 173.49, 142.69, 128.51, 128.41, 125.82, 77.41, 77.16, 76.91, 70.52, 42.06, 36.48, 36.20, 30.48, 29.02, 27.87, 19.86, 19.28.

HRMS (ESI-TOF) *m/z*: [M+H$^+$] calculated for $C_{17}H_{26}O_2$, 285.1831; found, 285.1827.

IR: ν 2959, 2931, 2873, 1733 cm^{-1}.

Specific optical rotation: -5.9194°, C = 1.265g/100mL, 23.1 °C, $CHCl_3$, 589 nm.

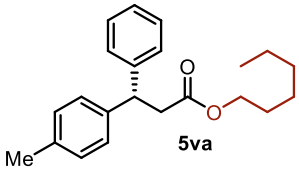

hexyl 3-phenyl-3-(*p*-tolyl)propanoate $C_{22}H_{28}O_2$

Isolation: 60 mL silica gel, dry load on celite. Load column with DCM. Eluent: 20% (5% Et_2O/DCM)/Hex. **R_f** = 0.12

32.7 mg (**5va**); 84% yield.

^{1}H NMR (500 MHz, $CDCl_3$) δ 7.30 – 7.20 (m, 4H), 7.17 (tt, *J* = 7.0, 1.8 Hz, 1H), 7.13 (td, *J* = 8.2, 2.1 Hz, 2H), 7.08 (d, *J* = 8.0 Hz, 2H), 4.51 (t, *J* = 8.1 Hz, 1H), 3.96 (t, *J* = 6.6 Hz, 2H), 3.03 (d, *J* = 8.1 Hz, 2H), 2.29 (s, 3H), 1.46 (p, *J* = 6.8 Hz, 2H), 1.36 – 1.14 (m, 6H), 0.87 (t, *J* = 7.1 Hz, 3H).

^{13}C NMR (126 MHz, $CDCl_3$) δ 172.12, 143.90, 140.67, 136.16, 129.36, 128.65, 127.76, 127.66, 126.57, 77.41, 77.16, 76.91, 64.77, 46.89, 41.09, 31.55, 28.66, 25.63, 22.66, 21.13, 14.17.

HRMS (ESI-TOF) *m/z*: [M+H$^+$] calculated for $C_{22}H_{28}O_2$, 325.2168; found, 325.2169.

IR: ν 2937, 2925, 2857, 1732 cm^{-1}.

Specific optical rotation: -1.5571°, C = 2.24g/100mL, 23.1 °C, $CHCl_3$, 589 nm.

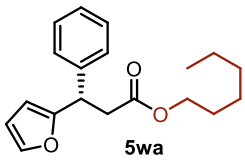

Hexyl (*S*)-3-(furan-2-yl)-3-phenylpropanoate $C_{19}H_{24}O_3$

Isolation: 60 mL silica gel, dry load on celite. Load column with DCM. Eluent: 30% (5% Et_2O/DCM)/Hex. R_f = 0.1

20.9 mg (**5wa**); 58%

yield.

^{1}H NMR (500 MHz, $CDCl_3$) δ 7.33 – 7.28 (m, 4H), 7.25 – 7.20 (m, 2H), 6.28 (dt, *J* = 3.0, 1.4 Hz, 1H), 6.05 (dt, *J* = 3.1, 1.0 Hz, 1H), 4.55 (t, *J* = 7.9 Hz, 1H), 4.00 (t, *J* = 6.7 Hz, 2H), 3.09 (dd, *J* =

15.5, 7.9 Hz, 1H), 2.90 (dd, *J* = 15.5, 7.9 Hz, 1H), 1.53 – 1.47 (m, 2H), 1.33 – 1.19 (m, 6H), 0.88 (t, *J* = 7.1 Hz, 3H).

^{13}C NMR (126 MHz, $CDCl_3$) δ 171.60, 156.40, 141.82, 141.30, 128.73, 127.87, 127.16, 110.22, 105.83, 77.41, 77.16, 76.91, 64.92, 41.61, 39.97, 31.54, 28.65, 25.63, 22.67, 14.16.

HRMS (ESI-TOF) *m/z*: [M+H$^+$] calculated for $C_{19}H_{24}O_3$, 323.1623; found, 323.1623.

IR: ν 2956, 2922, 2852, 1733, 1154 cm^{-1}.

Specific optical rotation: +41.8023°, C = 2.030g/100mL, 23.2 °C, $CHCl_3$, 589 nm.

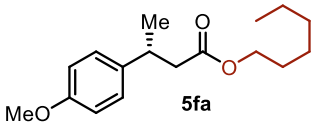

Hexyl (*R*)-3-(4-methoxyphenyl)butanoate $C_{17}H_{26}O_3$

Isolation: 60 mL silica gel, dry load on celite. Load column with DCM. Eluent: 30% (5% Et_2O/DCM)/Hex. R_f = 0.2

23.4 mg (**5fa**); 70% yield.

^{1}H NMR (500 MHz, $CDCl_3$) δ 7.17 – 7.11 (m, 2H), 6.85 – 6.81 (m, 2H), 4.00 (t, *J* = 6.7 Hz, 2H), 3.78 (s, 3H), 3.23 (h, *J* = 7.2 Hz, 1H), 2.57 (dd, *J* = 14.9, 7.3 Hz, 1H), 2.51 (dd, *J* = 14.9, 8.0 Hz, 1H), 1.57 – 1.49 (m, 2H), 1.32 – 1.20 (m, 9H), 0.88 (t, *J* = 6.9 Hz, 3H).

^{13}C NMR (126 MHz, $CDCl_3$) δ 172.71, 158.20, 138.01, 127.80, 113.97, 64.62, 55.37, 43.42, 35.94, 31.57, 28.72, 25.70, 22.67, 22.22, 14.16.

HRMS (ESI-TOF) *m/z*: [M+H$^+$] calculated for $C_{17}H_{26}O_3$, 301.1780; found, 301.1781.

IR: ν 2956, 2927, 2857, 1732, 1514, 1247 cm^{-1}.

Specific optical rotation: -18.6362°, C = 1.27g/100mL, 23.1 °C, $CHCl_3$, 589 nm.

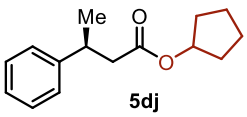

Cyclopentyl (*R*)-3-phenylbutanoate $C_{15}H_{20}O_2$

Isolation: 60 mL silica gel, dry load on celite. Load column with DCM. Eluent: 30% (5% Et_2O/DCM)/Hex. R_f = 0.12

17.8 mg (**5d*J***); 64% yield

^{1}H NMR (500 MHz, $CDCl_3$) δ 7.32 – 7.27 (m, 2H), 7.24 – 7.16 (m, 3H), 5.09 (tt, *J* = 6.1, 2.9 Hz, 1H), 3.25 (h, *J* = 7.2 Hz, 1H), 2.58 (dd, *J* = 14.8, 7.4 Hz, 1H), 2.51 (dd, *J* = 14.8, 7.9 Hz, 1H), 1.81 – 1.71 (m, 2H), 1.66 – 1.47 (m, 6H), 1.29 (d, *J* = 7.0 Hz, 3H).

^{13}C NMR (126 MHz, $CDCl_3$) δ 172.35, 145.87, 128.56, 126.93, 126.49, 43.37, 36.86, 32.73, 32.71, 23.81, 22.12.

HRMS (ESI-TOF) *m/z*: [M+H$^+$] calculated for $C_{15}H_{20}O_2$, 255.1361; found, 255.1362.

IR: ν 2962, 2919, 2873, 2850, 1728 cm^{-1}.

Specific optical rotation: -18.2237°, C = 1.49g/100mL, $CHCl_3$, 22.8 °C, 589 nm

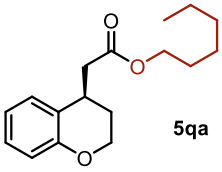

Hexyl (*R*)-2-(chroman-4-yl)acetate $C_{17}H_{24}O_3$

Isolation: 60 mL silica gel, dry load on celite. Load column with DCM. Eluent: 30% (5% Et_2O/DCM)/Hex. R_f = 0.1

21.6 mg (**5qa**); 65% yield.

^{1}H NMR (500 MHz, $CDCl_3$) δ 7.14 – 7.08 (m, 2H), 6.86 (td, *J* = 7.5, 1.3 Hz, 1H), 6.80 (dd, *J* = 8.1, 1.3 Hz, 1H), 4.23 – 4.14 (m, 2H), 4.12 (td, *J* = 6.8, 0.9 Hz, 2H), 3.36 (dq, *J* = 10.3, 5.2 Hz, 1H), 2.80 (dd, *J* = 15.5, 4.8 Hz, 1H), 2.53 (dd, *J* = 15.5, 10.0 Hz, 1H), 2.16 (dddd, *J* = 14.3, 8.7, 5.8, 4.2 Hz, 1H), 1.85 (dtd, *J* = 14.0, 5.4, 3.2 Hz, 1H), 1.64 (dq, *J* = 8.1, 6.7 Hz, 2H), 1.39 – 1.23 (m, 7H), 0.90 (t, *J* = 7.0 Hz, 3H).

^{13}C NMR (126 MHz, $CDCl_3$) δ 172.39, 154.69, 128.86, 127.97, 124.75, 120.54, 117.21, 64.99, 63.34, 41.55, 31.56, 30.68, 28.74, 27.52, 25.75, 22.69, 14.15.

HRMS (ESI-TOF) *m/z*: [M+H$^+$] calculated for $C_{17}H_{24}O_3$, 299.1623; found, 299.1633.

IR: ν 2938, 2926, 2857, 1731, 1224, 1162 cm^{-1}.

Specific optical rotation: -5.9385°, C = 1.80g/100mL, 22.8 °C, $CHCl_3$, 589 nm.

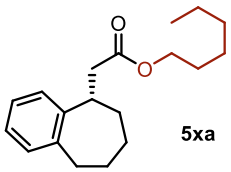

5xa

Hexyl (*S*)-2-(6,7,8,9-tetrahydro-5H-benzo[7]annulen-5-yl)acetate

$C_{19}H_{28}O_2$

Isolation: 60 mL silica gel, dry load on celite. Load column with DCM. Eluent: 10% (5% Et_2O/DCM)/Hex. R_f = 0.1

29.1 mg (**5xa**); 84% yield.

^{1}H NMR (500 MHz, $CDCl_3$) δ 7.17 – 7.04 (m, 4H), 4.06 (t, *J* = 6.7 Hz, 2H), 3.52 – 3.43 (m, 1H), 2.95 – 2.87 (m, 1H), 2.86 – 2.82 (m, 1H), 2.80 (dd, *J* = 15.1, 6.7 Hz, 1H), 2.70 (dd, *J* = 15.1, 8.9 Hz, 1H), 1.96 – 1.84 (m, 1H), 1.83 – 1.69 (m, 3H), 1.65 – 1.47 (m, 4H), 1.38 – 1.19 (m, 6H), 0.89 (t, *J* = 6.8 Hz, 3H).

^{13}C NMR (126 MHz, $CDCl_3$) δ 173.08, 144.07, 142.71, 129.87, 126.37, 126.24, 64.71, 40.82, 38.84, 36.17, 33.51, 31.56, 29.86, 28.74, 27.95, 25.73, 22.69, 14.15.

HRMS (ESI-TOF) *m/z*: [M+H$^+$] calculated for $C_{19}H_{28}O_2$, 289.2168; found, 289.2161.

IR: ν 2922, 2853, 1733 cm^{-1}.

Specific optical rotation: 10.8212°, C = 1.160g/100mL, 23.2 °C, $CHCl_3$, 589 nm.

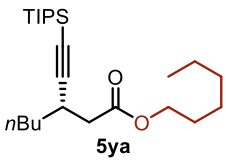

Hexyl (*S*)-3-((triisopropylsilyl)ethynyl)heptanoate $C_{24}H_{46}O_2Si$

Isolation: 60 mL silica gel, dry load on celite. Load column with DCM. Eluent: 20% (5% Et_2O/DCM)/Hex. **R_f** = 0.3

33.3 mg (**5ya**); 70% yield

^{1}H NMR (500 MHz, $CDCl_3$) δ 4.07 (td, *J* = 6.8, 1.6 Hz, 2H), 2.94 – 2.84 (m, 1H), 2.53 (dd, *J* = 15.2, 7.7 Hz, 1H), 2.43 (dd, *J* = 15.2, 7.2 Hz, 1H), 1.61 (dt, *J* = 8.3, 6.8 Hz, 2H), 1.55 – 1.39 (m, 5H), 1.39 – 1.24 (m, 9H), 1.06 – 1.03 (m, 18H), 1.01 – 0.97 (m, 1H), 0.89 (td, *J* = 7.2, 2.7 Hz, 6H).

^{13}C NMR (126 MHz, $CDCl_3$) δ 171.84, 110.62, 81.66, 64.88, 40.74, 34.47, 31.61, 29.49, 29.42, 28.74, 25.77, 22.69, 22.49, 18.75, 14.16, 14.14, 11.37.

HRMS (ESI-TOF) *m/z*: [M+H$^+$] calculated for $C_{24}H_{47}O_2Si$, 395.3345; found, 395.3353.

IR: ν 2929, 2864, 2167, 1739, 1463, 1162 cm^{-1}.

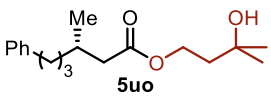

3-hydroxy-3-methylbutyl (*S*)-3-methyl-6-phenylhexanoate $C_{18}H_{28}O_3$

Isolation: 60 mL silica gel, dry load on celite. Eluent: (10% to 20%) EtOAc/Hex. **R_f** = 0.3

26.0 mg (**5uo**); 74% yield.

^{1}H NMR (500 MHz, $CDCl_3$) δ 7.30 – 7.27 (m, 2H), 7.20 – 7.15 (m, 3H), 4.24 (t, *J* = 6.9 Hz, 2H), 2.59 (ddd, *J* = 8.4, 6.8, 3.7 Hz, 2H), 2.29 (dd, *J* = 14.7, 6.0 Hz, 1H), 2.11 (dd, *J* = 14.8, 8.1 Hz, 1H), 1.98 (dq, *J* = 14.0, 7.2 Hz, 1H), 1.82 (t, *J* = 6.8 Hz, 2H), 1.72 – 1.56 (m, 2H), 1.56 – 1.53 (m, 2H), 1.37 (ddt, *J* = 13.4, 10.8, 5.6 Hz, 1H), 1.26 (s, 6H), 0.94 (d, *J* = 6.7 Hz, 3H).

^{13}C NMR (126 MHz, $CDCl_3$) δ 173.30, 142.64, 128.51, 128.42, 125.83, 70.21, 61.37, 42.05, 41.73, 36.45, 36.16, 30.43, 29.79, 28.98, 19.86.

HRMS (ESI-TOF) *m/z*: [M+H$^+$] calculated for $C_{18}H_{28}O_3Na$, 315.1936; found, 315.1929.

IR: ν 3442 (br), 2966, 2930, 2855, 1732, 1148 cm^{-1}.

3.8.3 HPLC Traces of Isolated Esters

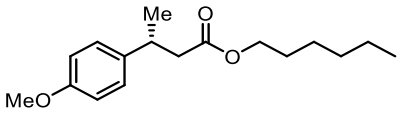

0.3%THF/Hex, 0.8 mL/min, CHIRALPAK IB-3, **97.0:3.0 e.r.**

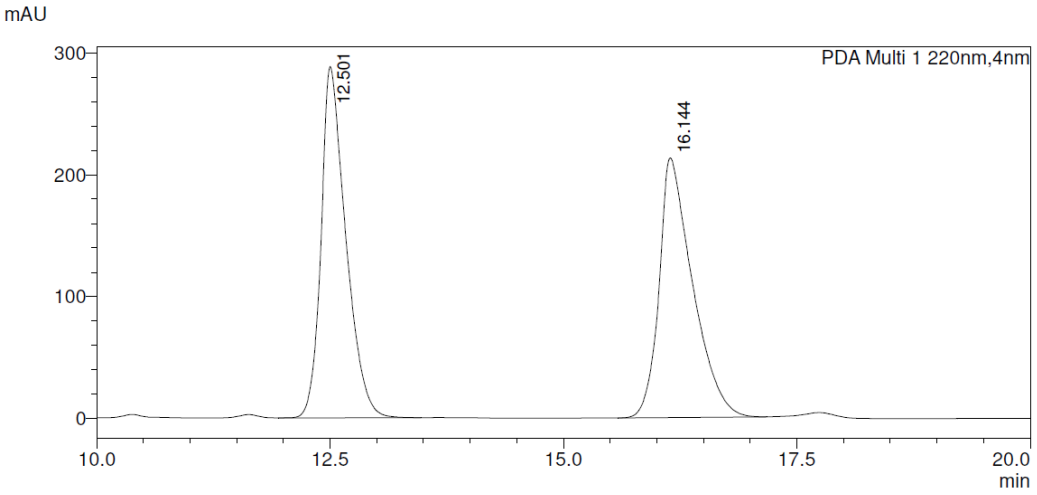

PDA Ch1 220nm

Peak#	Ret. Time	Area	Area%	Height	Height%
1	12.501	5304998	49.932	287965	57.503
2	16.144	5319540	50.068	212819	42.497
Total		10624538	100.000	500784	100.000

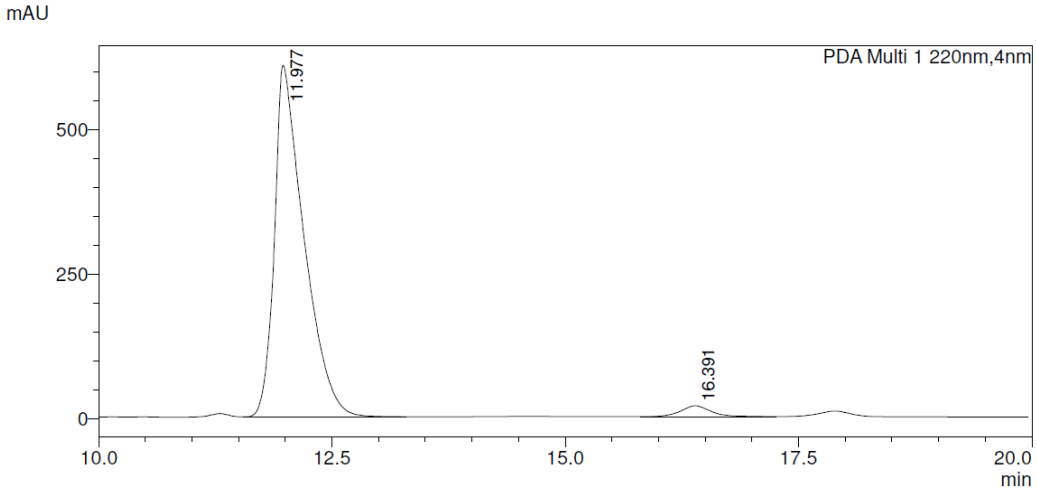

PDA Ch1 220nm

Peak#	Ret. Time	Area	Area%	Height	Height%
1	11.977	13436560	96.977	607738	97.015
2	16.391	418880	3.023	18700	2.985
Total		13855440	100.000	626438	100.000

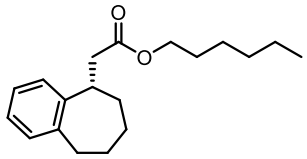

0.3%(95%hex, 5%EtOH, 0.2%TFA, 0.1%DEA), 99.7% hexanes, 0.8ml/min, CHIRALPAK IA-3

98.1:1.9 e.r.

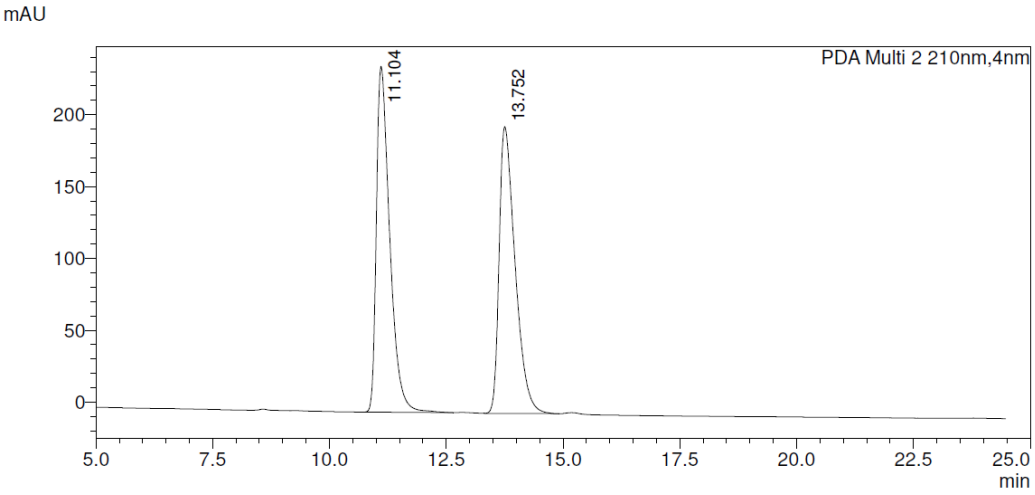

PDA Ch2 210nm

Peak#	Ret. Time	Area	Height	Area%
1	11.104	4786878	240525	50.223
2	13.752	4744335	199572	49.777
Total		9531213	440096	100.000

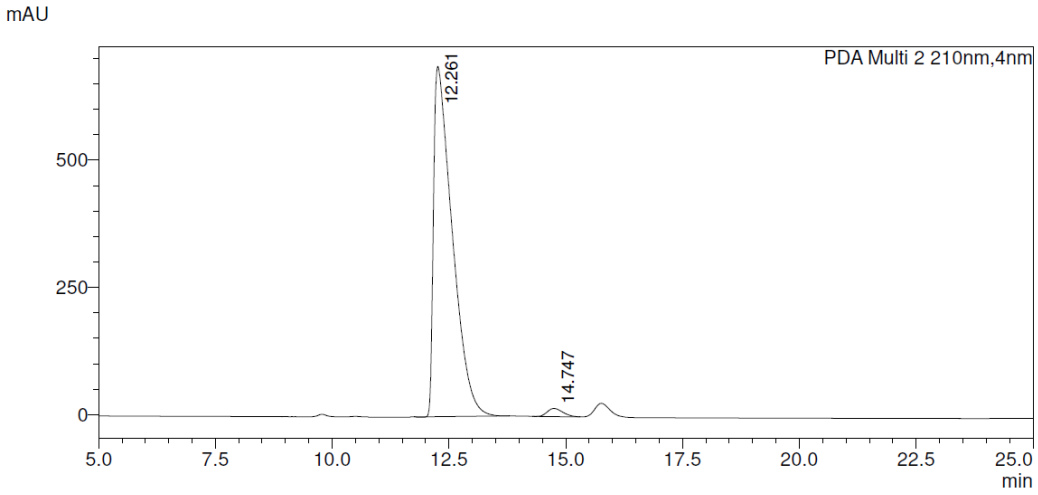

PDA Ch2 210nm

Peak#	Ret. Time	Area	Height	Area%
1	12.261	19173915	688179	98.073
2	14.747	376728	16244	1.927
Total		19550644	704422	100.000

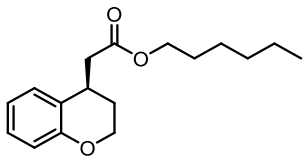

0.3%THF/Hex, 0.8 mL/min, CHIRALPAK IB-3

96.7:3.3 e.r.

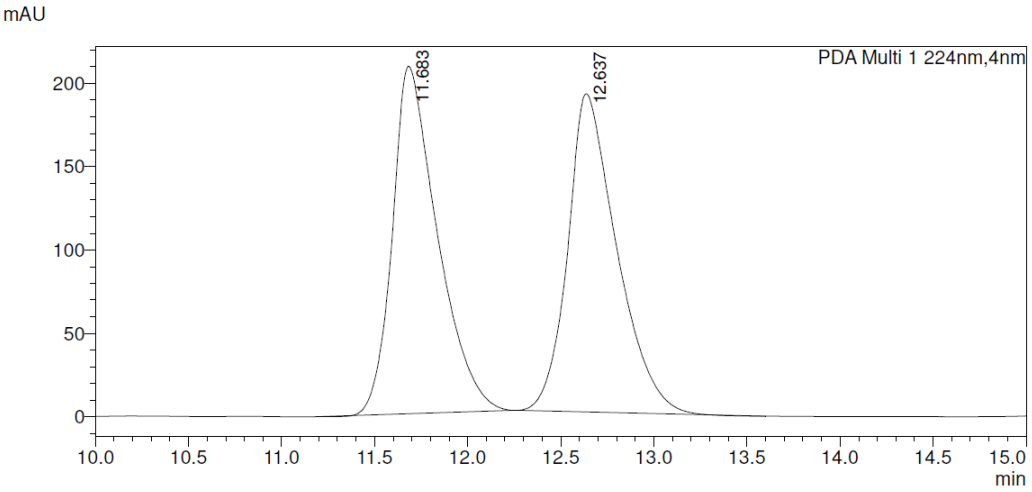

PDA Ch1 224nm

Peak#	Ret. Time	Area	Area%	Height	Height%
1	11.683	3507435	50.079	208320	52.195
2	12.637	3496379	49.921	190801	47.805
Total		7003813	100.000	399121	100.000

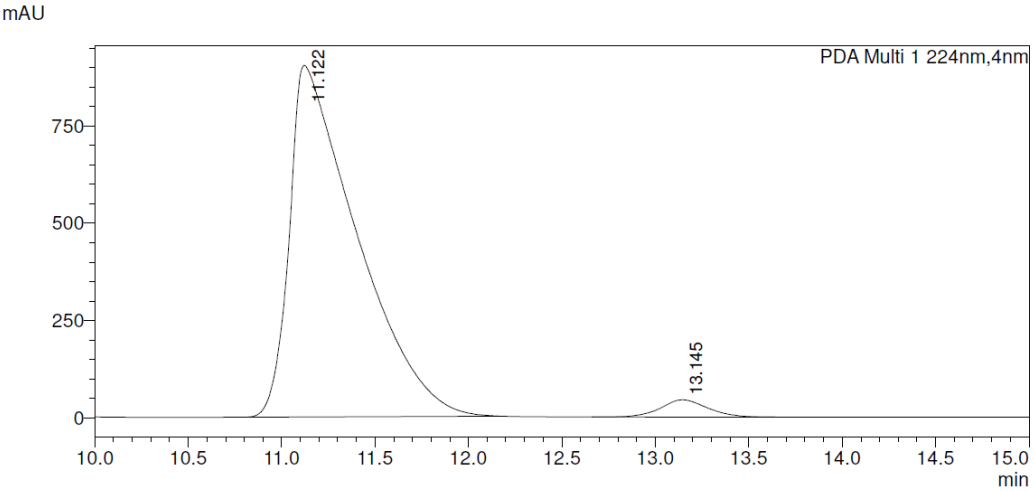

PDA Ch1 224nm

Peak#	Ret. Time	Area	Area%	Height	Height%
1	11.122	22729071	96.692	902909	95.315
2	13.145	777618	3.308	44379	4.685
Total		23506689	100.000	947288	100.000

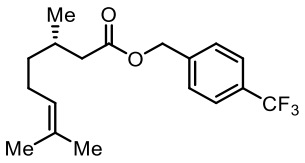

Saponified to citronellic acid, 1%(0.2%TFA/0.1%DEA/5%THF/Hex)/0.3%IPA/Hex, CHIRALPAK IC-3, **96.5:3.5 e.r.**

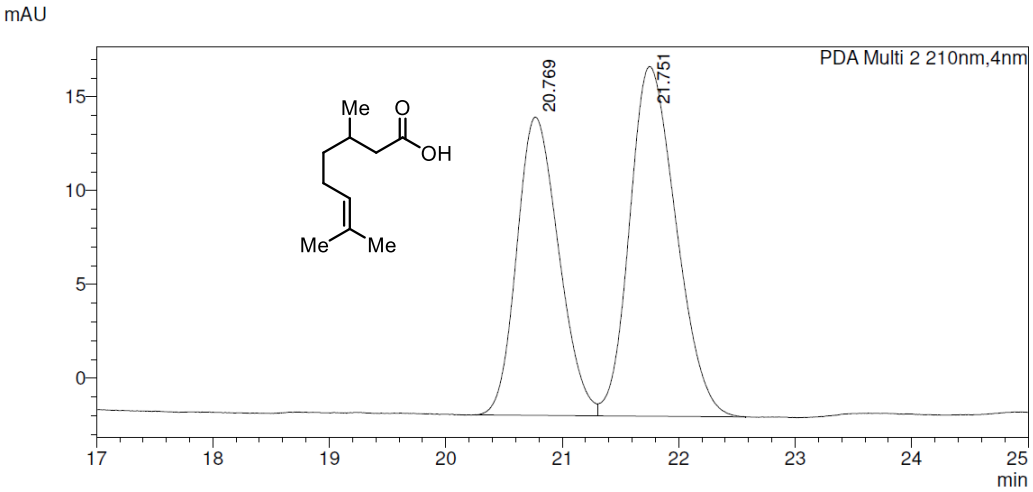

PDA Ch2 210nm

Peak#	Ret. Time	Area	Area%	Height	Height%
1	20.769	398717	43.456	15904	46.029
2	21.751	518801	56.544	18649	53.971
Total		917518	100.000	34553	100.000

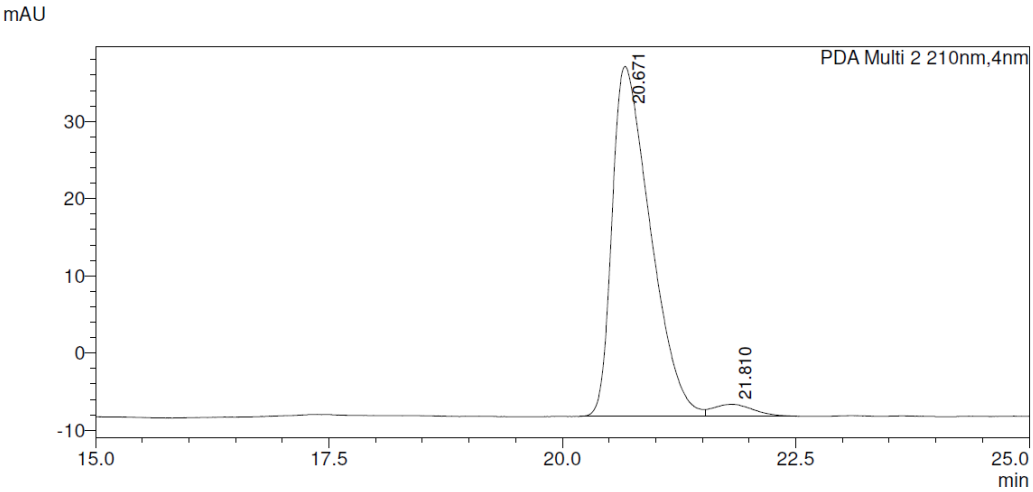

PDA Ch2 210nm

Peak#	Ret. Time	Area	Area%	Height	Height%
1	20.671	1295084	96.489	45343	96.675
2	21.810	47130	3.511	1559	3.325
Total		1342214	100.000	46902	100.000

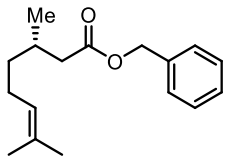

Saponified to citronellic acid, 1%(0.2%TFA/0.1%DEA/5%THF/Hex)/0.3%IPA/Hex,

CHIRALPAK IC-3, **96.6:3.4 e.r.**

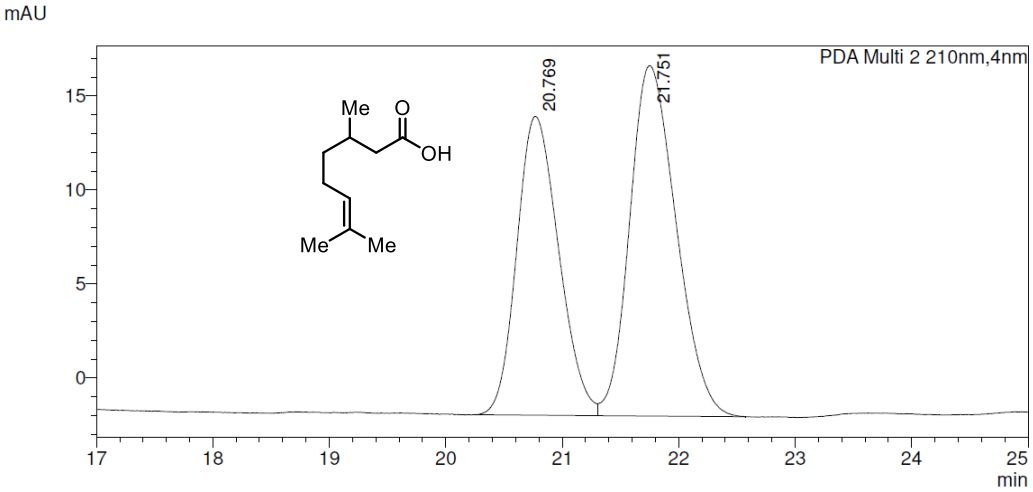

PDA Ch2 210nm

Peak#	Ret. Time	Area	Area%	Height	Height%
1	20.769	398717	43.456	15904	46.029
2	21.751	518801	56.544	18649	53.971
Total		917518	100.000	34553	100.000

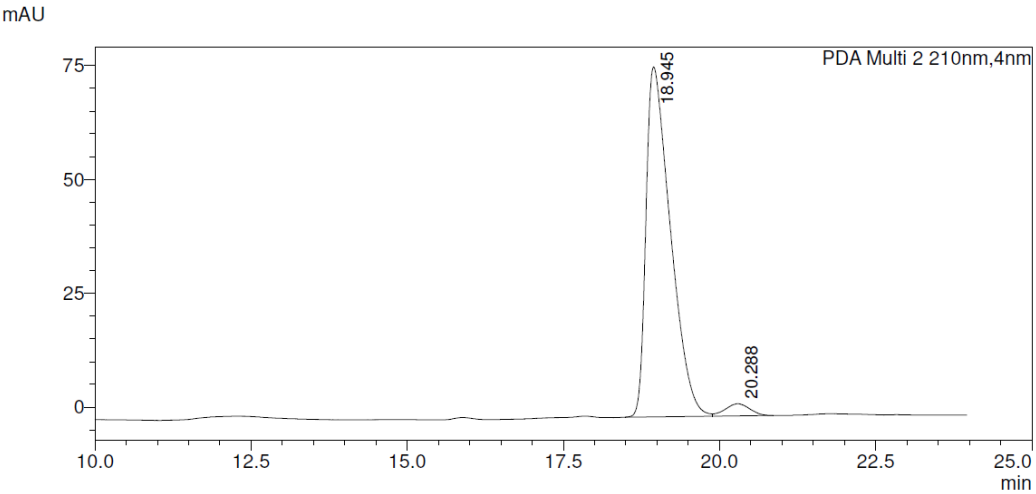

PDA Ch2 210nm

Peak#	Ret. Time	Area	Area%	Height	Height%
1	18.945	2087235	96.620	76769	96.643
2	20.288	73026	3.380	2667	3.357
Total		2160261	100.000	79436	100.000

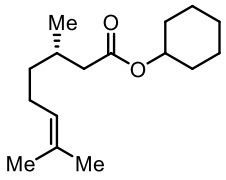

Saponified to citronellic acid, 1%(0.2%TFA/0.1%DEA/5%THF/Hex)/0.3%IPA/Hex,

CHIRALPAK IC-3, **95.7:4.3 e.r.**

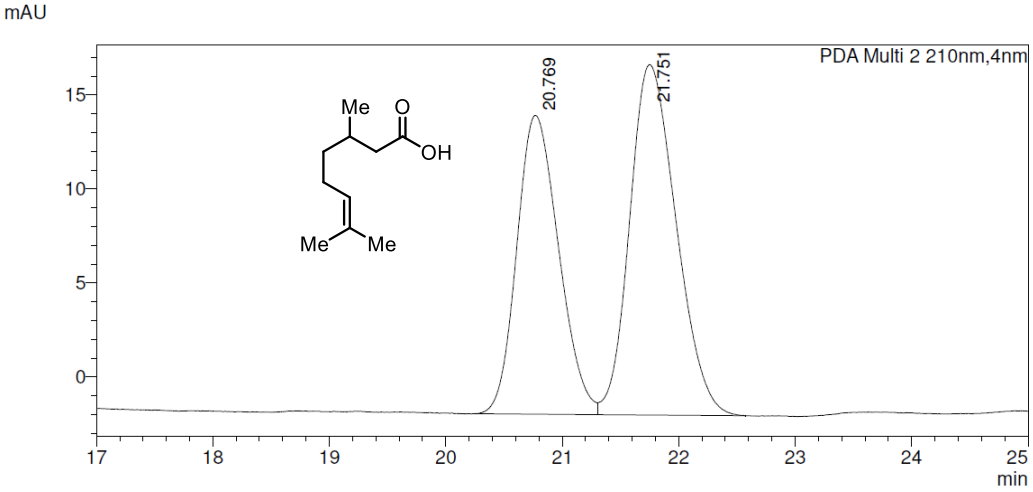

PDA Ch2 210nm

Peak#	Ret. Time	Area	Area%	Height	Height%
1	20.769	398717	43.456	15904	46.029
2	21.751	518801	56.544	18649	53.971
Total		917518	100.000	34553	100.000

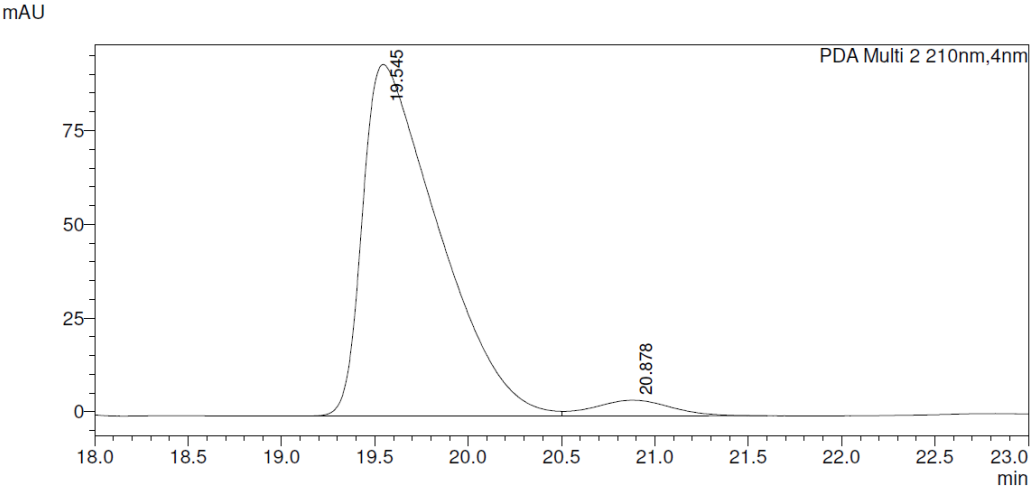

PDA Ch2 210nm

Peak#	Ret. Time	Area	Area%	Height	Height%
1	19.545	2656751	95.657	93715	95.698
2	20.878	120620	4.343	4213	4.302
Total		2777371	100.000	97928	100.000

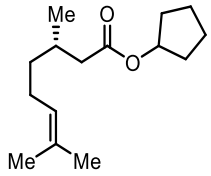

Saponified to citronellic acid, 1%(0.2%TFA/0.1%DEA/5%THF/Hex)/0.3%IPA/Hex, CHIRALPAK IC-3, **96.1:3.9 e.r.**

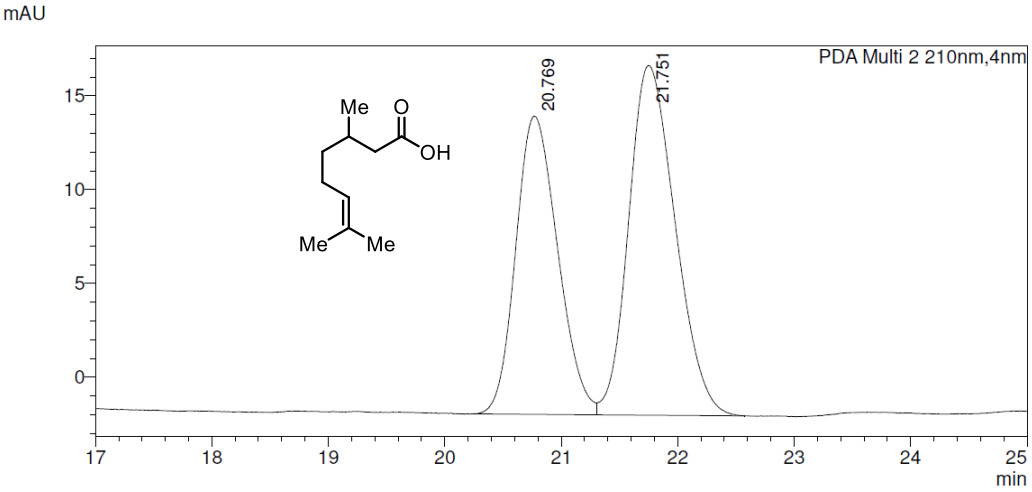

PDA Ch2 210nm

Peak#	Ret. Time	Area	Area%	Height	Height%
1	20.769	398717	43.456	15904	46.029
2	21.751	518801	56.544	18649	53.971
Total		917518	100.000	34553	100.000

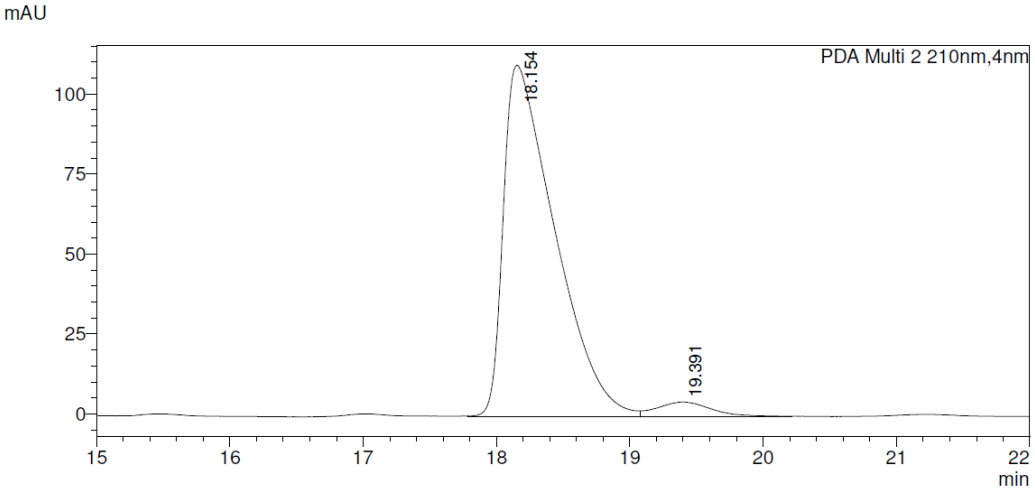

PDA Ch2 210nm

Peak#	Ret. Time	Area	Area%	Height	Height%
1	18.154	2940043	95.988	109630	96.128
2	19.391	122869	4.012	4415	3.872
Total		3062912	100.000	114045	100.000

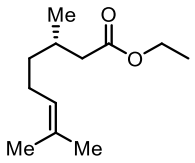

Saponified to citronellic acid, 1%(0.2%TFA/0.1%DEA/5%THF/Hex)/0.3%IPA/Hex, CHIRALPAK IC-3, **97.9:2.1 e.r.**

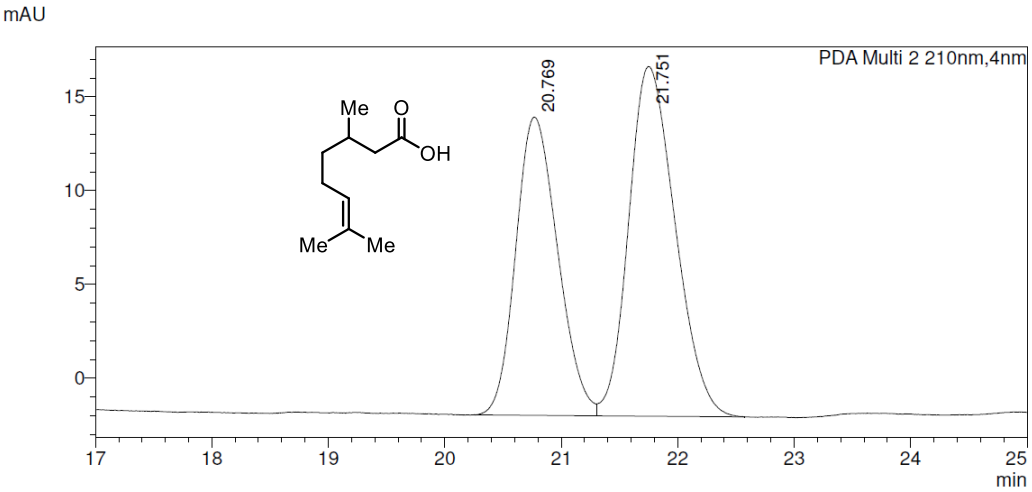

PDA Ch2 210nm

Peak#	Ret. Time	Area	Area%	Height	Height%
1	20.769	398717	43.456	15904	46.029
2	21.751	518801	56.544	18649	53.971
Total		917518	100.000	34553	100.000

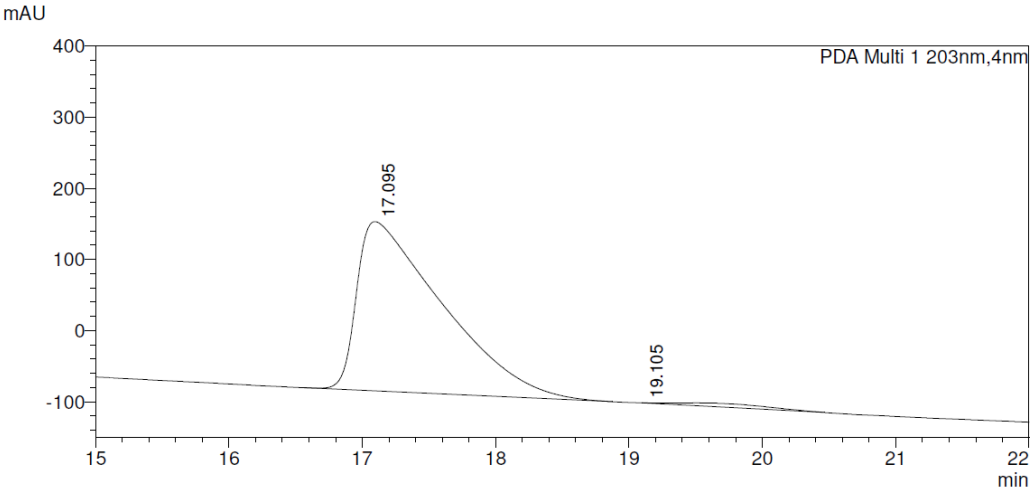

PDA Ch1 203nm

Peak#	Ret. Time	Area	Area%	Height	Height%
1	17.095	10613495	97.874	237961	99.976
2	19.105	230590	2.126	57	0.024
Total		10844085	100.000	238018	100.000

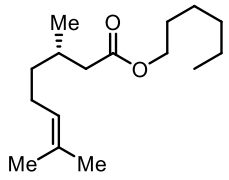

Saponified to citronellic acid, 1%(0.2%TFA/0.1%DEA/5%THF/Hex)/0.3%IPA/Hex, CHIRALPAK IC-3, **96.5:3.5 e.r.**

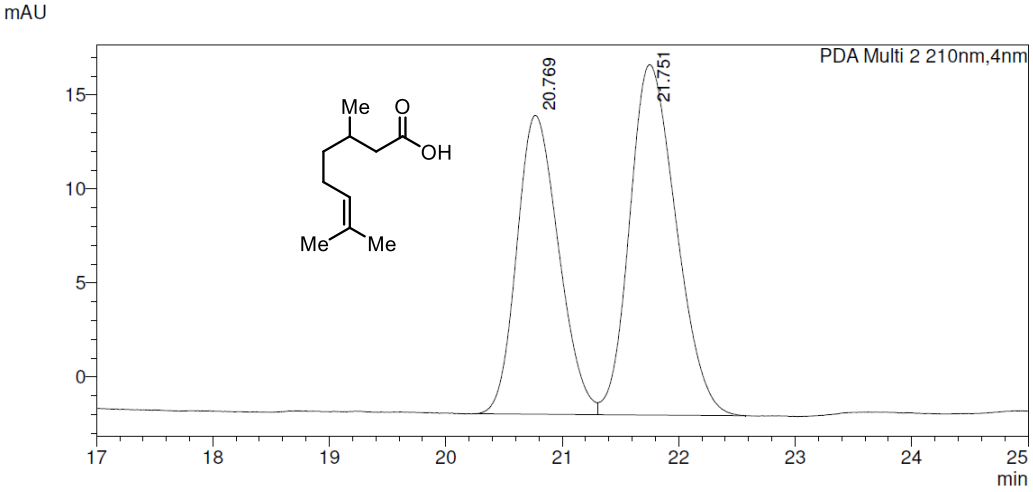

PDA Ch2 210nm

Peak#	Ret. Time	Area	Area%	Height	Height%
1	20.769	398717	43.456	15904	46.029
2	21.751	518801	56.544	18649	53.971
Total		917518	100.000	34553	100.000

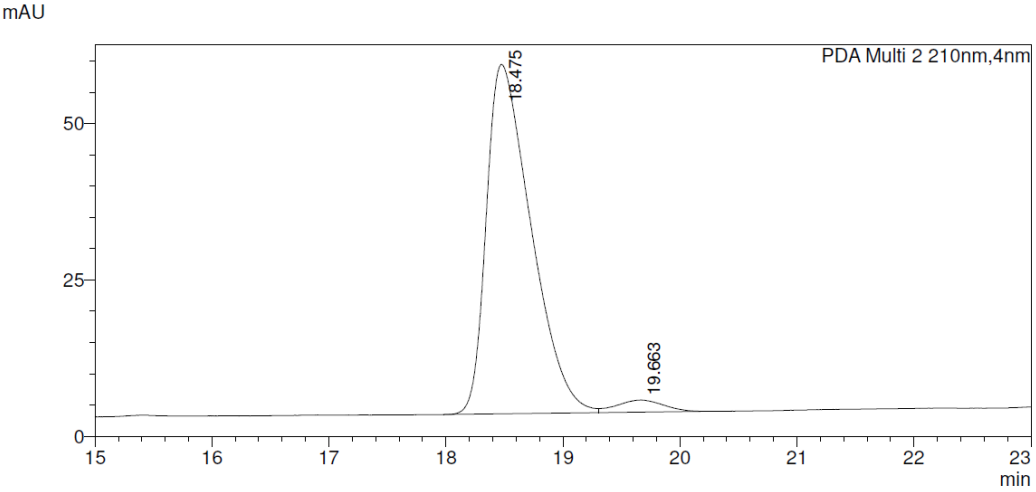

PDA Ch2 210nm

Peak#	Ret. Time	Area	Area%	Height	Height%
1	18.475	1482133	96.509	55810	96.665
2	19.663	53606	3.491	1926	3.335
Total		1535739	100.000	57736	100.000

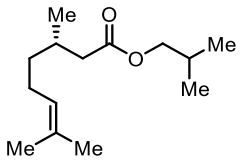

Saponified to citronellic acid, 1%(0.2%TFA/0.1%DEA/5%THF/Hex)/0.3%IPA/Hex, CHIRALPAK IC-3, **96.7:3.3 e.r.**

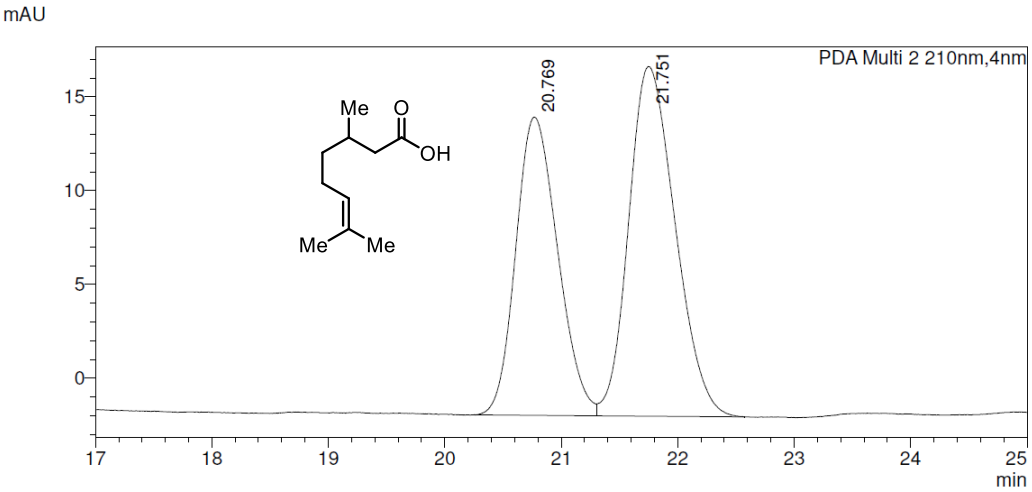

PDA Ch2 210nm

Peak#	Ret. Time	Area	Area%	Height	Height%
1	20.769	398717	43.456	15904	46.029
2	21.751	518801	56.544	18649	53.971
Total		917518	100.000	34553	100.000

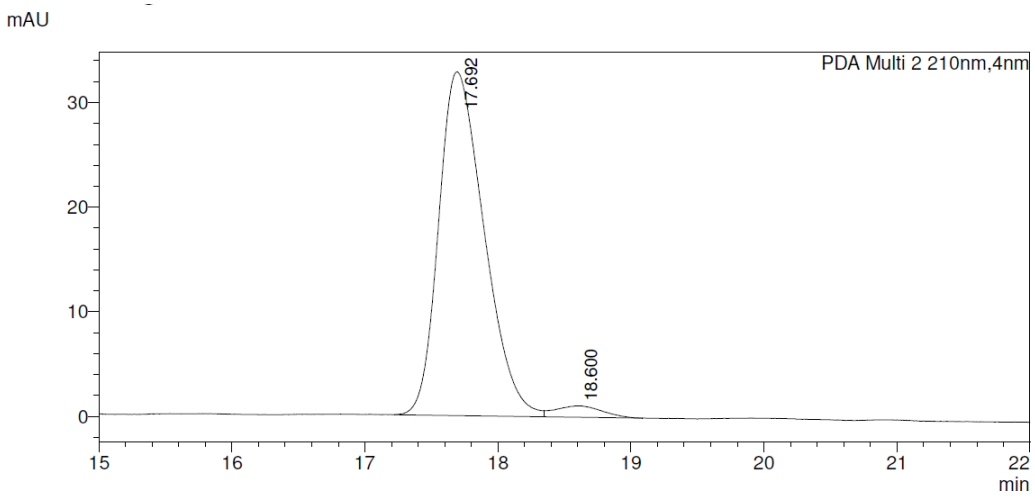

PDA Ch2 210nm

Peak#	Ret. Time	Area	Area%	Height	Height%
1	17.692	780574	96.700	32842	96.818
2	18.600	26636	3.300	1079	3.182
Total		807210	100.000	33921	100.000

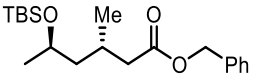

0.5%(0.2%TFA/0.1%DEA/5%THF/Hex)/0.3%IPA/Hex, CHIRALPAK IC-3

98.2:1.8 e.r.

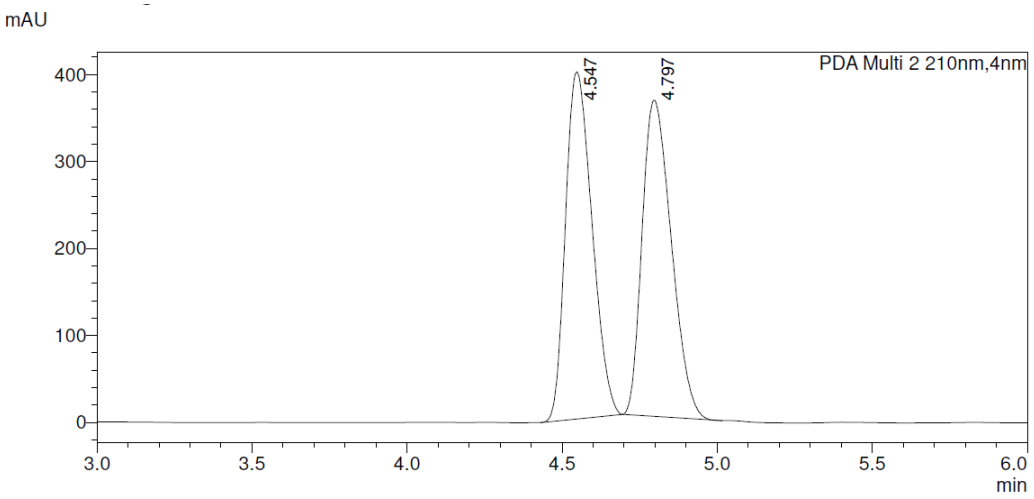

PDA Ch2 210nm

Peak#	Ret. Time	Area	Area%	Height	Height%
1	4.547	2373587	49.953	397759	52.286
2	4.797	2378047	50.047	362980	47.714
Total		4751634	100.000	760739	100.000

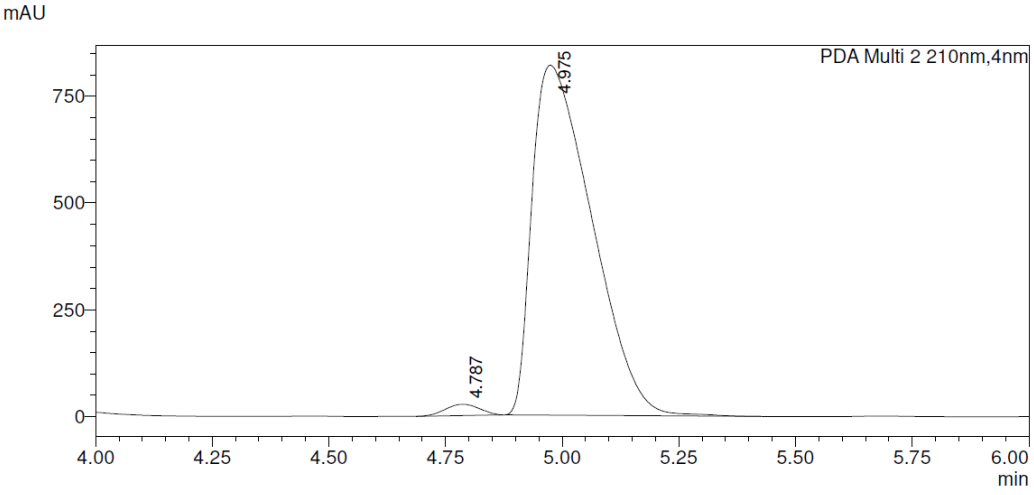

PDA Ch2 210nm

Peak#	Ret. Time	Area	Area%	Height	Height%
1	4.787	136020	1.825	26582	3.145
2	4.975	7318250	98.175	818552	96.855
Total		7454270	100.000	845134	100.000

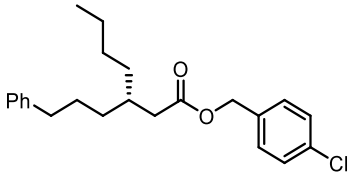

Saponified to carboxylic acid, **97.6:2.4 e.r.**

60%[1%(0.2%TFA/0.1%DEA/5%THF/Hex)/0.3%IPA/Hex]/40%Hex, CHIRALPAK IA-3

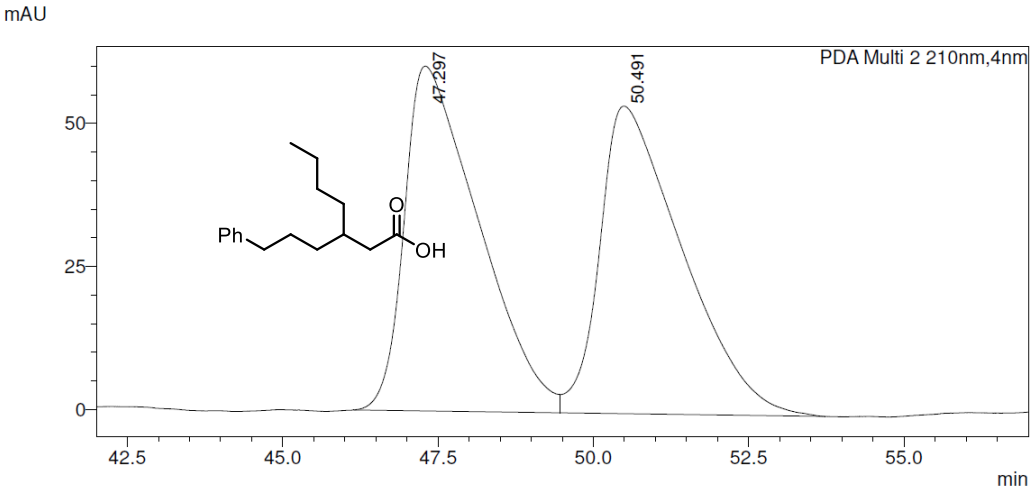

PDA Ch2 210nm

Peak#	Ret. Time	Area	Area%	Height	Height%
1	47.297	5024968	50.244	60259	52.849
2	50.491	4976235	49.756	53763	47.151
Total		10001202	100.000	114022	100.000

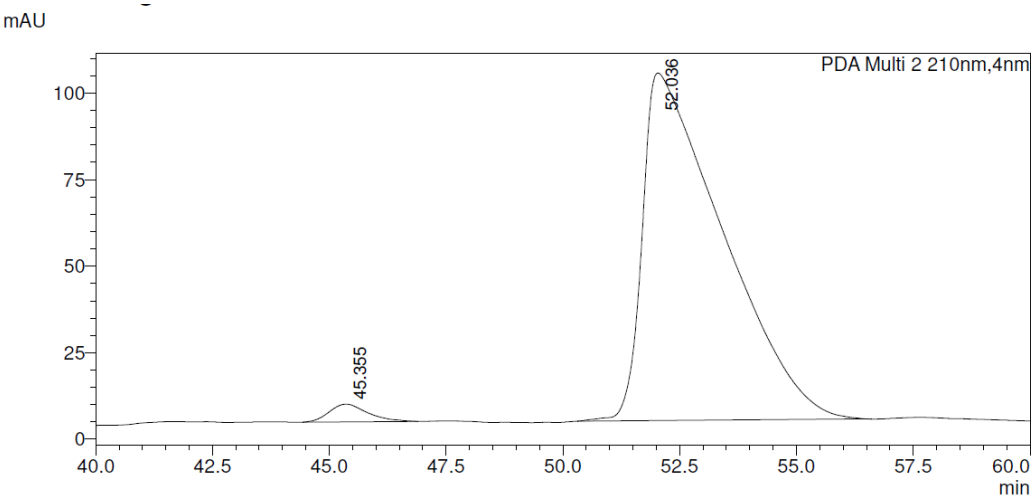

PDA Ch2 210nm

Peak#	Ret. Time	Area	Area%	Height	Height%
1	45.355	292202	2.375	5121	4.858
2	52.036	12013123	97.625	100287	95.142
Total		12305325	100.000	105408	100.000

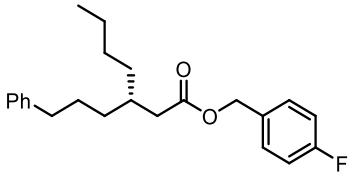

Saponified to carboxylic acid, **99.7:0.3 e.r.**

60%[1%(0.2%TFA/0.1%DEA/5%THF/Hex)/0.3%IPA/Hex]/40%Hex, CHIRALPAK IA-3

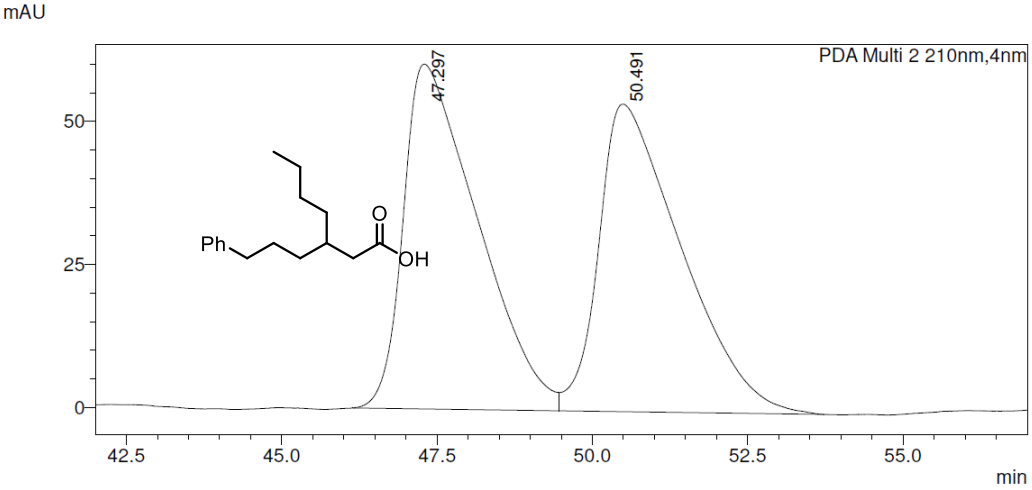

PDA Ch2 210nm

Peak#	Ret. Time	Area	Area%	Height	Height%
1	47.297	5024968	50.244	60259	52.849
2	50.491	4976235	49.756	53763	47.151
Total		10001202	100.000	114022	100.000

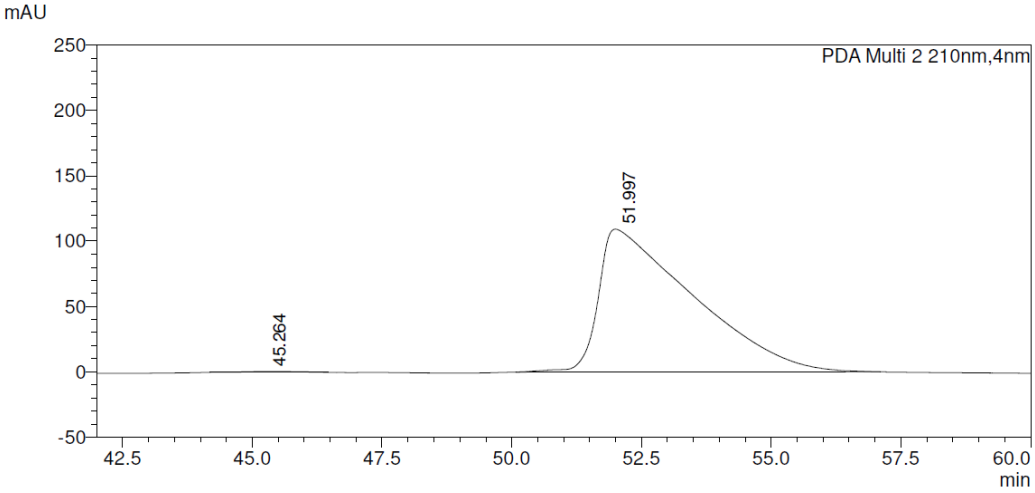

PDA Ch2 210nm

Peak#	Ret. Time	Area	Area%	Height	Height%
1	45.264	44358	0.320	596	0.542
2	51.997	13838175	99.680	109311	99.458
Total		13882534	100.000	109907	100.000

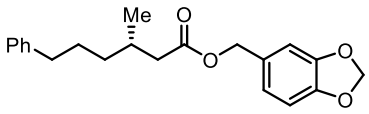

2.5%(0.2%TFA/0.1%DEA/5%EtOH/Hex)97.5%Hex, CHIRALPAK IC-3

97.7:2.3 e.r.

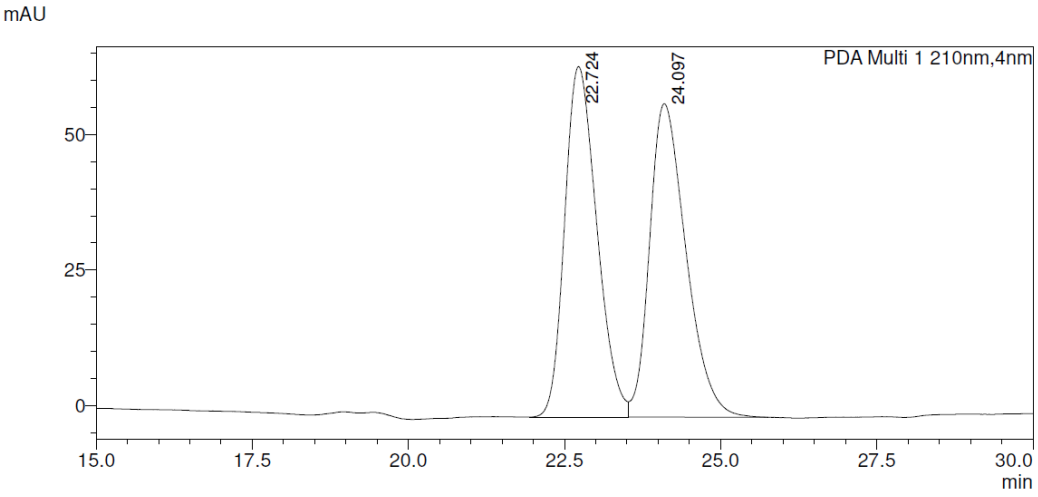

PDA Ch1 210nm

Peak#	Ret. Time	Area	Area%	Height	Height%
1	22.724	2320117	49.725	64589	52.785
2	24.097	2345734	50.275	57773	47.215
Total		4665851	100.000	122362	100.000

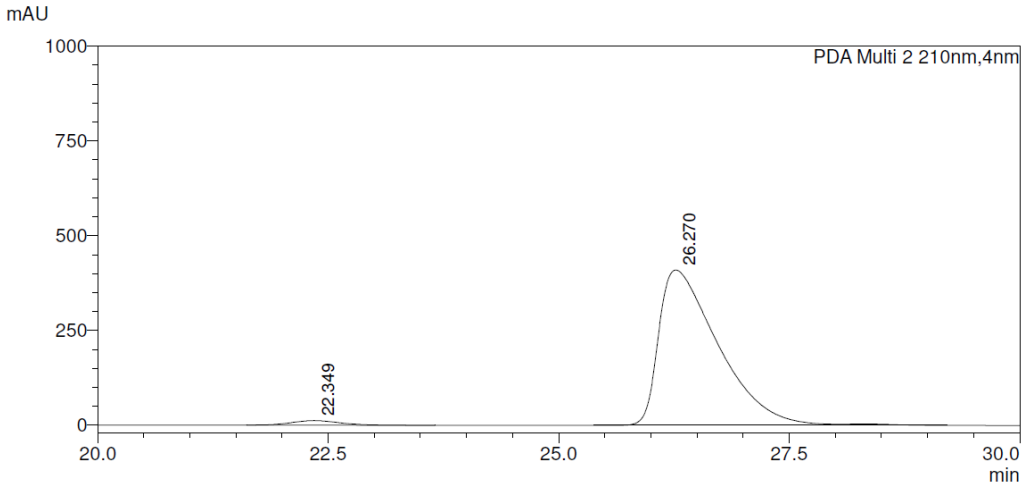

PDA Ch2 210nm

Peak#	Ret. Time	Area	Area%	Height	Height%
1	22.349	429953	2.271	11863	2.813
2	26.270	18499587	97.729	409831	97.187
Total		18929540	100.000	421694	100.000

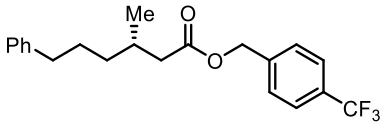

0.3%(0.2%TFA/0.1%DEA/5%EtOH/Hex)/99.7%Hex, CHIRALPAK IC-3

95.3:4.7 e.r.

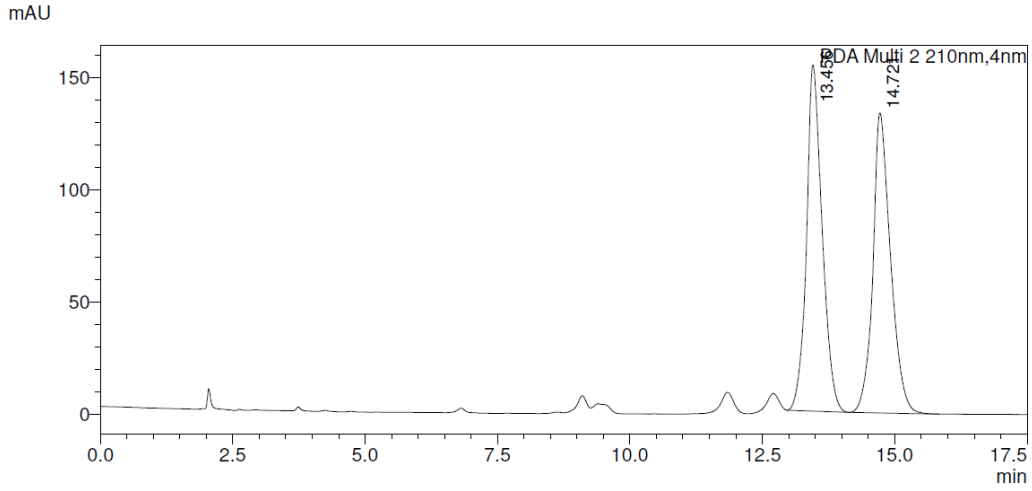

PDA Ch2 210nm

Peak#	Ret. Time	Area	Area%	Height	Height%
1	13.456	3185332	50.593	154362	53.576
2	14.721	3110651	49.407	133756	46.424
Total		6295984	100.000	288118	100.000

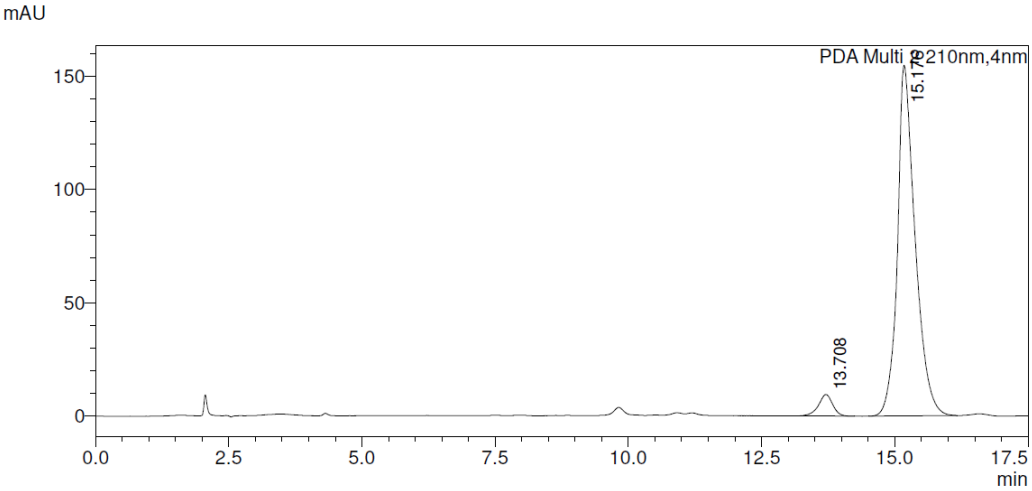

PDA Ch2 210nm

Peak#	Ret. Time	Area	Area%	Height	Height%
1	13.708	175854	4.684	9467	5.770
2	15.176	3578364	95.316	154600	94.230
Total		3754218	100.000	164068	100.000

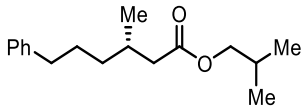

0.3%THF/Hex, CHIRALPAK IC-3

99.4:0.6 e.r.

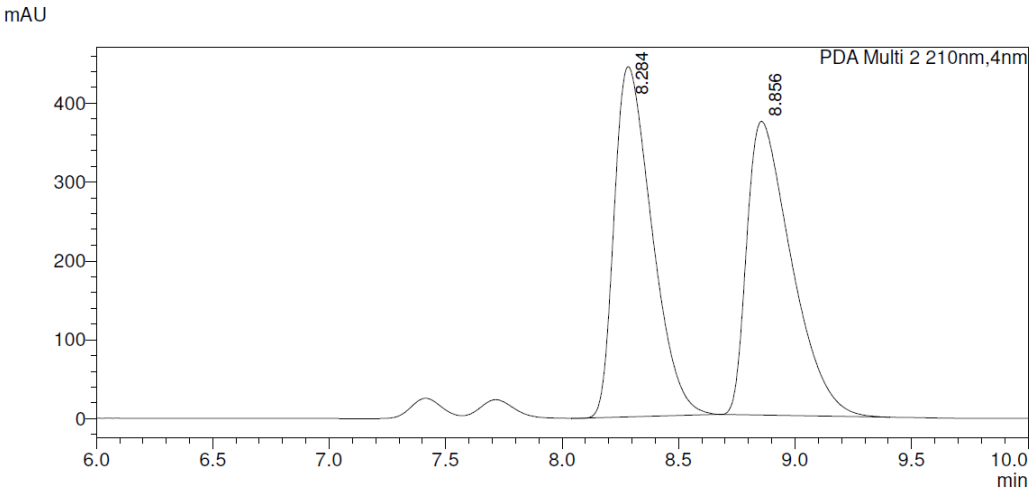

PDA Ch2 210nm

Peak#	Ret. Time	Area	Area%	Height	Height%
1	8.284	4997191	50.160	443719	54.389
2	8.856	4965409	49.840	372100	45.611
Total		9962600	100.000	815819	100.000

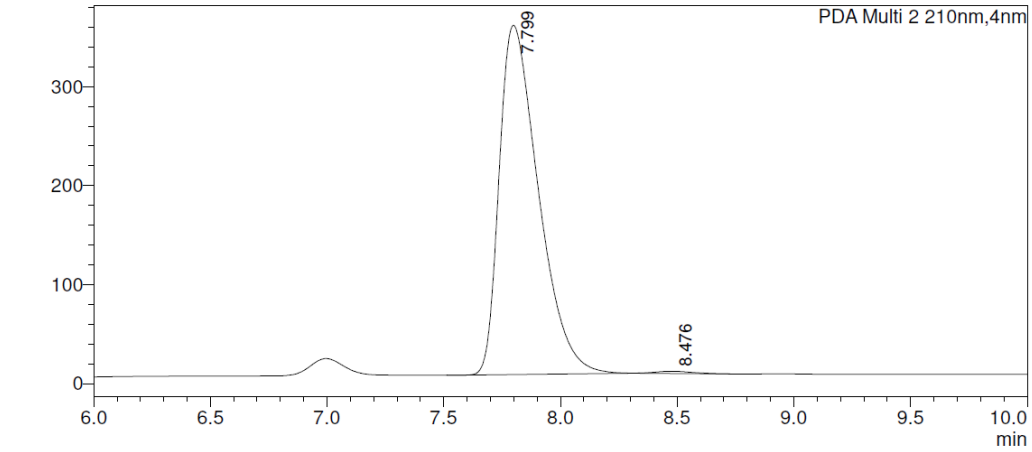

PDA Ch2 210nm

Peak#	Ret. Time	Area	Area%	Height	Height%
1	7.799	4124964	99.433	352563	99.399
2	8.476	23521	0.567	2133	0.601
Total		4148485	100.000	354696	100.000

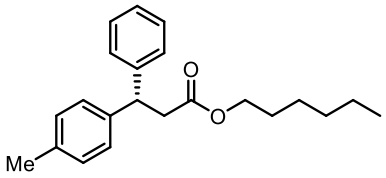

0.3%THF/Hex, 0.8 mL/min, CHIRALCEL O*J*-H

95.6:4.4 e.r.

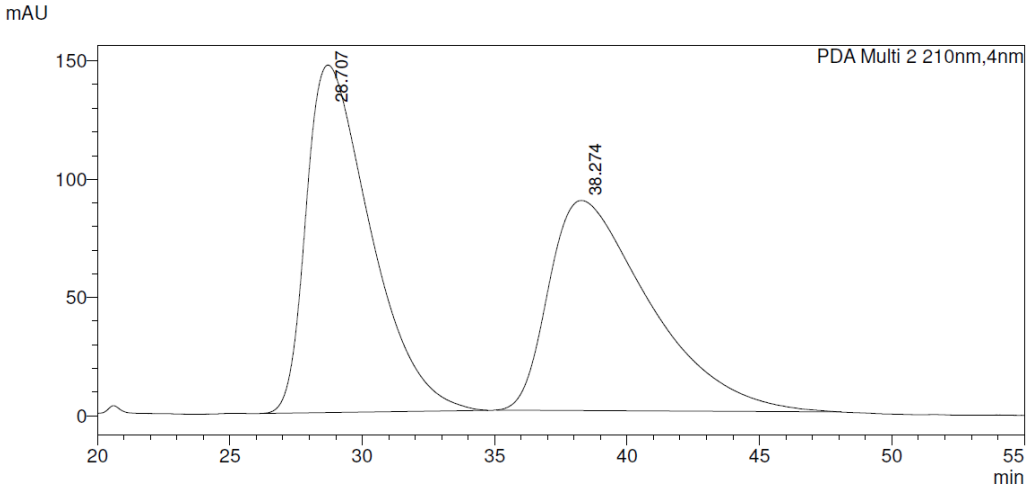

PDA Ch2 210nm

Peak#	Ret. Time	Area	Area%	Height	Height%
1	28.707	24896177	51.327	146884	62.319
2	38.274	23609238	48.673	88814	37.681
Total		48505415	100.000	235698	100.000

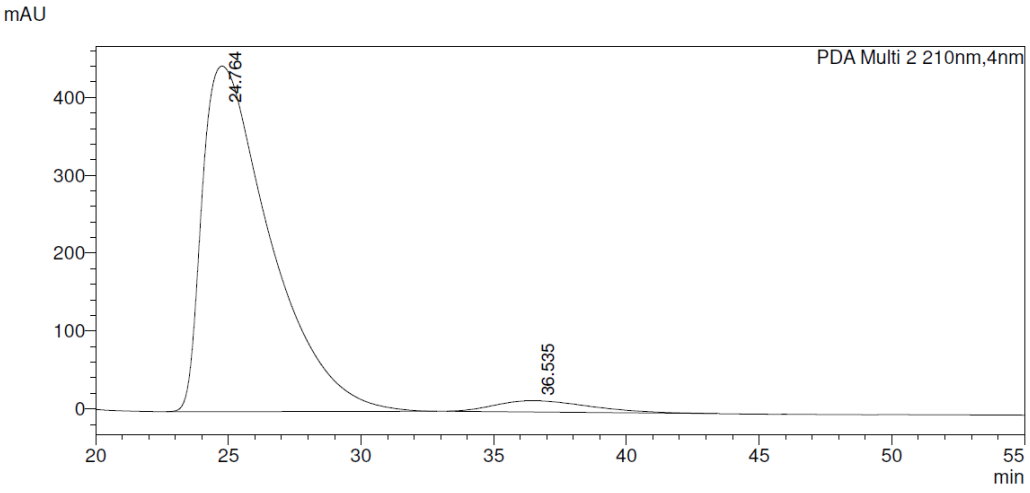

PDA Ch2 210nm

Peak#	Ret. Time	Area	Area%	Height	Height%
1	24.764	79183178	95.638	443657	96.817
2	36.535	3611696	4.362	14585	3.183
Total		82794873	100.000	458242	100.000

3.9 Allylic Amine Synthesis and Characterization

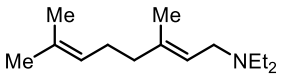

(*E*)-N,N-diethyl-3,7-dimethylocta-2,6-dien-1-amine

Synthesized according to literature precedent.[1]

^{1}H NMR (500 MHz, $CDCl_3$) δ 5.28 – 5.21 (m, 1H), 5.08 (tt, *J* = 6.9, 1.5 Hz, 1H), 3.05 (d, *J* = 6.9 Hz, 2H), 2.51 (q, *J* = 7.2 Hz, 4H), 2.09 (q, *J* = 7.4 Hz, 2H), 2.05 – 1.99 (m, 2H), 1.67 (s, 3H), 1.63 (s, 3H), 1.59 (s, 3H), 1.03 (t, *J* = 7.1 Hz, 6H).

^{13}C NMR (126 MHz, $CDCl_3$) δ 137.73, 131.57, 124.38, 121.99, 50.71, 46.81, 39.99, 26.59, 25.85, 17.82, 16.44, 11.98.

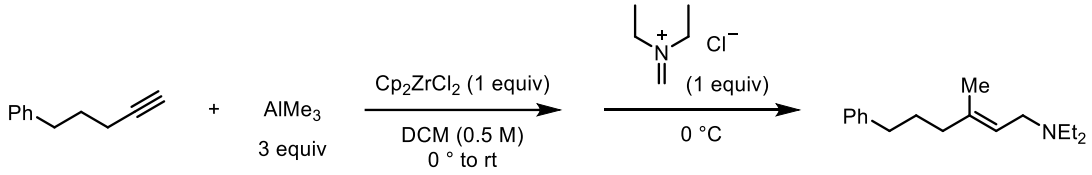

(*E*)-N,N-diethyl-3-methyl-6-phenylhex-2-en-1-amine: Zircocene dichloride (5.80 g, 20.0 mmol, 1.0 equiv) was added to a dry 250-mL round-bottomed flask under N_2 atmosphere followed by 40 mL dry methylene chloride. The mixture was cooled to 0 °C with stirring. Trimethylaluminum (2 M in Hexanes) (30 mL, 60.0 mmol, 3.0 equiv) was added slowly *via* syringe. The reaction mixture stirred at 0 °C for 10 min. The reaction mixture turned yellow after stirring. 5-phenyl-1-pentyne (3.0 mL, 20.0 mmol) was then added to the reaction mixture *via* syringe. After addition of the alkyne, the flask was warmed to rt and stirred overnight. The reaction flask was cooled to 0 °C followed by addition of *N*-ethyl-*N*-methyleneethanaminium chloride (2.42 g, 20 mmol, 1.0 equiv) in 10 mL dry methylene chloride (*N*-ethyl-*N*-methyleneethanaminium chloride solution was made in a N_2 glovebox). The reaction mixture stirred for an additional 2.5 h, after which it was quenched at 0 °C with sat. NH_4Cl. The crude reaction mixture was filtered over celite. The filtrate was dried with anhydrous Na_2SO_4, filtered, and the solvent was removed *in vacuo*. The crude oil was purified

via flash column chromatography on silica gel with 1% MeOH/10% Et_2O/89% (3% NH_3/DCM). The product was then distilled at reduced pressure (106–108 °C at 0.176 Torr) to yield 1.45 g (33%) of a clear, colorless oil.

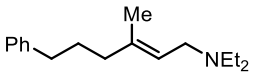

(*E*)-N,N-diethyl-3-methyl-6-phenylhex-2-en-1-amine $C_{17}H_{27}N$

^{1}H NMR (500 MHz, $CDCl_3$) δ 7.30 – 7.27 (m, 2H), 7.20 – 7.15 (m, 3H), 5.29 (tq, *J* = 6.8, 1.3 Hz, 1H), 3.07 (d, *J* = 6.8 Hz, 2H), 2.61 – 2.56 (m, 2H), 2.51 (q, *J* = 7.2 Hz, 4H), 2.06 (t, *J* = 7.5 Hz, 2H), 1.79 – 1.71 (m, 2H), 1.64 (s, 3H), 1.03 (t, *J* = 7.2 Hz, 6H).

^{13}C NMR (126 MHz, $CDCl_3$) δ 142.78, 137.61, 128.56, 128.39, 125.77, 122.18, 50.67, 46.85, 39.57, 35.65, 29.73, 16.42, 12.00.

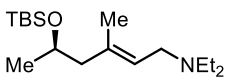

(*R*,*E*)-5-((tert-butyldimethylsilyl)oxy)-N,N-diethyl-3-methylhex-2-en-1-amine $C_{17}H_{37}NOSi$

Synthesized according to literature precedent.[1]

^{1}H NMR (500 MHz, $CDCl_3$) δ 5.28 (td, *J* = 6.6, 1.5 Hz, 1H), 3.93 (dt, *J* = 6.9, 5.9 Hz, 1H), 3.06 (d, *J* = 6.8 Hz, 2H), 2.51 (q, *J* = 7.1 Hz, 4H), 2.22 (dd, *J* = 13.1, 6.0 Hz, 1H), 2.06 (dd, *J* = 13.1, 6.8 Hz, 1H), 1.65 (s, 3H), 1.10 (d, *J* = 6.0 Hz, 3H), 1.03 (t, *J* = 7.2 Hz, 6H), 0.88 (s, 9H), 0.04 (d, *J* = 7.4 Hz, 6H).

^{13}C NMR (126 MHz, $CDCl_3$) δ 135.12, 124.68, 67.64, 50.67, 50.42, 46.86, 26.02, 23.57, 18.31, 17.16, 11.95, -4.40, -4.63.

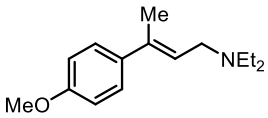

(*E*)-*N*,*N*-diethyl-3-(4-methoxyphenyl)but-2-en-1-amine $C_{15}H_{23}NO$

Synthesized according to literature precedent.[1]

^{1}H NMR (500 MHz, $CDCl_3$) δ 7.36 – 7.33 (m, 2H), 6.87 – 6.83 (m, 2H), 5.86 – 5.80 (m, 1H), 3.81 (s, 3H), 3.26 (dd, *J* = 6.7, 1.0 Hz, 2H), 2.58 (q, *J* = 7.1 Hz, 4H), 2.04 (s, 3H), 1.07 (t, *J* = 7.1 Hz, 6H).

^{13}C NMR (126 MHz, $CDCl_3$) δ 158.76, 136.23, 136.01, 126.80, 124.29, 113.68, 55.44, 51.53, 47.14, 16.24, 12.06.

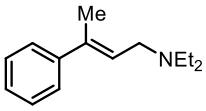

(*E*)-N,N-diethyl-3-phenylbut-2-en-1-amine $C_{14}H_{21}N$

Synthesized according to literature precedent.[1]

^{1}H NMR (500 MHz, $CDCl_3$) δ 7.43 – 7.39 (m, 2H), 7.34 – 7.29 (m, 2H), 7.25 – 7.21 (m, 1H), 5.91 (tq, *J* = 6.6, 1.4 Hz, 1H), 3.28 (dd, *J* = 6.6, 1.0 Hz, 2H), 2.58 (q, *J* = 7.2 Hz, 4H), 2.07 (d, *J* = 1.2 Hz, 3H), 1.07 (t, *J* = 7.1 Hz, 6H).

^{13}C NMR (126 MHz, $CDCl_3$) δ 143.68, 136.65, 128.33, 126.92, 125.95, 125.79, 51.53, 47.19, 16.23, 12.08.

Allylic diethylamine substrate **1v** was synthesized by the following method and the starting vinyl bromide was synthesized according to our previous report.[1]

Procedure: To a 50-ml round bottomed flask charged with a stir bar under inert atmosphere was added $Pd(OAc)_2$ (11 mg, 0.050 mmol, 1.0 mol %), PPh_3 (26 mg, 0.10 mmol, 2.0 mol %), KOH (0.560 g, 10 mmol, 2.0 equiv), starting material vinyl bromide (1.34g, 5 mmol, 1.0 equiv), 4-methyl boronic acid (0.880 g, 6.5 mmol, 1.3 equiv), 5 mL THF and 5 mL MeOH. The reaction was stirred at rt overnight followed by dilution with EtOAc, and washed by 1N NaOH solution

[1]Wu, Z.; Laffoon, S. D.; Nguyen, T. T.; McAlpin, J. D.; Hull, K. L. "Rhodium-Catalyzed Asymmetric Synthesis of β-Branched Amides," *Angew. Chem. Int. Ed.* **2017,** *56,* 1371-1375.

and brine. The organic lay was then dried over MgSO4, concentrated *in vacuo*, purified by Al_2O_3 column chromatography: 200 g Al_2O_3 + 12 g H_2O, 30 : 1 hexanes/ EtOAc with 0.5 % MeOH as eluent. The product was collected in 70% yield.

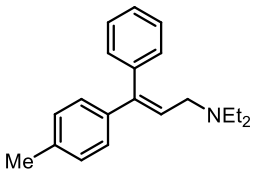

(*E*)-*N*,*N*-diethyl-3-phenyl-3-(p-tolyl)prop-2-en-1-amine $C_{20}H_{25}N$

^{1}H NMR (500 MHz, $CDCl_3$) δ 7.40 – 7.33 (m, 2H), 7.34 – 7.29 (m, 1H), 7.18 – 7.12 (m, 4H), 7.10 – 7.06 (m, 2H), 6.19 (t, *J* = 6.7 Hz, 1H), 3.15 (d, *J* = 6.8 Hz, 2H), 2.52 (q, *J* = 7.2 Hz, 4H), 2.32 (s, 3H), 0.96 (t, *J* = 7.1 Hz, 6H).

^{13}C NMR (126 MHz, $CDCl_3$) δ 143.24, 140.11, 139.65, 137.01, 129.97, 128.96, 128.21, 127.27, 127.15, 126.55, 51.86, 47.13, 21.20, 11.96.

Synthesized according the procedure cited for **1v**.

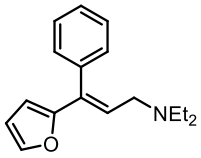

(*E*)-*N*,*N*-diethyl-3-(furan-2-yl)-3-phenylprop-2-en-1-amine $C_{17}H_{21}NO$

^{1}H NMR (500 MHz, $CDCl_3$) δ 7.41 – 7.32 (m, 4H), 7.25 – 7.22 (m, 2H), 6.40 (t, *J* = 7.0 Hz, 1H), 6.31 (dd, *J* = 3.3, 1.8 Hz, 1H), 5.80 (d, *J* = 3.3 Hz, 1H), 3.14 (d, *J* = 7.0 Hz, 2H), 2.52 (q, *J* = 7.1 Hz, 4H), 0.96 (t, *J* = 7.2 Hz, 6H).

^{13}C NMR (126 MHz, $CDCl_3$) δ 155.34, 142.06, 137.29, 133.58, 129.75, 128.25, 127.67, 124.13, 111.28, 108.14, 50.94, 47.02, 12.01.

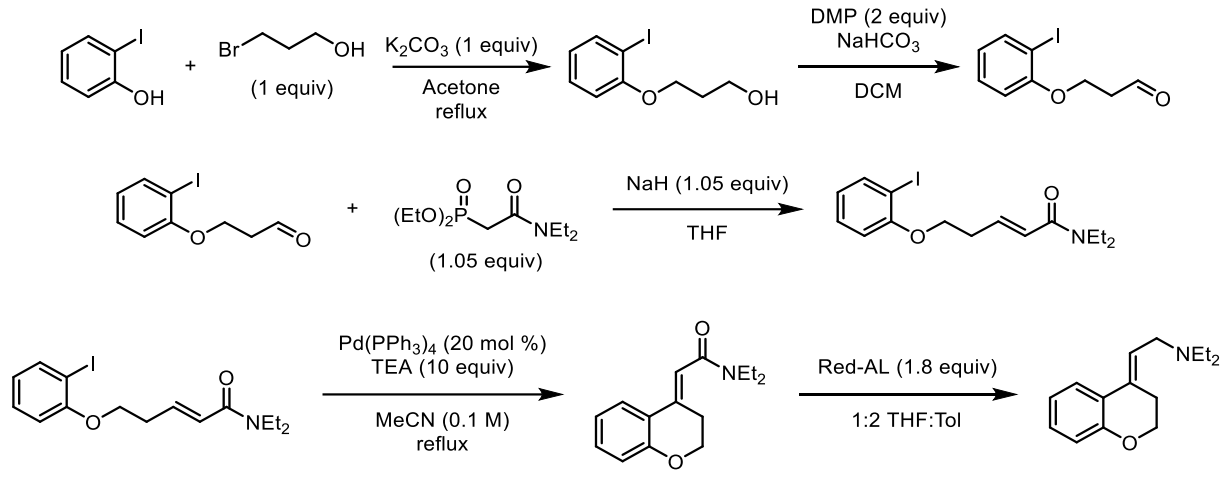

(*E*)-2-(chroman-4-ylidene)-*N*,*N*-diethylethan-1-amine: 2-iodophenol (4.4 g, 20 mmol), K_2CO_3 (2.8 g, 20 mmol, 1.0 equiv), **3-bromo-1-propanol** (1.8 mL, 20 mmol, 1.0 equiv), and acetone (20 mL) were added to a dried 250-mL round-bottomed flask equipped with a stir bar. A reflux condenser, and the reaction mixture was stirred at reflux overnight. The reaction flask was then cooled to room temperature. The crude reaction mixture was washed with DI H_2O and extracted with EtOAc. The aqueous layer was back-extracted with methylene chloride. The combined organic layers were dried over $MgSO_4$. The mixture was filtered to remove solids, and the solvent was removed *in vacuo*. The crude product was used without further purification.

A 500-mL round-bottomed flask with stir bar (not dried) was charged with **3-(2-iodophenoxy)propan-1-ol** (5.6 g, 20 mmol), $NaHCO_3$ (4 g, 47.6 mmol, 2.4 equiv), and wash bottle grade methylene chloride (100 mL). The reaction mixture was cooled to 0 °C with stirring. Dess-Martin periodinane (17 g, 40 mmol, 2.0 equiv) was added to the stirring reaction mixture in one portion, and the reaction continued stirring for 2.5 h. The reaction mixture was warmed to room temperature and filtered over a bed of celite. The filtrate was washed with sat. $NaHCO_3$. The combined aqueous layers were extracted with methylene chloride. The combined organic layers were dried over Na_2SO_4, filtered, and the solvent was removed *in vacuo*. The crude product was

purified *via* flash column chromatography over silica gel with 10% to 20% to 30% EtOAc/Hex. The product was obtained as an orange oil (4.2 g, 76% yield).

A 250-mL round-bottomed flask was equipped with a magnetic stir bar and dried. NaH (60% dispersion in mineral oil) (0.63 g, 15.75 mmol, 1.05 equiv) was added to the flask and then placed under N_2 atmosphere. Dry THF (25 mL) was added to the flask *via* syringe. The reaction flask was then cooled to 0 °C. **Diethyl (2-(diethylamino)-2-oxoethyl)phosphonate** was added dropwise *via* syringe. The reaction mixture was stirred until clear. **3-(2-iodophenoxy)propanal** was then added to the reaction flask and stirred overnight while slowly warming to room temperature. The reaction mixture was cooled to 0 °C and then quenched with sat. NH_4Cl. The solids were filtered and the filtrate was extracted with EtOAc. The combined organic layers were dried over $MgSO_4$, filtered, and the solvent was removed *in vacuo*. The crude oil was purified *via* silica gel flash column chromatography (10% to 50% EtOAc/Hex gradient).

A dry 250-mL 3-necked flask equipped with a stir bar was charged with $Pd(PPh_3)_4$ (1.2 g, 1 mmol, 0.20 equiv) under N_2 atmosphere. Triethylamine (7 mL, 50 mmol, 10 equiv), **(*E*)-*N*,*N*-diethyl-5-(2-iodophenoxy)pent-2-enamide** (1.9 g, 5 mmol), and MeCN (50 mL) were then added to the reaction flask sequentially *via* syringe. The flask was topped with a reflux condenser and heated to reflux overnight. The reaction mixture was then cooled to room temperature, and the solvent was removed *in vacuo*. The crude oil was washed with DI H_2O and extracted with methylene chloride. The combined organic layers were dried over $MgSO_4$, filtered, and the solvent was removed *in vacuo*. The crude oil was used without further purification.

A dry 100-mL round-bottomed flask equipped with a stir bar was dried and placed under N_2 atmosphere. To the flask was added dry THF (4 mL) and dry toluene (8 mL) followed by **(*E*)-2-(chroman-4-ylidene)-*N*,*N*-diethylacetamide** (0.98 g, 4 mmol). The reaction solution was

cooled to 0 °C. Red-AL (3.5 M in toluene) (2.4 mL, 7.2 mmol, 1.8 equiv) was added dropwise *via* syringe. The reaction flask was warmed to room temperature and stirred for 2.25 h. The reaction solution was cooled to 0 °C and quenched with NaOH (5 M aq.) The crude reaction mixture was extracted with EtOAc. The combined organic layers were dried over Na_2SO_4, filtered, and the solvent was removed *in vacuo*. The crude product was purified *via* silica gel flash column chromatography [1% MeOH/10% Et_2O/89% (3% to 7% NH_3 in DCM)]. The product was obtained in 0.583 g, 63%.

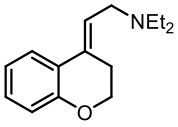

(*E*)-2-(chroman-4-ylidene)-*N*,*N*-diethylethan-1-amine $C_{15}H_{21}NO$

^{1}H NMR (500 MHz, $CDCl_3$) δ 7.57 (dd, *J* = 8.0, 1.6 Hz, 1H), 7.13 (ddd, *J* = 8.2, 7.2, 1.6 Hz, 1H), 6.89 (ddd, *J* = 7.9, 7.2, 1.3 Hz, 1H), 6.83 (dd, *J* = 8.2, 1.3 Hz, 1H), 6.15 (tt, *J* = 6.8, 1.8 Hz, 1H), 4.20 (dd, *J* = 6.1, 5.3 Hz, 2H), 3.25 (d, *J* = 6.9 Hz, 2H), 2.69 (ddt, *J* = 6.6, 4.9, 1.3 Hz, 2H), 2.57 (q, *J* = 7.2 Hz, 4H), 1.07 (t, *J* = 7.2 Hz, 6H).

^{13}C NMR (126 MHz, $CDCl_3$) δ 154.50, 130.23, 128.77, 124.11, 122.72, 120.94, 120.04, 117.59, 66.26, 50.55, 47.15, 26.26, 12.04.

Synthesized *via* HWE olefination followed by Red-AL reduction. Representative procedures shown above.

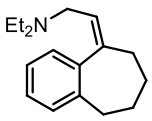

(*Z*)-*N*,*N*-diethyl-2-(6,7,8,9-tetrahydro-5H-benzo[7]annulen-5-ylidene)ethan-1-amine $C_{17}H_{25}N$

^{1}H NMR (500 MHz, $CDCl_3$) δ 7.17 – 7.09 (m, 3H), 7.02 – 6.97 (m, 1H), 5.64 (t, *J* = 6.8 Hz, 1H), 3.00 (d, *J* = 6.8 Hz, 2H), 2.77 – 2.67 (m, 2H), 2.47 (q, *J* = 7.1 Hz, 4H), 2.33 – 2.24 (m, 2H), 1.85 (p, *J* = 5.9 Hz, 2H), 1.72 – 1.61 (m, 2H), 0.92 (t, *J* = 7.1 Hz, 6H).

^{13}C NMR (125 MHz, CDCl3) δ 145.62, 141.73, 141.18, 129.12, 128.98, 126.92, 125.59, 124.99, 51.08, 46.81, 38.10, 36.63, 33.30, 27.87, 11.76.

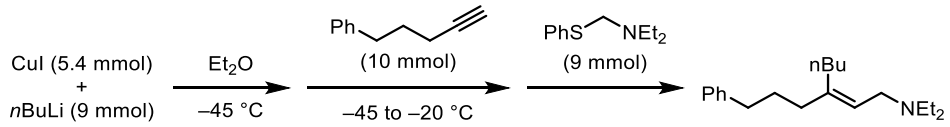

(*E*)-*N*,*N*-diethyl-3-(3-phenylpropyl)hept-2-en-1-amine: CuI (1.1 g, 5.4 mmol, 0.54 equiv) and Et_2O (40 mL) were added to a dry 100-mL Schlenk flask equipped with a stir bar under atmosphere of N_2. The flask was cooled to –45 °C. *n*-butyl lithium (1.6 M in hexanes) (6 mL, 9 mmol, 0.9 equiv) was added to the reaction flask *via* syringe. The reaction mixture stirred at temperature for 30 min. 5-phenyl-1-pentyne was then added to the reaction mixture *via* syringe. The reaction was stirred at –45 °C for an additional 10 min after which it was warmed to –20 °C and stirred for an additional 2 h. The flask was then cooled to –45 °C, and *N*-ethyl-*N*-((phenylthio)methyl)ethanamine was added to the reaction mixture *via* syringe. The flask was warmed to room temperature and allowed to stir overnight. The reaction mixture was then cooled to 0 °C and quenched with sat. NH_4Cl then NH_4OH (1 M aq.). The crude reaction mixture was filtered. The filtrate was extracted with EtOAc, dried over $MgSO_4$, and the solvent was removed

in vacuo. The crude oil was dissolved in Et_2O and extracted with HCl (1 M) x3. The combined aqueous layers were basified with 10% NaOH (aq.) and extracted with methylene chloride. The combined organic layers were dried over $MgSO_4$, filtered, and the solvent was removed *in vacuo*. The crude oil was purified *via* basic alumina flash column chromatography (12 g DI H_2O in 300 g basic alumina; 1% to 10% MeOH/5% to 10% Et_2O/pet. ether). The product was purified again *via* silica gel flash column chromatography [1% MeOH/10% Et_2O/89%(1% to 7% NH_3 in DCM)]. The product was obtained in 22% yield, 1.90 g.

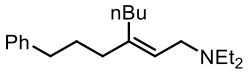

(*E*)-*N*,*N*-diethyl-3-(3-phenylpropyl)hept-2-en-1-amine $C_{20}H_{33}N$

^{1}H NMR (500 MHz, $CDCl_3$) δ 7.30 – 7.26 (m, 2H), 7.20 – 7.15 (m, 3H), 5.26 (t, J = 6.7 Hz, 1H), 3.07 (d, J = 6.7 Hz, 2H), 2.62 – 2.57 (m, 2H), 2.51 (q, J = 7.1 Hz, 4H), 2.11 – 1.98 (m, 4H), 1.78 – 1.69 (m, 2H), 1.35 – 1.26 (m, 4H), 1.03 (t, J = 7.1 Hz, 6H), 0.93 – 0.86 (m, 3H).

^{13}C NMR (126 MHz, $CDCl_3$) δ 142.83, 141.96, 128.55, 128.40, 125.77, 122.43, 50.49, 46.87, 36.76, 35.81, 30.89, 30.32, 30.02, 23.01, 14.19, 12.03.

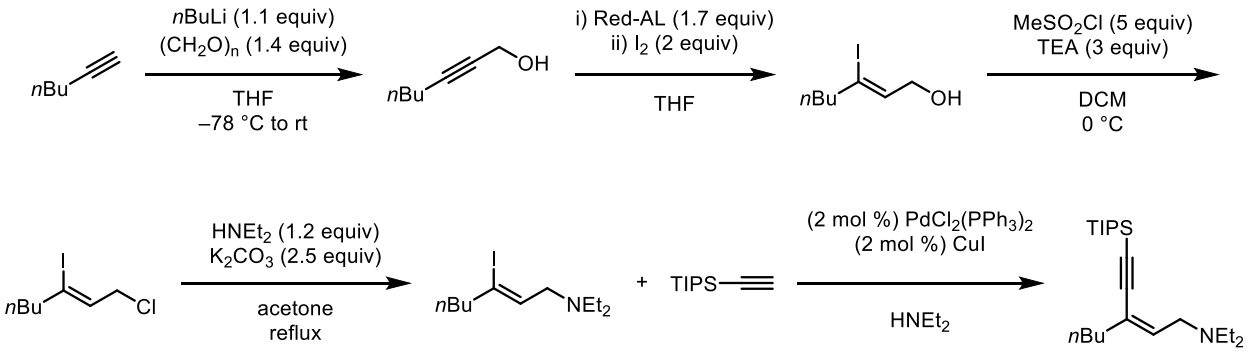

(*Z*)-*N*,*N*-diethyl-3-((triisopropylsilyl)ethynyl)hept-2-en-1-amine: A dry 250-mL 3-necked round bottomed flask was equipped with a stir bar and addition funnel and placed under N_2 atmosphere. **1-hexyne** (3.4 mL, 30.0 mmol) and 40 mL THF were added to the flask *via* syringe.

The flask was cooled to –78 °C followed by the addition of *n*BuLi (1.6 M in Hex) (18.8 mL, 1 equiv, 30 mmol) over 10 minutes. The reaction mixture was stirred for 1 h. **Paraformaldehyde** (1.4 g, 1.4 equiv, 42.0 mmol) was added to the reaction flask in one portion under positive pressure of N_2. The flask was then warmed to rt and stirred overnight. After cooling to 0 °C, the reaction was quenched with sat. NH_4Cl and extracted with EtOAc. The combined organic layers were dried over $MgSO_4$, filtered, and the solvent was removed *in vacuo*. The crude oil was distilled (7 torr, bp = 60-65 °C). Yield = 2.77g, 82%

A dry 500-mL round bottomed flask was equipped with a stir bar and placed under N_2. 100 mL THF was added to the flask *via* syringe followed by Red-AL (3.5 M in Toluene) (17.9 mL, 1.7 equiv, 62.7 mmol). The reaction flask was cooled to 0 °C. **Hept-2-yn-1-ol** (36.9 mmol) was diluted in 20 mL THF and transferred to the reaction flask *via* syringe. The reaction was warmed to rt and stirred for 4 h. The reaction mixture was then cooled to –10 °C followed by the addition of anhydrous EtOAc (10.1 mL, 2.8 equiv, 103.3 mmol). The reaction mixture was stirred for 25 min. The reaction was then cooled to –78 °C, then I_2 (18.7 g, 2 equiv, 73.8 mmol) was added in two portions against positive pressure N_2. The reaction mixture was stirred for an additional 1 h. 50 mL sat. sodium potassium tartrate was added to the reaction flask *via* syringe followed by 90 mL sat. $Na_2S_2O_3$. The mixture was stirred until clear then extracted with EtOAc. The combined organic layers were dried over $MgSO_4$, filtered, and then the solvent was removed *in vacuo*. The crude oil was purified *via* silica gel flash column chromatography (5% to 25% EtOAc/Hex). The product was obtained in 8.8 g, 99% yield.

A dry 500-mL round bottomed flask was equipped with a stir bar and placed under N_2. Triethylamine (15.3 mL, 3 equiv, 110.1 mmol) and 140 mL methylene chloride were transferred to the flask *via* syringe followed by **(*Z*)-3-iodohept-2-en-1-ol** (36.7 mmol). The flask was cooled

to 0 °C, and methanesulfonyl chloride (8.5 mL, 3 equiv, 110.1 mmol) was added. The reaction mixture was stirred at 0 °C for 7 h. Methanesulfonyl chloride (5.7 mL, 2 equiv, 73.4 mmol) was added to the reaction flask at 0 °C. The reaction was then warmed to rt and allowed to stir overnight. The reaction mixture was diluted with methylene chloride under ambient atmosphere then washed with 1 M HCl, sat. $NaHCO_3$, then brine. The organic layer was dried over $MgSO_4$, filtered and the solvent was removed *in vacuo*. The crude oil was purified *via* silica gel flash column chromatography. The product was obtained in 89% yield (8.45 g).

A 500-mL round bottomed flask was equipped with a stir bar and charged with K_2CO_3 (11.3 g, 2.5 equiv, 81.8 mmol), diethylamine (4.1 mL, 1.2 equiv, 39.2 mmol), and **(*Z*)-1-chloro-3-iodohept-2-ene** (32.7 mmol). The flask was fitted with a reflux condenser, and the reaction mixture was heated to reflux overnight. The flask was then cooled to rt, and the reaction mixture was washed with DI H_2O and extracted with EtOAc. The combined organic layers were dried over $MgSO_4$, filtered, and the solvent was removed *in vacuo*. The crude product was distilled (0.18 Torr, 60-70 °C) and obtained in 86% yield.

A dry 500-mL round bottomed flask was dried and equipped with a stir bar. In a N_2 filled glove box, $PdCl_2(PPh_3)_2$ (70.2 mg, 0.02 equiv, 0.1 mmol) and CuI (19.0 mg, 0.02 equiv, 0.1 mmol) were transferred to the flask. The flask was fitted with a septum, removed from the glove box, and placed on a standard Schlenk line under N_2 atmosphere. Diethylamine (10 mL) was added to the flask *via* syringe. **(*Z*)-N,N-diethyl-3-iodohept-2-en-1-amine** (1.48 g, 5 mmol) was transferred to the flask, and the reaction mixture was stirred for 10 min. **Ethynyltriisopropylsilane** (1.4 mL, 1.2 equiv, 6 mmol) was added to the reaction mixture *via* syringe, and the reaction continued to stir at rt overnight. The crude reaction mixture was filtered over celite then concentrated *in vacuo*. The

crude oil was purified by basic alumina flash column chromatography (100 g Al_2O_3 + 6 g H_2O). Eluent: (0.5% MeOH/ 1% Et_2O/ Pet. Ether) yield: 1.7 g, 98%.

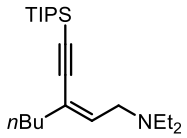

(*Z*)-*N*,*N*-diethyl-3-((triisopropylsilyl)ethynyl)hept-2-en-1-amine $C_{22}H_{43}NSi$

^{1}H NMR (500 MHz, $CDCl_3$) δ 5.79 (tt, J = 7.0, 1.2 Hz, 1H), 3.37 (d, J = 7.0 Hz, 2H), 2.54 (q, J = 7.2 Hz, 4H), 2.15 (td, J = 7.3, 1.1 Hz, 2H), 1.52 (tt, J = 8.5, 6.7 Hz, 2H), 1.31 (dq, J = 14.6, 7.3 Hz, 2H), 1.10 – 1.08 (m, 21H), 1.04 (t, J = 7.1 Hz, 6H), 0.89 (t, J = 7.3 Hz, 3H).

^{13}C NMR (126 MHz, $CDCl_3$) δ 134.96, 126.05, 105.45, 95.60, 52.94, 47.14, 36.97, 30.47, 22.02, 18.81, 14.04, 12.06, 11.47.

3.10 Literature Cited

(1) Tsakos, M.; Schaffert, E. S.; Clement, L. L.; Villadsen, N. L.; Poulsen, T. B. *Nat. Prod. Rep.* 2015, **32**, 605.

(2) (a) Walker, S. D.; Borths, C. J.; DiVirgilio, E.; Huang, L.; Liu, P.; Morrison, H.; Sugi, K.; Tanaka, M.; Woo, J. C. S.; Faul, M. M. *Org. Process Res. Dev.* 2011, **15**, 570. (b) Angibaud, P. R.; Pilatte, I. N. C.; Querolle, O. A. G. PCT Int. Appl. WO 20131719034 A1 20131205, 2013. (c) Aslanian, R. G.; Berlin, M. Y.; Huang, Y.; McCormick, K. D.; Mutahi, M. W.; Shih, N.-Y.; Ting, P. C.; Tom, W. C.; Zheng, J. PCT Int. Appl. WO 2007002057 A1 20010104, 2007.

(3) Catalytic examples of the Tishchenko reaction: (a) Horino, H.; Ito, T.; Yamamoto, A. *Chem. Lett.* 1978, **7**, 17. (b) Seki, T.; Nakajo, T.; Onaka, M. *Chem. Lett.* 2006, **35**, 824.

(c) Ogata, Y.; Kawasaki, A. *Tetrahedron* 1969, **25**, 929. (d) Hoshimoto, Y.; Ohashi, M.; Ogoshi, S. *J. Am. Chem. Soc.* 2011, **133**, 4668.

(4) Catalytic oxidative esterification: (a) Rout, S. K.; Guin, S.; Ghara, K. K.; Banerjee, A.; Patel, B. K. *Org. Lett.* 2012, **14**, 3982. (b) Gopinath, R.; Patel, B. K. *Org. Lett.* 2000, **2**, 577. (c) Lerebours, R.; Wolf, C. *J. Am. Chem. Soc.* 2006, **128**, 13052. (d) Powell, A. B.; Stahl, S. S. *Org. Lett.* 2013, **15**, 5072. (e) Travis, B. R.; Sivakumar, M.; Hollist, G. O.; Borhan, B. *Org. Lett.* 2003, **5**, 1031.

(5) Transfer hydrogenative esterification: (a) Owston, N. A.; Nixon, T. D.; Parker, A. J.; Whittlesey, M. K.; Williams, J. M. J. *Synthesis* 2009, 1578. (b) Whittaker, A. M.; Dong, V. M. *Angew. Chem. Int. Ed.* 2015, **54**, 1312. (c) Tschaen, B. A.; Schmink, J. R.; Molander, G. A. *Org. Lett.* 2013, **15**, 500.

(6) Dehyrdogenative esterification: (a) Prechtl, M. H. G.; Wobser, K.; Theyssen, N.; Ben-David, Y.; Milstein, D.; Leitner, W. *Catal. Sci. Technol.* 2012, **2**, 2039. (b) Cheng, J.; Zhu, M; Wang, C.; Li, J.; Jiang, X.; Wei, Y.; Tang, W.; Xue, D.; Xiao, J. *Chem. Sci.* 2016, **7**, 4428. (c) Zhang, J.; Leitus, G.; Ben-David, Y.; Milstein, D. *J. Am. Chem. Soc.* 2005, **127**, 10840.

(7) Catalytic asymmetric conjugate reduction: [Cu] (a) Appella, D. H.; Moritani, Y.; Shintani, R.; Ferreira, E. M.; Buchwald, S. L. *J. Am. Chem. Soc.* 1999, **121**, 9473. (b) Lipshutz, B. H.; Servesko, J. M.; Taft, B. R. *J. Am. Chem. Soc.* 2004, **126**, 8352. (c) Hou, C.-J.; Guo, W.-L.; Hu, X.-P.; Deng, J.; Zheng, Z. *Tetrahedron:* Asymmetry 2011, **22**, 195. [Co] (d) Leutenegger, U.; Madin, A.; Pfaltz, A. *Angew. Chem. Int. Ed.* 1989, **28**, 60. [Rh] (e) Tsuchiya, Y.; Kanazawa, Y.; Shiomi, T.; Kobayashi, K.; Nishiyama, H. *Synlett* 2004, 2493. (f) Kanazawa, Y.; Tsuchiya, Y.; Kobayashi, K.; Shiomi, T.; Itoh, J.-

i.; Kikuchi, M.; Yamamoto, Y.; Nishiyama, H. *Chem. Eur. J.* 2005, **12**, 63. [Ni] (g) Guo, S.; Zhou, J. *Org. Lett.* 2016, **18**, 5344.

(8) Catalytic enantioselective conjugate addition: [Cu] (a) Wang, S.-Y.; Ji, S.-J.; Loh, T.-P. *J. Am. Chem. Soc.* 2007, **129**, 276. (b) López, F.; Harutyunyan, S. R.; Meetsma, A.; Minnaard, A. J.; Feringa, B. L. *Angew. Chem. Int. Ed.* 2005, **44**, 2752. [Rh] (c) Takaya, Y.; Senda, T.; Kurushima, H.; Ogasawara, M.; Hayashi, T. *Tetrahedron:* Asymmetry, 1999, **10**, 4047. (d) Sakuma, S.; Sakai, M.; Itooka, R.; Miyaura, N. *J. Org. Chem.* 2000, **65**, 5951. (e) Paquin, J.-F.; Stephenson, C. R. J.; Defieber, C.; Carreira, E. M. *Org. Lett.* 2005, **7**, 3821. For a review, see: (f) Harutyunyan, S. R.; Hartog, T. d.; Geurts, K.; Minnaard, A. J.; Feringa, B. L. *Chem. Rev.* 2008, **108**, 2824.

(9) Khumsubdee, S.; Burgess, K. *ACS Catal.* 2013, **3**, 237.

(10) (a) Tani, K.; Yamagata, T.; Otsuka, S.; Akutagawa, S.; Kumobayashi, H.; Taketomi, T.; Takaya, H.; Miyashita, A.; Noyori, R. *J. Chem. Soc., Chem. Commun.* 1982, 600. (b) Tani, K.; Yamagata, T.; Akutagawa, S.; Kumobayashi, H.; Taketomi, T.; Takaya, H.; Miyashita, A.; Noyori, R.; Otsuka, S. *J. Am. Chem. Soc.* 1984, **106**, 5208. (c) Inoue, S.-i.; Takaya, H.; Tani, K.; Otsuka, S.; Sato, T.; Noyori, R. *J. Am. Chem. Soc.* 1990, **112**, 4897. (d) Nova, A.; Ujaque, G.; Albéniz, A. C.; Espinet, P. *Chem. Eur. J.* 2008, **14**, 3323. (e) Yoshimura, T.; Maeda, S.; Tetsuya, T.; Sawamura, M.; Morokuma, K.; Mori, S. *Chem. Sci.* 2017, **8**, 4475.

(11) (a) Wu, Z.; Laffoon, S. D.; Nguyen, T. T.; McAlpin, J. D.; Hull, K. L. *Angew. Chem. Int. Ed.* 2017, **56**, 1371. (b) Wu, Z.; Hull, K. L. *Chem. Sci.* 2016, **7**, 969.

(12) Hanson, S. K.; Heinekey, D. M.; Goldberg, K. I. *Organometallics* 2008, **27**, 1454.

(13) Tejel, C.; Ciriano, M. A.; Passarelli, V. *Chem. Eur. J.* 2011, **17**, 91.

CHAPTER 4: TANDEM ASYMMETRIC ALLYLIC AMINE ISOMERIZATION AND REDUCTIVE AMINATION UNDER RHODIUM CATALYSIS

This chapter has been adapted from the following publication:

Wu, Z.; Laffoon, S. D.; Hull, K. L. Asymmetric Synthesis of γ-Branched Amines via Rhodium-Catalyzed Reductive Amination. *Nat. Commun.* **2018**, *9*, 1185.

4.1 Abstract

This chapter describes the development of a general asymmetric route for the one-pot synthesis of chiral γ-branched amines through the highly enantioselective isomerization of allylamines, followed by enamine exchange and subsequent chemoselective reduction. This protocol is suitable for establishing various tertiary stereocenters, including those containing dialkyl, diaryl, cyclic, trifluoromethyl, difluoromethyl, and silyl substituents, which allows for a rapid and modular synthesis of many chiral γ-branched amines. To demonstrate the synthetic utility, Terikalant and Tolterodine are synthesized using this method with high levels of enantioselectivity.

4.2 Motivation and Background

Chapters 2 and 3 describe the one-step synthesis of chiral, β-branched amides and esters via Rh-catalyzed enantioselective isomerization of allylic amines, followed by enamine exchange, and subsequent oxidation.[1] The slow oxidation of the more sterically hindered diethyl enamine (**i**, when R=ethyl, Figure 4.2a) compared to facile oxidation of enamine (**ii**) leads to exclusive

formation of the desired amide product (**iii**). Based on this report, we proposed that chiral enamine intermediate (**ii**) could instead be reduced to afford the valuable enantiopure γ-branched amine (**v**).

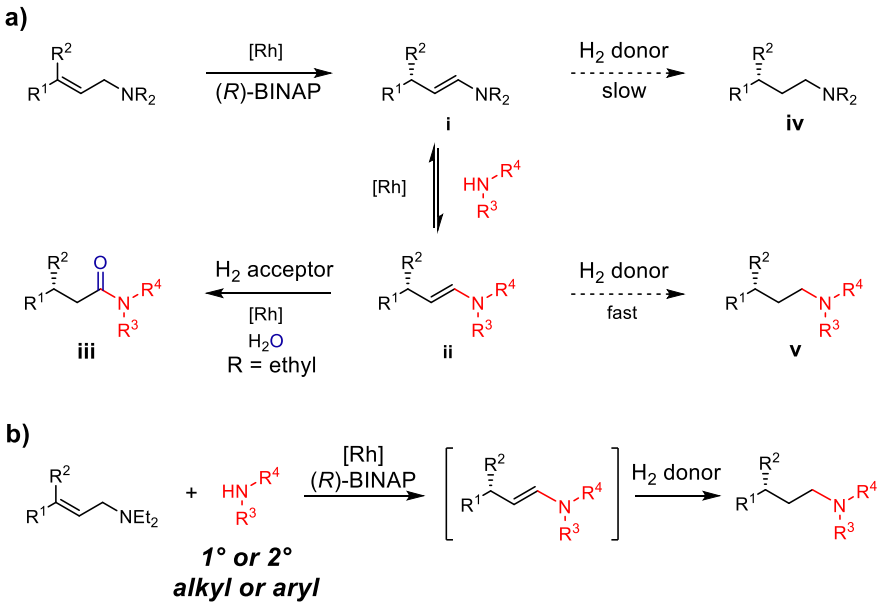

Figure 4.1. Design of a tandem asymmetric isomerization—enamine exchange—reduction process. The chemoselectivity is determined by the relative reduction rate of intermediates **i** and **ii**. When R = ethyl, exclusive formation of β-branched amide **iii** is observed in the presence of hydrogen acceptor. **b**, One-pot synthesis of chiral γ-branched amine from allylic amine, exogenous amine nucleophile, and hydrogen donor.

We report herein a nucleophilic amination of allylic amines with exogenous amine nucleophiles to afford chiral, γ-branched amines via a transfer hydrogenation (Figure 4.1b). Both primary and secondary alkyl/aryl amines are effective nucleophiles, coupling with allylic diethylamine precursors to afford various γ-branched amine products with excellent enantioselectivities in a two-step one-pot manner.

4.3 Developing Conditions for Reductive Amination

To establish a method for the selective conversion of allylic amines to enantiopure γ-branched amines, we began our investigation by examining a variety of hydrogen donors in the reductive amination of geranyl diethylamine (**1a**) with morpholine (**2b**) under slightly modified conditions from our previous report.[21] Compared to the oxidative process, the reduction is more

Table 4.1. Selected optimization of reductive amination of allylic amines.[a]

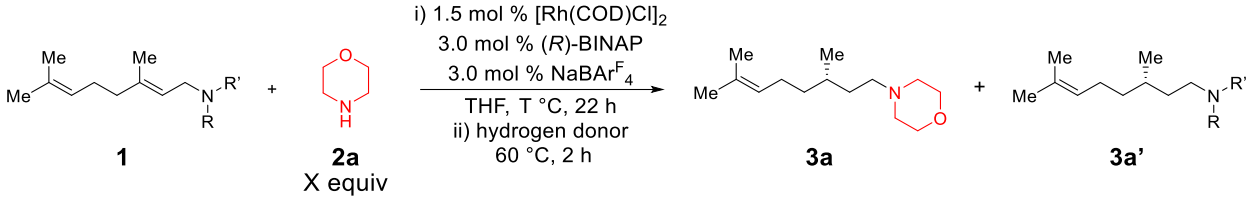

Entry	1	R, R'	T (°C)	X	Hydrogen donor	Yield **3a** (%)[b]	Yield **3a'** (%)[b]
1	**1a**	Et, Et	40	1.2	^{i}PrOH	< 1 [c]	5
2	**1a**	Et, Et	40	1.2	MeOH	< 1 [c]	2
3	**1a**	Et, Et	40	1.2	HCO_2NH_4	12	20
4	**1a**	Et, Et	40	1.2	HCOOH	88 (96.2:3.8 er)	10
5	**1a**	Et, Et	60	2.0	HCOOH	87	8
6	**1a**	Et, Et	60	3.0	HCOOH	88	5
7	**1b**	Me, Me	80	1.2	HCOOH	53 (96.4:3.6 er)	43
8	**1c**	*i*-Pr, *i*-Pr	80	1.2	HCOOH	80 (77.6:22.4 er)	< 1
9	**1d**	Cy, H	80	1.2	HCOOH	44	28

a) General reaction conditions: geranyl amine (**1**) (0.12 mmol, 1.0 equiv, *E*/*Z* = 97.5:2.5), morpholine (**2a**), hydrogen donor (3.0 equiv), THF (1.2 M). The absolute configuration of **3a** was assigned by analogy. b) *In situ* yield determined by GC or NMR analysis. c) Enamine of **3a** was observed as the major product. er: enantiometric ratio.

challenging as the hydrogenated starting material (Figure 4.1a, **iv**) was often observed as the major byproduct in the amidation reaction.[1] Therefore, an appropriate selection of a hydrogen donor and starting material (R group) to allow for the rapid and chemoselective reduction of intermediate (**ii**) was the key challenge in our investigation. No conversion of **1a** was observed in the presence of H_2 donors, presumably due to protonation of the basic allylic nitrogen atom or coordination to the cationic catalyst, thereby impeding the initiation of the 1,3-hydride shift.[2] Sequential addition of the hydrogen donor after the isomerization/enamine exchange step led to higher conversion of starting material, with HCO_2H showing superior reactivity and selectivity (Table 4.1, entries 1-4). Increasing the equivalency of amine nucleophile improved the ratio of **3a**/**3a'**, but did not increase the yield of the desired product **3a** (Table 4.1, entries 4-6). Different allylic amine precursors (**1b-d**) were then tested to compare both chemo- and enantioselectivity (Table 4.1, entries 7-9). Elevated temperature was required to achieve high conversion for these substrates. Less sterically hindered dimethylamino substate **1b** afforded poor chemoselectivity and high enantioselectivity;

however, bulkier allylic diisopropylamine **1c** showed greater chemoselectivity but poor enantioselectivity. Secondary amine precursor **1d** was less reactive and selective under these conditions.

4.4 Expanding Reaction Scope

With these optimized conditions in hand, the amine nucleophile scope was investigated (Figure 4.2). Secondary cyclic amines such as morpholine (**3a**), Boc-protected piperazine (**3b**), tetrahydroisoquinoline (**3c**) and 2-(piperazin-1-yl) pyrimidine (**3d**) all gave similarly excellent yields and enantiometric ratios. Without the addition of amine, **3e** could be obtained in high yield and e.r. Surprisingly, more sterically hindered acyclic dialkyl amines **3f** and **3g** (compared to diethylamine) were effective nucleophiles in this reaction, indicating that the volatility of the resulting diethylamine byproduct is likely playing a larger role than steric hindrance in determining the chemoselectivity (*vide infra*). Enantiopure α-branched amine **2g** afforded the desired product **3g** and **3g'** with high e.r. (>97:3) and d.r. (>20:1), demonstrating that the isomerization is not affected by the chirality of the nucleophile, but is instead controlled by the ligand. Importantly, no racemization of the chiral amine nucleophile occurred under the reaction conditions.

Under slightly modified conditions, primary aryl and alkyl amines were coupled with allylic diethylamine electrophiles to afford the chiral secondary amines, respectively. In these cases, $NaBH_4$ proved to be a superior reductant than HCO_2H. Both electron rich (**3i**) and poor (**3j**) anilines afforded the desired chiral amines with identically excellent enantiomeric ratios. In the presence of primary alkyl amines (with the exception of $tBuNH_2$ **2m**), the isomerization of allylic diethylamine was completely prohibited; therefore, a sequential addition of nucleophile was required to reach high yields. Primary alkyl amines, α to 1°(**3k**), 2°(**3l**), and 3° (**3m**) carbons, all

afforded desired products with moderate to good yields and excellent enantioselectivity. A nucleophile containing a tethered tertiary nitrogen atom (**3n**) was well tolerated.

A survey of 3,3-disubstituted allylic amine electrophiles revealed that a wide variety of tertiary stereocenters can be installed under these reductive amination conditions (Figure 4.3). Several 3,3-aryl,alkyl allylic diethylamines (**5a-c**) were tested and all afforded products with good yields and enantioselectivities. An ortho substituent on the aryl ring (**5c**) has no effect on the enantioselectivity of the isomerization, and the standard reaction conditions were amenable to aryl bromides, with no proteodebromination byproducts observed. The use of β,β-dialkyl allylic

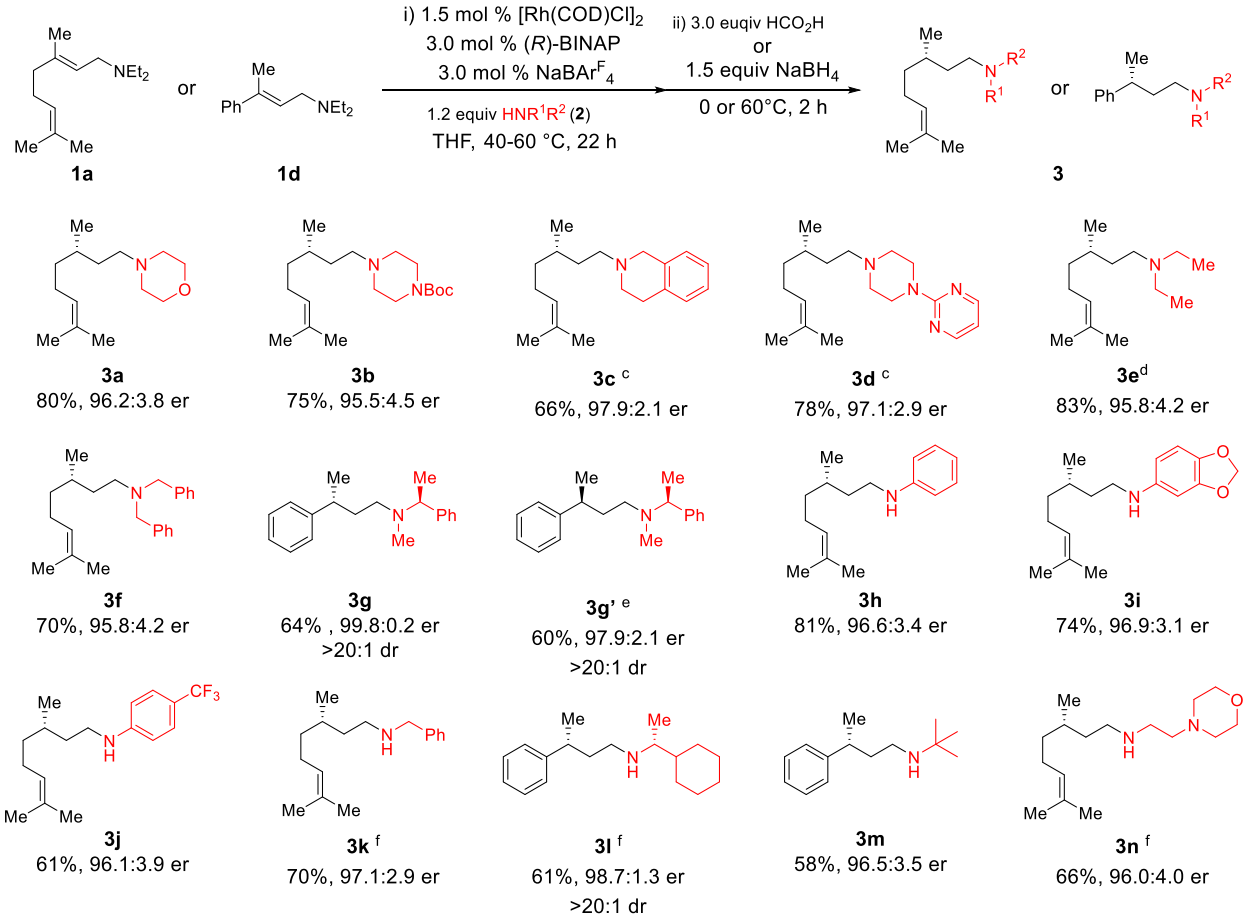

Figure 4.2. Scope of amine nucleophiles for the reductive amination of allylamine. a) General reaction conditions: **1a** (0.24 mmol, 1.0 equiv, *E*/*Z* = 97.5:2.5, 40 °C for 1st step) or **1b** (0.24 mmol, 1.0 equiv, *E*/*Z* > 99:1, 60 °C for 1st step) nucleophile **2** (1.2 equiv), hydrogen donor (3.0 equiv), THF (1.2 M). b) For **3a-3g**, HCO_2H used as H_2 donor at 60 °C for 2nd step; For **3h-3n**, $NaBH_4$ (1.5 equiv) used as reductant at 0°C to rt for 2nd step. c) **2d** and **2e** added together with HCO_2H. d) No nucleophile added. e) (*S*)-BINAP used. f) **2k**, **2l**, and **2n** added after isomerization. See supplemental methods for details. dr: diastereomeric ratio.

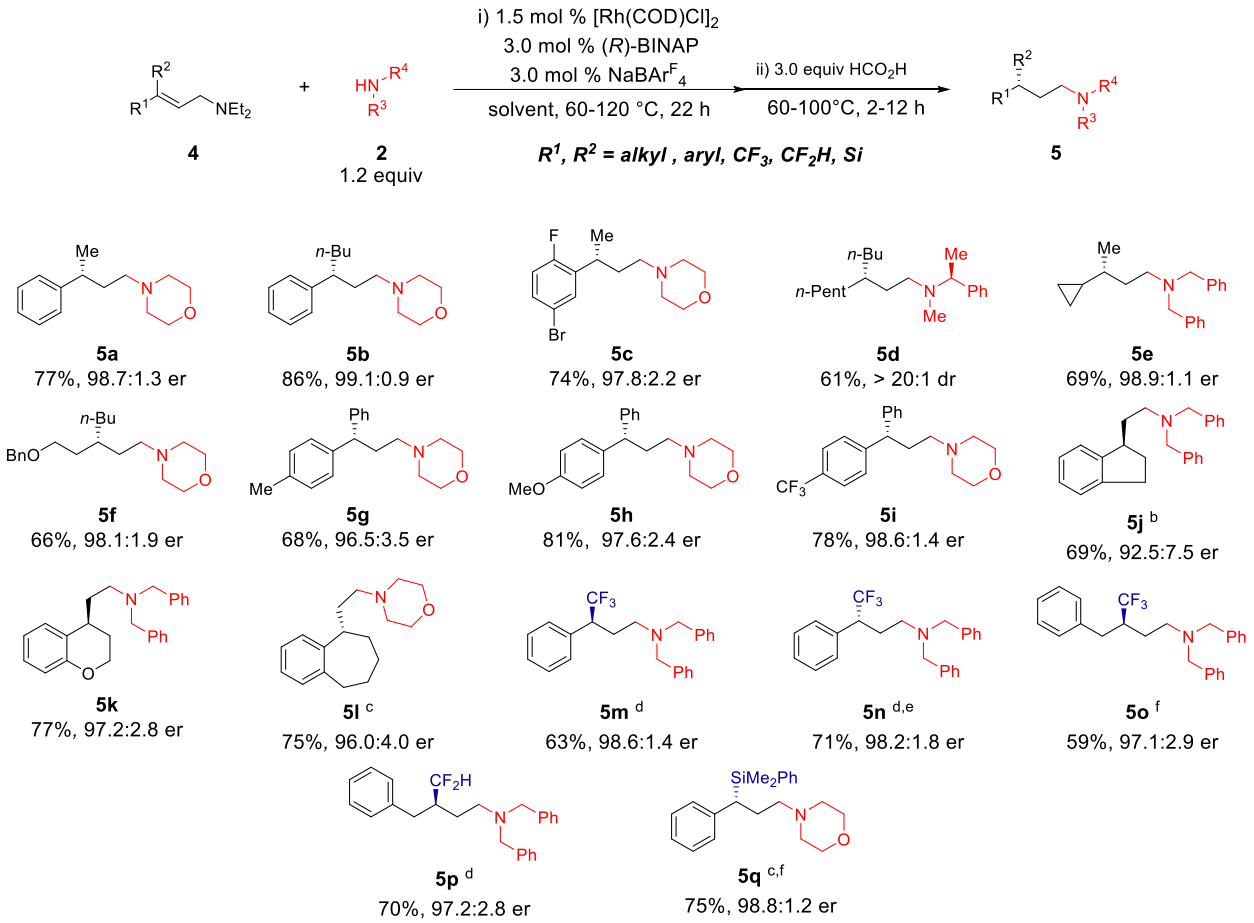

Figure 4.3. Scope of allylamine. a) General reaction conditions: allylic diethylamine **4** (0.24 mmol, 1.0 equiv, *E*/*Z* > 99:1 unless otherwise noted), nucleophile **2** (1.2 equiv), HCO_2H (3.0 equiv), THF (1.2 M). b) Substrate *E*/*Z* = 96.7:3.3. c) Substrate *Z*/*E* > 99:1. d) 1,4-dioxane used. e) Substrate *Z*/*E*=95.6:4.4. f) Toluene used. See supplemental methods for details. The absolute configuration of product is determined by alkene configuration.

diethylamine (**5d-f**) was successful, enabling the highly enantioselective synthesis of γ-dialkyl amines, even with minimally differentiated substituents (**5d**, *n*-Pent vs *n*-Bu). When more challenging 3,3-diaryl allylic diethylamines (**5j-i**) were subjected to the reaction conditions, amine products bearing γ-diaryl stereocenters, a common moiety in pharmaceutical agents, can be formed with excellent enantioselectivity.[3–6] Substrates bearing electron-rich (**5h**) and electron-poor (**5i**) aryl substituents afforded good yields and excellent enantiomeric ratios. This method can be used to set stereocenters containing sterically and electronically similar phenyl and para-tolyl groups with excellent selectivity (**5g**, 96.5:3.5 er). Chiral γ-cyclic amines containing five-, six-, and seven-

membered rings (**5j-l**) could be obtained as well with high enantioselectivity under identical conditions.[7,8]

Due to the superior reactivity and broad substrate tolerance of this catalyst, we sought to further develop this method for the construction of highly valuable stereocenters containing CF_3, CF_2H, and SiR_3 substituents (Figure 4.3). In order to effect suitable conversion, modification of the reaction solvent and increased temperatures were required. This may be attributed to the difficult isomerization of the more hindered allylic amines. Under these new conditions, difficult to synthesize enantiopure γ-trifluromethylated (**5m-o**) and difluoromethylated (**5p**) amines can be accessed with moderate to good yields and excellent enantioselectivities.[9,10] It is worth noting that the (*Z*)-CF_3 allylic amine (**5b**) was slightly more reactive under these conditions compared to the (*E*)-isomer (**5n**), as higher conversion was observed for **5m**. Phenyldimethylsilyl substituted allylic diethylamines (**5q**) afforded good yields and enantioselectivities under these conditions as well. It is noteworthy that the chiral silyl group can be installed, as this can be converted to a range of functionalities.[11]

This methodology was applied in the enantioselective syntheses of biologically active Terikalant and Tolterodine as illustrated in Figure 4.4. Substrate **4k** and nucleophile **2o** were prepared according to literature procedures. The presence of **2o** proved to inhibit the isomerization of allylic amine **4k**. Therefore, the addition of nucleophile along with formic acid after the isomerization step was found effective, giving 75% yield as well as excellent e.r. (96.7:3.3) for Terikalant (Figure 4.5a), a significant improvement over the current synthesis utilizing chiral resolution.[12] A highly enantioselective synthesis of (*R*)-Tolterodine was then demonstrated in Figure 4.5b.[13–15] The (*E*)-vinyl bromide **6**, prepared from trans-cinnamyl chloride,[16] was coupled with aryl boronic acid **7** to afford the diastereopure (*Z*)-allylic amine **8** in 91% yield. A sequential

addition of catalyst, hydrogen donor, and strong acid afforded the desired (*R*)-Tolterodine in 88% overall yield and 96.0:4.0 e.r. Although diisopropylamine was not a sufficient nucleophile to perform the enamine exchange with the diethyl enamine, the isomerization of allylic diisopropylamine **8** also proceeds in a highly enantioselective fashion. It is worth noting that the reaction was carried out on the 1.0 mmol scale with half the catalyst loading compared to the aminations performed on the smaller scale. Compared to state-of-the-art Tolterodine synthesis, which requires the ortho-hydroxyl substituent to direct the asymmetric hydrogenation,[15] our method allows for a modular and rapid synthesis of Tolterodine derivatives, including those without the ortho-hydroxyl functionality (**5g-i**).

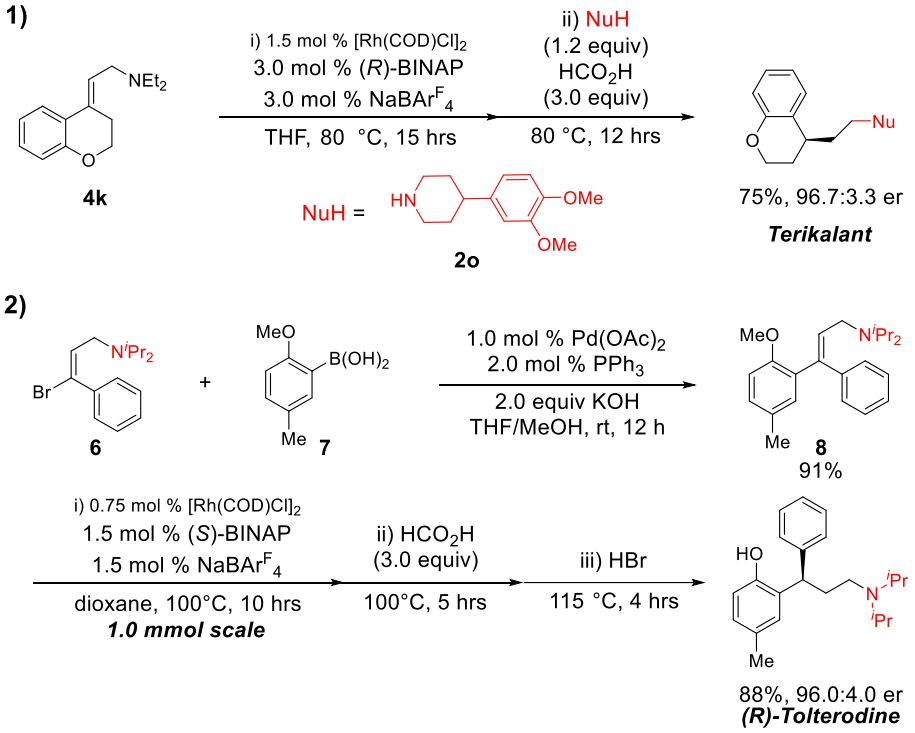

Figure 4.4. Synthetic application of rhodium-catalyzed asymmetric reductive amination of allylamines. a, Enantioselective synthesis of Terikalant from allylic diethylamine **4k**. **b**, Enantioselective and modular synthesis of (*R*)-Tolterodine from vinyl bromide **6**. See supplemental methods for details.

4.5 Investigating Reaction Selectivity

To gain insight into the overall selectivity of this tandem process, a series of control reactions were carried out under optimized conditions (Figure 4.5a-d). The selectivity of the enamine exchange step was first investigated. In general, less sterically hindered amine nucleophiles (compared to diethylamine) led to higher selectivity of desired product enamine **9** over the diethylenamine **10a** (Figure 4.5a). For sterically similar dibutylamine and dibenzylamine, **9** was found to be the major product, presumably due to a combination of the relative amine volatilities, stoichiometry of the reaction, and enamine stability. When equimolar amounts of nucleophile and substrate were subjected to the reaction conditions, similar product distributions were observed regardless of the permutation of allylic amine versus nucleophile (Figure 4.5b). This implies that the exchanging product distribution is controlled by a thermodynamic equilibrium under standard reaction conditions. When the nucleophiles and hydrogen donor were added simultaneously into the reaction after the isomerization step (Figure 4.5c), the observed selectivities are similar to those shown in Figure 4.6a, indicating that the exchange step is faster than the reduction. Finally, various secondary amine nucleophiles were studied under standard conditions (Figure 4.5d). Higher selectivities were observed compared to those in Figure 4.5a, implying that the reduction of desired enamine intermediates is faster than the diethylenamine **10a**. Therefore, the chemoselectivity of this two-step one-pot reaction comes from both steps, favoring the desired product. A proposed mechanism is shown in Figure 4.6: the basic nitrogen atom of the allylic amine substrate coordinates to the cationic rhodium to form **A**, followed by β-hydride elimination and re-insertion of in situ generated conjugated iminium **B** to afford the chiral enamine **C**. A thermally controlled enamine exchange leads to **D**, which then undergoes subsequent transfer hydrogenation upon addition of formic acid. A rhodium-mediated transfer hydrogenation

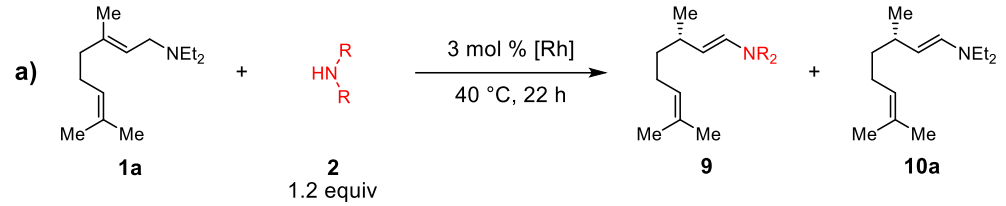

R	Me	Bu	Bn	-(CH2)2O(CH2)2-
conversion of 1a	>95%	>95%	>95%	>95%
9/10a ratio	3.5	1.6	2.4	4.8

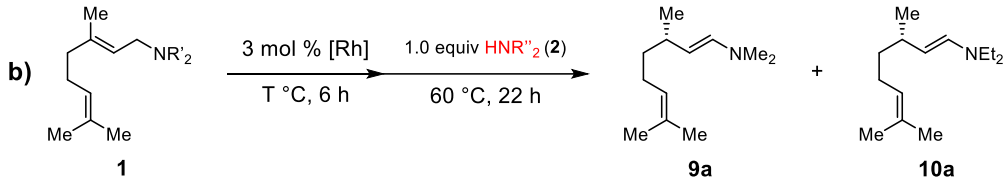

R'	Me	Et
R''	Et	Me
T (°C)	60	40
conversion of 1	>95%	>95%
9a/10a ratio	2.8	3.0

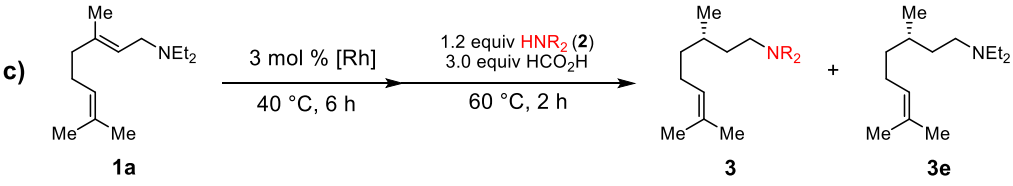

R	Bu	Bn	-(CH2)2O(CH2)2-
3 yield	64%	64%	73%
3e yield	36%	30%	15%
3/3e ratio	1.8	2.1	4.9

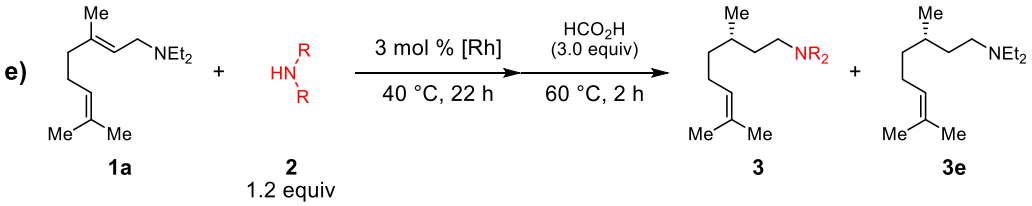

R	Me	Bu	Bn	*i*Pr	-(CH2)2O(CH2)2-
3 yield	79%	65%	85%	<1%	88%
3e yield	13%	35%	15%	96%	10%
3/3e ratio	6.1	1.9	5.7	<0.1	8.8

Figure 4.5. Control experiments and proposed catalytic cycles. a, Selectivity of the enamine exchange step. **b**, Thermodynamic equilibrium for the enamine exchange. **c**, Selectivity of the transfer hydrogenation step (simultaneous addition of amine and hydrogen donor). **d**, Chemoselectivity for various secondary amine nucleophiles under standard conditions. **e**, Proposed catalytic cycles: enantioselective isomerization and transfer hydrogenation, X=BAr_4^F.

mechanism is proposed, as lower conversion was observed in the absence of metal catalyst when investigating the reduction of pre-made enamine. An in situ formed rhodium formate species **F** can undergo decarboxylation to generate Rh hydride species **G**.[17,18] Subsequent iminium **E** inserts into Rh–H **G** to give the desired chiral γ-branched amine and regenerate rhodium formate **F**.

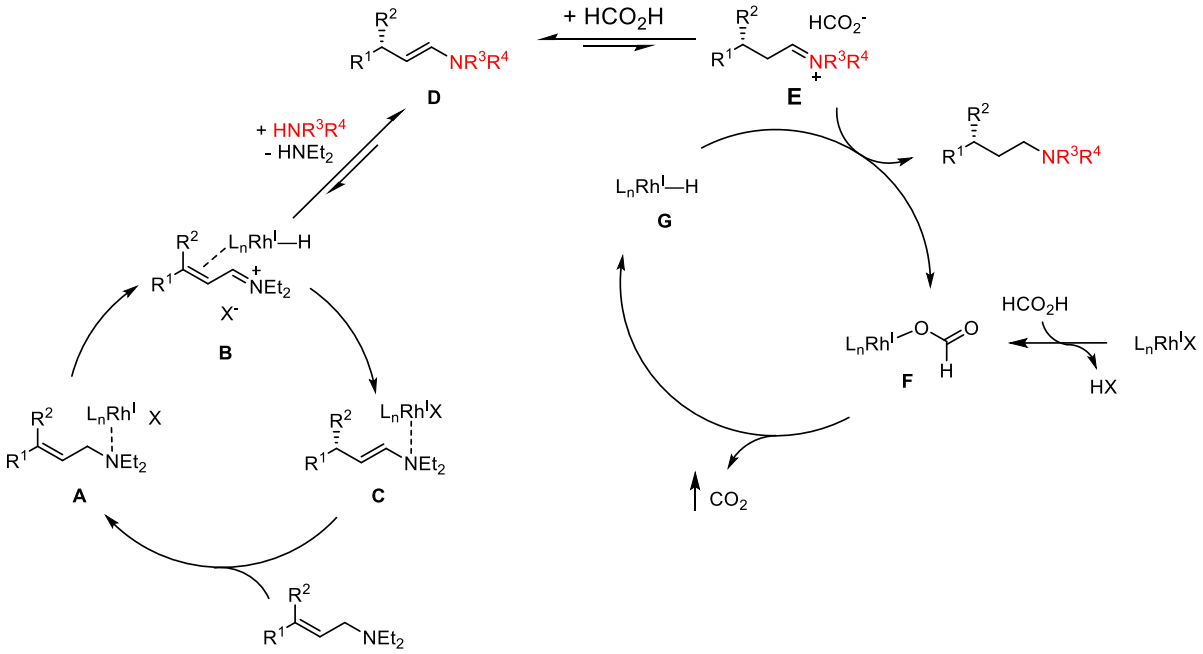

Figure 4.6. Proposed reaction mechanism.

4.6 Conclusion

We have developed conditions for a highly enantioselective, modular synthesis of chiral γ-branched amines. This method enables a rapid assembly of various stereocenters as well as amine functionalities via a tandem isomerization–enamine exchange–transfer hydrogenation process. Stereocenters bearing diaryl, cyclic, fluoroalkyl and silyl substituents are established using same catalyst under similar conditions.

4.7 Supporting Information

4.7.1 Direct asymmetric synthesis of γ-branched amines

$[Rh(COD)Cl]_2$ (2.0 mg, 1.5 mol %), (*R*)-BINAP (4.5 mg, 3.0 mol %), $NaBAr_4^F$ (6.4 mg, , 3.0 mol %), and THF (0.2 mL) were added to a oven-dried 4 mL vial equipped with a stir bar in the glove box under nitrogen atmosphere. To the vial was added sequentially allylic diethylamine (**1**, 0.24 mmol, 1.0 equiv), and secondary amine (**2**, 0.29 mmol, 1.2 equiv). The resulting solution was allowed to stir for 22 h at 40 °C (unless otherwise noted). After 22 h, formic acid (0.36 mmol, 3.0 equiv) was added into reaction vial via syringe and the reaction was allowed to stir for another 2 h at 60 °C (unless otherwise noted). The reaction crude was quenched by the addition of DCM, concentrated *in vacuo* and then purified by basic alumina chromatography to afford the desired product **3**.

4.7.2 General procedure for trisubstituted allylic amine synthesis

Allylic diethylamine substrates **1a-1e, 4a, 4b, 4d, 4f, 4i, 4k** were synthesized according to our previous report. The ^1H and ^{13}C NMRs are marched with literature.[19]

Allylic diethylamine substrates **4c** and **4e** were synthesized by following method, modified from our previous report.[19]

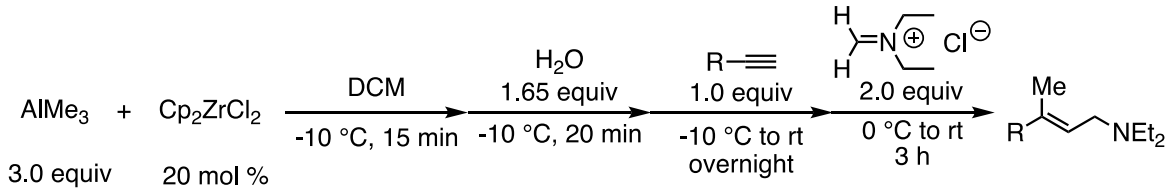

Procedure: To a dry 100 mL schlenk flask was charged with a stir bar and 0.292 g Cp_2ZrCl_2 (1 mmol, 20 mmol %), purged with nitrogen followed by the addition of 25 mL DCM. Cooled to -10 °C, 7.5 mL 2 M $AlMe_3$/hexanes solution (15 mmol, 3.0 equiv) was added slowly. The reaction

was allowed to stir at -10 °C for 15 min followed by the slow addition of 168 µL H_2O (8.2 mmol, 1.65 equiv). The resµting mixture was stirred vigorously at -10 °C for 20 min then added the alkyne (5 mmol, 1.0 equiv). The reaction flask was then was then warmed up to rt and stir overnight. A solution of the iminium chloride salt (10 mmol, 2 equiv) in 5 mL dry DCM was added slowly to the flask at 0 °C, then reaction was warmed up to rt and stir for another 3 hrs . The reaction is quenched by careful addition of 2 M NaOH solution at 0 °C, then filtered through ceilite and washed with warm DCM. The resulting mixture was then extract by DCM three time and combined organic layers were dried by Na_2SO_4, concentrated *in vacuo*, and distilled under vacuum to afford desired allylic diethylamines.

4.7.3 Synthesis and Characterization of Allylic Amines

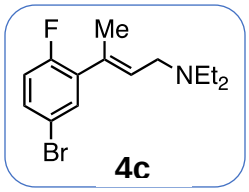

(*E*)-3-(5-bromo-2-fluorophenyl)-*N*,*N*-diethylbut-2-en-1-amine (4c), prepared according to previously described procedure in 60% yield.

^{1}H NMR (500 MHz, $CDCl_3$) δ: 7.36 (dd, J = 6.8, 2.6 Hz, 1H), 7.30 (ddd, J = 8.7, 4.3, 2.6 Hz, 1H), 6.90 (dd, J = 10.2, 8.7 Hz, 1H), 5.73 (t, J = 6.6 Hz, 1H), 3.25 (d, J = 6.6 Hz, 2H), 2.58 (q, J = 7.2 Hz, 4H), 2.01 (s, 3H), 1.07 (t, J = 7.1 Hz, 6H).

^{13}C NMR (125 MHz, $CDCl_3$) δ: 159.06 (d, J = 247.5 Hz), 134.53 (d, J = 15.7 Hz), 132.48 (d, J = 4.6 Hz), 132.32 , 131.08 (d, J = 8.4 Hz), 130.28 , 117.57 (d, J = 24.6 Hz), 116.46 (d, J = 3.4 Hz), 50.92 , 47.20 , 17.20 (d, J = 3.8 Hz), 12.09.

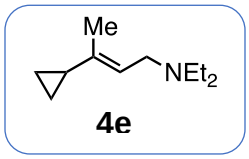

(*E*)-3-cyclopropyl-*N*,*N*-diethylbut-2-en-1-amine (4e), prepared according to previously described procedure in 78% yield.

^{1}H NMR (500 MHz, $CDCl_3$) δ: 5.29 (t, *J* = 6.8 Hz, 3H), 3.05 (d, *J* = 6.8 Hz, 2H), 2.49 (q, *J* = 7.2 Hz, 4H), 1.54 (s, 3H), 1.42 – 1.33 (m, 1H), 1.02 (t, *J* = 7.2 Hz, 6H), 0.57 – 0.51 (m, 2H), 0.46 – 0.42 (m, 2H).

^{13}C NMR (125 MHz, $CDCl_3$) δ: 138.44, 120.19, 50.66, 46.81, 19.01, 14.54, 11.91, 4.61.

Allylic diethylamine substrate **4g** was synthesized by following method[20] and the starting vinyl bromide was synthesized according to our previous report[19] and literature.[20]

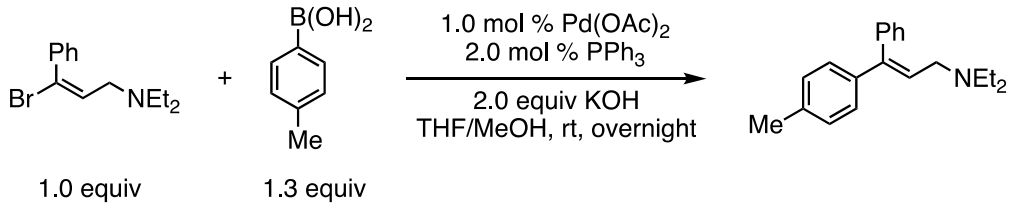

Procedure: To a 50 ml round bottom flask was charged with a stir bar and 11 mg $Pd(OAc)_2$ (0.050 mmol, 1.0 mol %), 26 mg PPh_3 (0.10 mmol, 2.0 mol %), 0.560 g KOH (10 mmol, 2.0 equiv), starting material vinyl bromide (1.34g, 5 mmol, 1.0 equiv) ,0.880 g 4-methyl boronic acid (6.5 mmol, 1.3 equiv) and 5 mL THF and 5 mL MeOH. The reaction was stirred at rt overnight followed by dilution with EtOAc, and washed by 1 N NaOH solution and brine. The organic layer was then dried over $MgSO_4$, concentrated *in vacuo*, purified by Al_2O_3 column chromatography: 200 g Al_2O_3 + 12 g H_2O, 30 : 1 hexanes/ EtOAc with 0.5% MeOH as eluent.

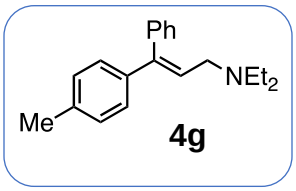

(*E*)-*N*,*N*-diethyl-3-phenyl-3-(p-tolyl)prop-2-en-1-amine (4g), prepared according to previously described procedure in 70% yield.

^{1}H NMR (500 MHz, $CDCl_3$) δ: 7.40 – 7.34 (m, 2H), 7.33 – 7.28 (m, 1H), 7.20 – 7.12 (m, 4H), 7.11 – 7.05 (m, 2H), 6.19 (t, J = 6.7 Hz, 1H), 3.15 (d, J = 6.7 Hz, 2H), 2.52 (q, J = 7.1 Hz, 4H), 2.32 (s, 3H), 0.96 (t, J = 7.1 Hz, 6H).

^{13}C NMR (125 MHz, $CDCl_3$) δ: 143.23, 140.11, 139.65, 137.01, 129.97, 128.96, 128.21, 127.27, 127.15, 126.55, 51.86, 47.13, 21.20, 11.96.

The cyclic allylic diethylamine substrates **4j and 4l** were synthesized by following method[21] and the starting diethyl (2-(diethylamino)-2-oxoethyl) phosphonate was synthesized according to our previous report[19] and literature.[21]

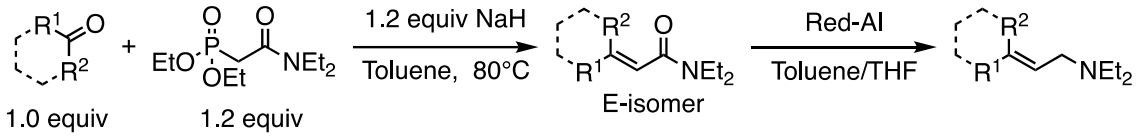

Olefination: A dry 100mL round-bottom flask was charged with a stir bar and 0.48g NaH (60 wt %, 12 mmol, 1.2 equiv), purged with nitrogen followed by the addition of 15 mL toluene. Cooled to 0 °C, diethyl (2-(diethylamino)-2-oxoethyl)phosphonate was added dropwise (2.8 mL, 12 mmol, 1.2 equiv). The reaction was allowed to stir at 0 °C for 30 min until the solution become clear. Ketone was added dropwise (10 mmol, 1.0 equiv) to the reaction over 5 min, then warmed up to 80 °C, stirring overnight. The reaction was quenched with sat. NH_4Cl solution, and the aqueous layer was extracted with DCM three times. The combined organic layers were dried over $MgSO_4$, and purified by silica column chromatography.

Reduction: To a dry 20 mL round-bottom flask was charged with a stir bar, purged with N_2 three times, followed by the addition of unsaturated amide (4.0 mmol), dry THF (3 mL) and dry toluene (6 mL, V(tol)/V(THF)=2). The flask was then cooled in ice bath, and added RedAl solution (2.0 equiv, 3.5 M) dropwised. The reaction was allowed to stir at 0 °C for 2 hours then warmed up to rt for another 4 hours. The reaction crude was cooled in ice bath and quenched by the addition of 10 mL 5 M NaOH solution and 20 mL toluene. After stirring for 30 minutes, the crude was transferred to a separatory funnel. Organic layer was separated, washed by 5 M NaOH solution

twice, dried over $MgSO_4$, concentrated *in vacuo* and further purified by Al_2O_3 column chromatography.

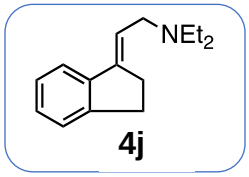

4j

(*E*)-2-(2,3-dihydro-1H-inden-1-ylidene)-*N*,*N*-diethylethan-1-amine (**4j**), prepared according to previously described procedure at 25% overall yield.

^{1}H NMR (500 MHz, $CDCl_3$) δ: 7.51 – 7.44 (m, 1H), 7.25 – 7.23 (m, 1H), 7.21 – 7.14 (m, 2H), 6.05 (ddd, J = 7.0, 4.3, 2.6 Hz, 1H), 3.25 (d, J = 6.8 Hz, 2H), 3.06 – 2.90 (m, 2H), 2.80 – 2.71 (m, 2H), 2.58 (q, J = 7.2 Hz, 4H), 1.07 (t, J = 7.2 Hz, 6H).

^{13}C NMR (125 MHz, $CDCl_3$) δ: 146.06, 144.18, 141.52, 127.87, 126.57, 125.38, 120.33, 116.74, 52.33, 47.08, 30.28, 28.12, 12.04.

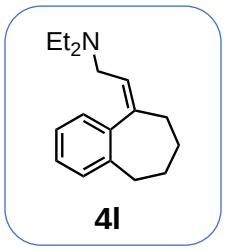

4l

(*Z*)-*N*,*N*-diethyl-2-(6,7,8,9-tetrahydro-5H-benzo[7]annulen-5-ylidene)ethan-1-amine (**4l**), prepared according to previously described procedure at 46% overall yield.

^{1}H NMR (500 MHz, $CDCl_3$) δ: 7.17 – 7.09 (m, 3H), 7.02 – 6.97 (m, 1H), 5.64 (t, J = 6.8 Hz, 1H), 3.00 (d, J = 6.8 Hz, 2H), 2.77 – 2.67 (m, 2H), 2.47 (q, J = 7.1 Hz, 4H), 2.33 – 2.24 (m, 2H), 1.85 (p, J = 5.9 Hz, 2H), 1.72 – 1.61 (m, 2H), 0.92 (t, J = 7.1 Hz, 6H).

^{13}C NMR (125 MHz, $CDCl_3$) δ: 145.62, 141.73, 141.18, 129.12, 128.98, 126.92, 125.59, 124.99, 51.08, 46.81, 38.10, 36.63, 33.30, 27.87, 11.76.ppm.

The (*E*)-selective β-CF_3 or CF_2H substituted allylic diethylamine substrates **4m, 4o,** and **4p** were synthesized by following method.[22]

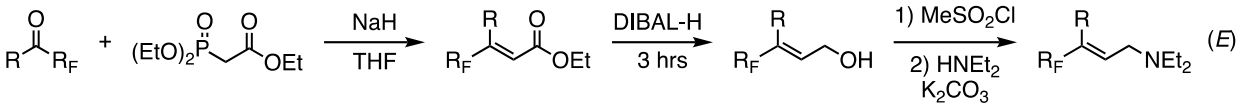

Olefination: A dry 100mL round-bottom flask was charged with a stir bar and 0.60 g NaH (60 wt %, 15 mmol, 1.5 equiv), purged with nitrogen followed by the addition of 30 mL THF. Cooled to 0 °C, ethyl 2-(diethoxyphosphoryl)acetate was added dropwise (3.0 mL, 15 mmol, 1.5 equiv). The reaction was allowed to stir at 0 °C for 30 min until the solution become clear. Fluoroakyl ketone was added dropwise (10 mmol, 1.0 equiv) to the reaction over 5 min, then warmed up to 50 °C, stirring overnight. The reaction was quenched with sat. NH_4Cl solution, and the aqueous layer was extracted with DCM three times. The combined organic layers were dried over $MgSO_4$, concentrated *in vacuo* and purified by silica column chromatography to afforded (E)-R_F-substituted allylic ester. (Yields: 60% to 80% for desired isomer)

Reduction: To a dry 250 mL round-bottom flask was charged with a stir bar, purged with N_2 three times, followed by the addition of unsaturated ester (4.8 mmol), dry THF (24 mL). The flask was then cooled in ice bath, then added DIBAL-H solution (2.5 equiv, 1 M in hexanes) dropwise. The reaction was allowed to stir at 0 °C for 2 hours then quenched by the addition of 10 mL sat. Rochelle salt solution. After stirring at rt overnight, the crude was extracted with Et_2O three times, combined organic lay dried over $MgSO_4$, concentrated *in vacuo* and used for next step without further purification.

Chlorination: To a dry 50 mL round-bottom flask was charged with a stir bar, purged with N_2 three times, followed by the addition of allylic alcohol (4.6 mmol), dry DCM (20 mL), and 1.9 mL $Et_{3\ N}$ (13.8 mmol, 3.0 equiv). The flask was then cooled in ice bath, then added $MeSO_2Cl$ (13.8 mmol, 3.0 equiv) dropwise. The reaction was allowed to stir at 0 °C for 5 hours followed by the addition of another 2.0 equiv of $MeSO_2Cl$. The resulting mixture was then warmed up to rt, and stirred overnight. The reaction crude was diluted in DCM, washed sequentially with 1 N HCl

solution, sat. $NaHCO_3$ solution and brine. The organic layer was then dried over $MgSO_4$, concentrated *in vacuo* and purified by silica column chromatography to afforded the corresponding allylic chloride. (Yield: 85% to 95%, two steps)

S_N2: To a dry 50 mL round-bottom flask was charged with a stir bar, allylic chloride (4.0 mmol), $HNEt_2$ (6.0 mmol, 1.5 equiv), K_2CO_3 (10 mmol, 2.5 equiv), and 22 mL acetone. The reaction mixture was then refluxed under N_2 at 70 °C overnight. The reaction crude was then filtered through celite, concentrated *in vacuo* to remove solvent, re-diluted in Et_2O, extracted with 1 N HCl three time. The aqueous layer was then basified by the addition of 3 N NaOH solution, (pH>11) and extracted with DCM three times. The combined DCM layers were $MgSO_4$, concentrated *in vacuo* and distilled under vacuum to afford the desired allylic amines (Yields: 82% to 88%)

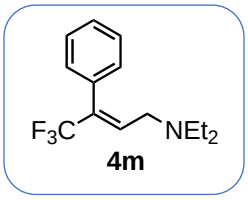

4m

(*E*)-*N,N*-diethyl-4,4,4-trifluoro-3-phenylbut-2-en-1-amine (4m), prepared according to previously described procedure.

^{1}H NMR (500 MHz, $CDCl_3$) δ: 7.44 – 7.36 (m, 3H), 7.25 – 7.21 (m, 2H), 6.55 (ddt, J = 6.6, 5.0, 1.6 Hz, 1H), 3.13 – 2.94 (m, 2H), 2.46 (q, J = 7.1 Hz, 4H), 0.95 (t, J = 7.1 Hz, 6H).

^{13}C NMR (125 MHz, $CDCl_3$) δ: 134.83 (q, J = 5.3 Hz), 132.38 (q, J = 29.7 Hz), 132.04, 129.52, 128.57, 128.40, 123.22 (q, J = 273.2 Hz), 50.39, 47.12, 11.81.

^{19}F NMR (471 MHz, $CDCl_3$) δ -65.91 (d, J = 1.9 Hz).

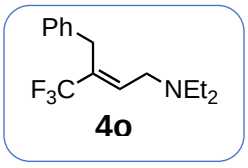

4o

(*E*)-3-benzyl-*N,N*-diethyl-4,4,4-trifluorobut-2-en-1-amine (4o), prepared according to previously described procedure.

^{1}H NMR (500 MHz, $CDCl_3$) δ: 7.32 – 7.27 (m, 2H), 7.24 – 7.20 (m, 1H), 7.19 – 7.16 (m, 2H), 6.45 (t, J = 6.2 Hz, 1H), 3.60 (s, 2H), 3.18 (dq, J = 5.1, 2.4 Hz, 2H), 2.49 (q, J = 7.1 Hz, 4H), 1.00 (t, J = 7.1 Hz, 6H).

^{13}C NMR (125 MHz, $CDCl_3$) δ: 137.92, 135.13 (q, J = 5.8 Hz), 129.40 (q, J = 28.6 Hz), 128.77, 128.33, 126.71, 124.30 (q, J = 273.4 Hz), 50.52, 47.45, 31.89, 12.11.

^{19}F NMR (471 MHz, $CDCl_3$) δ: -67.01 (d, J = 2.2 Hz).

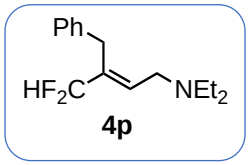

4p

(*E*)-3-benzyl-*N*,*N*-diethyl-4,4-difluorobut-2-en-1-amine (4p), prepared according to previously described procedure.

^{1}H NMR (500 MHz, $CDCl_3$) δ: 7.31 – 7.26 (m, 2H), 7.22 – 7.17 (m, 3H), 6.10 – 6.05 (m, 1H), 5.99 (t, J = 56.1 Hz, 1H), 3.57 (s, 2H), 3.17 (dt, J = 6.8, 3.7 Hz, 2H), 2.49 (q, J = 7.1 Hz, 3H), 1.00 (t, J = 7.2 Hz, 6H).

^{13}C NMR (125 MHz, $CDCl_3$) δ: 138.58, 134.22 (t, J = 9.9 Hz), 133.73 (t, J = 20.5 Hz), 128.63, 128.51, 126.41, 117.00 (t, J = 237.6 Hz), 50.37, 47.25, 31.10 (t, J = 1.8 Hz), 11.96.

^{19}F NMR (471 MHz, $CDCl_3$) δ: -114.38 (d, J = 55.8 Hz).

The (*Z*)-selective β-CF_3 substituted allylic diethylamine substrates **4n** was synthesized by following method.[23]

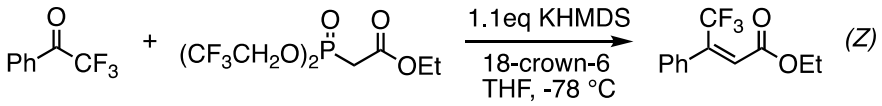

Olefination: A dry 50 mL round-bottom flask was charged with a stir bar and 1.76 g KHMDS (8.8 mmol, 1.1 equiv) and 2.56 g 18-crown-6 (9.6 mmol, 1.2 equiv) purged with nitrogen followed by the addition of 15 mL THF. Cooled to -78 °C, ethyl 2-(bis(2,2,2-trifluoroethoxy)phosphoryl)acetate was added dropwise (8.8 mmol, 1.1 equiv). The reaction was allowed to stir at -78 °C for 45 min followed by the addition of trifluoroacetophenone (8.0 mmol,

1.0 equiv) to the reaction, stirred at -78 °C for another 3 h then warmed up to rt, quenched with sat. NH_4Cl solution, and the aqueous layer was extracted with DCM three times. The combined organic layers were dried over $MgSO_4$, concentrated *in vacuo* and purified by silica column chromatography to afford (Z)-R_F-substituted allylic ester at 58% yield.

Reduction, **Chlorination, and SN_2** were carried out under same conditions as described above.

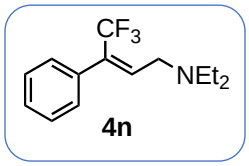

4n

(*Z*)-*N*,*N*-diethyl-4,4,4-trifluoro-3-phenylbut-2-en-1-amine (4n), prepared according to previously described procedure. Purity: Z/E=22:1.

^{1}H NMR (500 MHz, $CDCl_3$) δ: δ 7.42 – 7.30 (m, 5H), 6.19 (td, J = 6.2, 0.9 Hz, 1H), 3.49 (dq, J = 5.8, 2.8 Hz, 2H), 2.58 (q, J = 7.1 Hz, 4H), 1.07 (t, J = 7.1 Hz, 6H).

^{13}C NMR (125 MHz, $CDCl_3$) δ: 140.93 (q, J = 2.8 Hz), 136.28 (q, J = 1.8 Hz), 132.15 (q, J = 30.5 Hz), 128.41, 128.29, 128.15, 124.03 (q, J = 275.7 Hz), 51.29 (q, J = 2.4 Hz), 47.49, 12.09.

^{19}F NMR (471 MHz, $CDCl_3$) δ: -57.30 (d, J = 3.1 Hz).

β-Silyl substituted allylic diethylamine substrate **4q** was synthesized by following method, modified from literature.[24]

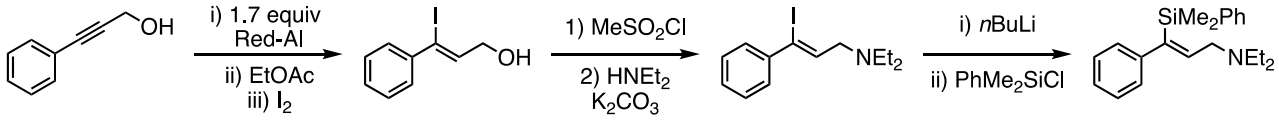

Hydroalumination:[6] To a dry 100 mL schlenk flask was charged with a stir bar, purged with N_2 three times, followed by the addition of dry THF (30 mL) and 2.8 mL RedAl solution (8.5 mmol, 1.7 equiv). The flask was then cooled in ice bath, then added 5 mL THF solution of 3-phenyl-2-propyn-1-ol (5.0 mmol, 1.0 equiv) dropwise. The reaction was allowed to warm up to rt and stir

for 4 hours. Then, the reaction flask was then cooled to ⁻10 °C followed by the slow addition of 2.0 mL EtOAc to quench excess Red-Al then stirred at -10 °C for another 15 min. The resulting mixture was then cooled to ⁻78 °C, followed by the addition of I_2 (10 mmol, 2.0 equiv) in one portion under nitrogen flow. The reaction crude was then allowed to stir at ⁻78 °C for another hour before being quenched by 15 mL sat. Rochelle salt solution and 25 mL sat. $Na_2S_2O_3$ solution at 0 °C. The biphasic mixture was then stirred vigorously at rt overnight, and extracted by Et_2O three times. The combined organic layer was then dried over $MgSO_4$, concentrated *in vacuo* and used for next step without further purification.

Chlorination and SN_2 were carried out under same conditions as described above.

Vinyl silane synthesis: To a dry 200 mL schlenk flask was charged with a stir bar, purged with N_2 three times, followed by the addition of dry THF (25 mL) and starting vinyl iodine (5.0 mmol, 1.0 equiv). The flask was then cooled to ⁻78 °C, followed by the slow addition of nBuLi (12 mmol, 2.4 equiv) over 10 min. The resulting crude was allowed to stir at ⁻78 °C for another 30 min, before the addition of chloro(dimethyl)phenylsilane (15 mmol, 3.0 equiv). The resulting mixture was allowed to stir at ⁻78 °C for another 2 hours followed by being quenched with sat. $NaHCO_3$ solution, extracted by Et_2O three times. The combined organic layer was then dried over $MgSO_4$, concentrated *in vacuo* and further purified by Al_2O_3 column chromatography.

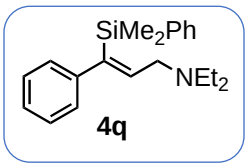

4q

(*Z*)-3-(dimethyl(phenyl)silyl)-*N*,*N*-diethyl-3-phenylprop-2-en-1-amine (4q), prepared according to previously described procedure.

^{1}H NMR (500 MHz, $CDCl_3$) δ: δ 7.62 – 7.55 (m, 2H), 7.35 (dd, J = 4.8, 1.9 Hz, 3H), 7.29 – 7.23 (m, 2H), 7.21 – 7.14 (m, 1H), 7.12 – 7.05 (m, 2H), 6.33 (t, J = 6.3 Hz, 1H), 3.10 (d, J = 6.3 Hz, 2H), 2.40 (q, J = 7.1 Hz, 4H), 0.91 (t, J = 7.1 Hz, 6H), 0.34 (s, 6H).

^{13}C NMR (125 MHz, $CDCl_3$) δ: 146.66, 146.50, 142.37, 139.34, 133.99, 129.11, 128.02, 127.97, 127.72, 125.73, 54.79, 46.89, 12.04, -0.34.

4.7.4 General procedure for Rh-catalyzed reductive amination of allylic diethylamine with secondary amine nucleophiles (General procedure A)

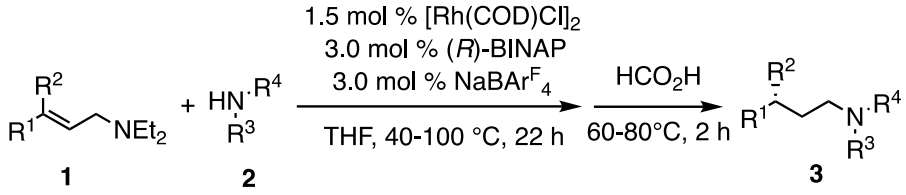

General procedure A: $[Rh(COD)Cl]_2$ (2.0 mg, 0.0036 mmol, 1.5 mol %), (*R*)-BINAP (4.5 mg, 0.0072 mmol, 3.0 mol %), $NaBAr_4^F$ (6.4 mg, 0.0072 mmol, 3.0 mol %), and THF (0.2 mL) were added to a 4 mL vial equipped with a stir bar in the glove box under nitrogen atmosphere. To the vial was added sequentially allylic diethylamine (**1**, 0.24 mmol, 1.0 equiv), and secondary amine (**2**, 0.29 mmol, 1.2 equiv). The resulting solution was allowed to stir for 22 h at 40 °C (unless otherwise noted). After 22 h, formic acid (0.36 mmol, 3.0 equiv) was added into reaction vial via syringe and the reaction was allowed to stir for another 2 h at 60 °C (unless otherwise noted). The reaction crude was quenched by the addition of DCM, concentrated *in vacuo* and then purified by basic alumina chromatography to afford the desired product **3**.

General procedure for Rh-catalyzed reductive amination of allylic diethylamine with aryl amine nucleophiles (General procedure B)

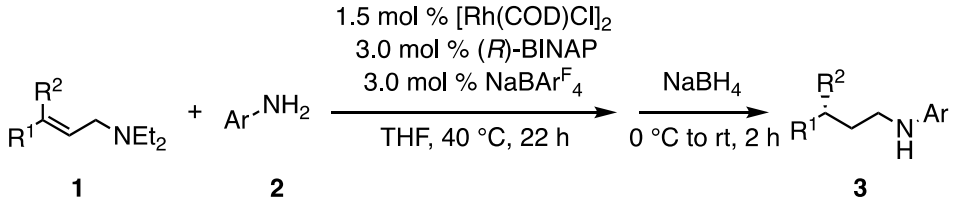

General procedure B: $[Rh(COD)Cl]_2$ (2.0 mg, 0.0036 mmol, 1.5 mol %), (*R*)-BINAP (4.5 mg, 0.0072 mmol, 3.0 mol %), $NaBAr_4^F$ (6.4 mg, 0.0072 mmol, 3.0 mol %), and THF (0.2 mL) were added to a 4 mL vial equipped with a stir bar in the glove box under nitrogen atmosphere. To the vial was added sequentially allylic diethylamine (**1**, 0.24 mmol, 1.0 equiv), and aryl amine (**2**, 0.29 mmol, 1.2 equiv). The resulting solution was allowed to stir for 22 h at 40 °C (unless otherwise noted). After 22 h, the reaction vial was cooled to 0 °C followed by the addition of $NaBH_4$ (0.18 mmol, 1.5 equiv) and 1.0 ml MeOH. The resulting mixture was allowed to stir at 0 °C for 1 h then warmed up to rt for another 1 h. The crude reaction was quenched by the addition of DCM, concentrated *in vacuo* and then re-dissolved in DCM, washed with sat. $NaHCO_3$ solution. The organic layer was dried over $MgSO_4$, concentrated *in vacuo*, and purified by silica gel chromatography to afford the desired product **3**.

General procedure for Rh-catalyzed reductive amination of allylic diethylamine with primary alkyl amine nucleophiles (General procedure C)

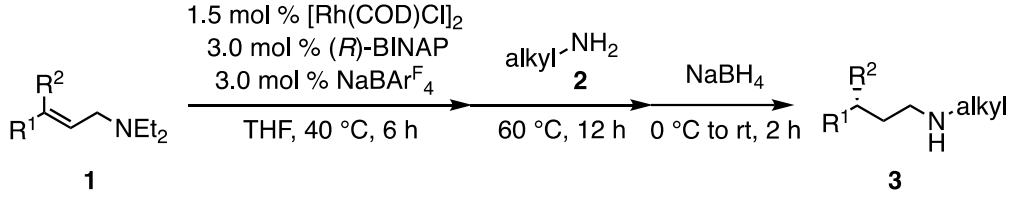

General procedure C: $[Rh(COD)Cl]_2$ (2.0 mg, 0.0036 mmol, 1.5 mol %), (*R*)-BINAP (4.5 mg, 0.0072 mmol, 3.0 mol %), $NaBAr_4^F$ (6.4 mg, 0.0072 mmol, 3.0 mol %), THF (0.2 mL), and allylic diethylamine (**1**, 0.24 mmol, 1.0 equiv) were added to a 4 mL vial equipped with a stir bar in the glove box under nitrogen atmosphere. The resulting solution was allowed to stir for 6 h at 40 °C (unless otherwise noted), followed by the addition of primary alkyl amine (**2**, 0.29 mmol, 1.2 equiv) then continued stirring at 60 °C for another 12 h. After 12 h, the reaction vial was cooled

to 0 °C followed by the addition of $NaBH_4$ (0.18 mmol, 1.5 equiv) and 1.0 ml MeOH. The resulting mixture was allowed to stir at 0 °C for 1 h then warmed up to rt for another 1 h. The reaction crude was then quenched by the addition of DCM, concentrated *in vacuo* and then re-dissolved in DCM, washed with sat. $NaHCO_3$ solution. The organic layer was dried over $MgSO_4$, concentrated *in vacuo*, and purified by basic alumina chromatography to afford the desired product **3**.

4.7.5 Characterization of Final Compounds

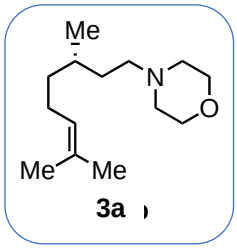

3a

(*S*)-4-(3,7-dimethyloct-6-en-1-yl)morpholine (3a): Prepared according to General procedure A from geranyl diethyl amine (**1a**) with morpholine (**2a**) in 80% isolated yield.

Column Chromatography Condition: 100 g Al_2O_3 + 9 g H_2O, 30 : 1 hexanes/ EtOAc with 0.5% MeOH to 15 : 1 hexanes/ EtOAc with 1.0% MeOH as gradient eluent.

^{1}H NMR (500 MHz, $CDCl_3$) δ: 5.09 (t, J = 7.1 Hz, 1H), 3.71 (t, J = 4.7 Hz, 4H), 2.49 – 2.39 (m, 4H), 2.40 – 2.26 (m, 2H), 2.08 – 1.87 (m, 2H), 1.68 (s, 3H), 1.60 (s, 3H), 1.52 (ddt, J = 12.5, 10.3, 5.5 Hz, 1H), 1.48 – 1.40 (m, 1H), 1.37 – 1.27 (m, 2H), 1.17 (m, 1H), 0.89 (d, J = 6.6 Hz, 3H).

^{13}C NMR (125 MHz, $CDCl_3$) δ: 131.33, 124.93, 67.19, 57.41, 54.07, 37.37, 33.72, 31.19, 25.86, 25.62, 19.86, 17.80.

HRMS (ESI-TOF) *m/z*: [M+H$^+$] calculated for $C_{14}H_{28}NO$, 226.2171; found, 226.2175.

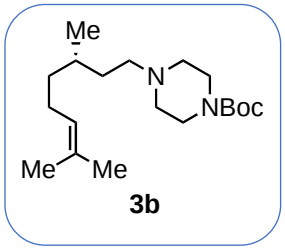

3b

tert-butyl (*S*)-4-(3,7-dimethyloct-6-en-1-yl)piperazine-1-carboxylate (3b): Prepared according to General procedure A from geranyl diethyl amine (**1a**) with *tert*-butyl piperazine-1-carboxylate (**2b**) in 75% isolated yield.

Column Chromatography Condition: 100 g Al_2O_3 + 9 g H_2O, 30 : 1 hexanes/ EtOAc with 0.5% MeOH as eluent.

^{1}H NMR (500 MHz, $CDCl_3$) δ: 5.08 (t, J = 7.0 Hz, 1H), 3.43 (m, 4H), 2.46 – 2.22 (m, 6H), 2.09 – 1.85 (m, 2H), 1.68 (s, 3H), 1.59 (s, 3H), 1.55 – 1.49 (m, 2H), 1.45 (s, 9H), 1.31 (m, 2H), 1.22 – 1.10 (m, 1H), 0.88 (d, J = 6.5 Hz, 3H).

^{13}C NMR (125 MHz, $CDCl_3$) δ: 154.91, 131.34, 124.91, 79.68, 56.98, 53.31, 37.35, 33.94, 31.20, 28.58, 25.86, 25.61, 19.84, 17.80.

HRMS (ESI-TOF) *m/z*: [M+H$^+$] calculated for $C_{19}H_{37}N_2O_2$, 325.2855; found, 325.2850.

Nucleophiles **2c** and **2d** were observed to slow down the isomerization of allylic amine **1a**, therefore the addition of **2c** or **2d** together with formic acid led to increased conversion of **1a**.

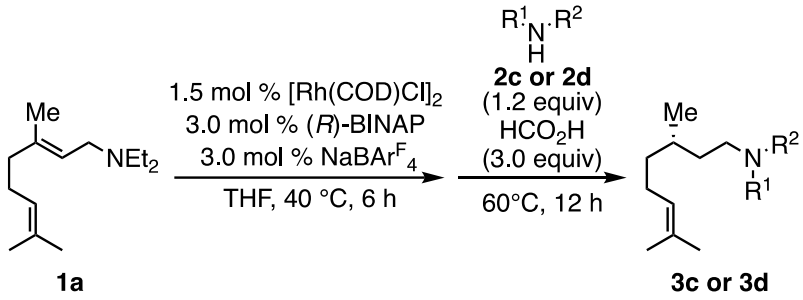

1a **3c or 3d**

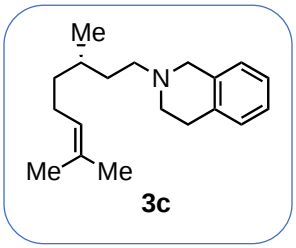

3c

(*S*)-2-(3,7-dimethyloct-6-en-1-yl)-1,2,3,4-tetrahydroisoquinoline (3c): Prepared according to modified General procedure A from geranyl diethyl amine (**1a**) with 1,2,3,4-tetrahydroisoquinoline (**2c**) in 66% isolated yield.

Column Chromatography Condition: 100 g Al_2O_3 + 6 g H_2O, 50 : 1 hexanes/ EtOAc with 0.5% MeOH to 30 : 1 hexanes/ EtOAc with 1.0% MeOH as gradient eluent.

^{1}H NMR (500 MHz, $CDCl_3$) δ: 7.16 – 7.07 (m, 3H), 7.05 – 6.97 (m, 1H), 5.11 (t, J = 6.9 Hz, 1H), 3.63 (s, 2H), 2.91 (t, J = 6.0 Hz, 2H), 2.73 (td, J = 6.0, 3.1 Hz, 2H), 2.52 (dt, J = 9.5, 5.5 Hz, 2H),

2.10 – 1.88 (m, 2H), 1.69 (s, 3H), 1.67 – 1.63 (m, 1H), 1.61 (s, 3H), 1.55 – 1.48 (m, 1H), 1.46 – 1.32 (m, 2H), 1.24 – 1.15 (m, 1H), 0.93 (d, J = 6.6 Hz, 3H)..

^{13}C NMR (125 MHz, $CDCl_3$) δ: 135.09, 134.53, 131.30, 128.76, 126.73, 126.17, 125.66, 125.00, 56.73, 56.49, 51.25, 37.44, 34.39, 31.27, 29.30, 25.88, 25.66, 19.91, 17.82.

HRMS (ESI-TOF) *m/z*: [M+H$^+$] calculated for $C_{19}H_{30}N$, 272.2378; found, 272.2377.

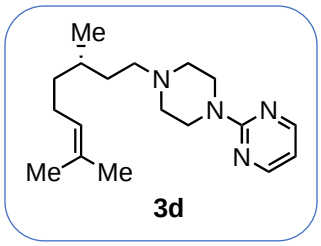

3d

(*S*)-2-(4-(3,7-dimethyloct-6-en-1-yl)piperazin-1-yl)pyrimidine (3d): Prepared according to modified General procedure A from geranyl diethyl amine (**1a**) with 2-(piperazin-1-yl)pyrimidine (**2d**) in 83% isolated yield.

Column Chromatography Condition: 100 g Al_2O_3 + 9 g H_2O, 30 : 1 hexanes/ EtOAc with 0.5% MeOH to 15 : 1 hexanes/ EtOAc with 1.0% MeOH as gradient eluent.

^{1}H NMR (500 MHz, $CDCl_3$) δ: 8.30 (d, J = 4.7 Hz, 2H), 6.47 (t, J = 4.7 Hz, 1H), 5.09 (t, J = 7.0 Hz, 1H), 3.92 – 3.76 (br, 4H), 2.54 – 2.45 (br, 4H), 2.44 – 2.30 (m, 2H), 2.09 – 1.87 (m, 2H), 1.68 (s, 3H), 1.60 (s, 3H), 1.58 – 1.53 (m, 1H), 1.51 – 1.43 (m, 1H), 1.39 – 1.29 (m, 2H), 1.22 – 1.13 (m, 1H), 0.90 (d, J = 6.6 Hz, 3H).

^{13}C NMR (125 MHz, $CDCl_3$) δ: 161.83, 157.83, 131.34, 124.93, 190.91 57.10, 53.41, 43.84, 37.37, 34.01, 31.27, 25.87, 25.63, 19.87, 17.81.

HRMS (ESI-TOF) *m/z*: [M+H$^+$] calculated for $C_{18}H_{31}N_4$, 303.2549; found, 303.2549.

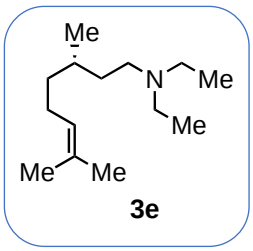

3e

(*S*)-*N*,*N*-diethyl-3,7-dimethyloct-6-en-1-amine (3e): Prepared according to General procedure A from geranyl diethyl amine (**1a**) without any nucleophilic amine added in 83% isolated yield.

Column Chromatography Condition: 100 g Al_2O_3 + 9 g H_2O, 30 : 1 hexanes/ EtOAc with 0.5% MeOH as eluent.

^{1}H NMR (500 MHz, $CDCl_3$) δ: 5.09 (t, J = 7.1 Hz, 1H), 2.51 (q, J = 7.1, 4H), 2.46 – 2.36 (m, 2H), 1.97 (qq, J = 14.5, 7.1 Hz, 2H), 1.67 (d, J = 1.6 Hz, 3H), 1.59 (s, 3H), 1.53 – 1.38 (m, 2H), 1.36 – 1.21 (m, 2H), 1.16 (m, 1H), 1.01 (t, J = 7.1 Hz, 6H), 0.88 (d, J = 6.5 Hz, 3H).

^{13}C NMR (125 MHz, $CDCl_3$) δ: 131.21, 125.05, 50.97, 47.05, 37.44, 34.01, 31.31, 25.87, 25.66, 19.90, 17.77, 11.84.

HRMS (ESI-TOF) *m/z*: [M+H$^+$] calculated for $C_{14}H_{30}N$, 212.2378; found, 212.2385.

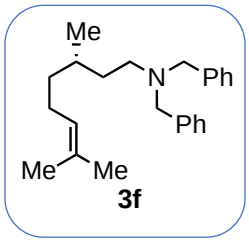

3f

(*S*)-*N*,*N*-dibenzyl-3,7-dimethyloct-6-en-1-amine (3f): Prepared according to General procedure A from geranyl diethyl amine (**1a**) with dibenzylamine (**2f**) in 70% isolated yield.

Column Chromatography Condition: silica gel, 20 : 1 hexanes/ EtOAc as eluent.

^{1}H NMR (500 MHz, $CDCl_3$) δ: δ 7.39 – 7.34 (m, 4H), 7.33 – 7.28 (m, 4H), 7.24 – 7.18 (m, 2H), 5.06 (tq, J = 7.1, 1.4 Hz, 1H), 3.58 (d, J = 13.7 Hz, 2H), 3.50 (d, J = 13.7 Hz, 2H), 2.43 (t, J = 7.3 Hz, 2H), 2.04 – 1.83 (m, 2H), 1.67 (brs, 3H), 1.57 (brs, 4H, overlap), 1.52 – 1.42 (m, 1H), 1.37 – 1.27 (m, 1H), 1.27 – 1.17 (m, 1H), 1.13 – 1.00 (m, 1H), 0.76 (d, J = 6.5 Hz, 3H).

^{13}C NMR (125 MHz, $CDCl_3$) δ: 140.17, 131.13, 128.93, 128.24, 126.83, 125.08, 58.42, 51.44, 37.26, 34.15, 30.52, 25.87, 25.61, 19.75, 17.79.

HRMS (ESI-TOF) *m/z*: [M+H$^+$] calculated for $C_{24}H_{34}N$, 336.2691; found, 336.2695.

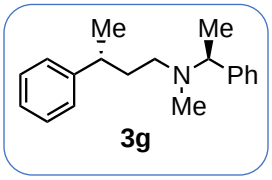

3g

(*R*)-*N*-methyl-3-phenyl-*N*-((*S*)-1-phenylethyl)butan-1-amine (3g): Prepared according to General procedure A from (*E*)-*N*,*N*-diethyl-3-phenylbut-2-en-1-amine (**1b**) with (*S*)-*N*-methyl-1-phenylethan-1-amine (**2g**) and (*R*)-BNIAP as ligand in 64% isolated yield.

Column Chromatography Condition: 100 g Al_2O_3 + 3 g H_2O, 50 : 1 hexanes/ EtOAc with 0.5% MeOH to 30 : 1 hexanes/ EtOAc with 1.0% MeOH as gradient eluent.

^{1}H NMR (500 MHz, $CDCl_3$) δδ 7.31 – 7.23 (m, 5H), 7.23 – 7.19 (m, 2H), 7.19 – 7.12 (m, 3H), 3.52 (q, J = 6.8 Hz, 1H), 2.70 (h, J = 7.1 Hz, 1H), 2.38 (ddd, J = 12.6, 9.4, 6.0 Hz, 1H), 2.18 (ddd, J = 12.5, 9.3, 5.3 Hz, 1H), 2.13 (s, 3H), 1.79 (dddd, J = 13.3, 9.4, 8.0, 5.3 Hz, 1H), 1.71 (ddt, J = 13.4, 9.3, 6.2 Hz, 1H), 1.30 (d, J = 6.8 Hz, 3H), 1.20 (d, J = 6.9 Hz, 3H).

^{13}C NMR (125 MHz, $CDCl_3$) δ: 147.74, 144.08, 128.42, 128.16, 127.82, 127.08, 126.77, 125.94, 63.22, 52.72, 38.47, 37.96, 35.76, 22.66, 18.24.

HRMS (ESI-TOF) *m/z*: [M+H$^+$] calculated for $C_{19}H_{26}N$, 268.2065; found, 268.2073.

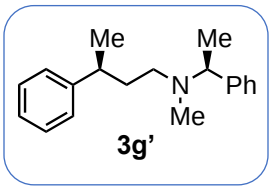

3g'

(*S*)-*N*-methyl-3-phenyl-*N*-((*S*)-1-phenylethyl)butan-1-amine (3g'): Prepared according to General procedure A from (*E*)-*N*,*N*-diethyl-3-phenylbut-2-en-1-amine (**1b**) with (*S*)-*N*-methyl-1-phenylethan-1-amine (**2g**) and (*S*)-BNIAP as ligand in 60% isolated yield.

Column Chromatography Condition: 100 g Al_2O_3 + 3 g H_2O, 50 : 1 hexanes/ EtOAc with 0.5% MeOH to 30 : 1 hexanes/ EtOAc with 1.0% MeOH as gradient eluent.

^{1}H NMR (500 MHz, $CDCl_3$) δ: 7.30 – 7.26 (m, 3H), 7.25 – 7.18 (m, 4H), 7.17 – 7.11 (m, 3H), 3.49 (q, J = 6.7 Hz, 1H), 2.70 (h, J = 7.0 Hz, 1H), 2.36 – 2.20 (m, 2H), 2.12 (s, 3H), 1.81 – 1.67 (m, 2H), 1.26 (d, J = 6.8 Hz, 3H), 1.17 (d, J = 7.0 Hz, 3H).

^{13}C NMR (125 MHz, $CDCl_3$) δ: 147.77, 144.23, 128.41, 128.19, 127.80, 127.07, 126.79, 125.93, 63.34, 52.58, 38.60, 37.79, 35.65, 22.48, 18.55.

HRMS (ESI-TOF) *m/z*: [M+H$^+$] calculated for $C_{19}H_{26}N$, 268.2065; found, 268.2066.

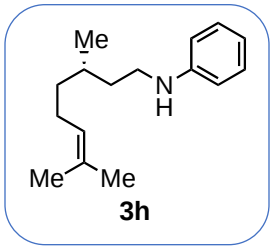

3h

(*S*)-*N*-(3,7-dimethyloct-6-en-1-yl)aniline (3h): Prepared according to General procedure B from geranyl diethyl amine (**1a**) with aniline (**2h**) in 81% isolated yield.

Column Chromatography Condition: silica gel, 50 : 1 hexanes/ EtOAc as eluent.

^{1}H NMR (500 MHz, $CDCl_3$) δ: 7.22 – 7.11 (m, 2H), 6.75 – 6.66 (m, 1H), 6.64 – 6.58 (m, 2H), 5.11 (t, J = 7.0 Hz, 1H), 3.60 (brs, 1H), 3.26 – 3.00 (m, 2H), 2.12 – 1.91 (m, 2H), 1.70 (s, 3H), 1.68 – 1.63 (m, 1H), 1.61 (s, 3H), 1.59 – 1.54 (m, 1H), 1.49 – 1.34 (m, 2H), 1.28 – 1.17 (m, 1H), 0.95 (d, J = 6.6 Hz, 3H).

^{13}C NMR (125 MHz, $CDCl_3$) δ: 148.64, 131.49, 129.36, 124.79, 117.27, 112.87, 42.12, 37.24, 36.84, 30.58, 25.88, 25.62, 19.75, 17.83.

HRMS (ESI-TOF) *m/z*: [M+H$^+$] calculated for $C_{16}H_{26}N$, 232.2065; found, 232.2064.

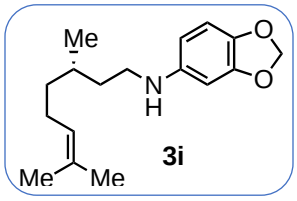

3i

(*S*)-*N*-(3,7-dimethyloct-6-en-1-yl)benzo[d][1,3]dioxol-5-amine (3i): Prepared according to General procedure B from geranyl diethyl amine (**1a**) with benzo[*d*] [1,3]dioxol-5-amine aniline (**2i**) in 74% isolated yield.

Column Chromatography Condition: silica gel, 30 : 1 hexanes/ EtOAc as eluent.

^{1}H NMR (500 MHz, $CDCl_3$) δ: 6.65 (d, J = 8.2 Hz, 1H), 6.24 (d, J = 2.3 Hz, 1H), 6.04 (dd, J = 8.3, 2.3 Hz, 1H), 5.85 (s, 2H), 5.12 (t, J = 7.0 Hz, 1H), 3.35 (brs, 1H), 3.15 – 2.91 (m, 2H), 2.13 – 1.88 (m, 2H), 1.69 (s, 3H), 1.66 – 1.62 (m, 1H), 1.61 (s, 3H), 1.57 – 1.50 (m, 1H), 1.46 – 1.31 (m, 2H), 1.28 – 1.14 (m, 1H), 0.94 (d, J = 6.5 Hz, 3H).

^{13}C NMR (125 MHz, $CDCl_3$) δ: 148.46, 144.52, 139.55, 131.49, 124.78, 108.75, 104.44, 100.65, 96.00, 43.15, 37.24, 36.85, 30.58, 25.88, 25.61, 19.75, 17.83.

HRMS (ESI-TOF) *m/z*: [M+H$^+$] calculated for $C_{17}H_{26}NO_2$, 276.1964; found, 276.1961.

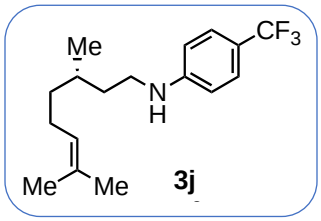

(*S*)-*N*-(3,7-dimethyloct-6-en-1-yl)-4-(trifluoromethyl)aniline (3j): Prepared according to General procedure B from geranyl diethyl amine (**1a**) with 4-trifluoro-methyl aniline (**2j**) in 61% isolated yield (as a mixture of 12:1 desired product and hydrogenated product).

Column Chromatography Condition: silica gel, 99 : 1 hexanes/ EtOAc as eluent.

^{1}H NMR (500 MHz, $CDCl_3$) δ: δ 7.32 (d, J = 8.6 Hz, 2H), 6.51 (d, J = 8.4 Hz, 2H), 5.05 – 4.99 (m, 1H), 3.87 (brs, 1H), 3.21 – 2.84 (m, 2H), 2.06 – 1.80 (m, 2H), 1.62 (d, J = 1.3 Hz, 3H), 1.60 – 1.55 (m, 1H), 1.53 (d, J = 1.4 Hz, 3H), 1.51 – 1.45 (m, 1H), 1.44 – 1.35 (m, 1H), 1.34 – 1.25 (m, 1H), 1.17 – 1.10 (m, 1H), 0.88 (d, J = 6.6 Hz, 3H)..

^{13}C NMR (125 MHz, $CDCl_3$) δ: 151.04, 131.72, 126.82 (q, J = 3.8 Hz), 125.28 (q, J = 270.2 Hz), 124.75, 118.72 (q, J = 32.7 Hz), 111.92, 41.76, 37.26, 36.63, 30.59, 25.98, 25.69, 19.80, 17.93.

^{19}F NMR (471 MHz, $CDCl_3$) δ: -61.30.

HRMS (ESI-TOF) *m/z*: [M+H$^+$] calculated for $C_{17}H_{25}NF_3$, 300.1939; found, 300.1947.

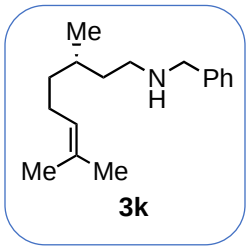

(*S*)-*N*-benzyl-3,7-dimethyloct-6-en-1-amine (3k): Prepared according to General procedure C from geranyl diethyl amine (**1a**) with benzylamine (**2k**) in 70% isolated yield.

Column Chromatography Condition: 100 g Al_2O_3 + 9 g H_2O, 20 : 1 hexanes/ EtOAc with 0.5% MeOH to 10 : 1 hexanes/ EtOAc with 1.0% MeOH as gradient eluent.

^{1}H NMR (500 MHz, $CDCl_3$) δ: 7.34 – 7.30 (m, 4H), 7.26 – 7.21 (m, 1H), 5.09 (dddd, J = 7.1, 5.7, 2.9, 1.4 Hz, 1H), 3.79 (s, 2H), 2.72 – 2.58 (m, 2H), 2.06 – 1.88 (m, 2H), 1.68 (d, J = 1.3 Hz, 3H), 1.59 (s, 3H), 1.56 – 1.44 (m, 2H), 1.39 – 1.28 (m, 2H), 1.21 – 1.10 (m, 1H), 0.88 (d, J = 6.5 Hz, 3H).

^{13}C NMR (125 MHz, $CDCl_3$) δ: 140.70, 131.31, 128.51, 128.25, 127.00, 124.97, 54.35, 47.60, 37.43, 37.38, 30.77, 25.87, 25.64, 19.78, 17.80.

HRMS (ESI-TOF) *m/z*: [M+H$^+$] calculated for $C_{17}H_{28}N$, 246.2222; found, 246.2228.

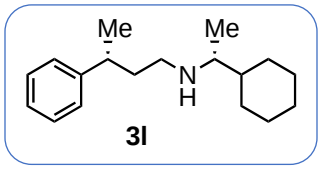

(*R*)-*N*-((*R*)-1-cyclohexylethyl)-3-phenylbutan-1-amine (3l): Prepared according to General procedure C from (*E*)-*N*,*N*-diethyl-3-phenylbut-2-en-1-amine (**1b**) with (*R*)-1-cyclohexylethan-1-amine (**2l**) in 61% isolated yield.

Column Chromatography Condition: 100 g Al_2O_3 + 9 g H_2O, 30 : 1 hexanes/ EtOAc with 0.5% MeOH to 15 : 1 hexanes/ EtOAc with 1.0% MeOH as gradient eluent.

^{1}H NMR (500 MHz, $CDCl_3$) δ: δ 7.32 – 7.27 (m, 2H), 7.22 – 7.15 (m, 3H), 2.77 (h, J = 7.1 Hz, 1H), 2.63 – 2.53 (m, 1H), 2.42 – 2.29 (m, 2H), 1.80 – 1.68 (m, 4H), 1.67 – 1.57 (m, 3H), 1.25 (d, J = 6.9 Hz, 4H, overlap), 1.20 – 1.04 (m, 4H), 0.99 – 0.92 (m, 1H), 0.91 (d, J = 6.4 Hz, 3H).

^{13}C NMR (125 MHz, $CDCl_3$) δ: 147.49, 128.49, 127.07, 126.06, 57.93, 46.03, 43.12, 39.00, 38.35, 30.07, 28.09, 26.92, 26.80, 26.66, 22.74, 16.87.

HRMS (ESI-TOF) *m/z*: [M+H$^+$] calculated for $C_{18}H_{30}N$, 260.2378; found, 260.2381.

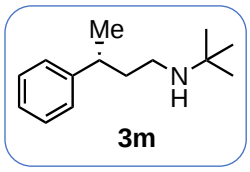

3m

(*R*)-*N*-(tert-butyl)-3-phenylbutan-1-amine (3m): Prepared according to General procedure B from (*E*)-*N*,*N*-diethyl-3-phenylbut-2-en-1-amine (**1b**) with t-butylamine (**2m**) in 58% isolated yield.

Column Chromatography Condition: silical gel, 30 : 1 hexanes/ EtOAc to 10 : 1 hexanes/ EtOAc as gradient eluent.

^{1}H NMR (500 MHz, $CDCl_3$) δ: 7.39 – 7.30 (m, 3H), 7.26 – 7.19 (m, 2H), 2.84 (h, J = 7.0 Hz, 1H), 2.62 – 2.43 (m, 2H), 1.87 – 1.75 (m, 2H), 1.31 (d, J = 6.9 Hz, 3H), 1.08 (s, 9H).

^{13}C NMR (125 MHz, $CDCl_3$) δ: 147.38, 128.47, 127.07, 126.06, 50.34, 40.91, 39.60, 38.34, 29.16, 22.80.

HRMS (ESI-TOF) *m/z*: [M+H$^+$] calculated for $C_{14}H_{24}N$, 206.1909; found, 206.1913.

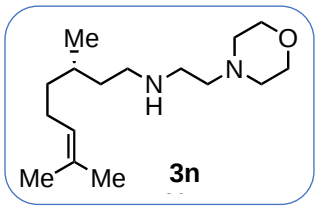

3n

(*S*)-3,7-dimethyl-N-(2-morpholinoethyl)oct-6-en-1-amine (3n): Prepared according to General procedure C from geranyl diethyl amine (**1a**) with 2-morpholinoethan-1-amine (**2n**) in 66% isolated yield.

Purification: No column chromatography needed. Reaction crude was concentrated to remove solvent then re-dissolve in Et_2O followed by an acid/base extraction to afford the desired product **3n**.

^{1}H NMR (500 MHz, $CDCl_3$) δ: δ 5.09 (ddt, J = 8.9, 7.2, 1.6 Hz, 1H), 3.93 – 3.48 (m, 4H), 2.71 (t, J = 6.2 Hz, 2H), 2.62 (dddd, J = 20.9, 11.4, 10.4, 5.7 Hz, 2H), 2.49 (t, J = 6.1 Hz, 2H), 2.45 – 2.40

(m, 4H), 1.96 (m, 2H), 1.81 (brs, 1H), 1.67 (d, J = 1.6 Hz, 3H), 1.59 (s, 3H), 1.57 – 1.44 (m, 2H), 1.40 – 1.28 (m, 2H), 1.18 – 1.11 (m, 1H), 0.88 (d, J = 6.4 Hz, 3H).

^{13}C NMR (125 MHz, $CDCl_3$) δ: 131.32, 124.92, 67.18, 58.42, 53.91, 48.14, 46.35, 37.36, 37.32, 30.80, 25.86, 25.64, 19.74, 17.79.

HRMS (ESI-TOF) *m/z*: [M+H$^+$] calculated for $C_{16}H_{33\ N2}O$, 269.2593; found, 269.2593.

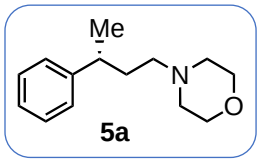

5a

(*R*)-4-(3-phenylbutyl)morpholine (5a): Prepared according to General procedure A from (*E*)-*N*,*N*-diethyl-3-phenylbut-2-en-1-amine (**4a**) with morpholine (**2a**) in 77% isolated yield.

Column Chromatography Condition: 100 g Al_2O_3 + 9 g H_2O, 30 : 1 hexanes/ EtOAc with 0.5% MeOH to 15 : 1 hexanes/ EtOAc with 1.0% MeOH as gradient eluent.

^{1}H NMR (500 MHz, $CDCl_3$) δ: 7.35 – 7.27 (m, 2H), 7.22 – 7.15 (m, 3H), 3.69 (t, J = 4.7 Hz, 4H), 2.75 (h, J = 7.1 Hz, 1H), 2.47 – 2.33 (m, 4H), 2.27 (ddd, J = 12.1, 8.5, 6.5 Hz, 1H), 2.19 (ddd, J = 12.1, 8.6, 6.6 Hz, 1H), 1.83 – 1.73 (m, 2H), 1.26 (d, J = 6.9 Hz, 3H).

^{13}C NMR (125 MHz, $CDCl_3$) δ: 147.30, 128.51, 127.08, 126.13, 67.18, 57.45, 53.94, 38.24, 35.18, 22.64.

HRMS (ESI-TOF) *m/z*: [M+H$^+$] calculated for $C_{14}H_{22}NO$, 220.1701; found, 220.1706.

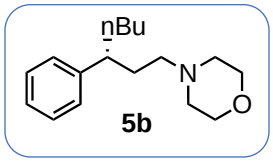

5b

(*R*)-4-(3-phenylheptyl)morpholine (5b): Prepared according to General procedure A from (*E*)-*N*,*N*-diethyl-3-phenylhept-2-en-1-amine (**4b**) with morpholine (**2a**) in 86% isolated yield.

Column Chromatography Condition: 100 g Al_2O_3 + 9 g H_2O, 30 : 1 hexanes/ EtOAc with 0.5% MeOH to 15 : 1 hexanes/ EtOAc with 1.0% MeOH as gradient eluent.

^{1}H NMR (500 MHz, $CDCl_3$) δ: 7.31 – 7.25 (m, 2H), 7.21 – 7.16 (m, 1H), 7.15 – 7.10 (m, 2H), 3.68 (t, J = 4.7 Hz, 4H), 2.53 (tt, J = 9.7, 5.4 Hz, 1H), 2.43 – 2.29 (m, 4H), 2.21 (ddd, J = 12.1, 10.2, 5.8 Hz, 1H), 2.10 (ddd, J = 12.1, 10.2, 4.9 Hz, 1H), 1.85 (ddt, J = 13.1, 10.5, 5.4 Hz, 1H), 1.76 – 1.68 (m, 1H), 1.67 – 1.50 (m, 2H), 1.38 – 1.00 (m, 4H), 0.82 (t, J = 7.2 Hz, 3H).

^{13}C NMR (125 MHz, $CDCl_3$) δ: 145.76, 128.41, 127.73, 126.08, 67.17, 57.46, 53.94, 44.27, 36.96, 33.75, 29.89, 22.88, 14.15.

HRMS (ESI-TOF) *m/z*: [M+H$^+$] calculated for $C_{17}H_{28}NO$, 262.2171; found, 262.2177.

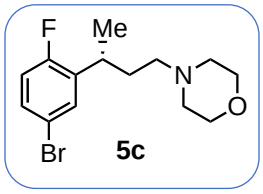

(*R*)-4-(3-(5-bromo-2-fluorophenyl)butyl)morpholine (5c): Prepared according to General procedure A from (*E*)-3-(5-bromo-2-fluorophenyl)-*N*,*N*-diethylbut-2-en-1-amine (**4c**) with morpholine (**2a**) in 74% isolated yield.

Column Chromatography Condition: 100 g Al_2O_3 + 9 g H_2O, 50 : 1 hexanes/ EtOAc with 0.5% MeOH to 15 : 1 hexanes/ EtOAc with 1.0% MeOH as gradient eluent.

^{1}H NMR (500 MHz, $CDCl_3$) δ: 7.32 (dd, J = 6.5, 2.5 Hz, 1H), 7.29 – 7.22 (m, 1H), 6.88 (dd, J = 9.9, 8.6 Hz, 1H), 3.68 (t, J = 4.7 Hz, 4H), 3.08 (h, J = 7.0 Hz, 1H), 2.44 – 2.34 (m, 4H), 2.29 (ddd, J = 12.3, 9.2, 6.0 Hz, 1H), 2.22 (ddd, J = 12.2, 9.3, 5.9 Hz, 1H), 1.86 – 1.68 (m, 2H), 1.25 (d, J = 6.9 Hz, 3H).

^{13}C NMR (125 MHz, $CDCl_3$) δ: 159.90 (d, J = 245.2 Hz), 136.23 (d, J = 16.3 Hz), 131.19 (d, J = 5.4 Hz), 130.34 (d, J = 8.4 Hz), 117.31 (d, J = 24.8 Hz), 116.79 (d, J = 3.2 Hz), 67.11, 57.06, 53.87, 33.80, 31.15, 31.14, 20.93.

HRMS (ESI-TOF) *m/z*: [M+H$^+$] calculated for $C_{14}H_{20}NOBrF$, 316.0712; found, 316.0716.

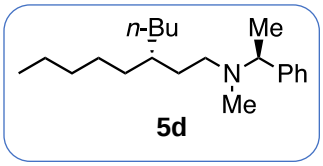

(*S*)-3-butyl-N-methyl-N-((S)-1-phenylethyl)octan-1-amine (5d): Prepared according to General procedure A from (*E*)-3-butyl-*N*,*N*-diethyloct-2-en-1-amine (**4d**) with (*S*)-*N*-methyl-1-phenylethan-1-amine (**2g**) in 61% isolated yield. $[\alpha]_D^{23}$ = -21.09 (*c* = 1.05)

Column Chromatography Condition: 100 g Al_2O_3 + 3 g H_2O, 50 : 1 hexanes/ EtOAc with 0.5% MeOH as eluent.

^{1}H NMR (500 MHz, $CDCl_3$) δ: 7.32 – 7.29 (m, 4H), 7.24 – 7.20 (m, 1H), 3.55 (q, J = 6.7 Hz, 1H), 2.40 (ddd, J = 12.5, 9.8, 6.0 Hz, 1H), 2.29 – 2.20 (m, 1H), 2.18 (s, 3H), 1.45 – 1.38 (m, 2H), 1.36 (d, J = 6.8 Hz, 3H), 1.32 – 1.22 (m, 6H), 1.22 – 1.10 (m, 9H), 0.87 (t, J = 7.1 Hz, 6H).

^{13}C NMR (125 MHz, $CDCl_3$) δ: 144.35, 128.19, 127.82, 126.81, 63.55, 52.39, 38.79, 35.89, 33.82, 33.60, 32.47, 31.03, 28.96, 26.41, 23.25, 22.85, 18.91, 14.29, 14.28.

HRMS (ESI-TOF) *m/z*: [M+H$^+$] calculated for $C_{21}H_{38}N$, 304.3004; found, 304.3006.

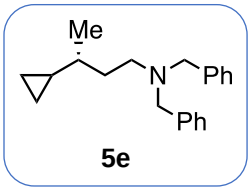

(*R*)-*N*,*N*-dibenzyl-3-cyclopropylbutan-1-amine (5e): Prepared according to General procedure A from (*E*)-3-cyclopropyl-*N*,*N*-diethylbut-2-en-1-amine (**4e**) with dibenzylamine (**2f**) in 69% isolated yield.

Column Chromatography Condition: silica gel, 30 : 1 hexanes/ EtOAc as eluent.

^{1}H NMR (500 MHz, $CDCl_3$) δ: 7.37 (d, J = 7.1 Hz, 4H), 7.31 (dd, J = 8.4, 6.7 Hz, 4H), 7.25 – 7.19 (m, 2H), 3.62 (d, J = 13.6 Hz, 2H), 3.51 (d, J = 13.6 Hz, 2H), 2.54 (ddd, J = 12.8, 9.0, 6.4 Hz, 1H), 2.46 (ddd, J = 12.7, 9.1, 5.1 Hz, 1H), 1.74 (ddt, J = 12.7, 9.2, 6.0 Hz, 1H), 1.54 – 1.39 (m, 1H), 0.84 (d, J = 6.6 Hz, 3H), 0.79 – 0.64 (m, 1H), 0.50 – 0.38 (m, 1H), 0.36 – 0.28 (m, 2H), 0.02 – -0.05 (m, 2H).

^{13}C NMR (125 MHz, $CDCl_3$) δ: 140.14, 128.98, 128.23, 126.83, 58.36, 51.49, 36.71, 34.59, 19.89, 18.35, 4.49, 3.23.

HRMS (ESI-TOF) *m/z*: [M+H$^+$] calculated for $C_{21}H_{28}N$, 294.2222; found, 294.2220.

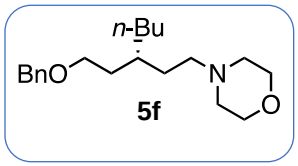

(*R*)-4-(3-(2-(benzyloxy)ethyl)heptyl)morpholine (5f): Prepared according to General procedure A from (*E*)-3-(2-(benzyloxy)ethyl)-*N*,*N*-diethylhept-2-en-1-amine (**4f**) with morpholine (**2a**) in 66% isolated yield.

Column Chromatography Condition: 100 g Al_2O_3 + 6 g H_2O, 15 : 1 hexanes/ EtOAc with 0.5% MeOH as eluent.

^{1}H NMR (500 MHz, $CDCl_3$) δ: 7.35 – 7.31 (m, 4H), 7.30 – 7.26 (m, 1H), 4.49 (s, 2H), 3.70 (t, J = 4.7 Hz, 4H), 3.49 (t, J = 6.9 Hz, 2H), 2.47 – 2.38 (m, 4H), 2.35 – 2.28 (m, 2H), 1.60 (qd, J = 6.8, 1.4 Hz, 2H), 1.53 – 1.49 (m, 1H), 1.48 – 1.42 (m, 2H), 1.29 – 1.23 (m, 8H), 0.88 (t, J = 6.8 Hz, 3H).

^{13}C NMR (125 MHz, $CDCl_3$) δ: 138.75, 128.48, 127.76, 127.64, 73.07, 68.70, 67.15, 57.10, 54.06, 33.93, 33.66, 33.34, 30.59, 28.84, 23.17, 14.25.

HRMS (ESI-TOF) *m/z*: [M+H$^+$] calculated for $C_{20}H_{34}NO_2$, 320.2590; found, 320.2598.

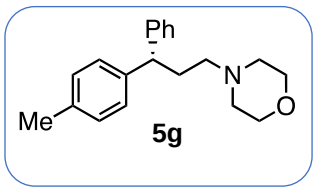

(*S*)-4-(3-phenyl-3-(p-tolyl)propyl)morpholine (5g): Prepared according to General procedure A from (*E*)-*N*,*N*-diethyl-3-phenyl-3-(p-tolyl)prop-2-en-1-amine (**4g**) with morpholine (**2a**) in 66% isolated yield.

Column Chromatography Condition: 100 g Al_2O_3 + 9 g H_2O, 30 : 1 hexanes/ EtOAc with 0.5% MeOH to 15 : 1 hexanes/ EtOAc with 1.0% MeOH as gradient eluent.

^{1}H NMR (500 MHz, $CDCl_3$) δ: 7.31 – 7.26 (m, 3H), 7.25 – 7.24 (m, 1H), 7.21 – 7.14 (m, 3H), 7.12 – 7.08 (m, 2H), 3.98 (t, J = 7.4 Hz, 1H), 3.77 – 3.68 (m, 4H), 2.46 – 2.37 (m, 4H), 2.32 (s, 3H), 2.30 – 2.27 (m, 2H), 2.27 – 2.20 (m, 2H).

^{13}C NMR (125 MHz, $CDCl_3$) δ: 145.19, 141.90, 135.81, 129.29, 128.57, 127.90, 127.81, 126.23, 67.19, 57.46, 53.94, 48.74, 32.61, 21.12.

HRMS (ESI-TOF) *m/z*: [M+H$^+$] calculated for $C_{20}H_{26}NO$, 296.2014; found, 296.2006.

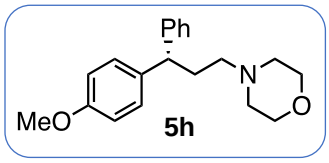

(*S*)-4-(3-(4-methoxyphenyl)-3-phenylpropyl)morpholine (5h): Prepared according to General procedure A from (*E*)-*N*,*N*-diethyl-3-(4-methoxyphenyl)-3-phenylprop-2-en-1-amine (**4h**) with morpholine (**2a**) in 81% isolated yield.

Column Chromatography Condition: 100 g Al_2O_3 + 8 g H_2O, 10 : 1 hexanes/ EtOAc with 1.0% MeOH as eluent.

^{1}H NMR (500 MHz, $CDCl_3$) δ: 7.29 – 7.26 (m, 1H), 7.25 – 7.21 (m, 3H), 7.20 – 7.13 (m, 3H), 6.89 – 6.76 (m, 2H), 3.95 (t, J = 7.6 Hz, 1H), 3.77 (s, 3H), 3.71 (t, J = 4.7 Hz, 5H), 2.49 – 2.36 (m, 4H), 2.31 – 2.24 (m, 2H), 2.24 – 2.15 (m, 2H).

^{13}C NMR (125 MHz, $CDCl_3$) δ: 158.06, 145.32, 137.04, 128.85, 128.57, 127.85, 126.22, 113.96, 67.18, 57.45, 55.35, 53.94, 48.27, 32.74.

HRMS (ESI-TOF) *m/z*: [M+H$^+$] calculated for $C_{20}H_{26}NO_2$, 312.1964; found, 312.1960.

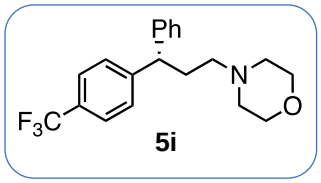

5i

(*S*)-4-(3-phenyl-3-(4-(trifluoromethyl)phenyl)propyl)morpholine (5i): Prepared according to General procedure A from (*E*)-*N*,*N*-diethyl-3-phenyl-3-(4-(trifluoromethyl)phenyl)prop-2-en-1-amine (**4i**) with morpholine (**2a**) in 78% isolated yield.

Column Chromatography Condition: 100 g Al_2O_3 + 9 g H_2O, 30 : 1 hexanes/ EtOAc with 0.5% MeOH to 15 : 1 hexanes/ EtOAc with 1.0% MeOH as gradient eluent.

^{1}H NMR (500 MHz, $CDCl_3$) δ: 7.53 (d, J = 7.9 Hz, 2H), 7.36 (d, J = 8.0 Hz, 2H), 7.33 – 7.27 (m, 2H), 7.25 – 7.18 (m, 3H), 4.17 – 4.03 (m, 1H), 3.71 (t, J = 4.7 Hz, 4H), 2.50 – 2.34 (m, 4H), 2.32 – 2.16 (m, 4H).

^{13}C NMR (125 MHz, $CDCl_3$) δ: 149.05, 143.86, 128.80, 128.65 (q, J = 32.4 Hz), 128.31, 127.94, 126.74, 125.56 (q, J = 3.8 Hz), 124.36 (q, J = 271.8 Hz), 67.16, 57.02, 53.90, 48.81, 32.34, 29.85.

^{19}F NMR (471 MHz, $CDCl_3$) δ: -62.75.

HRMS (ESI-TOF) *m/z*: [M+H$^+$] calculated for $C_{20}H_{23\,N}OF_3$, 350.1732; found, 350.1729.

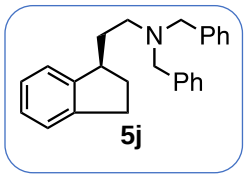

5j

(*R*)-*N*,*N*-dibenzyl-2-(2,3-dihydro-1H-inden-1-yl)ethan-1-amine (5j): Prepared according to General procedure A from (*E*)-2-(2,3-dihydro-1H-inden-1-ylidene)-*N*,*N*-diethylethan-1-amine (**4j**) with dibenzylamine (**2f**) in 69% isolated yield.

Column Chromatography Condition: silica gel, 99 : 1 hexanes/ EtOAc as eluent.

^{1}H NMR (500 MHz, $CDCl_3$) δ: 7.42 – 7.36 (m, 4H), 7.32 (t, J = 7.5 Hz, 4H), 7.24 (t, J = 7.4 Hz, 2H), 7.21 – 7.17 (m, 1H), 7.15 – 7.08 (m, 2H), 7.07 – 7.03 (m, 1H), 3.69 (d, J = 13.5 Hz, 2H), 3.52 (d, J = 13.6 Hz, 2H), 3.16 (ddd, J = 12.0, 9.9, 6.0 Hz, 1H), 2.84 (ddd, J = 15.8, 8.6, 4.5 Hz, 1H), 2.75 (dt, J = 15.9, 8.1 Hz, 1H), 2.61 (dd, J = 12.9, 7.6 Hz, 1H), 2.55 (ddt, J = 13.0, 8.4, 4.4 Hz,

1H), 2.16 – 2.07 (m, 1H), 2.03 (dtt, J = 12.4, 7.9, 4.1 Hz, 1H), 1.61 – 1.55 (m, 1H), 1.47 (dq, J = 12.4, 8.0 Hz, 1H).

^{13}C NMR (125 MHz, $CDCl_3$) δ: 147.77, 144.07, 140.03, 129.06, 128.33, 126.97, 126.32, 126.14, 124.50, 123.59, 58.58, 51.70, 42.74, 32.64, 32.22, 31.52.

HRMS (ESI-TOF) *m/z*: [M+H$^+$] calculated for $C_{25}H_{28}N$, 342.2222; found, 342.2221.

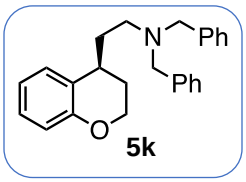

5k

(*S*)-*N*,*N*-dibenzyl-2-(chroman-4-yl)ethan-1-amine (5k): Prepared according to General procedure A from (*E*)-2-(chroman-4-ylidene)-*N*,*N*-diethylethan-1-amine (**4k**) with dibenzylamine (**2f**) in 77% isolated yield.

Column Chromatography Condition: silica gel, 30 : 1 hexanes/ EtOAc as eluent.

^{1}H NMR (500 MHz, $CDCl_3$) δ: 7.39 (d, J = 7.1 Hz, 4H), 7.33 (dd, J = 8.4, 6.7 Hz, 4H), 7.28 – 7.23 (m, 2H), 7.11 – 7.03 (m, 1H), 7.02 – 6.94 (m, 1H), 6.83 – 6.74 (m, 2H), 4.05 (dd, J = 6.5, 4.3 Hz, 2H), 3.74 (d, J = 13.5 Hz, 2H), 3.48 (d, J = 13.5 Hz, 2H), 2.94 (dq, J = 9.9, 5.0 Hz, 1H), 2.61 (dt, J = 12.9, 7.6 Hz, 1H), 2.51 (ddd, J = 12.7, 7.3, 4.7 Hz, 1H), 2.06 (dtd, J = 14.0, 7.7, 4.1 Hz, 1H), 1.84 – 1.70 (m, 1H), 1.62 (dddd, J = 14.2, 10.0, 7.0, 4.6 Hz, 1H), 1.51 – 1.40 (m, 1H).

^{13}C NMR (125 MHz, $CDCl_3$) δ: 154.64, 139.89, 129.12, 129.08, 128.38, 127.24, 127.07, 126.96, 120.24, 116.83, 63.54, 58.75, 50.54, 34.08, 31.06, 26.58.

HRMS (ESI-TOF) *m/z*: [M+H$^+$] calculated for $C_{25}H_{28}NO$, 358.2171; found, 358.2171.

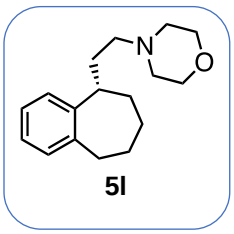

5l

(*S*)-4-(2-(6,7,8,9-tetrahydro-5H-benzo[7]annulen-5-yl)ethyl)morpholine (5l): Prepared according to General procedure A from (*Z*)-*N*,*N*-diethyl-2-(6,7,8,9-tetrahydro-5H-benzo[7]annulen-5-ylidene)ethan-1-amine (**4l**) with morpholine (**2a**) in 75% isolated yield.

Column Chromatography Condition: 100 g Al_2O_3 + 6 g H_2O, 30 : 1 hexanes/ EtOAc with 0.5% MeOH to 15 : 1 hexanes/ EtOAc with 1.0% MeOH as gradient eluent.

^{1}H NMR (500 MHz, Benzene-d_6) δ: 7.13 (dd, J = 7.5, 1.8 Hz, 1H), 7.10 (td, J = 7.2, 1.8 Hz, 1H), 7.06 (td, J = 7.1, 1.8 Hz, 1H), 7.03 (dd, J = 7.4, 1.8 Hz, 1H), 3.61 (t, J = 4.8 Hz, 4H), 2.90 (qd, J = 7.1, 2.3 Hz, 1H), 2.82 – 2.73 (m, 1H), 2.71 – 2.64 (m, 1H), 2.19 – 2.11 (m, 6H), 1.91 (dq, J = 13.8, 7.4 Hz, 1H), 1.79 – 1.44 (m, 7H).

^{13}C NMR (125 MHz, $CDCl_3$) δ: 145.14, 142.59, 130.03, 128.03, 126.06, 126.04, 67.15, 57.99, 54.02, 43.20, 36.26, 33.40, 29.85, 29.72, 28.22.

HRMS (ESI-TOF) *m/z*: [M+H$^+$] calculated for $C_{17}H_{26}NO$, 260.2014; found, 260.2017.

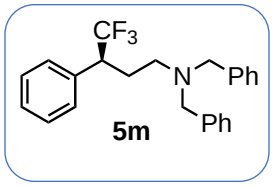

(*S*)-*N*,*N*-dibenzyl-4,4,4-trifluoro-3-phenylbutan-1-amine (5m): Prepared according to General procedure A from (*E*)-*N*,*N*-diethyl-4,4,4-trifluoro-3-phenylbut-2-en-1-amine (**4m**) with dibenzylamine (**2f**) in 63% isolated yield.

Column Chromatography Condition: silica gel, 50 : 1 hexanes/ EtOAc as eluent.

^{1}H NMR (500 MHz, $CDCl_3$) δ: 7.34 – 7.27 (m, 9H), 7.25 – 7.18 (m, 4H), 7.01 (dd, J = 7.5, 1.8 Hz, 2H), 3.67 (d, J = 13.5 Hz, 2H), 3.43 – 3.34 (m, 1H), 3.32 (d, J = 13.5 Hz, 2H), 2.37 (ddd, J = 12.1, 8.6, 6.1 Hz, 1H), 2.33 – 2.27 (m, 1H), 2.27 – 2.19 (m, 1H), 2.02 – 1.88 (m, 1H).

^{13}C NMR (125 MHz, $CDCl_3$) δ: 139.41, 134.82 (q, J = 1.9 Hz), 129.15, 129.13, 128.60, 128.39, 127.97, 127.31 (q, J= 279.5 Hz), 127.09, 58.46, 50.19, 47.49 (q, J = 26.6 Hz), 26.95 (q, J = 1.7 Hz).

^{19}F NMR (471 MHz, $CDCl_3$) δ: -69.58 (d, J = 9.8 Hz).

HRMS (ESI-TOF) *m/z*: [M+H$^+$] calculated for $C_{24}H_{25}NF_3$, 384.1939; found, 384.1927.

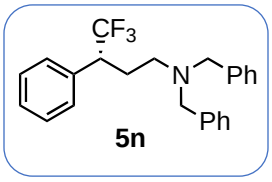

(*R*)-*N*,*N*-dibenzyl-4,4,4-trifluoro-3-phenylbutan-1-amine (5n): Prepared according to General procedure A from (*Z*)-*N*,*N*-diethyl-4,4,4-trifluoro-3-phenylbut-2-en-1-amine (**4n**) with dibenzylamine (**2f**) in 71% isolated yield.

Column Chromatography Condition: silica gel, 50 : 1 hexanes/ EtOAc as eluent.

^{1}H NMR (500 MHz, $CDCl_3$) δ: δ 7.35 – 7.24 (m, 9H), 7.24 – 7.17 (m, 4H), 7.08 – 6.95 (m, 2H), 3.67 (d, J = 13.4 Hz, 2H), 3.44 – 3.34 (m, 1H), 3.32 (d, J = 13.5 Hz, 2H), 2.43 – 2.33 (m, 1H), 2.32 – 2.20 (m, 2H), 1.94 (dtd, J = 15.2, 6.8, 3.3 Hz, 1H).

^{13}C NMR (125 MHz, $CDCl_3$) δ: 139.41, 134.82 (q, J = 1.8 Hz), 129.15, 129.13, 128.60, 128.39, 127.97, 127.31 (q, J= 279.0 Hz), 127.09, 58.47, 50.19, 47.49 (q, J = 26.6 Hz), 26.96 (q, J = 1.8 Hz).

^{19}F NMR (471 MHz, $CDCl_3$) δ: -69.58 (d, J = 9.8 Hz).

HRMS (ESI-TOF) *m/z*: [M+H$^+$] calculated for $C_{24}H_{25}NF_3$, 384.1939; found, 384.1952.

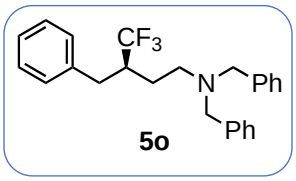

(*R*)-N,N,3-tribenzyl-4,4,4-trifluorobutan-1-amine (5o): Prepared according to General procedure A from (*E*)-3-benzyl-*N*,*N*-diethyl-4,4,4-trifluorobut-2-en-1-amine (**4o**) with dibenzylamine (**2f**) in 59% isolated yield.

Column Chromatography Condition: silica gel, 50 : 1 hexanes/ EtOAc as eluent.

^{1}H NMR (500 MHz, $CDCl_3$) δ: 7.30 (dd, J = 8.1, 6.8 Hz, 4H), 7.26 – 7.15 (m, 9H), 7.04 – 6.99 (m, 2H), 3.54 – 3.46 (m, 2H), 3.38 (d, J = 13.6 Hz, 2H), 2.94 – 2.81 (m, 1H), 2.54 – 2.45 (m, 2H), 2.45 – 2.34 (m, 2H), 1.82 (dtd, J = 14.5, 7.3, 4.9 Hz, 1H), 1.60 (ddt, J = 13.6, 7.7, 5.6 Hz, 1H).

^{13}C NMR (125 MHz, $CDCl_3$) δ: 139.40, 138.26, 129.28, 129.02, 128.58, 128.44 (q, *J* = 280.4 Hz), 128.33, 127.05, 126.61, 58.14, 50.53, 42.39 (q, J = 24.8 Hz), 34.40 (q, J = 2.9 Hz), 24.96 (q, J = 1.8 Hz).

^{19}F NMR (471 MHz, $CDCl_3$) δ: -70.26 (d, J = 8.3 Hz).

HRMS (ESI-TOF) *m/z*: [M+H$^+$] calculated for $C_{25}H_{27}NF_3$, 398.2096; found, 398.2090.

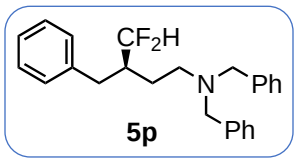

5p

(*R*)-*N*,*N*,3-tribenzyl-4,4-difluorobutan-1-amine (5p): Prepared according to General procedure A (*E*)-3-benzyl-*N*,*N*-diethyl-4,4-difluorobut-2-en-1-amine (**4p**) with dibenzyl-amine (**2f**) in 70% isolated yield.

Column Chromatography Condition: silica gel, 30 : 1 hexanes/ EtOAc as eluent.

^{1}H NMR (500 MHz, $CDCl_3$) δ: 7.34 – 7.28 (m, 7H), 7.26 – 7.22 (m, 4H), 7.21 – 7.16 (m, 1H), 7.08 – 7.02 (m, 2H), 5.54 (td, J = 56.7, 2.9 Hz, 1H), 3.57 – 3.48 (m, 2H), 3.44 (d, J = 13.4 Hz, 2H), 2.67 (dd, J = 13.9, 6.9 Hz, 1H), 2.49 – 2.47 (m, 1H), 2.45 (t, J = 6.8 Hz, 2H), 2.33 – 2.11 (m, 1H), 1.83 – 1.67 (m, 1H), 1.53 – 1.46 (m, 1H).

^{13}C NMR (125 MHz, $CDCl_3$) δ: 139.60, 139.00, 129.28, 129.11, 128.60, 128.37, 127.09, 126.42, 117.96 (t, J = 241.7 Hz), 58.37, 50.35, 41.73 (t, J = 19.1 Hz), 33.89 (dd, J = 6.2, 3.6 Hz), 24.20 (t, J = 3.9 Hz).

^{19}F NMR (471 MHz, $CDCl_3$) δ: -124.91 (ddd, J = 277.9, 56.8, 15.6 Hz), -126.24 (ddd, J = 277.8, 56.7, 17.6 Hz).

HRMS (ESI-TOF) *m/z*: [M+H$^+$] calculated for $C_{25}H_{28}NF_2$, 380.2190; found, 380.2182.

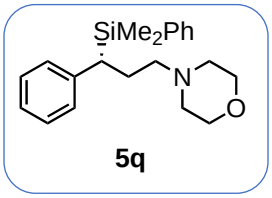

(*R*)-4-(3-(dimethyl(phenyl)silyl)-3-phenylpropyl)morpholine (5q): Prepared according to General procedure A from (*Z*)-3-(dimethyl(phenyl)silyl)-*N*,*N*-diethyl-3-phenylprop-2-en-1-amine (**4q**) with morpholine (**2a**) in 75% isolated yield.

Column Chromatography Condition: 100 g Al_2O_3 + 9 g H_2O, 30 : 1 hexanes/ EtOAc with 0.5% MeOH to 15 : 1 hexanes/ EtOAc with 1.0% MeOH as gradient eluent.

^{1}H NMR (500 MHz, $CDCl_3$) δ: 7.42 – 7.36 (m, 2H), 7.39 – 7.28 (m, 3H), 7.23 – 7.15 (m, 2H), 7.12 – 7.05 (m, 1H), 6.98 – 6.91 (m, 2H), 3.65 (t, J = 4.7 Hz, 4H), 2.32 – 2.23 (m, 5H), 2.20 (ddd, J = 12.1, 7.9, 6.0 Hz, 1H), 2.11 (dt, J = 12.1, 7.7 Hz, 1H), 1.90 (dt, J = 8.1, 7.0 Hz, 2H), 0.25 (s, 3H), 0.16 (s, 3H).

^{13}C NMR (125 MHz, $CDCl_3$) δ: 142.71, 137.57, 134.24, 129.19, 128.20, 128.00, 127.75, 124.75, 67.11, 58.83, 53.86, 34.51, 26.45, -3.73, -5.29.

HRMS (ESI-TOF) *m/z*: [M+H$^+$] calculated for $C_{21}H_{30}NOBSi$, 340.2097; found, 340.2091.

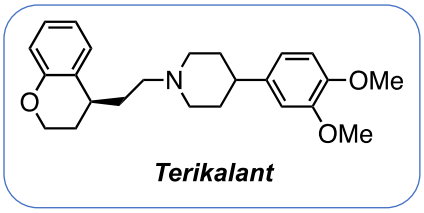

***(S)*-1-(2-(chroman-4-yl)ethyl)-4-(3,4-dimethoxyphenyl)piperidine (Terikanlant):** Prepared according to General procedure A from (*E*)-2-(chroman-4-ylidene)-*N*,*N*-diethylethan-1-amine (**4k**) with 4-(3,4-dimethoxyphenyl) piperidine[7] in 75% isolated yield.

Column Chromatography Condition: 100 g Al_2O_3 + 6 g H_2O, 12 : 1 hexanes/ EtOAc with 0.5% MeOH to 6 : 1 hexanes/ EtOAc with 1.0% MeOH as gradient eluent.

^{1}H NMR (500 MHz, $CDCl_3$) δ: 7.20 (d, J = 7.6 Hz, 1H), 7.13 (ddd, J = 8.7, 7.4, 1.7 Hz, 1H), 6.90 (td, J = 7.4, 1.3 Hz, 1H), 6.87 – 6.80 (m, 4H), 4.31 – 4.19 (m, 2H), 3.91 (s, 3H), 3.90 (s, 3H), 3.23

– 3.06 (m, 2H), 2.94 (dq, J = 10.2, 5.3 Hz, 1H), 2.55 (t, J = 7.7 Hz, 2H), 2.49 (dt, J = 11.7, 4.2 Hz, 1H), 2.21 – 2.03 (m, 4H), 1.95 – 1.75 (m, 6H).

^{13}C NMR (125 MHz, $CDCl_3$) δ: 154.61, 148.92, 147.42, 139.23, 129.22, 127.47, 126.34, 120.27, 118.66, 116.95, 111.25, 110.24, 63.62, 56.71, 56.03, 55.91, 54.85, 54.43, 42.50, 33.91, 33.89, 33.85, 32.19, 27.24.

HRMS (ESI-TOF) *m/z*: [M+H$^+$] calculated for $C_{24}H_{32}NO_3$, 382.2382; found, 382.2375.

Enantioselective Synthesis of (*R*)-Tolterodine

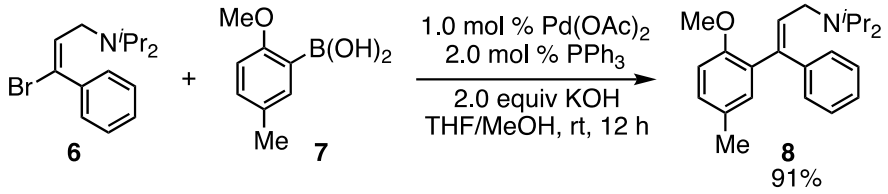

Vinyl bromide 6 was prepared from *trans*-cinnamyl chloride according to literature.[20]

Suzuki coupling: To a oven-dried 100 ml round bottom flask was charged with a stir bar, purged with N_2 three times then added 11 mg $Pd(OAc)_2$ (0.050 mmol, 1.0 mol %), 26 mg PPh_3 (0.10 mmol, 2.0 mol %), 0.560 g KOH (10 mmol, 2.0 equiv), starting material vinyl bromide (1.48g, 5 mmol, 1.0 equiv) ,0.996 g (2-methoxy-5-methylphenyl)boronic acid **7**(6.5 mmol, 1.3 equiv) and 20 mL THF and 20 mL MeOH. The reaction was stirred at rt overnight followed by dilution with EtOAc, and washed by 1 N NaOH solution and brine. **Acid-base extraction**: the organic layer was concentrated *in vacuo*, re-dissolved in Et_2O, and extracted with 3 N HCl solution three times. The resulting acidic aqueous layer was then basified by the addition of 5N NaOH solution until the pH > 11, followed by the extraction with DCM. The combined organic layers was then dried over $MgSO_4$, concentrated *in vacuo*, purified

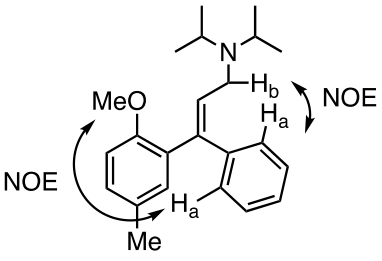

8

by **Al_2O_3 column chromatography**: 200 g Al_2O_3 + 8 g H_2O, 50 : 1 hexanes/ EtOAc with 0.5% MeOH as eluent to afford allylic amine **8** in 91% isolated yield. For **1n**: **^{1}H NMR** (500 MHz, $CDCl_3$) δ: 7.30 – 7.26 (m, 2H), 7.24 – 7.19 (m, 1H), 7.18 – 7.14 (m, 2H), 7.06 – 7.00 (m, 2H), 6.72 (d, J = 8.0 Hz, 1H), 5.89 (t, J = 6.4 Hz, 1H), 3.51 (s, 3H), 3.28 (d, J = 6.4 Hz, 2H), 3.06 (p, J = 6.5 Hz, 2H), 2.29 (t, J = 0.8 Hz, 3H), 0.96 (d, J = 6.6 Hz, 12H). **^{13}C NMR** (125 MHz, $CDCl_3$) δ: 155.24, 141.08, 138.59, 134.18, 133.49, 131.64, 129.79, 129.20, 128.69, 127.55, 126.42, 111.95, 55.99, 48.96, 43.99, 20.96, 20.62. The geometry of double bond was confirmed by NOE experiment (See **Supplementary Figure 64** for details).

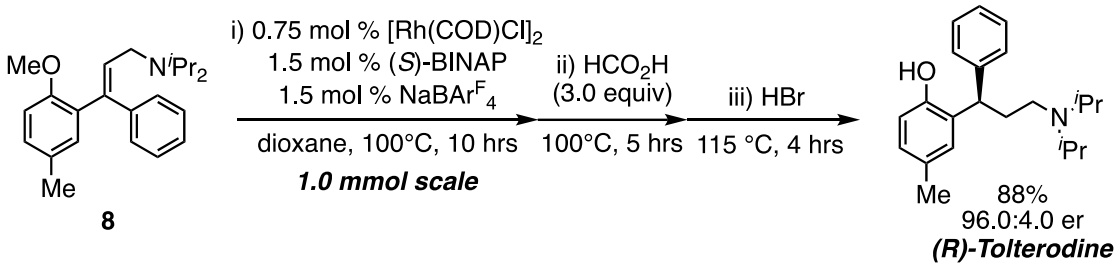

Tolterodine synthesis: $[Rh(COD)Cl]_2$ (4.0 mg, 0.75 mol %), (*S*)-BINAP (9.6 mg, 1.5 mol %), $NaBAr_4^F$ (12.8 mg, 1.5 mol %), and 1,4-dioxane (0.8 mL) were added to a 20 mL vial equipped with a stir bar in the glove box under nitrogen atmosphere. To the vial was added allylic diisopropylamine (**8**, 1.0 mmol, 1.0 equiv). The resulting solution was allowed to stir for 10 h at 100 °C. After 10 h, formic acid (3.0 mmol, 3.0 equiv) was added into reaction vial via syringe and the reaction was allowed to stir for another 5 h at 100 °C. The reaction crude was then diluted in DCM, filtered through basic alumina, and concentrated *in vacuo* (to get rid of 1,4-dioxane solvent). The residue was then transferred into another 20 mL vial, followed by the addition of HBr solution (2.2 mL, 13.2 equiv) and HOAc (2.0 mL), and allowed to stir at 115 °C for 4 h. After 4 h, the reaction crude was then diluted in water, extracted with EtOAc three times. Combined organic

layers were washed with 1 N NaOH solution three times. The pH of last basic wash was verified to be >10. The organic layer was washed with brine, dried over $MgSO_4$, concentrated *in vacuo* and then purified by basic alumina chromatography to afford the desired product **(*R*)-Tolterodine** in 88% isolated yield.

Column Chromatography Condition: 100 g Al_2O_3 + 5 g H_2O, 15 : 1 hexanes/ EtOAc with 0.5% MeOH to 8 : 1 hexanes/ EtOAc with 1.0% MeOH as gradient eluent.

^{1}H NMR (500 MHz, $CDCl_3$) δ: 10.33 (brs, 1H), 7.33 (d, J = 4.3 Hz, 4H), 7.23 (h, J = 4.3 Hz, 1H), 6.85 (dd, J = 8.2, 2.1 Hz, 1H), 6.80 (d, J = 8.1 Hz, 1H), 6.53 (d, J = 2.5 Hz, 1H), 4.49 (dd, J = 11.3, 4.0 Hz, 1H), 3.23 (p, J = 6.7 Hz, 2H), 2.73 (dt, J = 12.7, 3.6 Hz, 1H), 2.50 – 2.25 (m, 2H), 2.12 (s, 3H), 2.10 – 2.03 (m, 1H), 1.13 (d, J = 6.7 Hz, 6H), 1.08 (d, J = 6.6 Hz, 6H).

^{13}C NMR (125 MHz, $CDCl_3$) δ: 153.34, 144.88, 132.55, 129.53, 128.78, 128.66, 128.42, 127.88, 126.28, 118.32, 48.03, 42.21, 39.46, 33.37, 20.91, 20.10, 19.69.

HRMS (ESI-TOF) *m/z*: [M+H$^+$] calculated for $C_{22}H_{32}NO$, 326.2484; found, 326.2489.

4.7.6 Control Experiment of Enamine Reduction

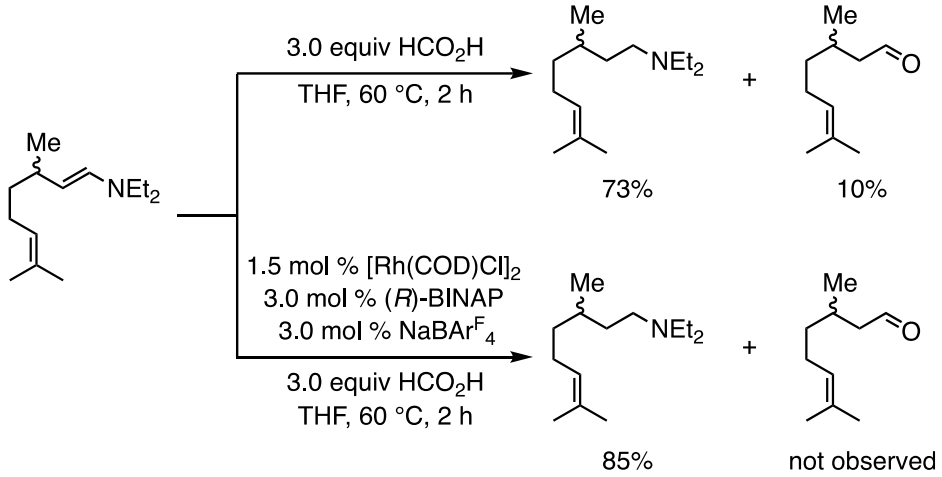

Figure 4.7. Control experiments

Procedure: A pre-made geranyl diethyl enamine was subjected to reduction conditions with and without the rhodium catalyst as shown above. After 2 hours, the reaction crude was concentrated under vacuum, and analyzed using NMR spectroscopy in $CDCl_3$.

4.7.7 HPLC Separation

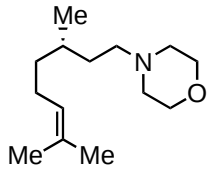

3a

25% (95% hexanes, 5% EtOH, 0.2%TFA, 0.1%DEA), 75% hexanes, 1.0 mL/min, CHIRALPAK® IA3

er = 96.2:3.8

$[\alpha]_D^{23}$ = +5.26 (*c* = 1.03)

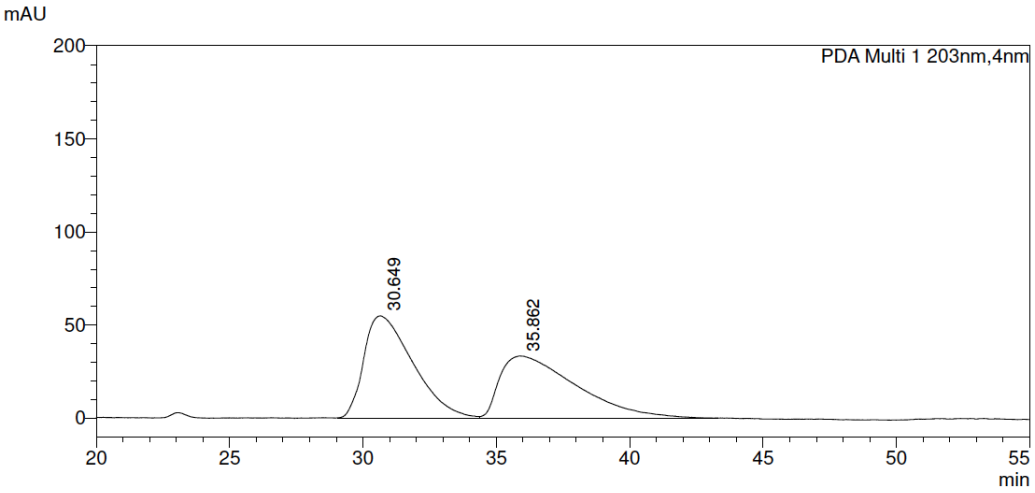

PDA Ch1 203nm

Peak#	Ret. Time	Area	Height	Area%
1	30.649	7045334	54875	51.550
2	35.862	6621600	33379	48.450
Total		13666934	88254	100.000

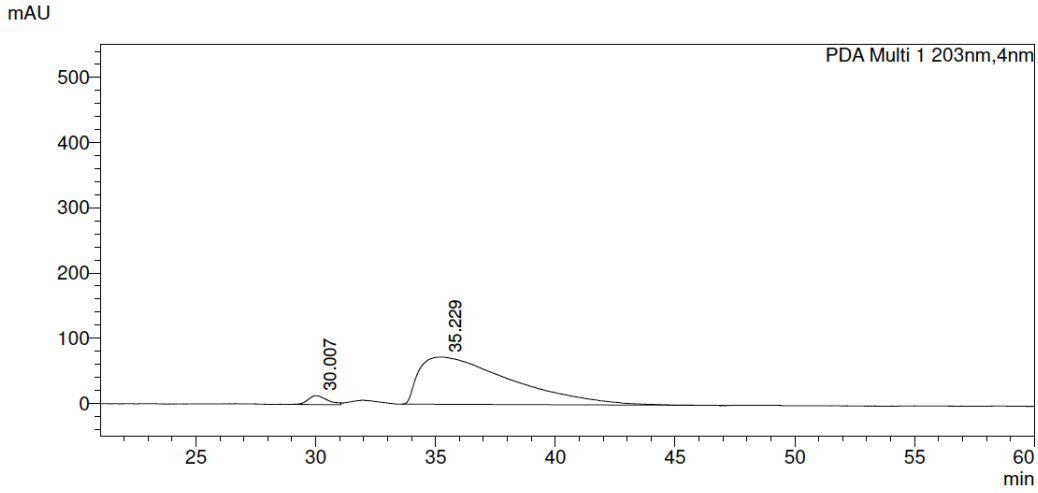

PDA Ch1 203nm

Peak#	Ret. Time	Area	Height	Conc.	Area%
1	30.007	760599	13701	0.000	3.751
2	35.229	19514962	72457	0.000	96.249
Total		20275561	86158		100.000

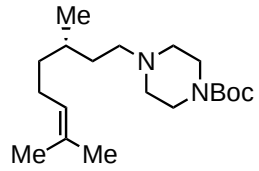

3b

10% (95% hexanes, 5% EtOH, 0.2%TFA, 0.1%DEA), 90% hexanes, 0.8 mL/min, CHIRALCEL® OJ-H

er = 95.5:4.5

$[\alpha]_D^{23}$ = +0.96 (*c* = 1.06)

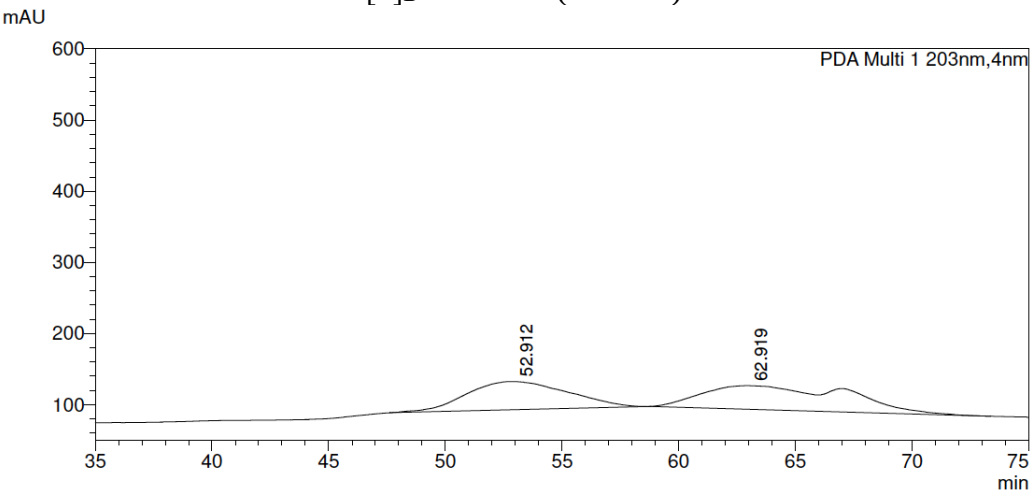

PDA Ch1 203nm

Peak#	Ret. Time	Area	Height	Area%
1	52.912	12004307	39668	44.341
2	62.919	15068254	33358	55.659
Total		27072561	73026	100.000

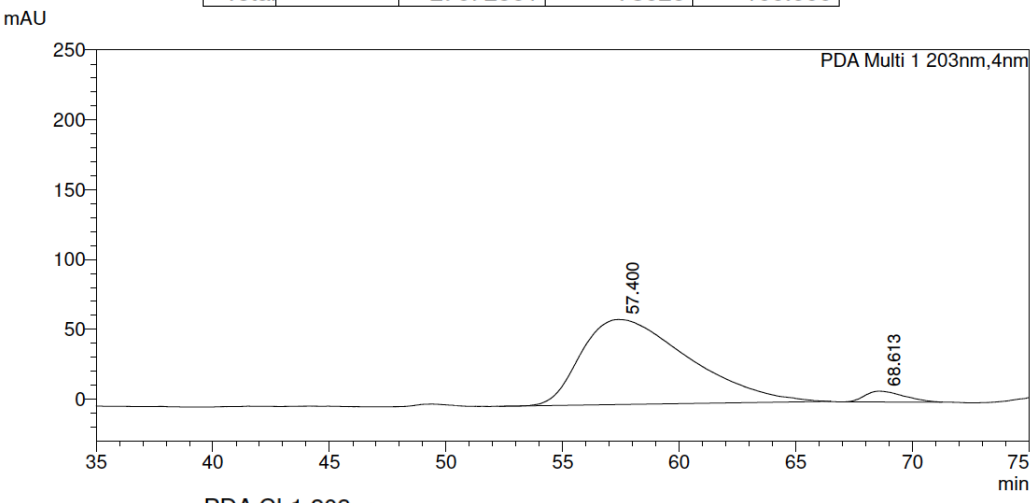

PDA Ch1 203nm

Peak#	Ret. Time	Area	Height	Area%
1	57.400	19593618	60894	95.537
2	68.613	915277	7851	4.463
Total		20508895	68745	100.000

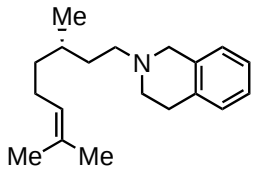

3c

15% (95% hexanes, 5% EtOH, 0.2%TFA, 0.1%DEA), 85% hexanes, 0.5 mL/min, CHIRALPAK® IA3

er = 97.9:2.1

$[\alpha]_D^{23}$ = +4.99 (*c* = 1.22)

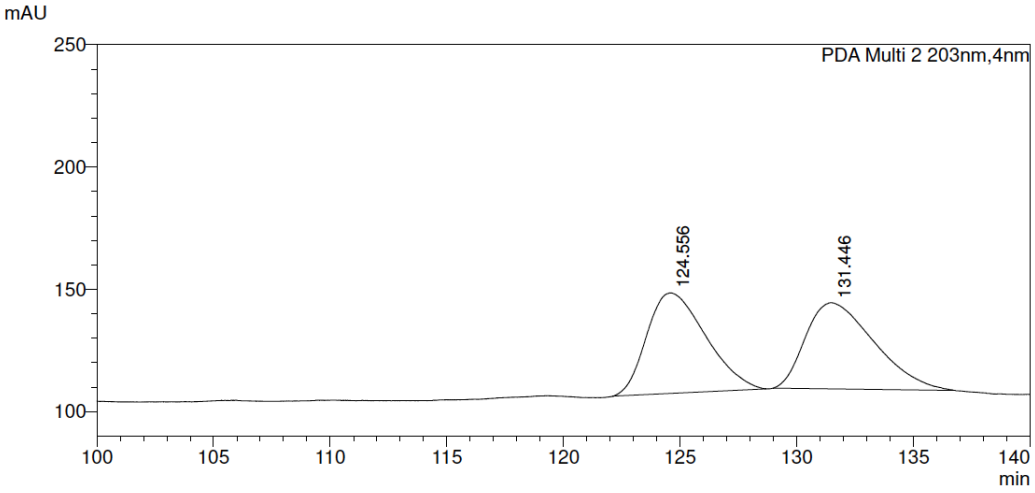

PDA Ch2 203nm

Peak#	Ret. Time	Area	Height	Area%
1	124.556	7224948	41143	50.072
2	131.446	7204093	35251	49.928
Total		14429041	76394	100.000

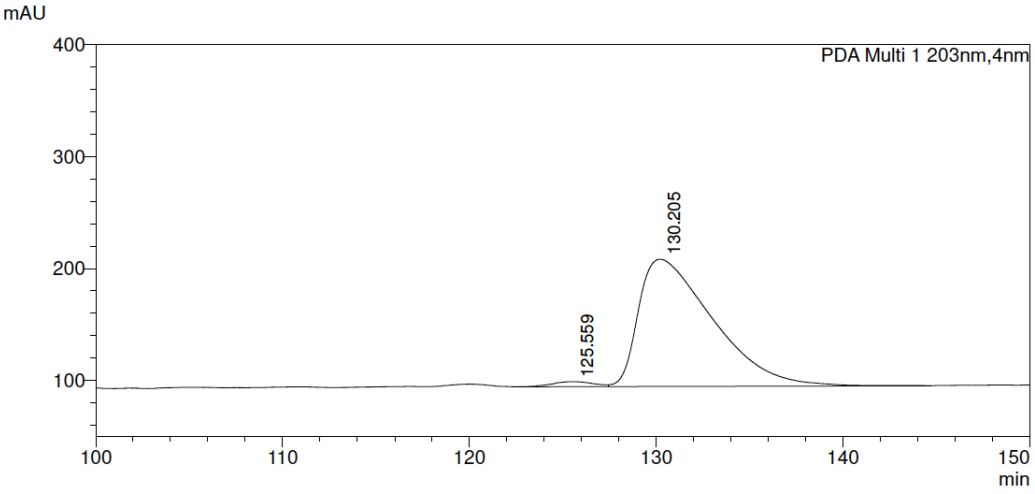

PDA Ch1 203nm

Peak#	Ret. Time	Area	Height	Area%
1	125.559	683713	4457	2.133
2	130.205	31377640	113789	97.867
Total		32061352	118247	100.000

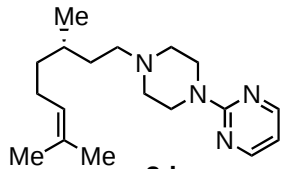

3d

35% (95% hexanes, 5% EtOH, 0.2%TFA, 0.1%DEA), 65% hexanes, 0.8 mL/min, CHIRALCEL® OJ-H

er = 97.1:2.9

$[\alpha]_D^{23}$ = +6.54 (*c* = 1.24)

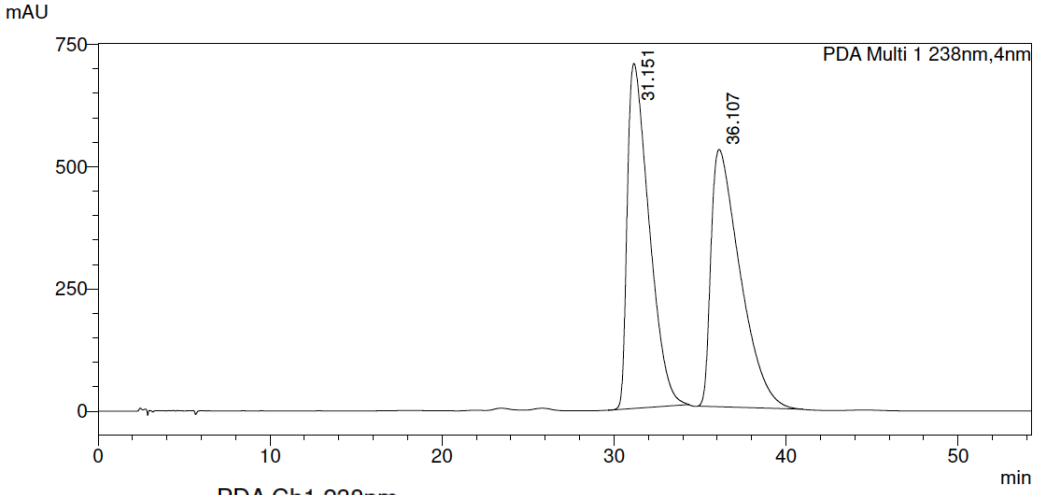

PDA Ch1 238nm

Peak#	Ret. Time	Area	Height	Area%
1	31.151	62093344	705329	50.009
2	36.107	62071201	526124	49.991
Total		124164545	1231453	100.000

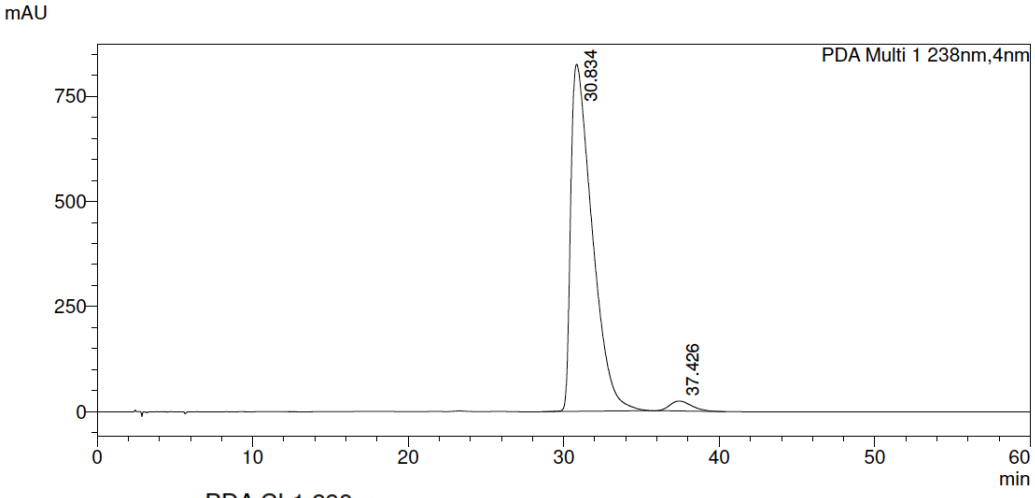

PDA Ch1 238nm

Peak#	Ret. Time	Area	Height	Area%
1	30.834	79102148	824737	97.129
2	37.426	2338378	23773	2.871
Total		81440526	848509	100.000

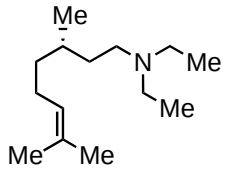

3e

25% (95% hexanes, 5% EtOH, 0.2%TFA, 0.1%DEA), 75% hexanes, 0.8 mL/min, CHIRALCEL® OJ-H

er = 95.8:4.2

$[\alpha]_D^{23}$ = +5.90 (*c* = 1.5.0)

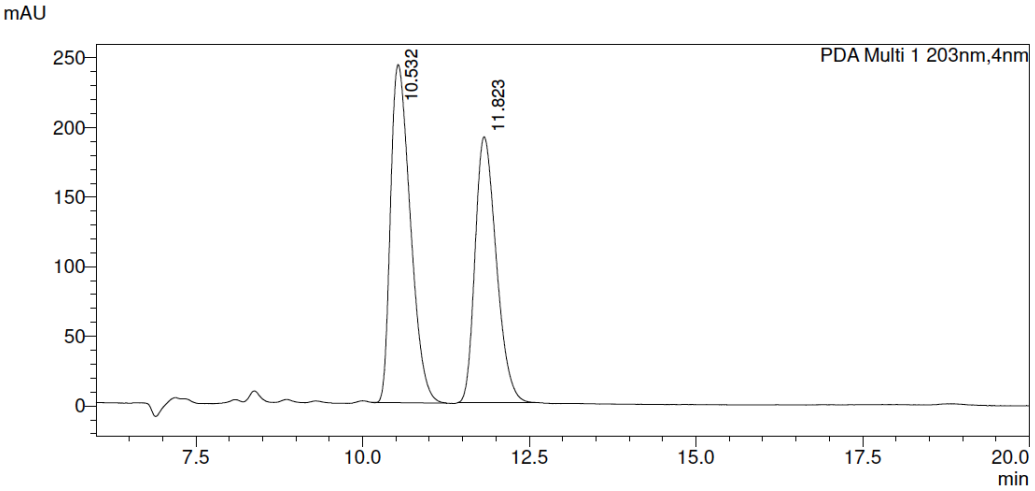

PDA Ch1 203nm

Peak#	Ret. Time	Area	Height	Area%
1	10.532	5023170	242833	54.239
2	11.823	4238093	190933	45.761
Total		9261263	433765	100.000

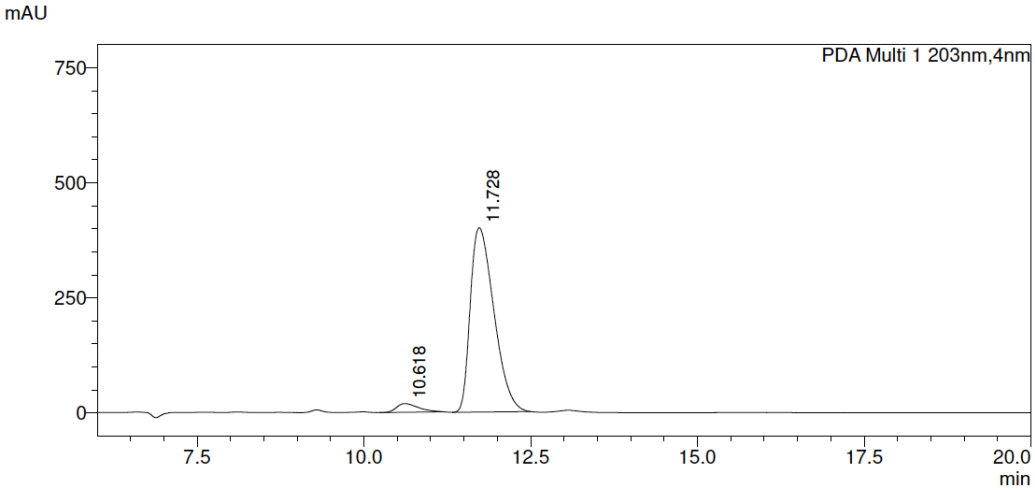

PDA Ch1 203nm

Peak#	Ret. Time	Area	Height	Area%
1	10.618	437245	19164	4.230
2	11.728	9900026	400551	95.770
Total		10337271	419715	100.000

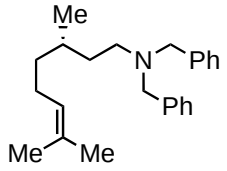

3f

50% (95% hexanes, 5% EtOH, 0.2%TFA, 0.1%DEA), 50% hexanes, 0.8 mL/min, CHIRALCEL® OJ-H

er = 95.8 : 4.2

$[\alpha]_D^{23}$ = -0.90 (*c* = 1.27)

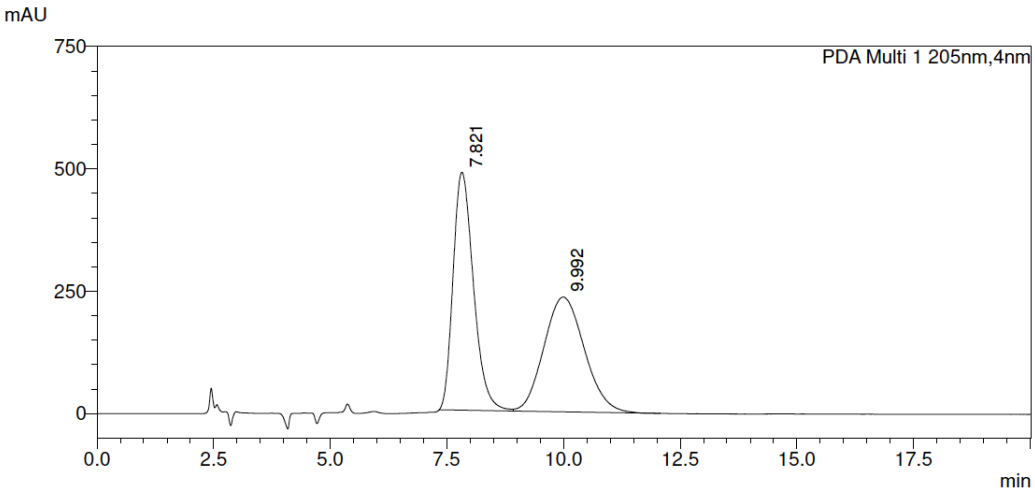

PDA Ch1 205nm

Peak#	Ret. Time	Area	Height	Conc.
1	7.821	14809676	486321	51.130
2	9.992	14155320	234507	48.870
Total		28964995	720828	

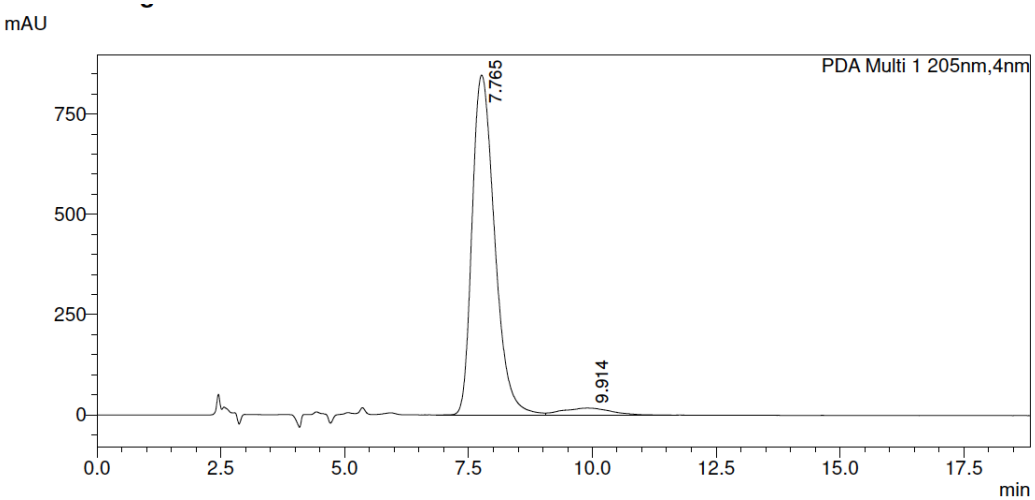

PDA Ch1 205nm

Peak#	Ret. Time	Area	Height	Area%
1	7.765	26853663	847280	95.821
2	9.914	1171290	17301	4.179
Total		28024953	864581	100.000

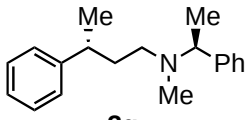

3g

50% (95% hexanes, 5% EtOH, 0.2%TFA, 0.1%DEA), 50% hexanes, 0.8 mL/min, CHIRALCEL® OJ-H

er = 99.8:0.2

$[\alpha]_D^{23}$ = -53.81 (*c* = 1.41)

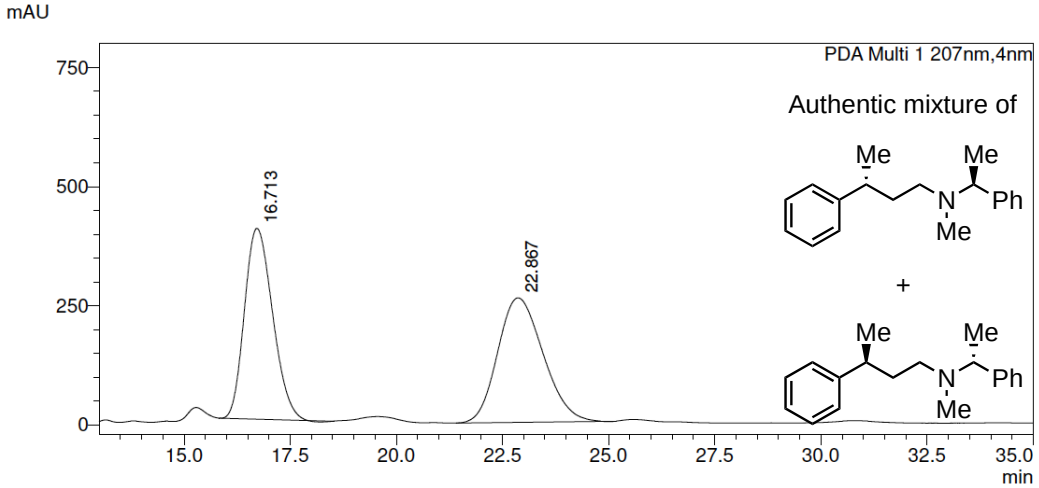

PDA Ch1 207nm

Peak#	Ret. Time	Area	Height	Area%
1	16.713	18488064	400696	48.737
2	22.867	19445966	261542	51.263
Total		37934029	662238	100.000

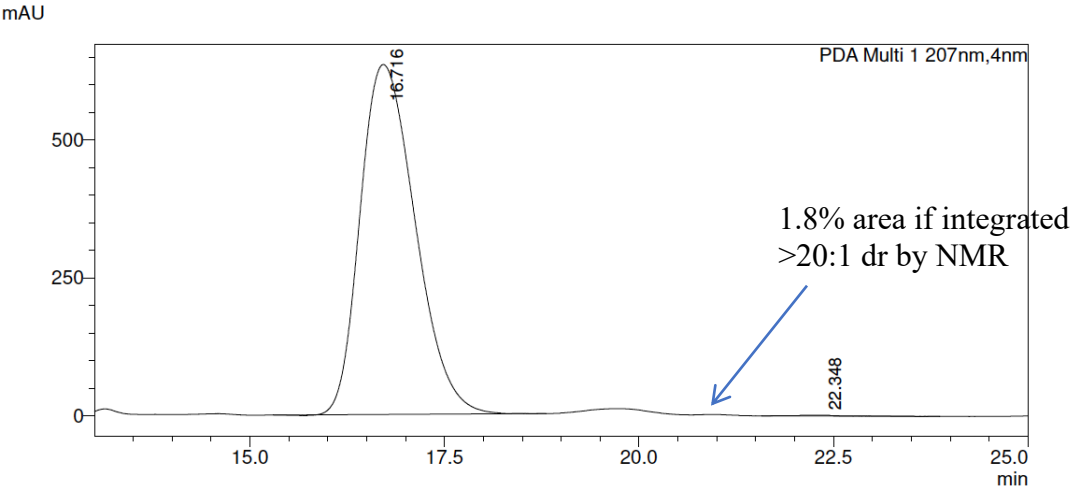

PDA Ch1 207nm

Peak#	Ret. Time	Area	Height	Area%
1	16.716	31186056	633830	99.841
2	22.348	49778	1370	0.159
Total		31235834	635199	100.000

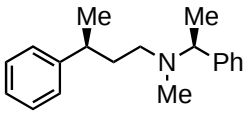

3g'

50% (95% hexanes, 5% EtOH, 0.3%TFA, 0.1%DEA), 50% hexanes, 0.8 mL/min, CHIRALPAK® IB3

er = 97.9:2.1

$[\alpha]_D^{23}$ = +5.06 (*c* = 1.82)

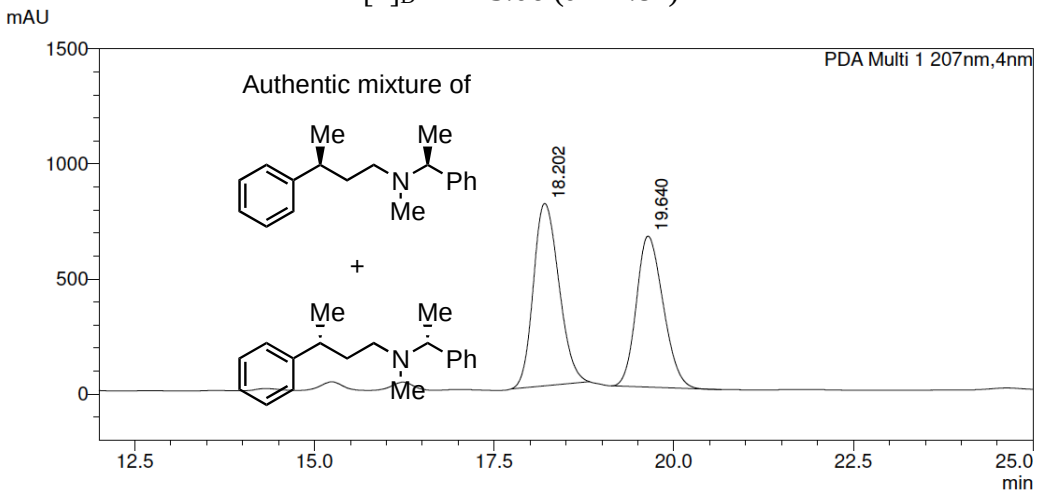

PDA Ch1 207nm

Peak#	Ret. Time	Area	Height	Area%
1	18.202	19620406	792191	53.392
2	19.640	17127349	656651	46.608
Total		36747755	1448842	100.000

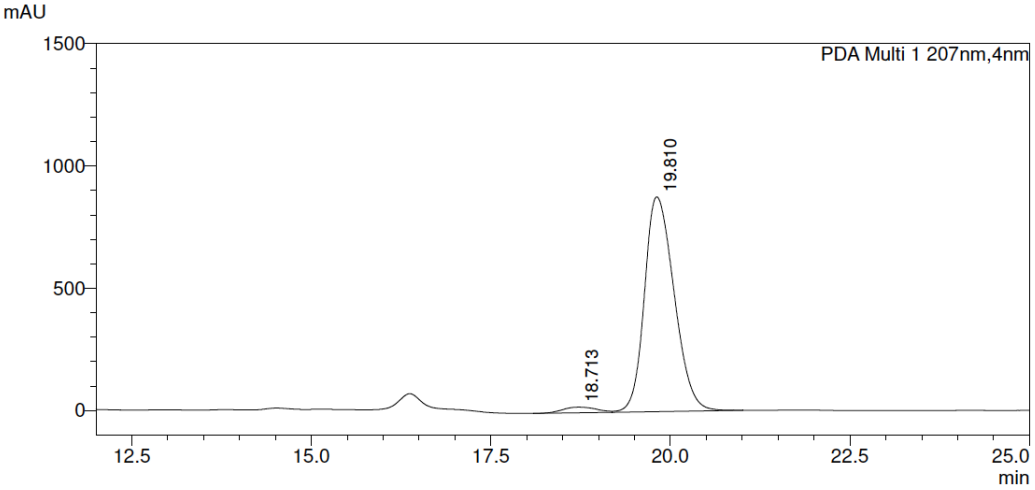

PDA Ch1 207nm

Peak#	Ret. Time	Area	Height	Area%
1	18.713	755220	23394	2.900
2	19.810	25288836	877926	97.100
Total		26044057	901320	100.000

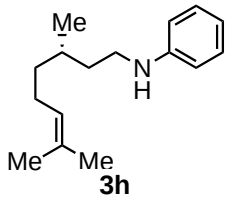

3h

10% (95% hexanes, 5% EtOH, 0.2%TFA, 0.1%DEA), 90% hexanes, 0.5 mL/min, CHIRALCEL® OJ-H

er = 96.6:3.4

$[\alpha]_D^{23}$ = +0.94 (*c* = 1.57)

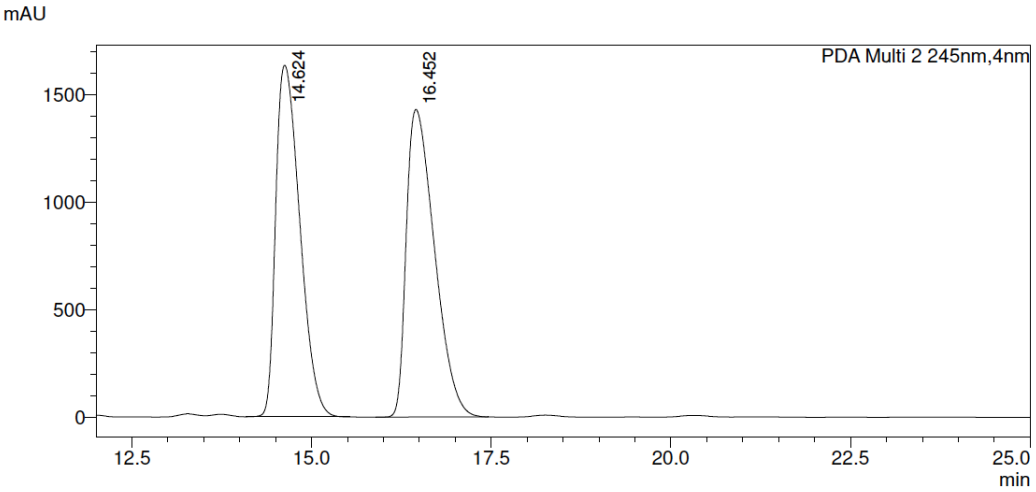

PDA Ch2 245nm

Peak#	Ret. Time	Area	Height	Area%
1	14.624	38080564	1633112	49.408
2	16.452	38992596	1428836	50.592
Total		77073160	3061948	100.000

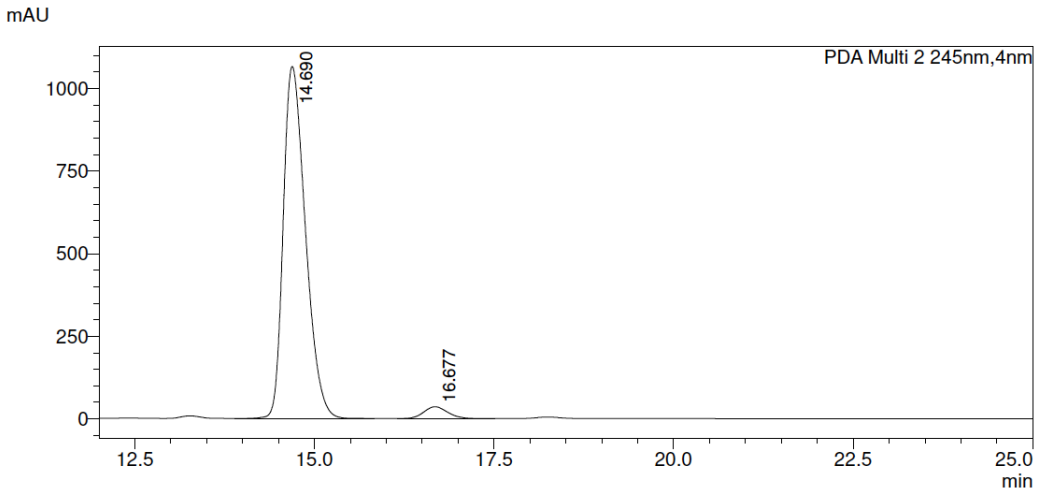

PDA Ch2 245nm

Peak#	Ret. Time	Area	Height	Area%
1	14.690	22874777	1065611	96.580
2	16.677	809936	35403	3.420
Total		23684713	1101015	100.000

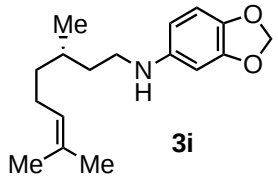

3i

15% (95% hexanes, 5% EtOH, 0.2%TFA, 0.1%DEA), 85% hexanes, 0.5 mL/min, CHIRALCEL® OJ-H

er = 96.9 : 3.1

$[\alpha]_D^{23}$ = +2.92 (*c* = 1.37)

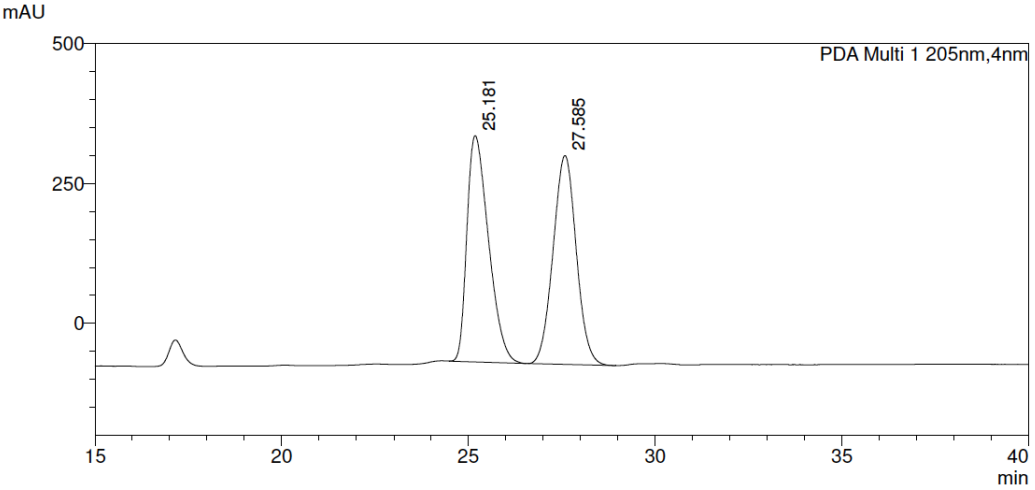

PDA Ch1 205nm

Peak#	Ret. Time	Area	Height	Area%
1	25.181	16289356	404945	50.201
2	27.585	16158952	373843	49.799
Total		32448308	778787	100.000

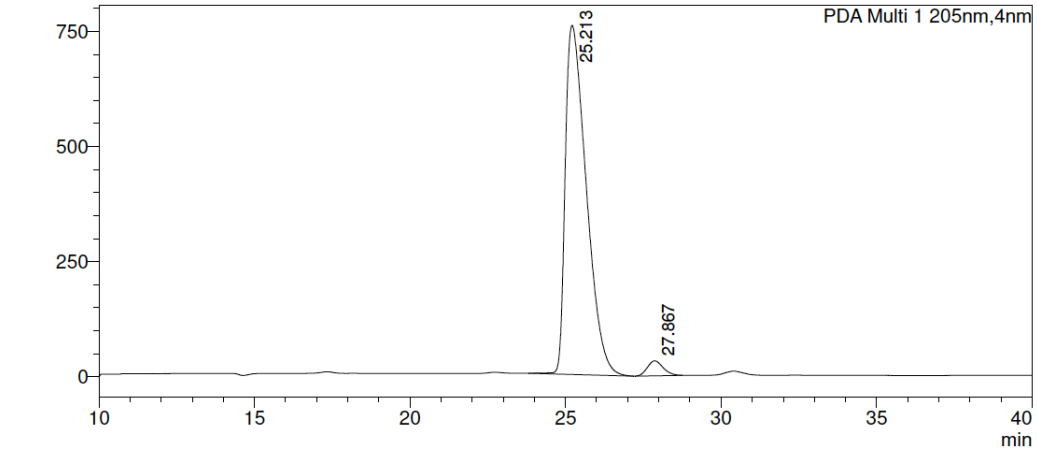

PDA Ch1 205nm

Peak#	Ret. Time	Area	Height	Area%
1	25.213	35595600	758232	96.865
2	27.867	1152161	32472	3.135
Total		36747762	790703	100.000

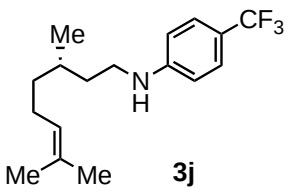

3j

3j was hydrogenated to **H2-3j** for the determination of er

8% (95% hexanes, 5% EtOH, 0.2%TFA, 0.1%DEA), 92% hexanes, 0.8 mL/min, CHIRALCEL® OJ-H

er = 96.1 : 3.9, $[\alpha]_D^{23}$ = +3.89 (*c* = 1.39)

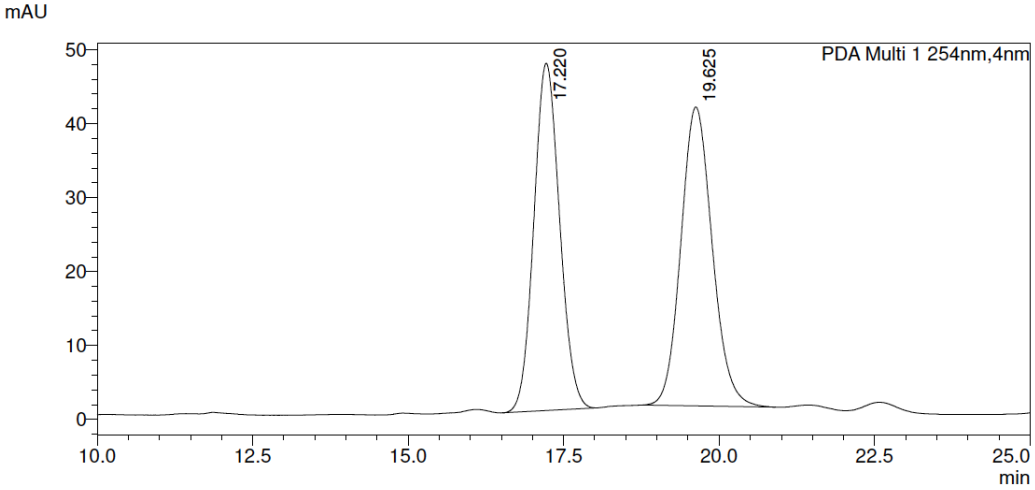

PDA Ch1 254nm

Peak#	Ret. Time	Area	Height	Area%
1	17.220	1353114	46965	48.812
2	19.625	1418984	40407	51.188
Total		2772098	87372	100.000

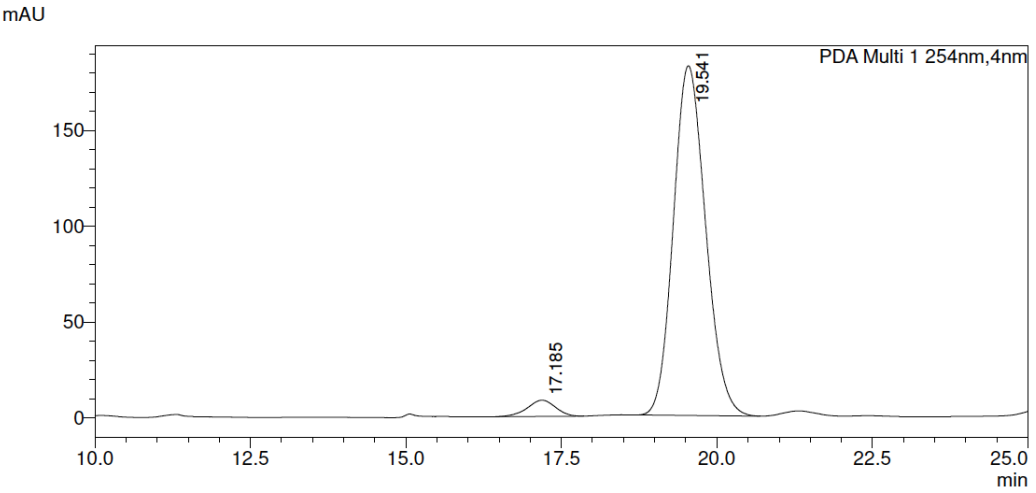

PDA Ch1 254nm

Peak#	Ret. Time	Area	Height	Area%
1	17.185	268082	8481	3.915
2	19.541	6579948	182416	96.085
Total		6848031	190897	100.000

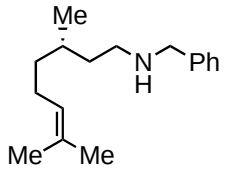

3k

15% (95% hexanes, 5% EtOH, 0.2%TFA, 0.1%DEA), 85% hexanes, 0.8 mL/min, CHIRALCEL® OJ-H

er = 97.1 : 2.9

$[\alpha]_D^{23}$ = +2.30 (*c* = 1.22)

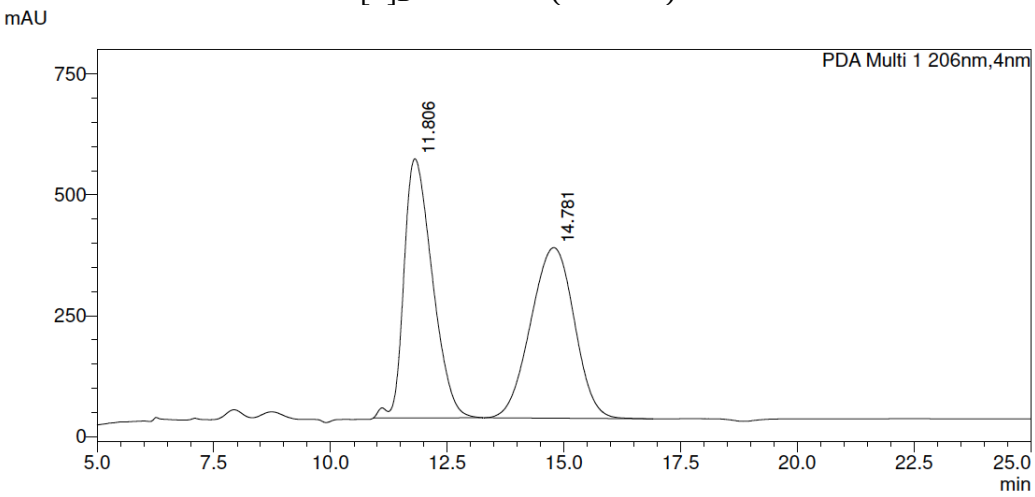

PDA Ch1 206nm

Peak#	Ret. Time	Area	Height	Area%
1	11.806	22727270	535977	49.791
2	14.781	22917725	352879	50.209
Total		45644995	888856	100.000

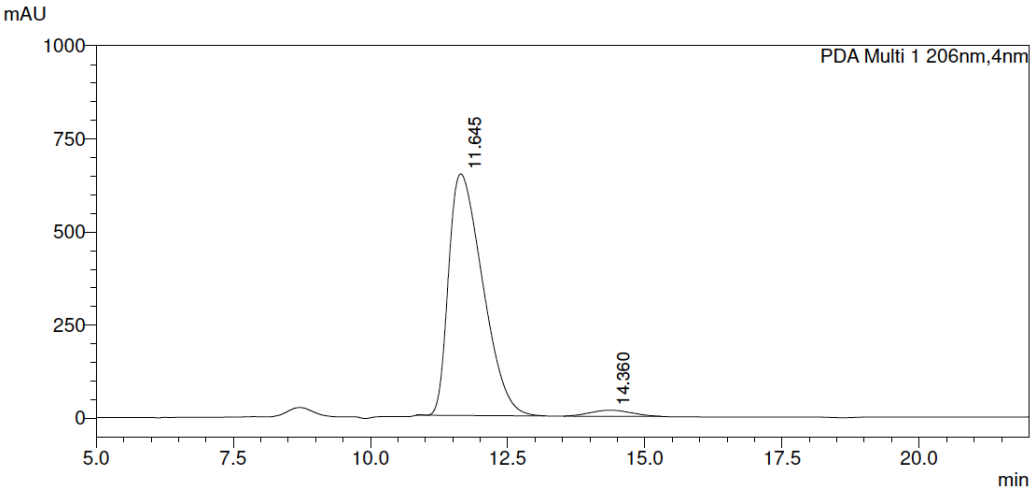

PDA Ch1 206nm

Peak#	Ret. Time	Area	Height	Area%
1	11.645	28053490	648611	97.093
2	14.360	839817	16129	2.907
Total		28893307	664740	100.000

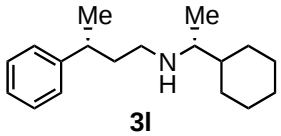

3l

50% (95% hexanes, 5% EtOH, 0.2%TFA, 0.1%DEA), 50% hexanes, 0.8 mL/min, CHIRALPAK® ID3

er = 98.7:1.3

$[\alpha]_D^{23}$ = -29.98 (*c* = 1.04)

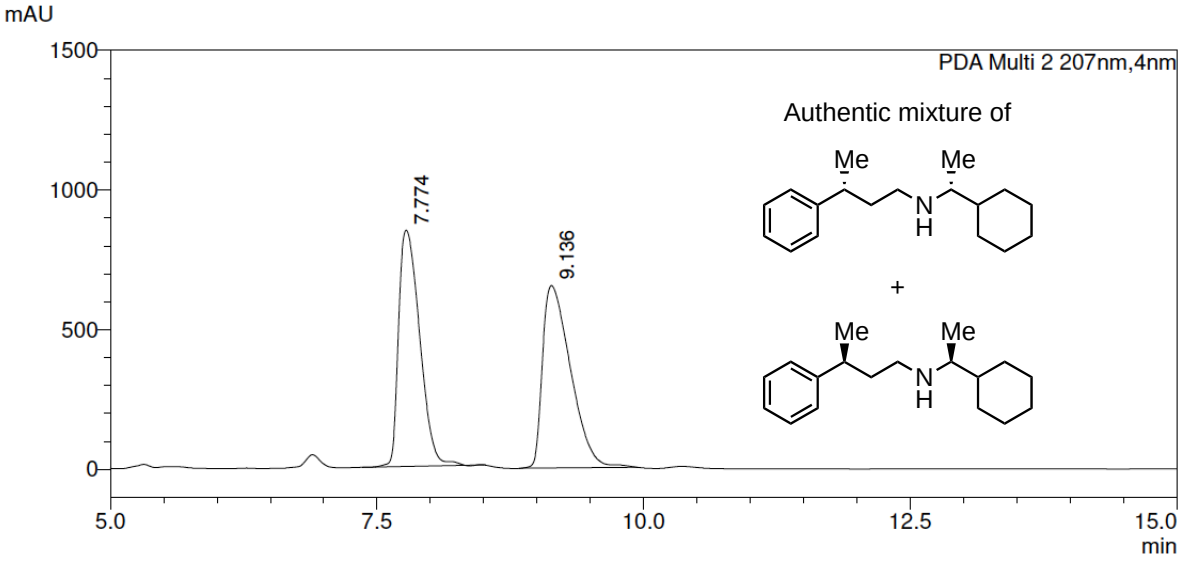

PDA Ch2 207nm

Peak#	Ret. Time	Area	Height	Area%
1	7.774	11673670	846410	49.351
2	9.136	11980896	653596	50.649
Total		23654566	1500006	100.000

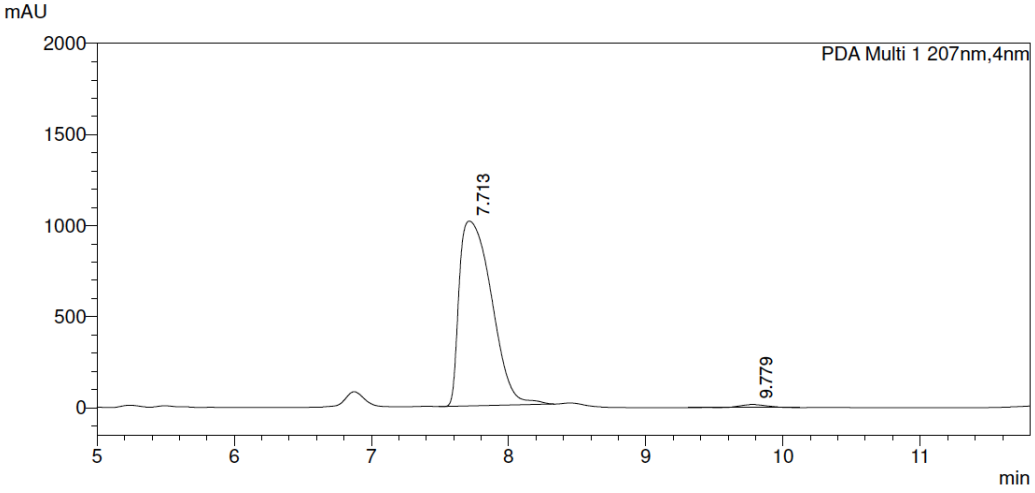

PDA Ch1 207nm

Peak#	Ret. Time	Area	Height	Area%
1	7.713	16698897	1014797	98.661
2	9.779	226615	16468	1.339
Total		16925513	1031265	100.000

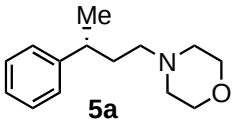

5a

100% (95% hexanes, 5% EtOH, 0.2%TFA, 0.1%DEA), 0.8 mL/min, CHIRALCEL® OJ-H

er = 98.7:1.3

$[\alpha]_D^{23}$ = -22.61 (*c* = 1.15)

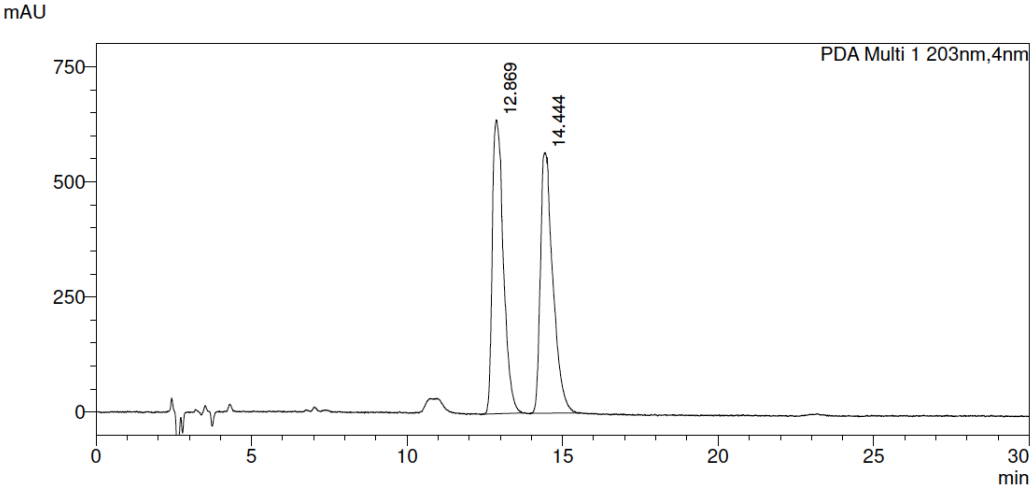

PDA Ch1 203nm

Peak#	Ret. Time	Area	Height	Area%
1	12.869	15832954	638093	49.993
2	14.444	15837223	566309	50.007
Total		31670178	1204401	100.000

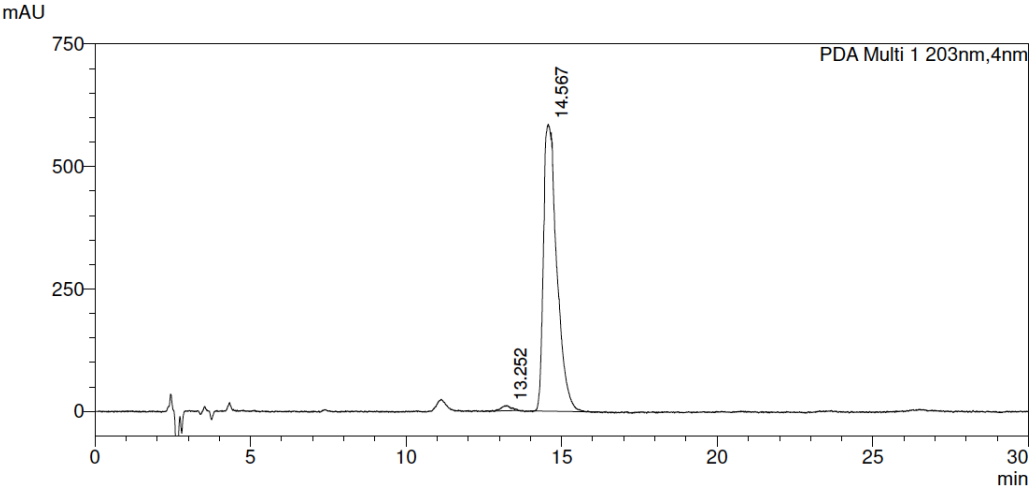

PDA Ch1 203nm

Peak#	Ret. Time	Area	Height	Area%
1	13.252	231539	10478	1.306
2	14.567	17495432	585933	98.694
Total		17726971	596411	100.000

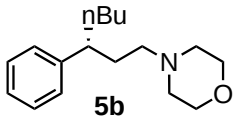

5b

50% (95% hexanes, 5% EtOH, 0.2%TFA, 0.1%DEA), 50% hexanes, 0.8 mL/min, CHIRALPAK® IA3

er = 99.1:0.9

$[\alpha]_D^{23}$ = -10.85 (*c* = 2.12)

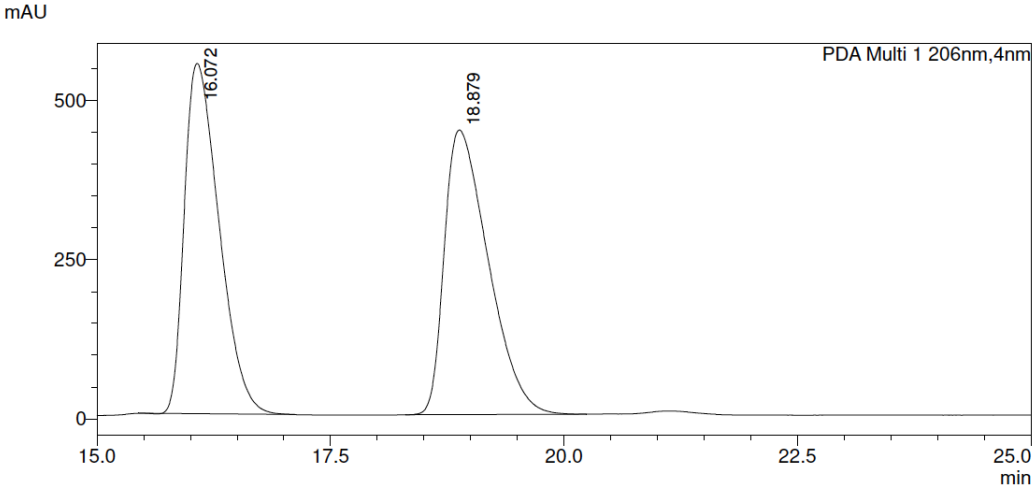

PDA Ch1 206nm

Peak#	Ret. Time	Area	Height	Area%
1	16.072	14246867	550302	49.306
2	18.879	14648200	447090	50.694
Total		28895068	997392	100.000

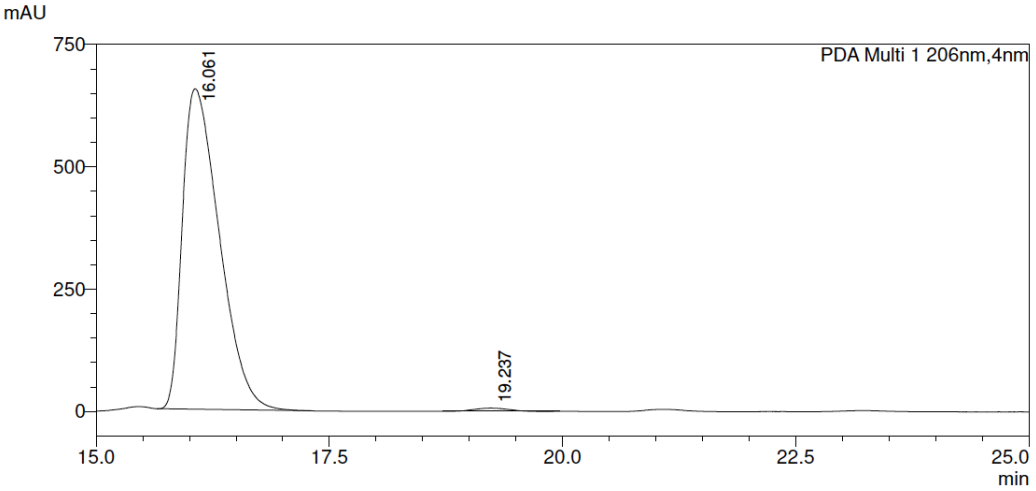

PDA Ch1 206nm

Peak#	Ret. Time	Area	Height	Area%
1	16.061	18071421	655107	99.088
2	19.237	166303	6740	0.912
Total		18237725	661847	100.000

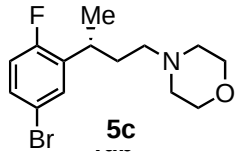

5c

30% (95% hexanes, 5% EtOH, 0.2%TFA, 0.1%DEA), 70% hexanes, 0.8 mL/min, CHIRALPAK® IA3

er = 97.8:2.2

$[\alpha]_D^{23}$ = -33.09 (*c* = 1.06)

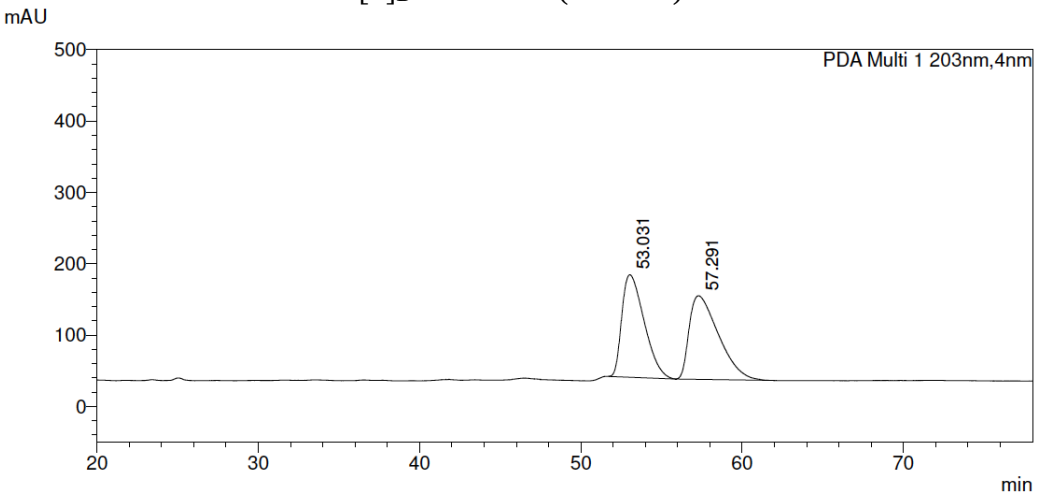

PDA Ch1 203nm

Peak#	Ret. Time	Area	Height	Area%
1	53.031	13837009	143708	48.335
2	57.291	14790355	117209	51.665
Total		28627365	260917	100.000

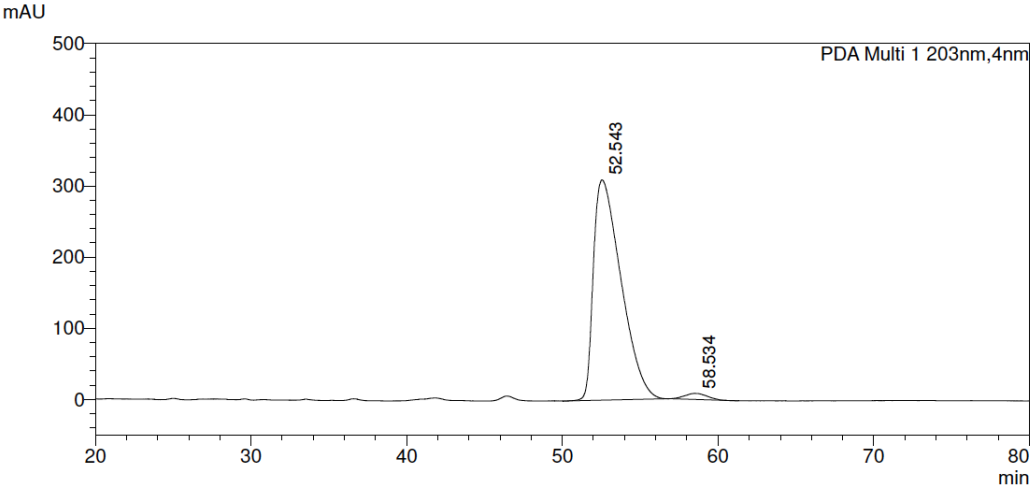

PDA Ch1 203nm

Peak#	Ret. Time	Area	Height	Area%
1	52.543	38237378	309568	97.804
2	58.534	858562	8644	2.196
Total		39095940	318212	100.000

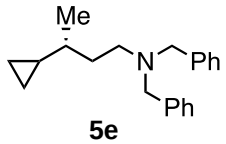

5e

10% (95% hexanes, 5% EtOH, 0.2%TFA, 0.1%DEA), 90% hexanes, 0.8 mL/min, CHIRALCEL® OJ-H

er = 98.9 : 1.1

$[\alpha]_D^{23}$ = 8.84 (*c* = 1.74)

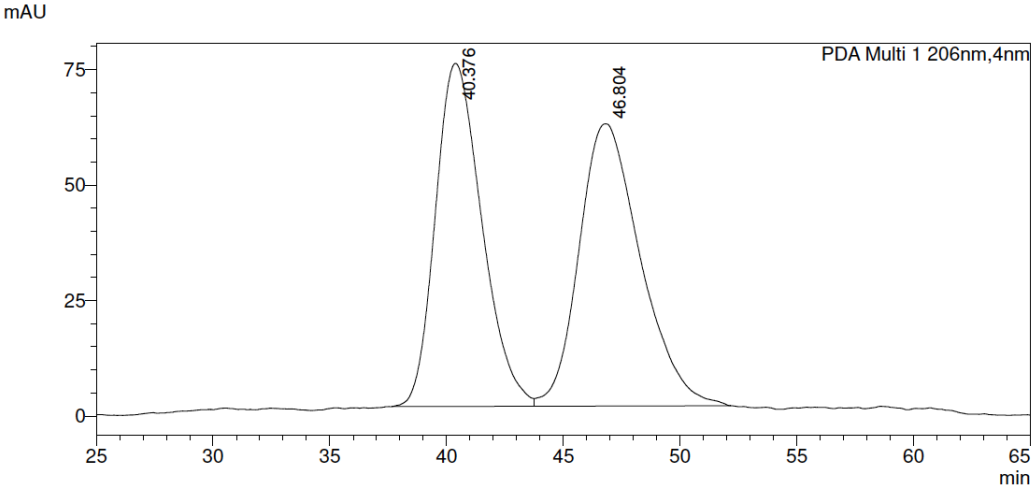

PDA Ch1 206nm

Peak#	Ret. Time	Area	Height	Area%
1	40.376	10298183	74278	47.947
2	46.804	11180038	61121	52.053
Total		21478221	135400	100.000

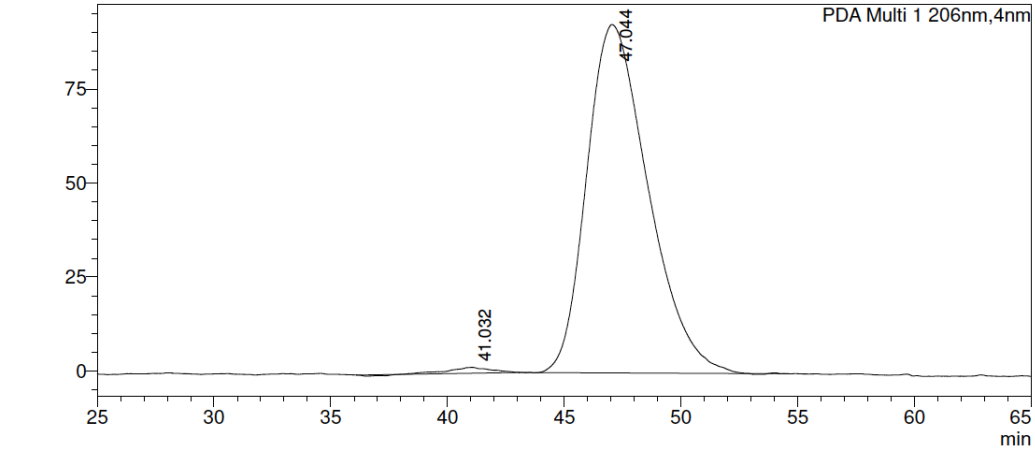

PDA Ch1 206nm

Peak#	Ret. Time	Area	Height	Area%
1	41.032	190116	1562	1.107
2	47.044	16985697	92714	98.893
Total		17175813	94276	100.000

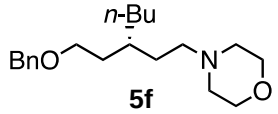

5f

50% (95% hexanes, 5% EtOH, 0.2%TFA, 0.1%DEA), 50% hexanes, 0.8 mL/min, CHIRALCEL® OJ-H

er = 98.1 : 1.9

$[\alpha]_D^{23}$ = 0.72 (*c* = 1.77)

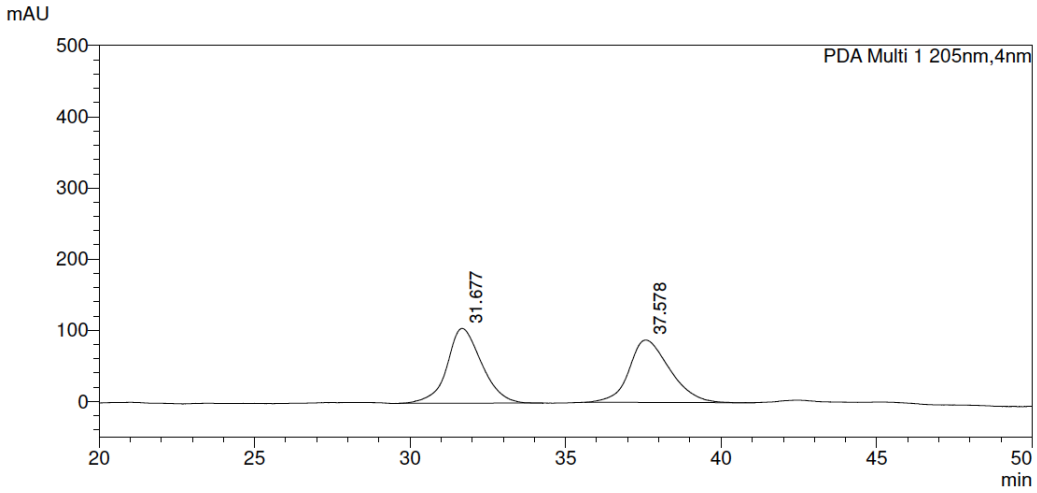

PDA Ch1 205nm

Peak#	Ret. Time	Area	Height	Area%
1	31.677	8177026	105089	50.601
2	37.578	7982873	87695	49.399
Total		16159899	192784	100.000

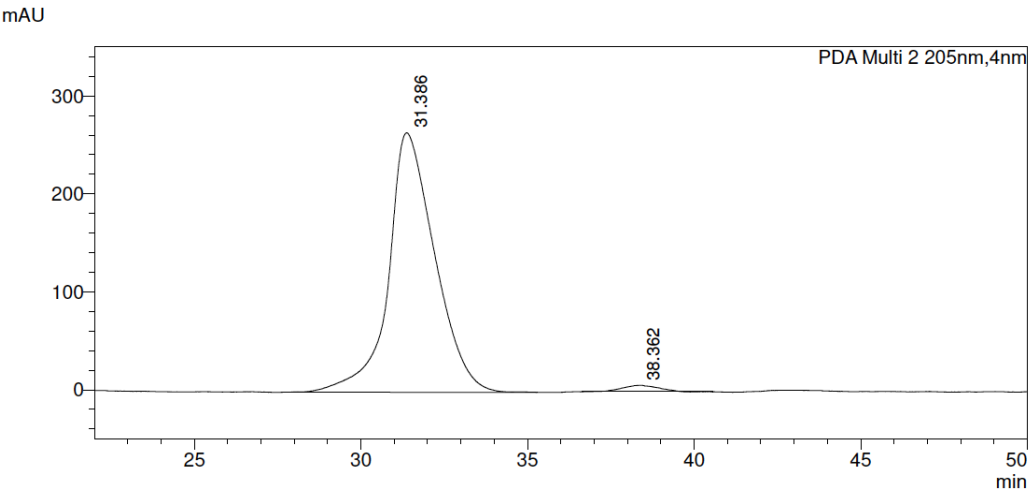

PDA Ch2 205nm

Peak#	Ret. Time	Area	Height	Area%
1	31.386	25684603	264916	98.079
2	38.362	503084	6450	1.921
Total		26187686	271367	100.000

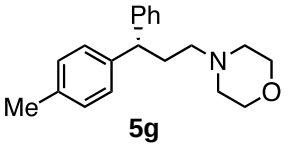

5g

50% (95% hexanes, 5% EtOH, 0.2%TFA, 0.1%DEA), 50% hexanes, 0.8 mL/min, CHIRALCEL® OJ-H

er = 96.5 : 3.5

$[\alpha]_D^{23}$ = 2.63 (*c* = 2.28)

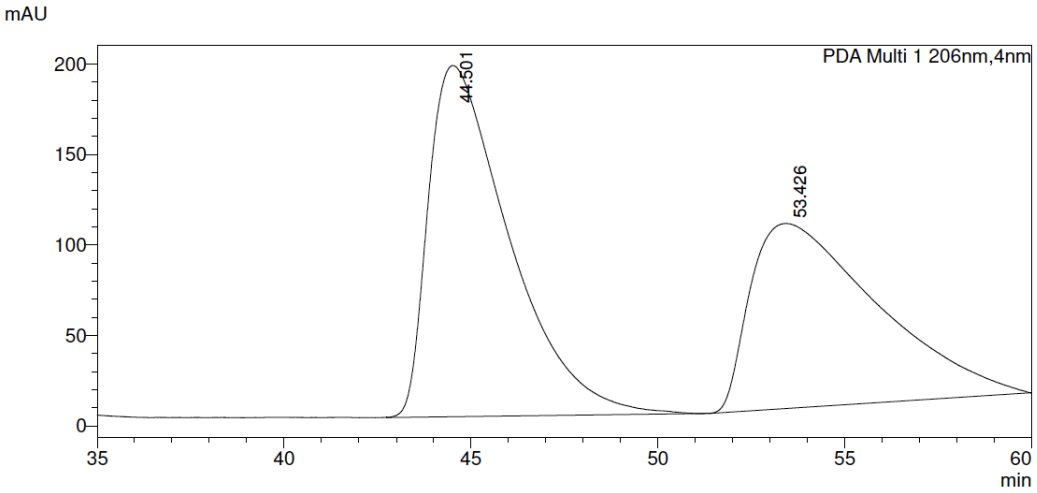

PDA Ch1 206nm

Peak#	Ret. Time	Area	Height	Area%
1	44.501	29184938	193973	54.829
2	53.426	24044256	102258	45.171
Total		53229194	296230	100.000

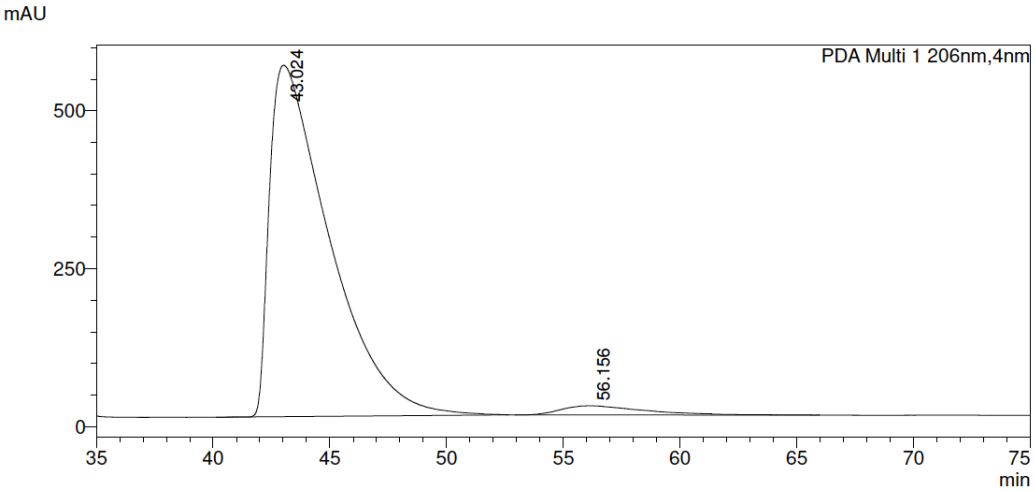

PDA Ch1 206nm

Peak#	Ret. Time	Area	Height	Area%
1	43.024	99442289	555842	96.538
2	56.156	3565794	14361	3.462
Total		103008083	570203	100.000

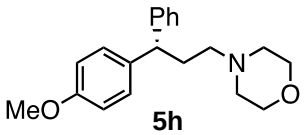

5h

100% (95% hexanes, 5% EtOH, 0.2%TFA, 0.1%DEA), 0.8 mL/min, CHIRALCEL® OJ-H

er = 97.6 : 2.4

$[\alpha]_D^{23}$ = 1.49 (*c* = 1.05)

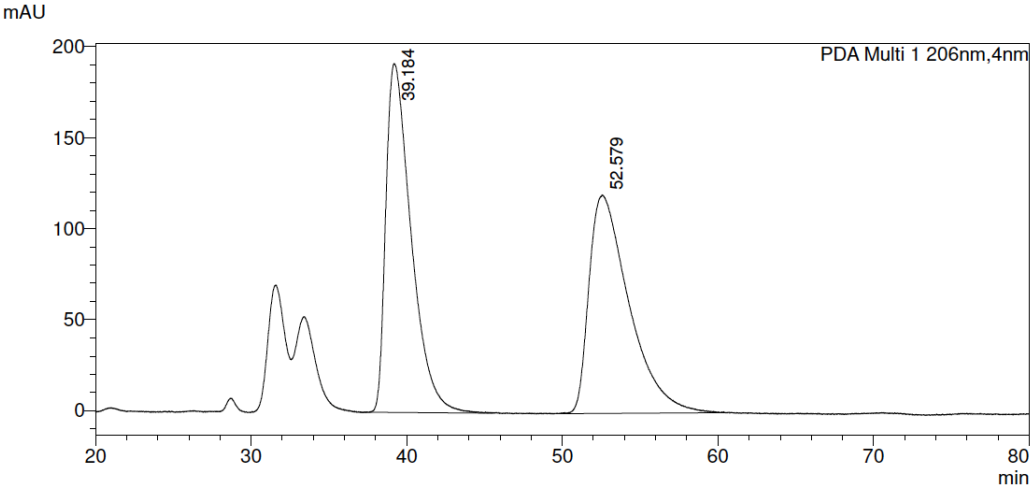

PDA Ch1 206nm

Peak#	Ret. Time	Area	Height	Area%
1	39.184	21696765	191679	50.302
2	52.579	21435894	120133	49.698
Total		43132658	311813	100.000

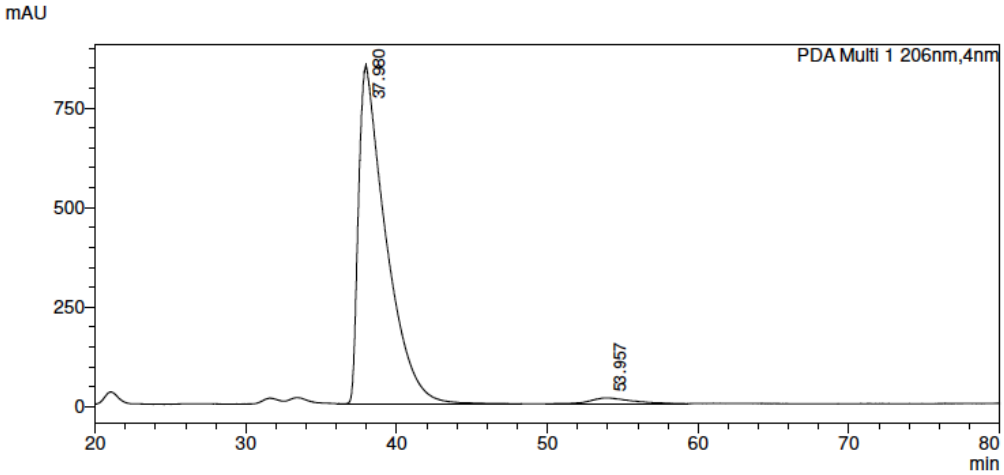

PDA Ch1 206nm

Peak#	Ret. Time	Area	Height	Area%
1	37.980	106654378	849883	97.624
2	53.957	2596321	14115	2.376
Total		109250699	863998	100.000

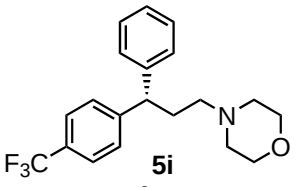

5i

50% (95% hexanes, 5% EtOH, 0.2%TFA, 0.1%DEA), 50% hexanes, 0.8 mL/min, CHIRALPAK® IA3

er = 98.6 : 1.4

$[\alpha]_D^{23}$ = -1.38 (*c* = 1.97)

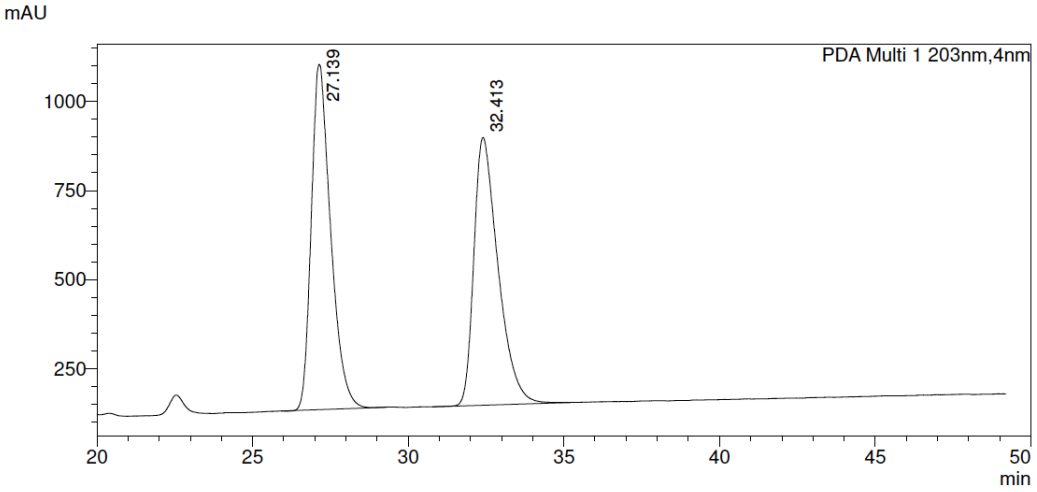

PDA Ch1 203nm

Peak#	Ret. Time	Area	Height	Area%
1	27.139	41885612	968486	50.790
2	32.413	40583421	750623	49.210
Total		82469033	1719109	100.000

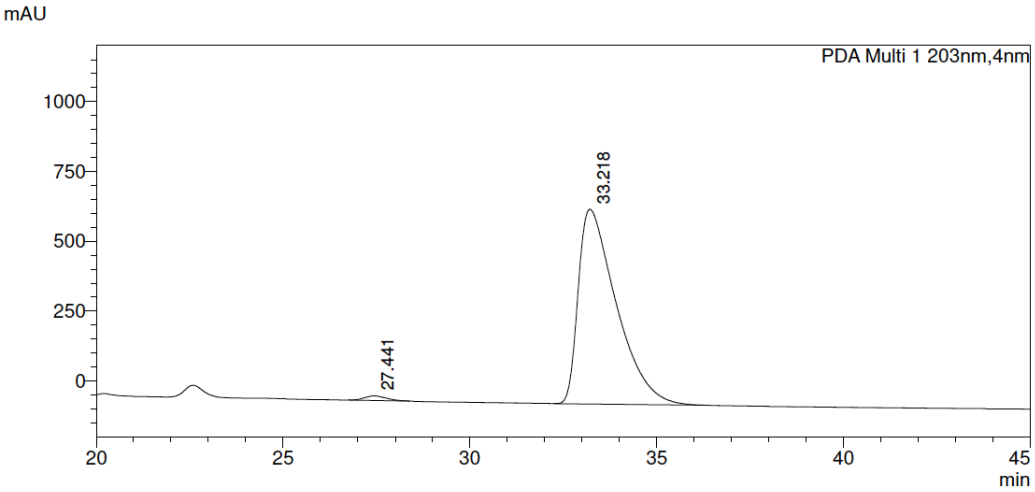

PDA Ch1 203nm

Peak#	Ret. Time	Area	Height	Area%
1	27.441	677383	16481	1.352
2	33.218	49413810	697168	98.648
Total		50091192	713649	100.000

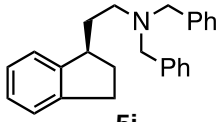

5j

100% (95% hexanes, 5% EtOH, 0.2%TFA, 0.1%DEA), 0.8 mL/min, CHIRALPAK® IB3

er = 92.5 : 7.5

$[\alpha]_D^{23}$ = 1.70 (*c* = 1.80)

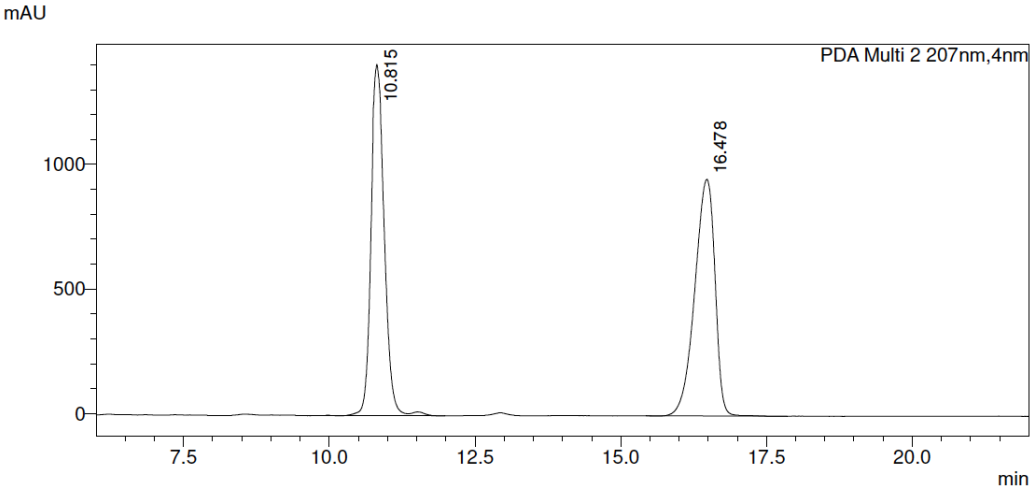

PDA Ch2 207nm

Peak#	Ret. Time	Area	Height	Area%
1	10.815	22292584	1408843	49.391
2	16.478	22841896	949498	50.609
Total		45134480	2358341	100.000

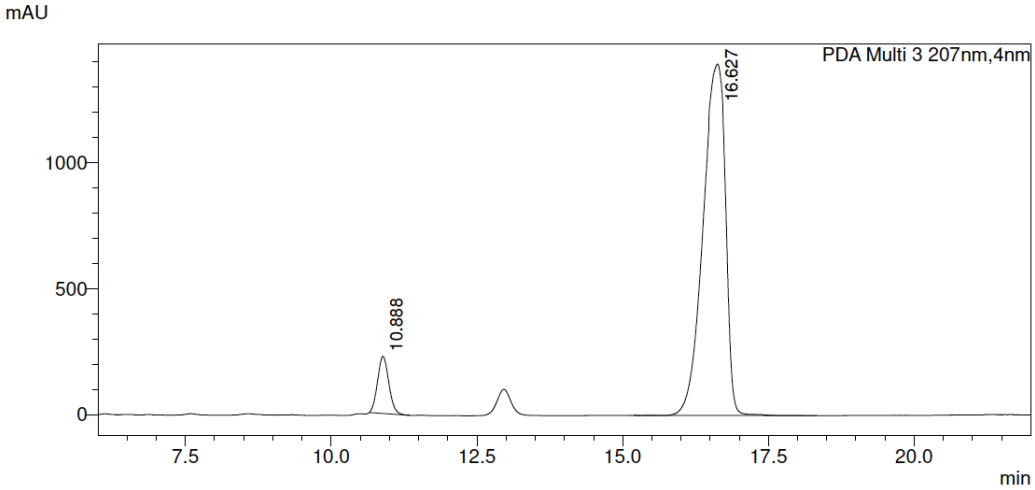

PDA Ch3 207nm

Peak#	Ret. Time	Area	Height	Area%
1	10.888	3039350	226339	7.505
2	16.627	37459855	1394936	92.495
Total		40499205	1621275	100.000

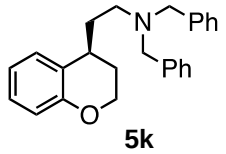

5k

100% (95% hexanes, 5% EtOH, 0.2%TFA, 0.1%DEA), 0.8 mL/min, CHIRALPAK® IB3

er = 97.2 : 2.8

$[\alpha]_D^{23}$ = -13.51 (*c* = 2.32)

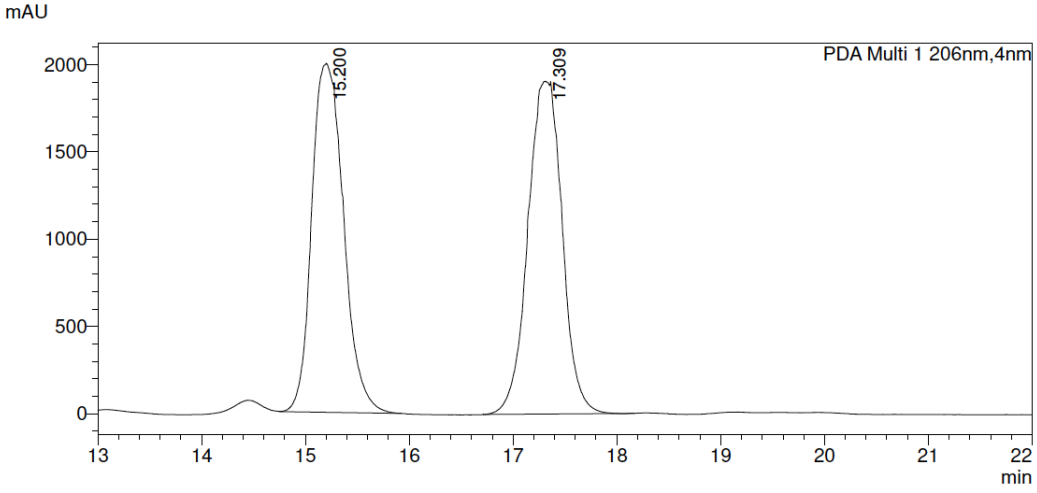

PDA Ch1 206nm

Peak#	Ret. Time	Area	Height	Area%
1	15.200	42613580	1997405	49.327
2	17.309	43777091	1907050	50.673
Total		86390672	3904456	100.000

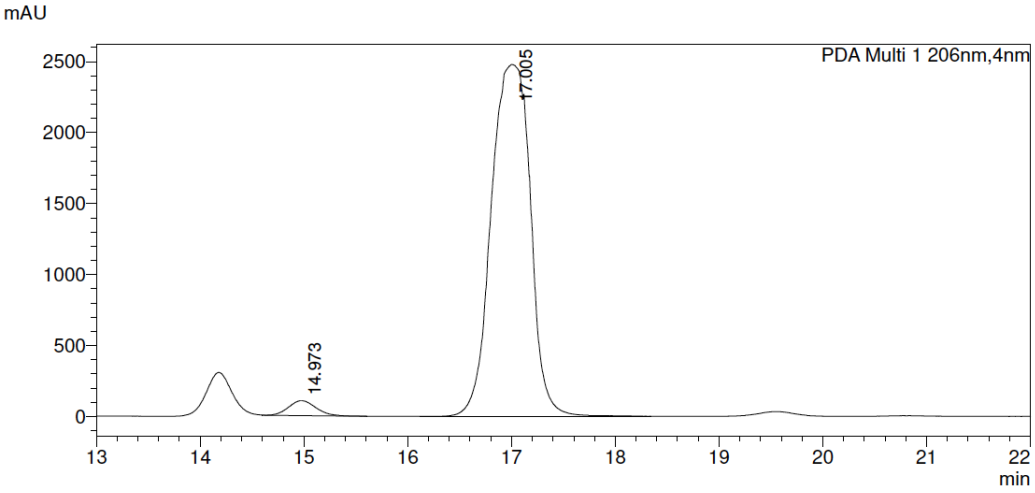

PDA Ch1 206nm

Peak#	Ret. Time	Area	Height	Area%
1	14.973	1902188	104915	2.842
2	17.005	65017948	2477029	97.158
Total		66920135	2581944	100.000

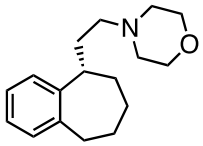

5l

50% (95% hexanes, 5% EtOH, 0.2%TFA, 0.1%DEA), 50% hexanes, 0.8 mL/min, CHIRALPAK® IB3

er = 96.0 : 4.0

$[\alpha]_D^{23}$ = 16.81 (*c* = 1.16)

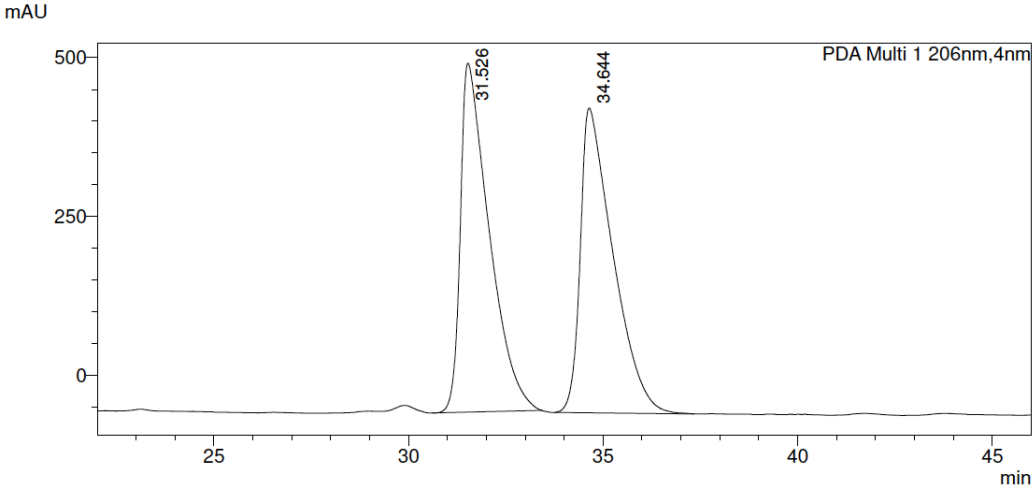

PDA Ch1 206nm

Peak#	Ret. Time	Area	Height	Area%
1	31.526	28259562	548678	50.192
2	34.644	28042812	478896	49.808
Total		56302374	1027574	100.000

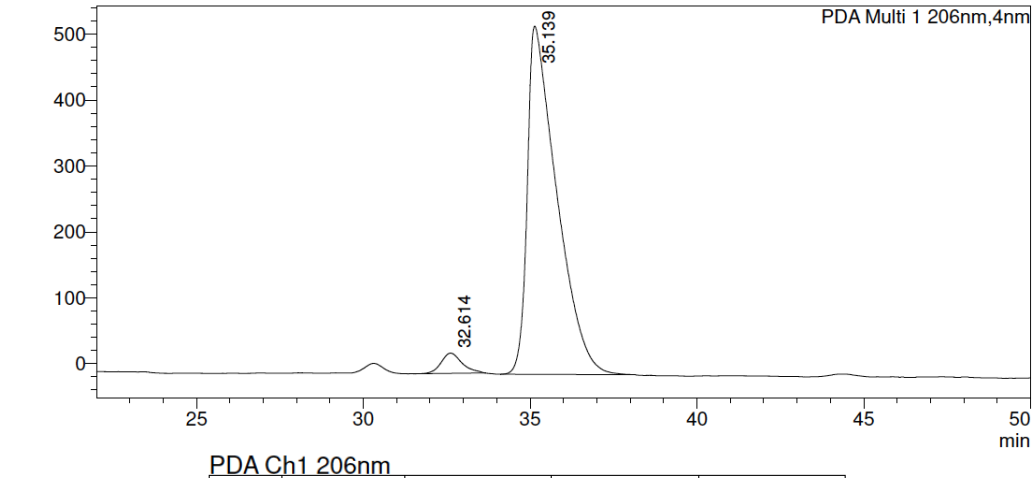

PDA Ch1 206nm

Peak#	Ret. Time	Area	Height	Area%
1	32.614	1343915	30711	3.967
2	35.139	32533565	528469	96.033
Total		33877480	559180	100.000

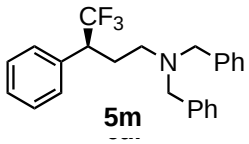

5m

100% (95% hexanes, 5% EtOH, 0.2%TFA, 0.1%DEA), 0.8 mL/min, CHIRALCEL® OJ-H

er = 98.6 : 1.4

$[\alpha]_D^{23}$ = 85.78 (*c* = 2.12)

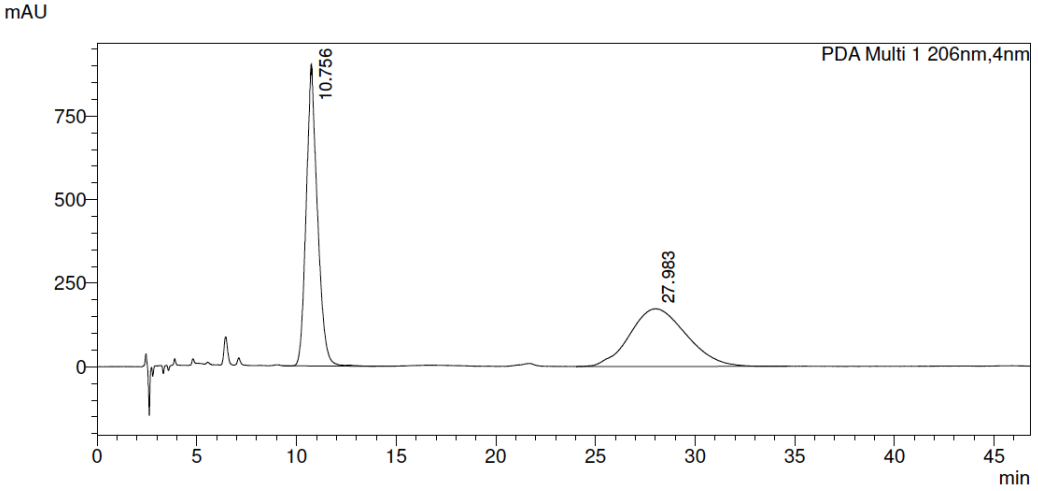

PDA Ch1 206nm

Peak#	Ret. Time	Area	Height	Area%
1	10.756	35119358	899382	50.822
2	27.983	33983624	172707	49.178
Total		69102982	1072088	100.000

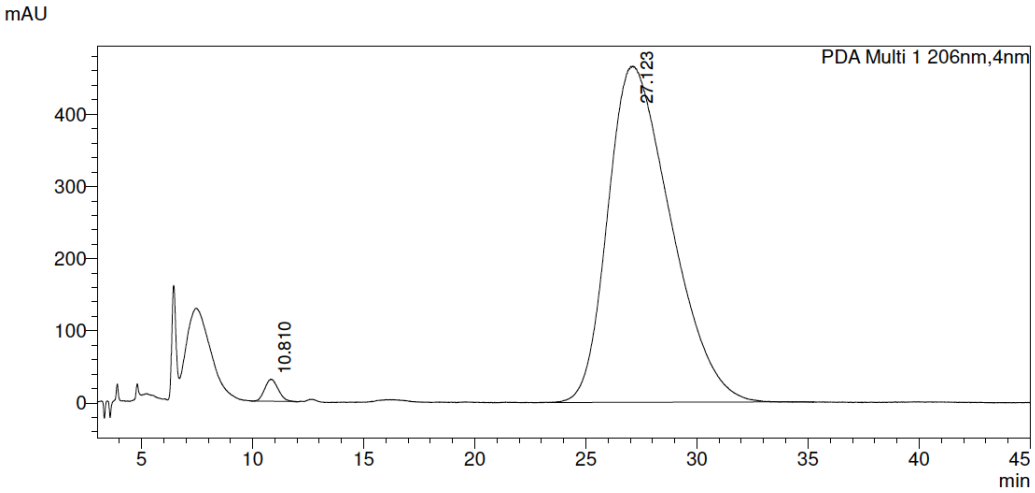

PDA Ch1 206nm

Peak#	Ret. Time	Area	Height	Area%
1	10.810	1258992	30385	1.352
2	27.123	91873672	465456	98.648
Total		93132664	495840	100.000

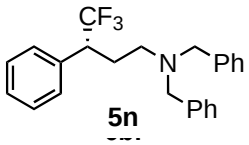

5n

100% (95% hexanes, 5% EtOH, 0.2%TFA, 0.1%DEA), 0.8 mL/min, CHIRALCEL® OJ-H

er = 98.2 : 1.8

$[\alpha]_D^{23}$ = -79.65 (*c* = 1.94)

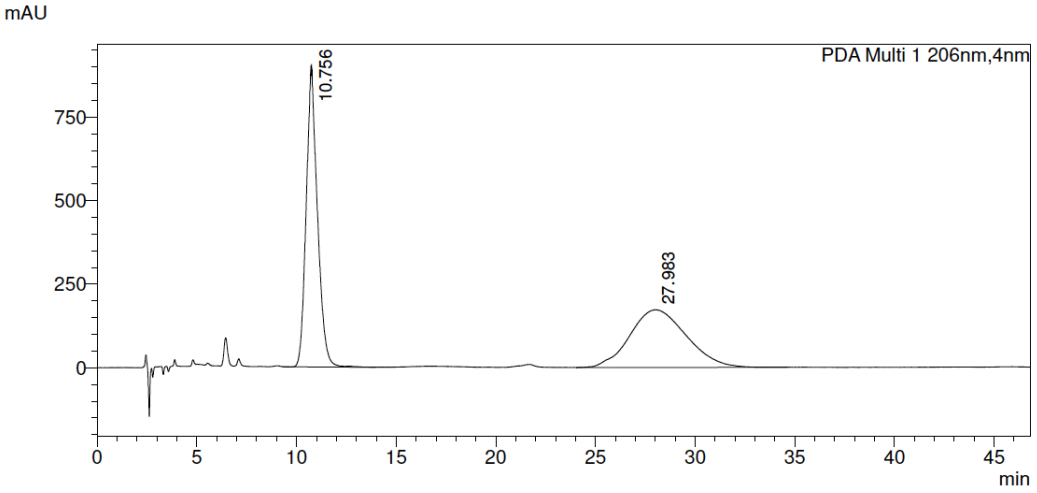

PDA Ch1 206nm

Peak#	Ret. Time	Area	Height	Area%
1	10.756	35119358	899382	50.822
2	27.983	33983624	172707	49.178
Total		69102982	1072088	100.000

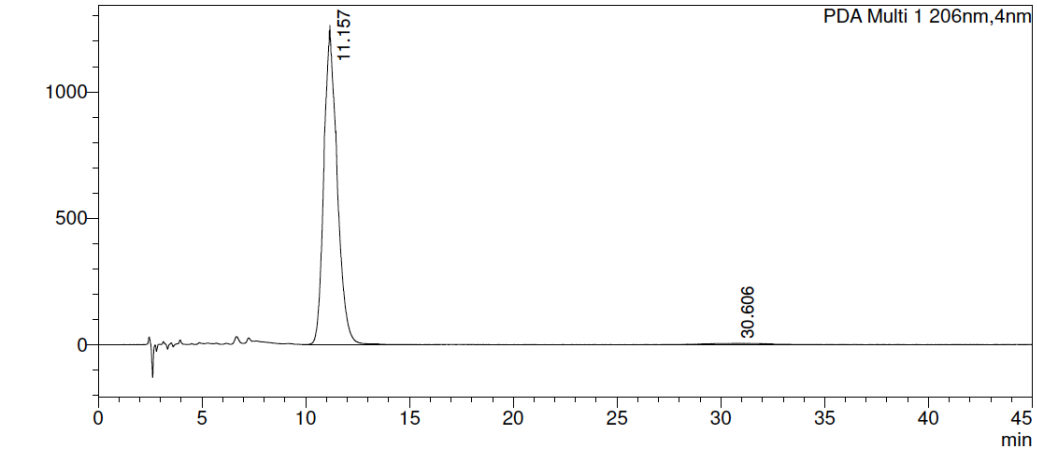

PDA Ch1 206nm

Peak#	Ret. Time	Area	Height	Area%
1	11.157	55511726	1243949	98.175
2	30.606	1032044	4753	1.825
Total		56543770	1248701	100.000

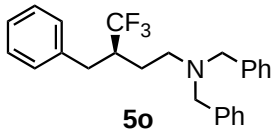

5o

25% (95% hexanes, 5% EtOH, 0.2%TFA, 0.1%DEA), 75% hexanes, 0.8 mL/min, CHIRALCEL® OJ-H

er = 97.1 : 2.9

$[\alpha]_D^{23}$ = -2.22 (*c* = 1.71)

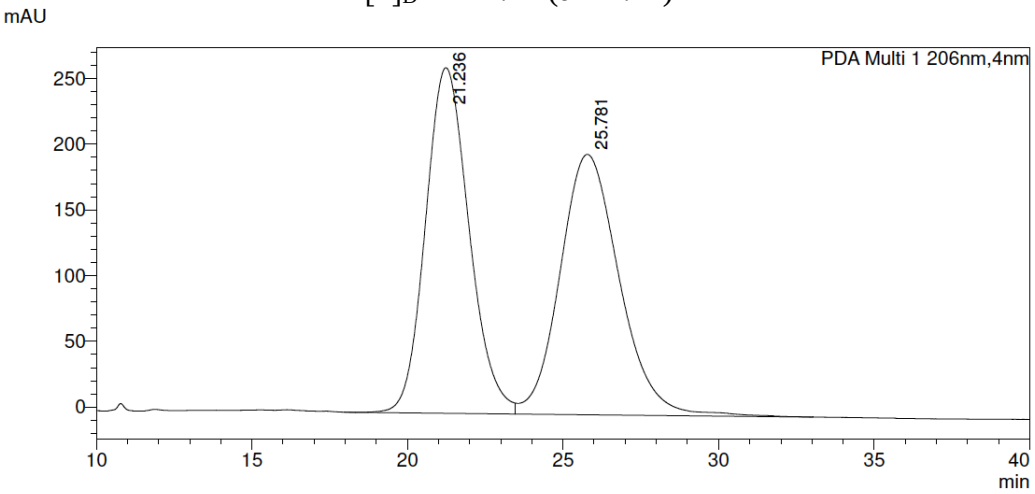

PDA Ch1 206nm

Peak#	Ret. Time	Area	Height	Conc.	Area%
1	21.236	25592581	262863	0.000	49.351
2	25.781	26265245	198023	0.000	50.649
Total		51857827	460887		100.000

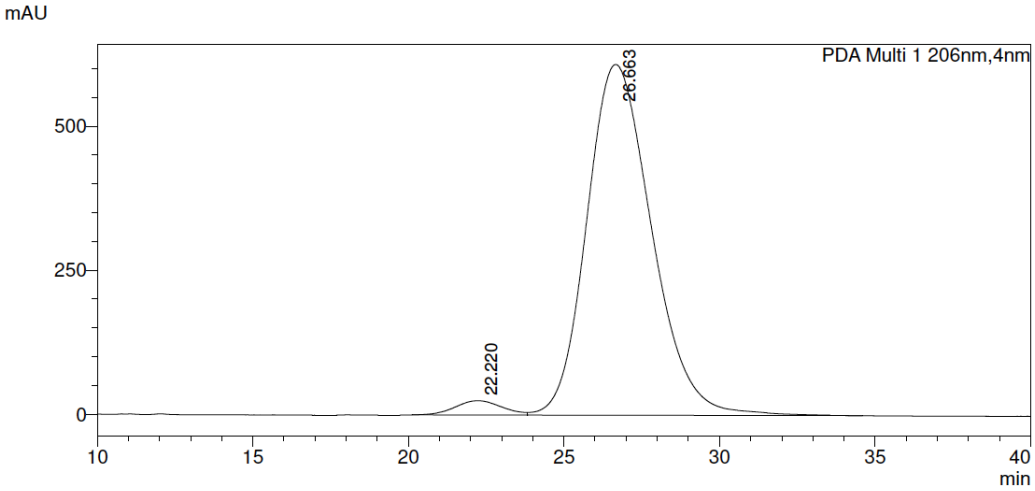

PDA Ch1 206nm

Peak#	Ret. Time	Area	Height	Area%
1	22.220	2608624	25026	2.867
2	26.663	88365204	608469	97.133
Total		90973828	633496	100.000

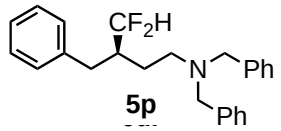

5p

100% (95% hexanes, 5% EtOH, 0.2%TFA, 0.1%DEA), 0.8 mL/min, CHIRALPAK® IB3

er = 97.2 : 2.8

$[\alpha]_D^{23}$ = 0.96 (*c* = 1.68)

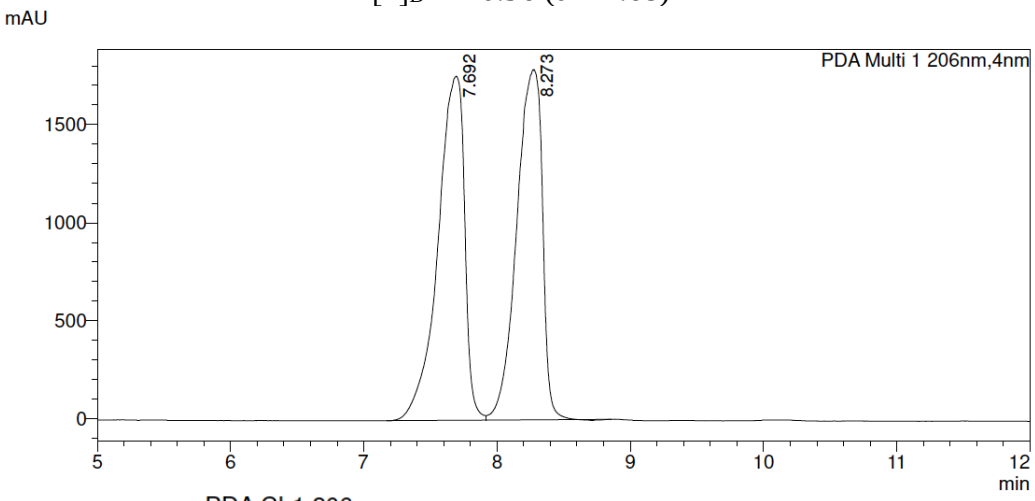

PDA Ch1 206nm

Peak#	Ret. Time	Area	Height	Area%
1	7.692	24454936	1752397	50.618
2	8.273	23857665	1782768	49.382
Total		48312601	3535164	100.000

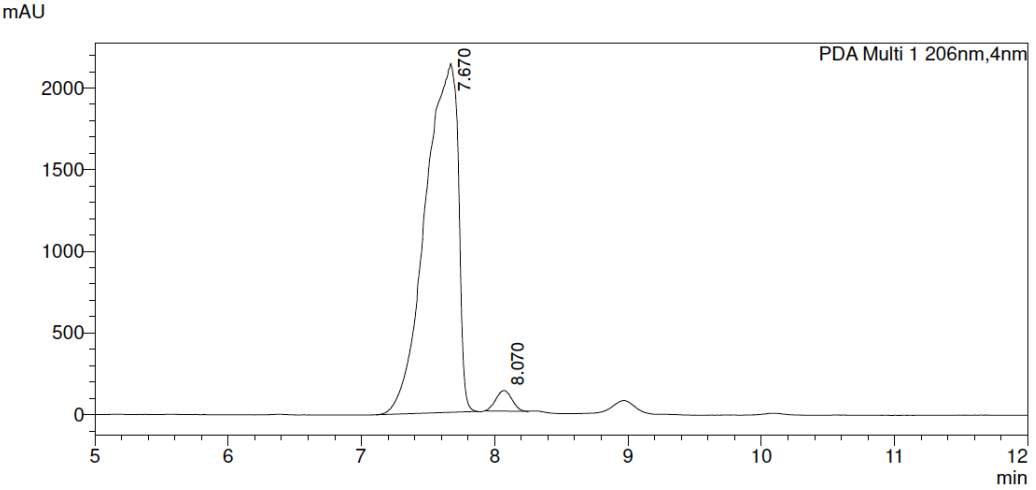

PDA Ch1 206nm

Peak#	Ret. Time	Area	Height	Area%
1	7.670	36625215	2132341	97.209
2	8.070	1051701	125602	2.791
Total		37676917	2257942	100.000

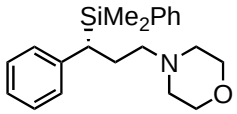

5q

50% (95% hexanes, 5% EtOH, 0.2%TFA, 0.1%DEA), 50% hexanes, 0.8 mL/min, CHIRALPAK® IA3

er = 98.8 : 1.2

$[\alpha]_D^{23}$ = 8.10 (*c* = 1.98)

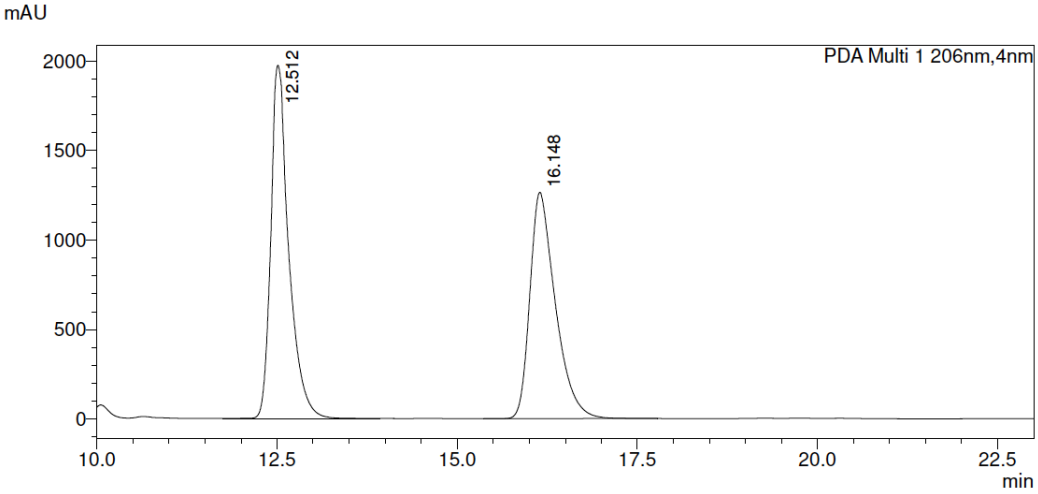

PDA Ch1 206nm

Peak#	Ret. Time	Area	Height	Area%
1	12.512	34134234	1972601	52.320
2	16.148	31106916	1265412	47.680
Total		65241150	3238013	100.000

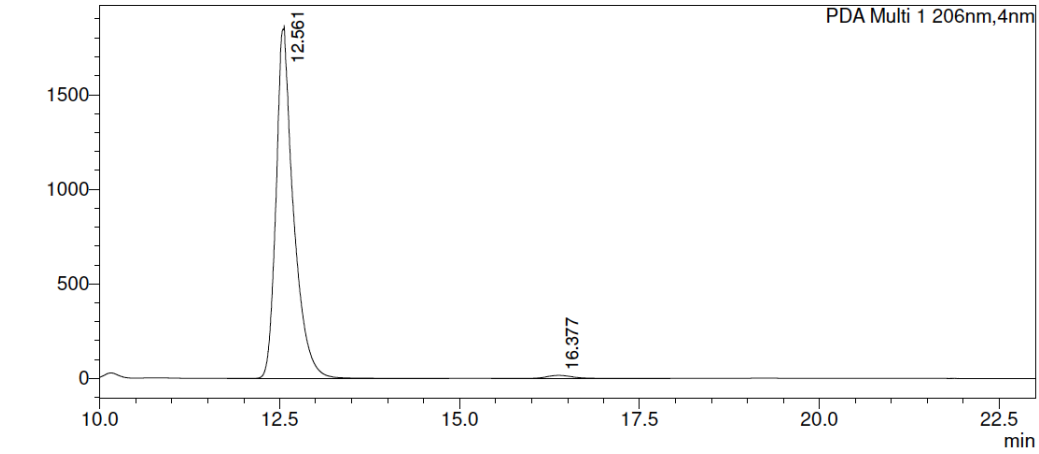

PDA Ch1 206nm

Peak#	Ret. Time	Area	Height	Area%
1	12.561	31258653	1846980	98.776
2	16.377	387503	16316	1.224
Total		31646156	1863296	100.000

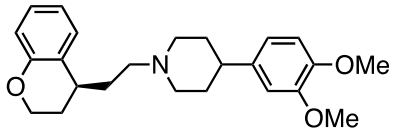

Terikalant

100% (95% hexanes, 5% EtOH, 0.2%TFA, 0.1%DEA), 0.8 mL/min, CHIRALPAK® IB3

er = 96.7 : 3.3

$[\alpha]_D^{23}$ = -8.85 (*c* = 2.68)

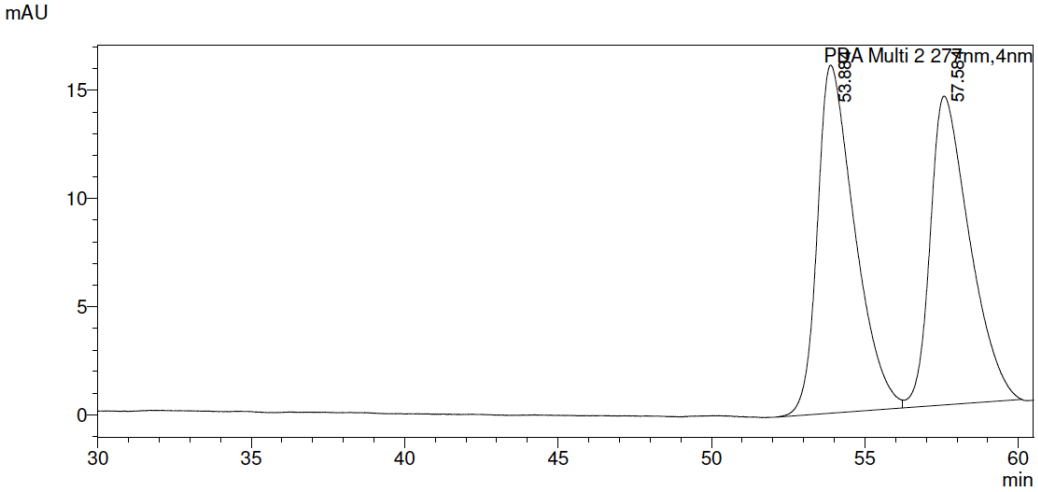

PDA Ch2 277nm

Peak#	Ret. Time	Area	Height	Conc.	Unit
1	53.884	1362921	16087	51.561	
2	57.584	1280383	14280	48.439	
Total		2643304	30367		

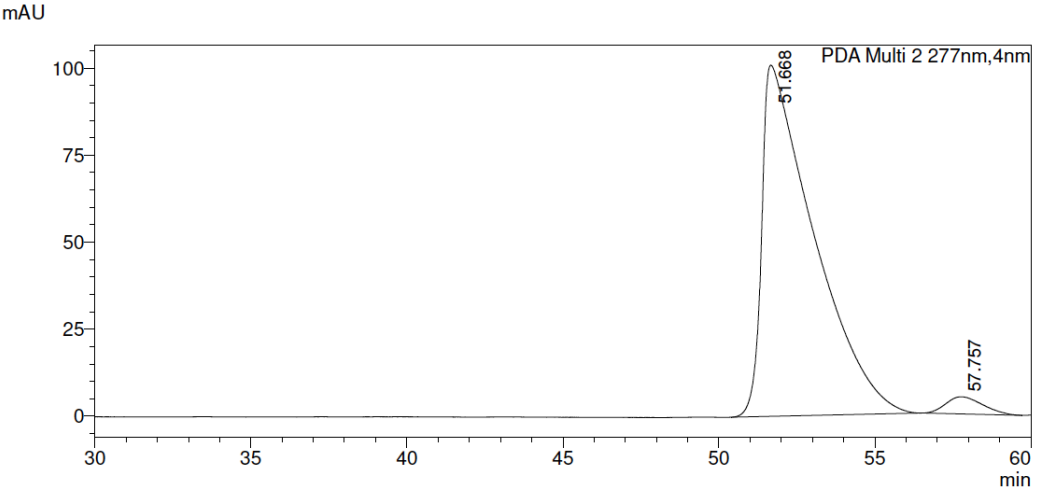

PDA Ch2 277nm

Peak#	Ret. Time	Area	Height	Area%
1	51.668	11746301	100998	96.657
2	57.757	406200	4951	3.343
Total		12152501	105950	100.000

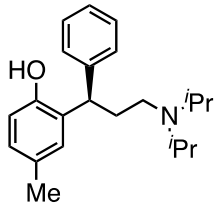

(R)-Tolterodine

50% (95% hexanes, 5% EtOH, 0.2%TFA, 0.1%DEA), 50% hexanes, 1.0 mL/min, CHIRALCEL® OJ-H

er = 96.0 : 4.0

$[\alpha]_D^{23}$ = 114.94 (*c* = 2.99)

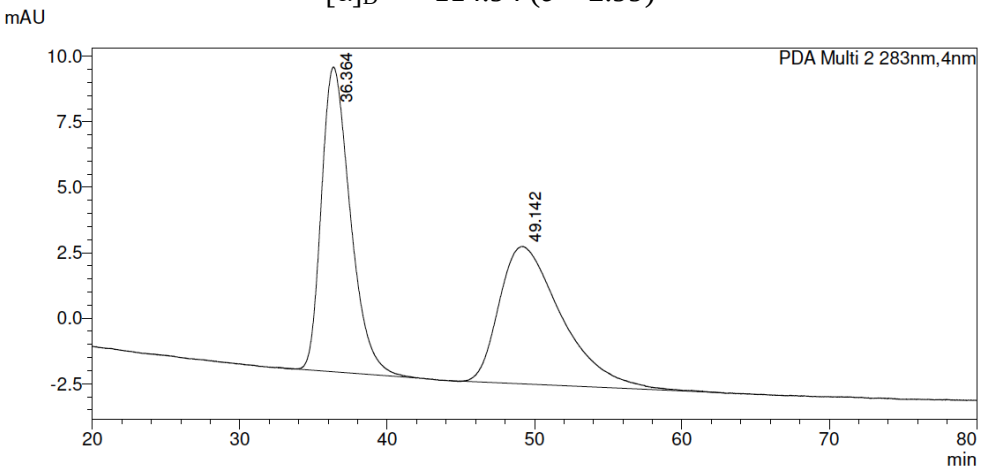

PDA Ch2 283nm

Peak#	Ret. Time	Area	Height	Area%
1	36.364	1589118	11634	50.698
2	49.142	1545382	5250	49.302
Total		3134500	16883	100.000

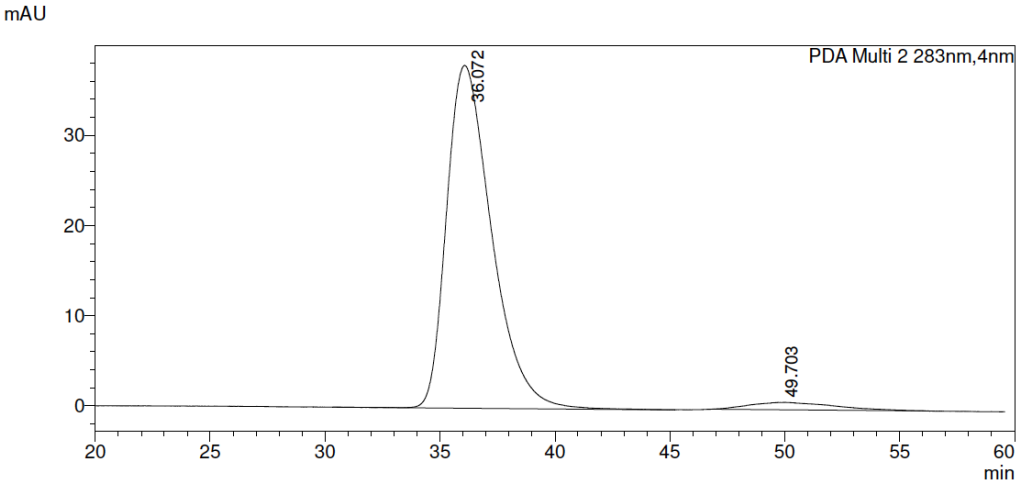

PDA Ch2 283nm

Peak#	Ret. Time	Area	Height	Area%
1	36.072	5179099	38025	95.994
2	49.703	216152	836	4.006
Total		5395251	38861	100.000

4.8 Literature Cited

(1) a) Wu, Z.; Laffoon, S. D.; Nguyen, T. T.; McAlpin, J. D.; Hull, K. L. Rhodium-Catalyzed Asymmetric Synthesis of β-Branched Amides. *Angew. Chem. Int. Ed.* **2017**, *56*, 1371–1375. b) Laffoon, S. D.; Wu, Z.; Hull, K. L. Rhodium-Catalyzed Asymmetric Synthesis of β-Branched Esters from Allylic Amines. *Chem. Comm.* **2018**, *54*, 7814–7817.

(2) Zhu, S.; Buchwald, S. L. Enantioselective CuH-Catalyzed Anti-Markovnikov Hydroamination of 1,1-Disubstituted Alkenes. *J. Am. Chem. Soc.* **2014**, *136*, 15913–15916.

(3) Lee, J. C. H.; McDonald, R.; Hall, D. G. Enantioselective preparation and chemoselective cross-coupling of 1,1-diboron compounds. *Nat. Chem.* **2011**, *3*, 894–899.

(4) Li, Y.; Dong, K.; Wang, Z.; Ding, K. Rhodium(I)-catalyzed enantioselective hydrogenation of substituted acrylic acids with sterically similar β,β-diaryls. *Angew. Chem. Int. Ed.* **2013**, *52*, 6748–6752.

(5) Yan, Q.; Kong, D.; Zhao, W.; Zi, G.; Hou, G. Enantioselective Hydrogenation of β,β-Disubstituted Unsaturated Carboxylic Acids under Base-Free Conditions. *J. Org. Chem.* **2016**, *81*, 2070–2077.

(6) Tolstoy, P.; Engman, M.; Paptchikhine, A.; Bergquist, J.; Church, T. L.; Leung, A. W.-M.; Andersson, P. G. Iridium-catalyzed asymmetric hydrogenation yielding chiral diarylmethines with weakly coordinating or noncoordinating substituents. *J. Am. Chem. Soc.* **2009**, *131*, 8855–8860.

(7) Guo, S.; Yang, P.; Zhou, J. (Steve). Nickel-catalyzed asymmetric transfer hydrogenation of conjugated olefins. *Chem. Commun.* **2015**, *51*, 12115–12117.

(8) Guo, S.; Zhou, J. N,N-Dimethylformamide as Hydride Source in Nickel-Catalyzed Asymmetric Hydrogenation of α,β-Unsaturated Esters. *Org. Lett.* **2016**, *18*, 5344–5347.

(9) Dong, K.; Li, Y.; Wang, Z.; Ding, K. Catalytic asymmetric hydrogenation of α-CF_3- or β-CF_3-Substituted acrylic acids using Rhodium(I) complexes with a combination of chiral and achiral ligands. *Angew. Chem. Int. Ed.* **2013**, *52*, 14191–14195.

(10) Chen, J.; Yuan, P.; Wang, L.; Huang, Y. Enantioselective β-Protonation of Enals via a Shuttling Strategy. *J. Am. Chem. Soc.* **2017**, *139*, 7045–7051.

(11) Colvin, E. W. Recent Synthetic Applications of Organosilicon Reagents. *Chem. Org. Silicon Compd.* **1998**, *2*, 1667–1685.

(12) Barreau, M.; Hardy, J.-C.; Martin, J.-P.; Renault, C. Benzopyran derivatives, their preparation and pharmaceutical compositions containing them. *US 4994470* (1990).

(13) Hedberg, C.; Andersson, P. Catalytic Asymmetric Total Synthesis of the Muscarinic Receptor Antagonist (R)-Tolterodine. *Adv. Synth. Catal.* **2005**, *347*, 662–666.

(14) Roesner, S.; Aggarwal, V. K. Enantioselective synthesis of (*R*)-tolterodine using lithiation/borylation–protodeboronation methodology. *Can. J. Chem.* **2012**, *90*, 965–974.

(15) Wang, X.; Guram, A.; Caille, S.; Hu, J.; Preston, J. P.; Ronk, M.; Walker, S. Highly Enantioselective Hydrogenation of Styrenes Directed by 2′-Hydroxyl Groups. *Org. Lett.* **2011**, *13*, 1881–1883.

(16) Limberger, J.; Claudino, T. S.; Monteiro, A. L. Stereoselective synthesis of (*E*)-3,3-diaryl and (*E*)-3-aryl-3-aryloxy allylamines and allylalcohols from trans-cinnamyl chloride and alcohol. *RSC Adv.* **2014**, *4*, 45558–45565.

(17) Fornika, R.; Dinjus, E.; Görls, H.; Leitner, W. Structure and reactivity of dimeric rhodium(I) formate complexes: X-ray crystal structure analysis of [{(cod)Rh(μ−κ2O,O′□HCO2)}2] and phosphane-induced hydride transfer to give an η3-cyclooctenyl complex. *J. Organomet. Chem.* **1996**, *511*, 145–155.

(18) Leitner, W.; Brown, J. M.; Leitner, W.; Brunner, H.; Leitner, W. Mechanistic Aspects of the Rhodium-Catalyzed Enantioselective Transfer Hydrogenation of α,β-Unsaturated Carboxylic Acids Using Formic Acid/Triethylamine (5:2) as the Hydrogen Source. *J. Am. Chem. Soc.* **1993**, *115*, 152–159.

(19) Wu, Z.; Laffoon, S. D.; Nguyen, T. T.; McAlpin, J. D.; Hull, K. L. Rhodium-Catalyzed Asymmetric Synthesis of β-Branched Amides. *Angew. Chem. Int. Ed.* **2017,** *56*, 1371–1375.

(20) Limberger, J.; Claudino, T. S.; Monteiro, A. L. Stereoselective synthesis of (*E*)-3,3-diaryl and (*E*)-3-aryl-3-aryloxy allylamines and allylalcohols from trans-cinnamyl chloride and alcohol. *RSC Adv.* **2014**, *4*, 45558–45565.

(21) Watanabe, M.; Hisamatsu, S.; Hotokezaka, H.; Furukawa, S. Reaction of lithiated senecioamide and related compounds with benzynes: Efficient syntheses of naphthols and naphthoquinones. *Chem. Pharm. Bull. (Tokyo).* **1986**, *34*, 2810–2820.

(22) Bizet, V.; Pannecoucke, X.; Renaud, J. L.; Cahard, D. Synthesis of β-CF_3 ketones from trifluoromethylated allylic alcohols by ruthenium catalyzed isomerization. *J. Fluor. Chem.* **2013**, *152*, 56–61.

(23) Eguchi, T.; Aoyama, T.; Kakinuma, K. Remarkable Reversal of Stereoselectivity Olefinations of a-Fluorinated in Wittig-Type Alkyl Aryl Ketones. *Tetrahedron Lett.* **1992**, *33*, 5545–5546.

(24) Corey, E. J.; Katzenellenbogen, J. A.; Posner, G. H. A new stereospecific synthesis of trisubstituted olefins. stereospecific synthesis of farnesol. *J. Am. Chem. Soc.* **1967**, *89*, 4245.

(25) Ohkawa, S. et al. Benzo-fused 5-membered heterocyclic compounds, their production and use. *U. S. Pat. Appl. Publ.* 20070149558 (2007).

CHAPTER 5: INTRODUCTION TO PART II

This chapter has been adapted from the following publication:

Greenlee, A. J.; Wendell, C. I.; Cencer, M. M.; Laffoon, S. D.; Moore, J. S. Kinetic and Thermodynamic Control in Dynamic Covalent Synthesis. *Trends Chem.* **2020** [online early access] doi: 10.1016/j.trechm.2020.09.005

5.1 Abstract

In recent years, dynamic covalent chemistry (DCC) has seen the synthesis of increasingly complex cyclooligomers, polymers, and diverse compound libraries. The reversible formation of covalent bonds characteristic of DCC reactions favors thermodynamic product distributions for simple unitopic reactions; however, kinetic effects are increasingly influential in reactions of multitopic precursors. This chapter discusses the interplay between thermodynamic and kinetic considerations in DCC synthesis with a focus on alkyne metathesis

5.2 Dynamic Covalent Chemistry (DCC)

DCC is an efficient synthetic strategy that utilizes multitopic precursors designed to form reversible covalent bonds, combining advantages of error correction during synthesis with the stability of a covalent compound as the final product. It has enabled the synthesis of a variety of molecular architectures, often isolated as a single, discrete species, including macrocycles,[1] cages,[2] and covalent organic frameworks.[3,4] Reversible bonds commonly in use include imine, boronic ester, hydrazone, disulfide, alkyne, oxime and alkene exchange (Figure 5.1). These structures have

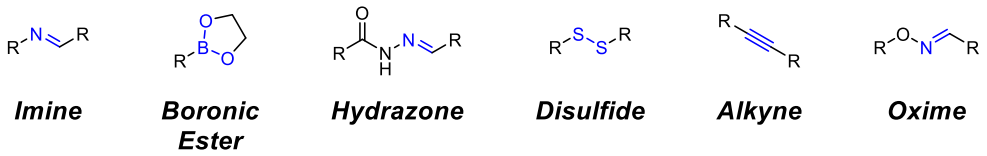

Figure 5.1. Common exchangeable bonds employed in DCC.

found applications in host-guest chemistry,[5] organic electronic materials,[6] information storage and retrieval,[7] catalysis,[8] biological applications,[9] chemical sensing,[10] and as building blocks for other materials, such as nanofibers.[11]

Most targets of DCC are constructed from a small number of different types of repeating units. Thus, DCC is commonly a cyclooligomerization process. The combination of a bimolecular oligomerization and intramolecular cyclization in the same reaction represents one challenge of dynamic covalent synthesis. Another challenge stems from the multitopic nature of DCC precursors. While the individual bond forming events are reversible, incorrectly joined structures may require multiple bond breakages to release an incorrectly placed precursor. Some erroneous structures fall out of dynamic equilibrium with the rest of the reaction network. Nonetheless, overcoming these challenges enables the synthetic efficiency of DCC reflected by the number of bonds made per operational step. Moreover, DCC product yields may approach quantitative, whereas cyclooligomerizations relying on strong irreversible bond formations tend to give low yields of final product, presumably because error correction is key to synthetic success.[12]

Due to the reversibility of each bond forming event, DCC is generally thought to operate under thermodynamic control. However, as DCC advances to increasingly complex targets, there is good reason to suggest that kinetic factors may become more important. The concatenation of multitopic precursors gives rise to a large number of structures on the way to the target product. These structures include polyhedra, polymers, and networks, and they may have very similar energies. This suggests a flat energy landscape, but complexes exhibiting multiple persistent bonds are stabilized, which produces a vast landscape with somewhat regular variation. Given the

complexity of DCC reaction networks and associated energy landscapes, synthetic intuition is unsuited to predict the outcome. Failures in experimental DCC often come at a high cost because multitopic, complex precursors require considerable structural optimization and synthetic overhead.[8] Predicting outcomes is therefore essential and may require computational modeling to ensure a full understanding of the underlying factors that shape the energy landscape.

5.3 Thermodynamic Control in DCC

The ability of dynamic systems to undergo reversible component exchange is key to the utility of DCC. Under thermodynamic control, even off-pathway intermediates typically error correct toward favorable product distributions on the timescale of the reaction (Figure 5.2).[13] In an example of thermodynamically driven alkyne metathesis, arylene ethynylene macrocycles are formed both by alkyne metathesis cyclooligomerization and by depolymerization-macrocyclization of linear poly(arylene ethynylene) species.[14] The product distribution is not dependent on reaction pathway which is a necessary condition to classify a given product distribution as thermodynamic rather than kinetic.

A depolymerization strategy was showcased in the synthesis of homochiral, BINOL based macrocyces through self-sorting alkyne metathesis DCC.[15] A heterochiral arylene ethynylene polymer containing both R- and S-BINOL repeating units was subjected to alkyne metathesis at RT resulting in formation of only homochiral R/S dimeric macrocycles. This selectivity was hypothesized to be a result of the difference in symmetry between hetero- and homochiral macrocycles. Calculations revealed that the enthalpic difference between the hetero- and homochiral structures is relatively small. However, the entropic difference between macrocycles of different symmetry was proposed to be a significant contribution to the overall DG of the

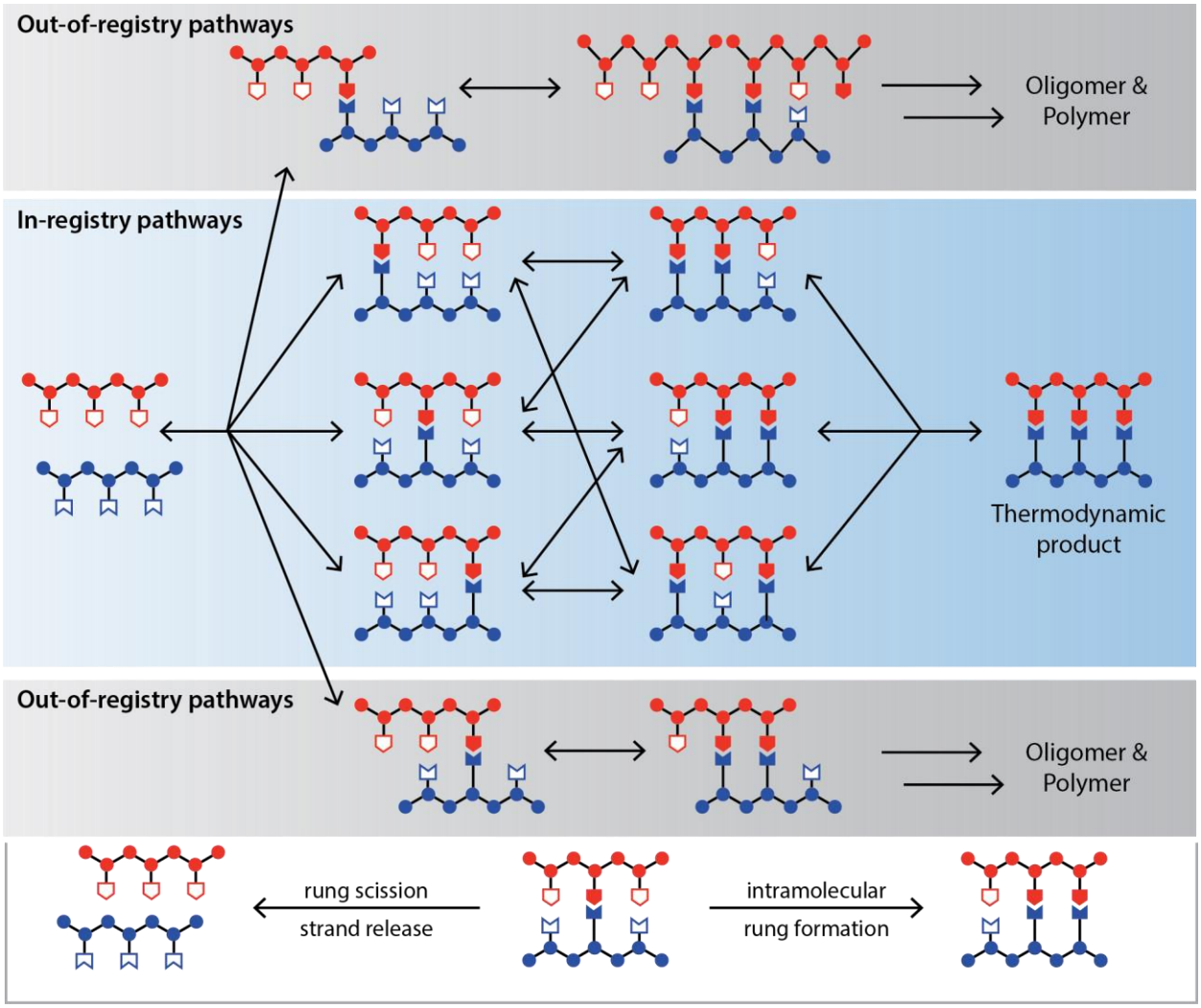

Figure 5.2. Reaction network of ladder formation under DCC. In-registry intermediates and products have correctly matched rungs where outer rungs bond to other outer rungs, and center rungs bond to other center rungs between two strands. Out-of-registry products have mismatched rung formation. Mismatched intermediates revert to free strands if rung scission is faster than intramolecular rung formation. Reproduced from reference 16.

reaction indicating thermodynamic selectivity.

Alkyne metathesis has become an increasingly popular tool of DCC as highly active and functional group tolerant catalyst systems have been developed. Alkyne metathesis has found wide application in both total synthesis and materials chemistry.[17] Alkyne metathesis is commonly catalyzed through the use of Schrock alkylydine complexes of molybdenum and tungsten (Figure 5.3). The catalytic cycle of AM is analogous to that of olefin metathesis and proceeds through cycloaddition and cycloreversion of metallacyclobutadiene intermediates. The reversibility of

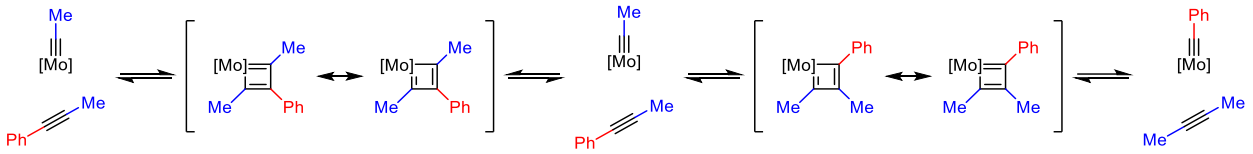

Figure 5.3. Reaction mechanism of alkyne metathesis with Schrock alkylidyne complexes.

alkyne metathesis is key to its utility in DCC; however, the equilibrium must be driven forward to obtain high yields of desired products. Propynylated precursors release volatile 2-butyne after metathesis which can be removed through high vacuum. To circumvent the need for vacuum driven conditions, the Moore group reported an efficient precipitation driven strategy to drive alkyne metathesis reactions to completion.[18] A key breakthrough in the development of alkyne metathesis DCC was made by Furstner and coworkers who have reported that alkyne metathesis can be efficiently driven forward by using propynylated substrates in conjunction with 5Å molecular sieves (MS) which effectively remove 2-butyne.[19] This strategy allows for more simple preparation of metathesis precursors and alleviates the need for bulky precipitating groups or a vacuum-driven system. [16a,20]

The reversibility of alkyne metathesis is key to its proclivity for self-correction. In AM-DCC using multitopic precursors, these reactions often proceed through initial formation of higher molecular weight oligomeric/polymeric products which then convert to a discrete product.[21,22] The Moore group has demonstrated that discrete macrocycles can be generated from polymeric precursors through a depolymerization-macrocyclization strategy. Polymer **1** was prepared through Sonogashira polymerization and determined to have a molecular weight (MW) of 11.4 kDa and polydispersity index of 1.8 (Figure 5.4).[23] Subjecting this polymer to alkyne metathesis conditions afforded macrocycle **2** in 70% yield after 24 hours.

Systems under thermodynamic control favor distributions that maximize entropy by generating structures with the fewest possible number of building blocks while minimizing angle

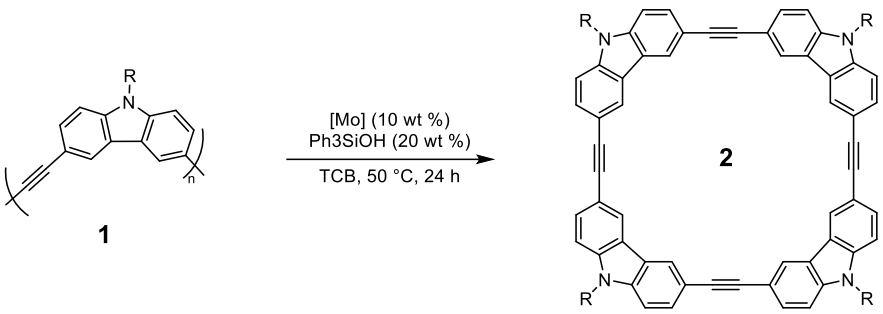

Figure 5.4. Synthesis of arylene(ethynylene) macrocycles via alkyne metathesis depolymerization.

strain of the resultant structures. These principles have enabled the intuitive design of a wide variety of cyclic molecular architectures on the basis of precursor topicity and geometry.[24] Furthermore, in systems with very flat energy landscapes, slight differences in thermodynamic stability lead to self-sorting and large amplifications of product concentrations, which can be further improved by increased catalyst loading and thermal cycling.[14,25-28]

While design principles such as precursor geometry and topicity are generally reliable predictors of product topology and stability, the complexity of DCC energy landscapes can lead to unpredicted reaction outcomes. Cooper and coworkers recently designed a computational screening procedure to predict the major products of imine condensation reactions based on product stability.[29] While many combinations of aldehyde and amine precursors produced the predicted imine cages, several pairings of precursors led to structures with unexpected topologies. In these cases, the less thermodynamically favored product was observed, and the energetic preference for the predicted structures was small (around 5 kJ mol^{-1}) compared to the observed products. The Zhang group reported similar phenomena in the synthesis of arylene ethynylene cages.[30] Slight variations in monomer size yielded structures with drastically different topologies, despite a consistent face-to-edge angle between substrates. Taken together, these results suggest that intuitive design rules are unreliable predictors of complex reaction outcomes, and that pathway-dependence may contribute to DCC syntheses in largely unexplored ways.

5.4 Kinetical Control in DCC

The reversible bonds used in DCC enable systems to undergo error correction. The faster the rate of exchange, the less prone the resulting system is to kinetic traps (Figure 5.5). In the synthesis of molecular ladders, hydrogen bonded rungs demonstrate much higher fidelity (98% vs. 62%) than an imine-linked ladder with an identical backbone, due in part to the high exchange rate of hydrogen bonding.[31,32] However, while rapid exchange speed rescues a system from a putative kinetic trap, all covalent bonds are susceptible to trapping under some circumstances. Rigid complex architectures, such as COFs and cages, typically synthesized via DCC tend to be predisposed towards kinetic control due to precursor multitopicity. Macrocycles with ditopic precursors require two bond breakage events before a precursor is released. After the first bond breakage, the two resulting reactive moieties are in close proximity and have a faster rate of

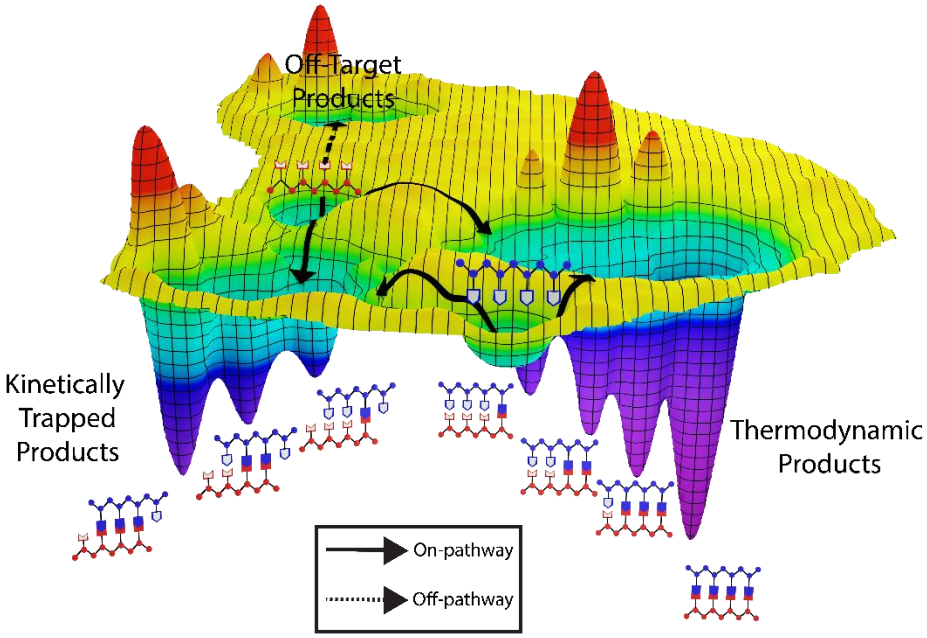

Figure 5.5. Generic energy landscape of ladder formation. In reactions with complex energy landscapes, species can become kinetically trapped even if reversible chemistry is used. Kinetic traps can persist if small barriers funnel material back to the trapped structure rather than out of the kinetic trap and toward a thermodynamic minimum. In the case of molecular ladders, out-of-registry products may be kinetic traps if rung scission is immediately followed by reformation of the rung. Kinetic factors such as proximity-induced high effective concentration prevent error correction in a dynamic system where the thermodynamic product is desired. Reproduced from reference 16.

recombination than two unlinked precursors, an effect which is exacerbated by the rigidity of the structures. If the rate of bond reformation is faster than the breakage of the second bond, the macrocycle may behave as a kinetic trap. Kinetic trap behavior is even more likely for structures which require three or four bond breakages, where precursors are tritopic or tetratopic and the partially broken structures have higher rigidity.[2,33] This is apparent in the synthesis of ladder compounds, which generally have [n]-topic precursors, where n is the number of rungs. These studies show that beyond a certain number of rungs the structures can no longer undergo error correction and tend to form myriad mismatched products instead.[7,34,35]

The Moore group has recently reported the synthesis of kinetically trapped tetrahedral organic cages through alkyne metathesis of tritopic precursors (Figure 5.6).[36] Precursor **3** was prepared as a structural analog of similar compounds which have been shown to have an alternating 'up-down-up' configuration of the 1,3,5-substitution of hexasubstituted arenes.[37] This conformation preorganizes **3** to undergo metathesis to adopt a conformation that favors formation

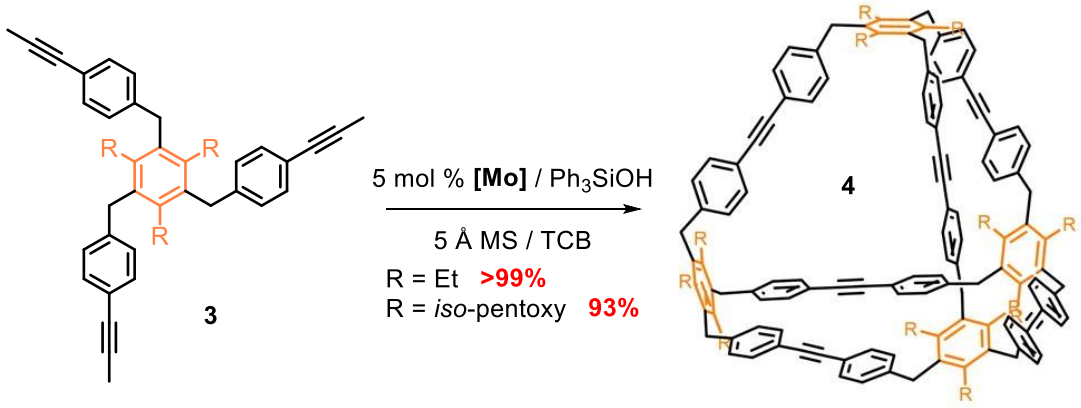

Figure 5.6. Synthesis of a kinetically trapped tetrahedral organic cage from a tritopic precursor under alkyne metathesis.

of a tetrameric organic cage.[36] Subjecting **3** to alkyne metathesis using only 5 mol% molybdenum catalyst afforded the tetrahedral cage **4** in near quantitative yield. Tetrahedral cage **4** was determined to be a kinetic trap and no longer dynamic under the alkyne metathesis conditions used for its synthesis.[36]

Precursor rigidity influences reaction outcomes by rendering certain transition states geometrically inaccessible. This is particularly relevant for reactions with conformationally restrictive transition states, such as the transition state leading to the metallacyclobutadiene intermediate in alkyne metathesis. Chapter 6 details the synthesis of a molecular Möbius strip under total kinetic diastereoselectivity arising from strain in the key metallacylobutadiene transition state.[37]

Solubility is often utilized as a tool for kinetically directing DCC synthesis. Heavily conjugated structures are common because they are rigid enough to be shape-persistent, but large, planar π surfaces contribute to insolubility due to π-π stacking, removing the compound from dynamic equilibrium and promoting its formation. Dichtel and coworkers developed a system which produces macrocycle only when it is insoluble in the reaction solvent; dissolving the macrocycle and allowing it to re-enter dynamic equilibrium leads to conversion into polymer, the putative thermodynamic product.[1] Many DCC syntheses are driven by precipitation.[38-40] Adding solubilizing groups or changing the size and planarity of the π surface allows modulation of solubility. Northrop and coworkers produce a planar and non-planar version of the same boronate ester cage by inserting ethynylene units into a biaryl backbone with a 90° twist.[38] They demonstrate that the more planar version is less soluble and more stable to protic solvents. The Moore group and others have the reported the synthesis of a number of novel macrocycles and cages through AM-DCC.[20,41-43] Precipitation-driven alkyne metathesis enabled the synthesis of macrocycle 6 as a precursor to a cycloparaphenyleneacetylene which effectively binds to C_{70}.[44] Macrocycle **6** is insoluble in 1,2,4-trichlorobenzene and falls out of the dynamic pool of exchangeable alkynes via precipitation.

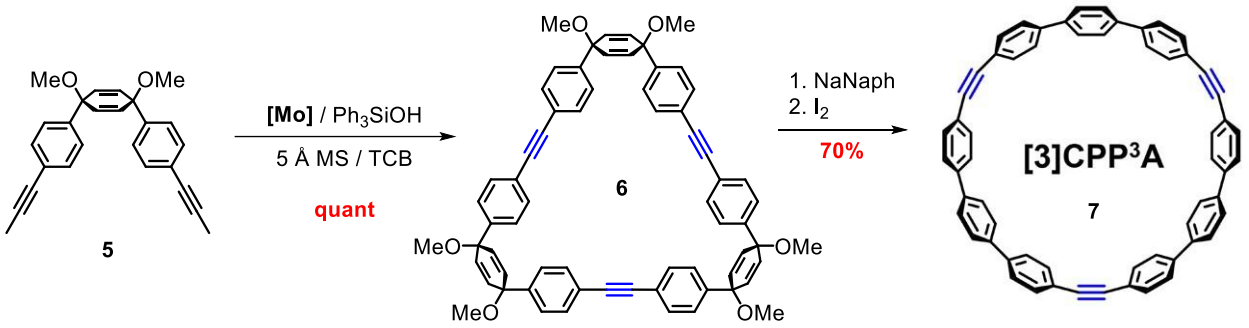

Figure 5.7. Precipitation driven cyclooligomerization alkyne metathesis.

In addition, supramolecular structures that form between cages and other complex products affect exchange rates. Dichtel and coworkers report an imine macrocycle that assembles into nanotubes which prevent further imine exchange, and Otto and coworkers report a similar effect.[11,45] In the synthesis of knots and catenanes from a DCL, multiple products are kinetically trapped as a result of intramolecular π-π stacking in ambiphilic molecules, analogous to the hydrophobic effect in protein folding.[46]

While kinetic traps may introduce synthetic obstacles, they sometimes provide products in higher yields than the same system under thermodynamic control. In some cases, the kinetic trap is also the thermodynamic product.[2,47] In other cases, the pathway-dependence of kinetically controlled systems can be leveraged. Multiple products may be accessible from the same precursors under different conditions, especially useful given the high synthetic overhead of DCC precursors.[11] Otto and coworkers have provided evidence that mechanical agitation has a strong influence on product distribution.[10,48] Slow addition of monomer has been demonstrated to produce COFs with larger crystal domains than a single-addition protocol.[49]

Scott and coworkers show that a high-fidelity synthesis of an information-bearing five rung imine ladder is only achieved by increasing and then decreasing the concentration of scandium (III) triflate, commonly used to promote imine exchange.[35] Maintaining catalyst concentration at consistent substoichiometric levels throughout the reaction leads to mismatched byproducts

instead; this dependence on pathway suggests that the information-bearing ladders are kinetic products. Lehn and coworkers have developed libraries of acyl hydrazones and imines generated from simple aldehyde, acyl hydrazine, and aniline building blocks.[7] In the presence of a metal cation with the appropriate coordination geometry, kinetically trapped species were favored. Upon precipitation of the directing metals, the libraries were expected to return to equilibrium, favoring formation of the more stable acyl hydrazone. However, because the exchange rate of imines and acyl hydrazones is on the order of weeks, the composition of the DCL remained unchanged on a relevant laboratory timescale, or until it was erased by thermal cycling. Furthermore, the library could be trained to adopt an altered kinetic equilibrium through the addition of a different metal cation, demonstrating the versatility of a simple system for information storage. In this case, kinetic factors allow access not only to targeted materials, but also to emergent properties from simple chemical systems.

5.5 Conclusion

While dynamic covalent chemistry is a relatively young field, consensus has already emerged around the importance of predicting reaction outcomes. Reversible covalent bonds combine the stability of covalent products with rapid error correction. However, not all linkages necessarily reversibly equilibrate and multitopicity of the resulting structures leads to complex reaction networks and energy landscapes. Unfortunately, the high overhead required to conceive of and develop precursors raises the cost of unpredictable outcomes.[7] Many researchers tend to overemphasize thermodynamic factors when planning a synthesis based on reversible covalent linkages even though the desired geometric complexity, rigidity, and extended conjugation often subject the synthesis to kinetic control. In response, computation has enhanced human intuition.

New approaches have begun to incorporate kinetic factors into computation shedding light on COF nucleation, ladder formation and trapping, and other processes with observable kinetic effects.[33,50] However, few studies to date have incorporated both kinetic and thermodynamic factors in computational prediction. Computational models will be vital to developing new precursor structures in the future of DCC.

The author thanks Oleg Davydovich and Dorothy Loudermilk for their contributions to the figures in this chapter.

5.6 Literature Cited

(1) Chavez, A. D.; Evans, A. M.; Flanders, N. C.; Bisbey, R. P.; Vitaku, E.; Chen, L. X.; Dichtel, W. R. Equilibration of imine-linked polymers to hexagonal macrocycles driven by self-assembly. *Chem. Eur. J.* **2018**, *24*, 3989–3993.

(2) Lee, S.; Yang, A.; Moneypenny II, T. P.; Moore, J. S. Kinetically trapped tetrahedral cages via alkyne metathesis. *J. Am. Chem. Soc.* **2016**, *138*, 2182–2185.

(3) Ma, T.; Kapustin, E. A.; Yin, S. X.; Liang, L.; Zhou, Z.; Niu, J.; Li, L.-H.; Wang, Y.; Su, J.; Li, J.; Wang, X.; Wang, W. D.; Wang, W.; Sun, J.; Yaghi, O. M. Single-crystal x-ray diffraction structures of covalent organic frameworks. *Science* **2018**, *361*, 48–52.

(4) Gasparini, G.; Dal Molin, M.; Lovato, A.; Prins, L. J. Dynamic Covalent Chemistry; *Supramolecular Chemistry: From Molecules to Nanomaterials.* **2012** (Gale, P. A., Steed, J.W. and Barbour, L.J., eds) John Wiley and Sons, Ltd.

(5) Slater, A. G.; Little, M. A.; Briggs, M. E.; Jelfs, K. E.; Cooper, A. I. A solution-processable dissymmetric porous organic cage. *Mol. Syst. Des. Eng.* **2018**, *3*, 223–227.

(6) Savino, C.; Ryan, R. P.; Knee, J. L.; Jimenez-Hoyos, C. A.; Northrop, B. H. Electronic spectroscopy of 2-phenyl-1,3,2-benzodioxaborole and its derivatives: Important building blocks of covalent organic frameworks. *J. Phys. Chem. A* **2020**, *124*, 529–537.

(7) Holub, J.; Vantomme, G.; Lehn, J.-M. Training a constitutional dynamic network for effector recognition: Storage, recall, and erasing of information. *J. Am. Chem. Soc.* **2016**, *138*, 11783–11791.

(8) Turcani, L.; Greenaway, R. L.; Jelfs, K. E. Machine learning for organic cage property prediction. *Chem. Mater.* **2019**, *31*, 714–727.

(9) Herrmann, A. Dynamic combinatorial/covalent chemistry: a tool to read, generate and modulate the bioactivity of compounds and compound mixtures. *Chem. Soc. Rev.* **2014**, *43*, 1899–1933.

(10) Evans, J.; Jelfs, K. E.; Day, G. M.; Doonan, C. J. Application of computational methods to the design and characterisation of porous molecular materials. *J. Chem. Soc. Rev.* **2017**, *46*, 3286–3301.

(11) Pal, A.; Malakoutikah, M.; Leonetti, G.; Tezcan, M.; Colomb-Delsuc, M.; Nguyen, V. D.; van der Gucht, J.; Otto, S. Controlling the structure and length of self-synthesizing supramolecular polymers through nucleated growth and disassembly. *Angew. Chem. Int. Ed.* **2015**, *54*, 7852–7856.

(12) Mastalerz, M. Porous shape-persistent organic cage compounds of different size, geometry, and function. *Acc. Chem. Res.* **2018**, *51*, 2411–2422.

(13) Zhang, W. and Jin, Y., eds *Principles of Dynamic Covalent Chemistry*; **2017** John Wiley & Sons, Ltd.

(14) Gross, D. E.; Moore, J. S. Arylene–Ethynylene macrocycles via depolymerization–macrocyclization. *Macromolecules* **2011**, *44*, 3685–3687.

(15) Sisco, S.; Moore, J. Homochiral Self-Sorting of Binol Macrocycles. *Chem. Sci.* **2014**, *5*, 81–85.

(16) Greenlee, A. J.; Wendell, C. I.; Cencer, M. M.; Laffoon, S. D.; Moore, J. S. Kinetic and Thermodynamic Control in Dynamic Covalent Synthesis. *Trends Chem.* **2020** [online early access] doi: 10.1016/j.trechm.2020.09.005

(17) (a) Fuerstner, A. Alkyne Metathesis on the Rise. *Angew. Chem. Int. Ed.* **2013**, *52*, 2794–2819. (b) Ehrhorn, H.; Tamm, M. Well-Defined Alkyne Metathesis Catalysts: Developments and Recent Applications. *Chem. Eur. J.* **2019**, *25*, 3190–3208.

(18) Zhang, W.; Moore, J. S. Arylene Ethynylene Macrocycles Prepared by Precipitation-Driven Alkyne Metathesis. *J. Am. Chem. Soc.* **2004**, *126*, 12796.

(19) Heppekausen, J.; Stade, R.; Goddard, R.; Fürstner, A. Practical New Silyloxy-Based Alkyne Metathesis Catalysts with Optimized Activity and Selectivity Profiles. *J. Am. Chem. Soc.* **2010**, *132*, 11045-11057.

(20) Pattillo, C. C. C., M.M.; Moore, J.S. Discussion Addendum For: Preparation of a Carbazole-Based Macrocycle Via Precipitation-Driven Alkyne Metathesis. *Org. Synth.* **2018**, *95*, 231–239.

(21) Moneypenny, T. P.; Yang, A.; Walter, N. P.; Woods, T. J.; Gray, D. L.; Zhang, Y.; Moore, J. S. Product Distribution from Precursor Bite Angle Variation in Multitopic Alkyne Metathesis: Evidence for a Putative Kinetic Bottleneck. *J. Am. Chem. Soc.* **2018**, *140*, 5825–5833.

(22) Zhang, C.; Wang, Q.; Long, H.; Zhang, W. A Highly C70 Selective Shape-Persistent Rectangular Prism Constructed through One-Step Alkyne Metathesis. *J. Am. Chem. Soc.* **2011**, *133*, 20995–21001.

(23) Gross, D.; Moore, J. Arylene Ethynylene Macrocycles Via Depolymerization Macrocyclization. *Macromolecules* **2011**, 3685–3687.

(24) Moneypenny II, T. P.; Yang, A.; Walter, N. P.; Woods, T. J.; Gray, D. L.; Zhang, Y.; Moore, J. S. Product distribution from precursor bite angle cariation in multitopic alkyne metathesis: Evidence for a putative kinetic bottleneck. *J. Am. Chem. Soc.* **2018**, *140*, 5825–5833.

(25) Sisco, S. W.; Moore, J. S. Homochiral self-sorting of BINOL macrocycles. *Chem. Sci.* **2014**, *5*, 81–85.

(26) Liu, X.; Warmuth, R. Solvent Effects in Thermodynamically Controlled Multicomponent Nanocage Syntheses. *J. Am. Chem. Soc.* **2006**, *128*, 14120–14127.

(27) Wei, T.; Furgal, J. C.; Jung, J. H.; Scott, T. F. Long, self-assembled molecular ladders by cooperative dynamic covalent reactions. *Polym. Chem.* **2017**, *8*, 520–527.

(28) Hartley, C. S.; Elliott, E. L.; Moore, J. S. Covalent assembly of molecular ladders. *J. Am. Chem. Soc.* **2007**, *129*, 4512–4513.

(29) Greenaway, R. L.; Santolini, V.; Bennison, M. J.; Alston, B. M.; Pugh, C. J.; Little, M. A.; Miklitz, M.; Eden-Rump, E. G. B.; Clowes, R.; Shakil, A.; Cuthbertson, H. J.; Armstrong, H.; Briggs, M. E.; Jelfs, K. E.; Cooper, A. I. High-throughput discovery of organic cages and catenanes using computational screening fused with robotic synthesis. *Nat. Commun.* **2018**, *9*, 2849.

(30) Wang, Q.; Yu, C.; Zhang, C.; Long, H.; Azarnoush, S.; Jin, Y.; Zhang, W. Dynamic covalent synthesis of aryleneethynylene cages through alkyne metathesis: Dimer, tetramer, or interlocked complex? *Chem. Sci.* **2016**, *7*, 3370–3376.

(31) Elliott, E. L.; Hartley, C. S.; Moore, J. S. Covalent ladder formation becomes kinetically trapped beyond four rungs. *Chem. Comm.* **2011**, *47*, 5028-5030.

(32) Swain, J. A.; Iadevaia, G.; Hunter, C. A. H-Bonded Duplexes based on a Phenylacetylene

Backbone. *J. Am. Chem. Soc.* **2018**, *140*, 11526–11536.

(33) Cencer, M. M.; Greenlee, A. J.; Moore, J. S. Quantifying error correction through a rule-based model of strand escape from an *n*-rung ladder. *J. Am. Chem. Soc.* **2020**, *142*, 162.

(34) Furgal, J. C.; van Dijck, J. M.; Leguizamon, S. C.; Scott, T. F. Accessing sequence specific hybrid peptoid oligomers with varied pendant group spacing. *Eur. Polym. J.* **2019**, *118*, 306–311.

(35) Leguizamon, S. C.; Scott, T. F. Sequence-selective dynamic covalent assembly of information-bearing oligomers. *Nat. Commun.* **2020**, *11*, 1–10.

(36) Lee, S.; Yang, A.; Moneypenny, T. P.; Moore, J. S. Kinetically Trapped Tetrahedral Cages Via Alkyne Metathesis. *J. Am. Chem. Soc.* **2016**, *138*, 2182–2185.

(37) Jiang, X.; Laffoon, S. D.; Chen, D.; Pérez-Estrada, S.; Danis, A. S.; Rodríguez-López, J.; Garcia-Garibay, M. A.; Zhu, J.; Moore, J. S. Kinetic control in the synthesis of a Möbius tris((ethynyl)[5]helicene) macrocycle using alkyne metathesis. *J. Am. Chem. Soc.* **2020**, *142*, 6493-6498.

(38) Smith, M. K.; Goldberg, A. R.; Northrop, B. H. The dynamic assembly of covalent organic polygons: Finding the optimal balance of solubility, functionality, and stability. *Eur. J. Org. Chem.* **2015**, *13*, 2928–2941.

(39) Chavez, A. D.; Smith, B. J.; Smith, M. K.; Beaucage, P. A.; Northrop, B. H.; Dichtel, W. R. Discrete, hexagonal boronate ester-linked macrocycles related to two-dimensional covalent organic frameworks. *Chem. Mater.* **2016**, *28*, 4884–4888.

(40) Ortiz, M.; Yu, C.; Jin, Y.; Zhang, W. Poly(aryleneethynylene)s: Properties, applications and synthesis through alkyne metathesis. *Topics Curr. Chem.* **2017**, *375*, 69.

(41) Zhang, W.; Moore, J. S. Arylene Ethynylene Macrocycles Prepared by Precipitation-Driven Alkyne Metathesis. *J. Am. Chem. Soc.* **2004**, *126*, 12796.

(42) Zhang, W.; Brombosz, S. M.; Mendoza, J. L.; Moore, J. S. A High-Yield, One-Step

Synthesis of O-Phenylene Ethynylene Cyclic Trimer Via Precipitation-Driven Alkyne Metathesis. *J. Org. Chem.* **2005**, *70*, 10198–10201.

(43) Zhang, W. C., H.M.; Moore, J.S. Preparation of a Carbazole-Based Macrocycle Via Precipitation-Driven Alkyne Metathesis. *Org. Synth.* **2007**, *84*, 177–191.

(44) Lee, S.; Chénard, E.; Gray, D. L.; Moore, J. S. Synthesis of Cycloparaphenyleneacetylene Via Alkyne Metathesis: C70complexation and Copper-Free Triple Click Reaction. *J. Am. Chem. Soc.* **2016**, *138*, 13814–13817.

(45) Strauss, M. J.; Evans, A. M.; Castano, I.; Li, R. L.; Dichtel, W. R. Supramolecular polymerization provides non-equilibrium product distributions of imine-linked macrocycles. *Chem. Sci.* **2020**, *11*, 1957–1963.

(46) Ponnuswamy, N.; Cougnon, F. B. L.; Pantoş, G. D.; Sanders, J. K. M. Homochiral and meso figure eight knots and a solomon link. *J. Am. Chem. Soc.* **2014**, *136*, 8243–8251.

(47) Castano, I.; Evans, A. M.; Li, H.; Vitaku, E.; Strauss, M. J.; Brédas, J.-L.; Gianneschi, N. C.; Dichtel, W. R. Chemical Control over Nucleation and Anisotropic Growth of Two-Dimensional Covalent Organic Frameworks. *ACS Cent. Sci.* **2019**, *5*, 1892–1899.

(48) Komáromy, D.; Stuart, M. C. A.; Santiago, G. M.; Tezcan, M.; Krasnikov, V. V.; Otto, S. Self-assembly can direct dynamic covalent bond formation toward diversity or specificity. *J. Am. Chem. Soc.* **2017**, *139*, 6234–6241.

(49) Li, J.; Nowak, P.; Fanlo-Virgós, H.; Otto, S. Catenanes from catenanes: quantitative assessment of cooperativity in combinatorial catenation. *Chem. Sci.* **2014**, *5*, 4968-4974.

(50) Li, H.; Chavez, A. D.; Li, H.; Li, H.; Dichtel, W. R.; Bredas, J.-L. Nucleation and growth of covalent organic frameworks from solution: The example of COF-5. *J. Am. Chem. Soc.* **2017**, *139*, 16310–16318.

CHAPTER 6: KINETIC CONTROL IN THE SYNTHESIS OF A MOLECULAR MÖBIUS STRIP USING ALKYNE METATHESIS

This chapter has been adapted from the following publication:

Jiang, X.; Laffoon, S. D.; Chen, D.; Pérez-Estrada, S.; Danis, A. S.; Rodríguez-López, J.; Garcia-Garibay, M. A.; Zhu, J.; Moore, J. S. "Kinetic Control in the Synthesis of a Möbius Tris((ethynyl)[5]helicene) Macrocycle Using Alkyne Metathesis," *J. Am. Chem. Soc.* **2020**, *142*, 6493–6498.

6.1 Abstract

The synthesis of conjugated Möbius molecules remains elusive since twisted and macrocyclic structures are low entropy species sporting their own synthetic challenges. Here we report the synthesis of a Möbius macrocycle in 84% yield from the alkyne metathesis of 2,13-bispropynyl[5]helicene. MALDI-MS, NMR, and X-ray diffraction indicated a trimeric product of two-fold symmetry with PPM/MMP configurations in the helicene subunits. Alternatively, a three-fold symmetric, PPP/MMM structure was determined by DFT calculation to be more thermodynamically stable, illustrating remarkable kinetic selectivity for this alkyne metathesis cyclooligomerization. Computational studies provided insight into the kinetic selectivity, demonstrating a difference of 15.4 kcal/mol in activation barriers between the PPM/MMP vs. PPP/MMM diastereodetermining steps. Computational (ACID and EDDB) and experimental (UV-Vis and fluorescence spectroscopy and cyclic voltammetry) studies revealed weak conjugation between the alkyne and adjacent helicene groups, as well as the lack of significant global aromaticity. The separation of PPM/MMP enantiomers was achieved via chiral HPLC at the analytical scale.

6.2 Background and Motivation

Dynamic covalent chemistry (DCC) is a powerful synthetic strategy for assembling complex structures via reversible reactions from simple building blocks. Such reactions, including alkyne metathesis, imine condensation, disulfide exchange, and boronic acid condensation have facilitated the preparation of organic architectures such as macrocycles, catenanes, cages, and extended frameworks.[1] Thermodynamically controlled DCC reactions enable error correction of intermediates along multiple reaction pathways, offering facile access to intricate connectivity and topology beyond the reach of conventional synthesis. We and others have developed alkyne metathesis cyclooligomerization[2] as a useful method for the efficient preparation of conjugated and shape-persistent molecules where step-wise synthetic strategies have fallen short.[3]

Limited examples of Möbius structures have been reported due to the challenges associated with synthesizing macrocycles and twisted structures.[4] Among them, many feature porhpyrinoid scaffolds due in part to the heightened structural rigidity offered by pyrrole moieties.[5] Two non-porphyrinoid Möbius structures with writhe-bearing subunits have been recently reported by Rissanen, Herges, and Durola, (Figure 6.1) with different synthetic strategies regarding the order of macrocyclization and writhe-formation.[6] While their successes are inspiring to theoretical and experimental chemists, both synthetic routes are lengthy with low overall yields (~1%). Very

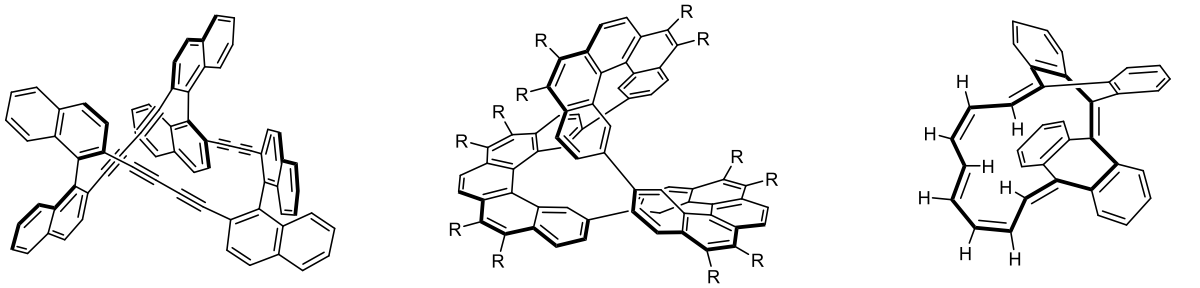

Figure 6.1 Previously reported Möbius hydrocarbons.

recently, Tanaka synthesized Möbius [*n*]cycloparaphenylene (CPP) analogues utilizing [2+2+2] cyclization with great enantioselectivity yet low overall yield.[7] To circumvent the limitations associated with stepwise macrocycle construction, we investigated a DCC-based assembly of simple monomers into molecular Möbius strips in a single step. We pursued a route toward a fully conjugated structure via alkyne metathesis given the influence Möbius topology holds over the aromaticity of an annulene.[8,9] Herein, we report the efficient synthesis of Möbius macrocycle **2** from the metathesis of 2,13-bispropynyl[5]helicene **1** (Figure 6.2).

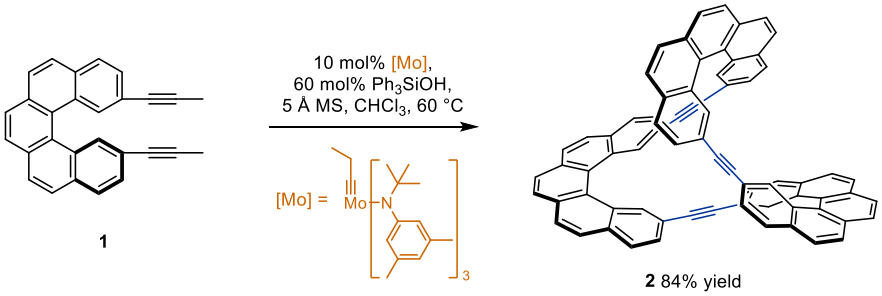

Figure 6.2 Synthesis of a Möbius tris((ethynyl)[5]helicene) macrocycle under Mo-catalyzed alkyne metathesis.

6.3 Reaction Conditions

Bispropynyl[5]helicene **1**, prepared from 2,13-dibromo[5]helicene[10] (90% yield), features a low inversion barrier of 25.6 kcal/mol, similar to that of the parent [5]helicene[11] (23.4 kcal/mol, see Table 6.9.1). The dynamic helicity makes **1** an ideal candidate for cyclooligomerization as chirality matching is allowed in the final ring closure step. Compound **1** was first subjected to alkyne metathesis conditions with 10 mol % of [EtC≡Mo(OSiPh$_3$)$_3$] at room temperature and 5 mM in CHCl$_3$. MALDI-MS analysis of the crude reaction mixture revealed that in addition to unconsumed starting material, ring-opened dimer, and higher molecular weight oligomers, a peak with *m/z* = 900.2838 (Figure 6.3A) corresponding to a ring-closed trimer (**2**) was observed. The ring-closed dimer **3** was never observed. Under the above reaction conditions, the trimeric product was formed in 23% yield as determined by NMR. To limit the formation of oligomeric products,

we diluted the reaction to 1 mM and increased the temperature to 40 °C, obtaining the ring-closed trimer in 38% NMR yield. Increasing the temperature to 60 °C at the same reaction concentration led to the optimized conditions giving an 84% yield by NMR. Solvent effect was also briefly explored, and reactions in toluene gave significantly lower yields at elevated temperatures due to competing precipitation.

6.4 Characterizing Product Symmetry

Regarding the symmetry of the macrocyclic product, four stereoisomers are possible, namely the *PPM* and *MMP* enantiomeric pair of **2** and the *PPP* and *MMM* enantiomeric pair of **4** (Figure 6.3B). Both diastereomers are twisted structures with Möbius topology. The *PPP*/*MMM* pair features three-fold symmetry and is triply twisted, while the *PPM*/*MMP* pair is C_2 symmetric and singly twisted. Single point energy calculations (M06-2X, B3LYP, and PBE0, at def2-TVZP

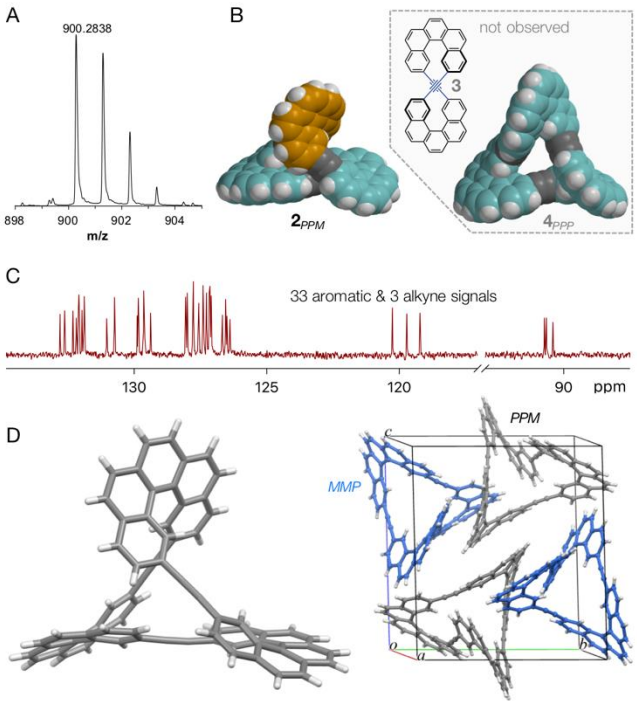

Figure 6.3. (A) MALDI-TOF mass spectrometry established the formation of a ring-closed trimeric species. (B) Space-filling models of DFT calculated structures of $\mathbf{2}_{PPM}$ and $\mathbf{4}_{PPP}$. (C) ^{13}C NMR spectrum showing 36 carbon signals. (D) Crystal structure of $\mathbf{2}_{PPM}$ (left) and the unit cell (right). Solvent molecules omitted for clarity.

level of theory, Table 6.2) showed that **2** is less stable than **4** by 1−2 kcal/mol, suggesting that **4** is the thermodynamically favored product. However, the ^{13}C NMR spectrum of the product is consistent with the exclusive formation of **2,** showing 33 aromatic and 3 alkynyl carbon resonances (Figure 6.3C). The unexpected kinetic selectivity and the *PPM*/*MMP* stereochemistry of the product were confirmed by X-ray diffraction (XRD) of single crystals grown from a hot ethyl acetate solution. The crystal structure of **2** was solved in the orthorhombic $P2_1/n$ space group, with two pairs of *PPM*/*MMP* enantiomers in each unit cell (Figure 6.3D). The XRD structure is very close to the DFT minimized structure, except that two of the three triple bonds deviate slightly from linearity (averaged bond angles 175°, 176°, and 178°).

6.5 Rationalizing Kinetic Diastereoselectivity

Since DCC reactions are typically under thermodynamic control, we were surprised that the less stable product **2** was formed exclusively in the reaction. In fact, thermodynamic driving forces are typically the sole factors considered when planning a DCC synthesis. To elucidate the origin of kinetic selectivity, DFT calculations (B3LYP/6-31G(d)/SDD) of the intermediates and transition states leading to structures $\mathbf{2}_{PPM}$ and $\mathbf{4}_{PPP}$ were performed (Figure 6.4). The rate determining steps in both pathways are the initial formation of metallacyclobutadiene (**TS1**). The activation energy for $\mathbf{TS1}_{PPP}$ formation is 37.0 kcal/mol, whereas the barrier for $\mathbf{TS1}_{PPM}$ formation is 21.6 kcal/mol. The 15.4 kcal/mol difference in activation energy accounts for the remarkable kinetic control in the synthesis. Notably, a single metallacyclobutadiene intermediate $\mathbf{IM}_{PPM}$ was located after $\mathbf{TS1}_{PPM}$, which quickly undergoes cycloreversion to give $\mathbf{2}_{PPM}$. This contrasts with the canonical observation of two discrete metallacyclobutadiene intermediates as were observed for $\mathbf{IM1}_{PPP}$ and $\mathbf{IM2}_{PPP}$. $\mathbf{TS2}_{PPM}$ was difficult to locate, most likely due to a small energy

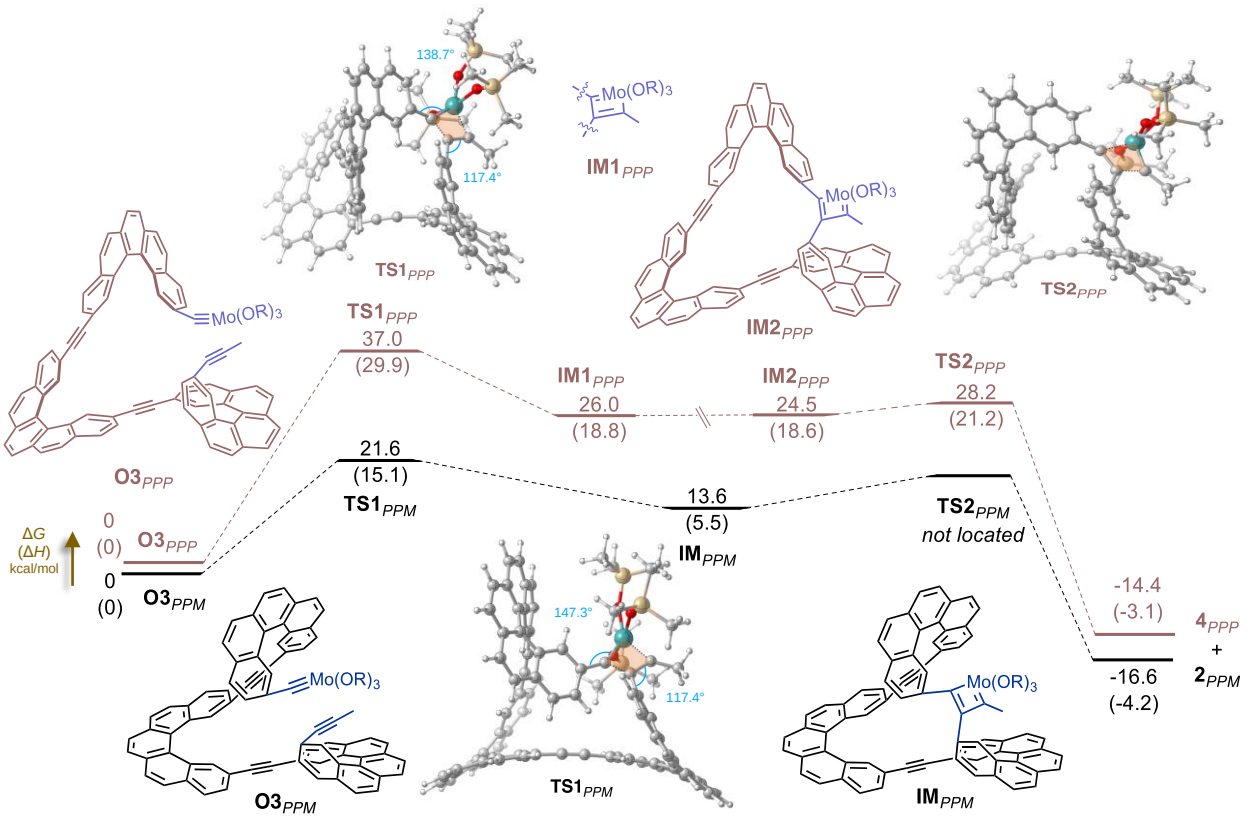

Figure 6.4. DFT calculated (B3LYP/6-31G(d)/SDD) relative Gibbs free energy and enthalpy (in parentheses) of intermediates and transition state structures in the formation of $\mathbf{2}_{PPM}$ and $\mathbf{4}_{PPP}$. Energies in both pathways are relative to the open trimers $\mathbf{O3}_{PPM}$ and $\mathbf{O3}_{PPP}$, respectively. Structures were optimized in the gas phase before the application of a solvation model (CH_3Cl, SMD). The rate determining steps in both pathways are the formation of metallacyclobutadiene (**TS1**). A simplified Me_3SiO- ligand was used in the calculation. The transition state structures were rendered in CYLview.[12] The metallacyclobutadiene structures are highlighted in orange, and bond angles in **TS1** are labeled in blue.

difference (an early transition state according to the Hammond Postulate) between $\mathbf{IM}_{PPM}$ and $\mathbf{TS2}_{PPM}$ (Figure 6.15). Free energy change from $\mathbf{TS1}_{PPM}$ to $\mathbf{2}_{PPM}$ is –38.2 kcal/mol and is consistent with the observation that $\mathbf{2}_{PPM}$ is kinetically stable under metathesis conditions in the presence of excess 1-phenyl-1-propyne (Figure 6.8).

Our experimental and computational studies illustrate unique kinetic sensitivity of alkyne metathesis, particularly for the preparation of rigid structures. This results from the strained four-membered metallacycles in the intermediates and transition states leading to product and their significant deviation from linearity. Specifically, a significantly higher level of bond angle

distortion was observed in **TS1**$_{PPP}$ (138.7° and 117.4°) than **TS1**$_{PPM}$ (147.3° and 117.4°) (from C_{Ar}–C_{sp}–Mo and C_{Ar}–C_{sp}–C_{sp} respectively), while no apparent difference was noticed in terms of dihedral angle or bond length (Figure 6.14). Therefore, seemingly stable and unstrained products may have surprisingly high energy barriers when constructed with alkyne metathesis. In the synthesis of **2**, such kinetic selectivity affords complete diastereocontrol.

6.6 Analyzing the Aromaticity of Compound 2

The optical properties of **2** were explored to probe its electronic structure. The UV-Vis and fluorescence excitation spectra of **2** are slightly red-shifted as compared to those of **1**, while the emission spectra were nearly identical (Figure 6.5). We attribute this to weak conjugation among the three helicene subunits in **2** and an increase of oscillator strength for the S_0-S_1 from **1** to **2**. The S_0-S_1 transition and other low energy transitions of **1** are symmetry forbidden and extremely weak, but the oscillator strength of the same transitions is higher for **2** (Table 6.4). The S_0-S_1 electric transition dipole of **2**$_{PPM}$ resembles the sum of those of the three helicene units, and the spatial arrangement of transition dipole moments of *P*- and *M*-helicene enables the otherwise forbidden transition (Figure 6.5C). The increased oscillator strength justifies the increased quantum yield of **2** over **1** (2.7% and 1.3% respectively). To further probe the electronic structure, comparative voltammetric measurements of **1** and **2** were performed (Figures 6.9-13). For the reduction process, the magnitude of the normalized peak currents (with respect to concentration and redox equivalents) indicates a single three-electron voltammetric wave for **2** (Figure 6.13). The lack of a stepwise behavior suggests that three electrons were accepted in redox centers that act independently of each other.[13] This strengthens conclusions regarding the additive behavior of the helicene units.

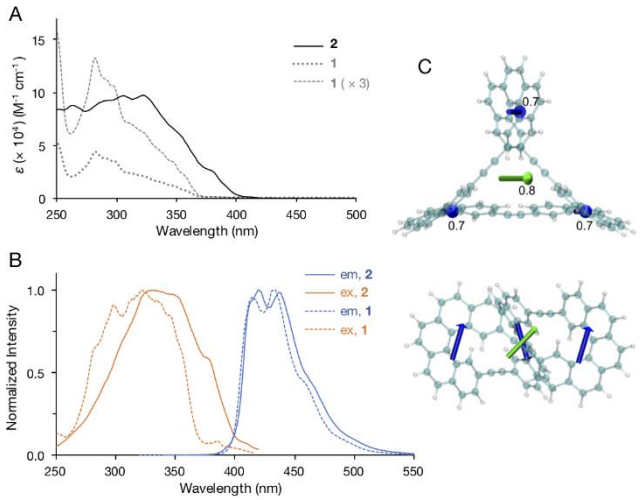

Figure 6.5. (A) UV-Vis and (B) fluorescence spectra of **1** and **2** in DCM. (C) The S_0-S_1 electric transition dipole moments (μ_e) of $\mathbf{2}_{PPM}$ (green arrow, the contribution of the acetylene carbons not includes) and the three helicene segments (blue arrows). Their absolute values are labeled (unit: Debye).

The photophysical and electrochemical properties described above are consistent with our theoretical interrogations of $\mathbf{2}_{PPM}$. The electron density of delocalized bonds (EDDB) plot shows that one set of *p* orbitals of the alkynes are parallel to the *p* orbitals of the adjacent helicenes, indicating significant conjugation between those moieties albeit less pronounced compared to the delocalization within the helicene units (Figure 6.6A, π-$EDDB_1$, pink). As expected, the *p* orbitals orthogonal to the helicene plane contribute negligible electron density to overall electron delocalization (Figure 6.6A, π-$EDDB_2$, yellow). While σ-delocalization is evident within the framework of the helicene fragments, almost zero σ-delocalization was observed along the bridging alkynyl bonds. Non-directional electron currents were observed at the alkynes in the anisotropic current (induced) density (ACID)[14] plot showing minimal helicene-helicene interactions with no significant global aromaticity (Figure 6.6B). Similar results were observed for an analogous compound reported by Herges and Durola,[6a] and the authors argued their system features global Möbius aromaticity with concurrent diatropic and paratropic ring currents. A larger extent of delocalization was observed for the T_1 excited state of **2**, resulting in an increased level of electron delocalization between the helicene and the alkyne units (Figure 6.18).

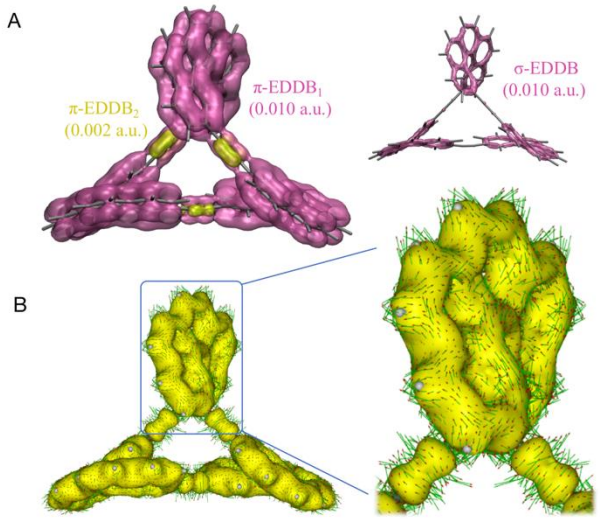

Figure 6.6. (A) Electron density of delocalized bonds (EDDB) of $\mathbf{2}_{PPM}$ showing π-$EDDB_1$ (45.98e, pink) and π-$EDDB_2$ (0.32e, yellow) and σ-EDDB (9.06e, pink) with their isovalues labeled. (B) Anisotropy of the induced current density (ACID) plots of $\mathbf{2}_{PPM}$ showing directional electron currents within each helicene units and non-directional electron currents at the alkynes (isovalue 0.015 a.u.). The external magnetic field vector is perpendicular to the ACID plots and points outward.

6.7 Future Directions and Conclusion

Chiral separation of the enantiomers of **2** was achieved on an analytical HPLC with a chiral stationary phase column (CHIRALPAK IB-3). However, preparatory scale separation of **2** was unsuccessful due to its limited solubility. Modification of the alkynes was attempted to address the limited solubility and electrochemical stability of macrocycle **2**. As shown in Figure 6.**7**, one of the three alkynes selectively reacts with tetrasubstituted cyclopentadienone **5**, and the Möbius topology is largely preserved in the product **6**. Subsequent cycloadditions were not observed, possibly due to the steric hindrance around the remaining alkynes. To examine the substrate scope of the reported synthetic strategy, alkyne metathesis was also attempted for two structurally related substrates. Compound **7** features an axially chiral binapthyl structure, which was key to the Möbius structure reported by Rissanen and Herges,[6b] and heterohelicene precursor **8** is structurally analogous to **1**; yet neither substrate gave any macrocycles via metathesis.

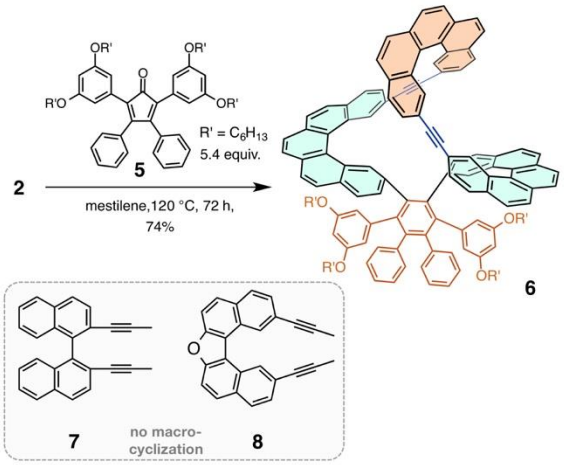

Figure 6.7. Cyclopentadienone **5** selectively reacted with one of the three alkynes in **2** to give compound **6** of pseudo 2-fold symmetry. Compounds **7** and **8** failed to form macrocyclic oligomers.

In conclusion, we demonstrate the use of alkyne metathesis in the preparation of Möbius tris((ethynyl)[5]helicene) macrocycle **2** through a synthetically efficient cyclooligomerization process. The high diastereoselectivity results from a 15.4 kcal/mol difference in activation energy during the cyclization step in favor of the *PPM*/*MMP* diastereomer. The findings reported here shed light on the kinetic aspects of alkyne metathesis cyclooligomerization that is different from other DCC reactions. While the lack of directional currents throughout the molecule in the ACID plot suggests a negligible global aromaticity, the alignment of p orbitals in the EDDB plots is set up for delocalization of π-electrons of the helicene and acetylene units in **2**.

6.8 Supporting Information

General

Unless stated otherwise, all compounds are used as received from commercial sources. Anhydrous chloroform and methanol were obtained from Sigma-Aldrich, and all other solvents were obtained from a solvent purification system. Reaction flasks are oven dried before cooled to room temperature under N_2. Silica gel (40–63 μm, 60 Å, bulk or pre-packed columns) was obtained

from Silicycle. TLC plates with flourescent indicator F254 were used and visualized with UV lamps.

Instruments

All alkyne metathesis reactions were performed in an Ar-filled glovebox as the catalyst is sensitive to poisoning by N_2. Solution ^{1}H and ^{13}C NMR spectra were acquired on a Bruker 500 MHz instrument with a 5-mm cryo probe. Mass spectra were obtained on Waters Q-TOF Ultima ESI (ESI-TOF) and Bruker Daltonics UltrafleXtreme MALDI TOFTOF (MALDI-TOF). DCTB (*trans*-2-[3-(4-tert-butylphenyl)-2-methyl-2-propenylidene]malononitrile) was used as the matrix, and C_{70} (840.0000) and [70]PCBM ([6,6]-phenyl C71 butyric acid methyl ester, 1030.0994) were used as MALDI standards for HRMS of **2**. Infrared (IR) spectra were acquired on a PerkinElmer Frontier FT-IR instrument with a KRS5 thallium bromide/iodide universal attenuated total reflectance accessory, and the peaks are reported in wavenumbers (cm^{-1}) together with their relative intensity (s = strong, m = medium, w = weak). EFOS Novacure UV Spot Curing System with a 100-W mercury lamp and light guide was used in the synthesis of dibromo[5]helicene.

6.8.1 Synthesis and Characterization

The synthesis of 2,13-dibromo-[5]helicene **S4** was achieved following literature procedures[15] with minor modifications:

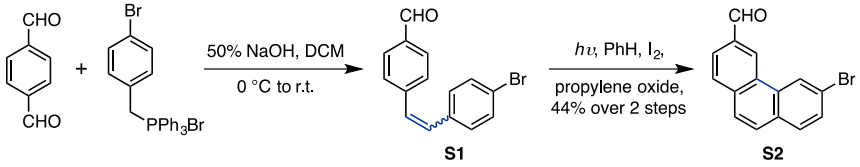

To a mixture of terephthalaldehyde (804 mg, 6.0 mmol) and (4-bromobenzyl)triphenylphosphonium bromide (3.07 g, 6.0 mmol) in DCM (100 mL) in an ice bath was added 50% (w/w) NaOH (4.0 mL) slowly. The ice bath was removed after the addition, and

the reaction was stirred at r.t. for 3 h before water (100 mL) was added. The organic layer was separated from the aqueous layer, which was extracted with DCM (30 mL) twice. The organic layers were collected, dried over Na_2SO_4, and evaporated under vacuum to give a yellow solid. The crude mixture was passed through a short plug of silica, and **S1** (mixture of cis/trans isomers) was used in the next step without further purification.

S1 was dissolved in benzene (800 mL), and propylene oxide (20 mL) and iodine (500 mg) were added to the flask. The solution was degassed by bubbling N_2 for 1h. A Pyrex (50% transmission at 320 nm) tube was inserted into the flask to insulate the optical guide of the UV light. After 50 h of irradiation, the solvent was removed and the residue was passed through a short plug of silica. Pure **S2** was obtained by washing the solid with hot ether; the mother liquor was concentrated to give brown solids, which were subjected to another cycle of photoreaction. The overall yield of **S2** was 737 mg (44%, over two steps).

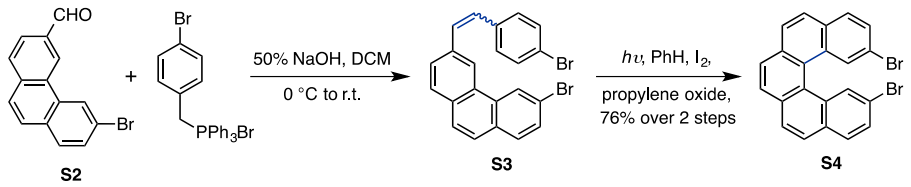

S2 S3 S4

To a mixture of **S2** (550 mg, 1.99 mmol) and (4-bromobenzyl)triphenylphosphonium bromide (1.11 g, 2.17 mmol) in DCM (50 mL) in an ice bath was added 50% (w/w) NaOH (2.2 mL) slowly. The ice bath was removed after the addition, and the reaction was stirred overnight before water (50 mL) was added. The organic layer was separated, and the aqueous layer was extracted with DCM (20 mL) twice. The combined organic layers were dried over Na_2SO_4 and evaporated under vacuum to give a yellow solid. Triphenylphosphine oxide was removed by passing the crude

mixture through a short plug of silica, and **S3** (mixture of cis/trans isomers) was used in the next step without further purification.

S3 was dissolved in benzene (500 mL) in a brown bottle, and propylene oxide (10 mL) and iodine (300 mg) were added to the solution. The solution was degassed by bubbling N_2 for 1h. A Pyrex (50% transmission at 320 nm) tube was inserted into the flask to insulate the optical guide of the UV light. *The cyclization of **S3** was much faster than that of **S1**, presumably because of the presence of two bromine atoms in the molecule.* After 5 h of irradiation, the solvent was removed to give a brown solid. Flash column chromatography (20% DCM in hexanes) gave 2,13-dibromo-[5]helicene (657 mg, 76% over two steps).

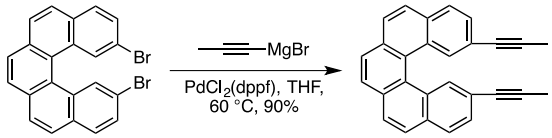

S4 **1**

To a solution of 2,13-dibromo-[5]helicene **S4** (109 mg, 0.25 mmol) and $PdCl_2$(dppf) (11 mg, 0.015 mmol, 6 mol %) in 2 mL THF was added propynylmagnesium bromide (0.5 M in THF, 2 mL, 1.0 mmol) under nitrogen atmosphere. The reaction mixture was stirred overnight at 60 ˚C before it was quenched with saturated NH_4Cl. The reaction mixture was extracted with EtOAc, and the combined organic layers were washed with brine and dried over $MgSO_4$. After the removal of solvent *in vacuo*, flash column chromatography (10–20% DCM in hexanes) gave the desired product **1** (80 mg, 90%) as an off-white solid.

^{1}H NMR (500 MHz, $CDCl_3$) δ 1.99 (s, 6H), 7.51 (dd, J = 8.3, 1.4 Hz, 2H), 7.90–7.81 (m, 8H), 8.57 (s, 2H). ^{13}C NMR (126 MHz, $CDCl_3$) δ 4.5, 80.1, 85.7, 120.5, 126.5, 126.6, 127.2, 127.3, 127.7, 129.2, 130.5, 131.6, 131.7, 132.5. IR υ (cm^{-1}): 843 (s), 1438 (w), 1502 (w), 1606 (w), 2223

(w), 2847 (w), 2912 (w), 3048 (w). HRMS (ESI-TOF, *m*/*z*): calculated for $C_{28}H_{19}$ $[MH]^+$: 354.1408; found: 354.1400.

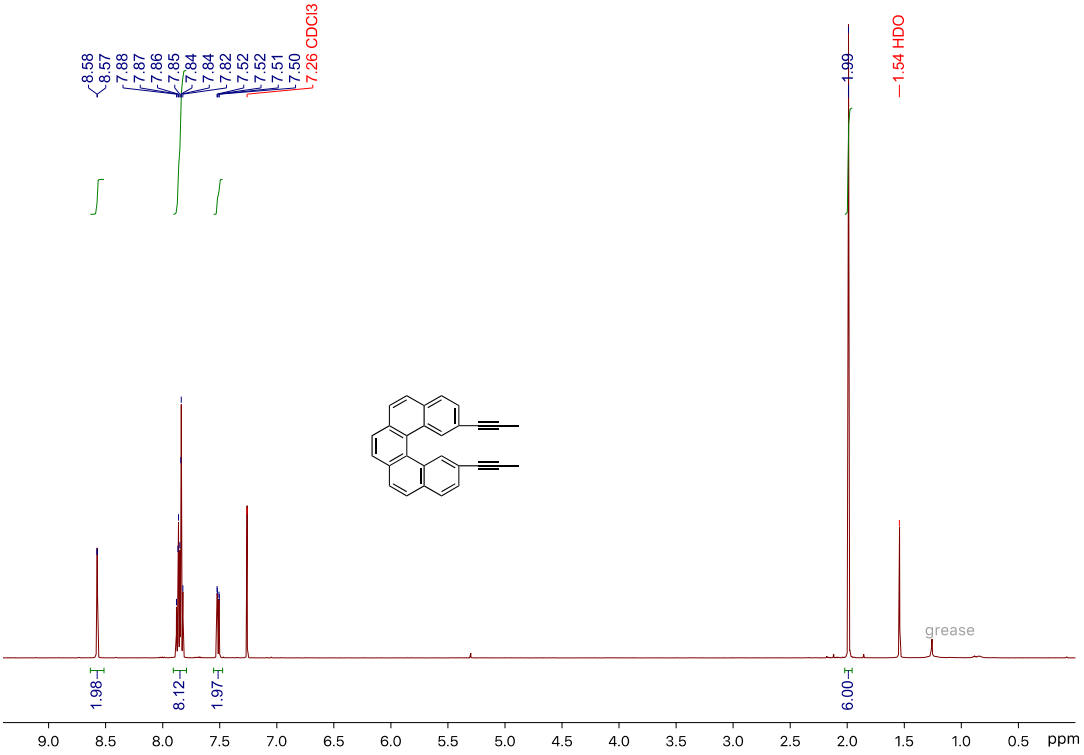

^{1}H NMR spectrum of **1** at 500 MHz in $CDCl_3$.

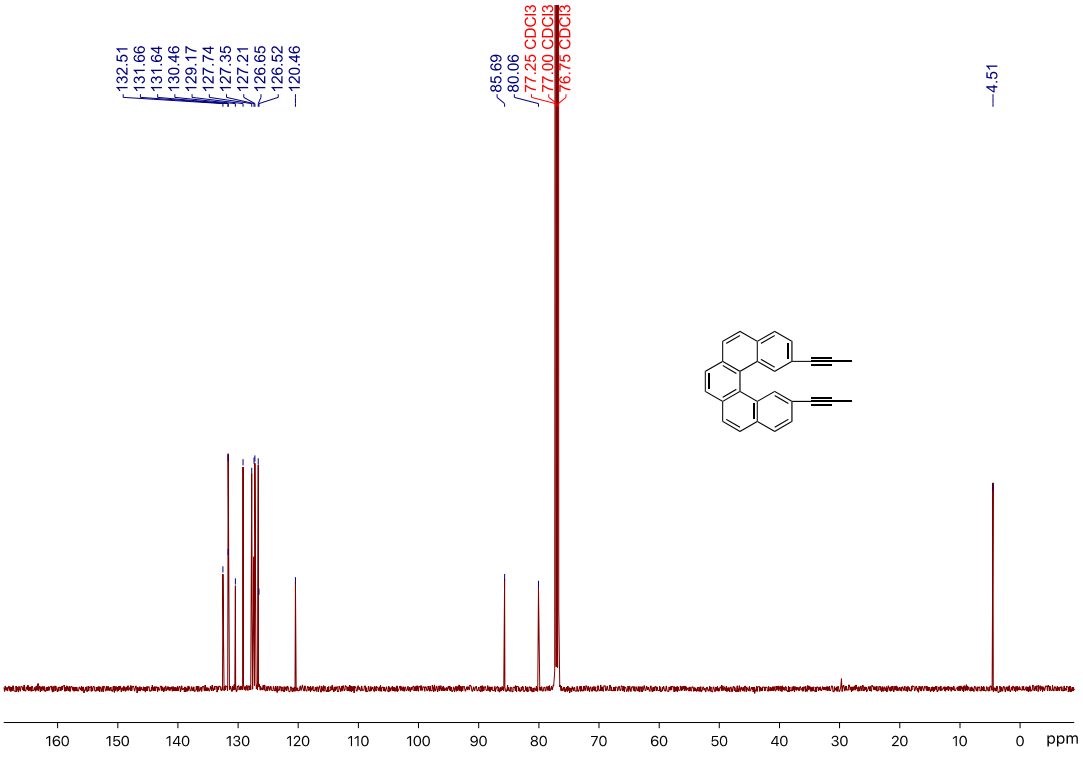

^{13}C NMR spectrum of **1** at 126 MHz in $CDCl_3$.

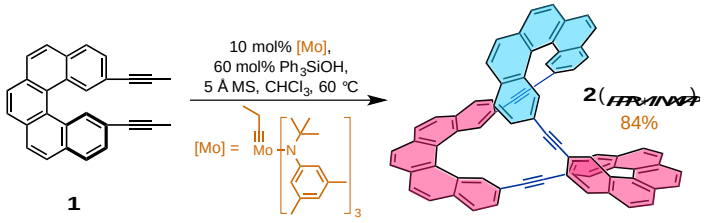

In an argon-filled glovebox, [Mo] (5.61 mg, 0.0085 mmol, 0.1 equiv) and triphenyl silanol (14.0 mg, 0.0508 mmol, 0.6 equiv) were added to a 7.5-mL vial (**I**) with a stir bar followed by $CHCl_3$ (3 mL). The solution was stirred at room temperature for 15 min to allow for catalyst pre-activation. Monomer **1** (30 mg, 0.085 mmol), 5 Å molecular sieves (168 mg, 1 gram per mmol of alkyne), and $CHCl_3$ (82 mL) were added to a separate flask (**II**) equipped with a stir bar. After stirring, the catalyst solution in vial **I** was transferred to flask **II** *via* syringe. The flask was capped with a new septum which was secured with electrical tape. The flask was brought out of the

glovebox and stirred at 60 °C overnight (no gas inlet). The reaction mixture was then cooled to r.t., filtered over celite, and concentrated to yield a brown solid. The crude solid was purified using flash column chromatography eluting with DCM in hexanes (10% to 30%). The product was obtained as a pale yellow solid (18.1 mg, 71% yield).

^{1}H NMR (500 MHz, $CDCl_3$) δ 7.73–7.79 (m, 4H), 7.80–7.89 (m, 12H), 7.91 (d, J = 4.1 Hz, 2H), 7.92 (dd, J = 8.5, 2.2 Hz, 4H), 7.89 (d, J = 7.9 Hz, 2H), 7.96 (d, J = 8.4 Hz, 2H), 8.02 (d, J = 8.6 Hz, 2H), 8.06 (dd, J = 8.1, 1.4 Hz, 2H), 8.10 (d, J = 8.1 Hz, 2H), 8.45 (s, 2H), 8.83 (s, 2H), 8.88 (s, 2H). ^{13}C NMR (126 MHz, $CDCl_3$) δ 90.4, 90.7, 90.7, 119.2, 119.7, 120.3, 126.4, 126.5, 126.5, 126.7, 127.1, 127.1, 127.2, 127.3, 127.4, 127.4, 127.6, 127.8, 127.8, 128.0, 128.1, 129.4, 129.6, 129.6, 129.8, 129.9, 130.7, 131.0, 131.9, 132.0, 132.1, 132.1, 132.2, 132.3, 132.6, 132.8. IR υ (cm^{-1}): 3043 (w), 2922 (w), 2851 (w), 2203 (w), 2032 (w), 1892 (w), 1608 (m), 1505 (m), 1142 (m), 909 (m), 838 (s). HRMS (MALDI-TOF, m/z): calculated for $C_{72}H_{36}$ $[M]^+$: 900.2817; found: 900.2838.

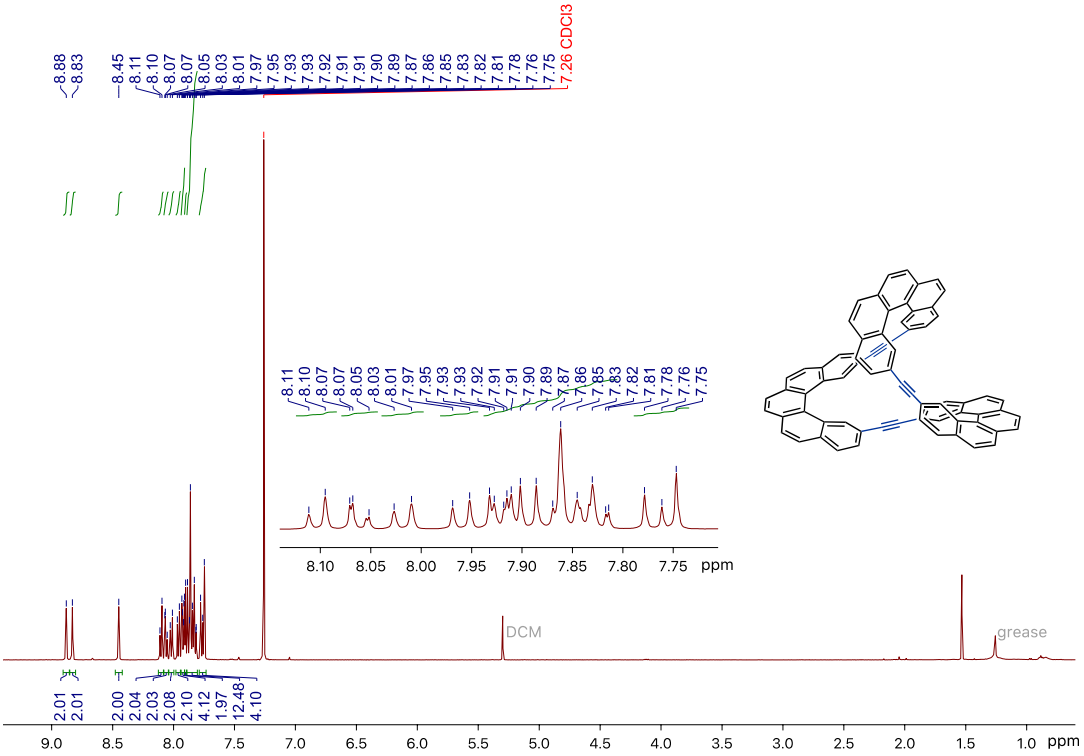

^{1}H NMR spectrum of **2** at 500 MHz in $CDCl_3$.

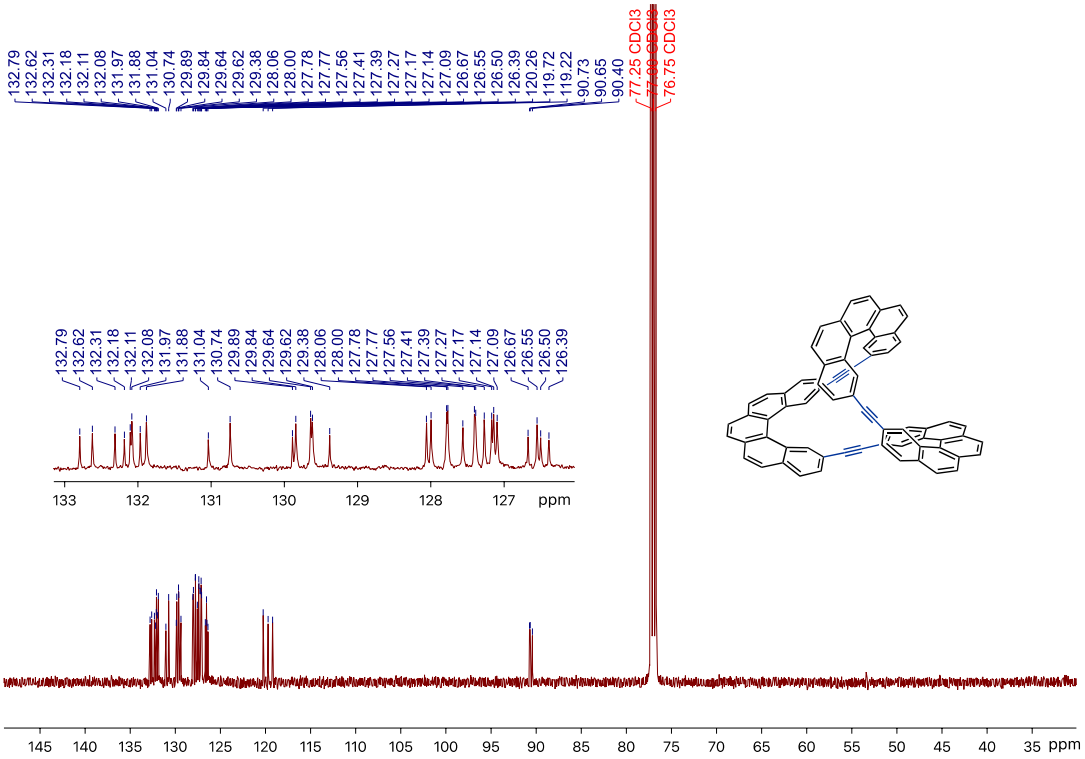

^{13}C NMR spectrum of **2** at 126 MHz in $CDCl_3$.

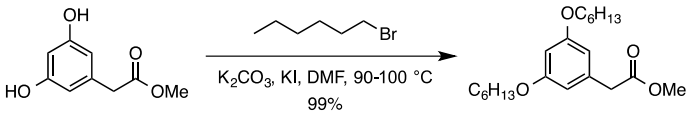

S5 **S6**

To a solution of 3,5-dihydoxyphenylacetic acid **S5** (5.27 g, 29.0 mmol) and 1-bromohexane (15.4 mL, 18.1 g, 110 mmol) in anhydrous DMF (50 mL) was added potassium carbonate (19.0 g, 137 mmol) and potassium iodide (1.0 g, 6.0 mmol), and the mixture was stirred at 90°C overnight. TLC analysis showed that the reaction was incomplete, so an additional 5.0 mL of 1-bromohexane (36 mmol) was added to the reaction, which was heated to 100°C for 24 h before the heating bath was removed, and water (100 mL) was added to the reaction. The product was extracted with ethyl acetate (200 mL), and the organic layer was subsequently washed with water, 1M LiCl solution, and brine, and dried over Na_2SO_4. The solvent was removed *in vacuo*, and the crude oil was subject to flash column chromatography (5−10% ethyl acetate in hexanes) to give the desired **S6** as a yellowish oil (9.50 g, 99%).

^{1}H NMR (500 MHz, $CDCl_3$) δ 0.90 (t, J = 6.4 Hz, 6H), 1.29−1.38 (m, 8H), 1.40−1.49 (m, 4H), 1.75 (app. quint, J = 7.1 Hz, 4H), 3.54 (s, 2H), 3.69 (s, 3H), 3.92 (t, J = 6.6 Hz, 4H), 6.36 (t, J = 2.2 Hz, 1H), 6.41 (d, J = 2.2 Hz, 2H). ^{13}C NMR (126 MHz, $CDCl_3$) δ 14.0, 22.6, 25.7, 29.2, 31.6, 41.5, 52.0, 68.0, 100.0, 107.7, 135.8, 160.3, 171.8. IR υ (cm^{-1}): 685 (w), 832 (w), 1061 (m), 1169 (s), 1460 (m), 1595 (s), 1741 (m), 2858 (w), 2930 (m). HRMS (ESI, TOF, m/z): calculated for $C_{21}H_{35}O_4$ $[MH]^+$: 351.2535, observed: 351.2532.

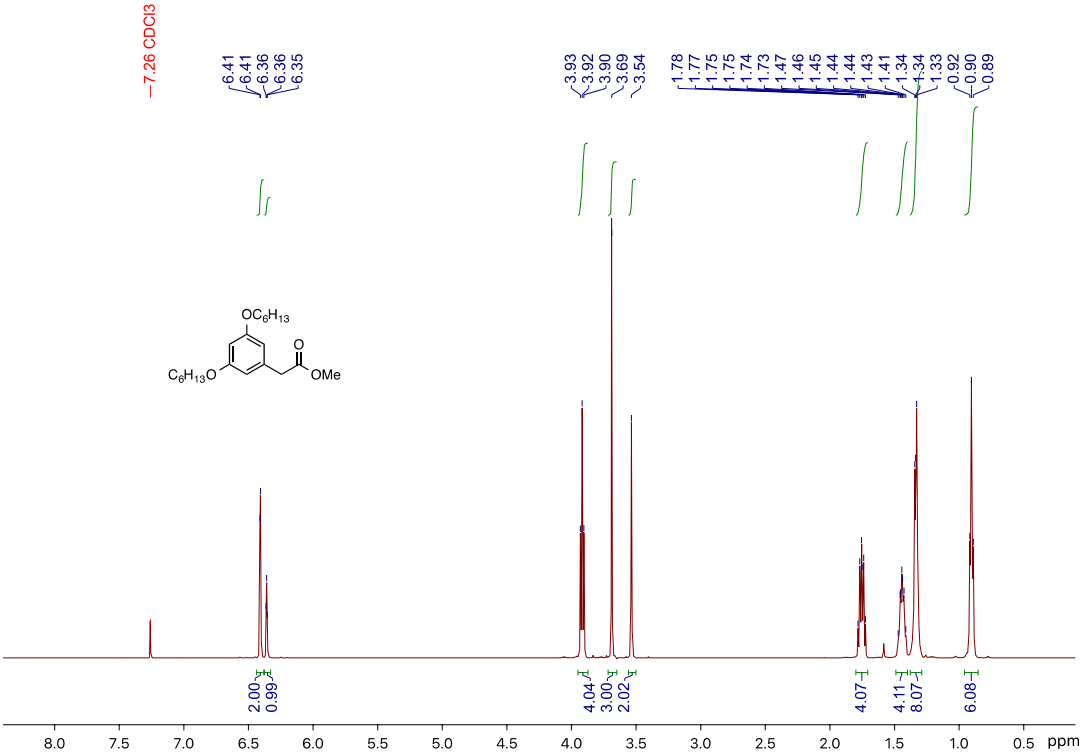

^{1}H NMR spectrum of **S6** at 500 MHz in $CDCl_3$.

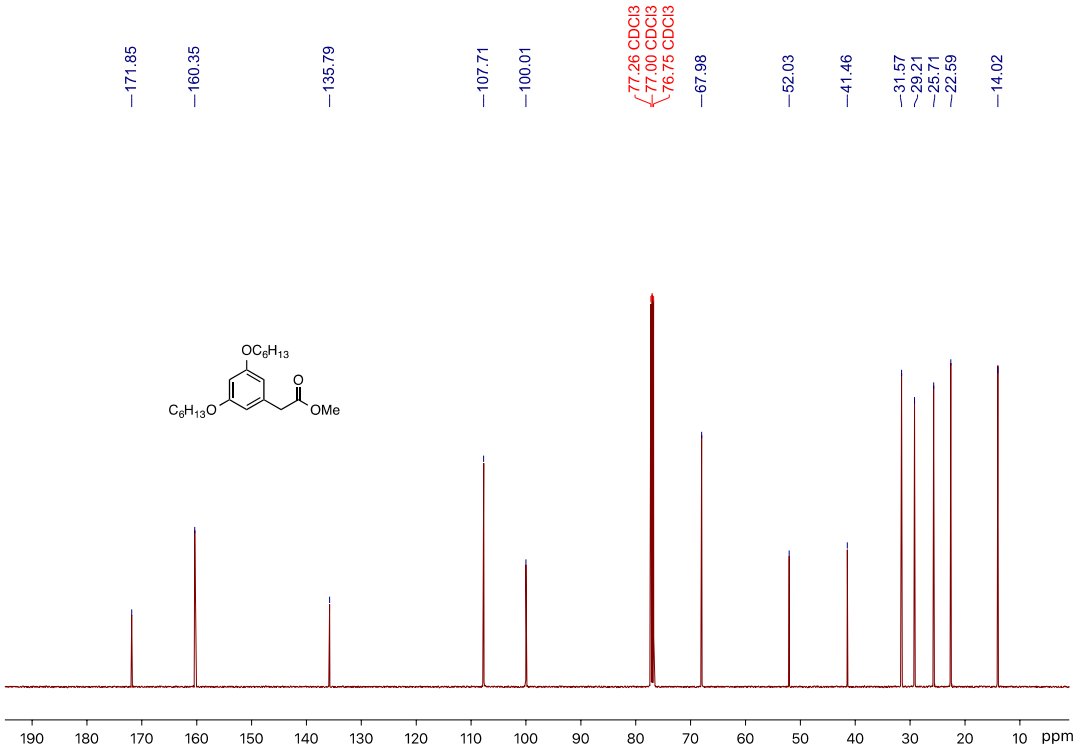

^{13}C NMR spectrum of **S6** at 126 MHz in $CDCl_3$.

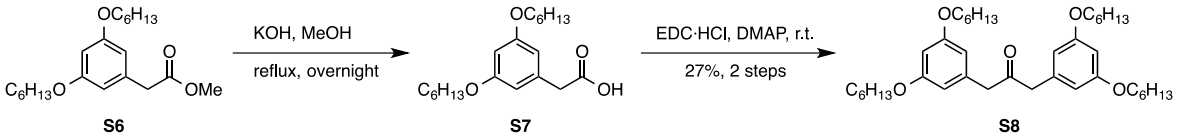

To a mixture of **S6** (4.17 g, 11.9 mmol), MeOH (1 mL), and water (30 mL) was added KOH (3.84 g, 68.5 mmol), and the reaction was heated to reflux overnight. The reaction mixture was allowed to cool down to rt before conc. HCl was slowly added to adjust its pH (< 3). The product was extracted with ethyl acetate, and the organic layer was washed with water and brine, and dried over Na_2SO_4. The solvent was removed *in vacuo*, and the crude **S7** was passed through a short plug of silica (EA) before it was concentrated and used in the next step.

To a solution of **S7** and DMAP (1.66 g, 13.6 mmol) in anhydrous DCM (25 mL) was added a slurry of EDC·HCl (2.61 g, 13.6 mmol) in anhydrous DCM (30 mL), and the reaction was stirred

overnight. A large portion of the solvent was removed, and celite was added to the flask. The resulting slurry was filtered through a plug of silica, and the solution was concentrated to give a brown oil. Flash column chromatography (2−10% ethyl acetate in hexanes) gave **S8** (972 mg, 27% over two steps) as a yellow oil.

^{1}H NMR (500 MHz, $CDCl_3$) δ 0.91 (t, J = 6.8 Hz, 12H), 1.29−1.38 (m, 16H), 1.40−1.49 (m, 8H), 1.75 (app. quint, J = 7.1 Hz, 8H), 3.61 (s, 4H), 3.89 (t, J = 6.7 Hz, 8H), 6.28 (t, J = 2.1 Hz, 4H), 6.35 (d, J = 2.1 Hz, 2H). ^{13}C NMR (126 MHz, $CDCl_3$) δ 14.0, 22.6, 25.7, 29.2, 31.6, 49.2, 68.0, 100.0, 107.9, 135.9, 160.5, 205.6. IR υ (cm^{-1}): 831 (w), 1059 (m), 1166 (s), 1456 (m), 1594 (s), 1713 (w), 2858 (w), 2930 (m). HRMS (ESI, TOF, m/z): calculated for $C_{39}H_{63}O_5$ $[MH]^+$: 611.4676, observed: 611.4677.

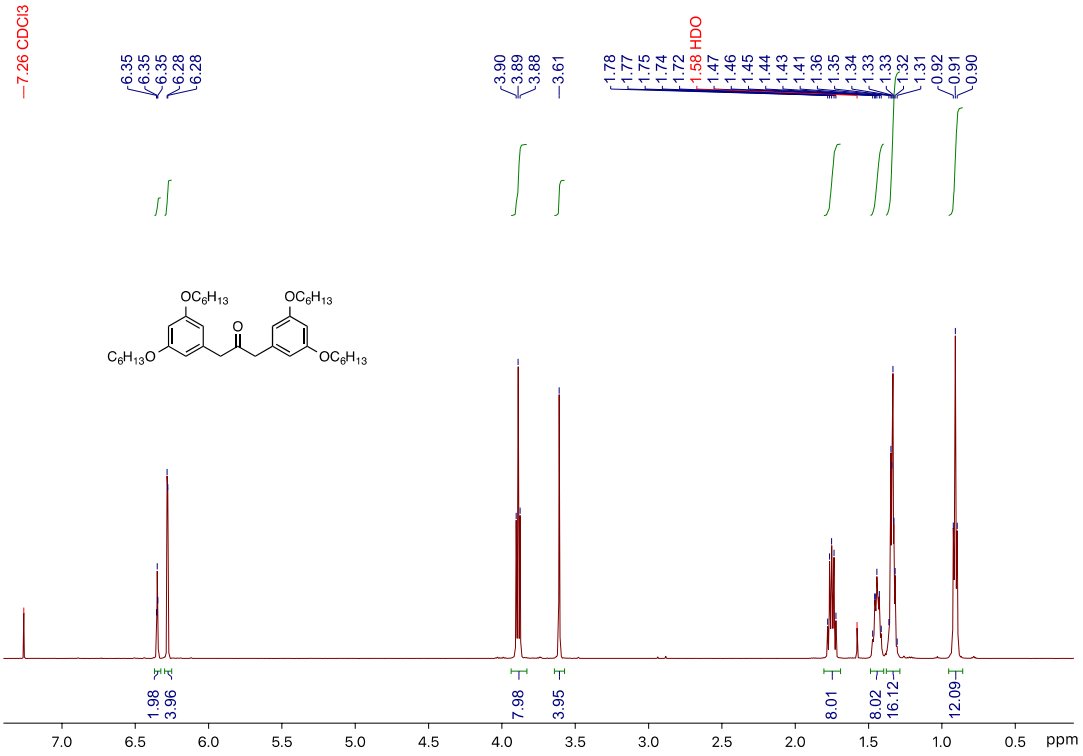

^{1}H NMR spectrum of **S8** at 500 MHz in $CDCl_3$.

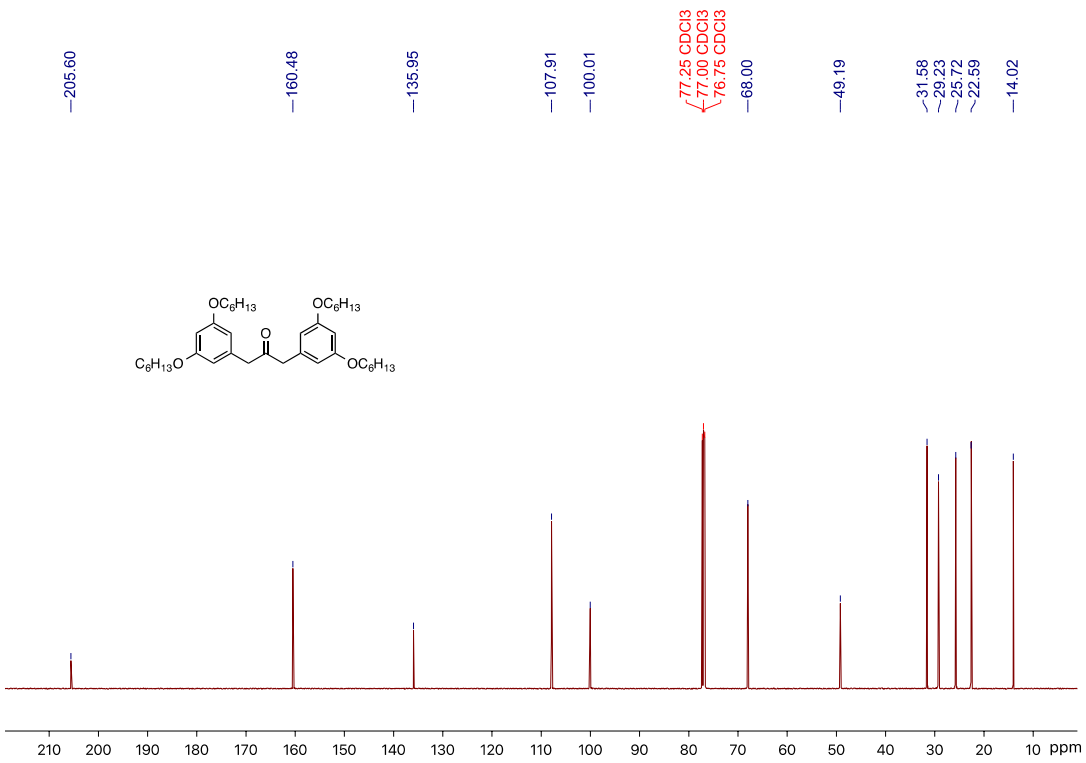

^{13}C NMR spectrum of **S8** at 126 MHz in $CDCl_3$.

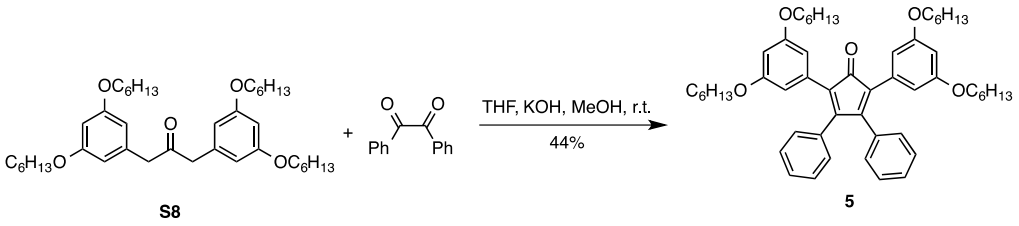

To a solution of **S8** (224 mg, 0.367 mmol) and benzil (77 mg, 0.367 mmol) in anhydrous THF (3 mL) was added a 5% (w/v) KOH solution in MeOH (0.25 mL), and the resulting mixture was stirred at r.t. for 48 h before it was concentrated under reduced pressure to give a dark violet crude. Flash column chromatography (5−10% ethyl acetate in hexanes) gave the desired product **5** as a violet oil (128 mg, 44%).

^{1}H NMR (500 MHz, $CDCl_3$) δ 0.89 (t, J = 6.9 Hz, 12H), 1.23−1.38 (m, 24H), 1.60−1.68 (m, 8H), 3.71 (t, J = 6.6 Hz, 8H), 6.33 (t, J = 2.2 Hz, 2H), 6.35 (d, J = 2.2 Hz, 4H), 6.95 (app. dd, J = 7.8, 1.5 Hz, 4H), 7.15−7.25 (m, 6H). ^{13}C NMR (126 MHz, $CDCl_3$) δ 14.0, 22.6, 25.6, 29.1, 31.5, 67.9, 102.0, 108.3, 125.3, 128.0, 128.4, 129.3, 132.1, 133.2, 154.6, 159.7, 199.9. IR υ (cm^{-1}): 697 (m), 846 (w), 1059 (m), 1159 (s), 1278 (m), 1432 (m), 1589 (s), 1712 (m), 2858 (w), 2929 (m). HRMS (ESI, TOF, m/z): $C_{53}H_{68}O_5$ $[MH]^+$: 785.5145, observed: 785.5154.

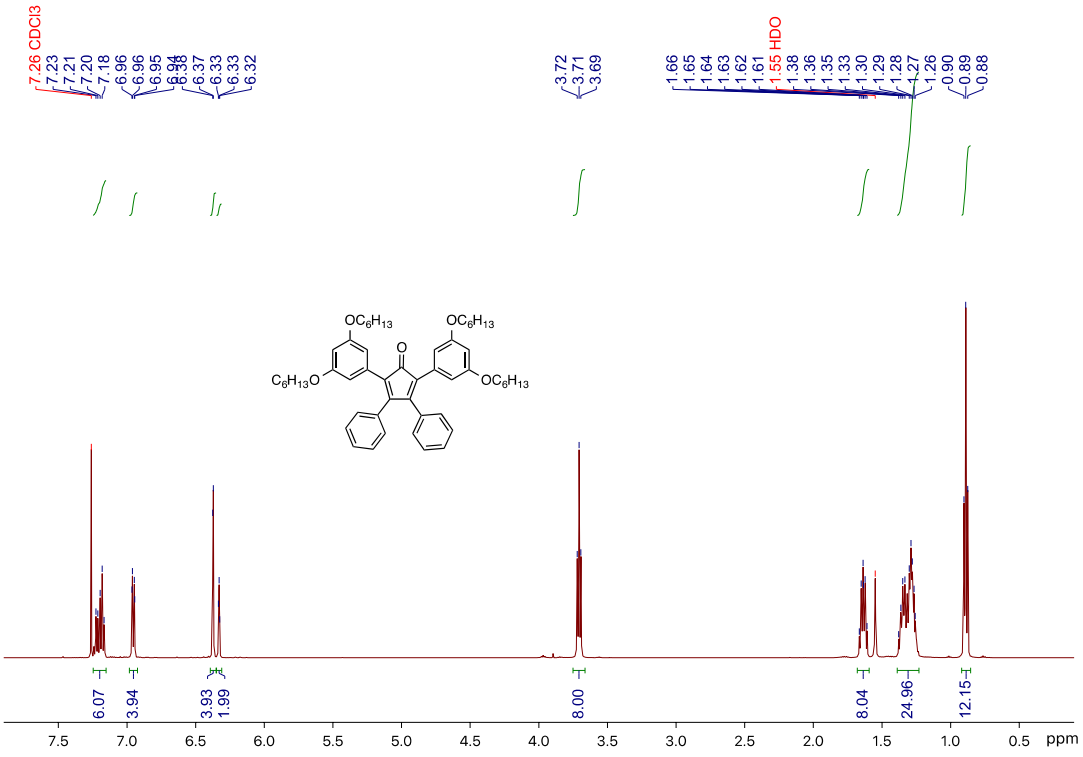

^{1}H NMR spectrum of **5** at 500 MHz in $CDCl_3$.

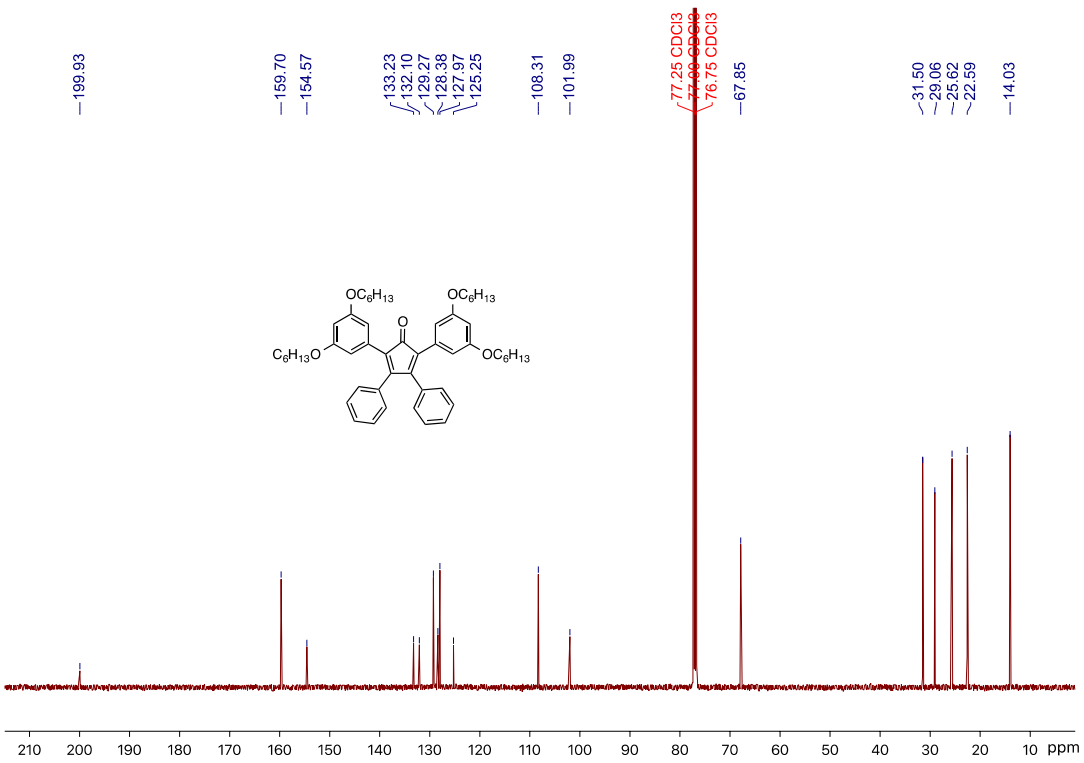

^{13}C NMR spectrum of **5** at 126 MHz in $CDCl_3$.

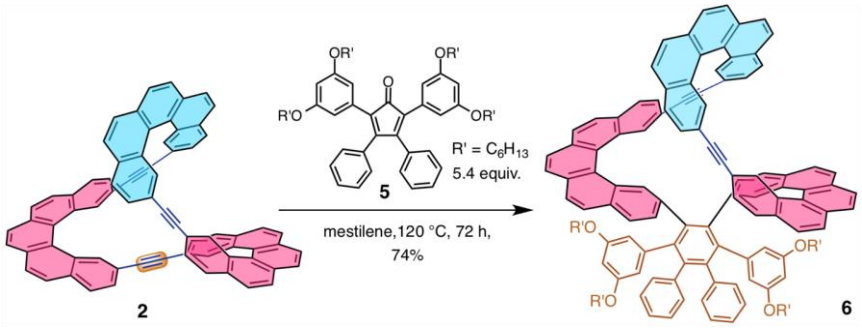

To a 5-mL vial was charged **2** (10.1 mg, 11.2 μmol), cyclopentadieneone **5** (47.3 mg, 60.2 μmol), and mesitylene (0.4 mL) under N_2. The vial was sealed and the reaction was heated to 120°C for 72 h. The mixture was directly adsorbed onto silica (> 2 g) and purified *via* flash column chromatography (2−10% ethyl acetate in hexanes). The fractions containing the desired product were collected and concentrated to give a pale yellow solid, which was subject to another round

of flash column chromatography (20−60% DCM in hexanes). The product was obtained as an off-white solid (13.8 mg, 74%).

^{1}H NMR (500 MHz, $CDCl_3$) δ 0.94 (t, J = 7.2 Hz, 6H), 1.00 (t, J = 7.3 Hz, 6H), 1.08−1.15 (m, 4H), 1.20−1.42 (m, 24H), 1.45−1.52 (m, 4H), 1.88 (dt, J = 8.8, 6.7 Hz, 8H), 2.55 (dt, J = 8.8, 6.6 Hz, 8H), 3.34 (dt, J = 9.5, 6.8 Hz, 2H), 3.51 (dt, J = 9.4, 6.8 Hz, 2H), 4.83 (s, 2H), 5.51 (s, 2H), 5.60 (t, J = 2.2 Hz, 2H), 6.47−6.57 (m, 4H), 6.61 (dd, J = 8.4, 1.1 Hz, 2H), 6.62−6.67 (m, 6H), 6.69 (dd, J = 8.3, 1.4 Hz, 2H), 7.36 (d, J = 8.4 Hz, 2H), 7.49 (dd, J = 8.3, 1.5 Hz, 2H), 7.53 (d, J = 8.7 Hz, 2H), 7.59 (d, J = 8.7 Hz, 2H), 7.64 (s, 2H), 7.78 (dd, J = 11.9, 8.3 Hz, 4H), 7.81−7.97 (m, 10H), 8.09 (d, J = 8.5 Hz, 2H), 8.19 (s, 2H), 8.31 (s, 2H), 8.50 (s, 2H). ^{13}C NMR (126 MHz, $CDCl_3$) δ 14.1, 14.2, 22.7, 22.8, 25.6, 28.9, 29.2, 31.5, 31.9, 66.8, 68.0, 90.2, 91.1, 99.9, 107.6, 110.5, 119.0, 121.8, 124.5, 124.9, 125.9, 126.0, 126.2, 126.2, 126.4, 126.5, 126.6, 126.8, 126.9, 127.0, 127.1, 127.2, 127.4, 127.7, 127.8, 128.0, 128.6, 129.5, 130.3, 130.6, 131.0, 131.3, 131.5, 131.5, 131.6, 131.7, 131.7, 132.0, 132.0, 132.2, 134.0, 134.3, 138.0, 138.4, 139.5, 140.3, 141.4, 141.5, 157.8, 158.0. IR υ (cm^{-1}): 3047 (w), 2927 (w), 2857 (w), 1592 (m), 1435 (w), 1378 (w), 1155 (m), 842 (s). LRMS (MALDI, TOF, m/z): $C_{124}H_{104}O_4$ $[M]^+$: 1656.8 (75%), 1657.8 (100%), 1658.8 (66%), 1659.8 (29%), observed: 1656.8 (88%), 1657.8 (100%), 1658.8 (66%), 1659.8 (30%).

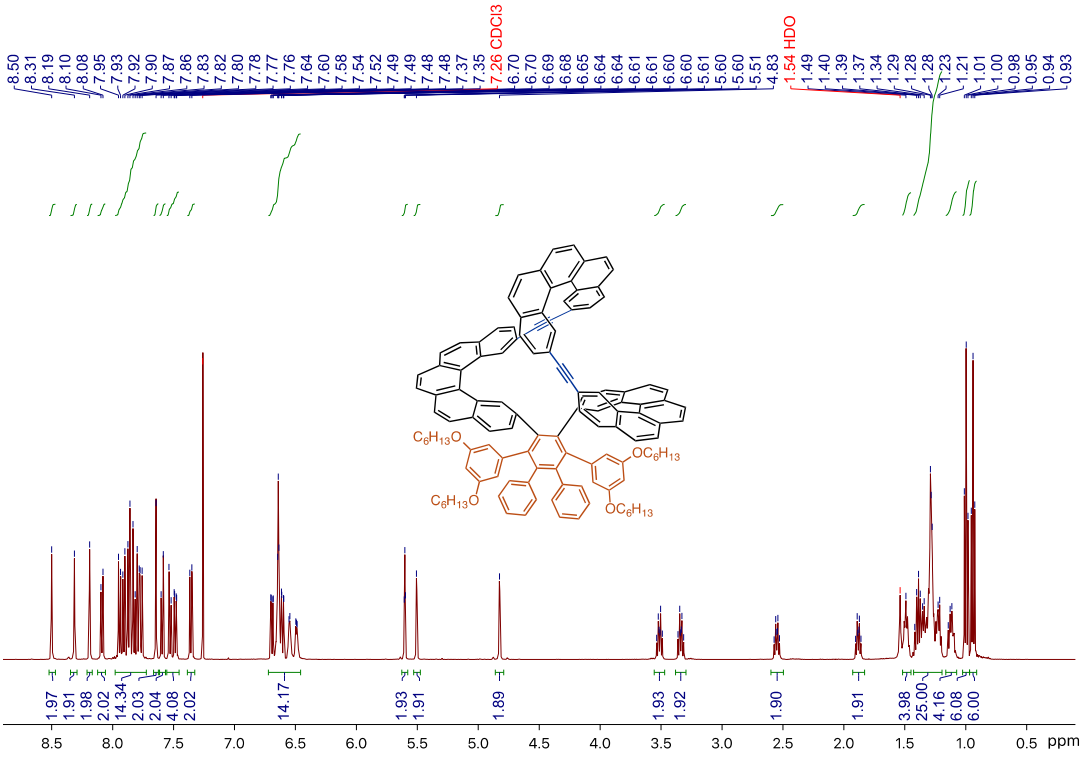

^{1}H NMR spectrum of **5** at 500 MHz in $CDCl_3$.

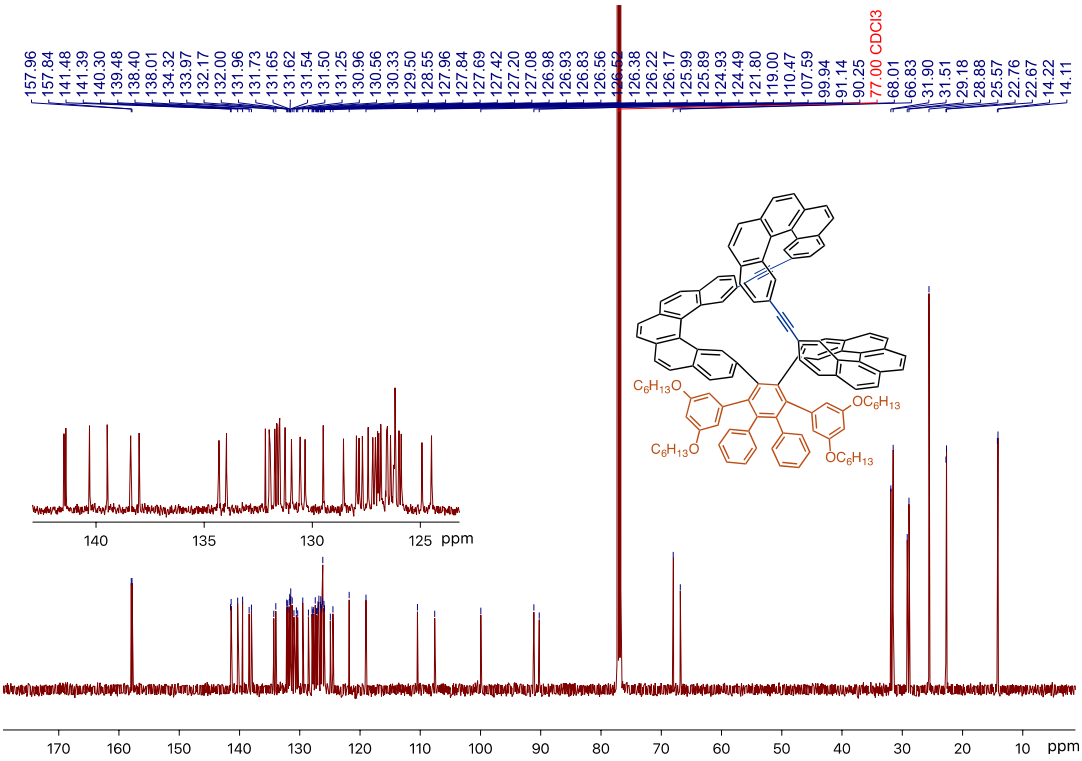

^{13}C NMR spectrum of **6** at 126 MHz in $CDCl_3$.

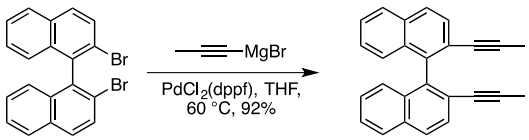

S9 **7**

$PdCl_2$(dppf) (53 mg, 0.06 equiv, 0.07 mmol) was added to a dry flask followed by 2,2'-dibromo-1,1'-binaphthalene **S9** (500 mg, 1.2 mmol) which was then placed under inert atmosphere. THF (24 mL) was transferred to the flask via syringe with stirring. 1-Propynyl-1-magnesium bromide solution (0.5 M in THF, 14.4 mL, 6.0 equiv, 7.2 mmol) was transferred to the reaction mixture dropwise via syringe. The reaction flask was then heated to 60 °C overnight. After cooling to rt, a saturated NH_4Cl (aq) solution was added to the reaction to quench any remaining organometallic species. The reaction mixture was extracted three times with ethyl acetate. The

combined organic layers were washed with brine then dried over $MgSO_4$. The solution was filtered followed by the removal of solvent *in vacuo*. The product **7** was purified *via* flash column chromatography eluting with DCM/Hexanes to give an off-white solid (365 mg, 92%).

^{1}H NMR (500 MHz, $CDCl_3$) δ 1.63 (s, 6H), 7.13 (d, J = 8.4 Hz, 2H), 7.25 (ddd, J = 8.2, 6.7, 1.3 Hz, 2H), 7.43 (ddd, J = 8.1, 6.7, 1.2 Hz, 2H), 7.63 (d, J = 8.5 Hz, 2H), 7.86 (d, J = 8.8 Hz, 2H), 7.88 (d, J = 7.7 Hz, 2H). ^{13}C NMR (126 MHz, $CDCl_3$) δ 4.3, 79.1, 89.5, 122.3, 125.9, 126.3, 126.4, 127.5, 127.8, 129.0, 132.5, 132.6, 139.5. IR υ (cm^{-1}): 750 (s), 817(s), 1375 (w), 1500(m), 1592(w), 2226(w), 2846 (w), 2913 (w), 3056 (w). HRMS (EI, TOF, m/z): $C_{26}H_{18}$ $[M]^+$: 330.1409, observed: 330.1412.

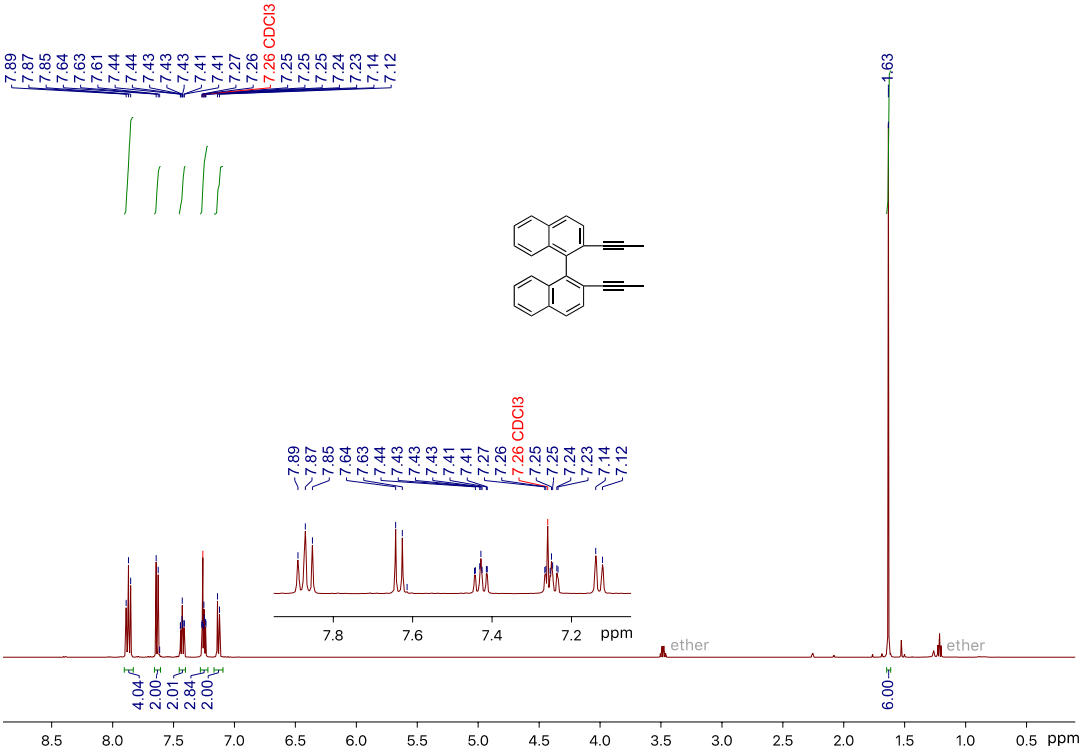

^{1}H NMR spectrum of **7** at 500 MHz in $CDCl_3$.

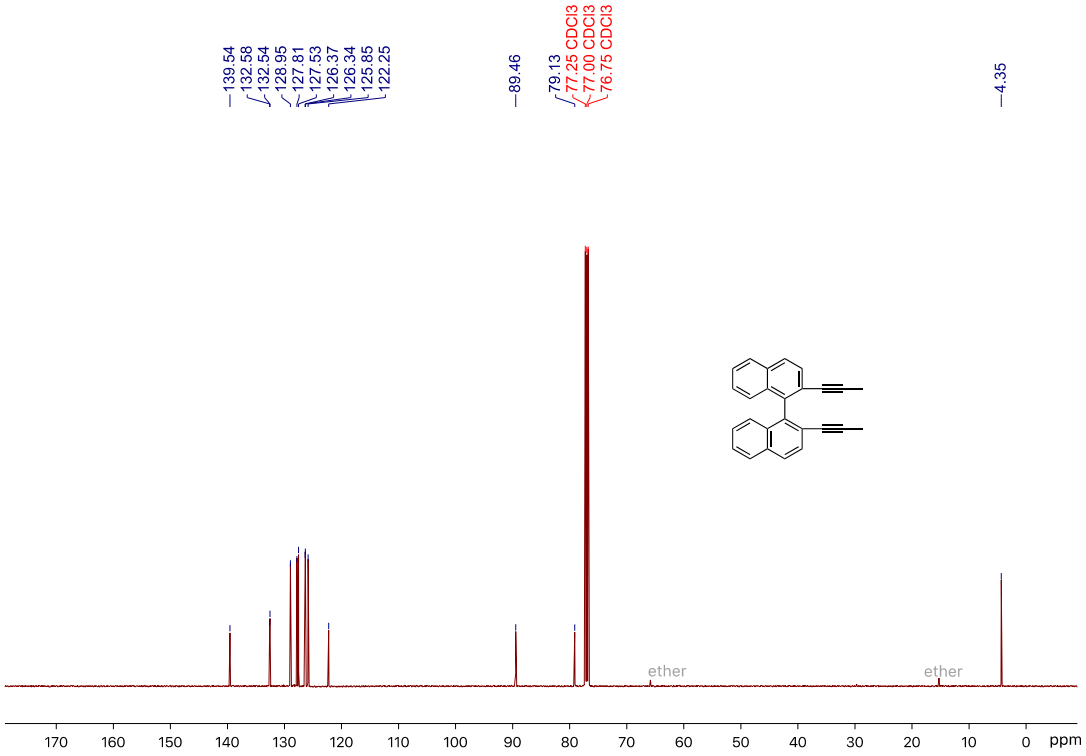

^{13}C NMR spectrum of **7** at 126 MHz in $CDCl_3$.

The synthesis of **S10**[16] and **S11**[17] was achieved using literature procedures with minor modifications:

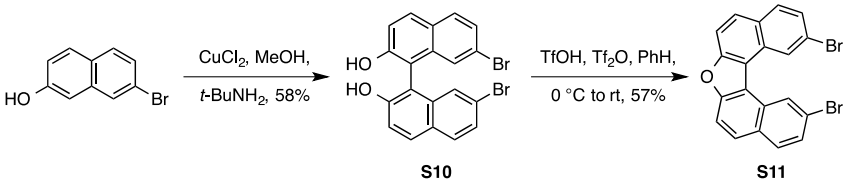

S10 **S11**

7-bromonaphthalen-2-ol (2.0 g, 9.0 mmol) along with $CuCl_2$ (2.4 g, 2.0 equiv, 18.0 mmol) was transferred to a dry 3-neck flask topped with an addition funnel and placed under inert atmosphere. Anhydrous MeOH (48 mL) was transferred to the flask *via* syringe and the solution was stirred at room temperature for 15 min. A solution of *tert*-butylamine (7.5 mL) in MeOH (27 mL) was added to the reaction mixture over 30 min *via* addition funnel. The reaction mixture stirred at rt overnight. The reaction was quenched at 0 °C by the addition of a 6 M solution of HCl until all solids

dissolved. Most of the MeOH was removed *in vacuo* followed by extraction of the solution into ethyl acetate three times. The combined organic layers were washed with brine and dried over Na_2SO_4. The mixture was filtered and concentrated *in vacuo*. The crude brown oil was dissolved in boiling toluene. The hot solution was filtered over a coarse glass frit. The filtrate was cooled to –20 °C overnight. White crystals of product were filtered out of the solution while still cold. The crystals were rinsed with cold (–20 °C) toluene and dried over vacuum. The product **S10** was collected as a white solid (First crop: 750 mg; second crop: 413 mg; 58% combined).

S10: ^{1}H NMR (500 MHz, $CDCl_3$) δ 5.01 (s, 2H), 7.23 (d, J = 1.8 Hz, 2H), 7.40 (d, J = 9.0 Hz, 2H), 7.48 (dd, J = 8.7, 1.9 Hz, 2H), 7.78 (d, J = 8.7 Hz, 2H), 7.97 (d, J = 8.9 Hz, 2H). ^{13}C NMR (126 MHz, $CDCl_3$) δ 153.76, 134.76, 131.91, 130.33, 128.12, 127.91, 126.09, 122.60, 118.43, 109.61.

7,7'-dibromo-[1,1'-binaphthalene]-2,2'-diol **S10** (200 mg, 0.45 mmol) was added to a dry flask which was then placed under inert atmosphere. Dry benzene (8 mL) was transferred to the flask *via* syringe, and the reaction mixture was cooled to 0 °C. Triflic acid (302 μL, 1.8 mmol, 4.0 equiv) was added to the reaction mixture *via* syringe. (*Note: No product was formed when the procedure in Ref. 3 was followed and TFA was used instead of TfOH*) A solution of triflic anhydride (160 μL, 1.8 mmol, 4.0 equiv) in benzene (2 mL) was transferred to the reaction mixture dropwise *via* syringe. The reaction mixture was warmed to room temperature and allowed to stir overnight. The reaction mixture was quenched with saturated $NaHCO_3$ solution and extracted with CH_2Cl_2. The combined organic layers were dried over $MgSO_4$. The solvent was removed *in vacuo* to yield an off-white solid **S11** (110 mg, 57%), which was used in the next reaction without further purification.

S11: ^{1}H NMR (500 MHz, $CDCl_3$) δ 9.25 (d, J = 1.4 Hz, 2H), 7.93 (dd, J = 8.8, 3.2 Hz, 4H), 7.84 (d, J = 8.9 Hz, 2H), 7.69 (dd, J = 8.7, 1.7 Hz, 2H). ^{13}C NMR (126 MHz, $CDCl_3$) δ 155.01, 131.16, 129.73, 129.67, 128.53, 128.07, 128.01, 121.06, 118.52, 113.24.

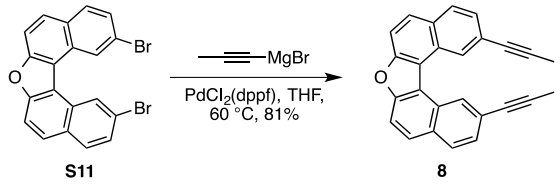

S11 **8**

To a dry flask was added 2,12-dibromodinaphtho[2,1-b:1',2'-d]furan **S11** (88 mg, 0.21 mmol) then $PdCl_2$(dppf) (9.2 mg, 0.0126 mmol, 0.06 equiv). The flask was placed under inert atmosphere followed by the addition of anhydrous THF (3 mL). 1-Propynyl-1-magnesium bromide solution (0.5 M in THF, 2.52 mL, 1.26 mmol, 6.0 equiv) was then transferred to the flask *via* syringe. The reaction mixture was heated to 60 °C overnight. After cooling to room temperature, the reaction was quenched with a saturated NH_4Cl solution and extracted with EtOAc. The combined organic layers were dried over $MgSO_4$, and the solvent was removed *in vacuo*. The product was purified using flash column chromatography eluting with DCM/Hexanes. Pure product was obtained as a pale yellow solid (57 mg, 81%).

^{1}H NMR (500 MHz, $CDCl_3$) δ 2.18 (s, 6H), 7.57 (dd, J = 8.4, 1.1 Hz, 2H), 7.80 (d, J = 8.8 Hz, 2H), 7.91 (d, J = 8.8 Hz, 2H), 7.97 (d, J = 8.4 Hz, 2H), 9.26 (s, 2H). ^{13}C NMR (126 MHz, $CDCl_3$) δ 4.5, 80.3, 86.8, 112.9, 119.0, 122.0, 127.0, 128.1, 128.2, 129.2, 129.3, 130.2, 154.7. HRMS (ESI, TOF, m/z): $C_{26}H_{17}O$ $[MH]^+$: 345.1279, observed: 345.1287.

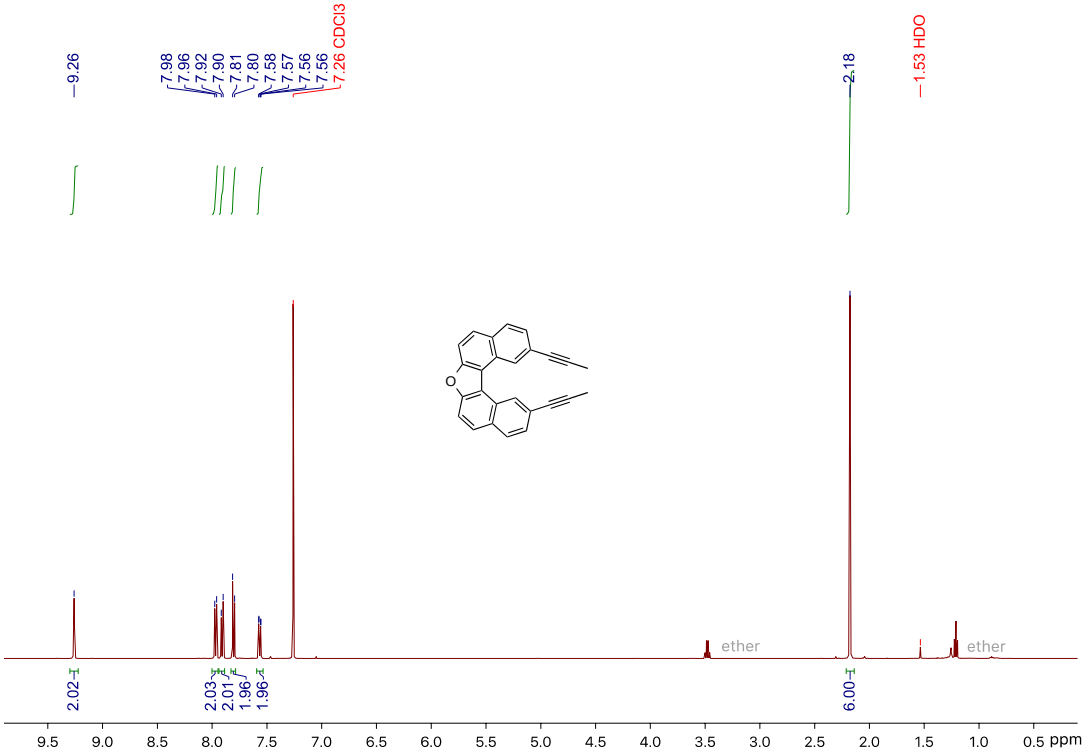

^{1}H NMR spectrum of **8** at 500 MHz in $CDCl_3$.

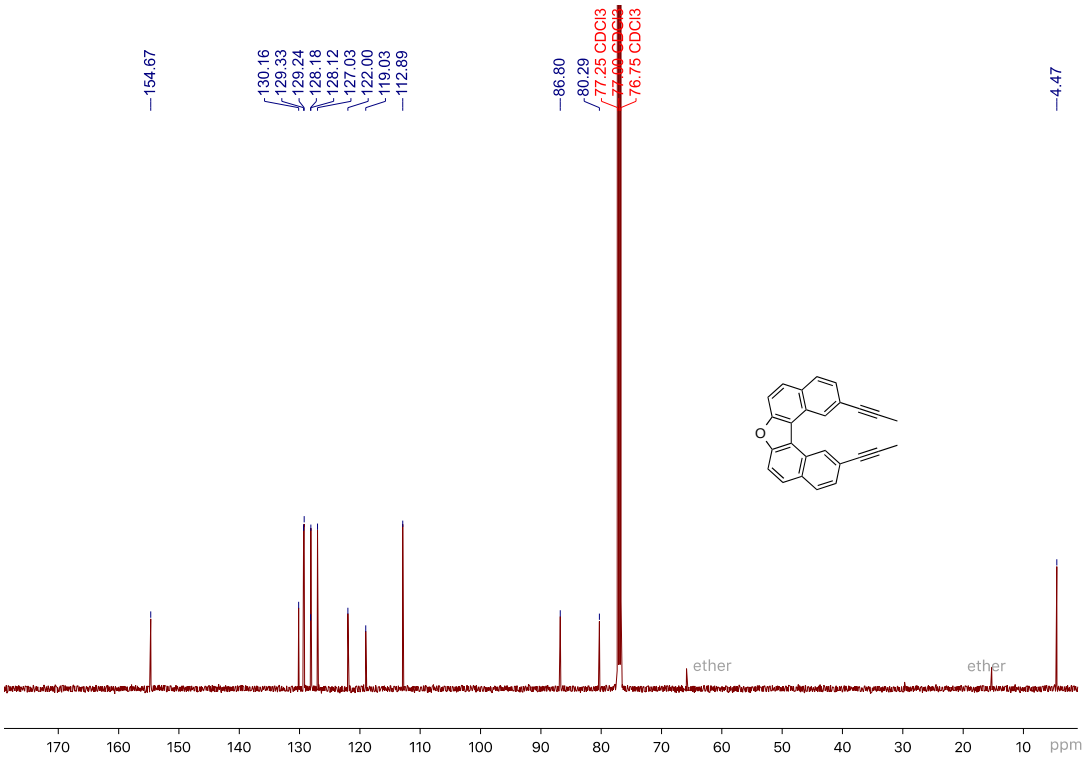

^{13}C NMR spectrum of **8** at 126 MHz in $CDCl_3$.

Scrambling Experiments

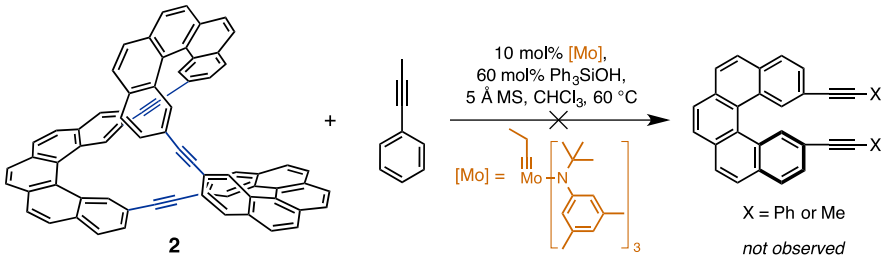

Scrambling experiments under alkyne metathesis conditions demonstrated the kinetic stability of **2** (mixture of both enantiomers) over other linear- or cyclic-oligomers. Trimer **2** was subjected to the alkyne metathesis conditions described above in the presence of 12 equiv. 1-phenyl-1-propyne. After 24 hours, no evidence of trimer ring-opening was observed by ^{1}H or ^{13}C NMR studies (**Figure**). Meanwhile, the formation of diphenylacetylene was observed, indicating that metathesis of 1-phenyl-1-propyne did proceed.

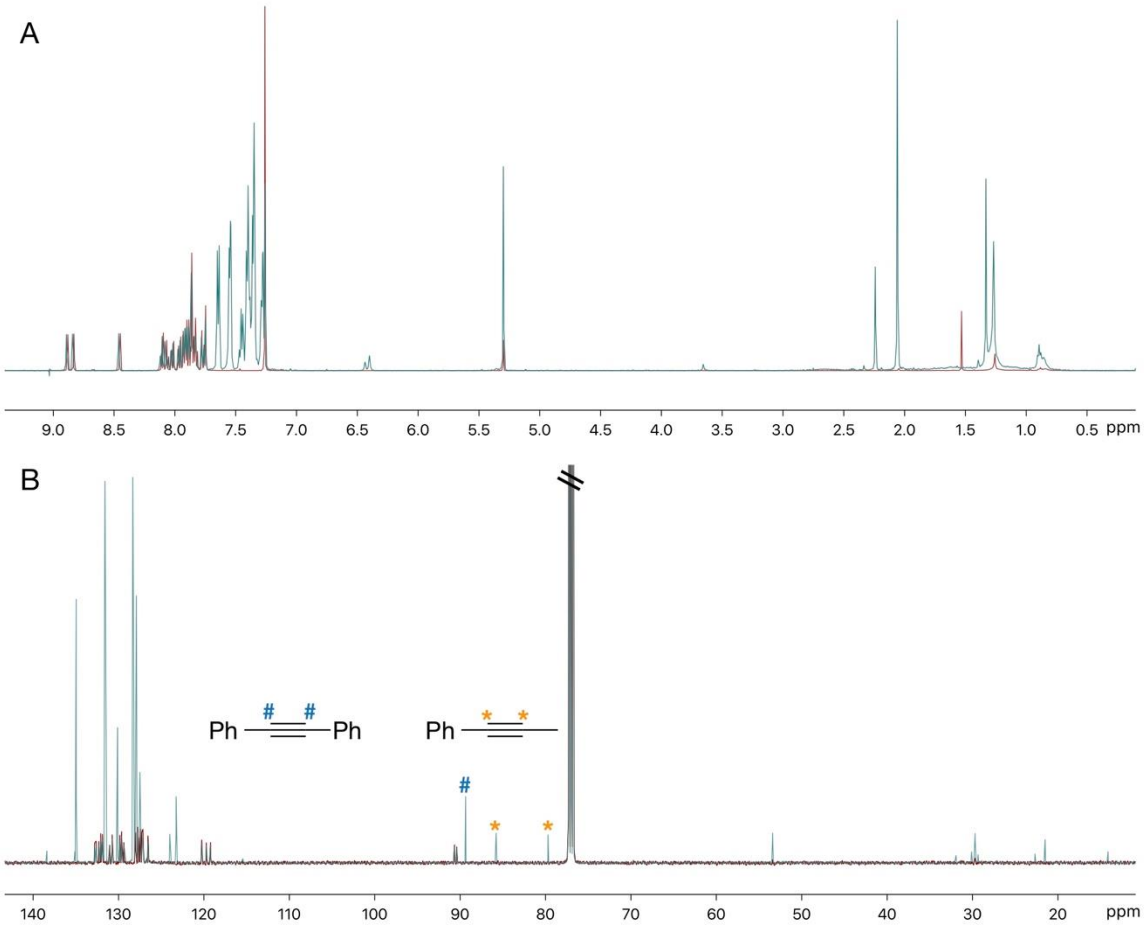

Figure 6.8. (A) The overlaid ^{1}H NMR and (B) ^{13}C NMR spectra of 2 (chestnut) and the crude product (cyan) of the scrambling experiment.

Crystallization and Single Crystal X-Ray Diffraction

A solution of trimer **2** in ethyl acetate in a vial was heated to reflux and was allowed to cool down on a stable shelf. Bright yellow crystals suitable for X-ray diffraction were formed overnight. A short prism of the crystal was covered in oil (Paratone-N, Exxon) before mounted onto a 0.3 mm cryo-loop (Hampton Research) for data collection with Mo K_{α} radiation at 100 K.

UV-Vis and Fluorescence Spectroscopy

UV-Vis spectra of **1** and **2** were obtained in spectrophotometric grade DCM at 9.0 and 3.0 μM, respectively. Fluorescence excitation and emission spectra of **1** and **2** were obtained in spectra grade DCM at ca. 3.0 and 1.0 μM, respectively. The solutions were purged with N_2 for 3 min to remove dissolved oxygen before each measurement. Diphenylanthracene in cyclohexane (90%) was used as the standard for quantum yield measurements.

Chiral HPLC Separation

Separation of enantiomers of **2** was achieved on an analytical HPLC by injection onto a ChiralPak IB-3column eluting with 2% to 10% IPA/Hexane over 20 minutes. Unfortunately, due to its limited solubility, the prep scale separation of **2** was not successful, and CD spectra of $\mathbf{2}_{PPM}$ and $\mathbf{2}_{MMP}$ were not obtained.

<Chromatogram>

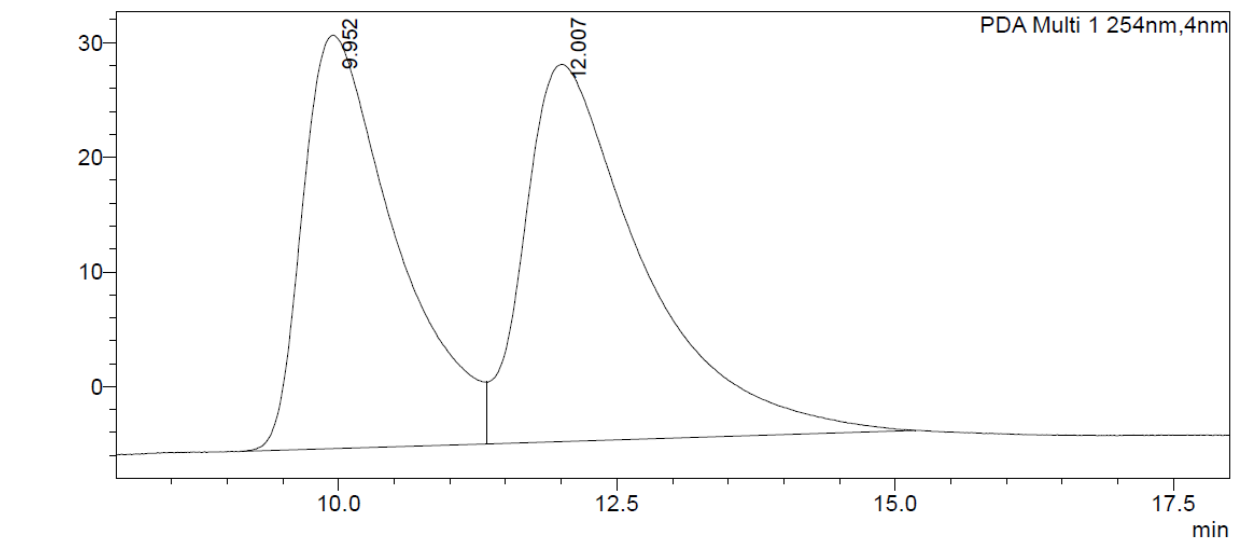

<Peak Table>

PDA Ch1 254nm

Peak#	Ret. Time	Area	Height	Conc.	Area%	Height%
1	9.952	2108963	36068	0.000	46.322	52.284
2	12.007	2443866	32917	0.000	53.678	47.716
Total		4552829	68986		100.000	100.000

6.8.2 Electrochemical Studies

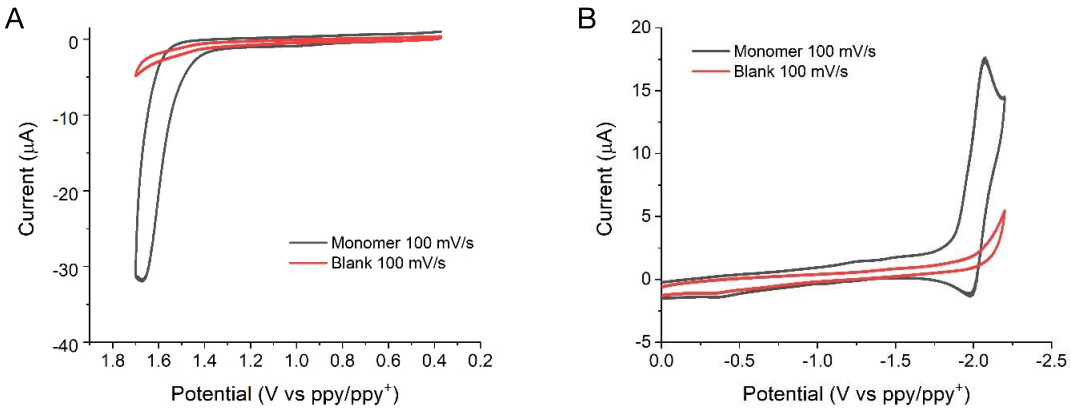

Figure 6.9. Cyclic voltammetry (CV) examining the first oxidation (A) and first reduction (B) of helicene 1.

CV was performed using solutions of 1.37 mM monomer and 0.125 M $TBAPF_6$ in MeCN (black trace) or 0.125 M $TBAPF_6$ in MeCN (red trace) in a glovebox under argon. The electrochemistry was performed at a scan rate of 100 mV/s utilizing a 2 mm Pt disc as a working electrode, a metal/ polypyrrole quasi-reference electrode (ppy/ppy^+), and a Pt wire as a counter electrode. Figure A displays an oxidative wave with an anodic peak at 1.675 V vs ppy/ppy^+, and the corresponding reverse cathodic wave is absent. Figure B displays a cathodic peak at -2.066 V vs ppy/ppy^+ and a smaller corresponding anodic peak at -1.972 V vs ppy/ppy^+. This equates to an approximate half wave potential for the 1^{st} reduction of -2.019 V vs ppy/ppy^+. The current generated from the anodic peak (A) is roughly twice that generated from the cathodic peak (B).

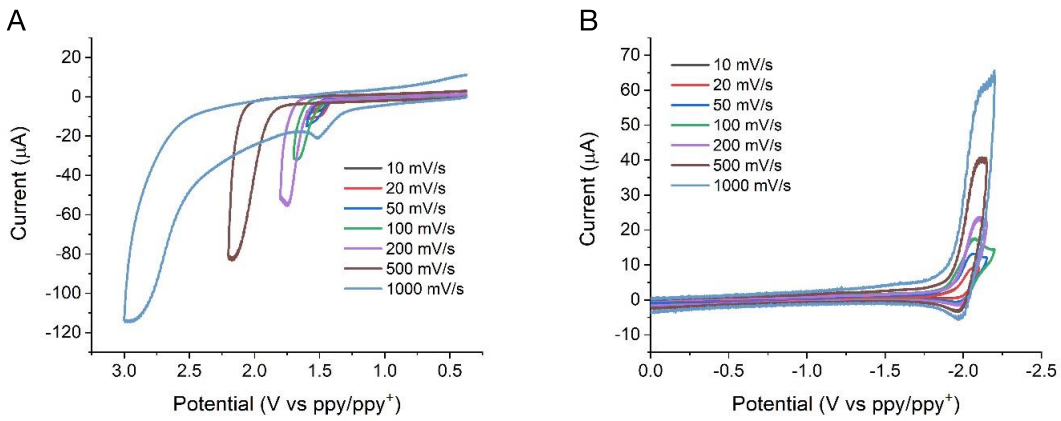

Figure 6.10. CV comparing the effect of scan rate on the 1st oxidation (A) and reduction (B) of helicene 1.

CV was performed with varying scan rates using a solution of 1.37 mM monomer and 0.125 M $TBAPF_6$ in MeCN in a glovebox under argon. The electrochemistry was performed utilizing a 2 mm Pt disc as a working electrode, ppy/ppy^+ reference electrode, and a Pt wire as a counter electrode. The 1st oxidation (A) demonstrated a large shift in potential upon increasing the scan rate and an absence of a corresponding cathodic peak even with probing at higher scan rates. In contrast, the 1st reduction (B) demonstrated very little shift upon increasing the scan rate and at faster scan rates the reverse anodic peak becomes more prominent. This indicates that the electrochemical products of the reduction are relatively more stable than the electrochemical oxidized species in Figure A.

Cyclic Voltammetry and Scan Rate Investigation of 2

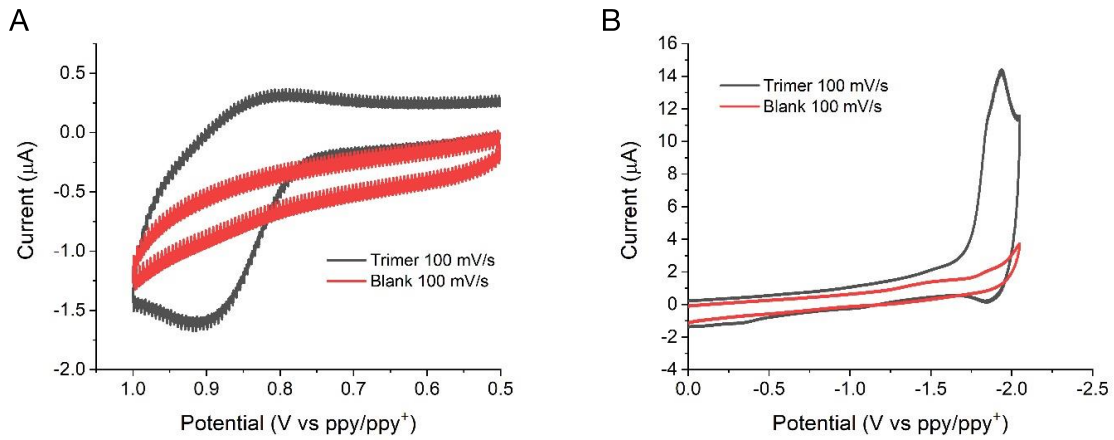

Figure 6.11. CV examining a prominent oxidative surface process (A) and the first reduction (B) of macrocycle 2.

CVs were performed using solutions of 376 μM of **2** and 0.125 M $TBAPF_6$ in MeCN (black trace) or 0.125 M $TBAPF_6$ in MeCN (red trace) in a glovebox under argon. The electrochemistry was performed at a scan rate of 100 mV/s utilizing a 2 mm Pt disc as a working electrode, ppy/ppy^+ reference electrode, and a Pt wire as a counter electrode. The oxidative process displayed an anodic peak at 0.914 V vs ppy/ppy^+, which is roughly 600 mV less anodic than the monomers 1st oxidation (Figure S1A). The y-offset in the blank is most likely due to a difference in sensitivity setting during the two measurements. Regardless, no peaks are observed in the blank, which indicates the observed process is faradaic. The 1st reduction (B) displays a cathodic peak at -1.938 V vs ppy/ppy^+ and corresponding anodic peak at -1.853 V vs ppy/ppy^+. This equates to an approximate half wave potential of 1.896 V vs ppy/ppy^+ for the 1st reduction. This is less 100 mV less cathodic than the corresponding 1st reduction for the monomer **1** (Figure S18B).

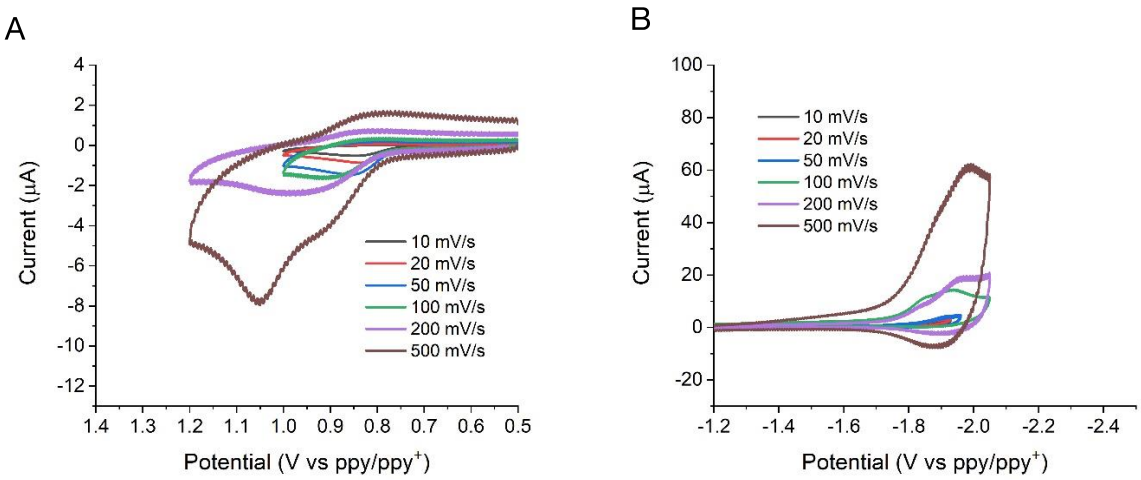

Figure 6.12. CV comparing the effect of scan rate on the oxidative surface process and 1st reduction of macrocycle 2.

CVs were performed using a solution of 376 μM macrocycle **2** and 0.1 M $TBAPF_6$ in MeCN in a glovebox under argon. The electrochemistry was performed at varied scan rates utilizing a 2 mm Pt disc as a working electrode, a ppy/ppy^+ reference electrode, and a Pt wire as a counter electrode. Unlike Figure S19A displaying a faradaic oxidation, the oxidative surface process observed for **2** (A) demonstrates a complex mixture of absorption and precipitation. Similar to Figure S19B, increasing the scan rate for the trimer reduction wave (B) causes the corresponding anodic peak to become more prominent.

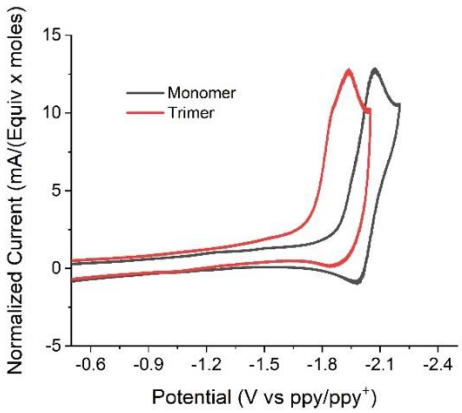

Figure 6.13. Comparison of monomer 1 (black trace) and macrocycle 2 (red trace) CV normalizing the cathodic currents.

Normalization was performed through dividing the current by the product of the number of moles in solution and the hypothesized number of redox active centers (monomer equal to one and trimer equal to three). The close correlation in normalized currents for the monomer and macrocycle CVs, as well as the presence of a single three-electron wave indicates that the global macrocycle structure is capable of accepting three electrons in redox centers that act independently of each other.

6.8.3 Computational Studies

General

All the DFT calculations in this study were carried out using the Gaussian 09 software package.[18] EDDB calculations were based on density matrix of natural atomic orbitals (NAOs) obtained using the NBO 6.0 program,[19] analyzed by the RunEDDB script.[20] Visualization of transition dipole moments was implemented by Multiwfn (v3.7)[21] and VMD (v1.9.3)[22] programs.

Unless stated otherwise, all DFT calculation were performed at B3LYP/6-31G(d) level of theory for C, H, O, and Si atoms, and B3LYP/SDD for Mo. Frequency calculations were performed to confirm that all optimized structures were minima and every transition state has only one imaginary frequency. Intrinsic reaction coordinate (IRC) calculations[23] confirmed the transition states are saddle points in the proposed potential energy surfaces (PES). SMD solvation models[24] were used for C, H, O, and Si atoms in PES calculations ($CHCl_3$), and the Stuttgart MWB28 pseudopotential and basis set were applied to only molybdenum atoms in the solvation models.[25] The SMD model (DCM) was also used in the TD-DFT calculation. The long-range corrected CAM-B3LYP functional[26] was used in the time-dependent DFT (TD-DFT)[27,28] and electron

density of delocalized bonds (EDDB)[29] calculations, in conjunction with basis sets 6-31G(d) for TD-DFT and 6-311G(d,p) for EDDB.

[5]Helicene Helicity Inversion Barrier

DFT calculation (in vacuum) suggests that the barriers of inversion at 298.15 K are essentially the same for [5]helicene and 2,13-diproprynyl-[5]helicene **1**. Coordinates of both compounds at the ground and transition states are in SI Appendix.

Table 6.1. Inversion barrier of parent and substituted [5]helicene.

	Inversion barrier (kcal mol^{-1})		
	ΔE	ΔH	ΔG
[5]helicene	24.3(8)	23.6(0)	24.3(5)
2,13-diproprynyl-[5]helicene **1**	24.4(4)	23.6(1)	25.6(1)

$\mathbf{2}_{PPM}$ and $\mathbf{4}_{PPP}$ Thermodynamic Stability

Both macrocycles **2** and **4** are optimized at B3LYP/6-31G(d) level of theory. High-level single-point energy calculations were performed on the optimized structures, suggesting that $\mathbf{4}_{PPP}$ is thermodynamically more stable than $\mathbf{2}_{PPM}$ by 1−2 kcal/mol. Minimal entropy/temperature contribution to the relative stability was observed (less than 0.1 kcal/mol over 100 K). ($\Delta E = E_{\mathrm{PPP}} - E_{\mathrm{PPM}}$)

Table 6.2. Thermodynamic stabilities of cyclic trimers **2** and **4**.

Methods	Relative energy differences (kcal/mol)			
	ΔE	ΔZPE	ΔH	ΔG
M06-2X/def2-TVZP	-1.1	-1.2	-1.2	-0.9
B3LYP/def2-TZVP	-2.9	-3.0	-3.0	-2.8
PBE0/def2TZVP	-2.1	-2.2	-2.2	-2.0

Mechanism for *PPM*/*PPP* Selectivity

The energy barriers of the last step of macrocyclic 3mer formation were studied. Basis set superposition error (BSSE) values calculated in gas phase for **2**$_{PPM}$···Mo and **4**$_{PPP}$···Mo are 0.00425 a.u. and 0.00332 a.u., respectively. The BSSE correction has been applied to the sum of product energies. Uncorrected energies are provided in parentheses.

Table 6.3. Relative energies of intermediates and transition states of **2**$_{PPM}$ and **4**$_{PPP}$ formation.

	O3	**TS1**	**IM1(IM)**	**IM2**	**TS2**	3mer + Mo
2$_{PPM}$ *G* (kcal/mol)	0.0	21.6	13.6	-	-	-16.5 (-13.8)
2$_{PPM}$ *H* (kcal/mol)	0.0	15.1	5.5	-	-	-4.2 (-1.6)
4$_{PPP}$ *G* (kcal/mol)	0.0	37.0	26.0	24.5	28.2	-14.4 (-12.3)
4$_{PPP}$ *H* (kcal/mol)	0.0	29.9	18.8	18.6	21.2	-3.1 (-1.0)

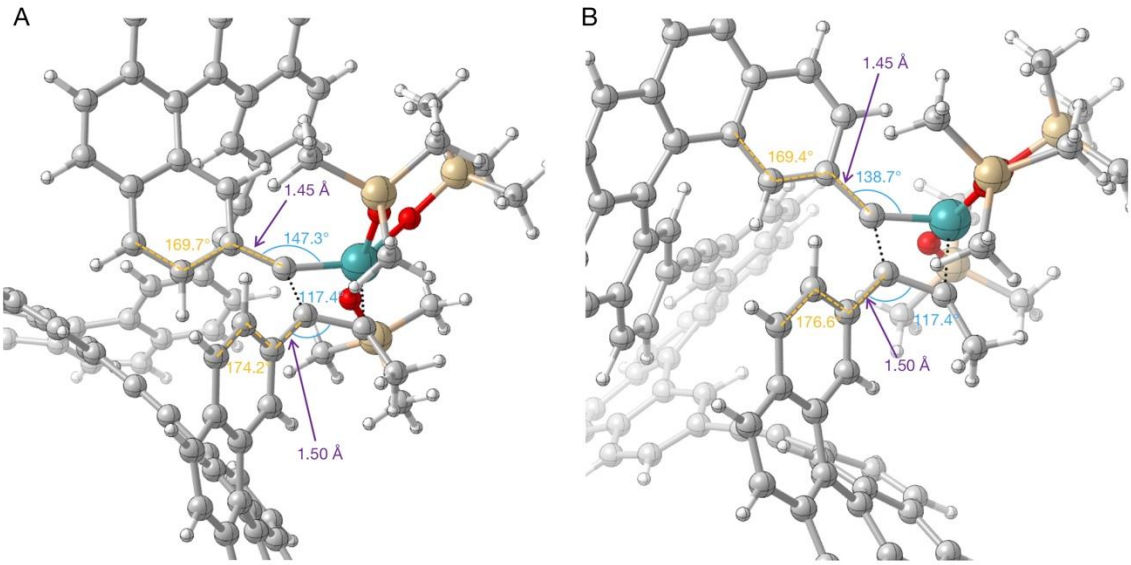

Figure 6.14. Key structure parameters, including bond angles (blue), bond length (purple), and dihedral angles (yellow) in TS1$_{PPM}$ **(A) and TS1**$_{PPP}$ **(B).**

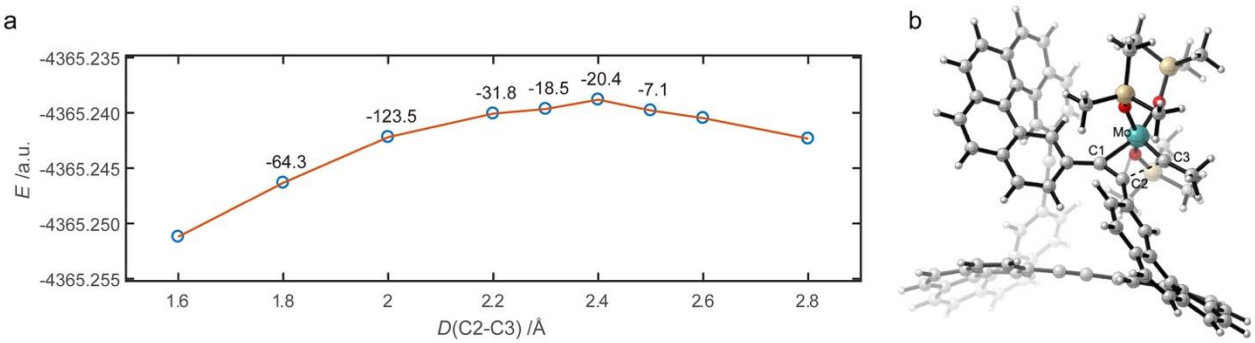

Figure 6.15. Relaxed potential energy surface (PES) scan (a) with fixed C2-C3 distances (b).

Imaginary frequencies correspond to the C2-C3 stretching vibration, and the values are given in cm^{-1}. Transition state searches based on the points including the one with the most negative imaginary frequency (C2-C3: 2.0 Å) and the one with highest energy (C2-C3: 2.4 Å), all failed to locate the **TS2** of PPM but directly lead to the product.

UV and ECD Spectra Prediction

The TD-DFT calculation was performed at CAM/6-31G(d) level of theory. A total of 10 and 50 states were calculated for the monomer and 3mer. The SMD was also applied to TD-DFT calculations in the singlet electronic state (solvent: DCM). The ECD of $\mathbf{2}_{PPM}$ is predicted to have a (+) peak at around 300 nm, and a (-) peak at approximately 380 nm.

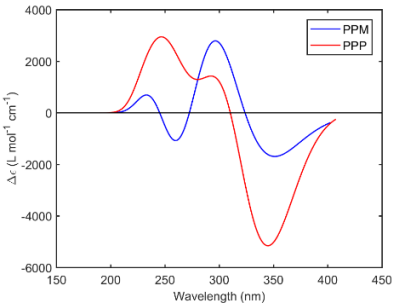

Figure 6.16. Calculated ECD of 2_{PPM} and 4_{PPP}.

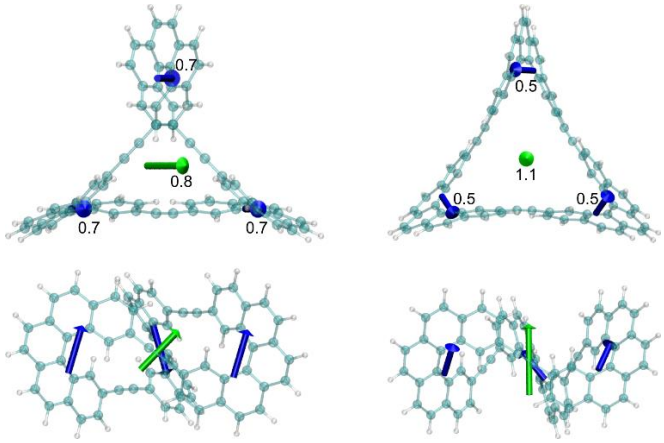

Figure 6.17. Electric transition dipole moments ($S_0 \rightarrow S_1$) of $\mathbf{2}_{PPM}$ (left) and $\mathbf{4}_{PPP}$ (right). Unit: Debye. Blue arrows indicate the contribution of transition dipole moments from helicene fragments, not including bridging moieties.

Table 6.4. Calculated oscillator strength of **1** (right, 10 states) and **2** (left, 50 states)

Index	Excit. energy(eV)	nm	Oscil.str.
1	3.4224	362.5237	0.0073
2	3.6167	343.04783	0.3322
3	3.6219	342.55532	0.2537
4	3.6354	341.28324	0.0002
5	3.6694	338.12097	0.5353
6	3.6887	336.35186	0.8579
7	3.9902	310.93707	0.7701
8	4.0003	310.15201	1.0035
9	4.0444	306.77013	0.0353
10	4.1825	296.64103	0.2784
11	4.2127	294.51447	0.5901
12	4.2611	291.16921	0.0311
13	4.2654	290.87567	0.0011
14	4.299	288.60226	0.7402
15	4.3461	285.47459	0.0179
16	4.3493	285.26455	0.3253
17	4.3828	283.08412	0.1002
18	4.4678	277.69844	0.149
19	4.4836	276.71985	0.2453
20	4.4926	276.16549	0.0602
21	4.5168	274.68586	0.0375
22	4.5825	270.74765	0.0099
23	4.7096	263.44087	0.0266
24	4.7138	263.20614	0.1152
25	4.741	261.69608	0.2973
26	4.7567	260.83232	0.0155
27	4.7774	259.70216	0.8144
28	4.8161	257.61531	0.1038
29	4.8831	254.08063	0.1246
30	4.8992	253.24565	0.3653
31	4.919	252.22629	0.0063

Index	Excit. energy(eV)	nm	Oscil.str.
1	3.6675	338.29614	0
2	3.8187	324.90143	0.1997
3	4.1565	298.4966	0.3642
4	4.3328	286.35088	0.0609
5	4.4539	278.5651	0.506
6	4.5023	275.57051	0.6415
7	4.7618	260.55296	0.021
8	4.9199	252.18015	0.2637
9	5.0559	245.39669	0.1907
10	5.0928	243.61866	0.5567

Table 6.4. (cont.)

32	4.9381	251.2507	0.199
33	4.9573	250.27759	0.0111
34	5.0022	248.03109	0.0043
35	5.03	246.66026	0.0115
36	5.0328	246.52303	0.0064
37	5.0658	244.91711	0.0146
38	5.0898	243.76225	0.0047
39	5.1036	243.10312	0.0452
40	5.1774	239.63787	0.005
41	5.1845	239.30969	0.1345
42	5.2045	238.39007	0.0623
43	5.219	237.72774	0.306
44	5.2192	237.71864	0.0356
45	5.2645	235.67311	0.2188
46	5.2813	234.92343	0.3211
47	5.2828	234.85672	0.012
48	5.3131	233.51736	0.0028
49	5.3593	231.50432	0.009
50	5.3681	231.12481	0.047

ACID and EDDB Plots

Anisotropy of the induced ring current density (ACID)[30,31] calculations were performed at the B3LYP/6-311G(d,p) level, using the continuous set of gauge transformation (CSGT)[32] method. EDDB calculation utilized the CAM-B3LYP functional with 6-311G(d,p) basis sets.

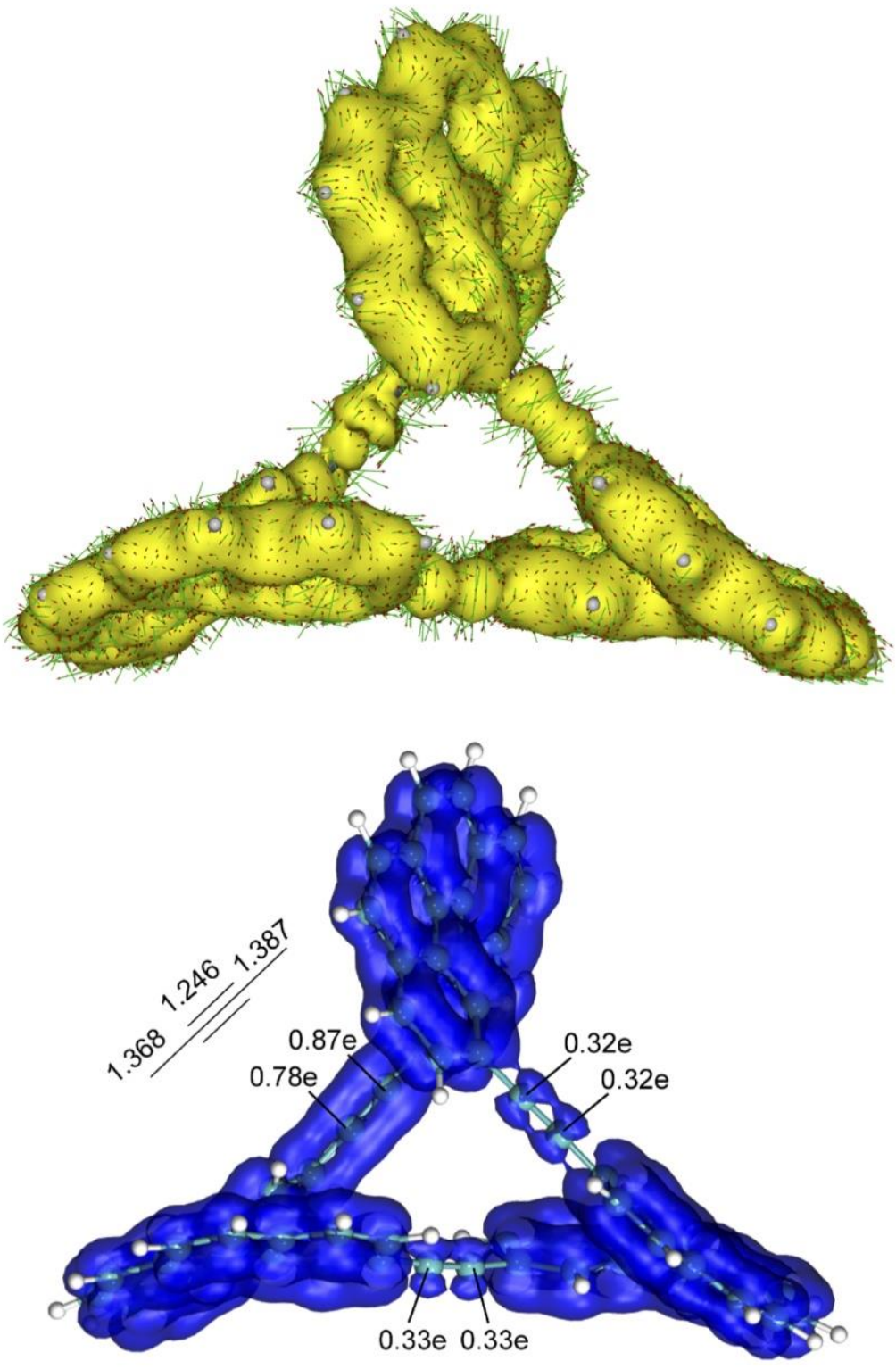

Figure 6.18. The ACID and EDDP plots of 2_{PPM} showing a higher level of conjugation through one of the three triple bonds at the T1 excited state.

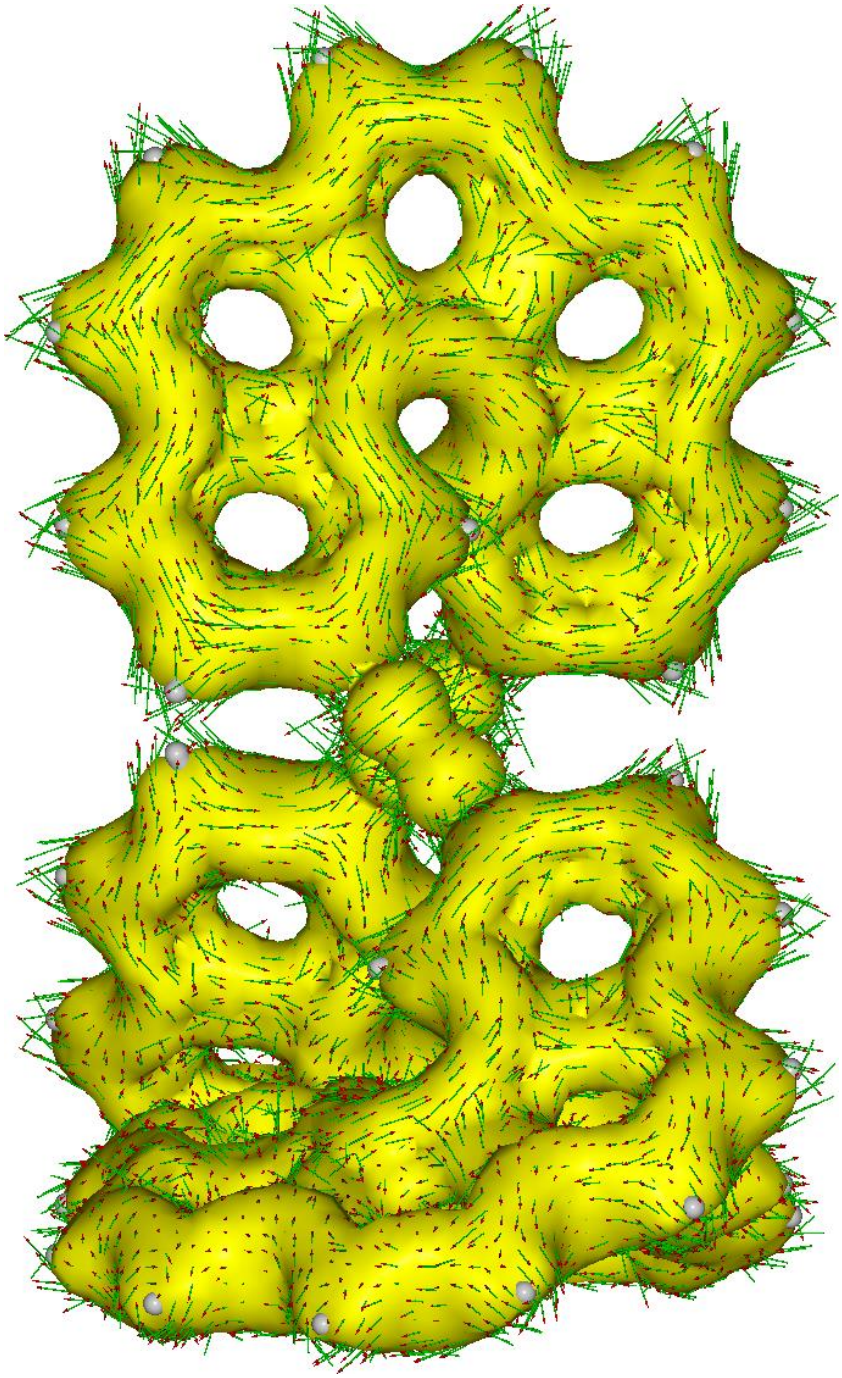

Figure 6.19. The ACID plot of 4*PPP*.

6.9 Literature Cited

(1) For recent books and reviews on DCC, see: (a) Dynamic Covalent Chemistry: Principles, Reactions, and Applications; Zhang, W., Jin, Y., Eds.; John Wiley & Sons, Ltd.: Chichester, UK, **2017**. (b) Dynamic Combinatorial Chemistry; Reek, J. N. H., Otto, S., Eds.; Wiley-VCH: Weinheim, Germany, **2010**. (c) Frei, P.; Hevey, R.; Ernst, B. Dynamic Combinatorial Chemistry: A New Methodology Comes of Age. *Chem. Eur. J.* **2019**, *25*, 60–73. (d) Rowan, S. J.; Cantrill, S. J.; Cousins, G. R. L.; Sanders, J. K. M.; Stoddart, J. F. Dynamic Covalent Chemistry. *Angew. Chem. Int. Ed.* **2002**, *41*, 898–952.

(2) (a) Hillenbrand, J.; Leutzsch, M.; Fürstner, A. Molybdenum Alkylidyne Complexes with Tripodal Silanolate Ligands: The Next Generation of Alkyne Metathesis Catalysts. *Angew. Chem. Int. Ed.* **2019**, *58*, 15690–15696. (b) Thompson, R. R.; Rotella, M. E.; Du, P.; Zhou, X.; Fronczek, F. R.; Kumar, R.; Gutierrez, O.; Lee, S. Siloxide Podand Ligand as a Scaffold for Molybdenum-Catalyzed Alkyne Metathesis and Isolation of a Dynamic Metallatetrahedrane Intermediate. *Organometallics* **2019**, *38*, 4054–4059. (c) Ehrhorn, H.; Tamm, M. Well-Defined Alkyne Metathesis Catalysts: Developments and Recent Applications. *Chem. Eur. J.* **2019**, *25*, 3190–3208. (d) Du, Y.; Yang, H.; Zhu, C.; Ortiz, M.; Okochi, K. D.; Shoemaker, R.; Jin, Y.; Zhang, W. Highly Active Multidentate Ligand-Based Alkyne Metathesis Catalysts. *Chem. Eur. J.* **2016**, *22*, 7959–7963. (e) Fürstner, A. Alkyne Metathesis on the Rise. *Angew. Chem. Int. Ed.* **2013**, *52*, 2794–2819.

(3) (a) Lee, S.; Yang, A.; Moneypenny, II, T. P.; Moore, J. S. Kinetically Trapped Tetrahedral Cages via Alkyne Metathesis. *J. Am. Chem. Soc.* **2016**, *138*, 2182–2185. (b) Wang, Q.; Zhang, C.; Noll, B. C.; Long, H.; Jin, Y.; Zhang, W. A Tetrameric Cage with D2h Symmetry through Alkyne Metathesis. *Angew. Chem. Int. Ed.* **2014**, *53*, 10663–10667.

(4) (a) Rzepa, H. S. Möbius Aromaticity and Delocalization. *Chem. Rev.* **2005**, *105*, 3697–3715. (b) Herges, R. Topology in Chemistry: Designing Möbius Molecules. *Chem. Rev.* **2006**, *106*, 4820–4842. (c) Yoon, Z. S.; Osuka, A.; Kim, D. Möbius Aromaticity and Antiaromaticity in Expanded Porphyrins. *Nat. Chem.* **2009**, *1*, 113–122.

(5) For reviews on Möbius structures of porphyrinoids, see: (a) Stępień, M.; Sprutta, N.; Latos-Grazyński, L. Figure Eights, Möbius Bands, and More: Conformation and Aromaticity of Porphyrinoids. *Angew. Chem. Int. Ed.* **2011**, *50*, 4288–4340. (b) Saito, S.; Osuka, A. Expanded Porphyrins: Intriguing Structures, Electronic Properties, and Reactivities. *Angew. Chem. Int. Ed.* **2011**, *50*, 4342–4373.

(6) (a) Naulet, G.; Sturm, L.; Robert, A.; Dechambenoit, P.; Röhricht, F.; Herges, R.; Bock, H.; Durola, F. Cyclic Tris-[5]Helicenes with Single and Triple Twisted Möbius Topologies and Möbius Aromaticity. *Chem. Sci.* **2018**, *9*, 8930–8936. (b) Schaller, G. R.; Topić, F.; Rissanen, K.; Okamoto, Y.; Shen, J.; Herges, R. Design and Synthesis of the First Triply Twisted Möbius Annulene. *Nat. Chem.* **2014**, *6*, 608–613.

(7) Nishigaki, S.; Shibata, Y.; Nakajima, A.; Okajima, H.; Masumoto, Y.; Osawa, T.; Muranaka, A.; Sugiyama, H.; Horikawa, A.; Uekusa, H.; Koshino, H.; Uchiyama, M.; Sakamoto, A.; Tanaka, K. Synthesis of Belt- and Möbius-Shaped Cycloparaphenylenes by Rhodium-Catalyzed Alkyne Cyclotrimerization. *J. Am. Chem. Soc.* **2019**, *141*, 14955–14960.

(8) Heilbronner, E. Hückel Molecular Orbitals of Möbius-Type Conformations of Annulenes. *Tetrahedron Lett.* **1964**, *5*, 1923–1928.

(9) Ajami, D.; Oeckler, O.; Simon, A.; Herges, R. Synthesis of a Möbius Aromatic Hydrocarbon. *Nature* **2003**, *426*, 819–821.

(10) Jhulki, S.; Mishra, A. K.; Chow, T. J.; Moorthy, J. N. Helicenes as All-in-One Organic Materials for Application in OLEDs: Synthesis and Diverse Applications of Carbo- and Aza[5]Helical Diamines. *Chem. Eur. J.* **2016**, *22*, 9375–9386.

(11) (a) Gingras, M.; Félix, G.; Peresutti, R. One Hundred Years of Helicene Chemistry. Part 2: Stereoselective Syntheses and Chiral Separations of Carbohelicenes. *Chem. Soc. Rev.* **2013**, *42*, 1007–1050. (b) Goedicke, C.; Stegemeyer, H. Resolution and Racemization of Pentahelicene. Tetrahedron Lett. 1970, 11, 937–940. (c) Berezhnaia, V.; Roy, M.; Vanthuyne, N.; Villa, M.; Naubron, J.-V.; Rodriguez, J.; Coquerel, Y.; Gingras, M. Chiral Nanographene Propeller Embedding Six Enantiomerically Stable [5]Helicene Units. *J. Am. Chem. Soc.* **2017**, *139*, 18508–18511.

(12) CYLview, 1.0b; Legault, C. Y., Université de Sherbrooke, **2009** (http://www.cylview.org)

(13) (a) Shen, M.; Rodríguez-López, J; Lee, Y.-T.; Chen, C.-T.; Fan. F.-R. F.; Bard, A. J. Electrochemistry and Electrogenerated Chemiluminescence of a Novel Donor-Acceptor FPhSPFN Red Fluorophore *J. Phys. Chem. C.* **2010**, *114*, 9772–9780 (b) Shen, M.; Rodríguez-López, J; Huang, J.; Liu, Q.; Zhu, X.-H.; Bard, A. J. Electrochemistry and Electrogenerated Chemiluminescence of Dithienylbenzothiadiazole Derivative. Differential Reactivity of Donor and Acceptor Groups and Simulations of Radical Cation-Anion and Dication-Radical Anion Annihilations *J. Am. Chem. Soc.* **2010**, *132*, 13453–13461.

(14) Geuenich, D.; Hess, K.; Köhler, F.; Herges, R. Anisotropy of the Induced Current Density (ACID), a General Method to Quantify and Visualize Electronic Delocalization. *Chem. Rev.* **2005**, *105*, 3758–3772.

(15) Jhulki, S.; Mishra, A. K.; Chow, T. J.; Moorthy, J. N. Helicenes as All-in-One Organic Materials for Application in OLEDs: Synthesis and Diverse Applications of Carbo- and Aza[5]Helical Diamines. *Chem. Eur. J.* **2016**, *22*, 9375–9386.

(16) Tagliavini, E.; Umani-Ronchi, A. Synthesis and Characterization of New Enantiopure 7,7′-Disubstituted 2,2′-Dihydroxy-1,1′-Binaphthyls: Useful Ligands for the Asymmetric Allylation Reaction of Aldehydes. *Eur. J. Org. Chem.* **2000**, 491–497.

(17) Schneider, J. F.; Nieger, M.; Nättinen, K.; Dötz, K. H. A Novel Approach to Functionalized Heterohelicenes via Chromium-Templated Benzannulation Reactions. *Synthesis* **2005**, *7*, 1109–1124.

(18) Frisch, M. J. et al. Gaussian 09, Revision E.01, Gaussian, Inc., Wallingford CT, 2013.

(19) Glendening, E. D.; Badenhoop, J. K.; Reed, A. E.; Carpenter, J. E.; Bohmann, J. A.; Morales, C. M.; Landis, C. R.; Weinhold, F. NBO 6.0. Theoretical Chemistry Institute, University of Wisconsin, Madison, 2013.

(20) Szczepanik, D. W. RunEDDB, available at: http://eddb.pl/runeddb/ (accessed in November 2019).

(21) Lu, T.; Chen, F. Multiwfn: A Multifunctional Wavefunction Analyzer. *J. Comput. Chem.* **2012**, *33*, 580–592.

(22) Humphrey, W.; Dalke, A.; Schulten, K. VMD: Visual Molecular Dynamics. *J. Mol. Graph.* **1996**, *14*, 33–38.

(23) Fukui, K. The Path of Chemical Reactions - The IRC Approach. *Acc. Chem. Res.* **1981**, *14*, 363–368.

(24) Marenich, A. V.; Cramer, C. J.; Truhlar, D. G. Universal Solvation Model Based on Solute Electron Density and on a Continuum Model of the Solvent Defined by the Bulk Dielectric Constant and Atomic Surface Tensions. *J. Phys. Chem. B* **2009**, *113*, 6378–6396.

(25) Andrae, D.; Häußermann, U.; Dolg, M.; Stoll, H.; Preuß, H. Energy-Adjusted Ab Initio Pseudopotentials for the Second and Third Row Transition Elements. *Theor. Chim. Acta* **1990**, *77*, 123–141.

(26) Yanai, T.; Tew, D. P.; Handy, N. C. A New Hybrid Exchange-Correlation Functional Using the Coulomb-Attenuating Method (CAM-B3LYP). *Chem. Phys. Lett.* **2004**, *393*, 51–57.

(27) Bauernschmitt, R.; Ahlrichs, R. Treatment of Electronic Excitations within the Adiabatic Approximation of Time Dependent Density Functional Theory. *Chem. Phys. Lett.* **1996**, *256*, 454–464.

(28) Scalmani, G.; Frisch, M. J.; Mennucci, B.; Tomasi, J.; Cammi, R.; Barone, V. Geometries and Properties of Excited States in the Gas Phase and in Solution: Theory and Application of a Time-Dependent Density Functional Theory Polarizable Continuum Model. *J. Chem. Phys.* **2006**, *124*, 094107.

(29) Szczepanik, D. W.; Andrzejak, M.; Dyduch, K.; Żak, E.; Makowski, M.; Mazur, G.; Mrozek, J. A Uniform Approach to the Description of Multicenter Bonding. *Phys. Chem. Chem. Phys.* **2014**, *16*, 20514–20523.

(30) Geuenich, D.; Hess, K.; Köhler, F.; Herges, R. Anisotropy of the Induced Current Density (ACID), a General Method to Quantify and Visualize Electronic Delocalization. *Chem. Rev.* **2005**, *105*, 3758–3772.

(31) Herges, R.; Geuenich, D. Delocalization of Electrons in Molecules. *J. Phys. Chem. A* **2001**, *105*, 3214–3220.

(32) Keith, T. A.; Bader, R. F. W. Topological Analysis of Magnetically Induced Molecular Current Distributions. *J. Chem. Phys.* **1993**, *99*, 3669–3682.